NASA Technical Paper 2283

April 1984

Effect of Aerodynamic and Angle-of-Attack Uncertainties on the Blended Entry Flight Control System of the Space Shuttle From Mach 10 to 2.5

Howard W. Stone and
Richard W. Powell

NASA

NASA Technical Paper 2283

1984

Effect of Aerodynamic and Angle-of-Attack Uncertainties on the Blended Entry Flight Control System of the Space Shuttle From Mach 10 to 2.5

Howard W. Stone and
Richard W. Powell

Langley Research Center
Hampton, Virginia

NASA
National Aeronautics
and Space Administration

Scientific and Technical Information Branch

CONTENTS

SUMMARY

A six-degree-of-freedom simulation analysis has been performed for the Space Shuttle Orbiter during entry from Mach 10 to 2.5 with realistic off-nominal conditions using the flight control system usually referred to as the blended entry digital autopilot specified in May 1978. The off-nominal conditions included the following: (1) aerodynamic uncertainties in extrapolating from wind-tunnel-derived characteristics to full-scale flight characteristics, (2) an error in deriving the angle of attack from onboard instrumentation, (3) the failure of two of the four reaction control-system thrusters on each side (design specification), and (4) a lateral center-of-gravity offset and vehicle asymmetries.

With combinations of the above off-nominal conditions, the control system performed satisfactorily with a few exceptions. The cases that did not exhibit satisfactory performance displayed the following main weaknesses. Marginal performance was exhibited at hypersonic speeds for a few cases with a sensed angle-of-attack error of 4°. At supersonic speeds the system tended to be oscillatory, particularly with increased rudder effectiveness. The system diverged for several cases because of the inability to hold lateral trim. Several system modifications were suggested to help solve these problems and to maximize safety on the first flight: alter the elevon-trim and speed-brake schedules to keep the elevon more positive at the higher supersonic speeds, delay switching to rudder trim until the rudder effectiveness is adequate, and reduce the overall rudder loop gain. These and other modifications were incorporated in a flight-control-system redesign in May 1979.

INTRODUCTION

A reusable Earth-to-orbit transportation system known as the Space Shuttle has been developed by the National Aeronautics and Space Administration (NASA). The Space Shuttle is designed to insert payloads of up to 29 500 kg into a near-Earth orbit, retrieve payloads already in orbit, and land with a payload of up to 14 500 kg. The Space Shuttle consists of an Orbiter, an external fuel tank, and two solid rocket boosters (SRB). The SRB's will be recovered after each launch for limited reuse. The external tank is designed for one use and is not recovered.

The Orbiter will have the capability to enter the Earth's atmosphere, glide up to a 2040-km cross range, and land horizontally. A closed-loop entry guidance system has been developed to provide the necessary commands for either the automatic flight control system or a pilot-operated, augmented flight control system. A general description of the Space Shuttle configuration and mission is given in reference 1, and the Orbiter avionics are described in reference 2.

The initial flights of the Space Shuttle are designed to verify the vehicle flight worthiness. The first flight was designed to demonstrate the safe ascent and return of the Orbiter and crew for conservative flight conditions. The vehicle was launched from the John F. Kennedy Space Center into a 220-km circular orbit inclined 38°. After approximately 20 orbits, a deorbit maneuver occurred, which was followed by the entry and landing at the Hugh L. Dryden Flight Research Facility of the Ames Research Center. A further description of this flight is presented in reference 3.

The NASA Langley Research Center performed evaluations of the guidance and flight control system as it evolved for the first mission. These evaluations were performed to cover system uncertainties thoroughly, identify weaknesses, and suggest appropriate modifications to maximize mission safety. The analysis reported herein is concerned with the flight control system, usually referred to as the blended entry digital autopilot, which was specified by the contractor in May 1978. This control system, which was developed under the guidance of the Lyndon B. Johnson Space Center, has evolved from the system analyzed in reference 4. The analysis of the flight control system was performed with the aid of a six-degree-of-freedom simulation with man-in-the-loop capability. The flight regime studied was from a Mach number of approximately 10 and an altitude of 50 km down to the initiation of the terminal-area-energy management (TAEM) guidance phase, which occurs at an altitude of approximately 26 km at a Mach number of 2.5. This 360-sec segment of the entry represents the period where the Orbiter performs its most extreme maneuvers, where the aerodynamic parameters are undergoing significant changes as the vehicle decelerates from hypersonic to low-supersonic velocities, and where the angle of attack is lowered from 36° to 10°. These simulation studies considered the center of gravity to be located at 66.25 percent of the body reference length with a lateral center-of-gravity offset of 0.0381 m (1.5 in.) toward the right wing (the maximum amount allowed by Shuttle design specifications). In addition, two of the four yaw thrusters on each side were assumed to be inoperable (off). The design specification calls for the Space Shuttle Orbiter to be able to fly safely with this condition. To these were added the aerodynamic uncertainties (ref. 5) that are intended to encompass any differences that might occur between the wind-tunnel data base and actual flight values. These uncertainties are based on the scatter in the wind-tunnel data and historical comparisons of flight and wind-tunnel data for various aircraft and lifting-body configurations. In addition to uncertainties, projected errors in deriving angle of attack from onboard instrumentation were included in the simulations. Since the Orbiter has no method of directly measuring angle of attack until velocity has been reduced to Mach 2.5, this error was initially estimated to be as much as ±4°. Without the aerodynamic uncertainties and the sensed angle-of-attack error, the flight control system is able to fly the entry mission safely.

Following the study reported in reference 4, the roll and yaw channels of the flight control system were extensively modified to decrease the sensitivity to errors in sensed angle of attack. The study described herein is similar to the study reported in reference 4 except for the modified control laws. The baseline preflight trajectory for the first Space Shuttle launch (STS-1) was studied with these aerodynamic uncertainties and angle-of-attack error, and control-system modifications were suggested to handle the problems that were encountered.

SYMBOLS

All coefficients and vehicle rates are in the body-axis system. Computer symbols used in the figures are shown in parentheses. Values are given in SI Units and, where considered useful, also in U.S. Customary Units. Measurements and calculations were made in U.S. Customary Units.

b	reference wing span, m
C_l	rolling-moment coefficient, Rolling moment/$q_\infty Sb$
C_{l_β}	effective-dihedral parameter, $\partial C_l/\partial\beta$, deg^{-1}

$C_{l_{\delta a}}$		rolling-moment coefficient due to aileron deflection, $\partial C_l/\partial \delta_a$, deg^{-1}
$C_{l_{\delta r}}$		rolling-moment coefficient due to rudder deflection, $\partial C_l/\partial \delta_r$, deg^{-1}
C_m		pitching-moment coefficient, Pitching moment/$q_\infty S\bar{c}$
C_n		yawing-moment coefficient, Yawing moment/$q_\infty Sb$
C_{n_β}		directional-stability parameter, $\partial C_n/\partial \beta$, deg^{-1}
$C_{n_{\delta a}}$		yawing-moment coefficient due to aileron deflection, $\partial C_n/\partial \delta_a$, deg^{-1}
$C_{n_{\delta r}}$		yawing-moment coefficient due to rudder deflection, $\partial C_n/\partial \delta_r$, deg^{-1}
C_Y		side-force coefficient, Side force/$q_\infty S$
C_{Y_β}		side-force coefficient due to sideslip angle, deg^{-1}
$C_{Y_{\delta r}}$		side-force coefficient due to rudder deflection, $\delta C_Y/\partial \delta_r$, deg^{-1}
$\bar{c}$		mean aerodynamic chord, m
DN_Y		stability-axis yaw rate due to side acceleration, deg/sec
g		acceleration due to gravity, where 1g = 9.8 m/sec^2 (32.152 ft/sec^2)
I_{sp}		specific impulse, sec
I_X		moment of inertia about body roll axis, $kg\text{-}m^2$
I_Y		moment of inertia about body pitch axis, $kg\text{-}m^2$
I_Z		moment of inertia about body yaw axis, $kg\text{-}m^2$
I_{XY}		product of inertia in body XY-plane, $kg\text{-}m^2$
I_{XZ}		product of inertia in body XZ-plane, $kg\text{-}m^2$
I_{YZ}		product of inertia in body YZ-plane, $kg\text{-}m^2$
M		Mach number
N_Y		side acceleration, g units
P_c		commanded roll rate, deg/sec
p	(P)	roll rate about body axis, deg/sec

p'		$= p + (180g \sin \theta \tan \phi)/\pi V_R$
q_∞		free-stream dynamic pressure, Pa
r		yaw rate about body axis, deg/sec
r'	(RPRIME)	$= r - (180g \sin \phi \cos \theta)\pi V_R$
S		reference area, m^2
V_R		Earth's relative velocity, m/sec
X,Y,Z		roll, pitch, and yaw body axes, respectively
α	(ALPHA)	angle of attack, deg
α_c	(ALPHAC)	commanded angle of attack, deg
β	(BETA)	sideslip angle, deg
Δ		increment
δ_a	(DELA)	aileron-deflection angle, [(Left elevon) - (Right elevon)]/2, deg
δ_{BF}	(DELBF)	body-flap-deflection angle (positive down), deg
δ_e	(DELE)	elevator-deflection angle (positive down), [(Left elevon) + (Right elevon)]/2, deg
δ_r	(DELR)	rudder-deflection angle (positive trailing edge left), deg
δ_{SB}	(DELSB)	speed-brake-deflection angle, deg
θ		pitch angle about body axis, deg
σ		standard deviation
ϕ	(PHI)	roll angle about body axis, deg
ϕ_c	(PHICM)	commanded roll angle, deg

Abbreviations:

DAP	digital autopilot
GDRC	scheduled rudder forward-loop gain
KGDA	scheduled aileron forward-loop gain
RCS	reaction control system

TAEM terminal-area-energy management

(YAWJET) number of yaw RCS thrusters firing (positive right side thrusters)

A dot over a symbol indicates the rate of change with time.

DESCRIPTION OF SPACE SHUTTLE ORBITER

The physical characteristics of the Orbiter are summarized in table I. The longitudinal center of gravity is located at 66.25 percent of the body reference length measured from the nose. A sketch of the Orbiter and its control effectors (control surfaces and reaction-control-system (RCS) thrusters) is shown in figure 1. The baseline trajectory is depicted on a world map in figure 2, and figure 3 shows the time history of selected nominal trajectory parameters.

Guidance System

The guidance system has separate algorithms for the three different guidance regimes: entry, terminal-area-energy management, and autoland. The entry guidance is designed to take the Orbiter from the atmospheric interface, at an altitude of 122 km, down to the initiation of the terminal-area-energy-management (TAEM) phase which occurs at an altitude of approximately 26 km at Mach 2.5. At an altitude of approximately 3 km, the autoland guidance is engaged and directs the Orbiter until touchdown. Since the current study was concerned with flight from $M \approx 10$ to 2.5, only the entry algorithm was needed. During entry, the angle of attack follows a preselected schedule, whereas roll angle is modulated to control both down range and cross range. Additional information on the guidance algorithm can be obtained in reference 6.

Flight Control System

The flight control system specified in May 1978 converts either guidance-system commands or pilot-control commands into aerodynamic control-surface deflections and reaction-control-system (RCS) thruster firings. It also takes rate gyro and accelerometer feedbacks and provides stability, damping, and turn-coordination outputs to these effectors. The aerodynamic control surfaces depicted in figure 1 include elevons (which are used as ailerons and elevators), a rudder with speed-brake capability, and a body flap for longitudinal trim. The RCS thrusters are used to supplement control about the roll, pitch, and yaw axes. The roll and pitch thrusters are used only during the early portion of the entry at low dynamic pressures. The yaw RCS thrusters are used down to Mach 1. The thrust level per thruster used in this study was 3870 N, and the I_{sp} was 289 sec. The flight control system, usually referred to as the blended entry digital autopilot (DAP), has several system changes throughout the trajectory depending upon the guidance algorithm and the relative effectiveness of the various control effectors. From the entry interface down to the TAEM interface, in the automatic mode, the control system nulls angle-of-attack errors by using the pitch thrusters (until dynamic pressure increases to 960 Pa) and the elevons. From the TAEM interface to landing, in the automatic mode, a normal-acceleration error is nulled by the elevons. In the manual mode, the control system converts stick deflections to rate commands. The body flap is a trim device used to maintain the average elevon deflection (elevator) near a preselected profile. Since the elevons are also used as ailerons, the aileron characteristics are a function of

the elevator deflection, and thus this preselected profile is used to help insure the proper aileron characteristics. The elevon and body-flap time histories for the nominal entry are shown in figure 4. The speed brake follows a schedule down to Mach 0.9, after which it follows a guidance-system command. Between Mach 10 and 0.9, the speed brake is used to provide a pitch-up moment to aid in longitudinal trim. Below Mach 0.9, the speed brake is used to control dynamic pressure. The nominal speed-brake time history is also shown in figure 4. A detailed description of the longitudinal channel and the speed-brake and body-flap channels is presented in appendix B of reference 6.

Control about the lateral-directional axes for a dynamic pressure less than 96 Pa is achieved with roll and yaw RCS thrusters only. As the dynamic pressure increases, the ailerons are added for control; and at a dynamic pressure of 480 Pa, the roll thrusters are turned off. From initial entry into the atmosphere down to about Mach 1.5, the control system operates in a "spacecraft mode," where the roll-rate command is directed to the yaw channel to produce a yawing rate and a small sideslip angle β. This β generates a rolling moment because of the positive effective dihedral of the Orbiter. In this mode, the ailerons are used for turn coordination and directional trim. The spacecraft mode was chosen for two reasons. First, the aerodynamics for this flight regime of the Orbiter are such that the vehicle exhibits roll-reversal characteristics; that is, if the ailerons are used to roll the vehicle with no yaw input from any other surface or RCS, the vehicle will start to roll in the desired direction and then roll in the opposite direction. The rudder is ineffective at flight conditions above Mach 4, and thus the RCS system would be required to provide much of the maneuver coordination. Second, to roll about the velocity vector at high values of α requires a large yawing moment about the body axis. After Mach 1.5, the control system switches to a more conventional aircraft mode where ailerons are used for roll control and the rudder is used for turn coordination. Between Mach 3 and 1.5, the flight control system is a blend between those two control modes which results in a blended-system designation. The roll and yaw channels of the flight control system are described in more detail in appendix A.

DESCRIPTION OF SIMULATION

The Reentry Flight Dynamics Simulator (RFDS) used for this study is a nonlinear, six-degree-of-freedom, interactive digital-computer program with man-in-the-loop capability developed by the Langley Research Center. The cockpit is not a replica of the Space Shuttle Orbiter cockpit, but it does have the instrumentation and controls necessary for engineering investigations. The vehicle response was recorded on time-history charts. A more complete simulation description is available in reference 6. A static aeroelastic model, described in appendix B, was added to the simulation for this study.

TEST CONDITIONS

The off-nominal conditions considered in this evaluation involved aerodynamics, vehicle asymmetries, sensed angle-of-attack errors, side accelerometer errors, and yaw RCS thruster failures. The Space Shuttle design specification requires that the Orbiter be able to fly safely with two of the four yaw thrusters on each side inoperable (off). Because of this requirement, all runs for the study had such a failure.

The nominal and off-nominal aerodynamics used in this study were obtained from reference 7. The off-nominal values were estimated 3σ envelopes of possible variations between wind-tunnel-derived characteristics and full-scale flight characteristics. Because a normal distribution was assumed, the variations could be either added to or subtracted from the nominal aerodynamics. The aerodynamic data base consisted of the six force and moment coefficients for the airframe with undeflected controls. These coefficients are functions of Mach number, angle of attack, and sideslip angle. To these are added the force and moment contribution of the control surfaces (functions of Mach number and angle of attack). The elevons (when used as an elevator), the body flap, and the speed brake are all considered to have nonlinear aerodynamic increments which are functions of Mach number, angle of attack, and surface position. Both the aileron and rudder have linear aerodynamics that are a function of Mach number and angle of attack, with the aileron aerodynamics also being a function of the average elevon position. The off-nominal aerodynamics are a function of Mach number.

All possible lateral-directional combinations involving moments generated by the bare airframe and the aileron were considered in this study. Table II shows the nomenclature used in the discussion of the results to describe these 16 cases of off-nominal conditions. Examination of the aerodynamic data of reference 7 revealed that the rudder derivatives $C_{l_{\delta r}}$, $C_{Y_{\delta r}}$, and $C_{n_{\delta r}}$, are approximately linearly dependent; therefore, they were varied together. In addition, none of the rudder derivatives were allowed to differ in sign from the nominal. Figure 4 of reference 4 shows the range of off-nominal lateral-directional stability and the aileron and rudder control effectiveness. The curves were generated by assuming that the angle of attack was exactly the angle commanded by the guidance algorithm and that the elevator position was the desired position used by the body-flap-control logic. The aileron is used for directional trim, as shown in appendix A of the present paper. This requirement places a great deal of dependence on $C_{n_{\delta a}}$. Reference 4 indicates that because of the uncertainity in the data, $C_{n_{\delta a}}$ could switch signs below Mach 5.5 and the magnitude could vary greatly above Mach 5.5. Thus, the control system should show a high sensitivity to uncertainties in $C_{n_{\delta a}}$. This sensitivity will be confirmed in the discussion of the results that follow.

Reference 7 also presents the longitudinal aerodynamic characteristics. However, longitudinal uncertainties were not, in general, included in the present study because reference 8 showed that variations in longitudinal aerodynamics do not impact the control of the Orbiter unless (1) the vehicle no longer can be trimmed or (2) the elevator must move to a position that adversely affects the aileron characteristics. This control system uses the body flap to maintain the proper elevator position; thus, no effects of pitching-moment variation would be expected until the body flap was forced to its limit and the elevator had to move from its desired position, which did not occur in the flight regime of this study.

Vehicle asymmetries, because of manufacturing uncertainty, have been estimated and were included in the modeling of the system. The values were given in coefficient form and are $\Delta C_l = 0.0004$, $\Delta C_n = -0.0002$, and $\Delta C_m = \pm 0.0034$. Also, a lateral center-of-gravity offset of 0.0381 m (1.5 in.) was included to account for manufacturing and payload-loading uncertainties.

Because angle of attack is not measured directly during the portion of the entry investigated in this study, it must be derived from the onboard inertial platform data. When error sources such as platform drift and winds are considered, angle of attack can be in error by as much as $\pm 4°$. Since the flight control system (see appendix A) uses angle of attack extensively, the system should be sensitive to this potential error in sensed α.

The accelerometer assembly is mounted in the forward avionics bay (ref. 2) and is subject to an estimated 3σ alignment uncertainty of 0.9°. Also, vehicle thermal deformation may contribute to misalignment errors. To simulate the possible alignment error, the sensed side acceleration used by the flight control system was modified to include a component of the normal acceleration in some of the simulation runs.

DISCUSSION OF RESULTS

In order to evaluate these off-nominal effects on the flying qualities of the Space Shuttle Orbiter, a test maneuver was devised to represent the maneuvering required during the entry phase. As noted earlier, the Orbiter flies a preselected angle-of-attack schedule and modulates the commanded value of ϕ to control both down range and cross range. The test maneuver was devised to maintain the initial ϕ for a short period of time, to roll 60° at maximum roll rate, and then to roll back 55°. The commanded angle of attack α_c was generated by the guidance algorithm. The test maneuver was initiated at Mach numbers of 10, 7.5, 5.0, and 4.2 along the entry profile, and the behavior of the Orbiter was examined. The length of time for the initial ϕ hold was varied with Mach number to get the roll to 60° and the reversal to occur at the most critical time. Unless otherwise noted, all cases were flown with the automatic control system - that is, with no pilot inputs.

System Performance at Hypersonic Speeds

At hypersonic speeds, the body-flap effectiveness in pitch was such that applying both the pitching-moment uncertainty and the increment due to vehicle asymmetry in the worst directions changed the body-flap deflection required for trim but not to its limit. Thus, the elevator remained at its desired value, and there was no apparent effect on the vehicle maneuver performance.

Figure 5 shows the vehicle response with the test maneuver initiated at Mach numbers of 10 and 7.5 with nominal aerodynamics, no error in sensed α, two yaw RCS thrusters on each side inoperable (off), and a lateral center-of-gravity offset of 0.0381 m (1.5 in.). The α profile shows the Orbiter transitioning from its initial value to lower values. The steps noted in the commanded angle-of-attack values occur because the guidance algorithm is interrogated every 1.92 sec; thus, the flight control sees the guidance commands as a series of step commands. The data indicate that th Orbiter performed the maneuver with no lateral oscillation and with very little sideslip. The yaw thrusters receive the roll-angle error signal and are fired to produce a body-axis yawing rate and small sideslip angle, thus allowing the effective dihedral to generate a rolling moment. The aileron is used to provide the turn coordination above Mach 1.5 according to the feedback control law

$$(\text{Gain}) \sin \alpha \, DN_Y + (\text{Gain } 1) \, r' \cot \alpha - p' + (\text{Gain } 2) \cos \alpha \, P_c = 0$$

where Gain 1 was approximately 1.0 and Gain 2 was negative and much less than 1.0 for Mach numbers greater than 3.0. The symbol DN_Y is a lagged side-force feedback with a gain which is a function of p above Mach 4.2. (See appendix A.) The sum of the r' and p' terms in the equation is approximately equal to the stability-axis yaw rate divided by sin α. When the difference between these two terms is zero, the rate of change of the sideslip angle is zero and the turn is "coordinated." Therefore, the change in the DN_Y term will be small. This side-acceleration term is in the control law to help control β when the angle of attack is not known very accurately and the term r' cot α - p' is not correct for true turn coordination. Thus, the overall effect of this control law is that $\dot{\beta}$ and β are minimized in the presence of substantial yawing rate. The yaw jets fire to establish and stop the maneuver and to limit sideslip. The aileron deflections required to coordinate the maneuver were approximately 0.05° and are difficult to see in figure 5. The apparent steady-state aileron deflection is the deflection required to trim the 0.0381-m (1.5-in.) lateral center-of-gravity offset.

Effect of sensed α errors.- Figures 6 and 7 show the vehicle performance with sensed angle-of-attack errors of -4° and 4°, respectively. A sensed α error of -4° causes the vehicle to fly 4° higher than the guidance command, and then all the signals, which are a function of α in the flight control system, are incorrect. Thus, in figure 6 the roll rate was smaller than that for nominal α and considerable yaw thruster firing was required to sustain the maneuver. The aileron was deflected in the positive direction from trim (compare figs. 5(a) and 6(a) at 40 sec), which should have resulted in a larger value of p. However, the adverse yaw due to aileron drove β positive, and the positive dihedral effect actually reduced p. In figure 7, where the vehicle performance with an α error of 4° is presented, the roll rate reached 5° per second, the vehicle tended to overshoot the ϕ_c value, and considerable yaw thruster firing was required to keep the maneuver rates from increasing even more. The aileron deflected in the negative direction from trim (compare figs. 5(a) and 7(a) at 40 sec), which drove β negative. This resulted in large roll rates which proved to be difficult to control.

Effect of off-nominal aerodynamics.- Without any error in sensed α, the flight control system has sufficient tolerance to handle adequately the entire off-nominal aerodynamic matrix given in table II at Mach 10 and 7.5. Several examples of the maneuver performance are presented in figures 8 and 9. There were minor differences in the p, r', β, δ_a, and yaw-jet time histories; but the maneuver performance was excellent.

Effects of combined off-nominal aerodynamics and sensed α errors.- With an α error of -4° at Mach 10, the off-nominal aerodynamics had little effect on the system performance as indicated in figure 10. Since the vehicle was holding an angle of attack that was 4° higher than the flight control system expected, the roll rate p was lower than nominal. The higher RCS fuel-consumption cases for the entire test matrix at Mach 10 are those shown in figure 10. The worst cases for an α error of -4° at Mach 7.5 are shown in figure 11. Comparing figures 10 and 11 with figures 6(a) and (b), respectively, shows that off-nominal aerodynamics has very little effect on maneuver performance at hypersonic speeds with a sensed α of -4°.

With a sensed α error of +4°, which caused the vehicle to fly 4° lower than the control system expected, the effect of off-nominal aerodynamics was more significant. The RCS fuel consumption increased by as much as 30 percent at Mach 10, β excursions greater than 1° were common, and roll-angle overshoots occurred frequently. Some Mach 10 cases are presented in figure 12.

With $C_{n_{\delta a}}$ less negative (cases 5 through 8 and 13 through 16 as shown in table II), less RCS fuel was consumed, but the maximum β excursions were larger. (Compare cases 3 and 7 in figs. 12(a) and (b), respectively.) The cases with positive increments in C_{n_β} and C_{l_β}, such as case 16 (see fig. 12(e)), resulted in the largest maximum sideslip excursions; whereas the cases with a negative increment in C_{n_β} and a positive increment in C_{l_β}, such as case 11 (see fig. 12(d)), consumed the most RCS fuel. More aileron effectiveness $\left(\text{positive increment in } C_{l_{\delta a}}\right)$ usually resulted in larger sideslip excursions and more RCS fuel consumed. Case 9 in figure 12(c) had the smallest maximum β excursion but was one of the largest fuel-consumption cases. The bare airframe characteristics were examined in the previous study. The characteristics at Mach 10 for nominal aerodynamics and case 11 with and without the α error of 4° were shown in table III of reference 4. This vehicle has two convergent lateral-directional oscillatory modes which vary in period and time to half-amplitude with aerodynamics and α. The conclusion in the previous study was that off-nominal aerodynamics and α errors did not significantly change the bare airframe characteristics, and thus any degradation in vehicle performance was due primarily to the control-system augmentation.

The maneuver performance at Mach 7.5 was very similar to the results at Mach 10. Figure 13 shows the results for six cases. Although none of the cases exhibited any control problems, the yaw-jet time histories showed that several cases were near the yaw-jet control-authority limit when trying to reverse or maintain the rolling rate. Cases 9 and 11 required one yaw jet all the time and two much of the time to maintain the rolling rate on the second reversal between 30 and 40 sec, and then two yaw jets were required for 6 to 7 sec to stop the rolling maneuver. Case 11 came very close to saturating the control system even though the maneuver itself looked good.

Some additional uncertainties were combined with case 11 to see if control could be maintained. Figure 14(a) shows the maneuver performance with a misalignment of 1° in the accelerometer assembly, which results in a component of the normal acceleration N_Z being sensed as a side acceleration. This puts a bias signal on the sensed N_Y used in the turn coordination in the flight control system. The roll rate for the first reversal was larger than nominal (see fig. 14(a)), and an overshoot in roll angle occurred. During the second reversal, the roll rate was less than nominal, and the maneuver was completed satisfactorily. The real-time simulation results indicated that the system performance became worse at slightly higher Mach numbers than for the maneuver shown in figure 14(a). The results for the same case with the maneuver occurring just prior to 2 sec are shown in figure 14(b). The roll-angle overshoot is slightly greater.

Figure 14(c) shows the effect of applying an uncertainty to C_{Y_β} for the aforementioned case. Since C_{Y_β} is nominally negative, applying a positive increment effectively decreased the side-acceleration feedback which resulted in slightly less β control and higher roll rates in the negative roll direction. As the figure shows, the C_{Y_β} increment resulted in a larger roll-angle overshoot and longer yaw-jet firings.

Figures 14(d) through (f) show the results of the same case with an accelerometer misalignment of -1° and both with and without the uncertainty in C_{Y_β}. During the roll reversal with positive p, shown in figure 14(d), two yaw jets were firing to decrease r', but the aileron was deflected to increase r'. Thus, the roll rate exceeded the nominal system design and was increasing until the roll-angle error signal changed signs. The rolling inertia then caused a large and unacceptable overshoot. A negative increment in C_{Y_β} effectively increased the N_Y feedback and kept p from becoming much greater than 5. (See fig. 14(e).) A positive increment in C_{Y_β} allowed p to become very large with a very large and unacceptable overshoot. (See fig. 14(f).) Thus, the system performance was unacceptable at hypersonic speeds with two failed yaw jet, a sensed α error of 4°, an accelerometer misalignment of -1°, and case 11 off-nominal aerodynamics with and without a positive increment on C_{Y_β}. The worst case (fig. 14(f)) was examined with all four jets operational. The system performance was satisfactory as is shown in figure 14(g).

In summary, the vehicle performance was satisfactory with the test maneuver initiated at Mach 10 or 7.5 for all cases with two yaw RCS thrusters on each side inoperable (off), a lateral center-of-gravity offset of 0.0381 m (1.5 in.), and off-nominal aerodynamics with and without a sensed α error of ±4°. The system appeared to be close to saturation in some cases for a sensed α error of 4°. Adding a 1° misalignment of the accelerometer assembly and a positive increment on C_{Y_β} did result in a large and unacceptable roll-angle overshoot.

System Performance at Supersonic Speeds

In the supersonic-speed range of interest in this study (Mach 5 to 2.5), the aerodynamic characteristics changed significantly, which forced some flight-control-system reconfiguration as well as gain scheduling. The gain on the N_Y feedback that is a function of p is terminated at Mach 4.2. The rudder is activated at Mach 4.5. As the Mach number decreased, the elevon had to deflect more negatively to trim the vehicle as the pitching-moment characteristics changed. As the elevon deflected more negatively, $C_{n_{\delta a}}$ tended to become more positive; and as Mach number decreased, $C_{n_{\delta a}}$ tended to be more positive. Since a negative $C_{n_{\delta a}}$ was used to provide lateral trim at the higher Mach numbers, a transition in the trim network took place. Also, the rudder began to be effective in the lower Mach number range. Since the rudder deflection and rate were limited when the speed brake was fully open, the speed brake had to be partially closed.

The analysis of this flight regime was accomplished with simulation initialization at Mach 5 and 4.2. Once again, the roll-reverse-roll maneuver was used to stress the system at several different times while the control system followed the guidance-commanded angle-of-attack schedule.

Effect of sensed α errors at Mach 5.- The Mach 5 maneuver performance with the maneuver occurring after 10 and 25 sec is shown in figure 15. The vehicle performed the maneuver very satisfactorily with both nominal α and sensed α errors. In some cases when the rudder was activated (Mach 4.5), a rudder-deflection spike, a β

spike, and a p spike occurred at the initiation of the roll reversal; and an oscillation in p, δ_r, and β followed the maneuver. For the longer runs (figs. 15(d), (e) and (f)), the transition from aileron trim to rudder trim is evident as δ_a faded to 0 and δ_r went to a negative value.

Effect of off-nominal aerodynamics at Mach 5.- All off-nominal aerodynamics cases listed in table II were run with nominal rudder effectiveness, but only the two worst cases (cases 3 and 7) are presented in figure 16. With the maneuver beginning just after 10 sec, it was completed satisfactorily for cases 3 and 7; but an oscillation in p, β, δ_a, and δ_r followed the maneuver. With the maneuver beginning just after 25 sec, the initiation of the roll reversal was accompanied by large p, β, and δ_r spikes; and for case 3, the system diverged. Cases 3 and 7 have the same bare-airframe characteristics which were given for case 7 in table V of reference 4 for this speed range. The bare airframe has four convergent aperiodic modes for these flight conditions. Thus, the control system itself must be the source of the oscillatory instability. The problem was believed to be caused by a forward-loop-gain mismatch between the rudder and the aileron. At the simulated Mach number and angle of attack for the cases, the rudder produces almost as much adverse rolling moment as yawing moment. Thus, to obtain the desired p, relatively large aileron and rudder deflections as well as yaw-jet pulses were required. The sideslip angle β became large, and the roll rate became excessive. The controllers were able to arrest the high rolling rate initially; but as the N_Y feedback was removed, β became excessive and the vehicle oscillation became severe.

The scheduled rudder forward-loop gain (GDRC) was reduced from 1000 to 750 above Mach 1.2. (See appendix A.) The Mach 5 maneuver performance for several cases, with the maneuver initiated at about 25 and 40 sec, is presented in figure 17. Both the nominal case and case 7 improved slightly with the reduced rudder gain. Case 3 improved significantly, but the maneuver was still unacceptable. There was a further slight improvement by reducing GDRC to 700. Also, 20- and 40-percent increases in the scheduled aileron forward-loop gain (KGDA), when coupled with GDRC = 750, produced a slight improvement over the case with nominal KGDA. Since other Shuttle program simulation studies and analyses have shown that GDRC = 750 was desirable, even though some stability margin for the nominal system may be lost, a GDRC value of 750 was used for the remainder of this analysis.

For cases 6 and 7 where $C_{n_{\delta a}}$ was more positive than nominal, the δ_a deflection for lateral trim reached approximately 3°. The maximum trim deflection allowed by the control system is 5°.

Off-nominal rudder characteristics (table II) were added to the other off-nominal aerodynamic characteristics. The results for several cases with increased rudder effectiveness, which aggravated the rudder instability, are presented in figure 18.

The Mach 5 maneuver-performance results for decreased rudder effectiveness are shown in figure 19. In all cases, the maneuver was completed satisfactorily without severe oscillations. However, in all cases the rudder was driven to the trim limit of 9° and the yaw jets were required to maintain trim. Case 7, the worst case, required one yaw jet full time and a second yaw jet most of the time to maintain trim. Other runs were made with case 7 to see if maneuvering while using most of the yaw-jet control authority for trim would cause the system to fail. The maneuver in

some runs was worse than that shown in figure 19(d), but control was adequate to complete the maneuver and maintain trim.

Effects of combined off-nominal aerodynamics and sensed α errors.- Some Mach 5 maneuver-performance results for a sensed α error of 4° and off-nominal aerodynamics (nominal rudder) are shown in figure 20. In several cases, the rudder instability continued to be a problem, although control was always maintained. For the cases where $C_{n_{\delta a}}$ was more positive than nominal, such as cases 5 and 14, δ_a was driven toward the trim limit of -5° as δ_e became more negative. For cases 5 and 14, considerable yaw-jet firing took place before the maneuver began to maintain trim, and large values of β (about 1.5° for case 14) were required for trim. To perform the first roll reversal, the jets fired in the opposite direction to that required for trim; and thus as β became more positive, the balance of roll due to β and roll due to aileron was upset. Then, a large negative roll rate occurred which the system had difficulty stopping, particularly for case 14 where the aileron was more effective in roll. Less control authority was available to roll back, since the jets were already required to help hold trim, and the rudder produced a negative rolling moment as it was deflected to augment the yaw jets. This problem was further aggravated by applying the off-nominal aerodynamic increment to the pitching moment in the direction that would move the elevon more negatively and by reducing the side-acceleration feedback by applying a positive increment to C_{Y_β}.

During simulation tests, an astronaut pilot used the roll-panel trim switch to help provide more symmetric p, but combinations were found where the pilot was unable to handle the vehicle in this flight regime.

One solution to this problem is to modify the body-flap schedule and keep the speed brake open longer, which tends to keep the elevon down. This will insure that $C_{n_{\delta a}}$ stays negative farther into the entry until the rudder has sufficient effectiveness to handle the trim requirements.

The results of four cases with decreased rudder effectiveness and a sensed α error of 4° are presented in figure 21. The less effective rudder decreased the oscillatory tendency exhibited in figure 20. However, cases 6 and 14 exhibited loss of control when the rudder ineffectiveness was added to the aileron trim problem discussed previously. The pilot's use of the roll-panel trim switch helped to avoid loss of control, but combinations were again found that he was unable to handle. This further demonstrated the requirement to schedule the speed brake and body flap for effective aileron trim until the rudder effectiveness is assured.

Increased rudder effectiveness and a sensed α error of 4° caused the response to be more oscillatory than that for the nominal rudder. This can be seen by comparing figures 20 and 22.

With a sensed α error of -4° and nominal rudder, the system was oscillatory after the rudder was activated, and the roll rate exhibited some asymmetry. Four representative off-nominal aerodynamic cases for these conditions are shown in figure 23.

The nominal aerodynamics and the two worst cases for increased rudder effectiveness (cases 3 and 7) are presented in figure 24. The response performance shows that the system was more oscillatory with increased rudder effectiveness. With decreased

rudder effectiveness, even with nominal aerodynamics, the control system required two yaw thrusters to hold trim as the rudder went to the trim limit (fig. 25). Case 3 appears to have divergent oscillation toward the end of the run, and cases 7 and 15 did diverge as the yaw thruster and the rudder were unable to maintain control. Again, the system must be modified to make sure that $C_{n_{\delta a}}$ has the proper sign until the rudder is effective.

Effect of sensed α errors at Mach 4.2.- The roll-reverse-roll maneuver was performed satisfactorily at 25 sec after initiation at Mach 4.2 for nominal and off-nominal angles of attack as shown in figure 26. The oscillatory tendency of the system was evident in each of the cases shown. Also, the improper turn coordination is evident because the angle-of-attack error decreased or increased p, as was shown at the higher Mach numbers.

Effect of off-nominal aerodynamics at Mach 4.2.- All cases listed in table II were run with nominal, decreased, and increased rudder effectiveness with the maneuver beginning 25 sec after initiation at Mach 4.2. With nominal rudder effectiveness, the maneuver was completed satisfactorily in all cases. However, cases 3 and 7, presented in figure 27, exhibited the system instability seen previously. The oscillatory tendency was present before and after the maneuver; and large p, β, δ_a, and δ_r spikes occurred at the initiation of the second reversal.

With decreased rudder effectiveness, the maneuver was satisfactorily completed in all cases even though during the maneuver the rudder reached its trim limit of 9° even with nominal aerodynamics, as shown in figure 28(a). In case 3, the combined trim deflection plus the deflection required to execute the roll reversal resulted in a rudder deflection greater than 20° (fig. 28(b)). The yaw thrusters were on at the same time, and thus the yaw control was nearly saturated. In case 6, shown in figure 28(c), the aileron was on the trim limit of 5° at the initiation of the run; but the system recovered, completed the maneuver, and maintained control throughout the run. Toward the end of each run presented, the rudder effectiveness increased as Mach number and angle of attack decreased, and the system control margin increased.

The nominal and the two worst cases with increased rudder effectiveness are presented in figure 29. The oscillatory tendency and the p, β, δ_a, and δ_r spikes at the beginning of the second reversal are similar to those of the previous cases. Again, the system appears to be marginally stable.

Effects of combined off-nominal aerodynamics and sensed α errors.- The response performance is shown in figure 30, with a sensed α error of -4° (the vehicle flies 4° higher than the system expects) and nominal rudder effectiveness. The three worst cases (cases 3, 5, and 7), which are shown in figure 30, all exhibit the asymmetric roll-rate characteristic that has been shown in previous results. Also, the rudder-deflection spike and the high roll rate at the beginning of the second roll reversal followed by the oscillation are typical of the high-rudder-gain problem discussed previously.

With decreased rudder effectiveness and a sensed α error of -4°, the rudder went to the trim limit, and two yaw thrusters were required to maintain the roll rate, at least part of the time, for the nominal-aerodynamics case shown in figure 31(a). Cases 3, 7, 11, and 15 all resulted in an unacceptable performance because the combination of two yaw thrusters that failed and very low rudder effectiveness were too much for the system. The two worst cases (cases 3 and 7) are presented in figures 31(b) and (c), respectively. Control was completely lost for case 7 as the vehicle rolled over. Revising the body-flap and speed-brake schedules

to provide more positive elevon deflection, and thus negative $C_{n_{\delta a}}$, and using the aileron for lateral trim to lower Mach numbers are probably the only ways to circumvent this problem.

Increased rudder effectiveness with a sensed α error of -4° produced the oscillatory tendency that occurred previously. The response results for nominal aerodynamics and two off-nominal aerodynamics cases are presented in figure 32. Case 7 was the worst with an excessive roll rate and large β with an oscillation preceding and following the maneuver.

The response results for two cases with a sensed α error of 4° and nominal rudder effectiveness are presented in figure 33. Case 3 exhibits the oscillatory tendency previously discussed and has the large roll-rate spikes at the initiation of the roll reversals. Case 5 has the additional problem that the aileron was on the trim limit and two jets were firing initially. As the rudder took over this trim function and the maneuver was made, the oscillaton amplitude was reduced. The aileron was on the trim limit for case 7, and the ensuing oscillation diverged. As has been mentioned previously, revision of the elevon-trim and speed-brake schedules to drive the elevon down (more positive) to provide more negative $C_{n_{\delta a}}$ is required to help alleviate the trim problem.

The response results with increased rudder effectiveness are presented in figure 34. The case with nominal aerodynamics performed satisfactorily, but the oscillatory tendency was evident. All the off-nominal aerodynamics cases with decreased aileron effectiveness (cases 1 through 8) exhibited marginal maneuver performance and the oscillatory tendency, although none lost control. Time histories of the two worst cases (cases 3 and 5) are presented in figure 34.

The response results for a few cases with decreased rudder effectiveness are presented in figure 35. The maneuver performance for nominal aerodynamics was very satisfactory even though the rudder did momentarily go to the trim limit. The maneuver was marginal for case 3 aerodynamics as the rudder deflection reached 19°. Again, the vehicle was untrimmed initially for case 5 aerodynamics. However, the oscillation converged, and the maneuver was accomplished even though the rudder drove to the trim limit.

In summary, at supersonic speeds (Mach 5 to 2.5) two basic design problems exist in the flight control system. With increased rudder effectiveness, the system tends to be oscillatory after the rudder is activated. The system diverged until the rudder forward-loop gain was reduced by 25 percent. With decreased rudder effectiveness, control was lost in several cases because of the inability to hold lateral trim. The rudder is too weak at Mach 4 to take over trim, and the aileron may be unable to trim because of the sign change in $C_{n_{\delta a}}$. Thus, the body-flap and speed-brake schedules must be modified to get a more positive elevon deflection and, therefore, a more negative $C_{n_{\delta a}}$ at lower Mach numbers.

CONCLUDING REMARKS

A six-degree-of-freedom simulation analysis has been performed for the Space Shuttle Orbiter during entry from Mach 10 to 2.5 with realistic off-nominal conditions using the flight control system referred to as the blended entry digital autopilot specified in May 1978. This flight control system has evolved from

previous studies of a similar approach. The off-nominal conditions included the following: (1) aerodynamic uncertainties in extrapolating from wind-tunnel-derived characteristics to full-scale flight characteristics, (2) an error in deriving the angle of attack from onboard instrumentation, (3) the failure of two of the four reaction control-system thrusters on each side (design specification), and (4) a lateral center-of-gravity offset and vehicle asymmetries. The effect of misalignment of the side accelerometer was also examined for a few cases.

With combinations of the aforementioned four off-nominal conditions, the control system performed satisfactorily with a few exceptions. The cases that did not exhibit satisfactory performance displayed the following main weaknesses. Marginal performance was exhibited at hypersonic speeds for a few cases with a sensed angle-of-attack error of 4°. (The vehicle flew 4° lower in angle of attack than the flight control system expected because of error.) At supersonic speeds the system tended to be oscillatory in roll rate, sideslip, and control deflections, particularly with increased rudder effectiveness. The system diverged for several cases because of the inability to hold lateral trim with the lateral center-of-gravity offset and vehicle asymmetries. Several system modifications were suggested to help solve these problems and to maximize safety on the first flight: alter the elevon-trim and speed-brake schedules to keep the elevon more positive at the higher supersonic speeds, delay switching to rudder trim until the rudder effectiveness is adequate and reduce the overall rudder loop gain. These and other modifications were incorporated in a flight-control-system redesign in May 1979.

Langley Research Center
National Aeronautics and Space Administration
Hampton, VA 23665
February 21, 1984

APPENDIX A

ROLL AND YAW CHANNELS OF FLIGHT CONTROL SYSTEM

The flight control system described in reference 6 was revised to solve the problems discussed in reference 4. The revised roll and yaw channels are described in this appendix.

Symbols

This flight control system was designed for measurements in the U.S. Customary Units. Therefore, units are given in both the SI and U.S. Customary Units.

AL	approach and landing guidance
ALPDG	angle of attack, deg
AUTO	autopilot control mode
BANKERR	control-system roll-angle error, deg
BETAF	control-system angle of sideslip, deg
BETDG	angle of sideslip, deg
COSALP	cosine of angle of attack
COSTHE	cosine of pitch angle
COTALP	cotangent of angle of attack
DACM	roll-rate error, deg/sec
DAM	roll-rotation hand-controller command, deg
DAMAX	roll-stick-command limit, deg
DAMS	shaped roll-stick command, deg
DAMSF	filtered roll-stick command, deg
DAMSFGN	gain to convert roll-stick command to rate command, (deg/sec)/deg
DAMTR	roll-panel-trim command
DAMTRS	roll-panel-trim rate, deg/sec
DAT	aileron-trim rate, deg/sec
DATR	aileron-trim rate due to crossfeed and forward loop, deg/sec
DATRI	aileron-trim rate due to crossfeed, deg/sec

DATRIM aileron-trim command, deg

DAY side-acceleration error, g units

DAYF filtered side-acceleration error

DELAC aileron-deflection command, deg

DNY stability-axis yaw rate due to side acceleration, deg/sec

DR preliminary rudder-deflection command, deg

DRC rudder-deflection command, deg

DRCC limited yaw-rate error for crossfeed, deg/sec

DRF filtered rudder-deflection command, deg

DRFS rudder-trim rate, deg/sec

DRFSI rudder-trim deflection, deg

DRJET yaw-jet-rate command, deg/sec

DRM rudder-pedal command, deg

DRMS shaped-rudder-pedal command, deg

DRMTR yaw-panel trim

DRRC yaw-rate error, deg/sec

EARLY flight-control-system subphase

ENTRY entry guidance

ERRBANK roll-angle error, deg

FADER signal fading logic

FLATURN flat-turn regime

GALR scheduled gain to blend between yaw-jet/aileron control and aileron/rudder control

GDA gain to convert roll-rate error into aileron command, deg/(deg/sec)

GDAY gain to schedule side-acceleration feedback to aileron and roll jets

GDRC scheduled gain used to obtain GGDRC, deg/(deg/sec)/Pa (deg/(deg/sec)/(lb/ft^2))

GGDRC gain to convert yaw-rate error to rudder-deflection command, deg/(deg/sec)

GLIN linear coefficient in roll-stick shaping, deg/deg

GNY gain to convert rudder-pedal command to side-acceleration command, (g units)/deg

GPC gain used to schedule roll-rate command to aileron

GPFBAY gain used to schedule high gain on side-acceleration feedback, (g units)/(deg/sec)

GPPHI gain to convert roll-angle error to roll-rate command, (deg/sec)/deg

GRH gain used to scale yaw-rate error

GTRR gain used to scale rudder-trim integrator

g acceleration due to gravity, where 1g = 9.8 m/sec^2 (32.152 ft/sec^2)

H1 flight-control fast-cycle time, sec

KGDA scheduled gain used to obtain GDA, deg/(deg/sec)/Pa (deg/(deg/sec)/(lb/ft^2))

MACH Mach number

MANRY pilot-commanded roll/yaw mode

NY side-acceleration feedback, g units

PAR coefficient of squared term in roll-stick shaping, deg/deg^2

PC commanded roll rate, deg/sec

PCC preliminary yaw-rate error, deg/sec

PCCO filtered preliminary yaw-rate error, deg/sec

PCLIM roll-rate-command limit, deg/sec

PDAC scaled aileron command, deg

PDACF filtered aileron command, deg

PDG sensed roll rate, deg/sec

PE turn-coordination roll-rate error, deg/sec

PEP aileron rate-trim signal for low dynamic pressure, deg/sec

PGAIN aileron-trim signal for low Mach number, deg

PHICM guidance-system roll-angle command, deg

PHICMS smoothed roll-angle-guidance command, deg

PHIDG sensed roll angle, deg

PP = PDG + (RTDG)(TANP)(SINTHE)/V, deg/sec

PTEM side-acceleration feedback gain, deg/sec

QB dynamic pressure, Pa (lb/ft^2)

RCS reaction control system

RDG sensed yaw rate, deg/sec

RFDS Reentry Flight Dynamics Simulator

RP = RDG - (RTDG)(SINPHI)(COSTHE)/V, deg/sec

RTDG = 57.3(g), $deg\text{-}m/sec^2$ ($deg\text{-}ft/sec^2$)

SINALP sine of angle of attack

SINPHI sine of roll angle

SINTHE sine of pitch angle

SMOOTHER guidance-command smoothing logic

TAEM terminal-area-energy-management guidance

TANP tangent of roll angle

TEMA lateral-acceleration command due to rudder-pedal input, g units

TEMB body-axis roll-rate command, deg/sec

UXC number of roll RCS thrusters commanded to fire

UZC number of yaw RCS thrusters commanded to fire

V airspeed, m/sec (ft/sec)

YALCM guidance yaw-rate command, deg/sec

YPT filtered acceleration due to yaw-panel trim, g units

YPTI acceleration due to yaw-panel trim, g units

z z-transform variable

Description of System

The block diagrams of the roll and yaw channels are presented in figures A1 and A2, respectively. The system was designed to minimize the time required to complete the flight-control calculations in the onboard digital computers. This was accomplished by operating various elements of the control laws at the minimum acceptable frequency; thus, a variation in computational frequency existed among the various signal paths of the flight control system. The frequency is indicated on the block diagrams either in the figure legend or by the dashed boxes around the control-system signal paths.

APPENDIX A

Computational frequency differences between the guidance system and flight control system resulted in a requirement to smooth the signals at the interface. This was accomplished by the SMOOTHER logic which is shown as a block in figure A1(a). Lateral-trim logic switching required a signal-fading logic indicated by the block FADER in figure A1(c). The SMOOTHER and FADER logics are described in detail in appendix B of reference 6.

Roll channel.- The aileron command and roll RCS command control laws are presented in figure A1. Figure A1(a) shows how either the roll-stick command (DAM) or the smoothed roll-angle-guidance command (PHICMS), depending on pilot selection (MANRY) in the cockpit, is converted to roll-rate command (PC). This command signal was directed to the yaw channel (fig. A2(b)) and to the aileron and roll RCS jet commands, as is shown in figure A1(b).

The Orbiter enters the Earth's atmosphere at approximately 40° angle of attack, holds this α until it decelerates to a Mach number of around 13, and then begins a slow transition in α, reaching 13° angle of attack near Mach 2.5. At the higher angles of attack, the stability-axis roll rate was obtained by using the yaw thruster to produce a body-axis yawing rate and letting the relatively large effective dihedral generate the body-axis rolling rate. The aileron was used only as a coordinating controller in maneuvering.

The gain GPC (fig. A1(b)) was very small at the higher Mach numbers because of the scheduled gain GALR, and thus only a small percentage of the roll rate commanded was directed to the roll thrusters and ailerons. At the lower Mach numbers, GPC was 1.0 and the commanded roll rate was directed entirely to the ailerons. Thus, the scheduled gain GALR was the mechanism by which the flight control system was blended from one type of system to another. Note, the roll jets (UXC = Jet command) were disengaged at a dynamic pressure of 479 Pa (10 lb/ft^2).

Crossfeed between the yaw channel and the roll channel DRRC was used to generate the aileron trim signal above Mach 4. (See fig. A1(c).) Below Mach 4, lateral trim was handled by the rudder-forward-loop integration. The 40-sec FADER was triggered at this Mach 4 switch to minimize the transient.

Yaw channel.- The rudder and yaw RCS command diagrams are presented in figure A2. Below Mach 4.5, the rudder was active and commands could be input through the rudder pedals DRM (fig. A2(a)). The system was designed, however, for the yaw channel to operate without requiring manual inputs through the rudder pedals. At the higher angles of attack, the stability-axis roll rate PC was used to generate a yaw-rate error (DRRC) (fig. A2(b)). At the lower angles of attack, the yaw-rate feedback RP is the predominant feedback signal and is sufficient to provide the desired turn coordination.

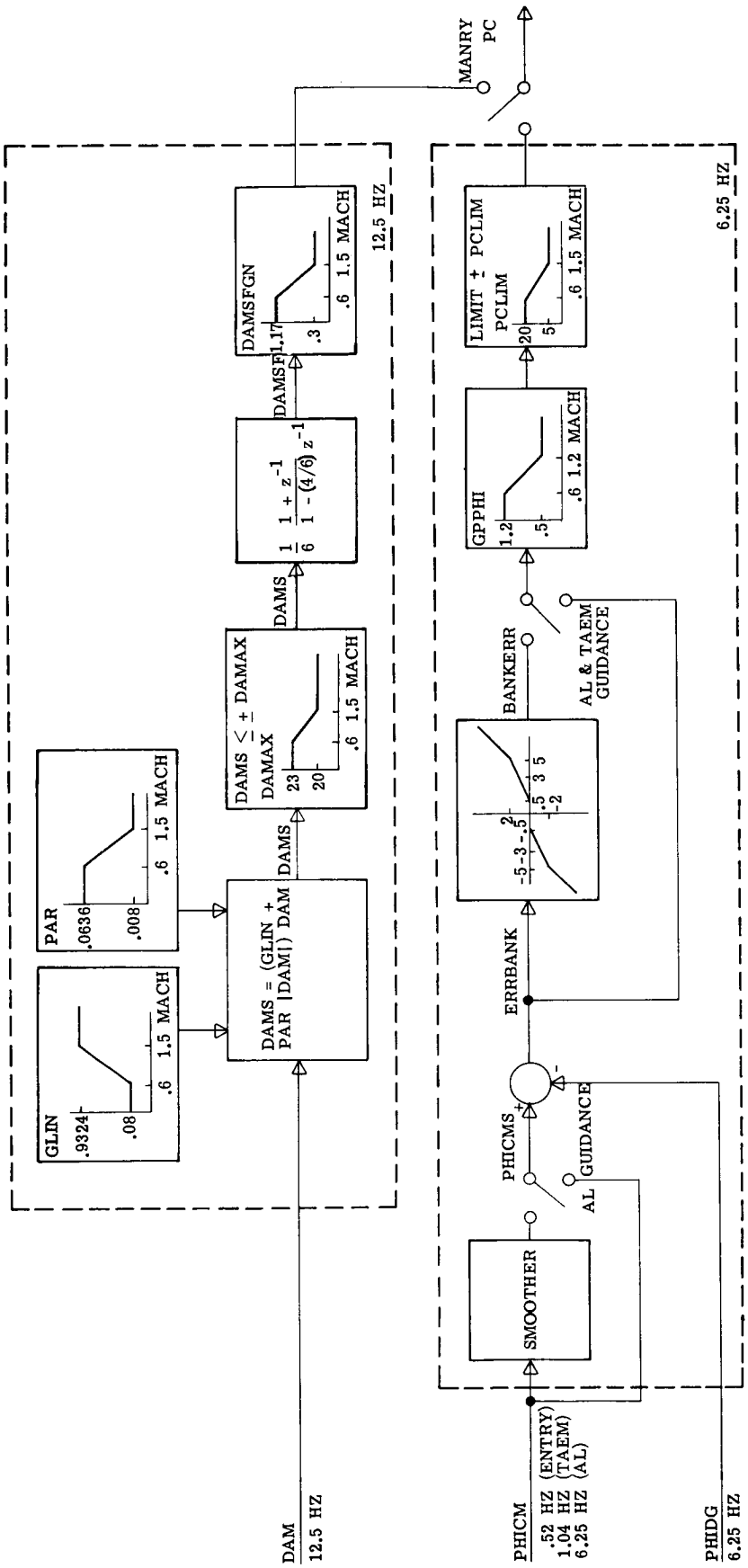

(a) Part I.

Figure A1.- Roll channel.

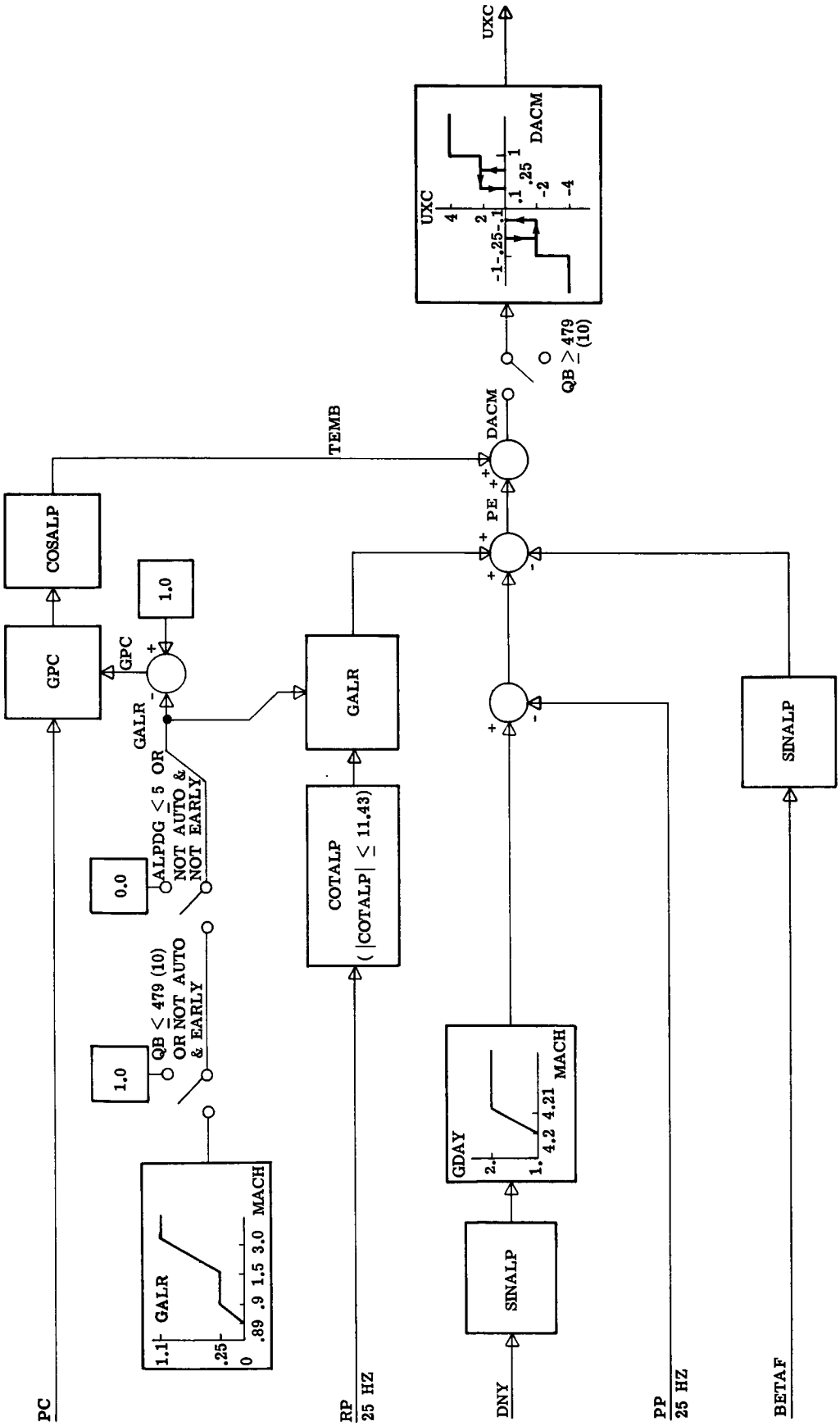

(b) Part II. Frequency of execution, 25 Hz.

Figure A1.- Continued.

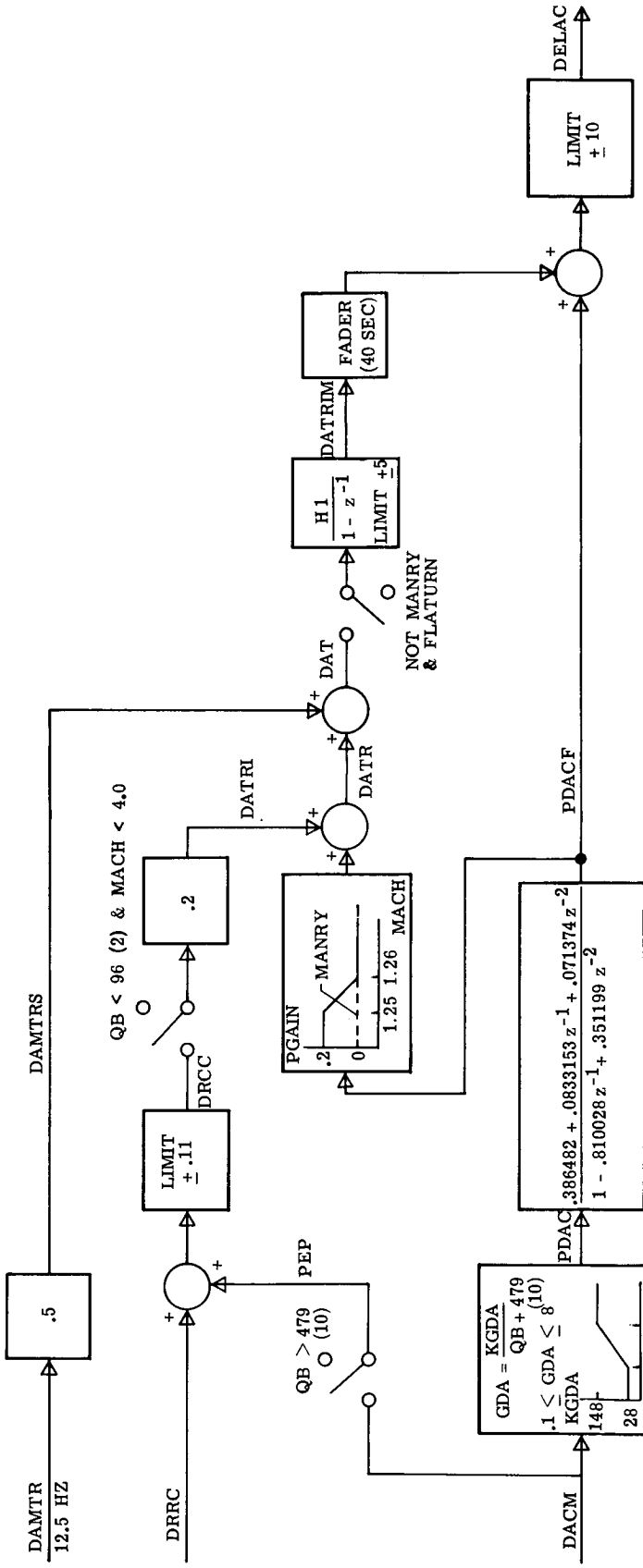

(c) Part III. Frequency of execution, 25 Hz.

Figure A1.- Concluded.

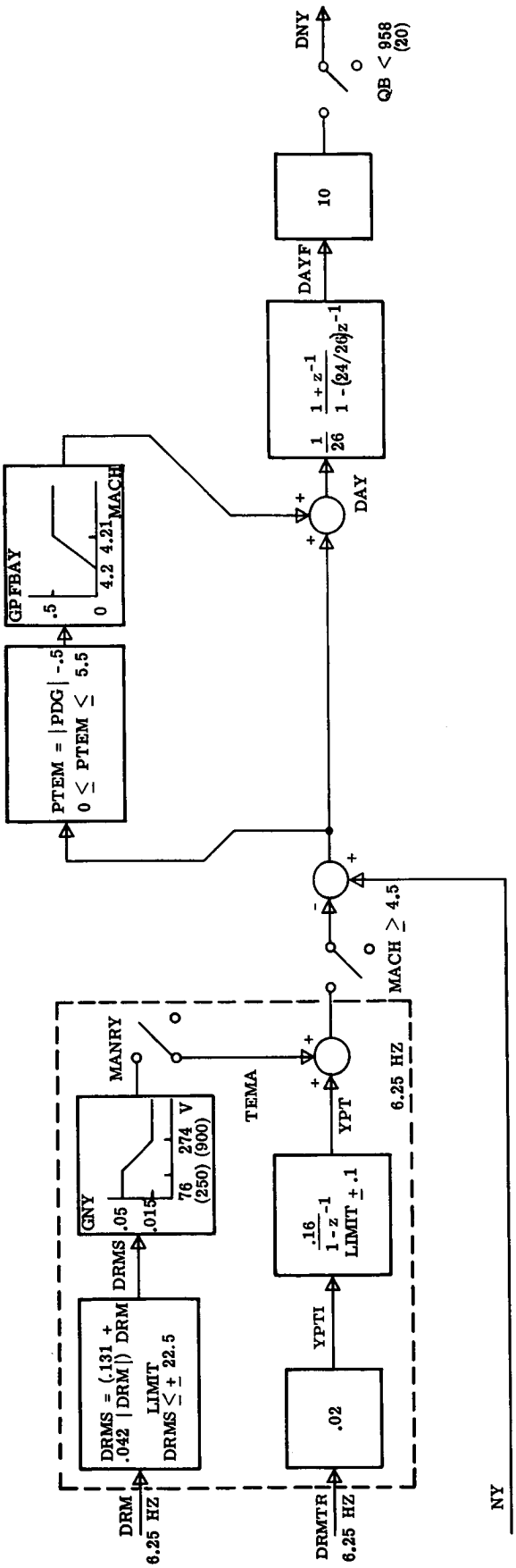

(a) Part I. Frequency of execution, 25 Hz unless otherwise noted.

Figure A2.- Yaw channel.

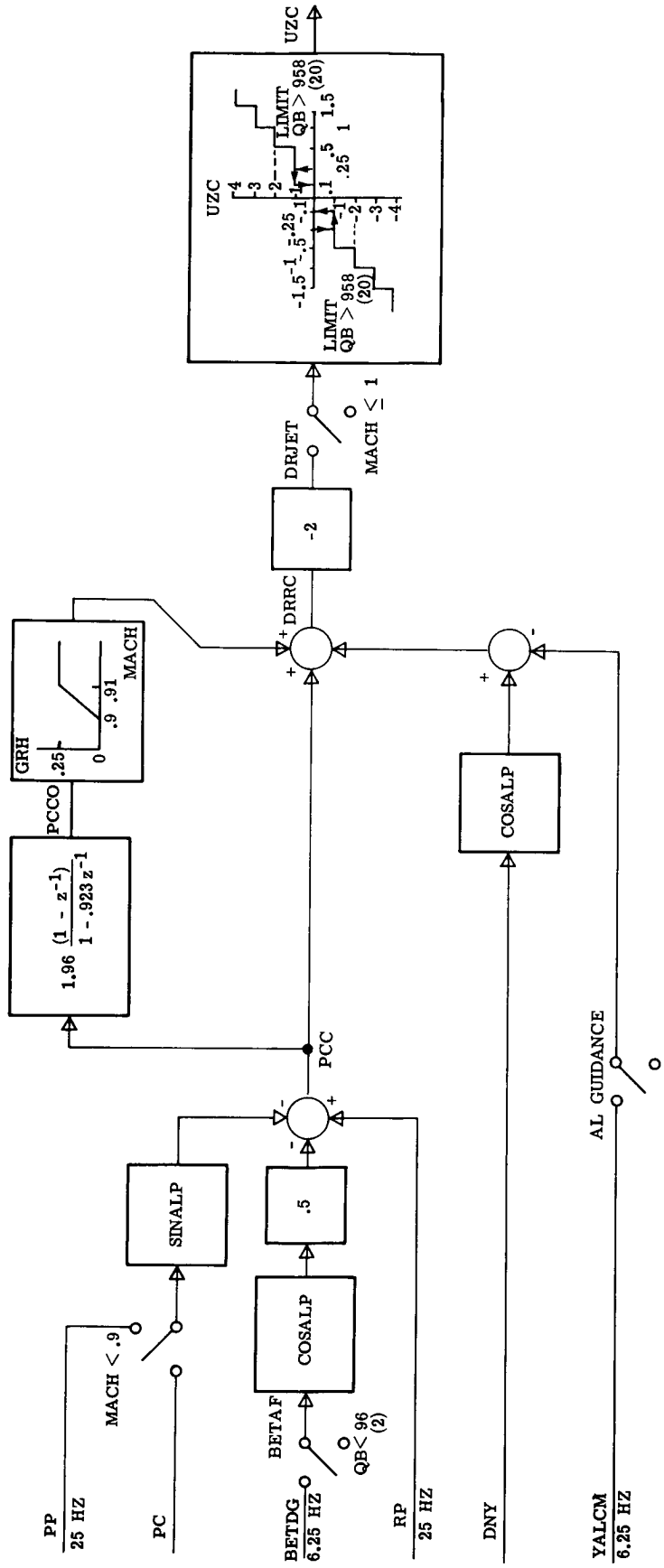

(b) Part II.

Figure A2.- Continued.

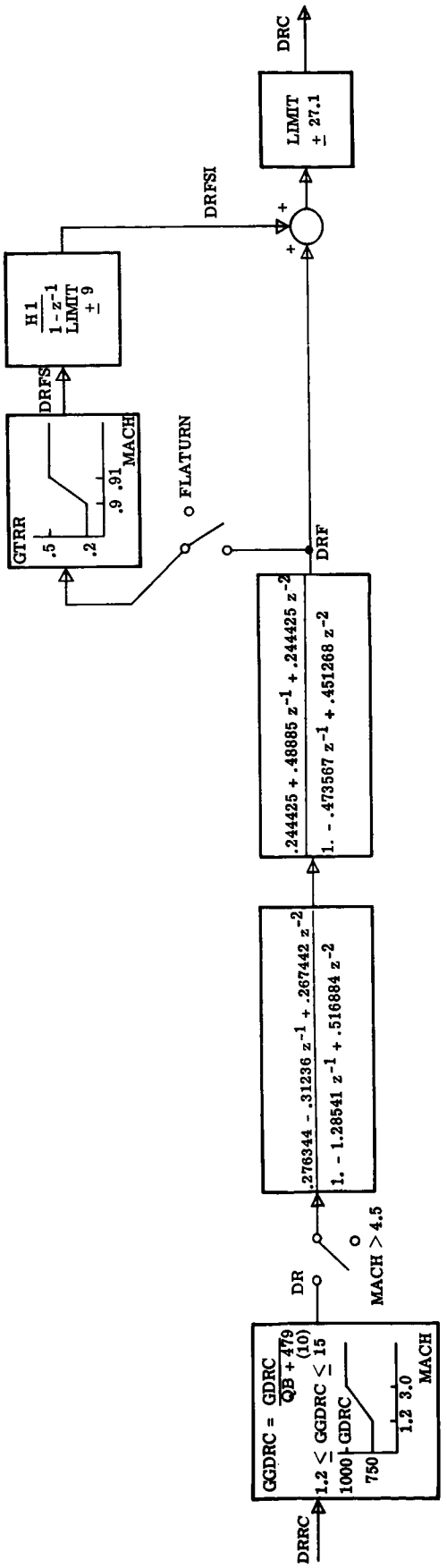

(c) Part III.

Figure A2.- Concluded.

APPENDIX B

AEROELASTIC MODEL

A static aeroelastic model developed for the Lyndon B. Johnson Space Center was used in the Reentry Flight Dynamics Simulator (RFDS). The model uses a series of curve fits to the aeroelastic data to generate factors or increments to be applied to the rigid-body aerodynamic coefficients. The curve fits were developed with dynamic pressure in U.S. Customary Units, and thus the coefficients in the equations are for U.S. Customary Units. To convert to S.I. Units, the coefficients must be multiplied by 47.880258. The purpose of this appendix is to present the formulation of this model.

Symbols

AE1	conversion factor for rudder derivatives
AE2	conversion factor for β derivatives
AE3	conversion factor for pitch and lift elevon effectiveness and aileron effectiveness in roll
AE6	conversion increment for lift
AE7	conversion increment for pitch
AE8	conversion factor for yaw due to aileron deflection
AE41	conversion factor for inner-elevon-panel hinge moment
AE42	conversion factor for outer-elevon-panel hinge moment
AE51	conversion factor for rudder hinge moment
AE52	conversion factor for rudder/speed-brake hinge moment due to sideslip
$C_{h_{e,i}}$	rigid-body inner-elevon-panel hinge-moment coefficient
$C_{h_{e,o}}$	rigid-body outer-elevon-panel hinge-moment coefficient
C_{h_β}	rigid-body rudder/speed-brake hinge-moment coefficient due to sideslip, deg^{-1}
$C_{h_{\delta r}}$	rigid-body rudder hinge-moment coefficient, deg^{-1}
C_L	rigid-body lift coefficient
C_{L_e}	rigid-body lift increment due to elevon deflection
C_{l_β}	rigid-body rolling-moment coefficient due to sideslip angle, deg^{-1}
$C_{l_{\delta a}}$	rigid-body rolling-moment coefficient due to aileron deflection, deg^{-1}

APPENDIX B

$C_{l_{\delta r}}$ rigid-body rolling-moment coefficient due to rudder deflection, deg^{-1}

C_m rigid-body pitching-moment coefficient

C_{m_e} rigid-body pitching-moment increment due to elevon deflection

C_{n_β} rigid-body yawing-moment coefficient due to sideslip angle, deg^{-1}

$C_{n_{\delta a}}$ rigid-body yawing-moment coefficient due to aileron deflection, deg^{-1}

$C_{n_{\delta r}}$ rigid-body yawing-moment coefficient due to rudder deflection, deg^{-1}

C_{Y_β} rigid-body side-force coefficient due to sideslip angle, deg^{-1}

$C_{Y_{\delta r}}$ rigid-body side-force coefficient due to rudder deflection, deg^{-1}

M Mach number

QB dynamic pressure, lb/ft^2

RFDS Reentry Flight Dynamics Simulator

α angle of attack, deg

β sideslip angle, deg

The notation $(\ )_{flex}$ signifies that the rigid-body coefficient in the parentheses has been converted to a flexible-body coefficient, and the notation $(\ )_{vert}$ signifies the rigid-body contribution of the vertical tail.

Conversion of Rigid-Body Coefficients to Flexible-Body Coefficients

The following equations were used to convert the rigid-body aerodynamic coefficients to the approximate flexible-body aerodynamic coefficients. The AE factors in each equation are the conversion factors which will be defined subsequently.

$$\left(C_{Y_{\delta r}}\right)_{flex} = AE1\ C_{Y_{\delta r}}$$

$$\left(C_{l_{\delta r}}\right)_{flex} = AE1\ C_{l_{\delta r}}$$

$$\left(C_{n_{\delta r}}\right)_{flex} = AE1\ C_{n_{\delta r}}$$

$$\left(C_{Y_\beta}\right)_{flex} = C_{Y_\beta} - (1 - AE2)\left(C_{Y_\beta}\right)_{vert}$$

$$\left(C_{l_\beta}\right)_{flex} = C_{l_\beta} - (1 - AE2)\left(C_{l_\beta}\right)_{vert}$$

$$\left(C_{n_\beta}\right)_{flex} = C_{n_\beta} - (1 - AE2)\left(C_{n_\beta}\right)_{vert}$$

$$\left(C_{L_e}\right)_{flex} = AE3\ C_{L_e}$$

$$\left(C_{m_e}\right)_{flex} = AE3\ C_{m_e}$$

$$\left(C_{l_{\delta a}}\right)_{flex} = AE3\ C_{l_{\delta a}}$$

$$\left(C_{n_{\delta a}}\right)_{flex} = AE8\ C_{n_{\delta a}}$$

$$\left(C_L\right)_{flex} = AE6 + C_L$$

$$\left(C_m\right)_{flex} = AE7 + C_m$$

$$\left(C_{h_{e,i}}\right)_{flex} = AE41\ C_{h_{e,i}}$$

$$\left(C_{h_{e,o}}\right)_{flex} = AE42\ C_{h_{e,o}}$$

$$\left(C_{h_\beta}\right)_{flex} = AE52\ C_{h_\beta}$$

$$\left(C_{h_{\delta r}}\right)_{flex} = AE51\ C_{h_{\delta r}}$$

The vertical-tail components $\left(C_{Y_\beta}\right)_{vert}$, $\left(C_{n_\beta}\right)_{vert}$, and $\left(C_{l_\beta}\right)_{vert}$ are given in tables BI, BII, and BIII, respectively.

APPENDIX B

The conversion factors are listed as follows according to Mach number:

For Mach numbers above 5:

$$AE1 = 1 - 0.0005\ QB$$

$$AE2 = 1 - 0.0002\ QB$$

$$AE3 = 0.995 - 0.0002\ QB$$

$$AE8 = 0.995 - 0.000175\ QB$$

$$AE6 = AE7 = 0$$

$$AE41 = AE42 = 1 - 0.0002\ QB$$

$$AE51 = 1 - 0.00015\ QB$$

$$AE52 = 1 - 0.00025\ QB$$

From Mach 5 to 3:

$$AE1 = 0.98 - 0.0006\ QB + (M - 3)(0.015 + 0.0005\ QB)$$

$$AE2 = 0.995 - 0.0003\ QB + (M - 3)(0.0025 + 0.00005\ QB)$$

$$AE3 = 0.995 - 0.00035\ QB + (M - 3)(0.000075\ QB)$$

$$AE8 = 0.995 - 0.0003\ QB + (M - 3)(0.0000633\ QB)$$

$$AE41 = AE42 = 1 - 0.0003\ QB + (M - 3)(0.00005\ QB)$$

$$AE51 = 0.995 - 0.0002\ QB + (M - 3)(0.0025 + 0.000025\ QB)$$

$$AE52 = 1 - 0.0004\ QB + (M - 3)(0.000075\ QB)$$

APPENDIX B

From Mach 3 to 2:

$$AE1 = 0.98 - 0.001\ QB + (M - 2)(0.03 + 0.0003\ QB)$$

$$AE2 = 0.985 - 0.0005\ QB + (M - 2)(0.01 + 0.0002\ QB)$$

$$AE3 = 0.99 - 0.0005\ QB + (M - 2)(0.005 + 0.00015\ QB)$$

$$AE8 = 0.99 - 0.00042\ QB + (M - 2)(0.005 + 0.000127\ QB)$$

$$AE51 = 0.995 - 0.0004\ QB + (M - 2)(0.0002\ QB)$$

$$AE52 = 0.99 - 0.0007\ QB + (M - 2)(0.01 + 0.0003\ QB)$$

From Mach 5 to 1.5:

$$AE6 = 0.00125 + 6 \times 10^{-6}\ QB + (M - 1.5)(-3.57143 \times 10^{-4} - 1.71429 \times 10^{-6}\ QB)$$

$$AE7 = -0.001 - 8 \times 10^{-6}\ QB + (M - 1.5)(2.85714 \times 10^{-4} + 2.285714 \times 10^{-6}\ QB)$$

From Mach 3 to 1.5:

$$AE41 = 0.985 - 0.00055\ QB + (M - 1.5)(0.01 + 0.000167\ QB)$$

$$AE42 = 0.99 - 0.00045\ QB + (M - 1.5)(0.006667 + 0.000133\ QB)$$

From Mach 2 to 1.5:

$$AE2 = 0.975 - 0.0005\ QB + 0.02(M - 1.5)$$

$$AE6 = 0.00125 + 6 \times 10^{-6}\ QB + (M - 1.5)(-3.57143 \times 10^{-4} - 1.71429 \times 10^{-6}\ QB)$$

$$AE7 = -0.001 - 8 \times 10^{-6}\ QB + (M - 1.5)(2.85714 \times 10^{-4} + 2.285714 \times 10^{-6}\ QB)$$

$$AE41 = 0.985 - 0.00055\ QB + (M - 1.5)(0.01 + 0.000167\ QB)$$

$$AE42 = 0.99 - 0.00045\ QB + (M - 1.5)(0.006667 + 0.000133\ QB)$$

$$AE51 = 0.99 - 0.0006\ QB + (M - 1.5)(0.01 + 0.0004\ QB)$$

$$AE52 = 0.965 - 0.0008\ QB + (M - 1.5)(0.05 + 0.0002\ QB)$$

From Mach 2 to 1.2:

$$AE1 = 0.9 - 0.00127075\ QB + (M - 1.2)(0.0875 + 0.000375\ QB)$$

$$AE3 = 0.96 - 0.00085\ QB + (M - 1.2)(0.0375 + 0.000348\ QB)$$

$$AE8 = 0.97 - 0.0007\ QB + (M - 1.2)(0.025 + 0.00036\ QB)$$

From Mach 1.5 to 1.2:

$$AE6 = 0.003 + 0.000052\ QB + (M - 1.2)(-5.8333 \times 10^{-3} - 1.5333 \times 10^{-4}\ QB)$$

$$AE7 = -0.003 - 4 \times 10^{-5}\ QB + (M - 1.2)(0.0066666 + 1.06666 \times 10^{-4}\ QB)$$

$$AE41 = 0.98 - 0.00085\ QB + (M - 1.2)(0.016667 + 0.001\ QB)$$

$$AE42 = 0.98 - 0.0006\ QB + (M - 1.2)(0.033333 + 0.0005\ QB)$$

$$AE51 = 0.96 - 0.0007\ QB + (M - 1.2)(0.1 + 0.000333\ QB)$$

$$AE52 = 0.985 - 0.0007\ QB - (M - 1.2)(0.066667 + 0.000333\ QB)$$

From Mach 1.5 to 0.95:

$$AE2 = 0.995 - 0.0003\ QB - (M - 0.95)(0.036364 + 0.00036364\ QB)$$

From Mach 1.2 to 0.95:

$$AE1 = 1.0 - 0.00087075\ QB - (M - 0.95)(0.4 + 0.0016\ QB)$$

$$AE3 = 0.985 - 0.0005\ QB - (M - 0.95)(0.1 + 0.0014\ QB)$$

$$AE41 = 1.0 - 0.0005\ QB - (M - 0.95)(0.08 + 0.0014\ QB)$$

$$AE42 = 1.0 - 0.0005\ QB - (M - 0.95)(0.08 + 0.0004\ QB)$$

$$AE51 = 0.97 - 0.0003\ QB - (M - 0.95)(0.04 + 0.0016\ QB)$$

$$AE52 = 1.0 - 0.0003\ QB - (M - 0.95)(0.06 + 0.0016\ QB)$$

From Mach 1.2 to 0.9:

$$AE6 = 0.005 + 0.000184\ QB + (M - 0.9)(-6.666666 \times 10^{-3} - 4.4 \times 10^{-4}\ QB)$$

$$AE7 = -2.7 \times 10^{-3} - 9.68 \times 10^{-5}\ QB + (M - 0.9)(-0.001 + 1.8933333 \times 10^{-4}\ QB)$$

$$AE8 = 0.995 - 0.00038\ QB - (M - 0.9)(0.025 + 0.0014\ QB)$$

From Mach 0.95 to 0:

$$AE1 = 1.0 - 0.0006\ QB - 0.5M^2(0.0006\ QB)$$

$$AE2 = 0.995 - 0.0003\ QB$$

$$AE3 = 0.99 - 0.0002\ QB - M(0.00526316 + 0.00031579\ QB)$$

$$AE41 = AE42 = 0.995 - 0.0002\ QB - M(0.0003\ QB)$$

$$AE51 = 0.99 - 0.0003\ QB - 0.021053M$$

$$AE52 = 1.0 - 0.0004\ QB + M(0.000105\ QB)$$

From Mach 0.9 to 0.6:

$$AE6 = 0.00125 + 0.000098\ QB + (M - 0.6)(0.0125 + 2.8666667 \times 10^{-4}\ QB)$$

$$AE7 = -0.001 - 4.4 \times 10^{-5}\ QB + (M - 0.6)(-1.16666 \times 10^{-3} - 2.12 \times 10^{-4}\ QB)$$

$$AE8 = 0.995 - 0.0002\ QB - (M - 0.6)(0.06 + 0.0004\ QB)$$

APPENDIX B

From Mach 0.6 to 0:

$$AE6 = 0.0015 + 0.000076\ QB + (M - 0.25)(0.6285714 \times 10^{-4}\ QB)$$

$$AE7 = -0.001 - 3.2 \times 10^{-5}\ QB + (M - 0.25)(9.28571 \times 10^{-3} - 1.085714 \times 10^{-4}\ QB)$$

$$AE8 = 0.995 - 0.00007\ QB - M(0.0002\ QB)$$

TABLE BI.- VERTICAL-TAIL COMPONENT OF $\left(C_{Y_\beta}\right)_{vert}$

α, deg	Values of $C_{Y_{\beta,vert}}$ at Mach numbers of -									
	0.25	0.60	0.90	0.95	1.05	1.2	1.55	2.0	3.0	5.0
-5	-0.0062	-0.0074	-0.0089	-0.0088	-0.0085	-0.0082	-0.0079	-0.0075	-0.0062	-0.0042
0	-.0060	-.0074	-.0089	-.0088	-.0084	-.0081	-.0077	-.0074	-.0060	-.0040
5	-.0058	-.0070	-.0084	-.0082	-.0080	-.0076	-.0072	-.0069	-.0055	-.0036
10	-.0056	-.0064	-.0072	-.0071	-.0069	-.0064	-.0057	-.0056	-.0044	-.0032
15	-.0056	-.0062	-.0054	-.0053	-.0050	-.0042	-.0030	-.0028	-.0026	-.0026
20	-.0058	-.0062	-.0030	-.0028	-.0022	-.0008	-.0024	-.0026	-.0002	-.0019
25	-.0058	-.0062	-.0030	-.0028	-.0022	-.0008	.0024	.0027	.0005	-.0008
30	-.0058	-.0062	-.0030	-.0028	-.0022	-.0008	.0024	.0012	.0000	-.0004
35	-.0058	-.0062	-.0030	-.0028	-.0022	-.0008	.0024	.0012	-.0002	-.0004

TABLE BII.- VERTICAL-TAIL COMPONENT OF $\left(C_{n_\beta}\right)_{vert}$

α, deg	Values of $C_{n_{\beta,vert}}$ at Mach numbers of -									
	0.25	0.60	0.90	0.95	1.05	1.2	1.55	2.0	3.0	5.0
-5	0.00315	0.00324	0.00388	0.00385	0.00372	0.00372	0.00367	0.00355	0.00285	0.00190
0	.00310	.00320	.00379	.00378	.00370	.00367	.00360	.00350	.00280	.00190
5	.00287	.00308	.00355	.00359	.00359	.00345	.00325	.00315	.00255	.00180
10	.00260	.00290	.00318	.00325	.00330	.00300	.00260	.00250	.00210	.00159
15	.00256	.00281	.00257	.00268	.00273	.00225	.00152	.00130	.00140	.00122
20	.00260	.00280	.00150	.00153	.00160	.00100	-.00026	-.00090	.00030	.00070
25	.00260	.00280	.00150	.00153	.00160	.00100	-.00026	-.00097	.00005	.00045
30	.00260	.00280	.00150	.00153	.00160	.00100	-.00026	-.00070	.00002	.00039
35	.00260	.00280	.00150	.00153	.00160	.00100	-.00026	-.00070	.00028	.00034

TABLE BIII.- VERTICAL-TAIL COMPONENT OF $\left(C_{l_\beta}\right)_{vert}$

α, deg	Values of $C_{l_\beta,vert}$ at Mach numbers of -									
	0.25	0.60	0.90	0.95	1.05	1.2	1.55	2.0	3.0	5.0
-5	-0.00221	-0.00241	-0.00269	-0.00270	-0.00273	-0.00263	-0.00237	-0.00225	-0.00185	-0.00115
0	-.00215	-.00235	-.00265	-.00266	-.00266	-.00260	-.00235	-.00220	-.00180	-.00110
5	-.00192	-.00215	-.00245	-.00245	-.00248	-.00238	-.00220	-.00205	-.00170	-.00105
10	-.00181	-.00200	-.00215	-.00220	-.00202	-.00202	-.00185	-.00180	-.00145	-.00100
15	-.00187	-.00205	-.00175	-.00181	-.00183	-.00150	-.00118	-.00110	-.00109	-.00081
20	-.00203	-.00225	-.00130	-.00133	-.00136	-.00086	.00022	.00035	-.00050	-.00050
25	-.00203	-.00225	-.00130	-.00133	-.00136	-.00086	.00022	.00045	.00005	-.00035
30	-.00203	-.00225	-.00130	-.00133	-.00136	-.00086	.00022	.00010	-.00005	-.00025
35	-.00203	-.00225	-.00130	-.00133	-.00136	-.00086	.00022	.00010	-.00013	-.00018

REFERENCES

1. Space Shuttle. NASA SP-407, 1976.

2. Carrier, L. M.; and Minor, R. G.: Space Shuttle Orbiter Avionics. A Collection of Technical Papers - AIAA 2nd Digital Avionics Systems Conference, Nov. 1977, pp. 146-156. (Available as AIAA Paper 77-1501.)

3. Brand, Vance D.: Return to Earth in the Space Shuttle. 1977 Report to the Aerospace Profession, Tech. Rev., vol. 13, no. 4, Soc. Exp. Test Pilots, c.1978, pp. 223-231.

4. Powell, Richard W.; and Stone, Howard W.: Analysis of the Space Shuttle Orbiter Entry Dynamics From Mach 10 to Mach 2.5 With the November 1976 Flight Control System. NASA TP-1667, 1980.

5. Young, James C.; and Underwood, Jimmy M.: The Development of Aerodynamic Uncertainties for the Space Shuttle Orbiter. A Collection of Technical Papers - 12th Aerodynamic Testing Conference, Mar. 1982, pp. 9-14. (Available as AIAA-82-0563.)

6. Rowell, Lawrence F.; Powell, Richard W.; and Stone, Howard W., Jr.: Development of the Reentry Flight Dynamics Simulator for Evaluation of Space Shuttle Orbiter Entry Systems. NASA TP-1700, 1980.

7. Aerodynamic Design Data Book. Volume 1: Orbiter Vehicle. NASA CR-160386, 1978.

8. Stone, Howard W.; and Powell, Richard W.: Entry Dynamics of Space Shuttle Orbiter With Longitudinal Stability and Control Uncertainties at Supersonic and Hypersonic Speeds. NASA TP-1084, 1977.

TABLE I.- PHYSICAL CHARACTERISTICS OF SPACE SHUTTLE ORBITER DURING ENTRY

Mass properties:	
Mass, kg	83 388
Moments of inertia:	
I_X, kg-m^2	1 169 236
I_Y, kg-m^2	8 729 397
I_Z, kg-m^2	8 991 771
I_{XY}, kg-m^2	3 868
I_{XZ}, kg-m^2	-218 615
I_{YZ}, kg-m^2	3 441
Wing:	
Reference area, m^2	249.91
Mean aerodynamic chord, m	12.06
Span, m	23.79
Elevon:	
Reference area, m^2	19.51
Mean aerodynamic chord, m	2.30
Rudder:	
Reference area, m^2	9.30
Mean aerodynamic chord, m	1.86
Body flap:	
Reference area, m^2	12.54
Mean aerodynamic chord, m	2.06

TABLE II.- OFF-NOMINAL AERODYNAMIC VARIATIONS[a]

Case	C_{n_β}	C_{l_β}	$C_{n_{\delta a}}$	$C_{l_{\delta a}}$
1	-	-	-	-
2	+	-	-	-
3	-	+	-	-
4	+	+	-	-
5	-	-	+	-
6	+	-	+	-
7	-	+	+	-
8	+	+	+	-
9	-	-	-	+
10	+	-	-	+
11	-	+	-	+
12	+	+	-	+
13	-	-	+	+
14	+	-	+	+
15	-	+	+	+
16	+	+	+	+

Rudder variations	$C_{Y_{\delta r}}$	$C_{n_{\delta r}}$	$C_{l_{\delta r}}$
Increased effectiveness	+	-	+
Decreased effectiveness	-	+	-

[a]A plus sign (+) indicates that aerodynamic variation is added to the nominal coefficient. A minus sign (-) indicates that aerodynamic variation is subtracted from the nominal coefficient.

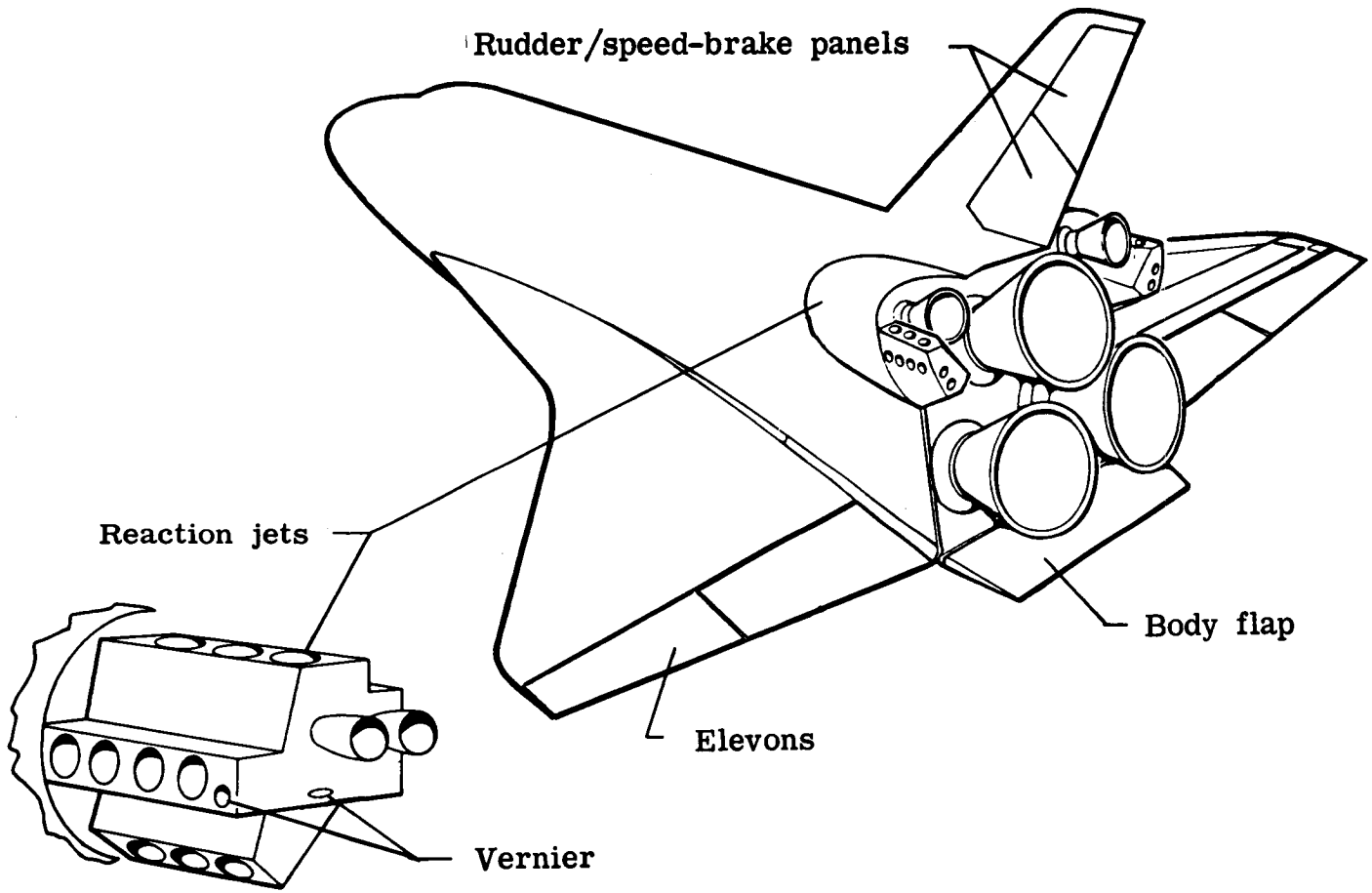

Figure 1.- Sketch of Space Shuttle Orbiter.

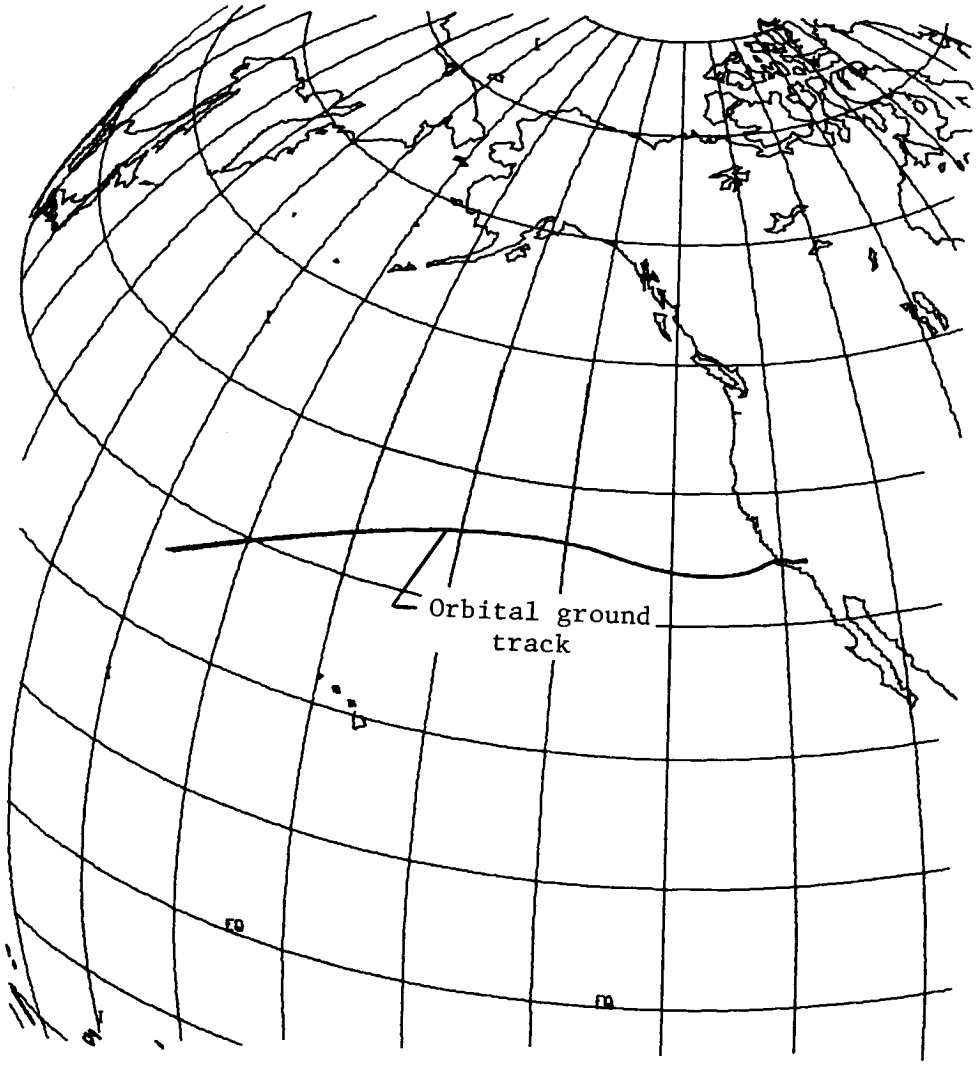

Figure 2.- Entry trajectory of Space Shuttle Orbiter for first flight.

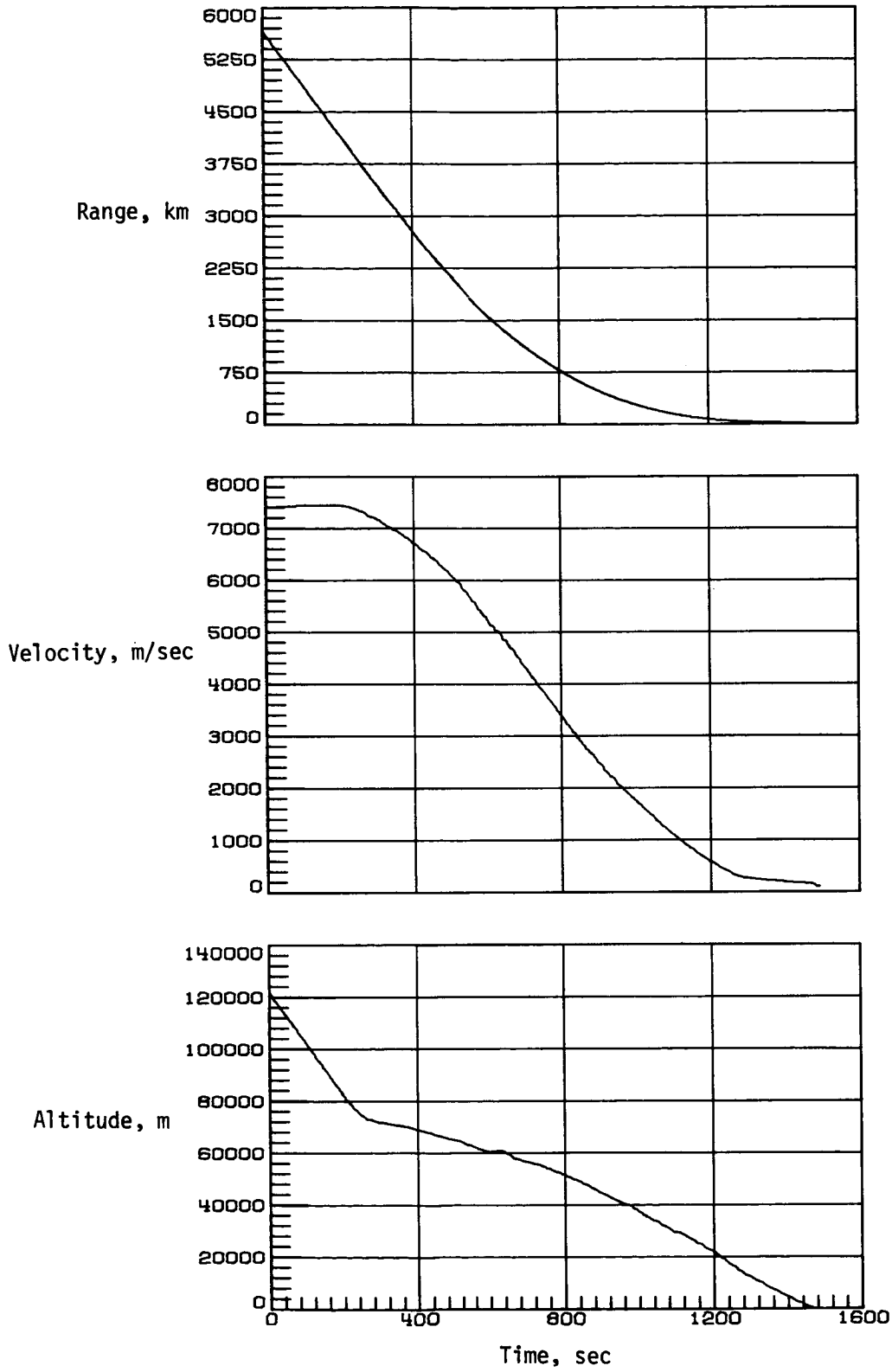

Figure 3.- Entry-trajectory parameters of Space Shuttle Orbiter for first flight.

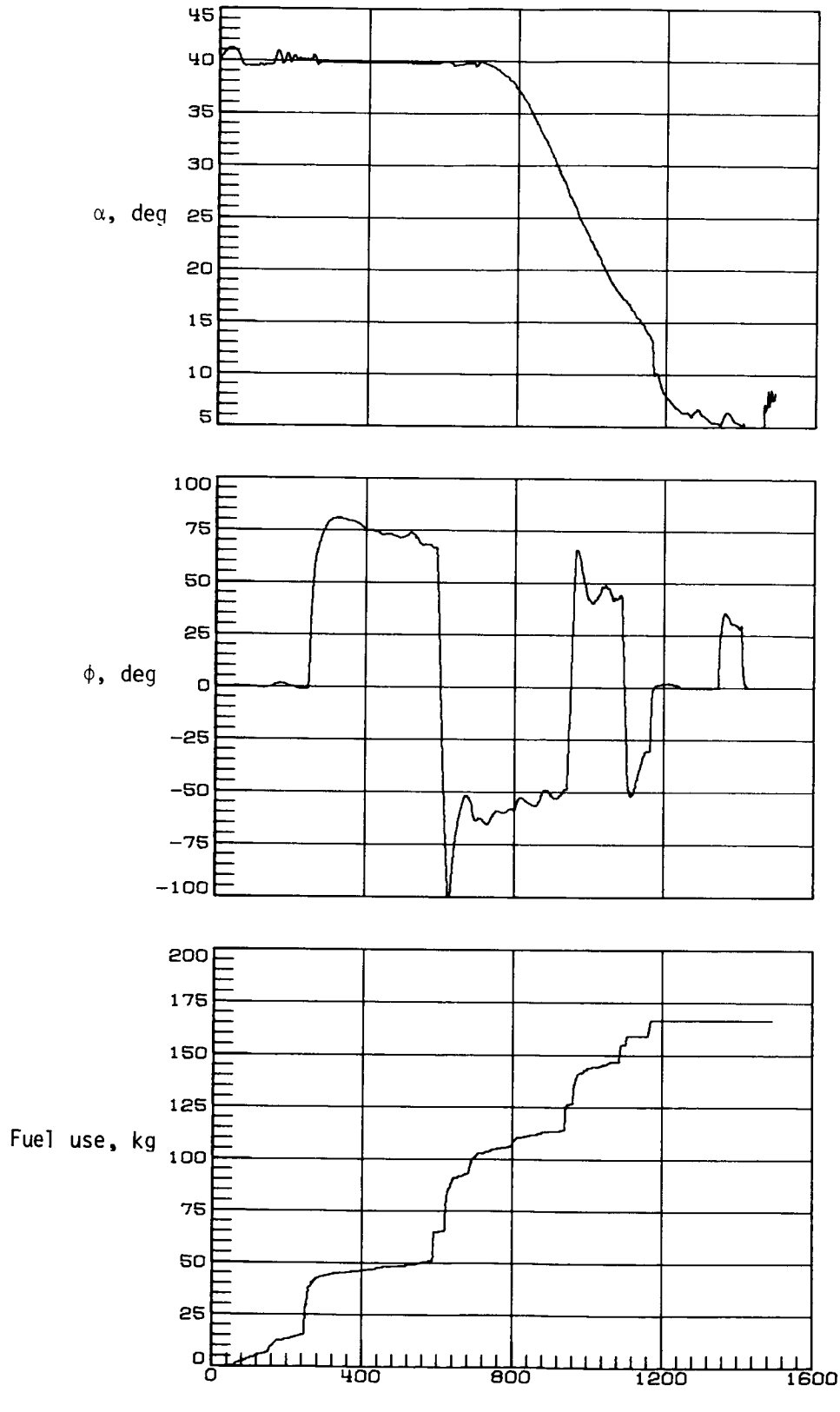

Figure 3.- Concluded.

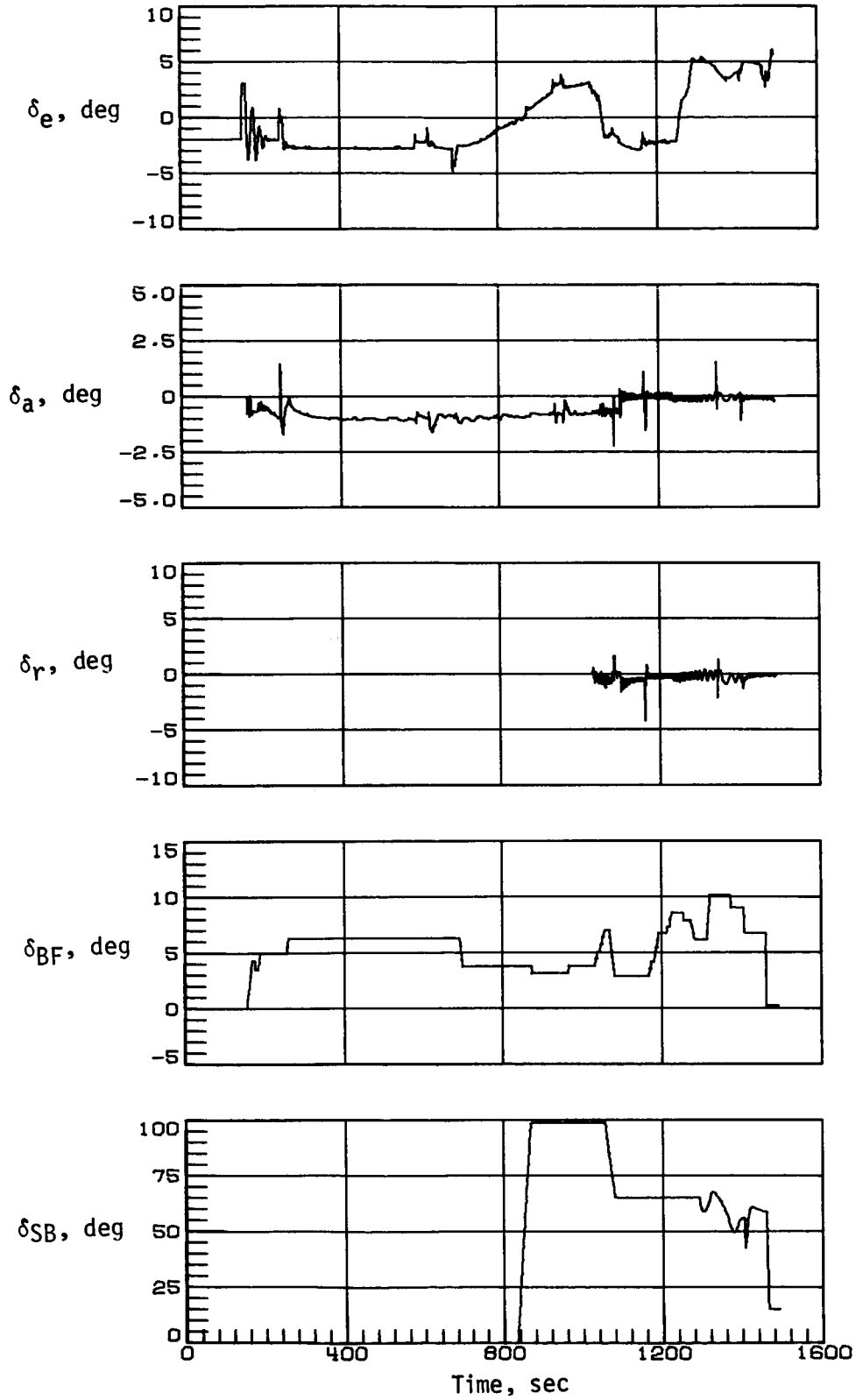

Figure 4.- Time history of nominal controls of Space Shuttle Orbiter.

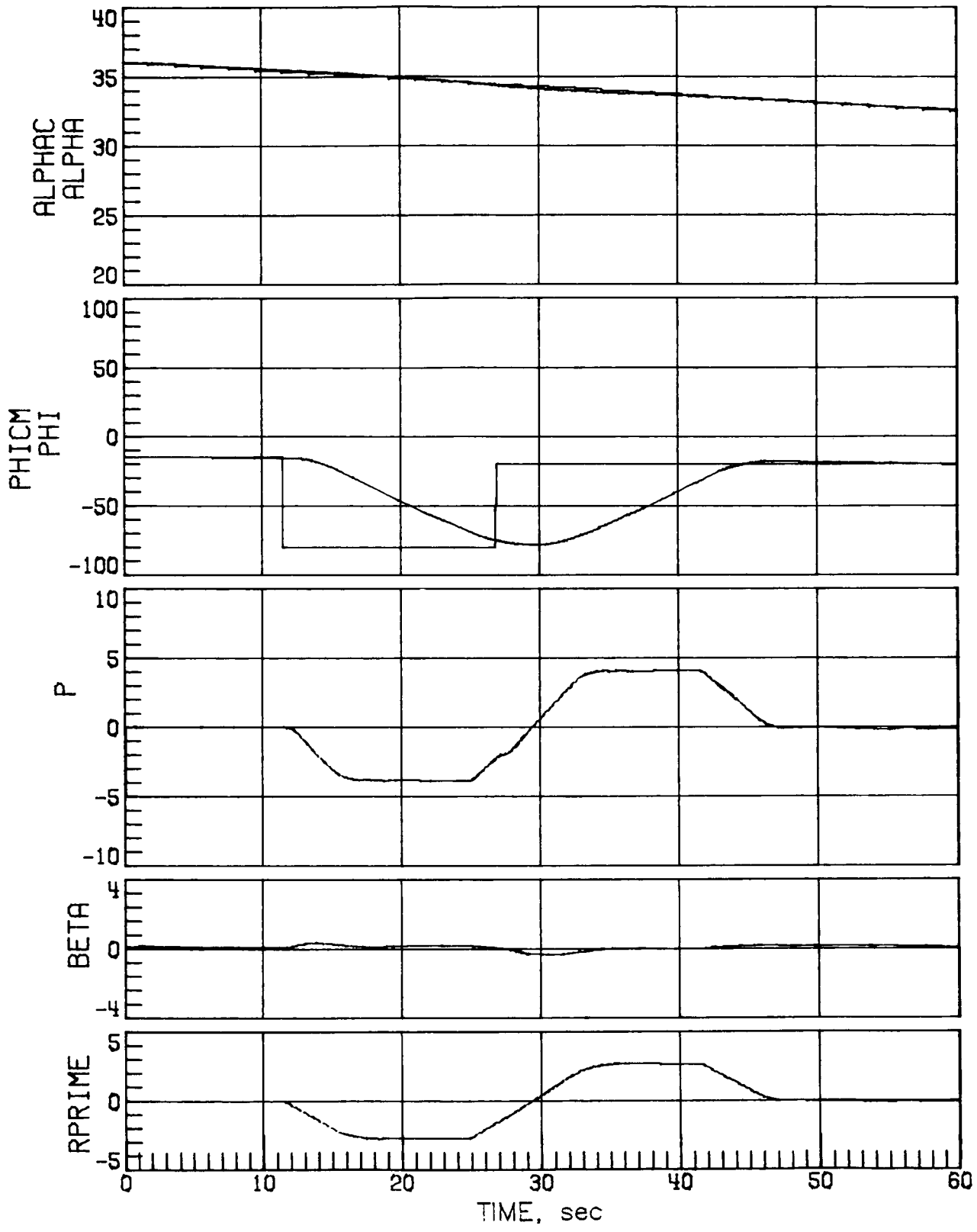

(a) Mach 10.

Figure 5.- Hypersonic maneuver performance for nominal conditions.

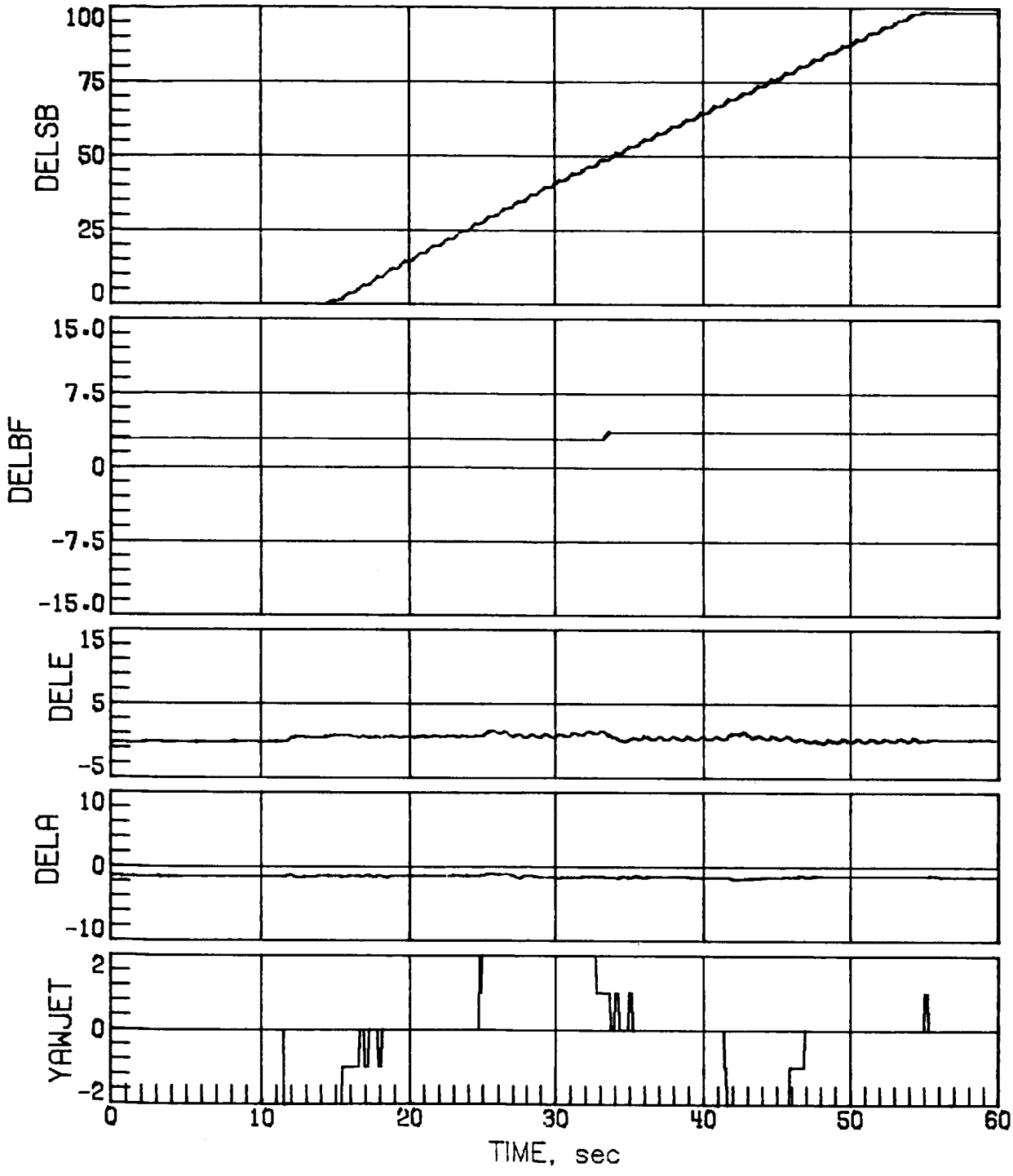

(a) Concluded.

Figure 5.- Continued.

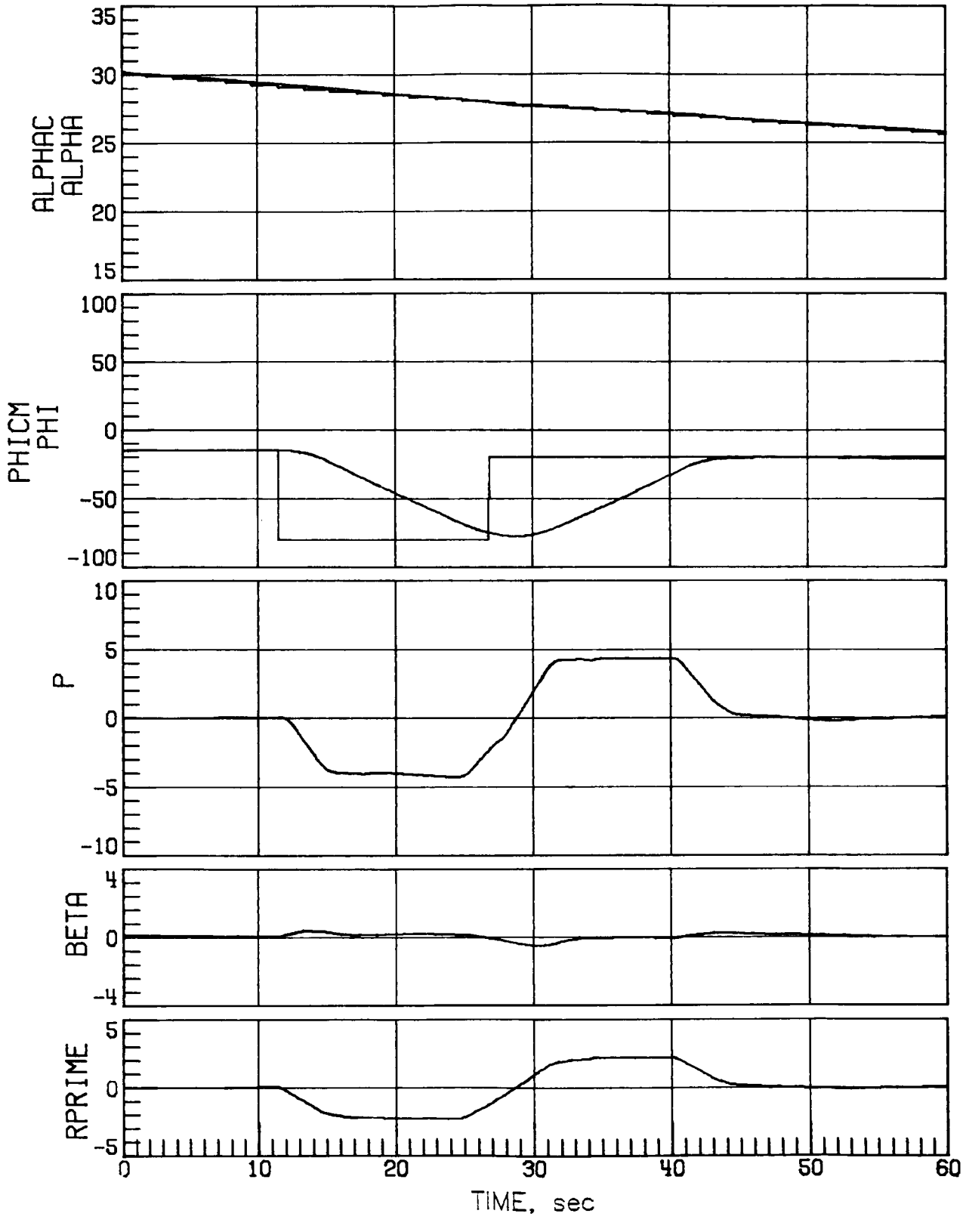

(b) Mach 7.5.

Figure 5.- Continued.

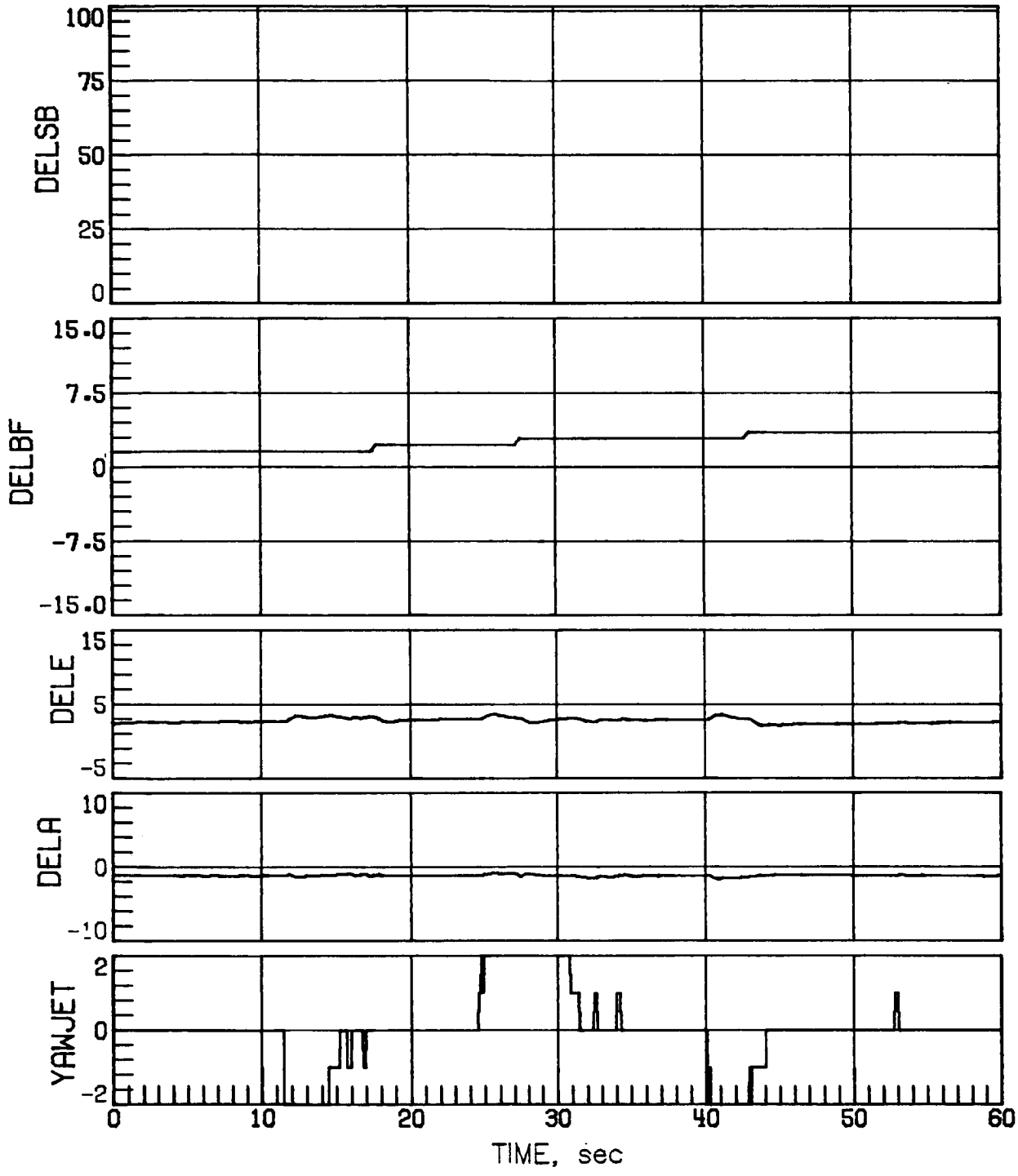

(b) Concluded.

Figure 5.- Concluded.

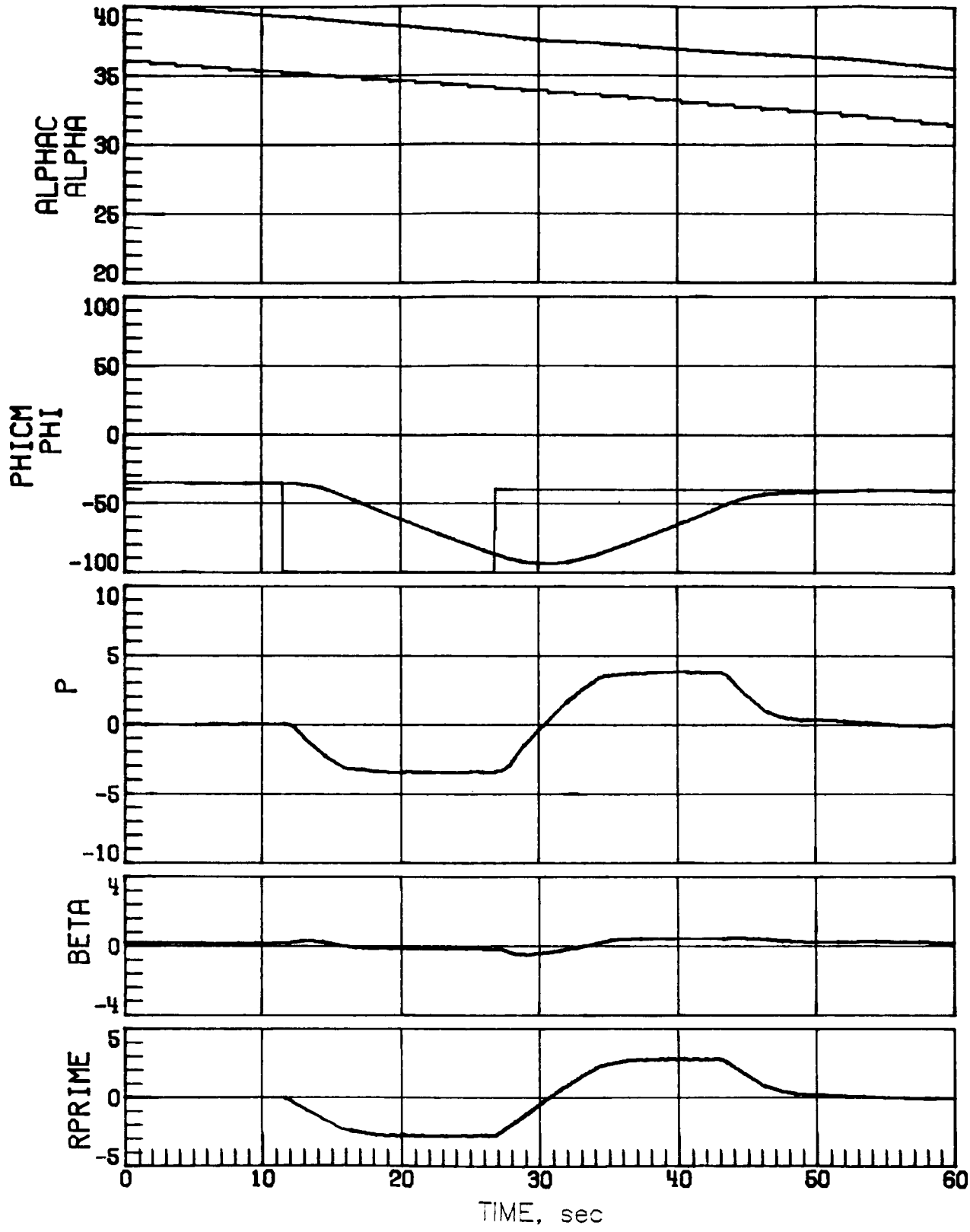

(a) Mach 10.

Figure 6.- Hypersonic maneuver performance for a low-sensed α error of 4°.

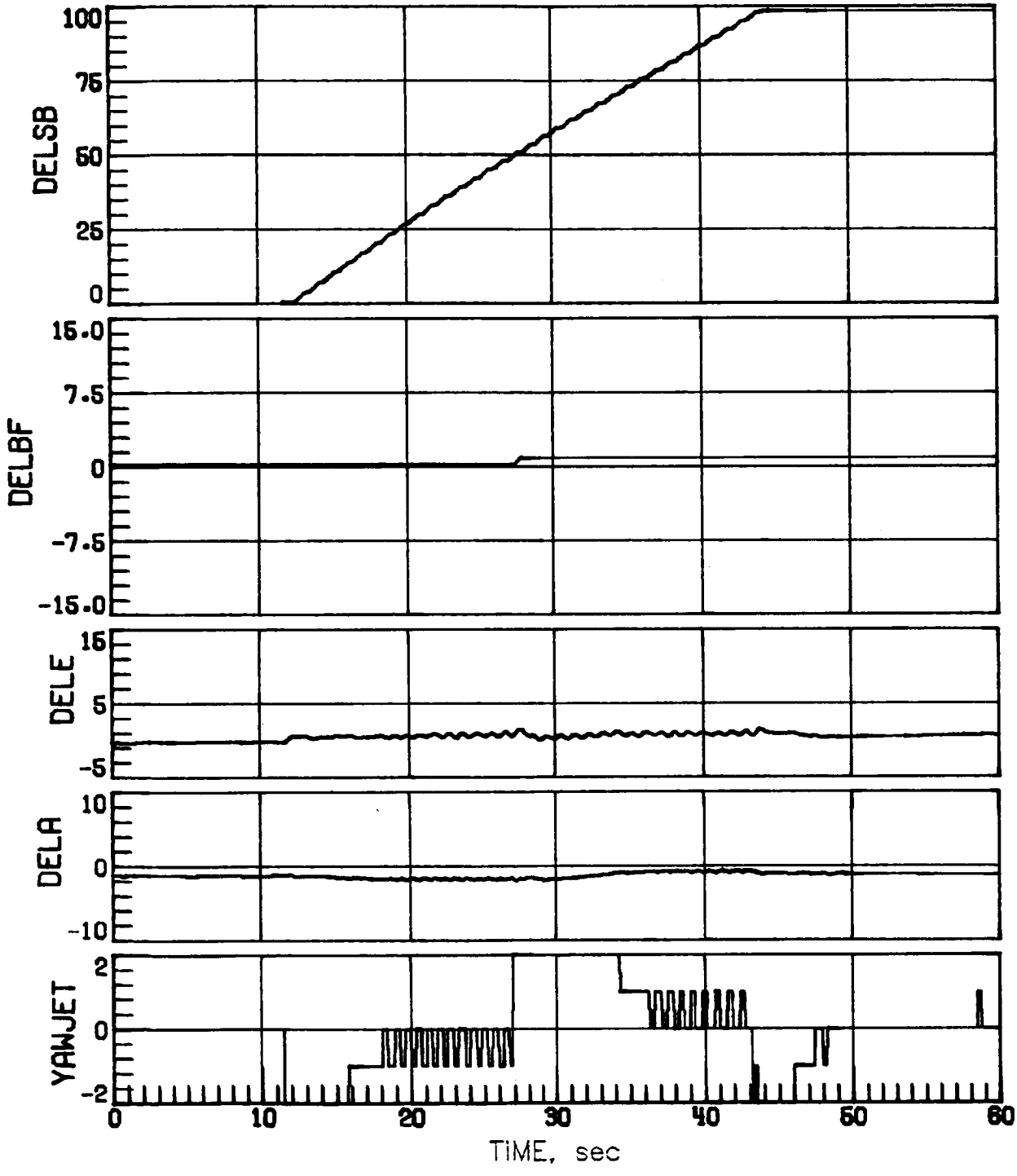

(a) Concluded.

Figure 6.- Continued.

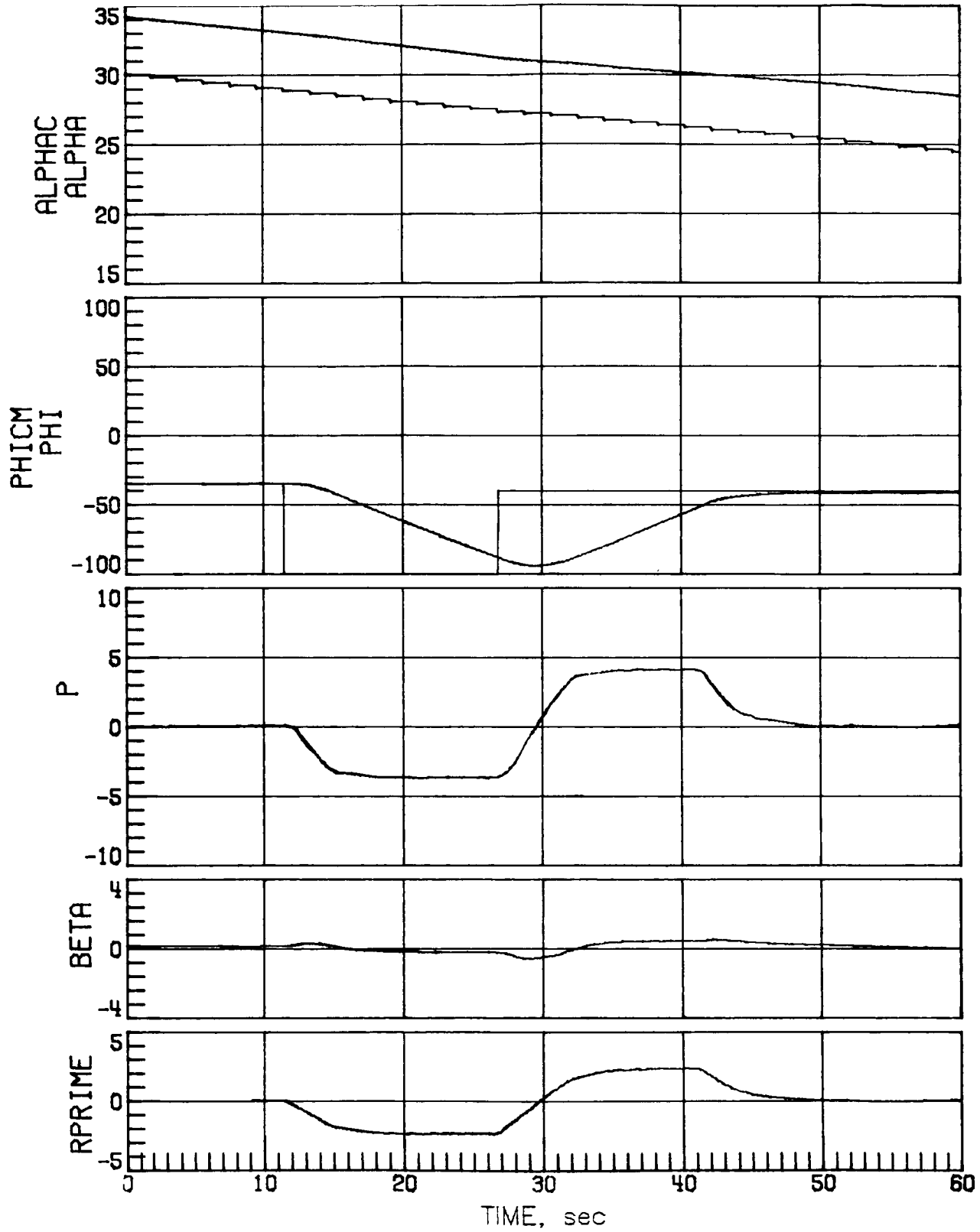

(b) Mach 7.5.

Figure 6.- Continued.

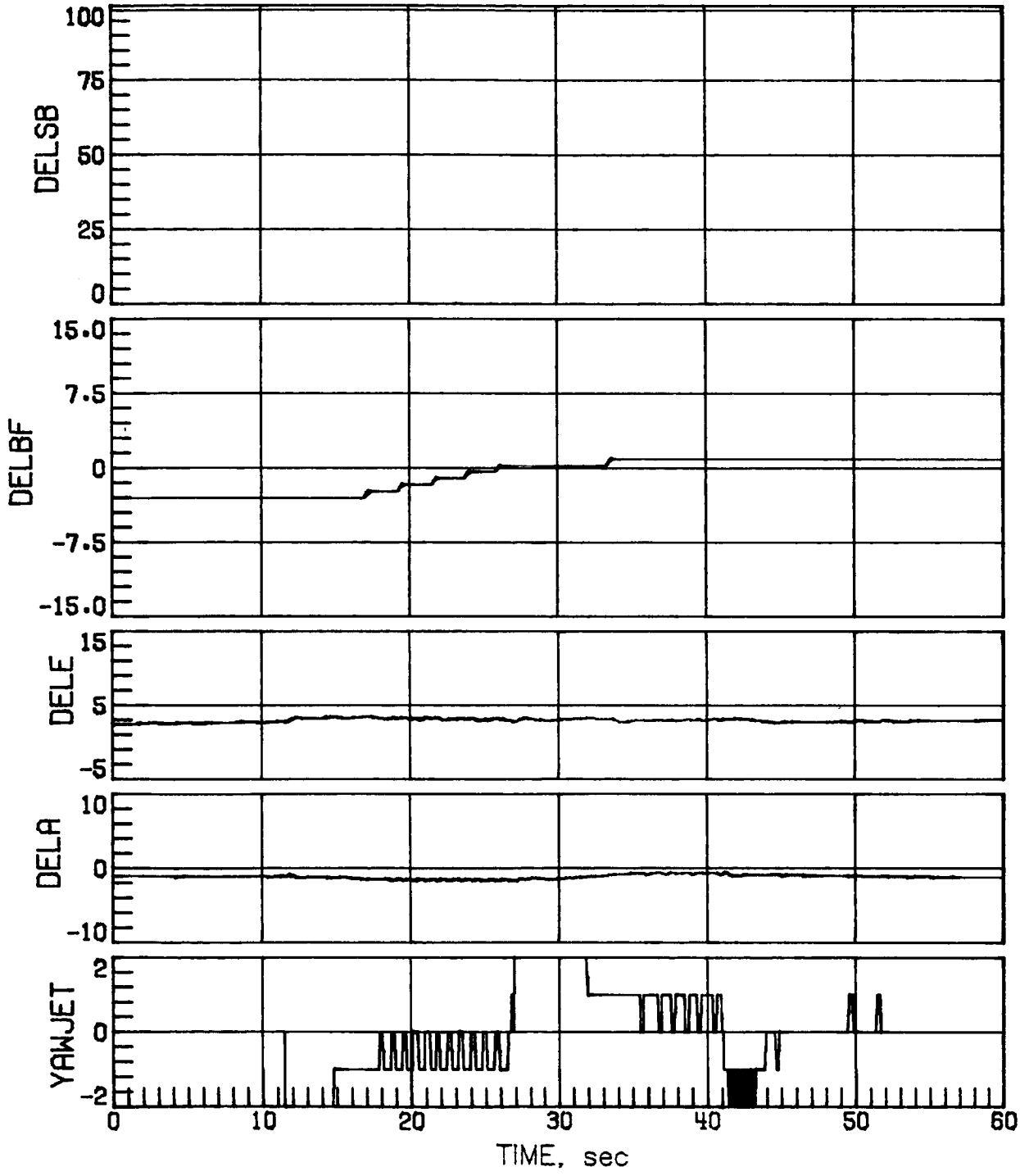

(b) Concluded.

Figure 6.- Concluded.

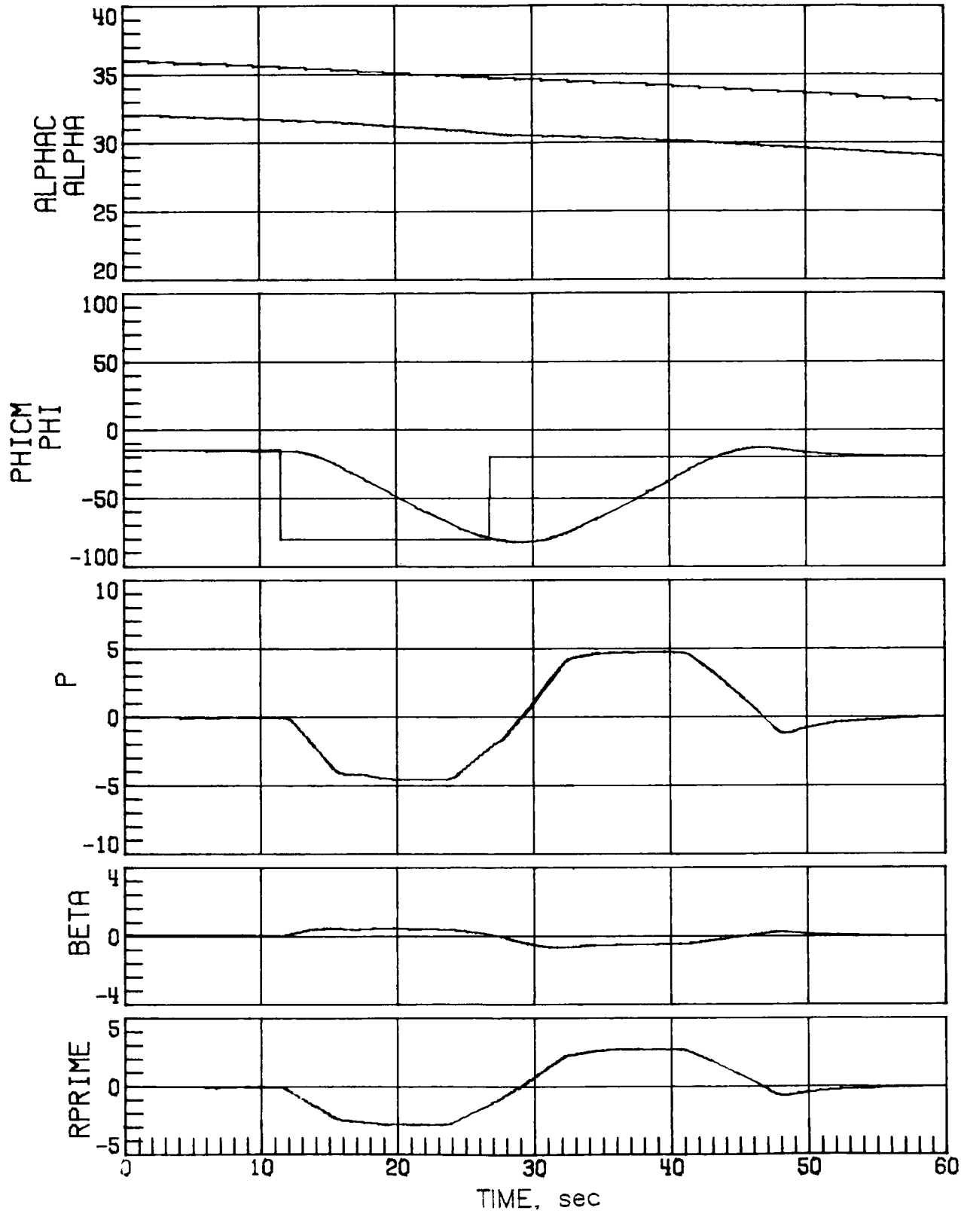

(a) Mach 10.

Figure 7.- Hypersonic maneuver performance for a high-sensed α error of 4°.

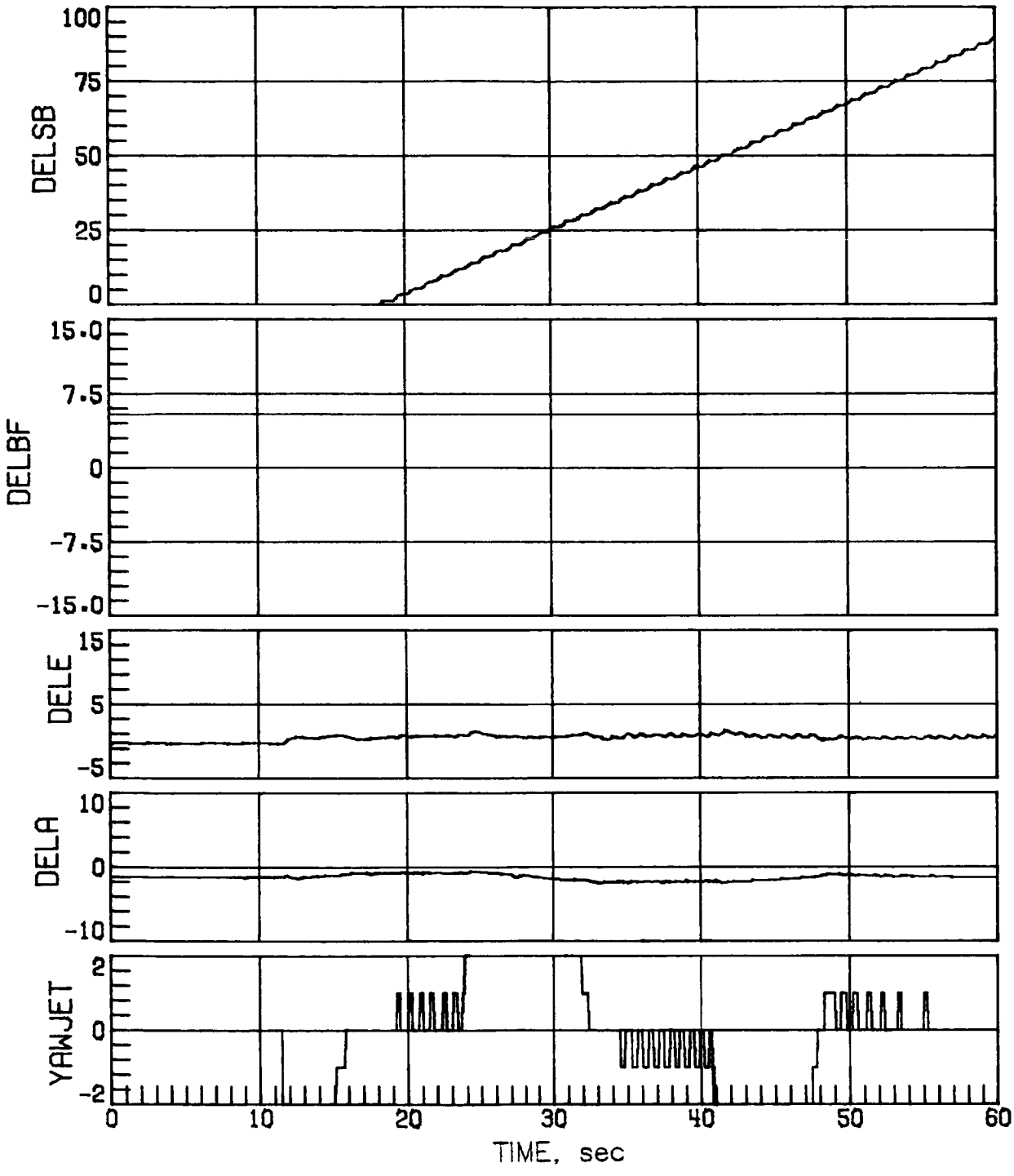

(a) Concluded.

Figure 7.- Continued.

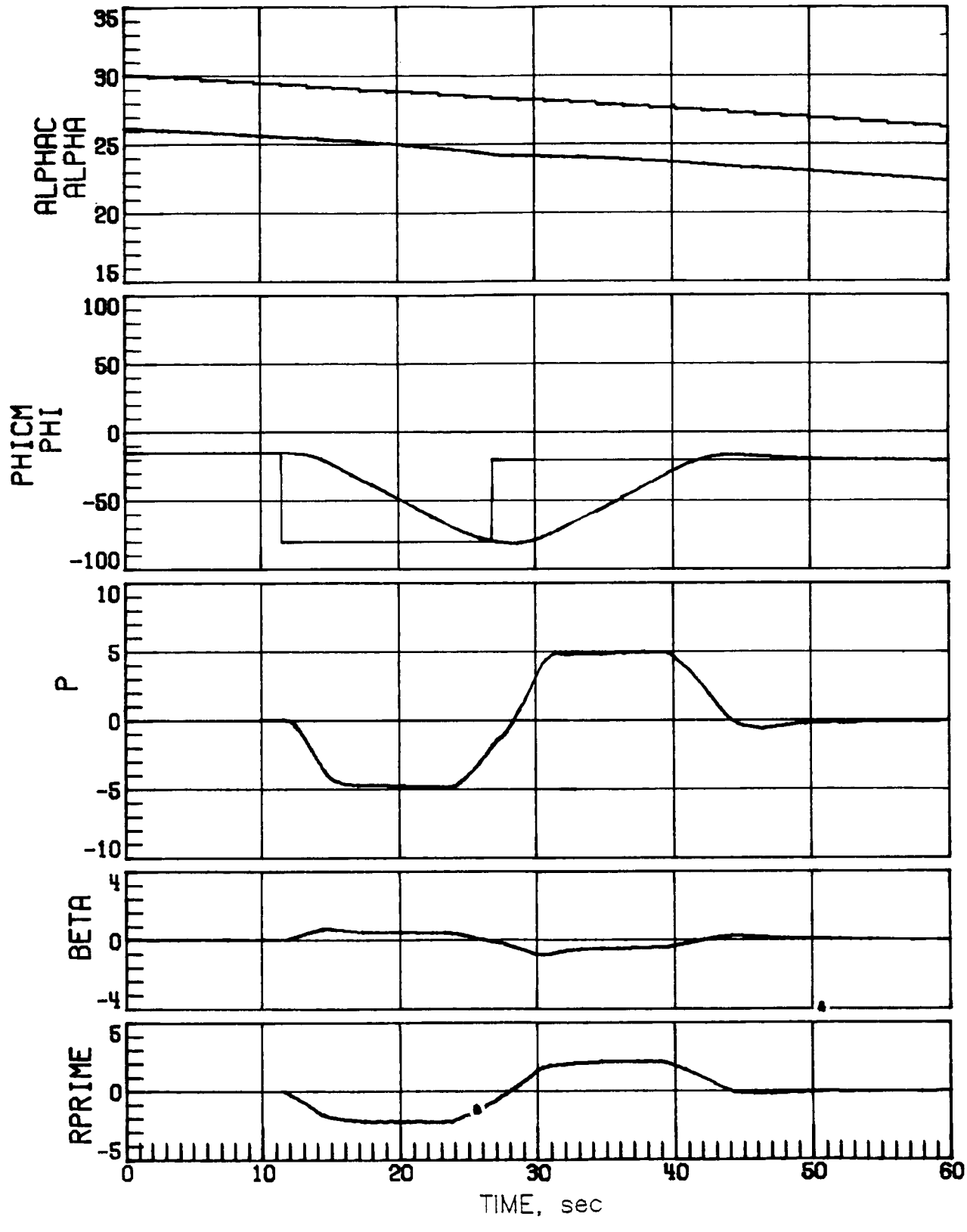

(b) Mach 7.5.

Figure 7.- Continued.

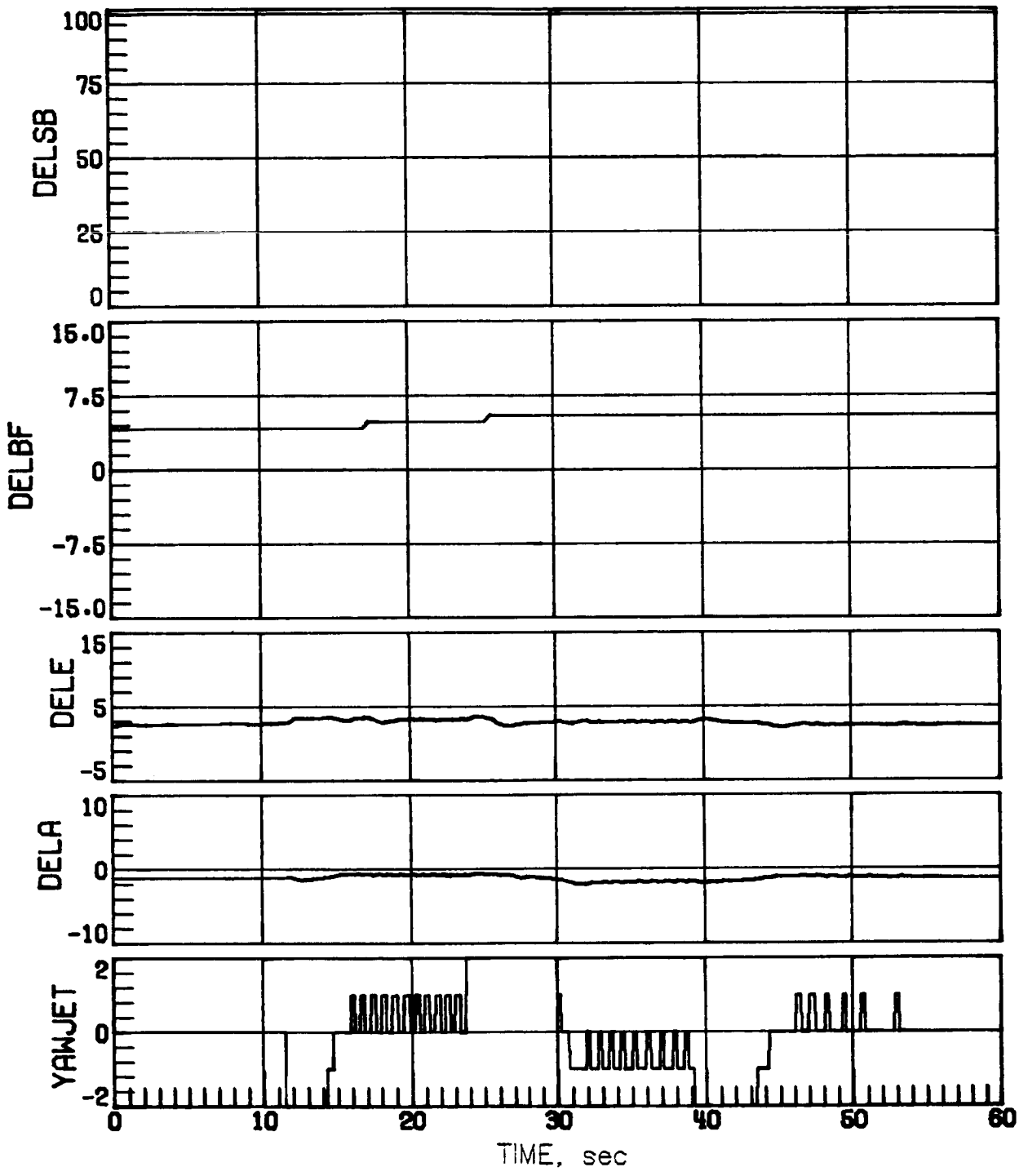

(b) Concluded.

Figure 7.- Concluded.

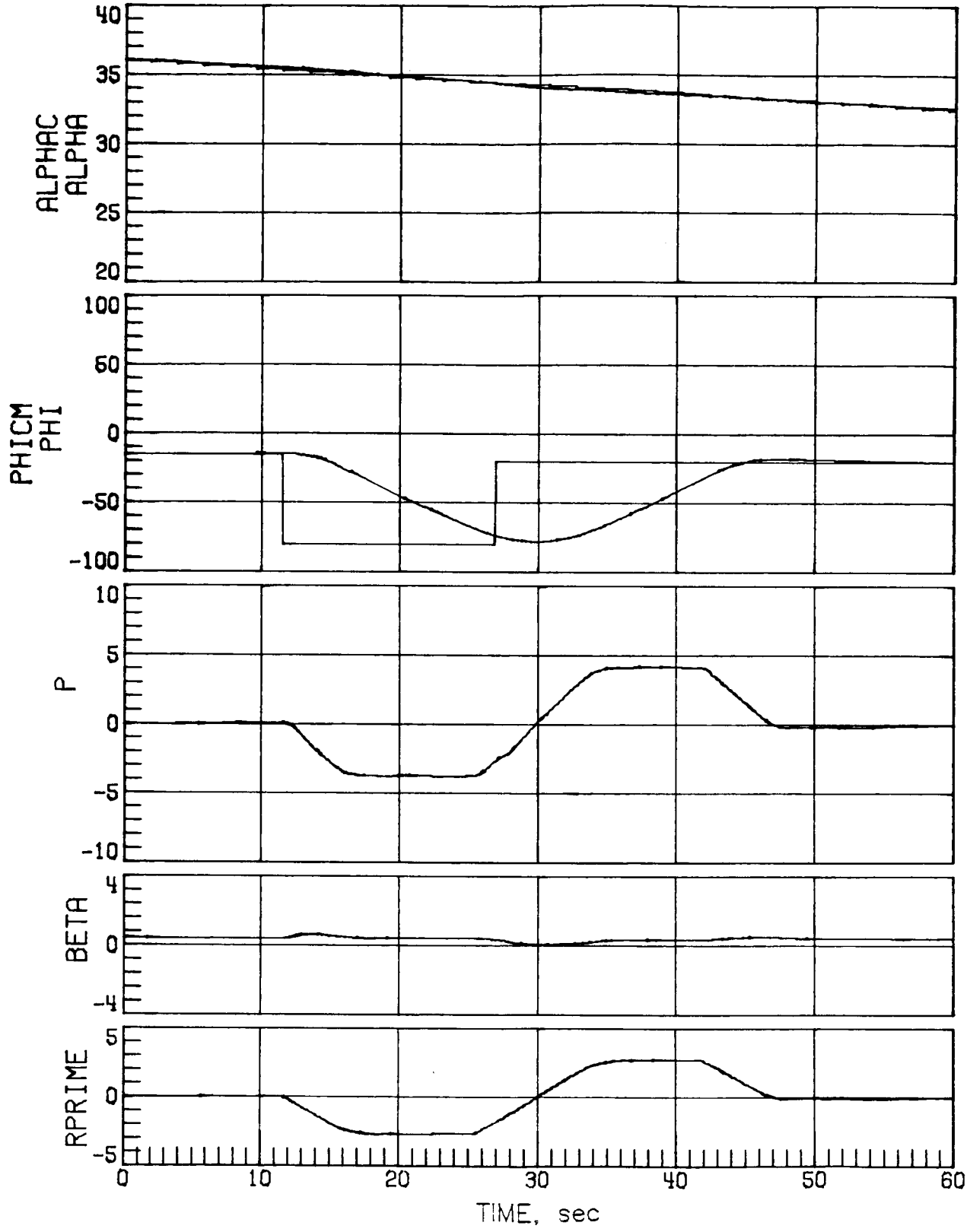

(a) Case 2.

Figure 8.- Mach 10 maneuver performance with off-nominal aerodynamics.

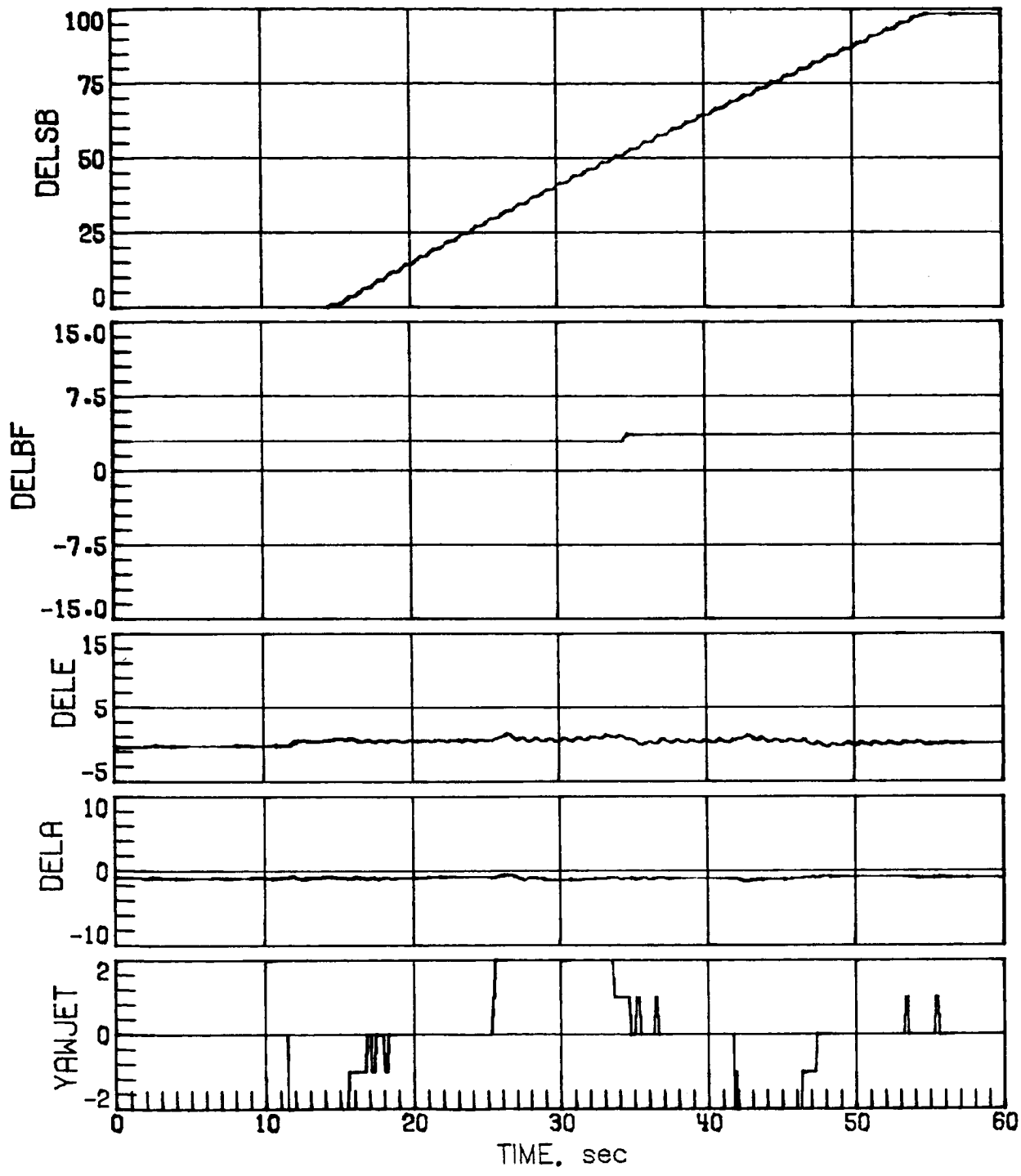

(a) Concluded.

Figure 8.- Continued.

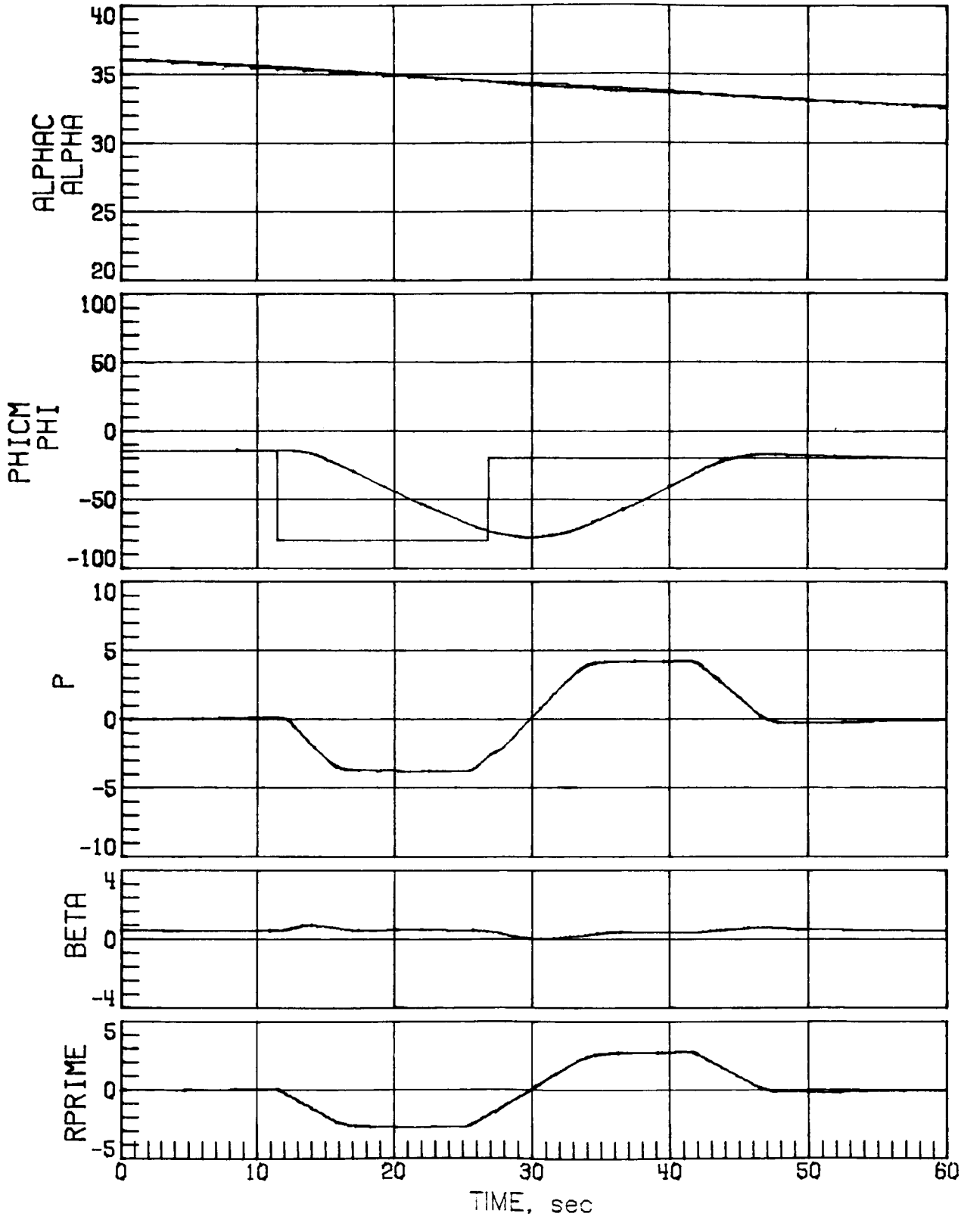

(b) Case 4.

Figure 8.- Continued.

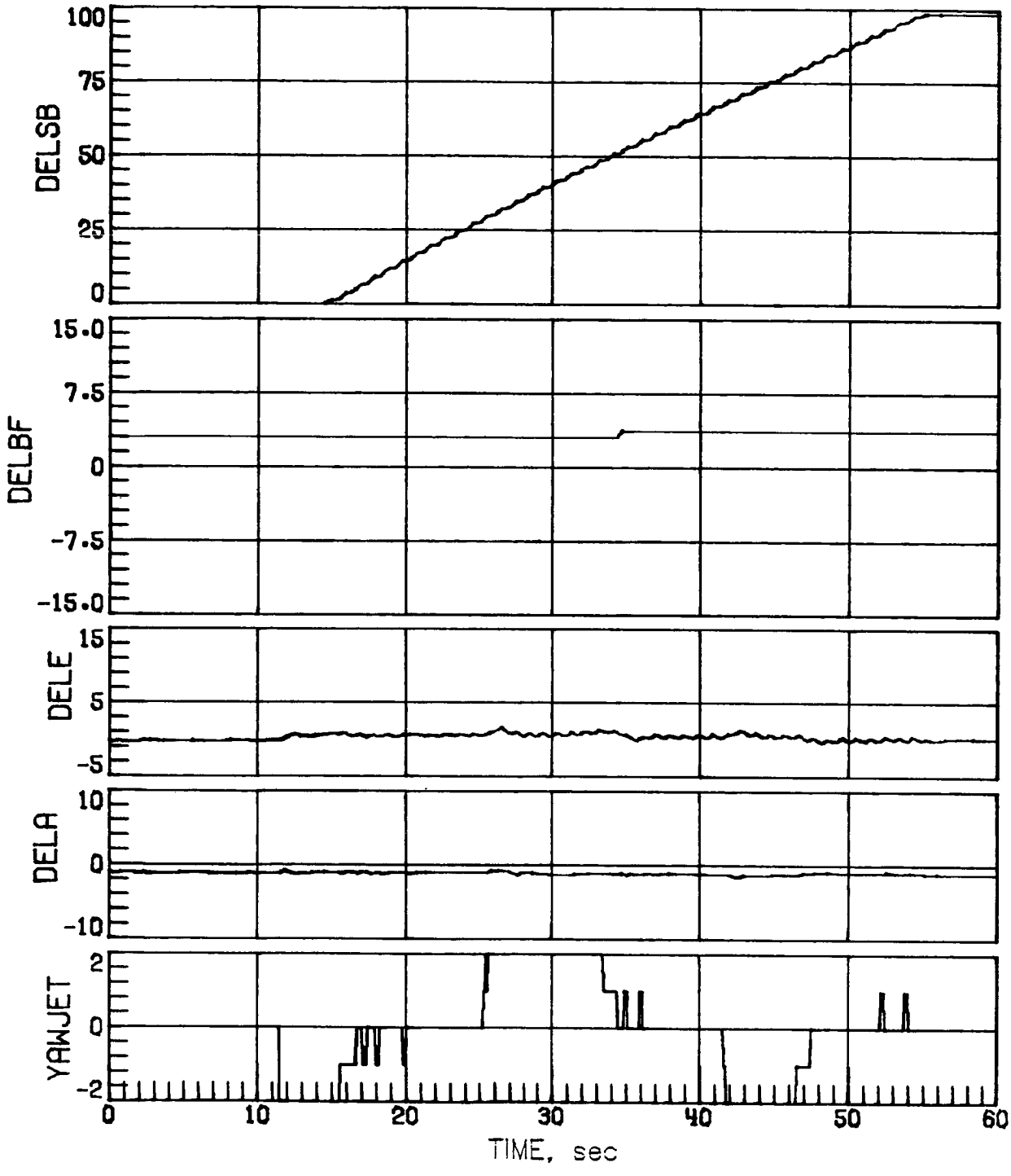

(b) Concluded.

Figure 8.- Continued.

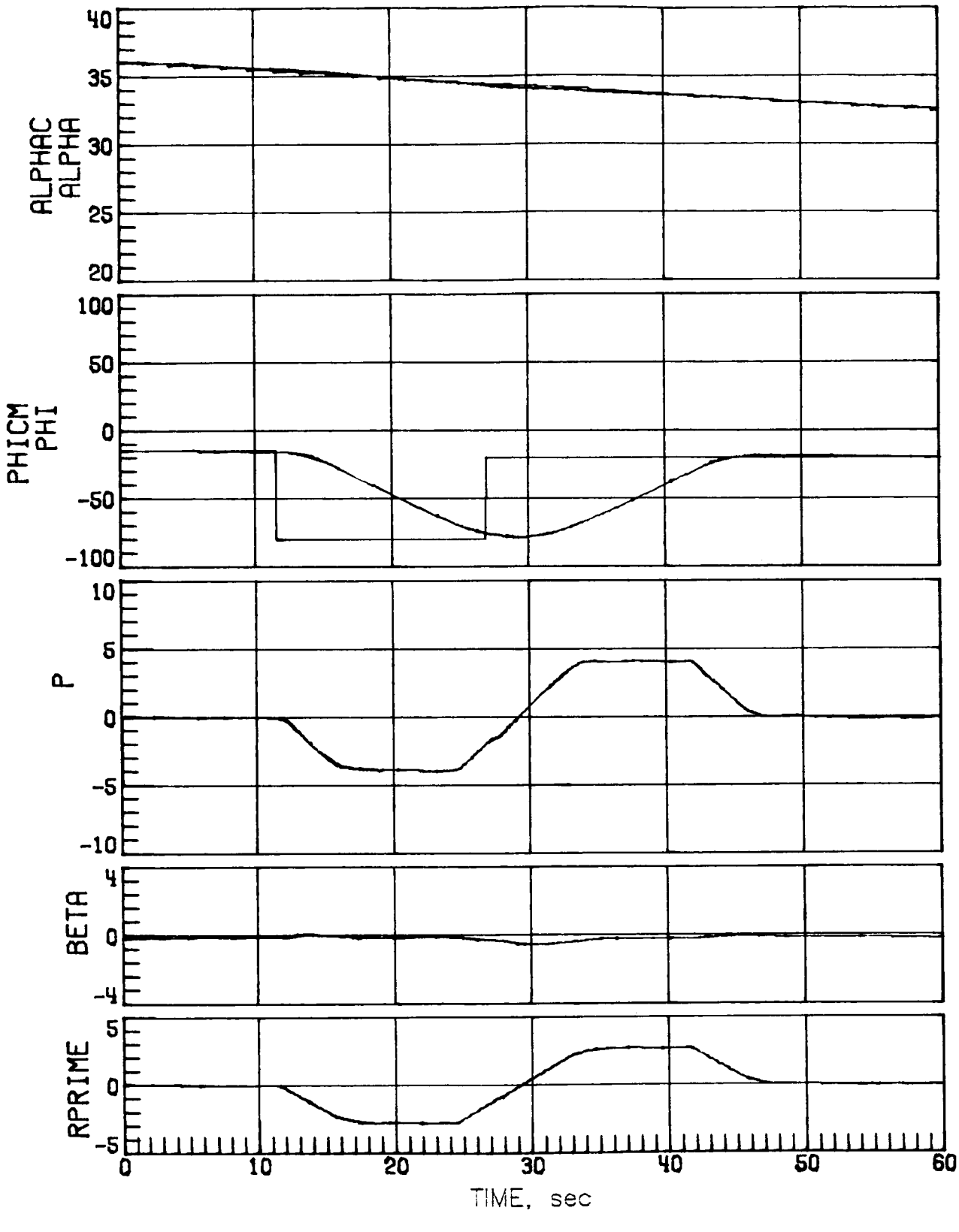

(c) Case 6.

Figure 8.- Continued.

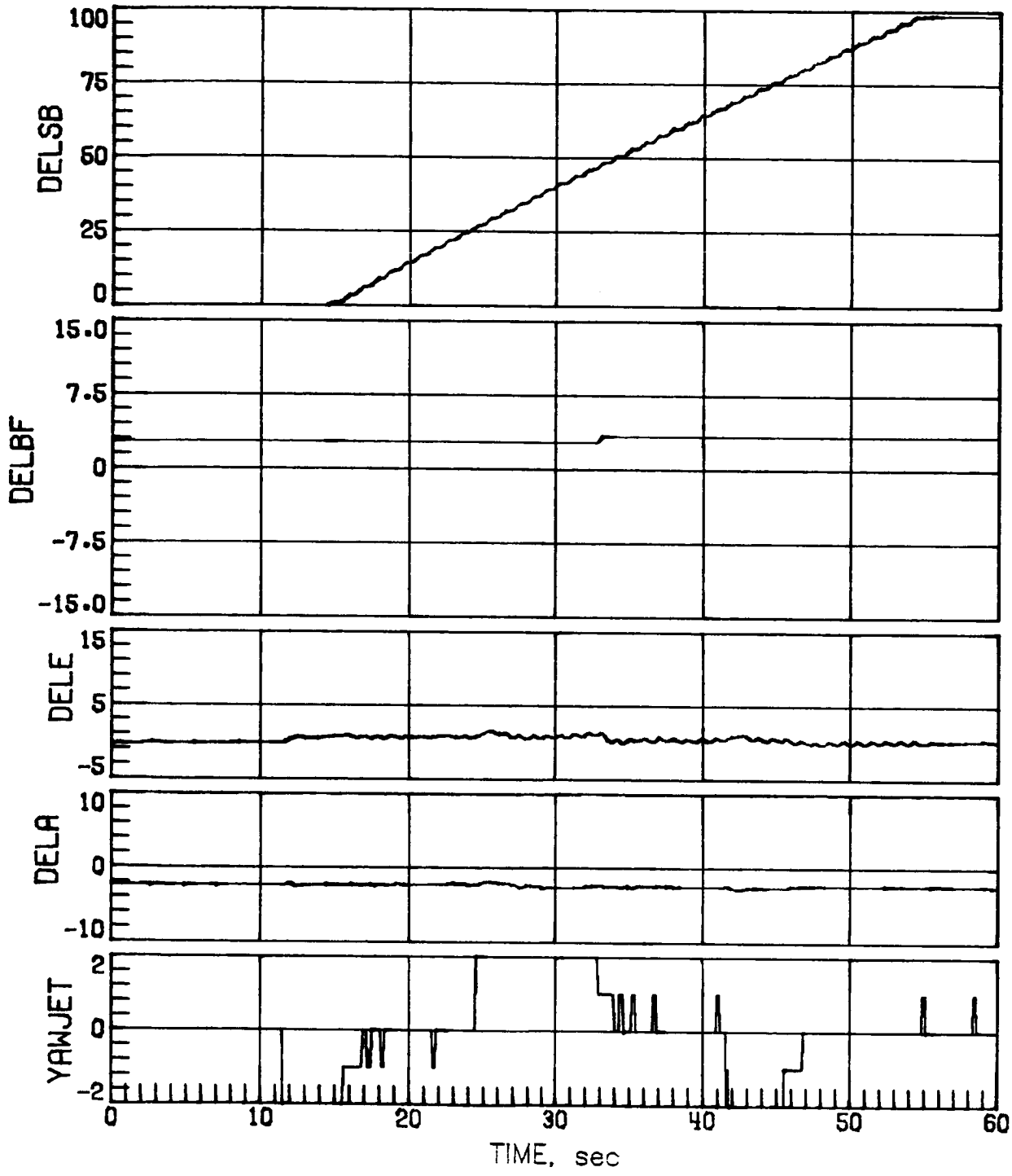

(c) Concluded.

Figure 8.- Continued.

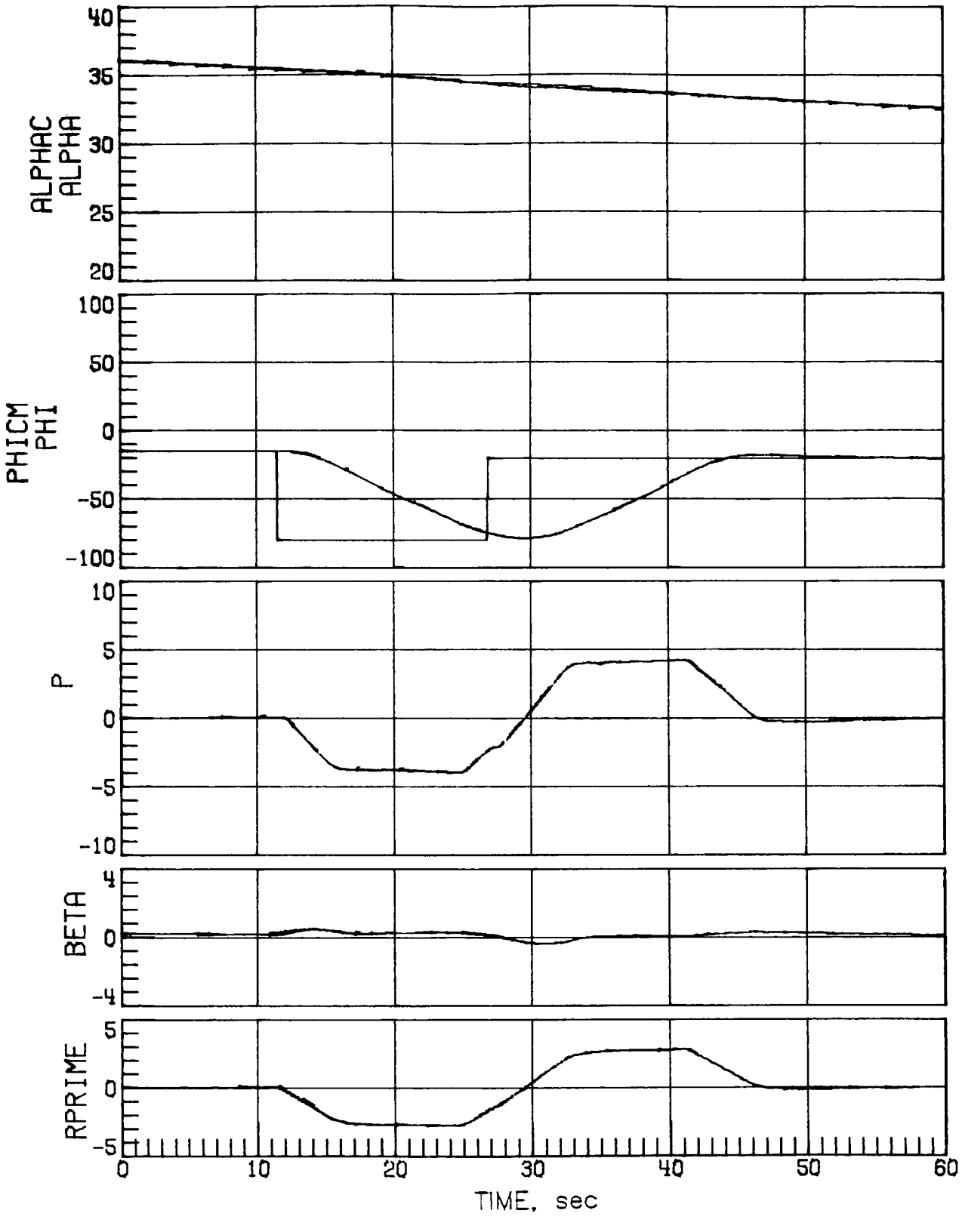

(d) Case 11.

Figure 8.- Continued.

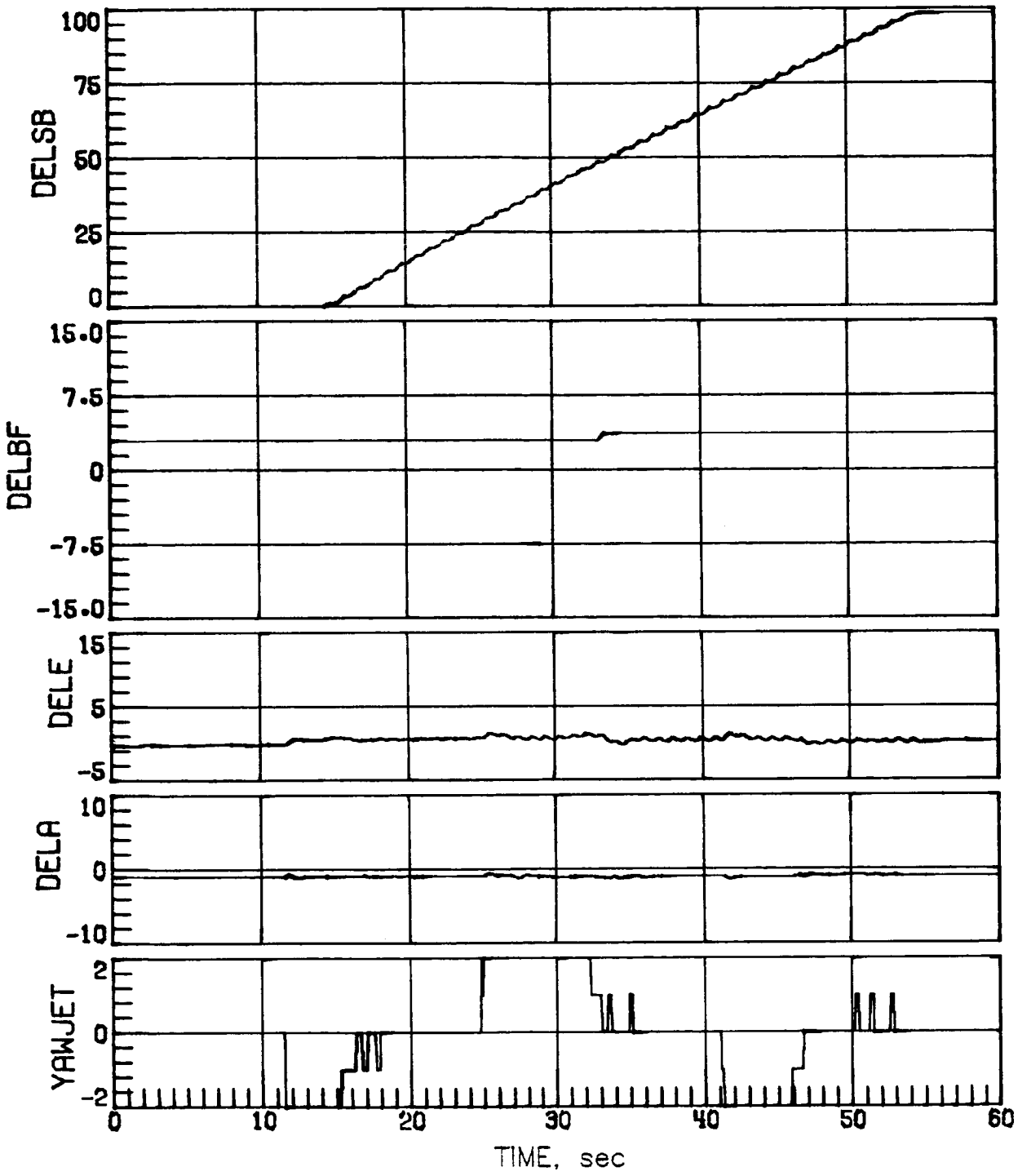

(d) Concluded.

Figure 8.- Continued.

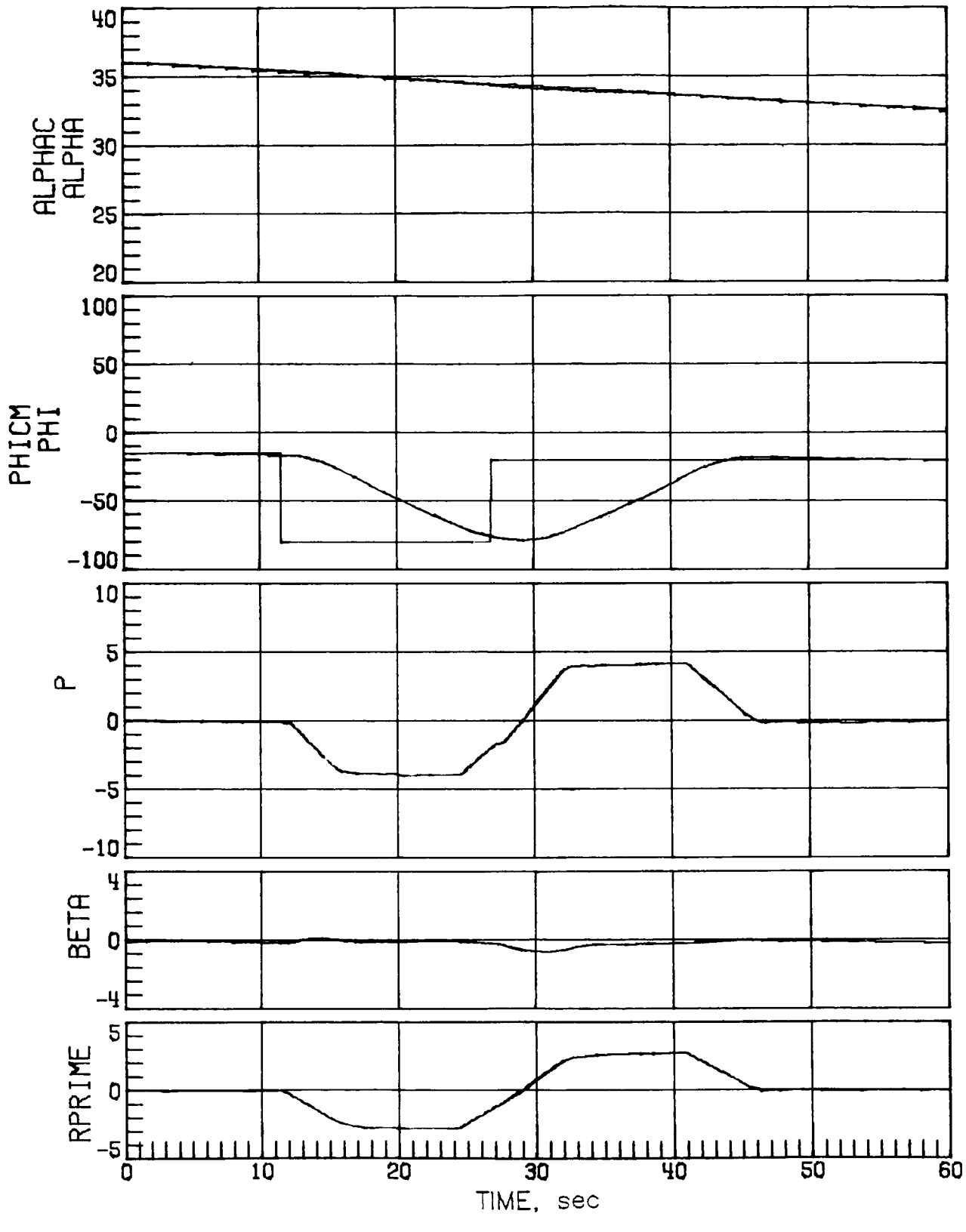

(e) Case 15.

Figure 8.- Continued.

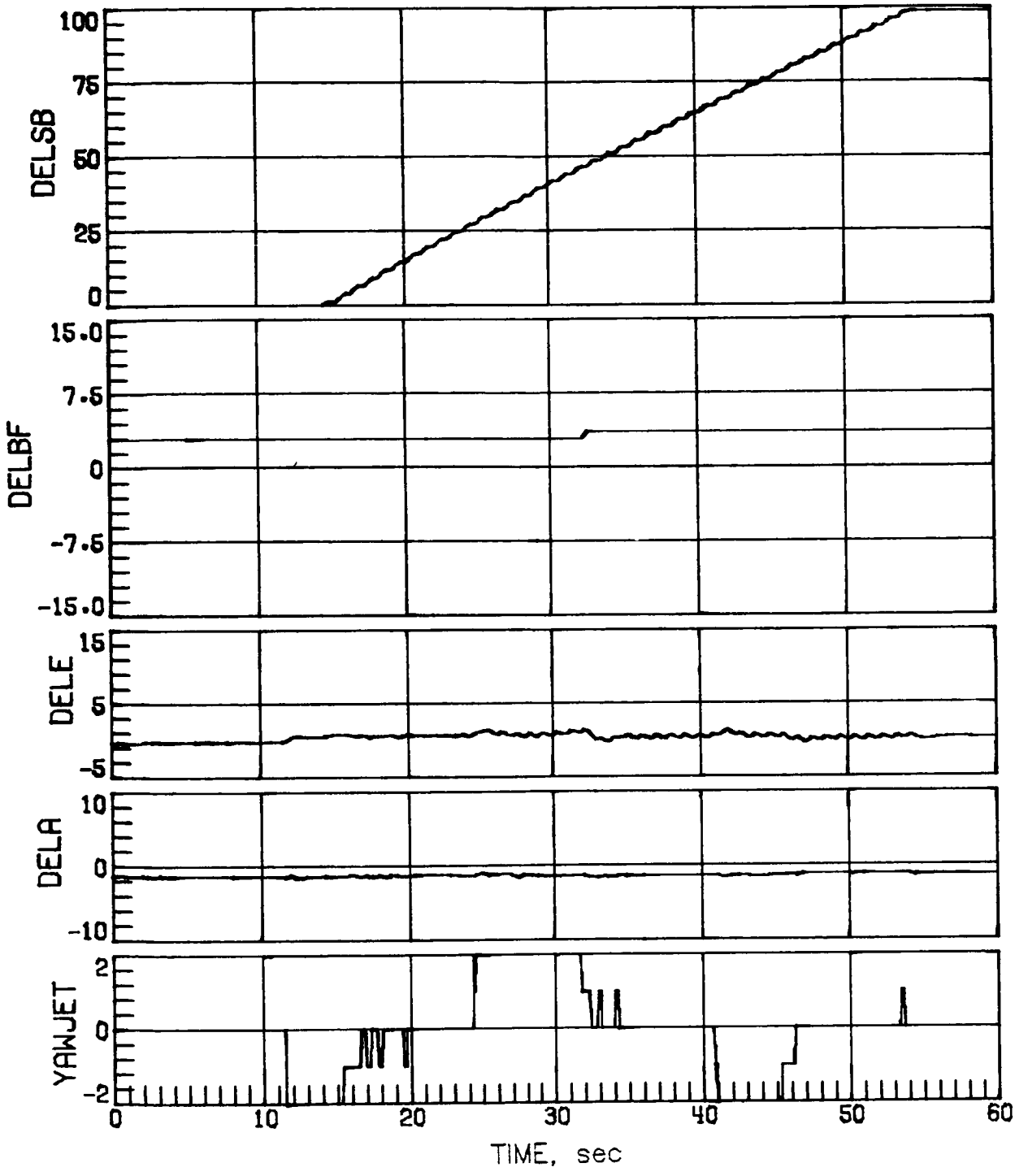

(e) Concluded.

Figure 8.- Concluded.

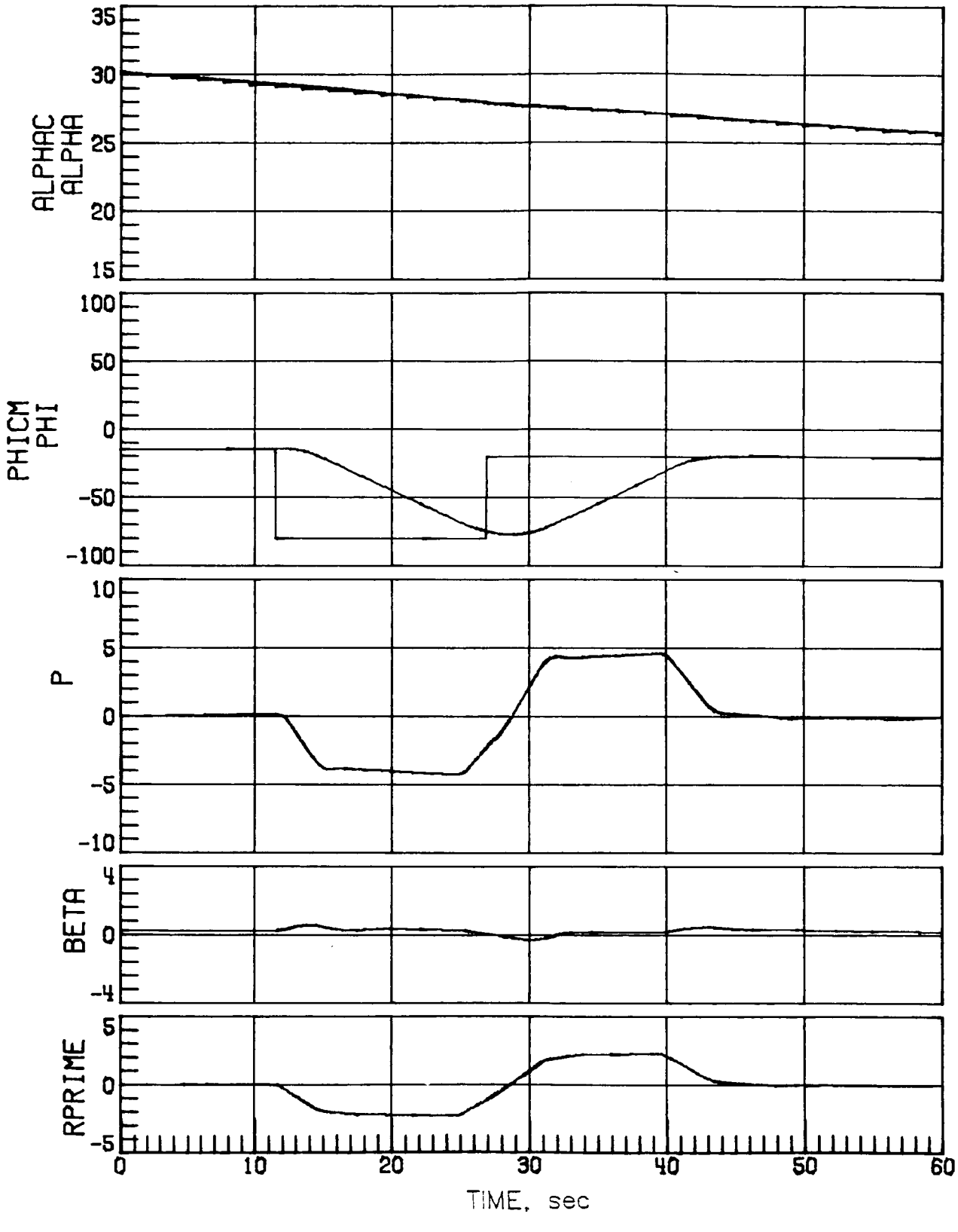

(a) Case 1.

Figure 9.- Mach 7.5 maneuver performance with off-nominal aerodynamics.

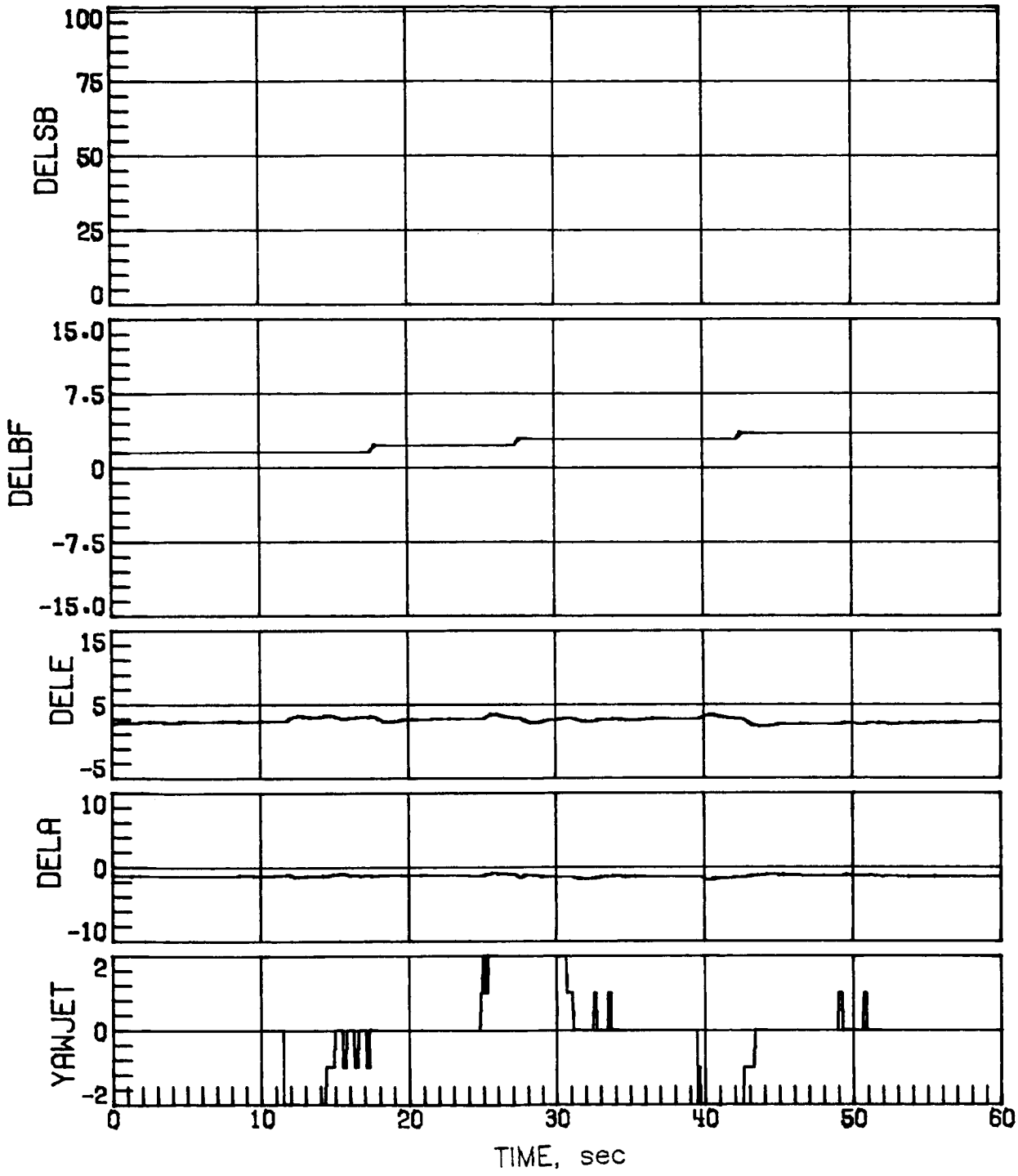

(a) Concluded.

Figure 9.- Continued.

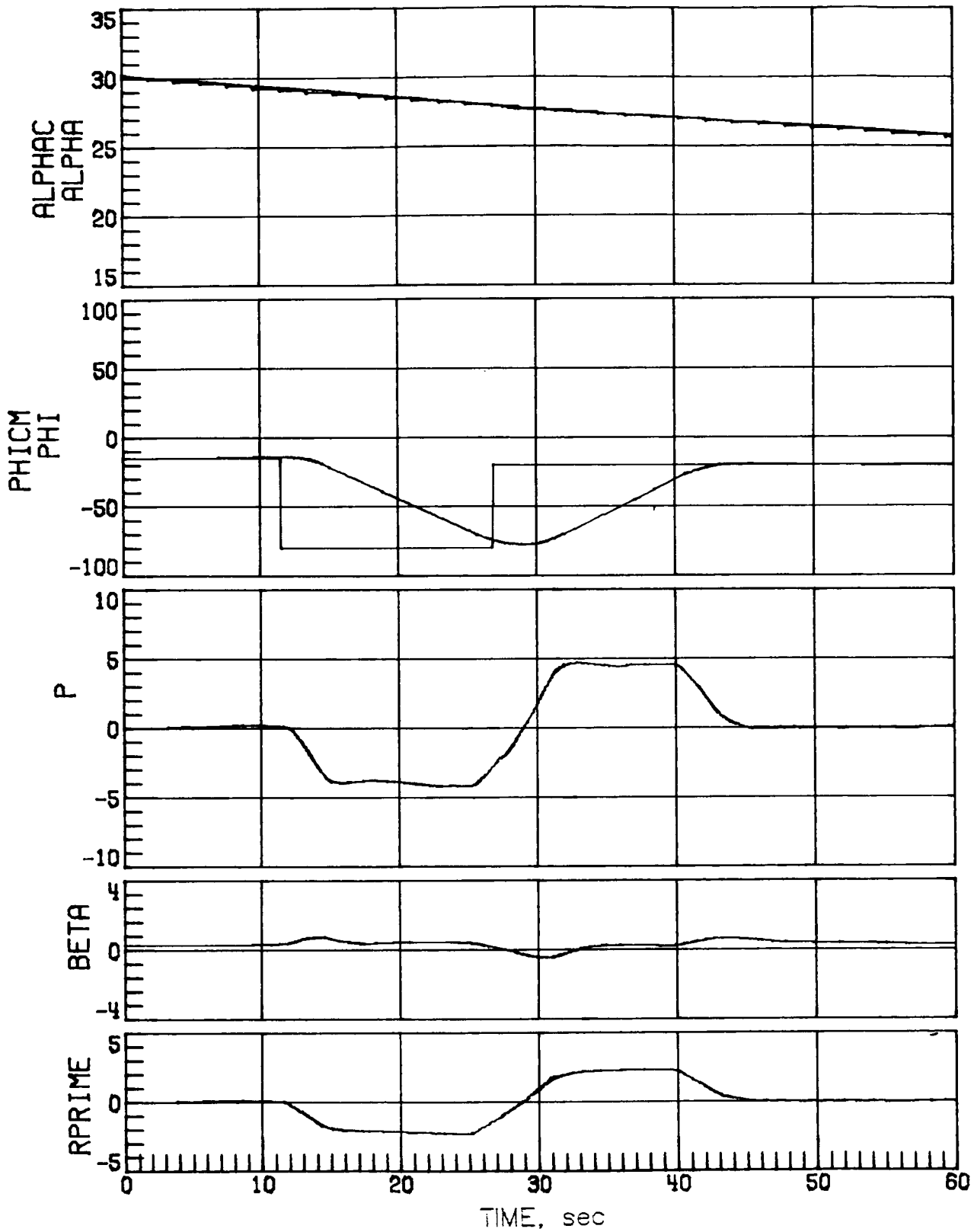

(b) Case 3.

Figure 9.- Continued.

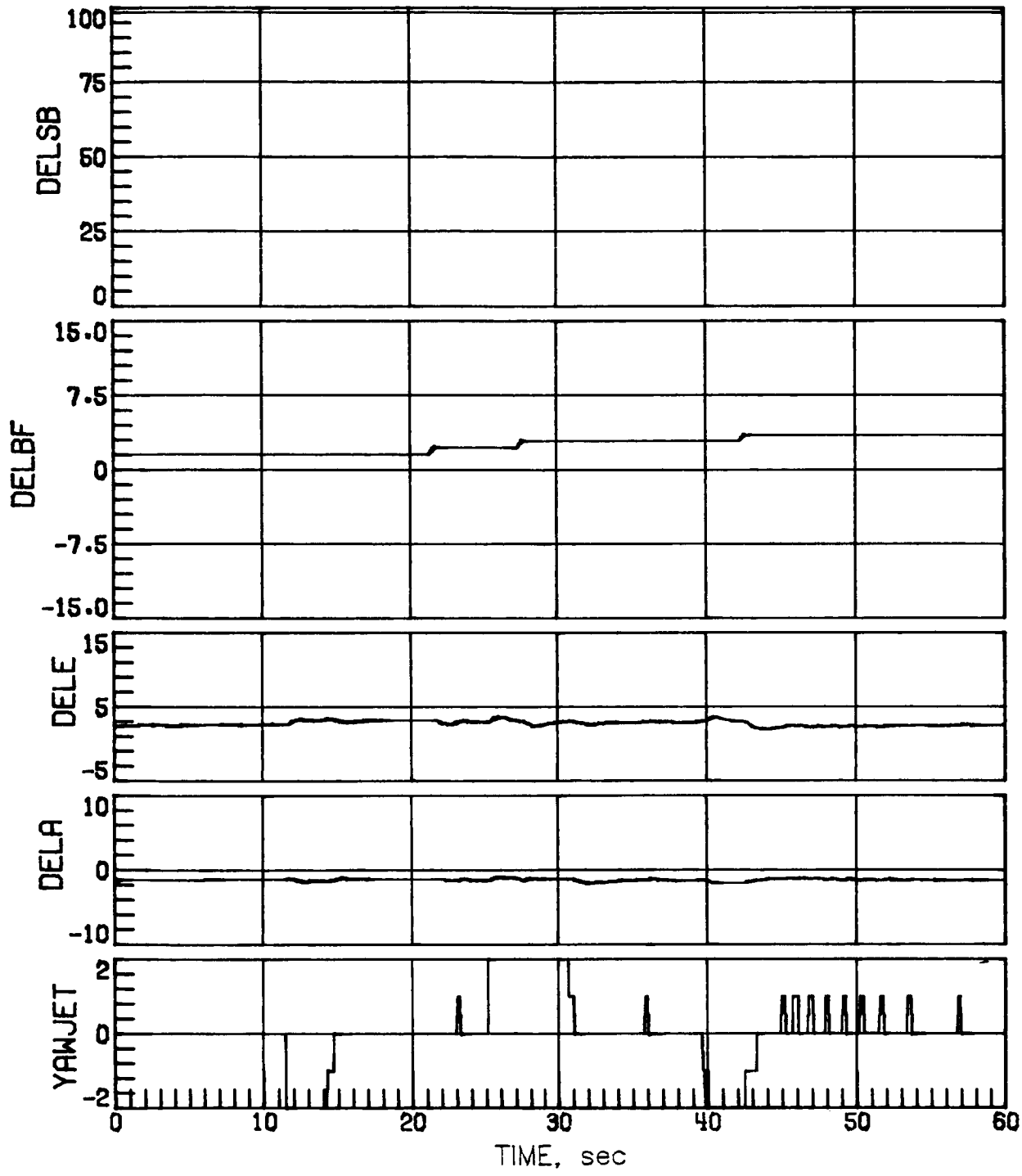

(b) Concluded.

Figure 9.- Continued.

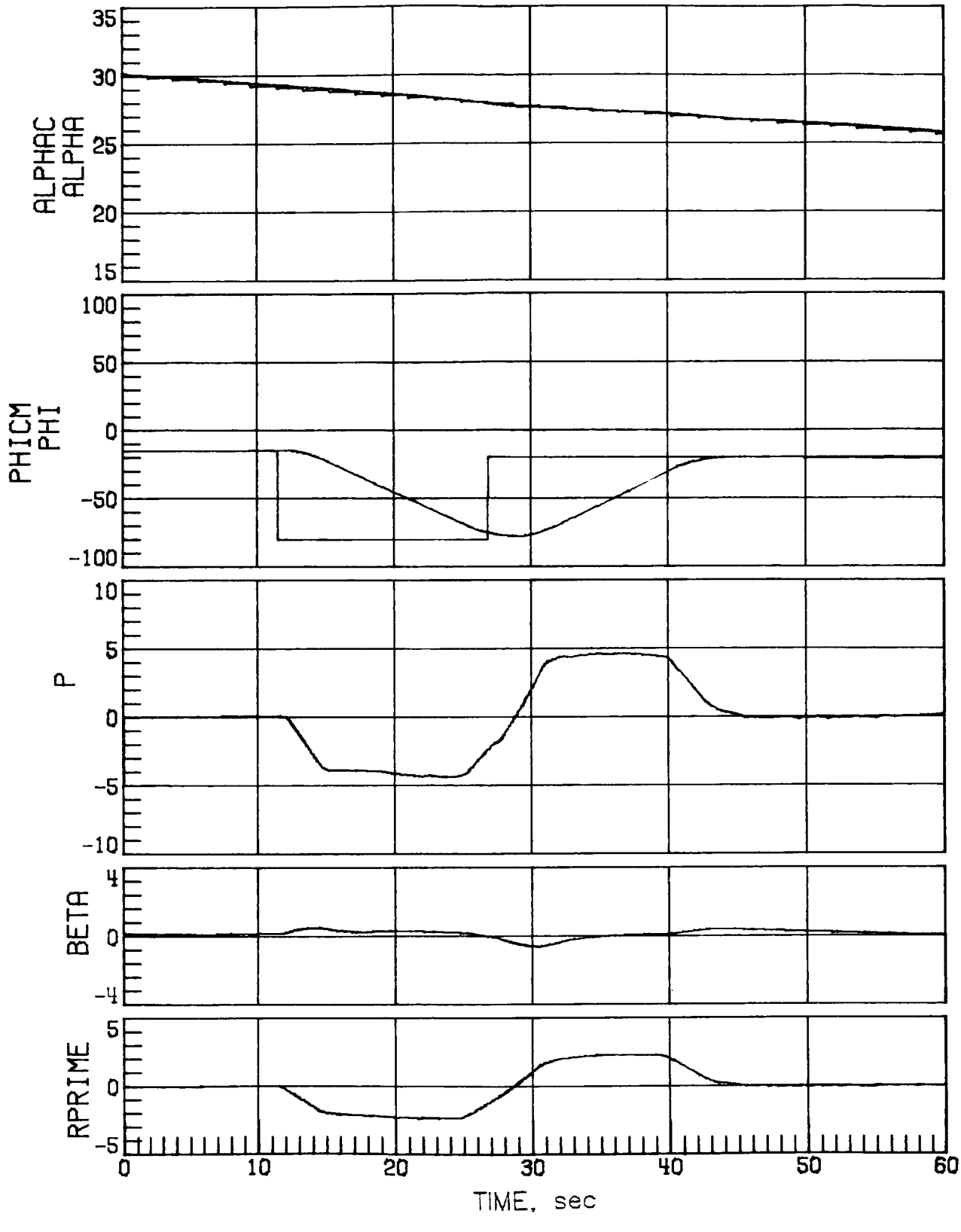

(c) Case 11.

Figure 9.- Continued.

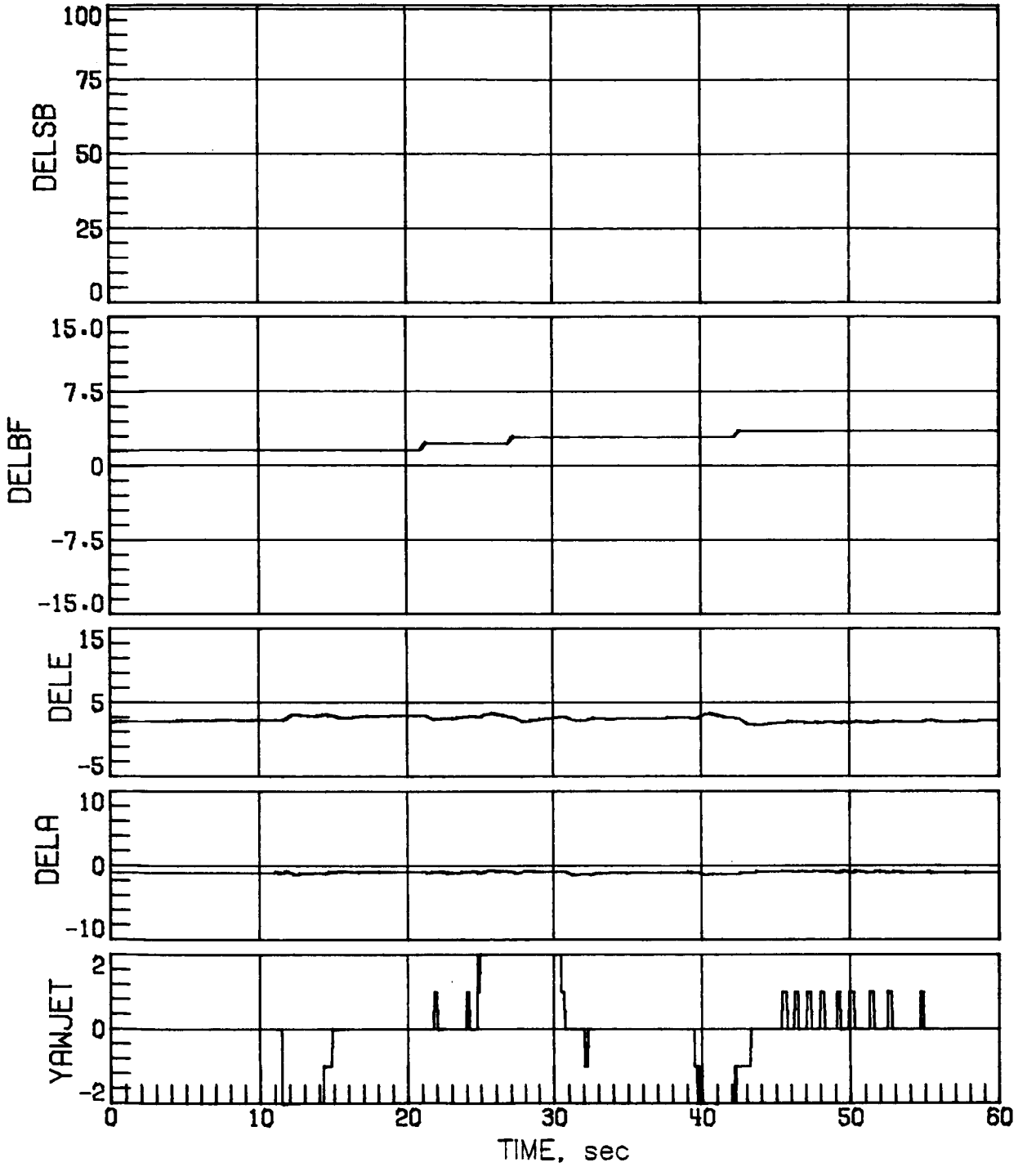

(c) Concluded.

Figure 9.- Continued.

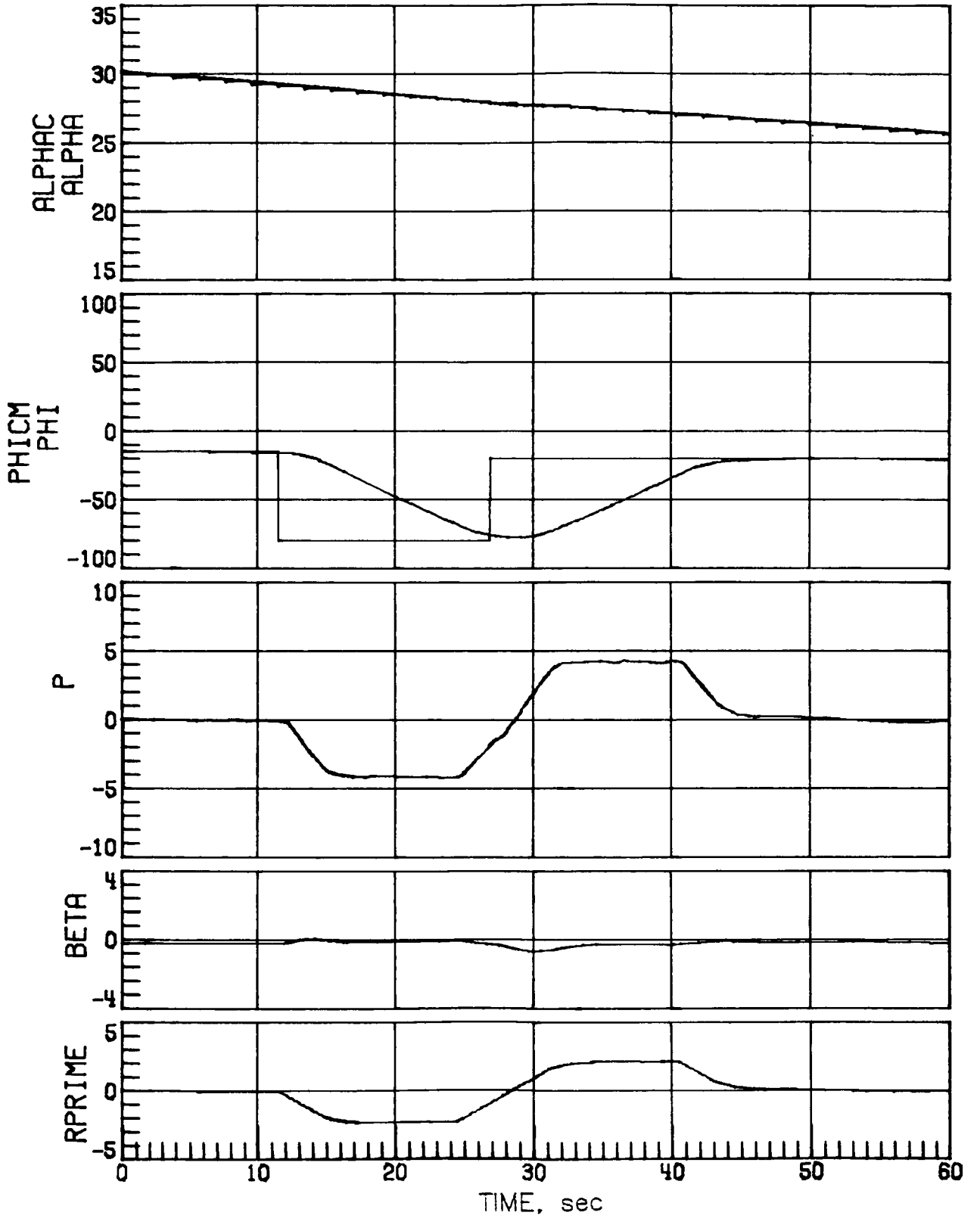

(d) Case 14.

Figure 9.- Continued.

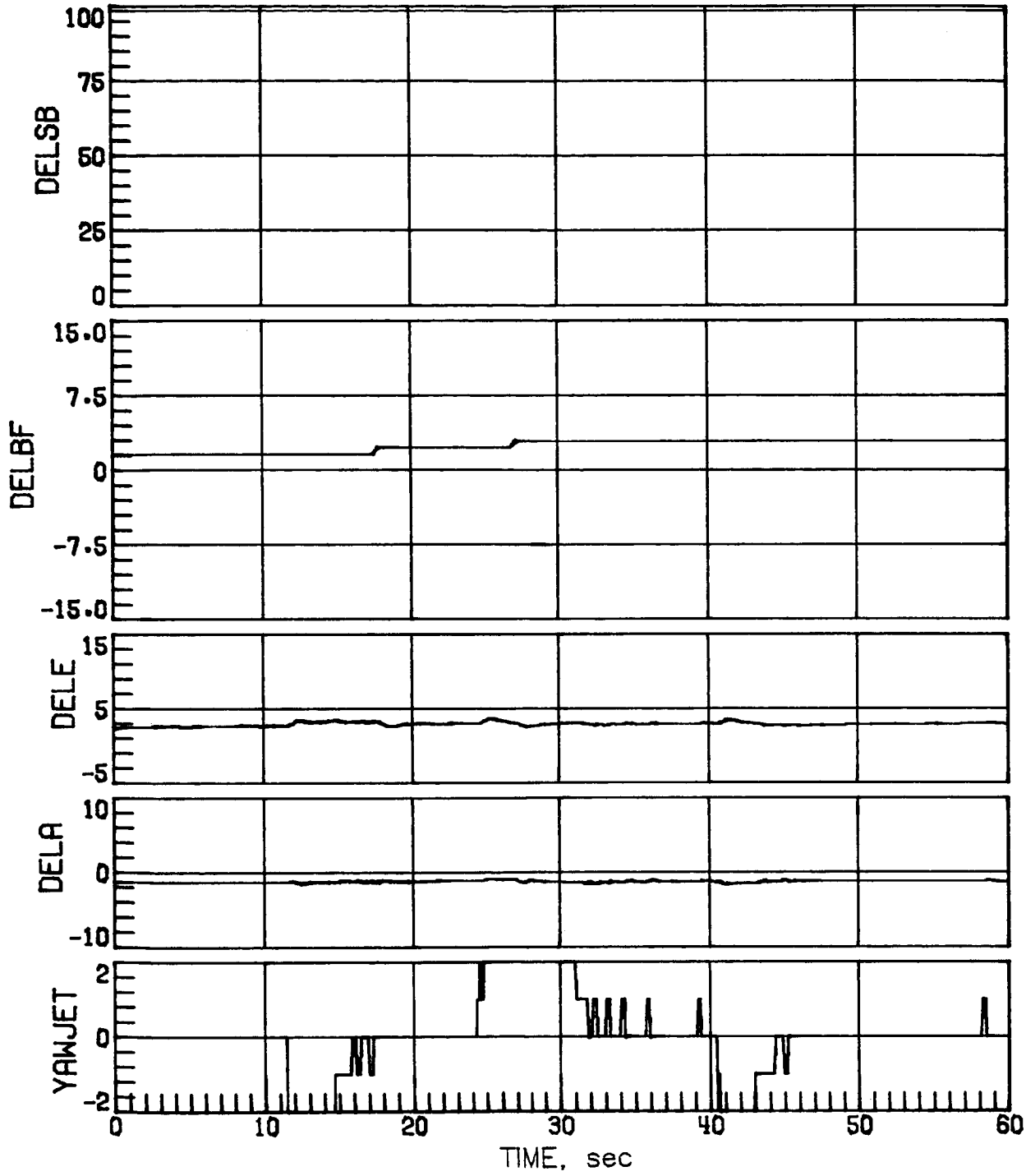

(d) Concluded.

Figure 9.- Continued.

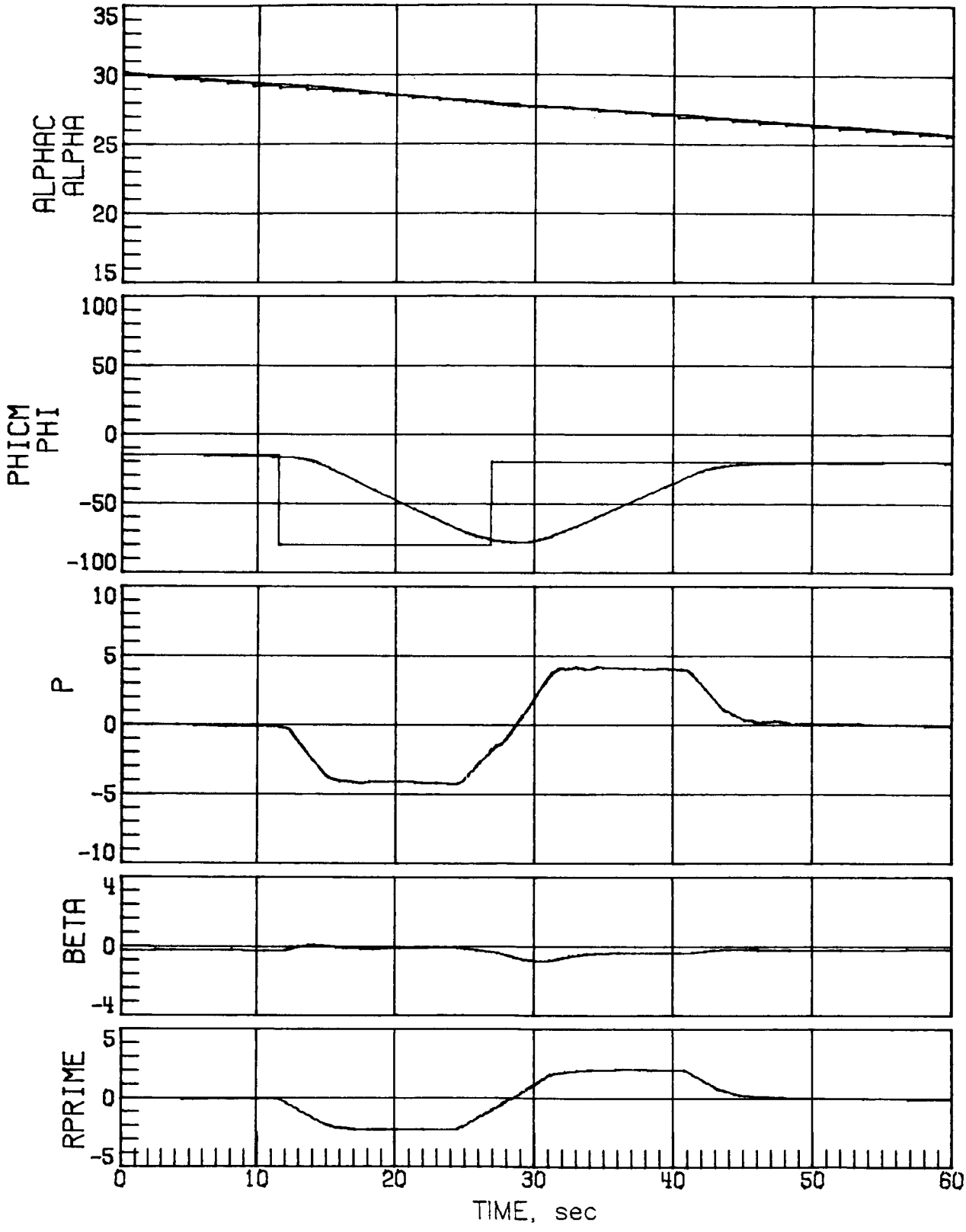

(e) Case 16.

Figure 9.- Continued.

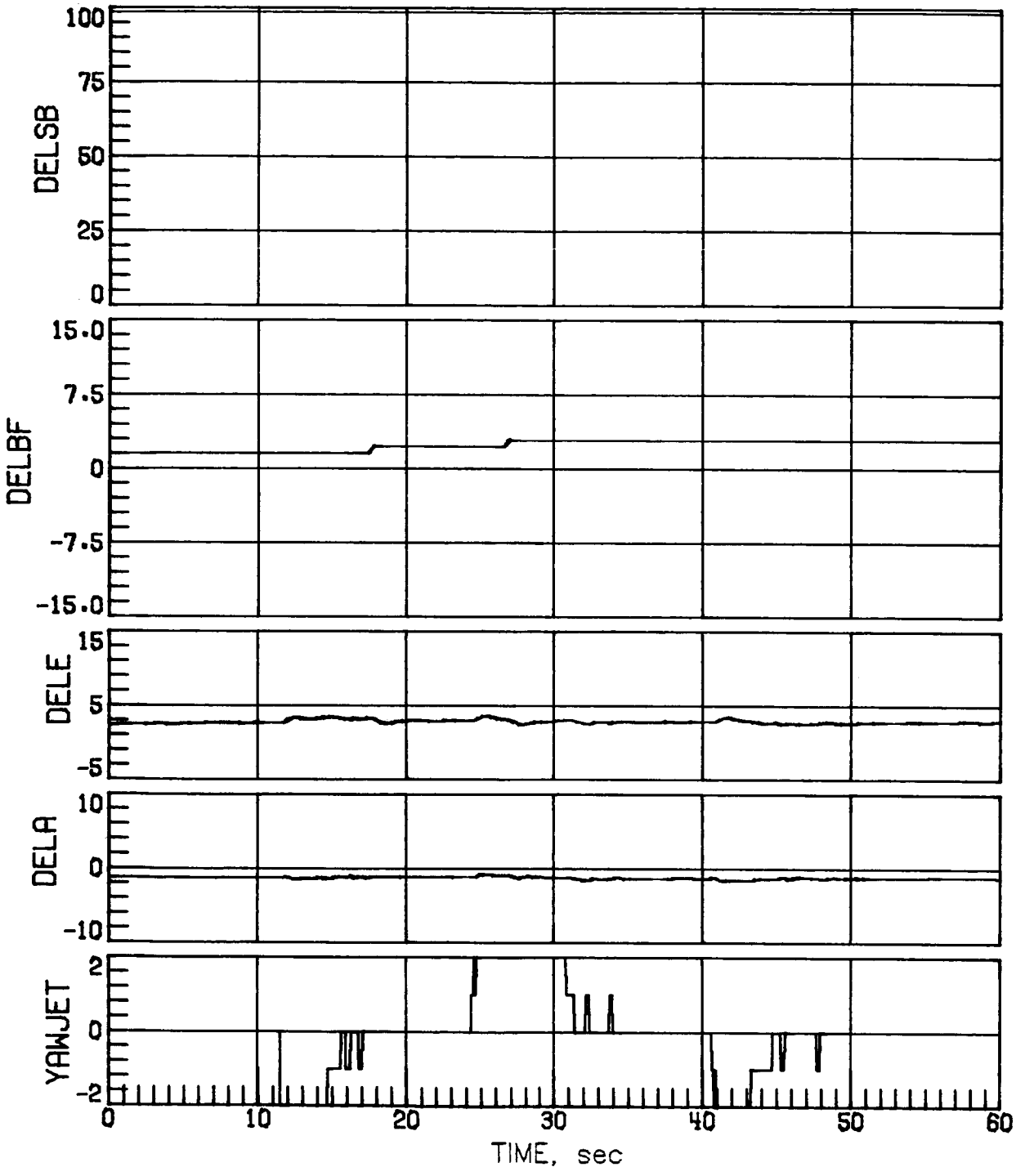

(e) Concluded.

Figure 9.- Concluded.

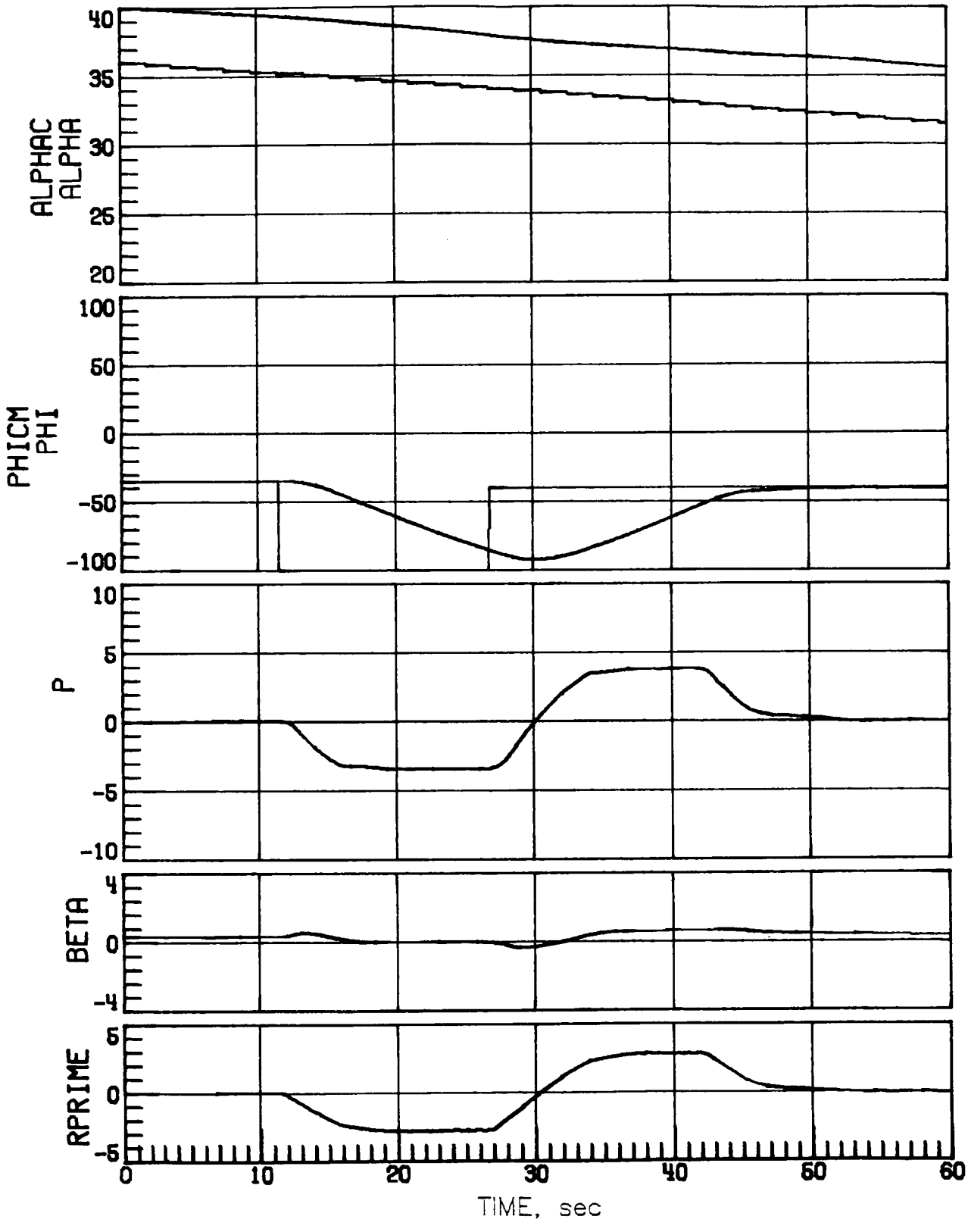

(a) Case 3.

Figure 10.- Mach 10 maneuver performance for a low-sensed α error of 4° with off-nominal aerodynamics.

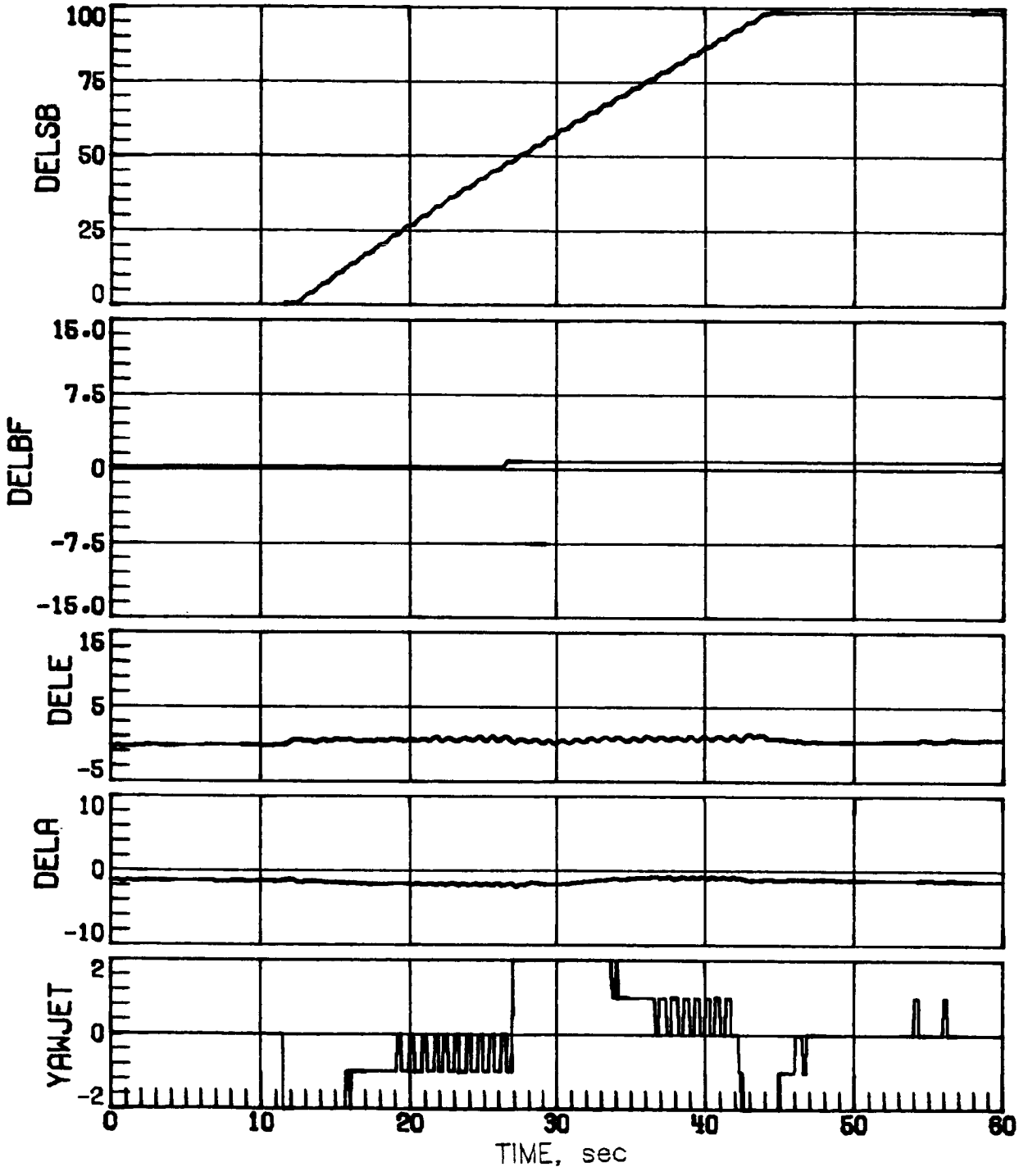

(a) Concluded.

Figure 10.- Continued.

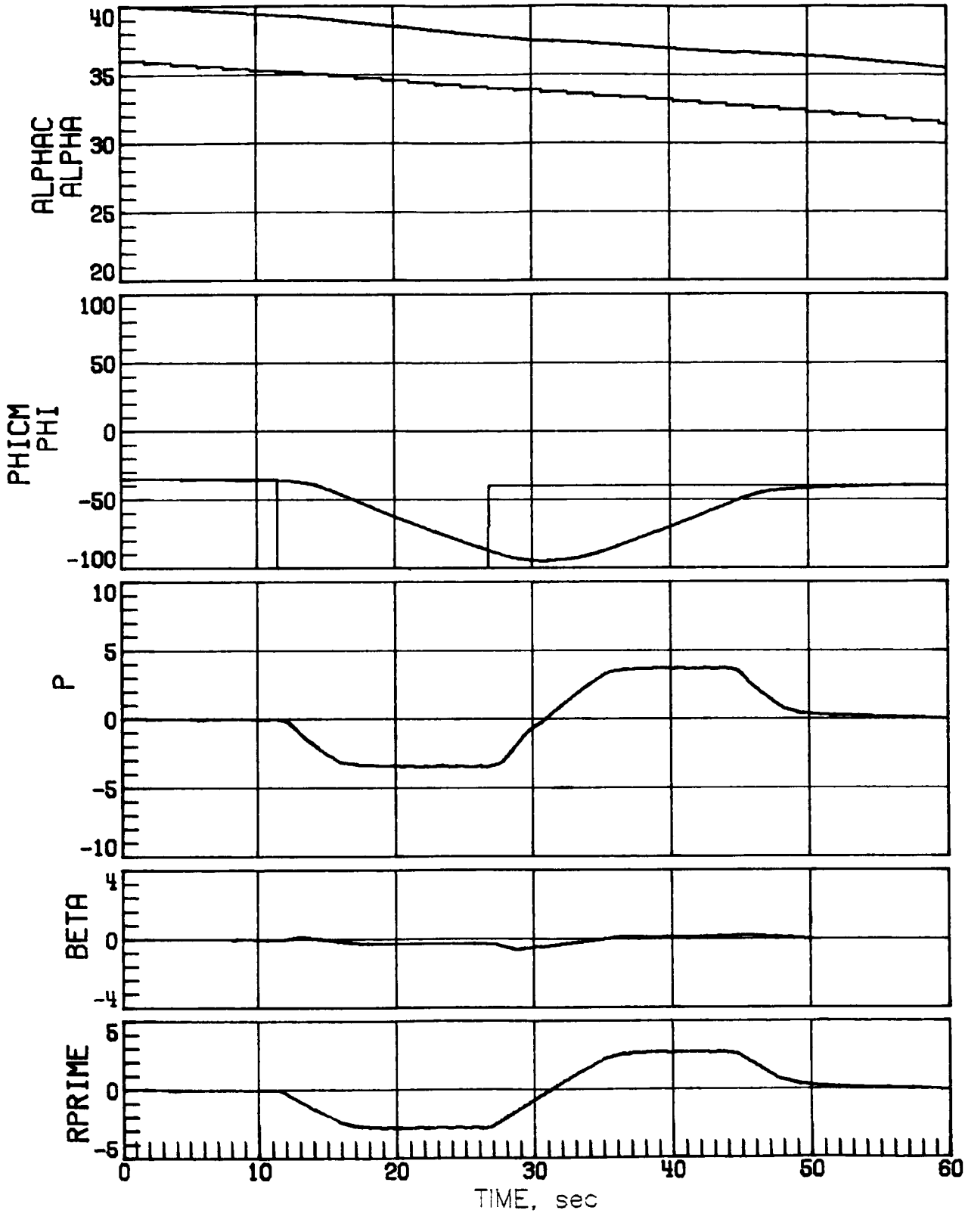

(b) Case 6.

Figure 10.- Continued.

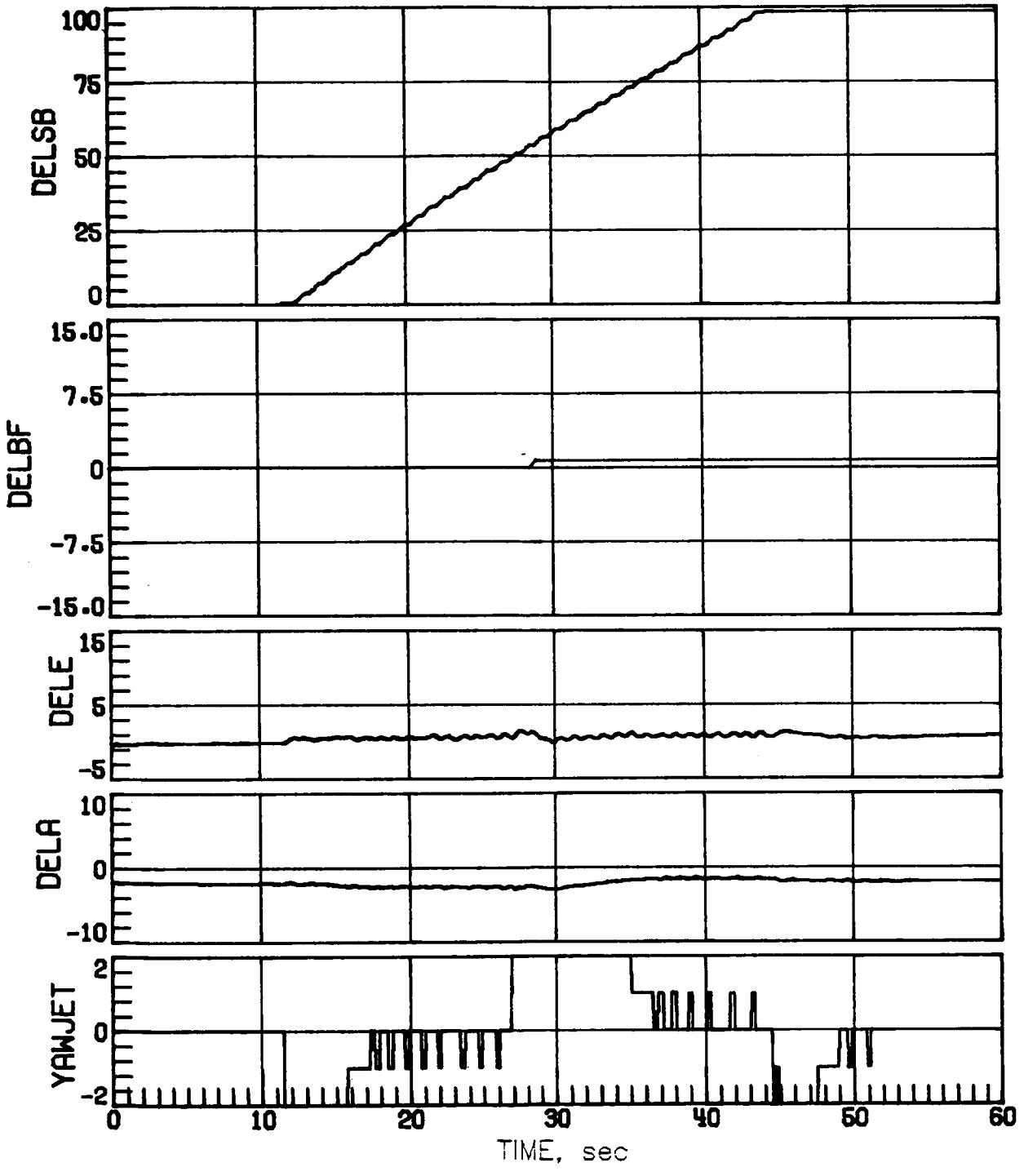

(b) Concluded.

Figure 10.- Continued.

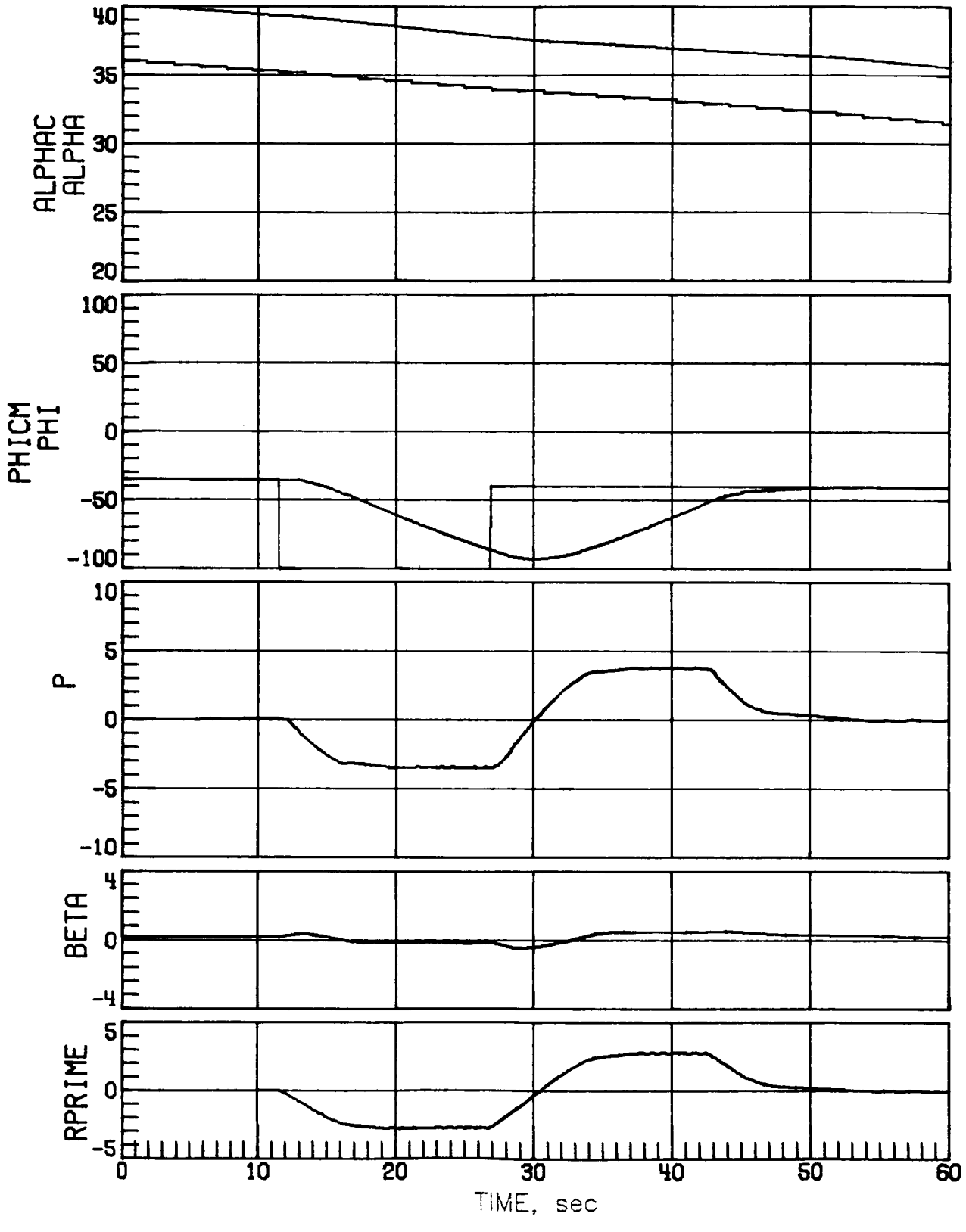

(c) Case 9.

Figure 10.- Continued.

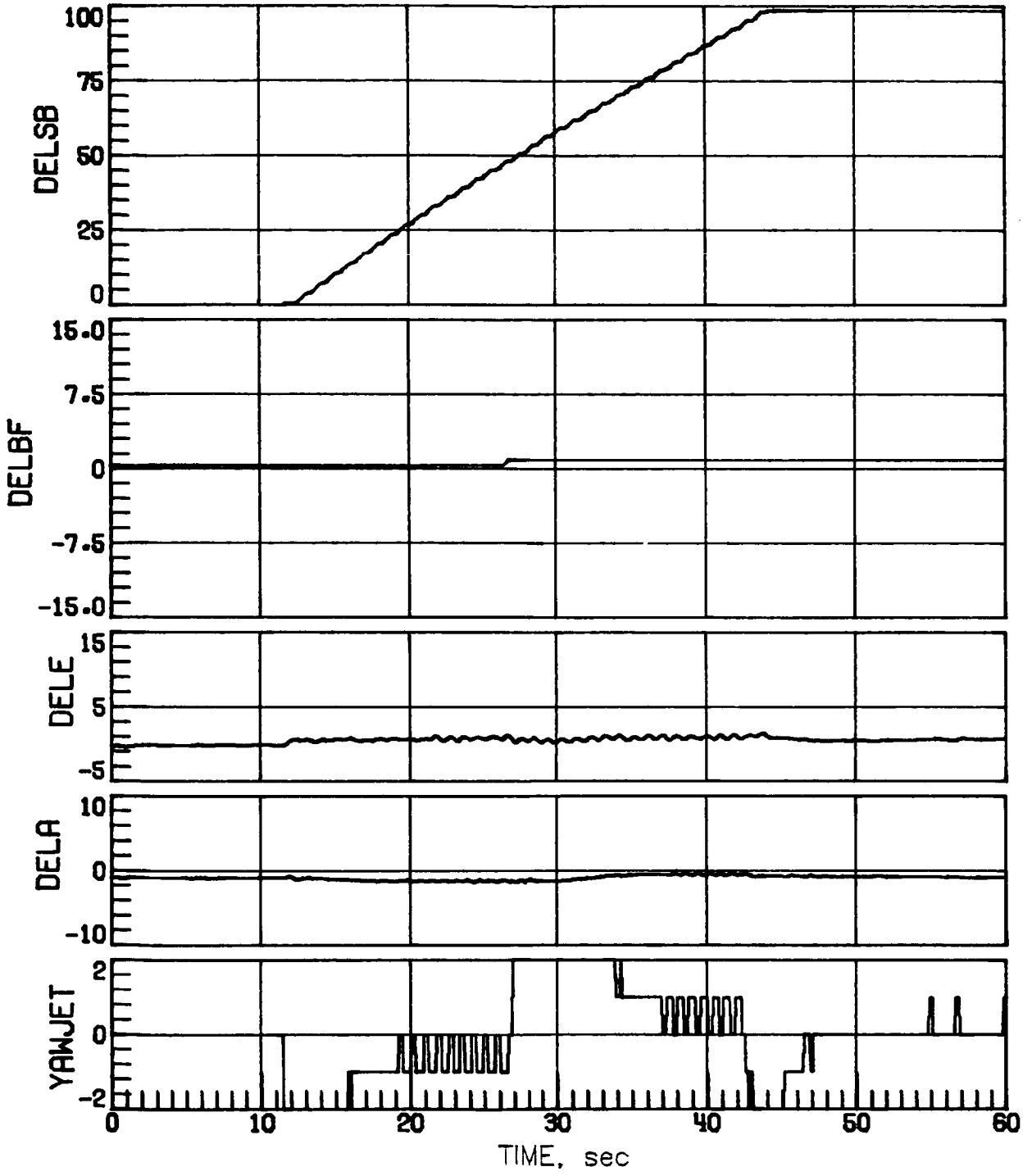

(c) Concluded.

Figure 10.- Continued.

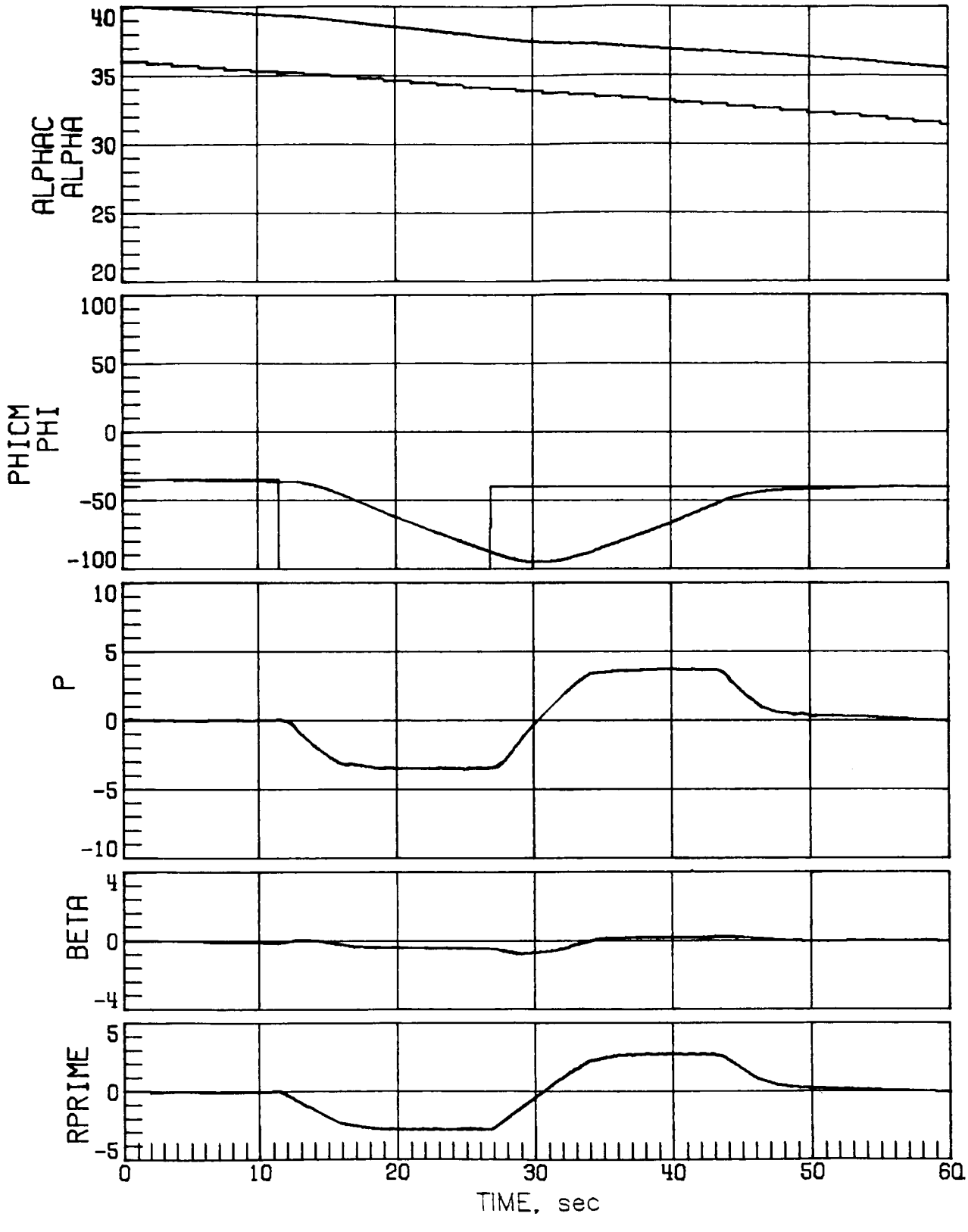

(d) Case 13.

Figure 10.- Continued.

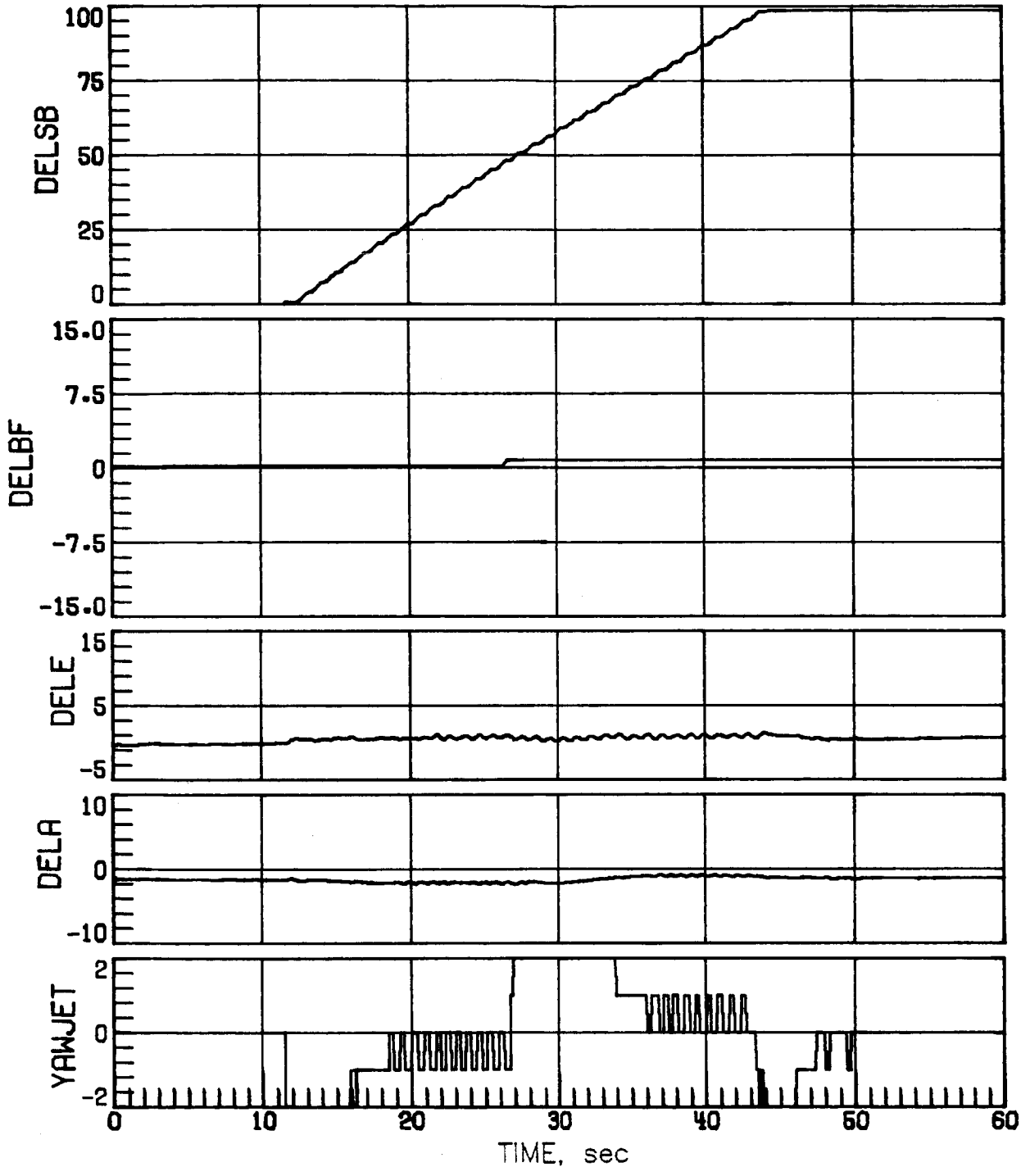

(d) Concluded.

Figure 10.- Concluded.

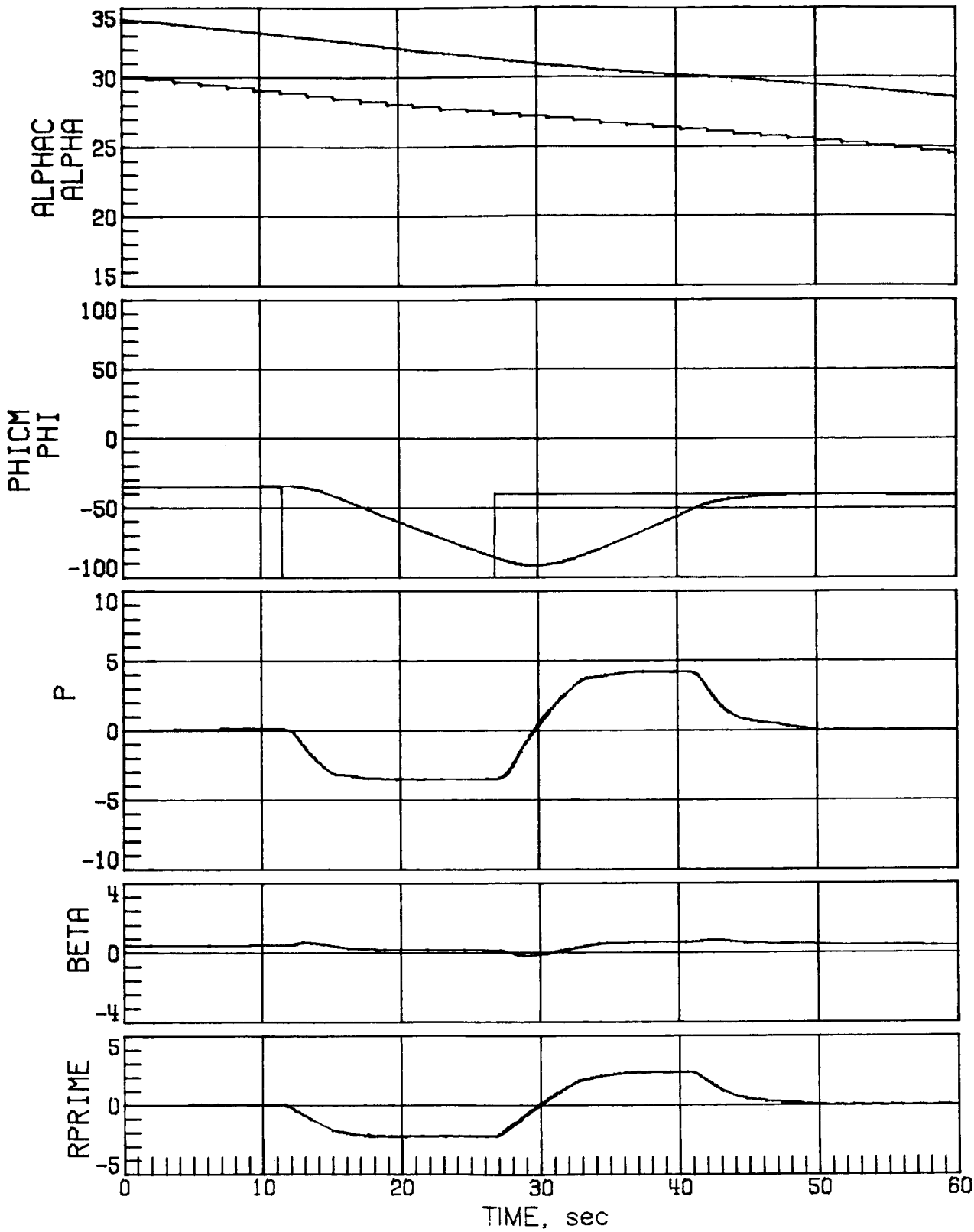

(a) Case 2.

Figure 11.- Mach 7.5 maneuver performance for a low-sensed α error of 4° with off-nominal aerodynamics.

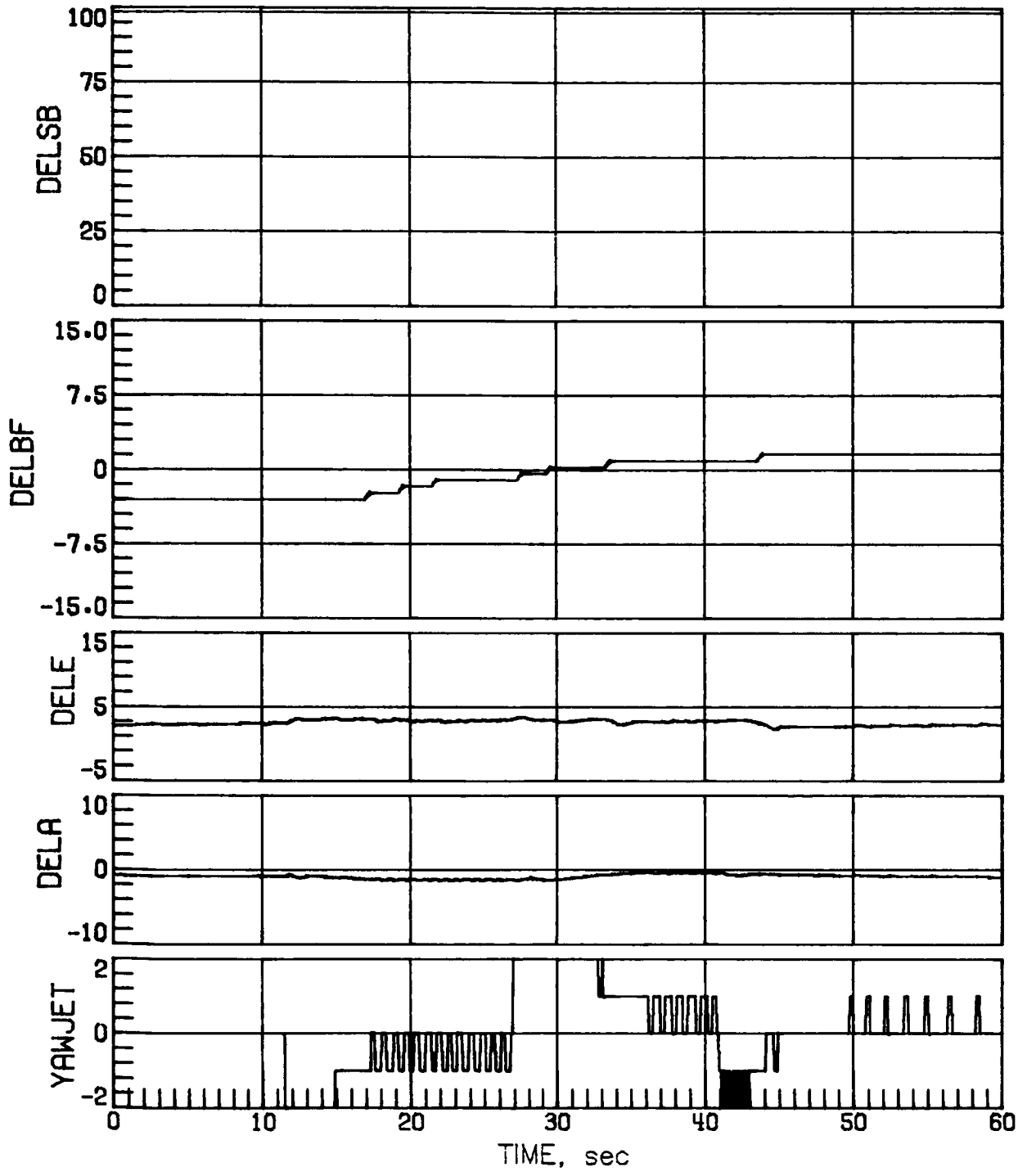

(a) Concluded.

Figure 11.- Continued.

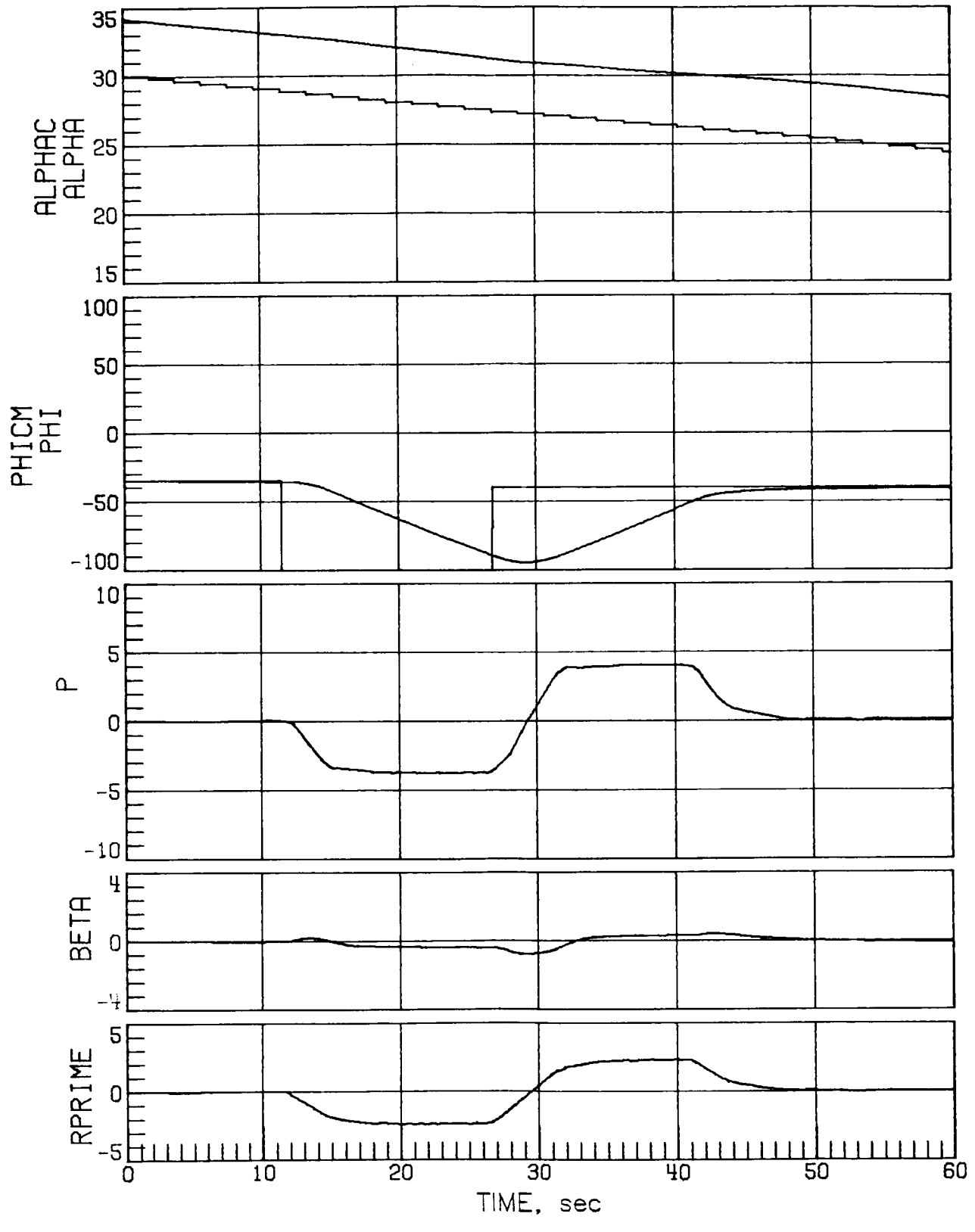

(b) Case 7.

Figure 11.- Continued.

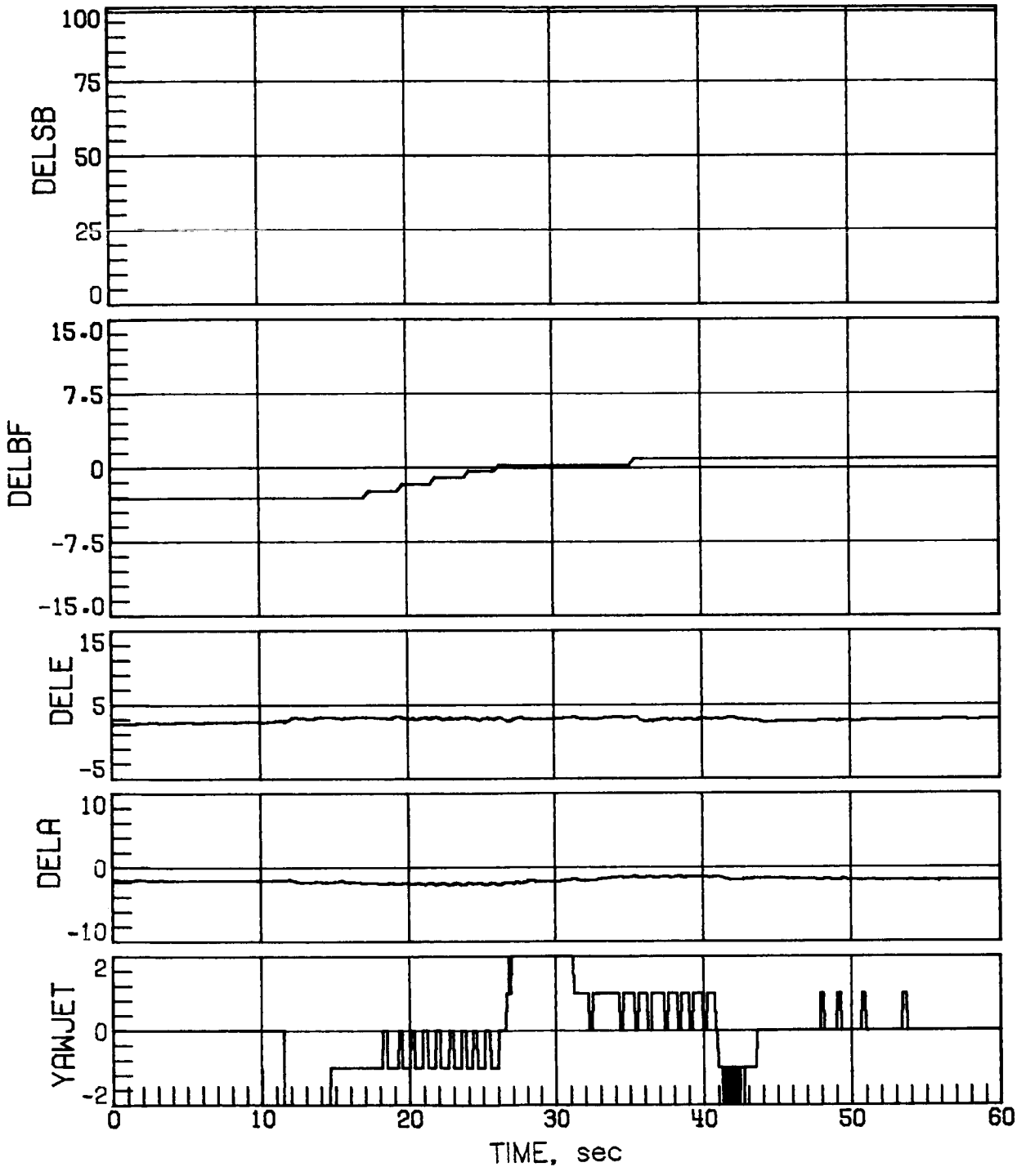

(b) Concluded.

Figure 11.- Continued.

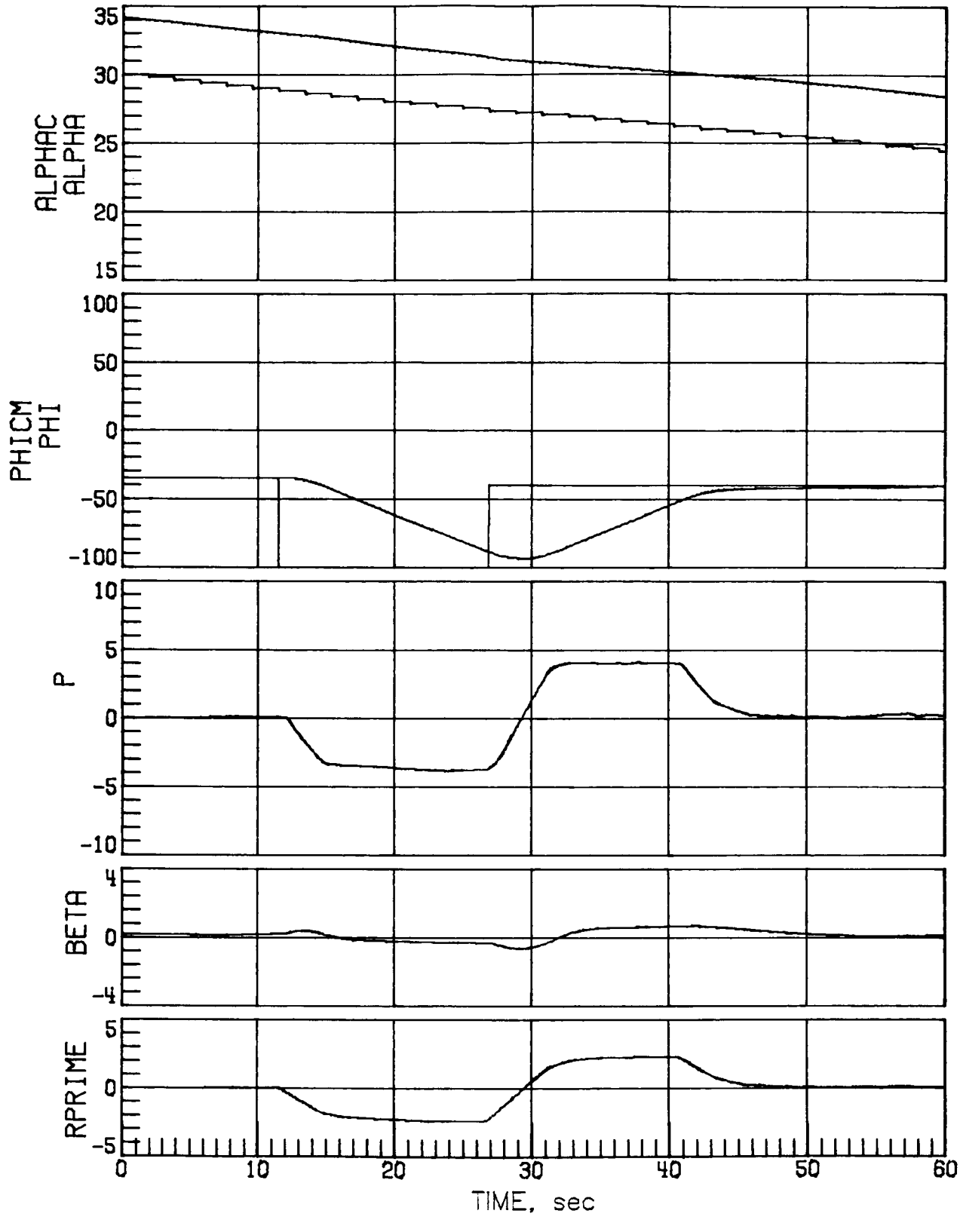

(c) Case 11.

Figure 11.- Continued.

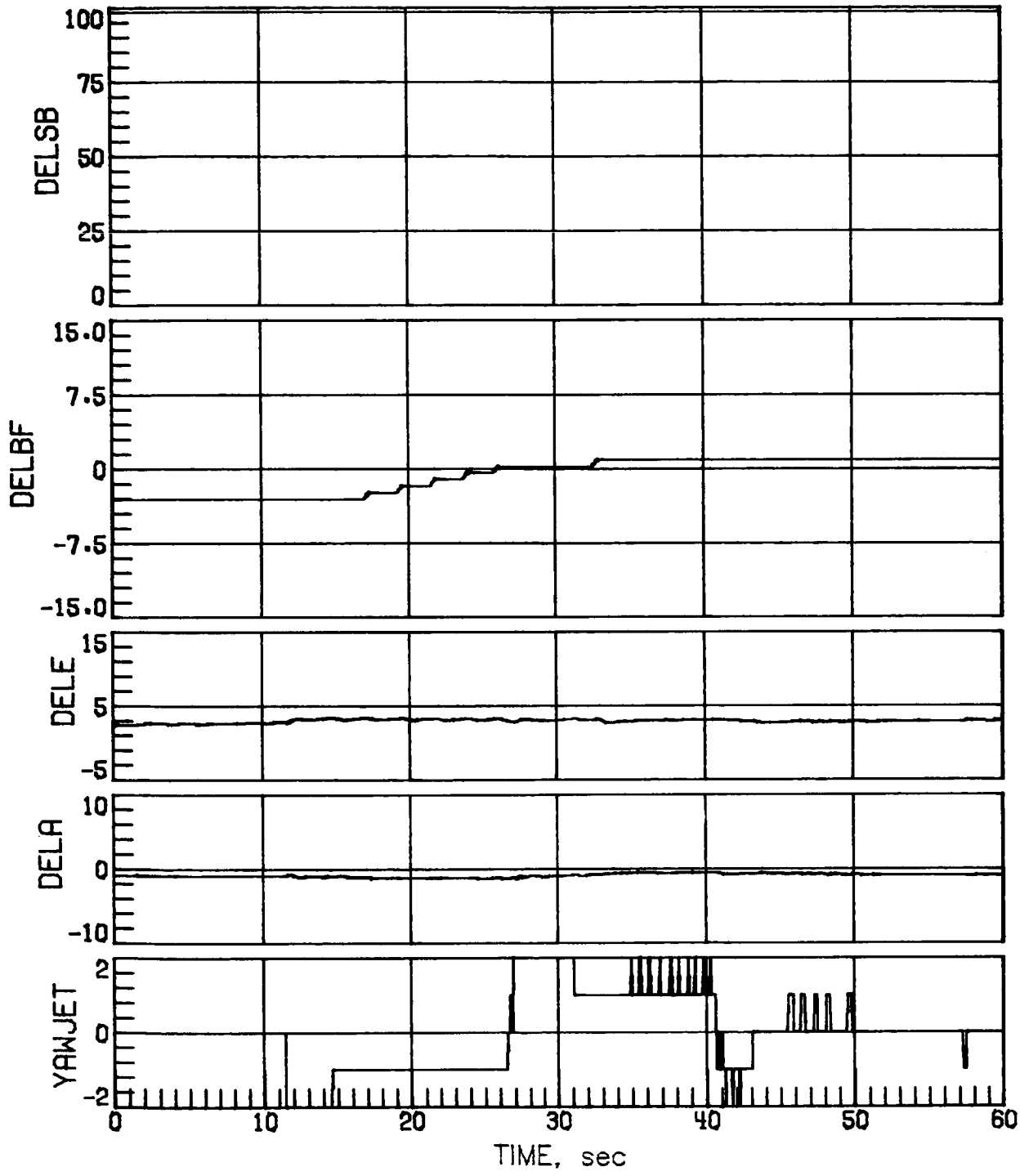

(c) Concluded.

Figure 11.- Continued.

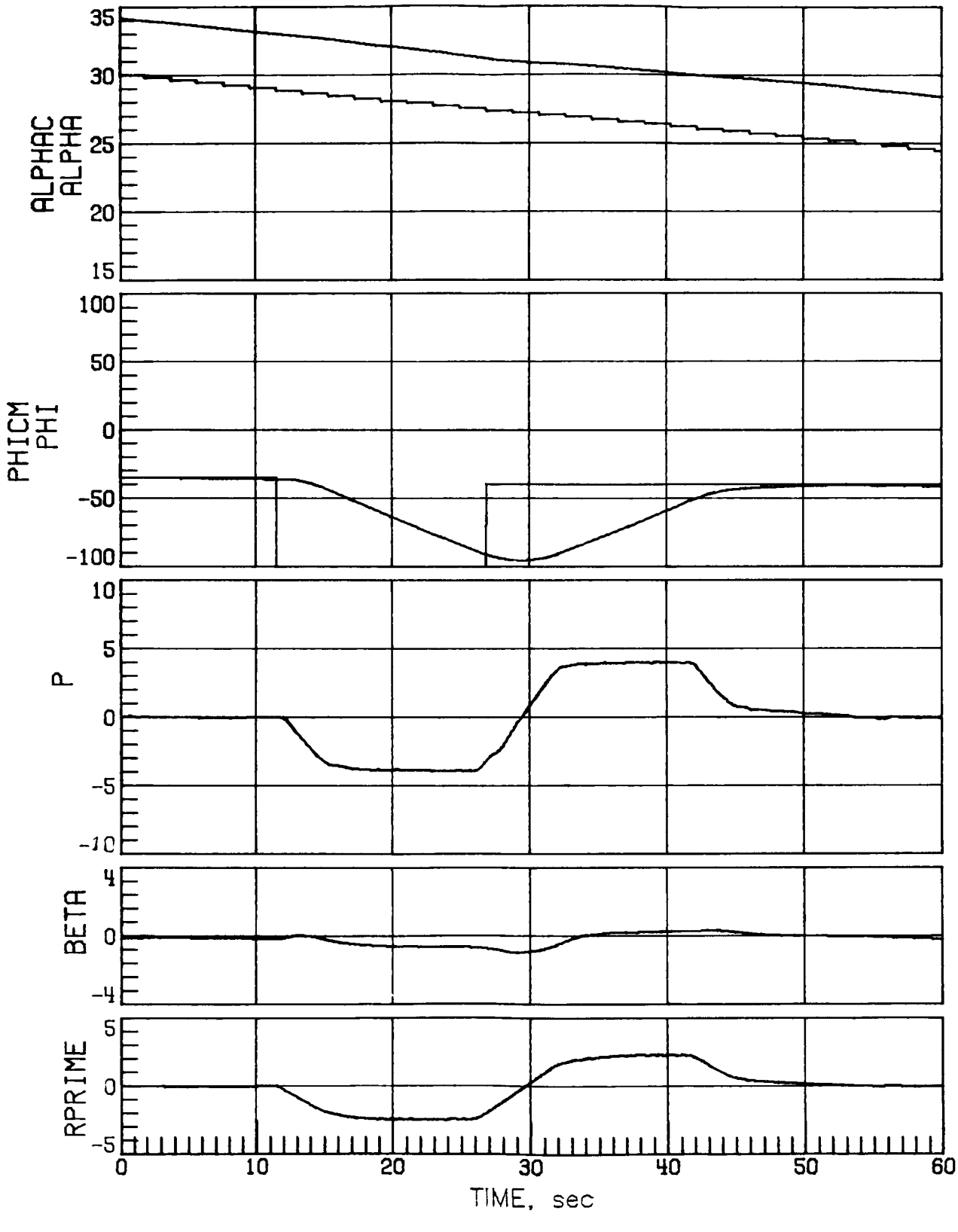

(d) Case 16.

Figure 11.- Continued.

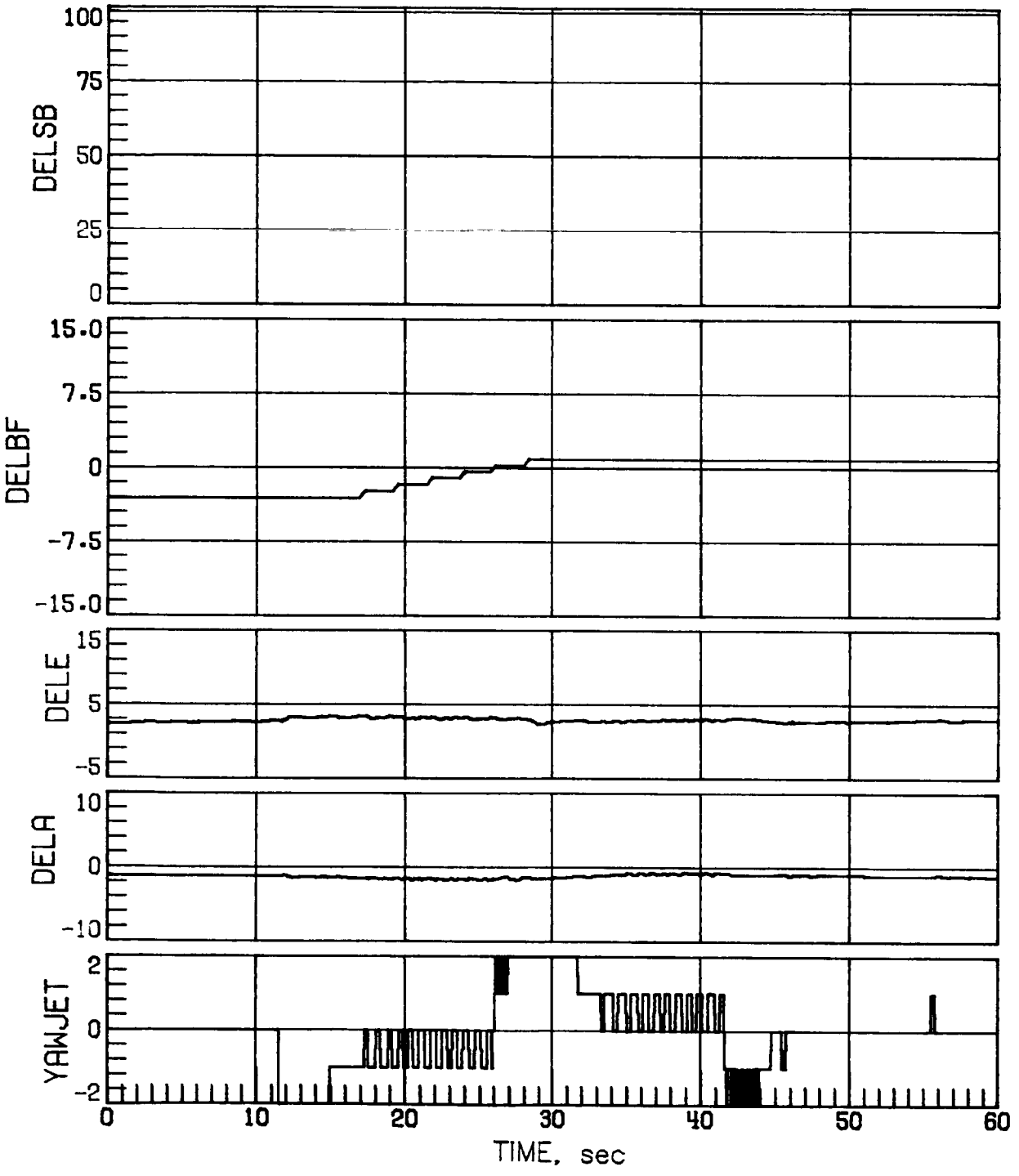

(d) Concluded.

Figure 11.- Concluded.

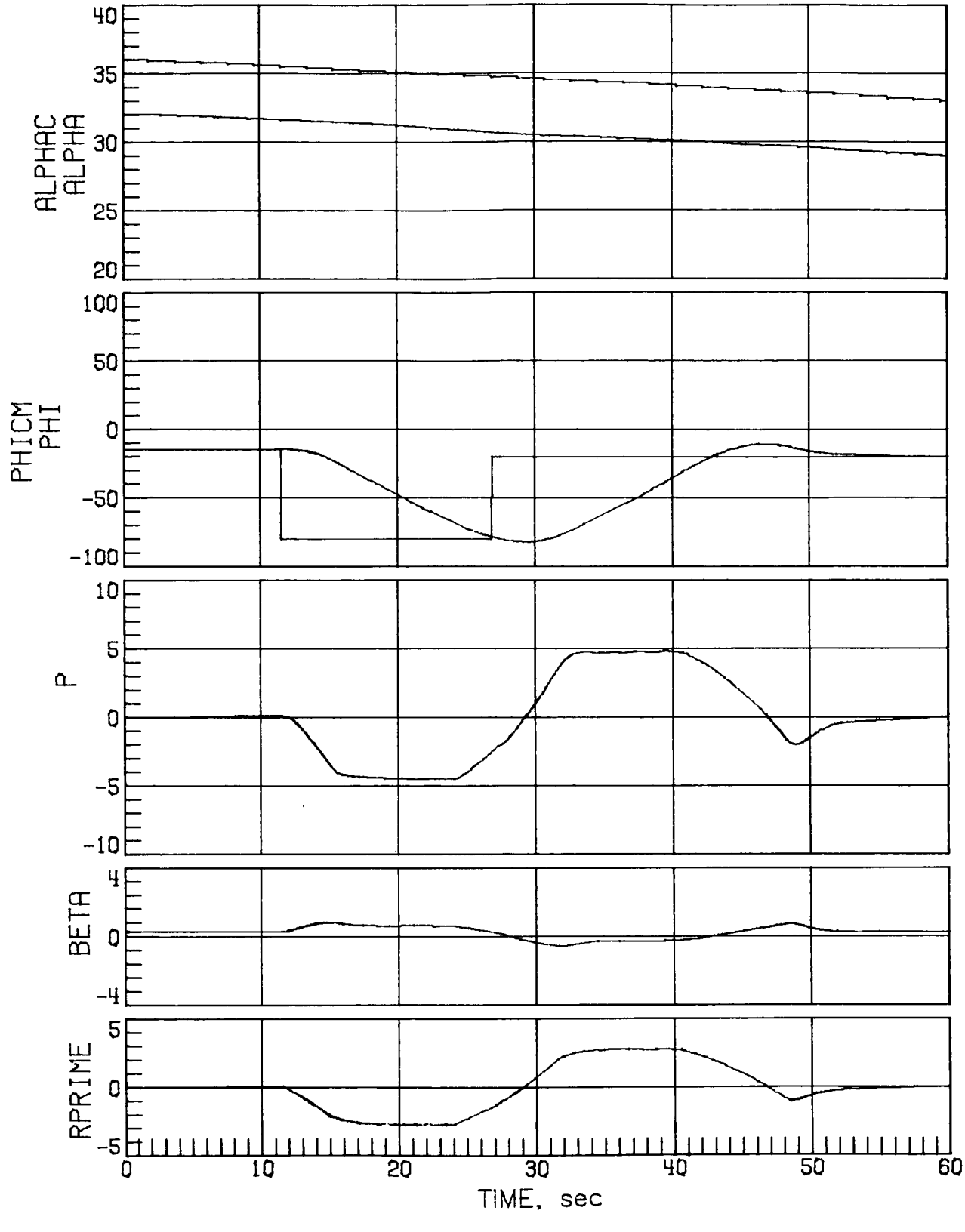

(a) Case 3.

Figure 12.- Mach 10 maneuver performance for a high-sensed α error of 4° with off-nominal aerodynamics.

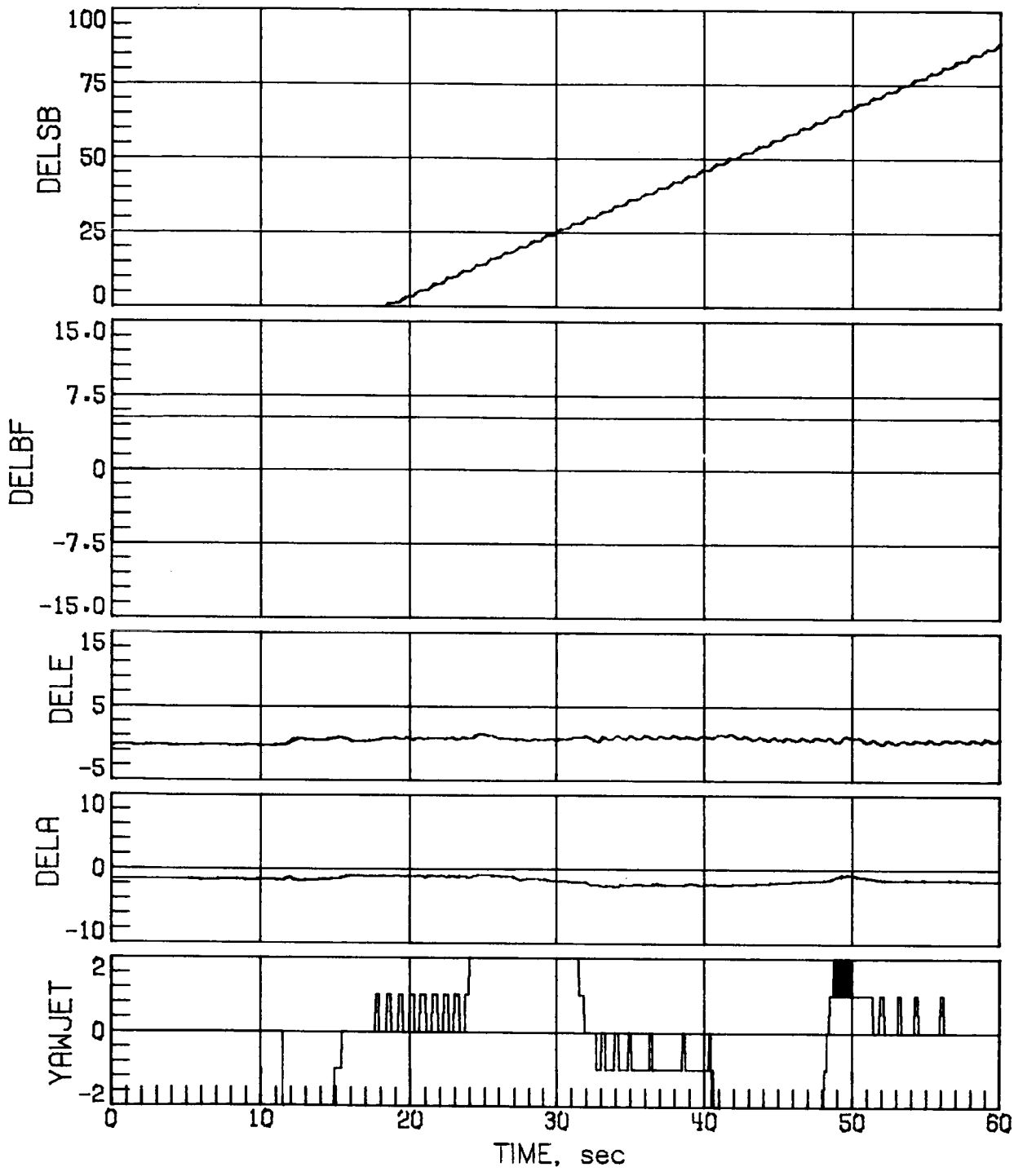

(a) Concluded.

Figure 12.- Continued.

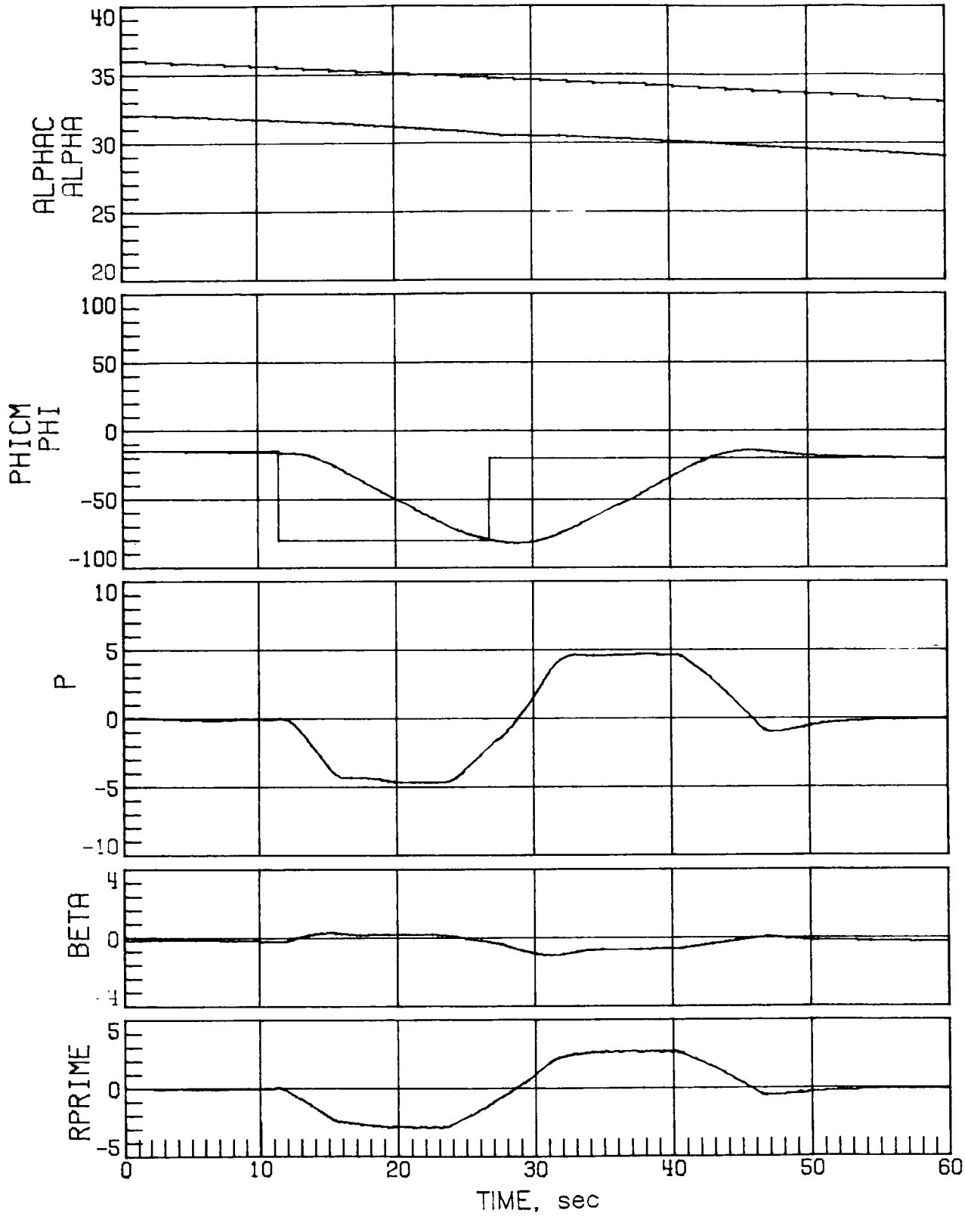

(b) Case 7.

Figure 12.- Continued.

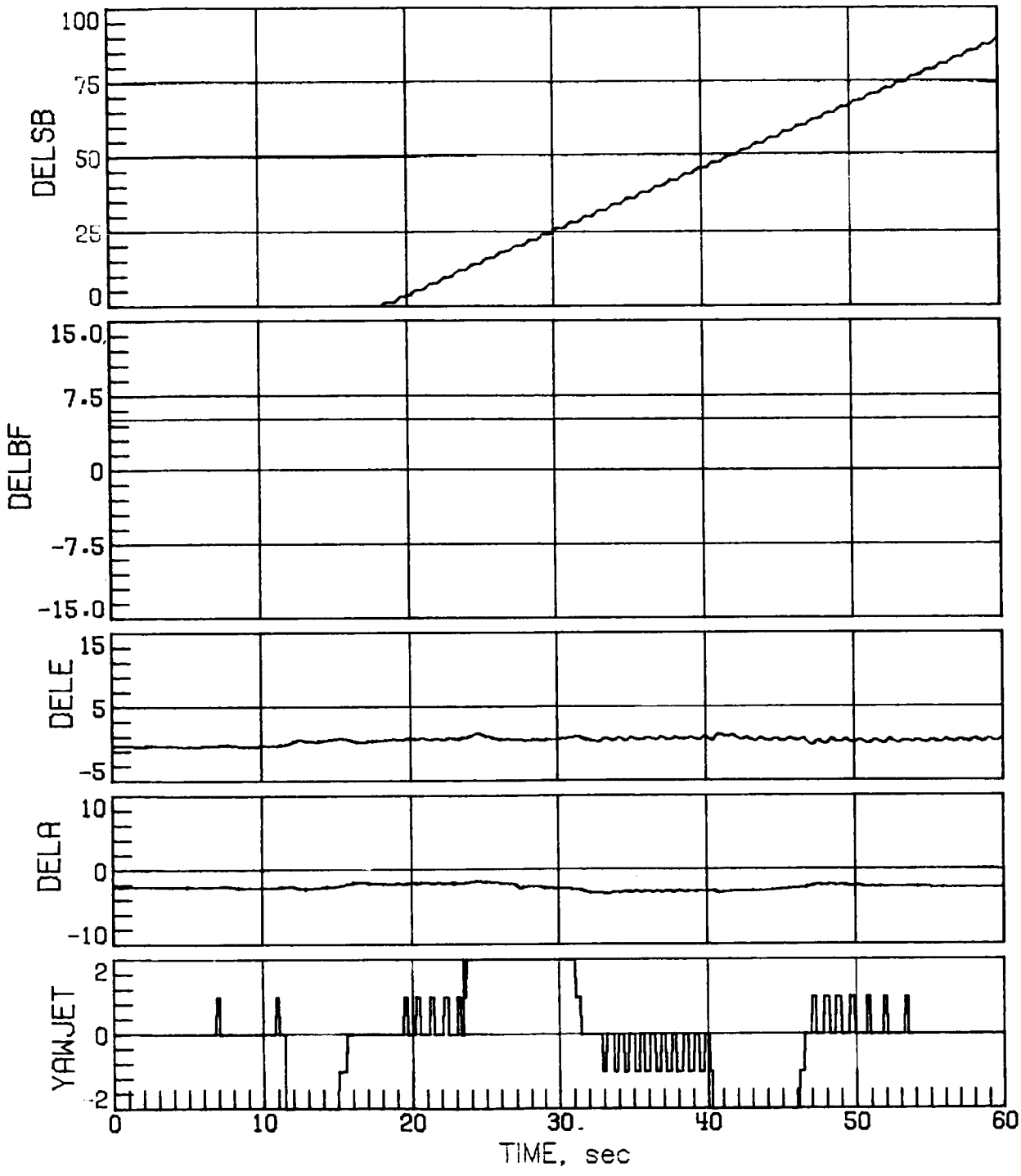

(b) Concluded.

Figure 12.- Continued.

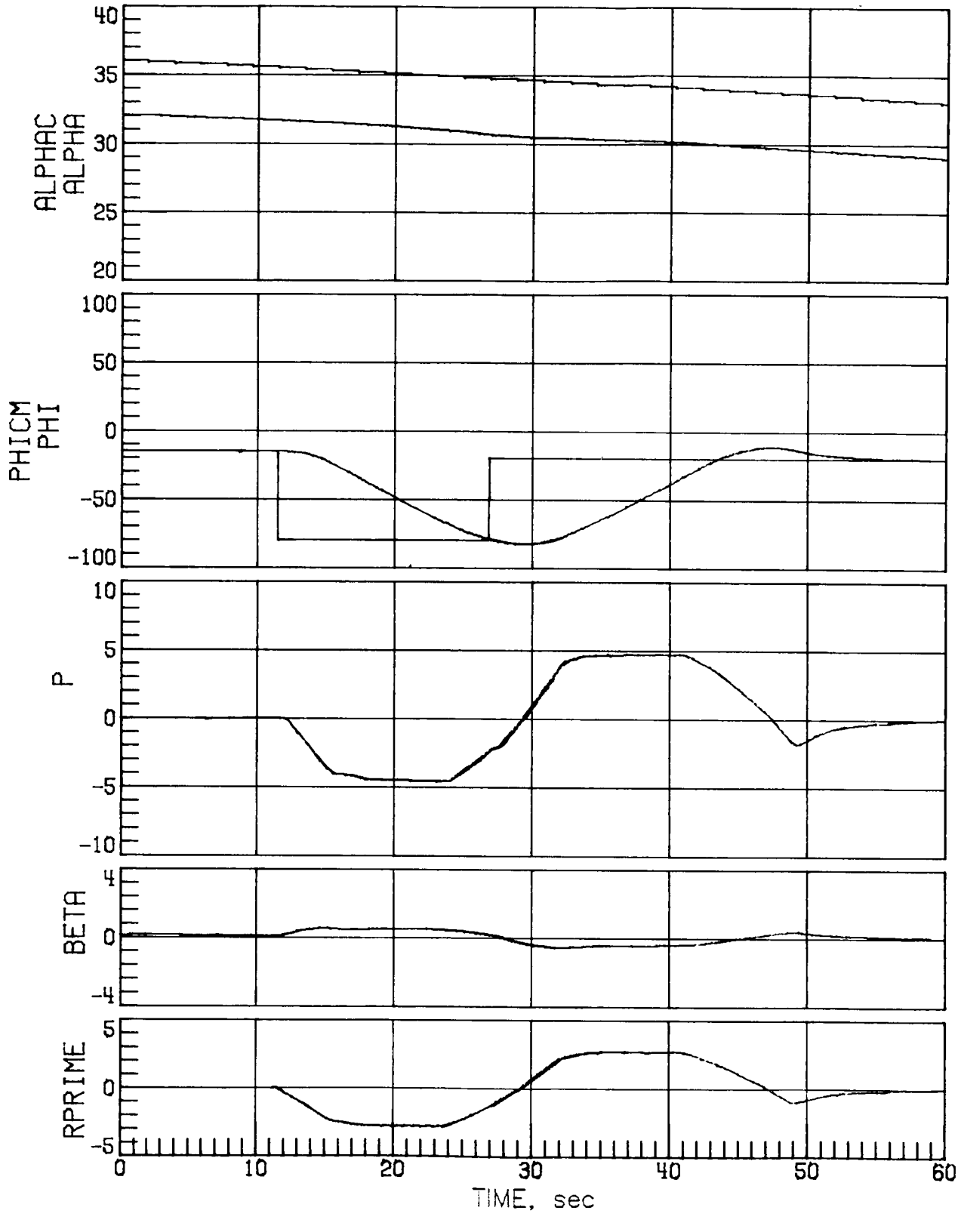

(c) Case 9.

Figure 12.- Continued.

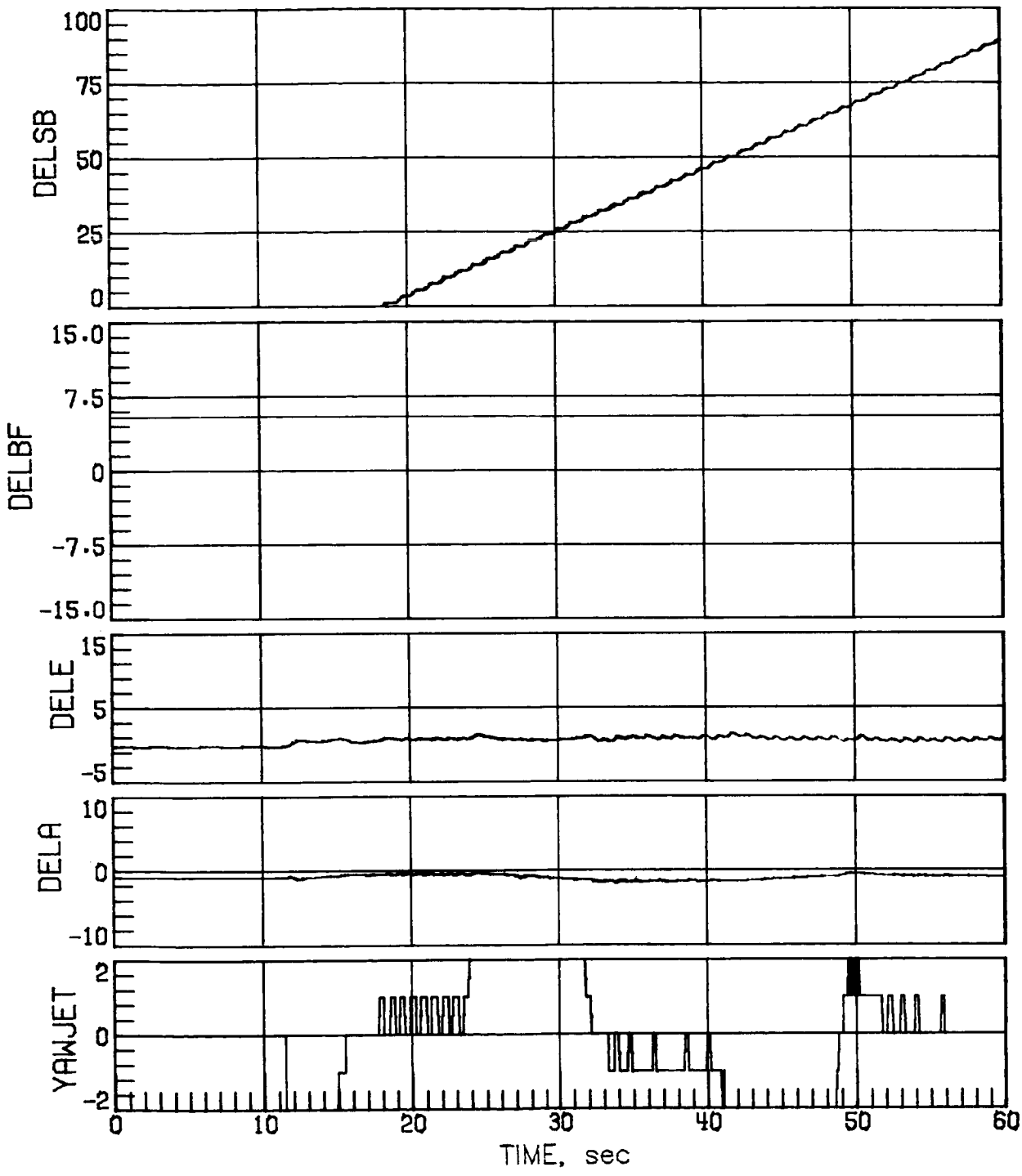

(c) Concluded.

Figure 12.- Continued.

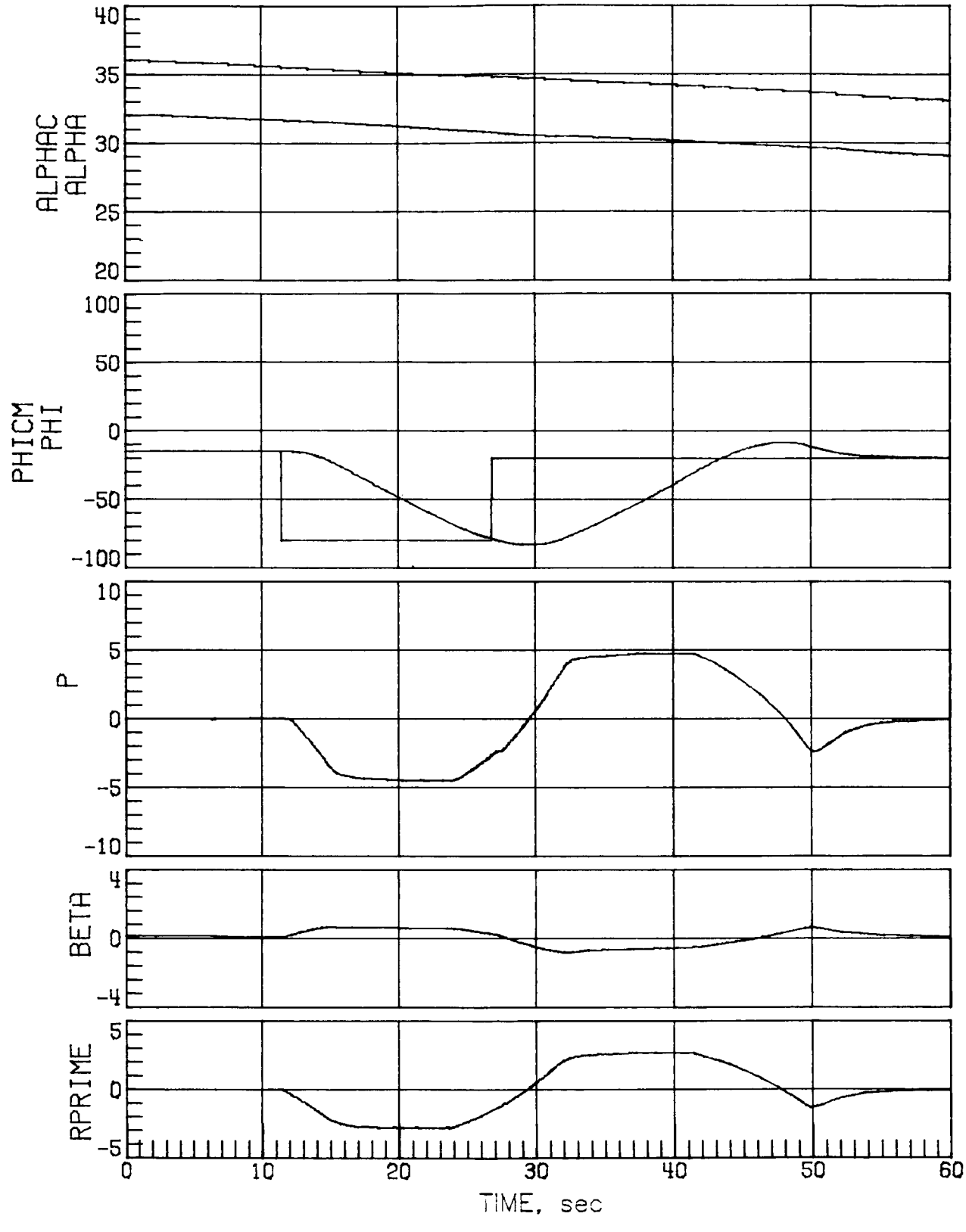

(d) Case 11.

Figure 12.- Continued.

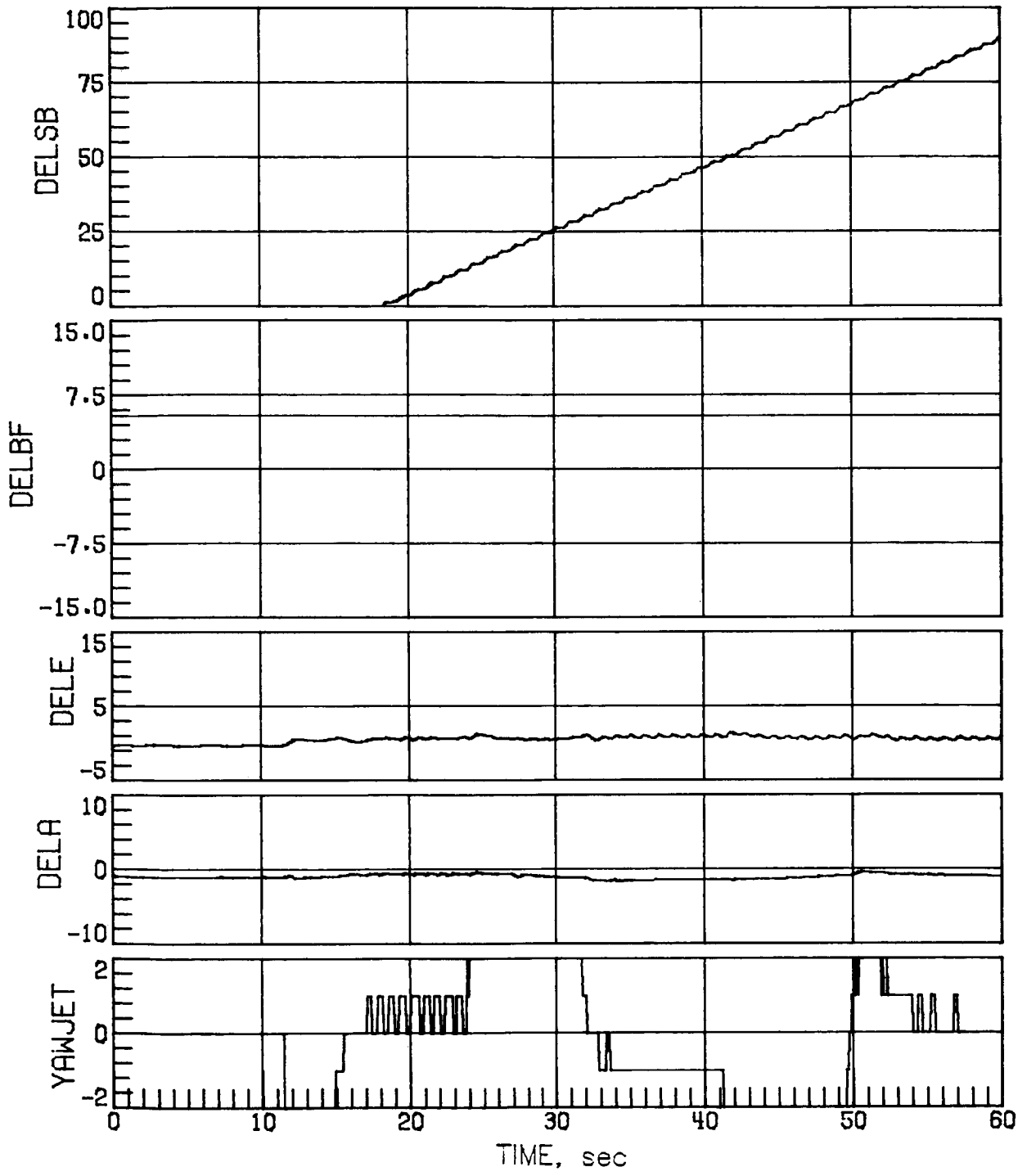

(d) Concluded.

Figure 12.- Continued.

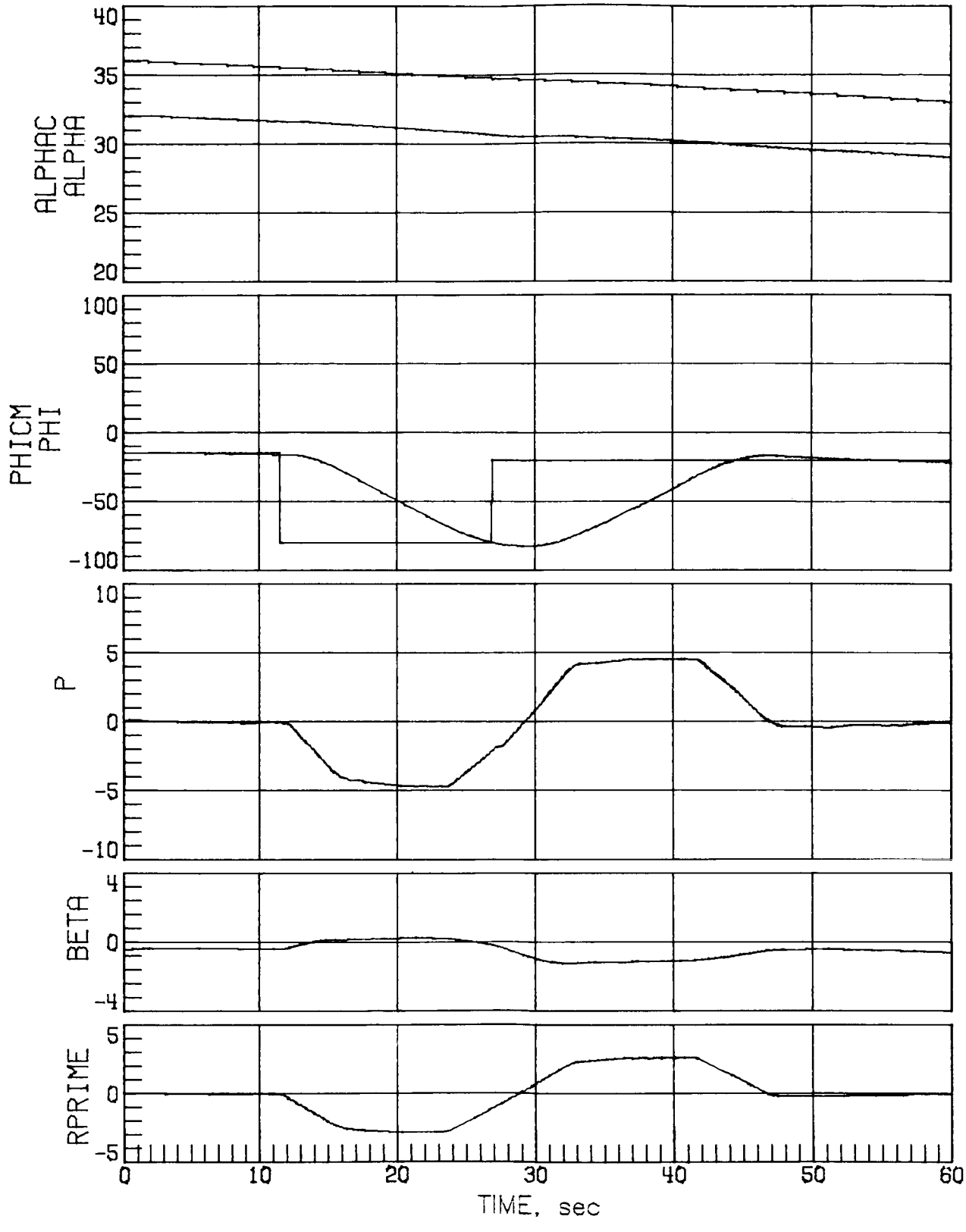

(e) Case 16.

Figure 12.- Continued.

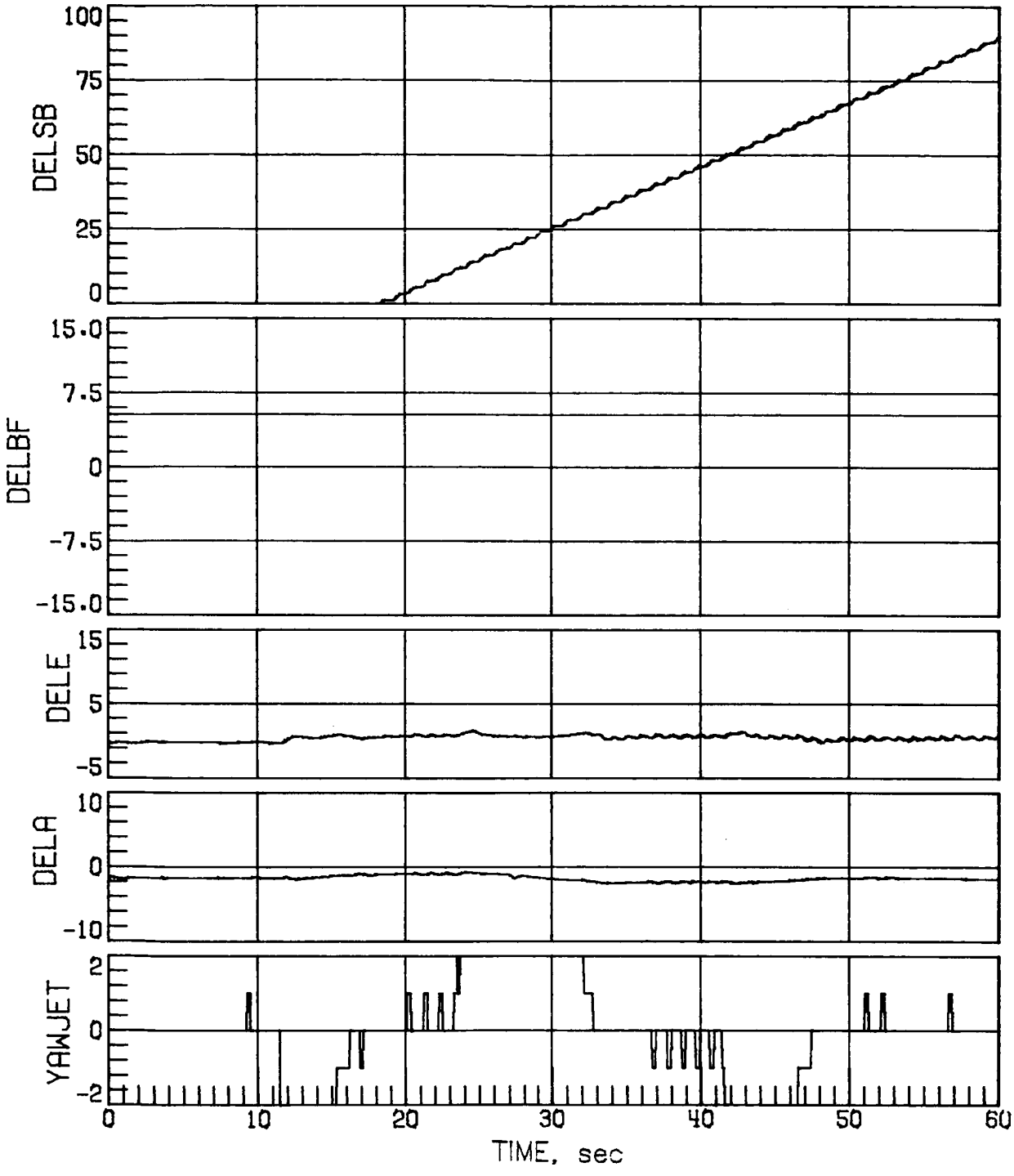

(e) Concluded.

Figure 12.- Concluded.

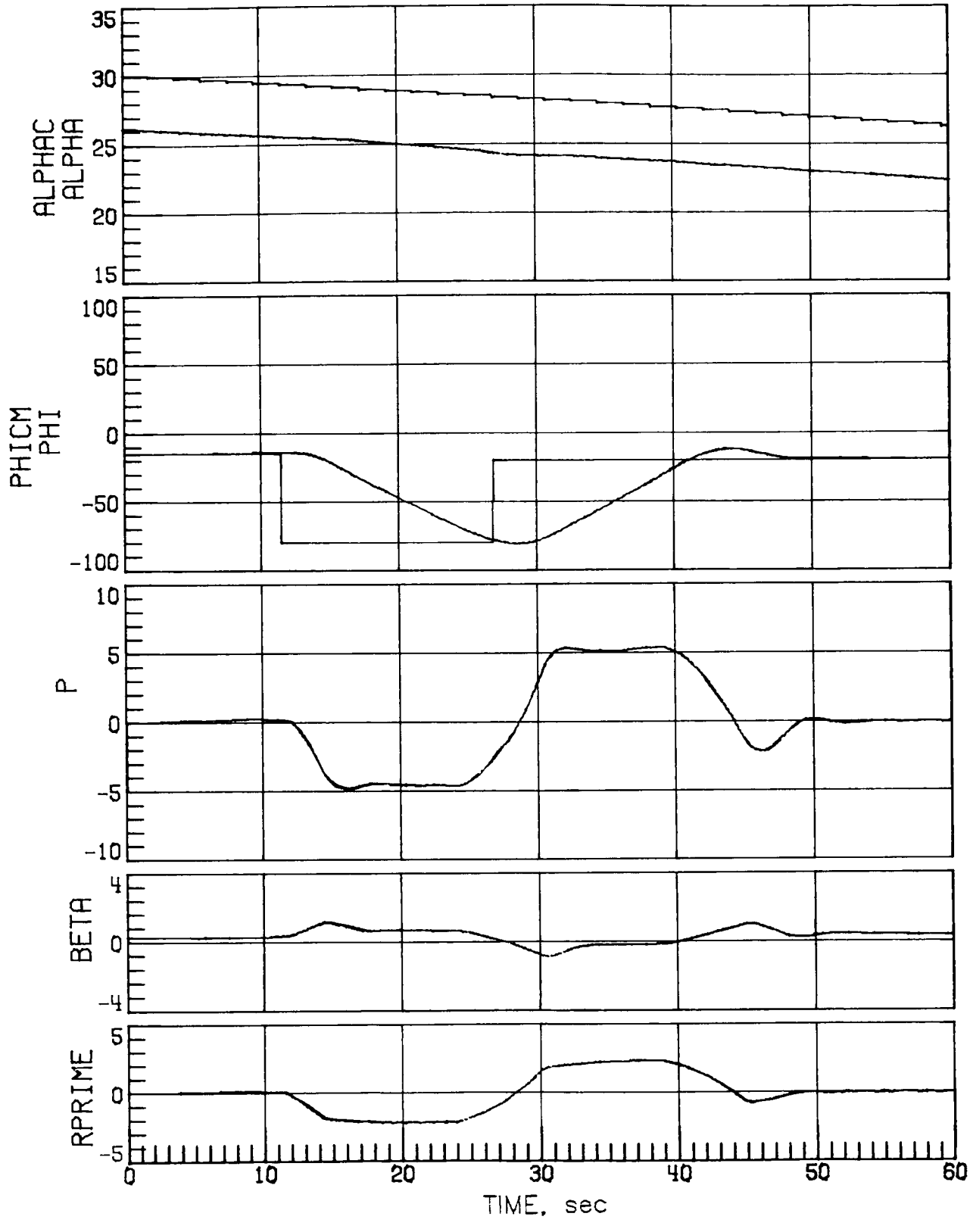

(a) Case 3.

Figure 13.- Mach 7.5 maneuver performance for a high-sensed α error of 4° with off-nominal aerodynamics.

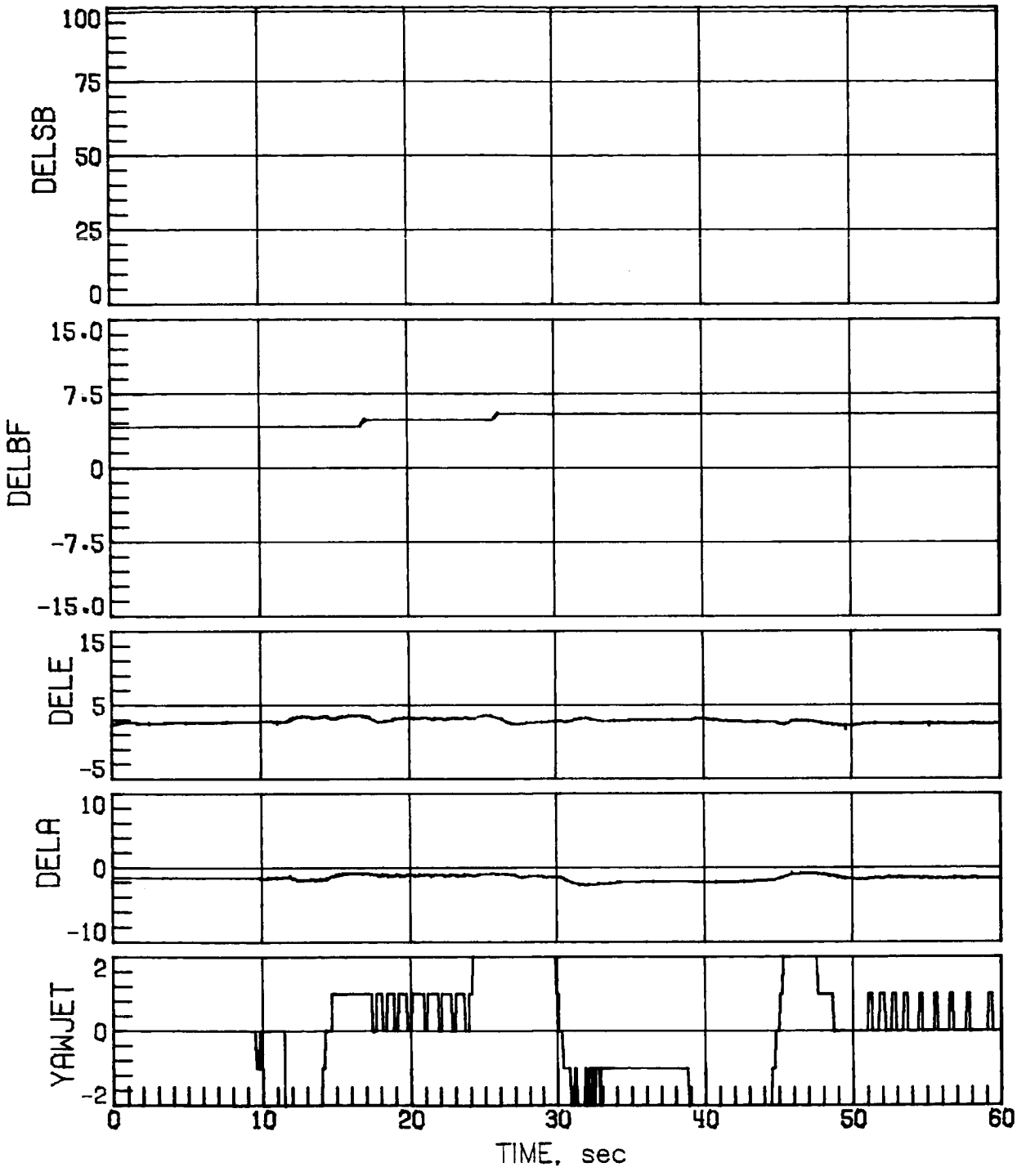

(a) Concluded.

Figure 13.- Continued.

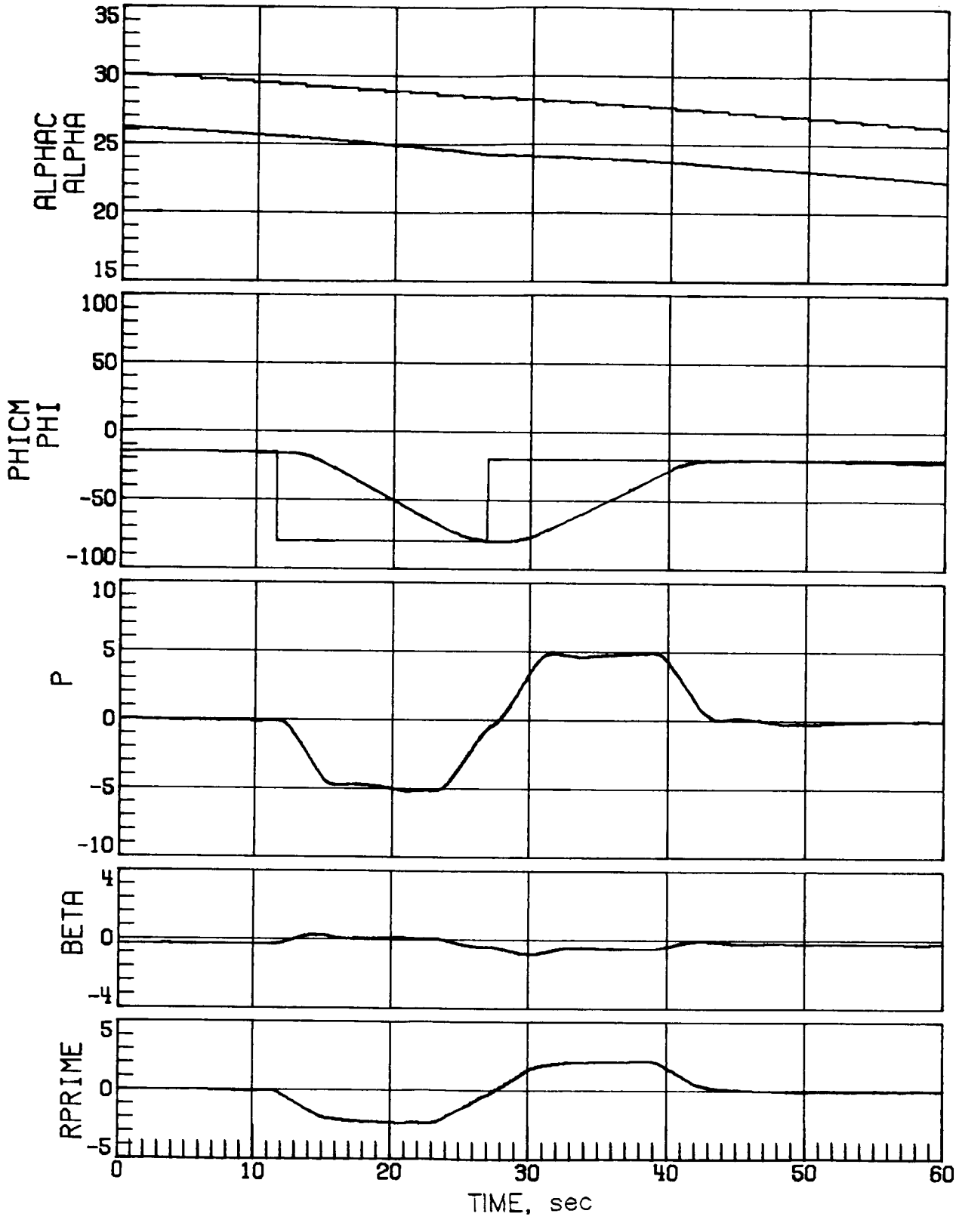

(b) Case 6.

Figure 13.- Continued.

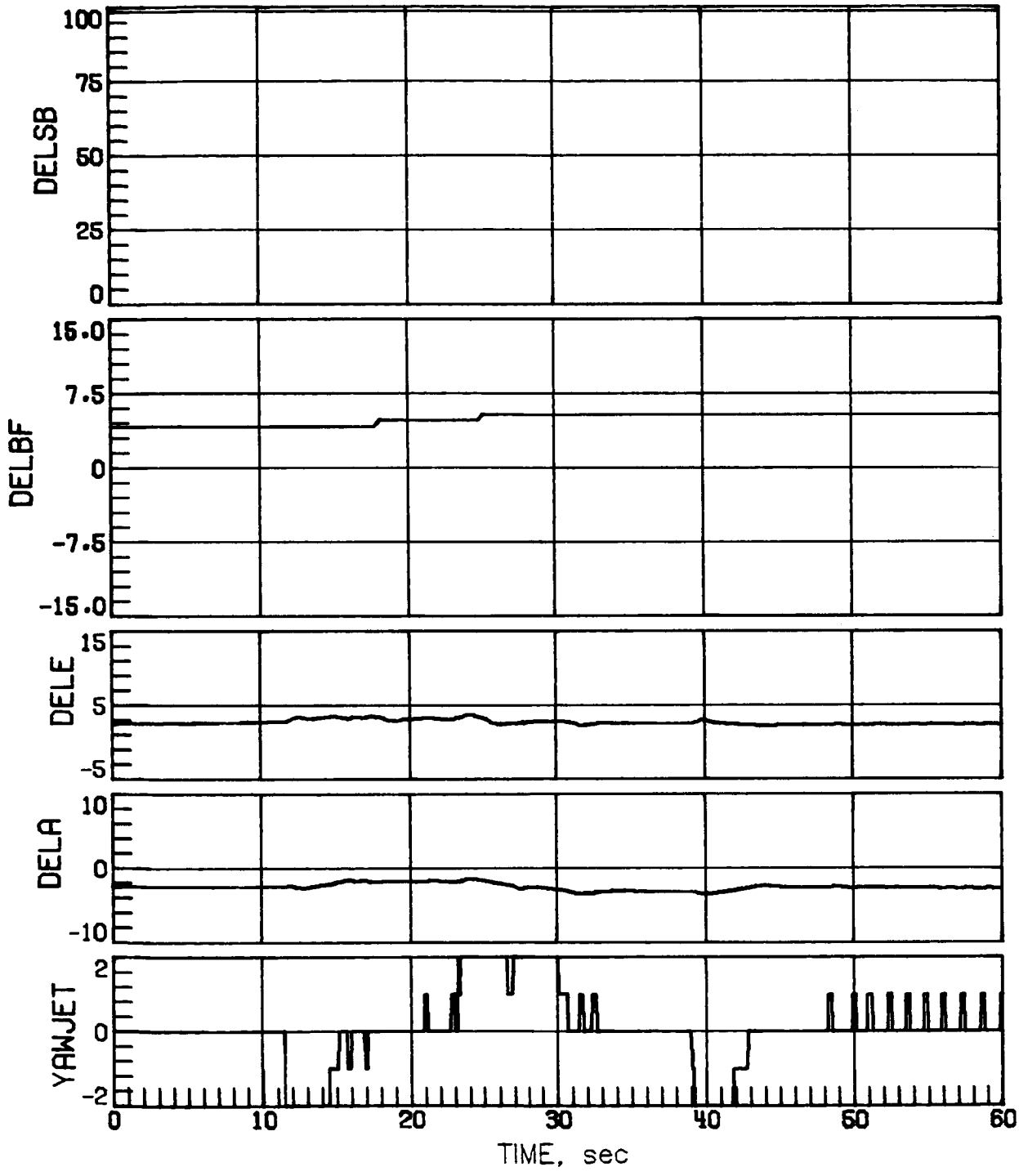

(b) Concluded.

Figure 13.- Continued.

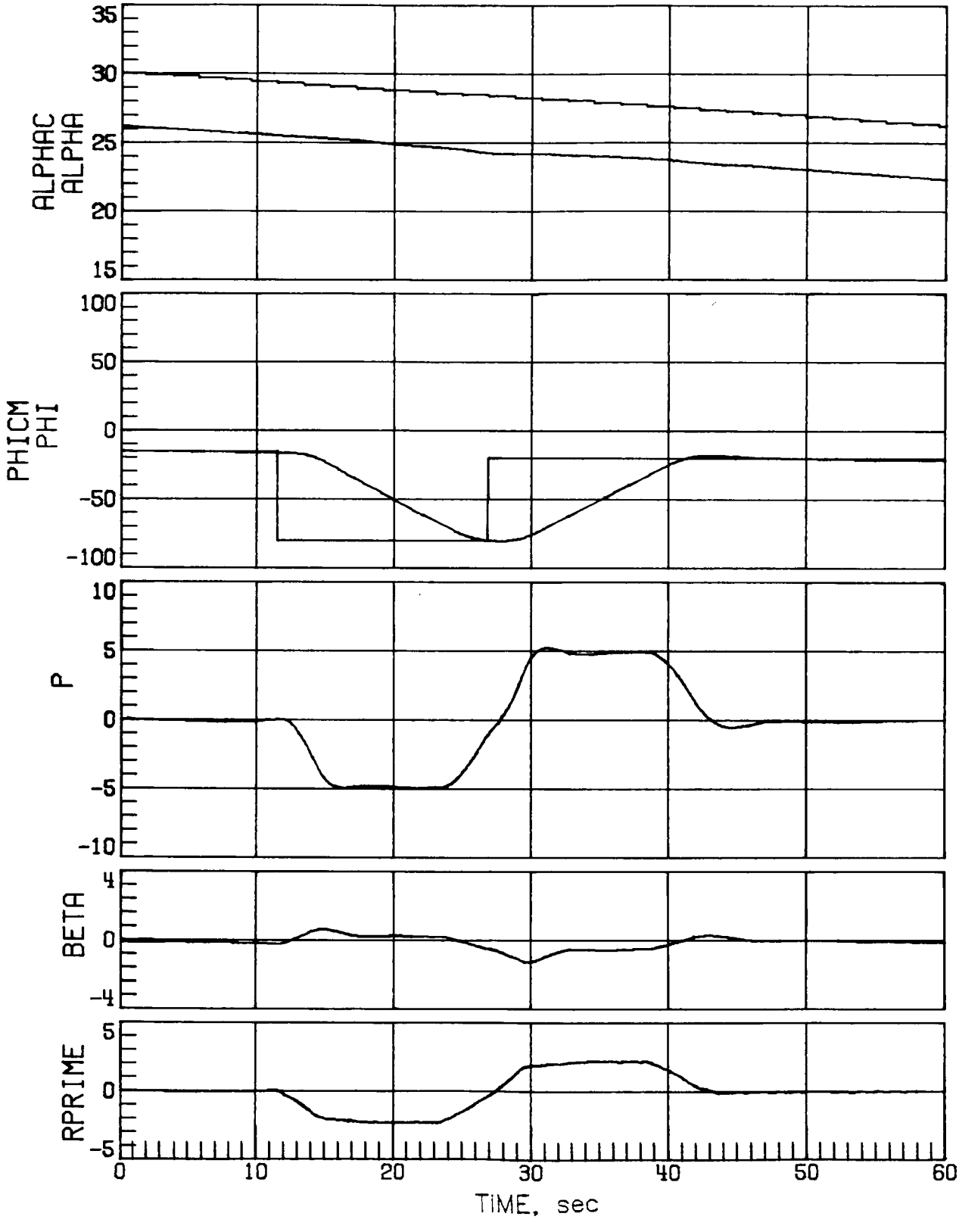

(c) Case 7.

Figure 13.- Continued.

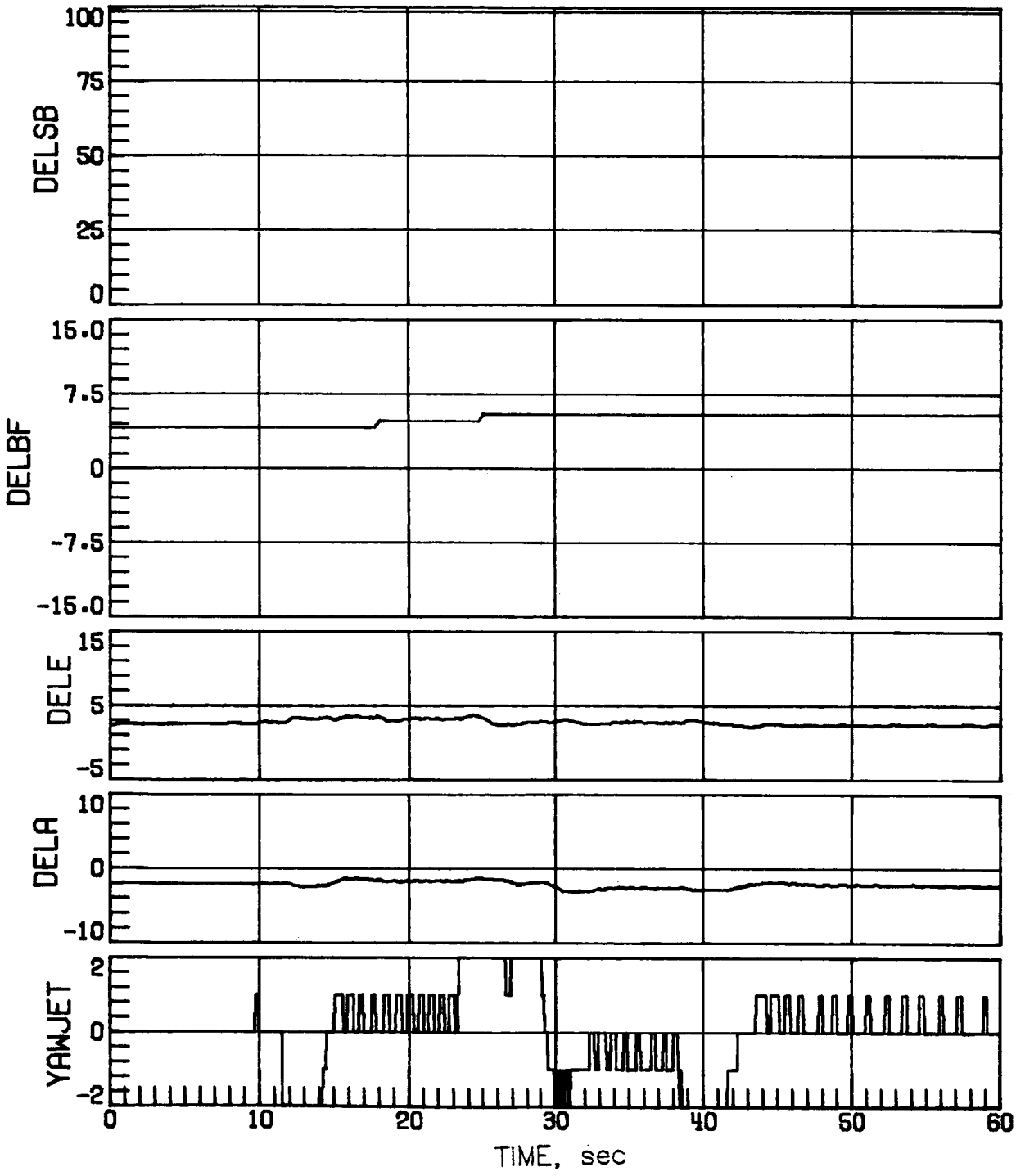

(c) Concluded.

Figure 13.- Continued.

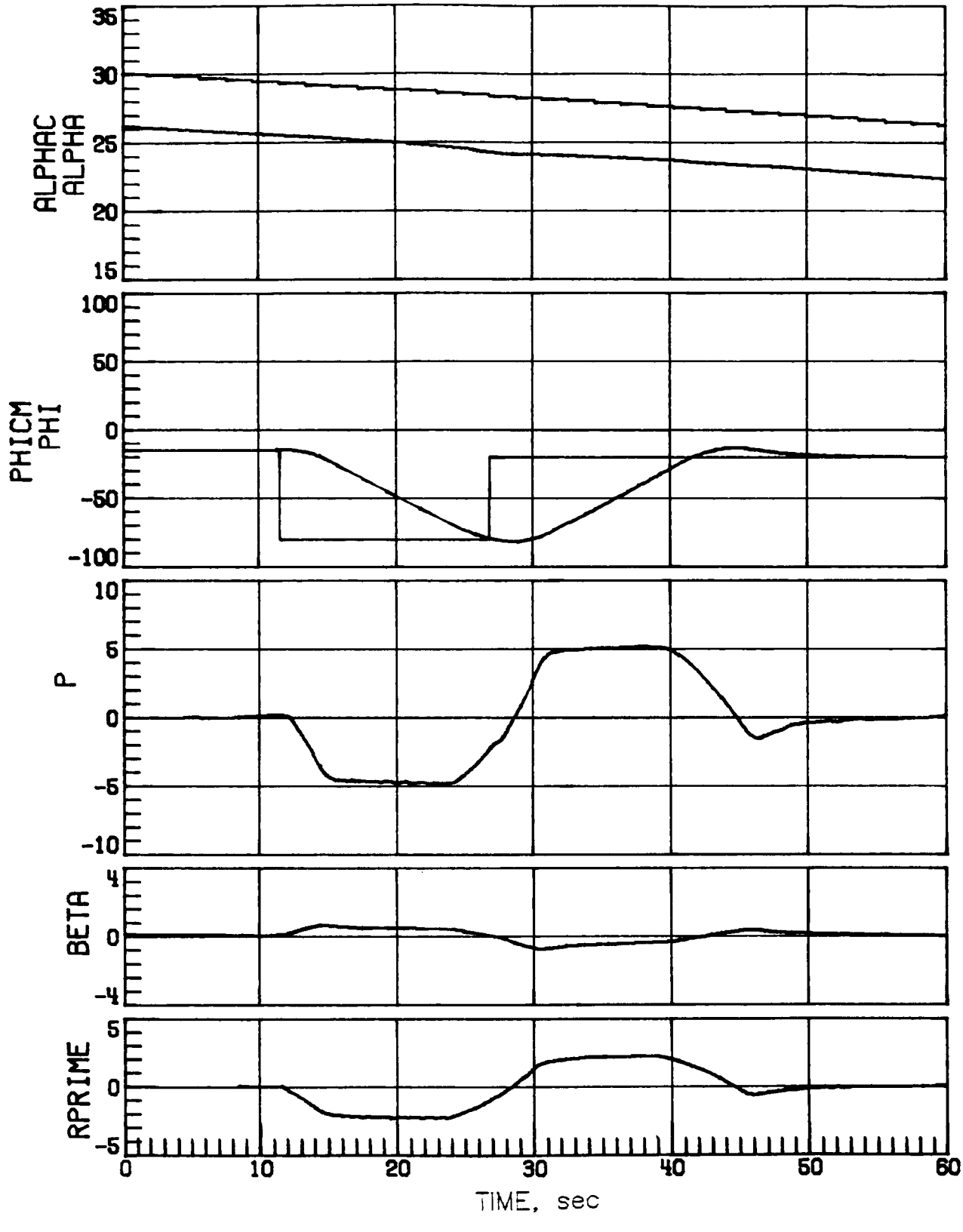

(d) Case 9.

Figure 13.- Continued.

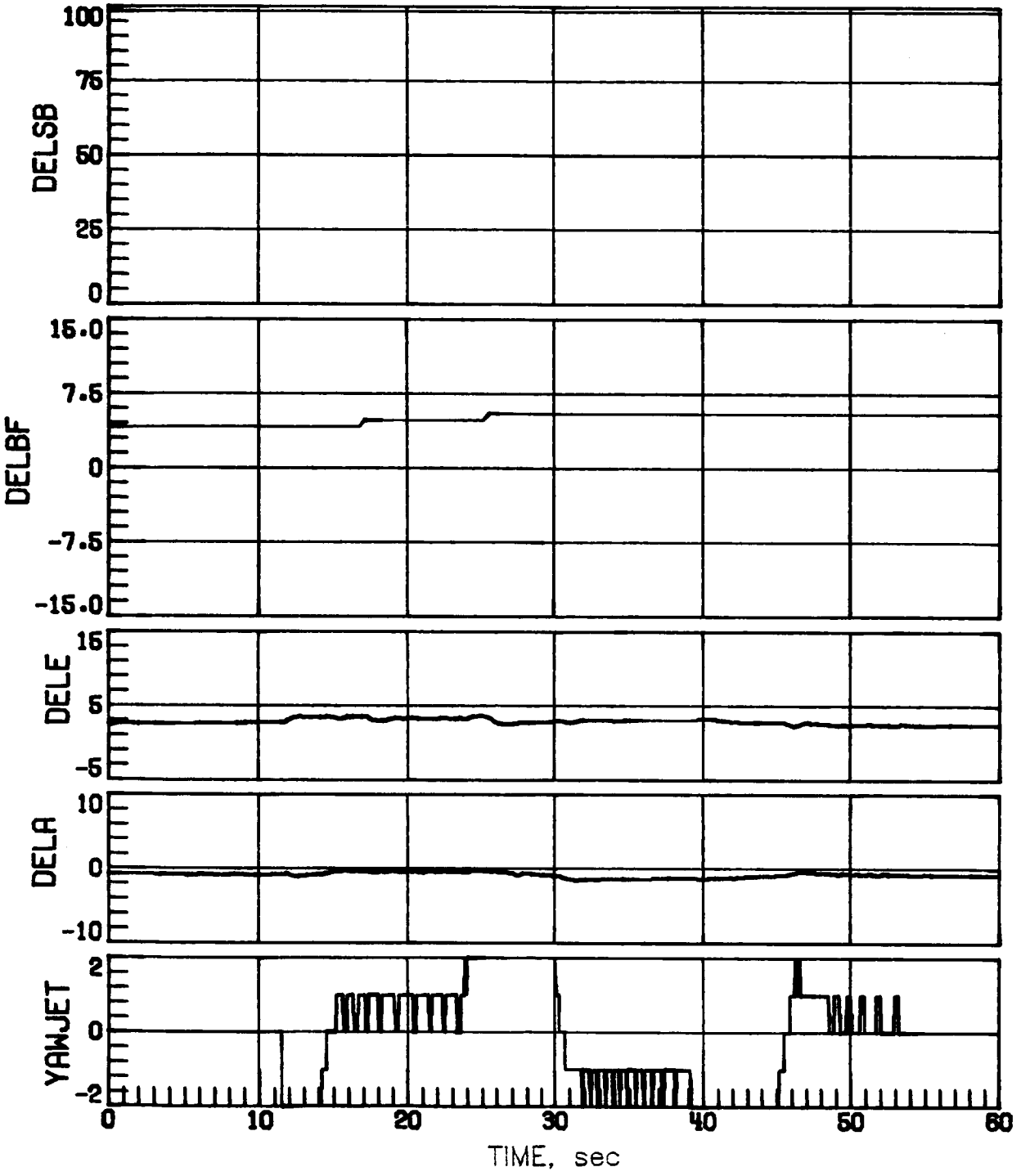

(d) Concluded.

Figure 13.- Continued.

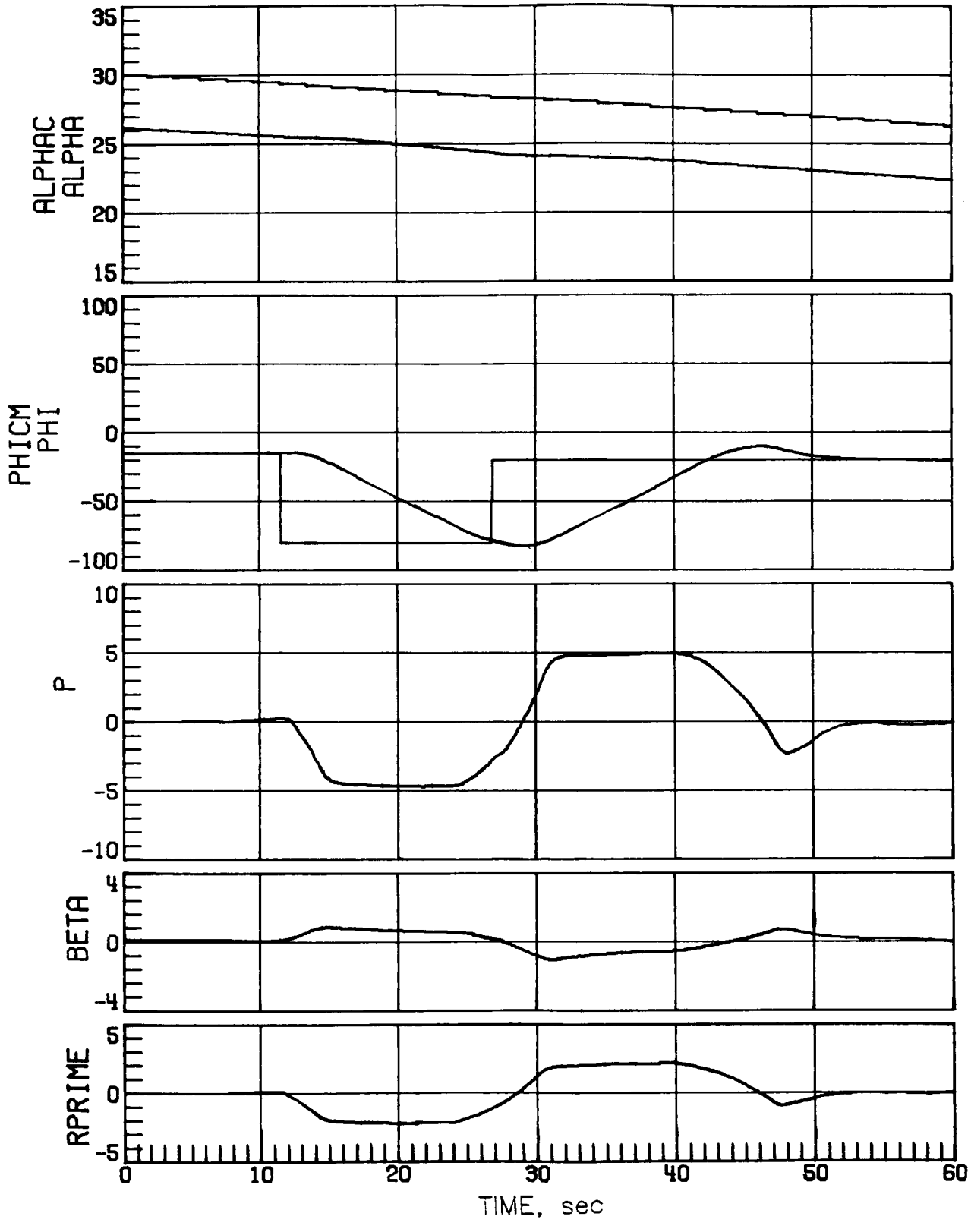

(e) Case 11.

Figure 13.- Continued.

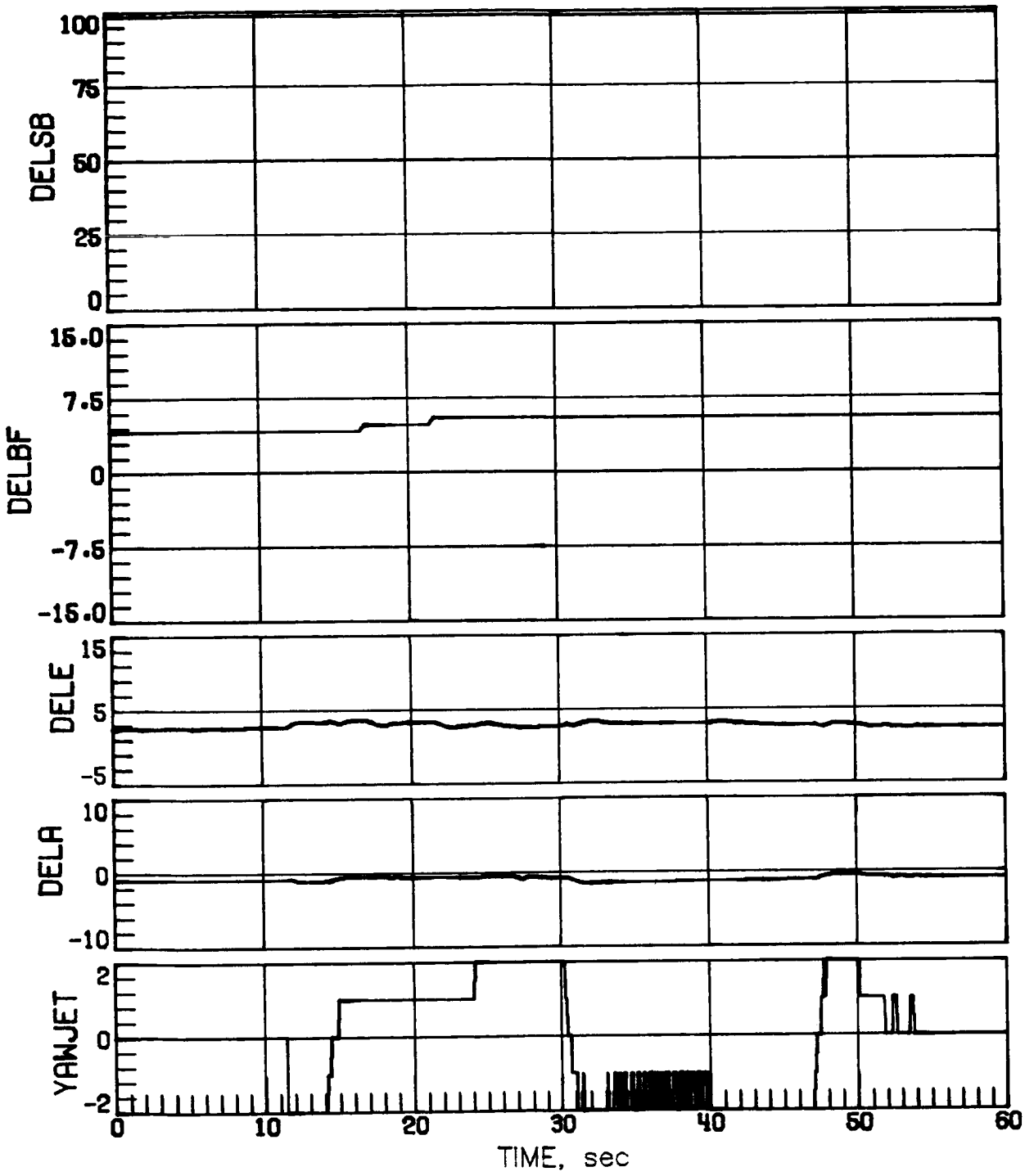

(e) Concluded.

Figure 13.- Continued.

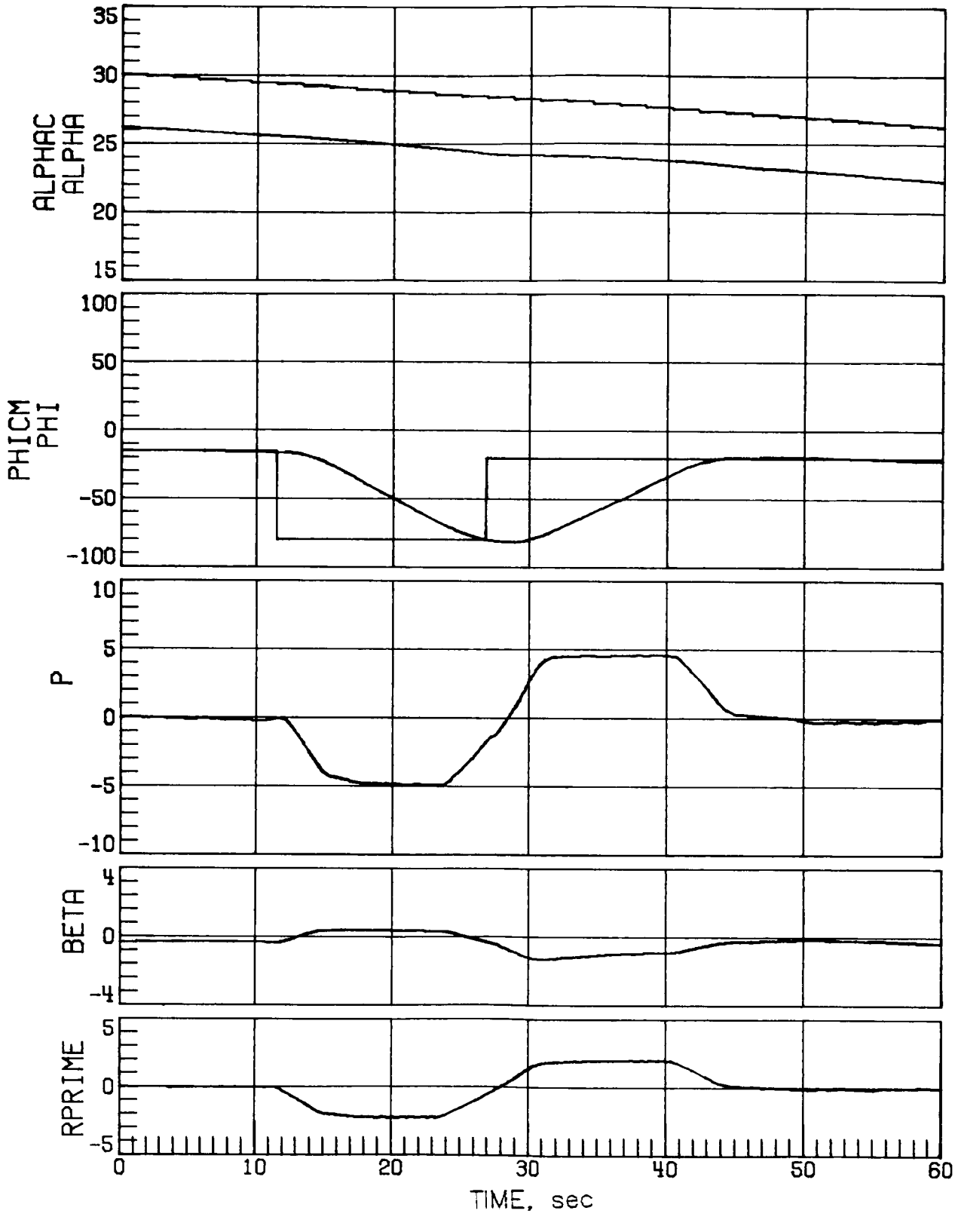

(f) Case 16.

Figure 13.- Continued.

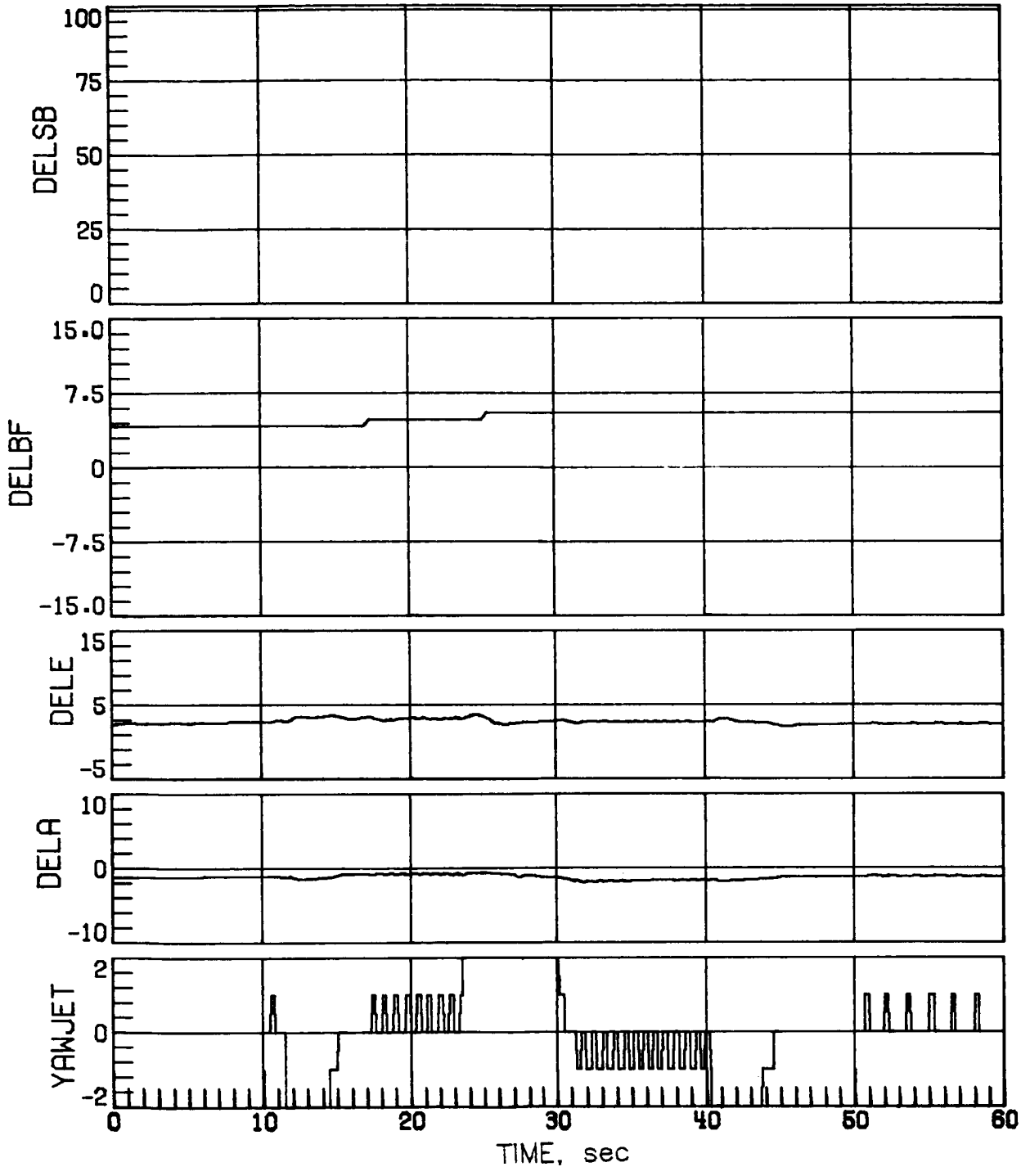

(f) Concluded.

Figure 13.- Concluded.

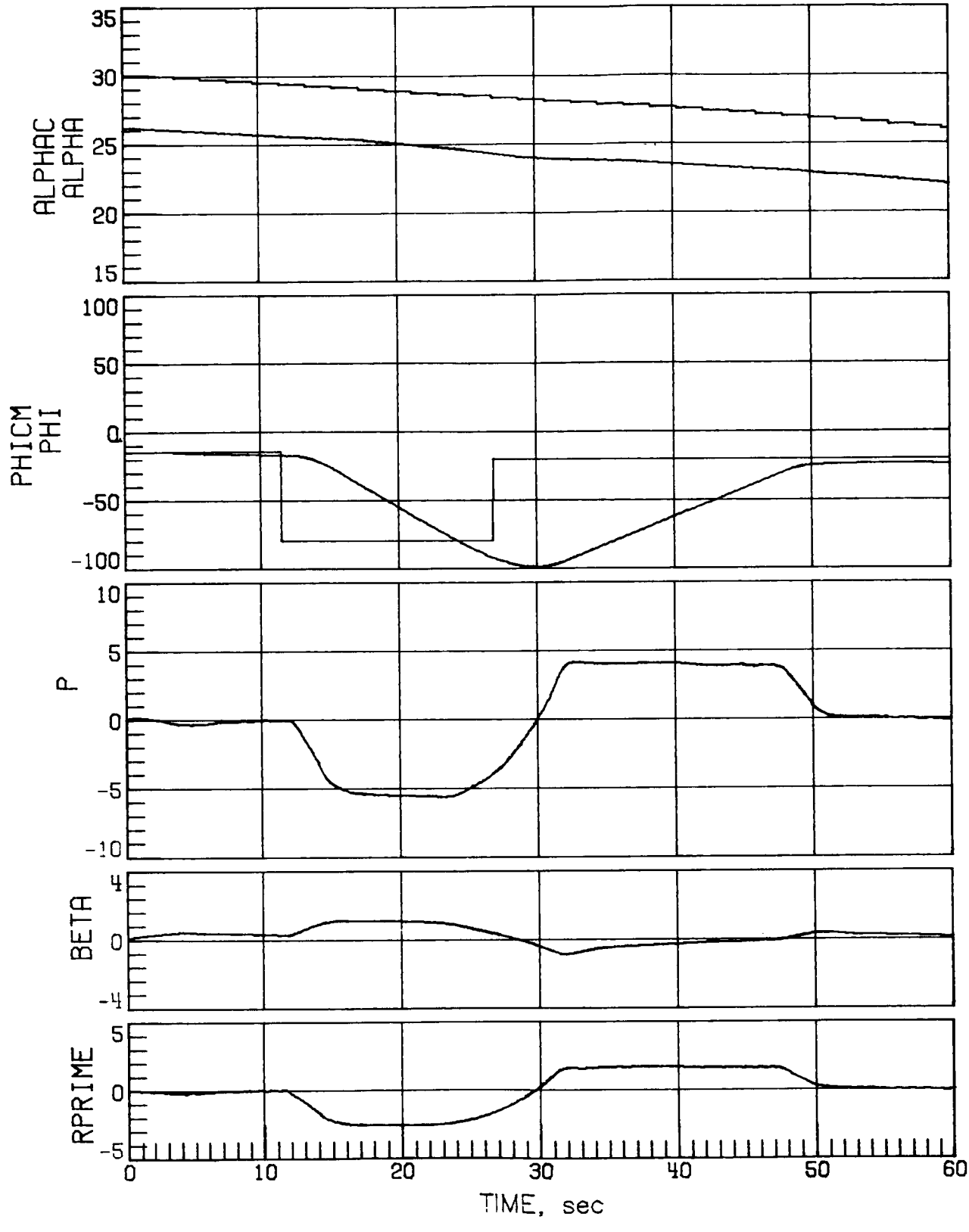

(a) N_Y misalignment of 1°.

Figure 14.- Mach 7.5 performance for a high-sensed α error of 4° with case 11 off-nominal aerodynamics.

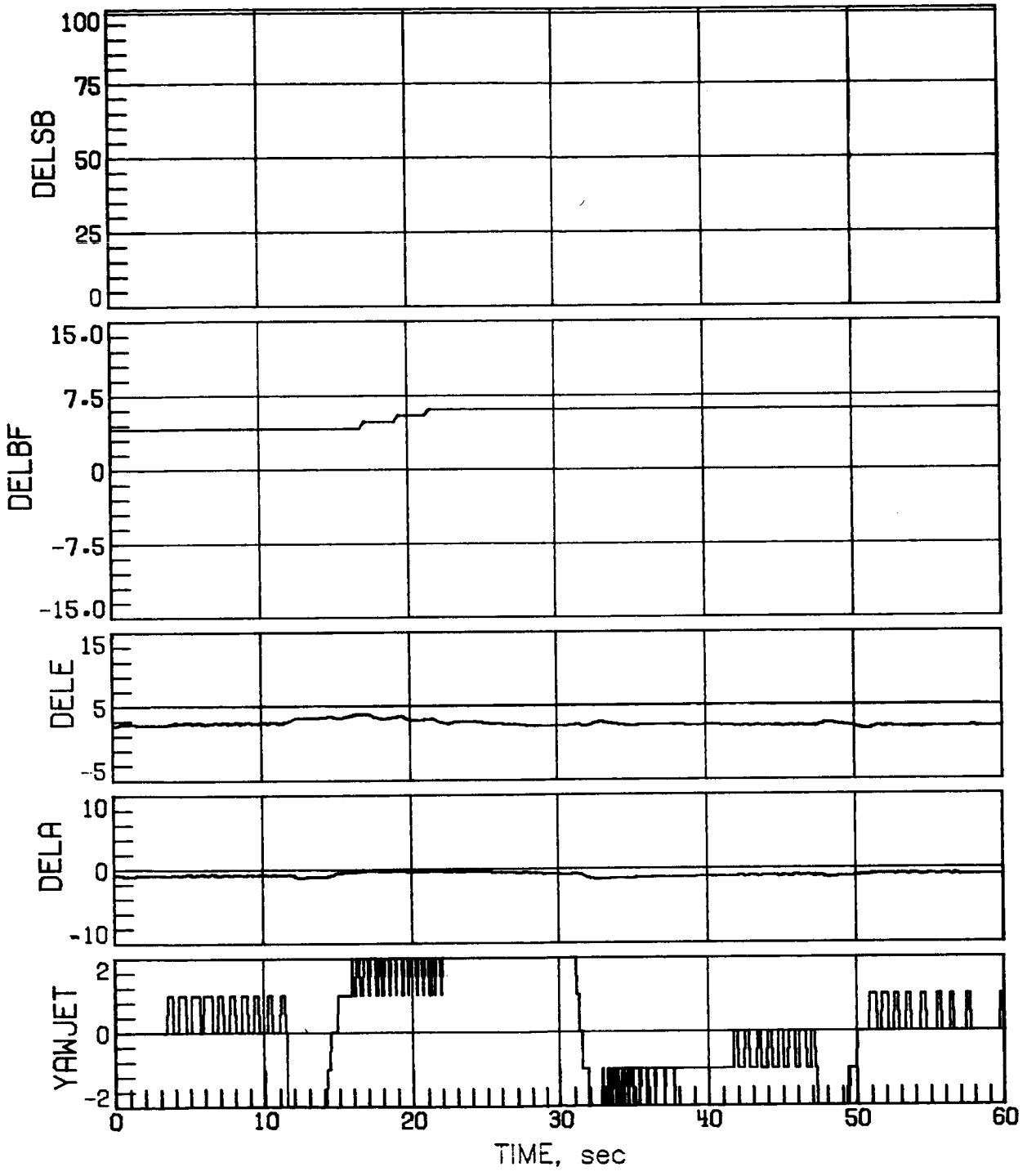

(a) Concluded.

Figure 14.- Continued.

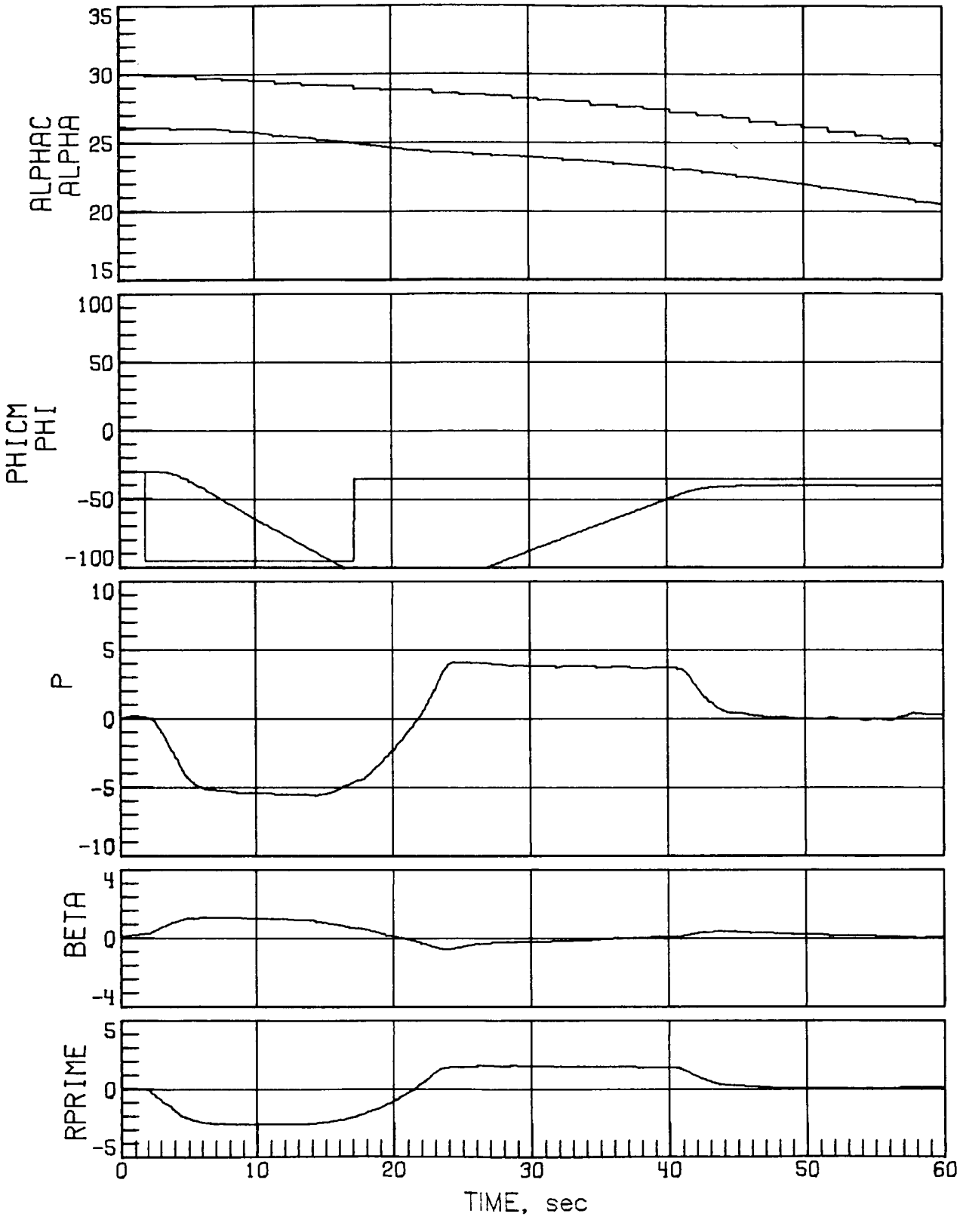

(b) N_Y misalignment of 1° with maneuver occurring prior to 2 sec.

Figure 14.- Continued.

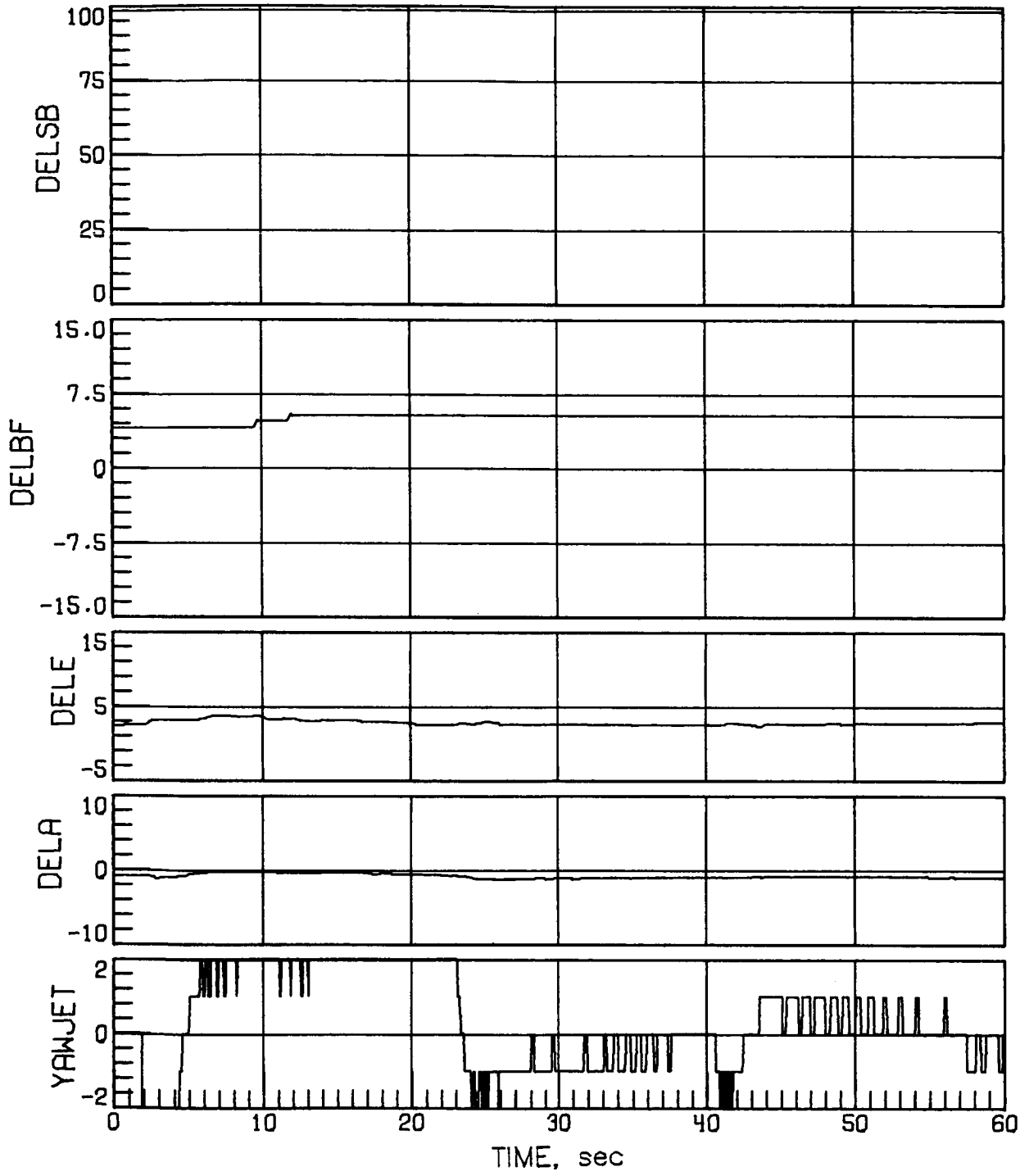

(b) Concluded.

Figure 14.- Continued.

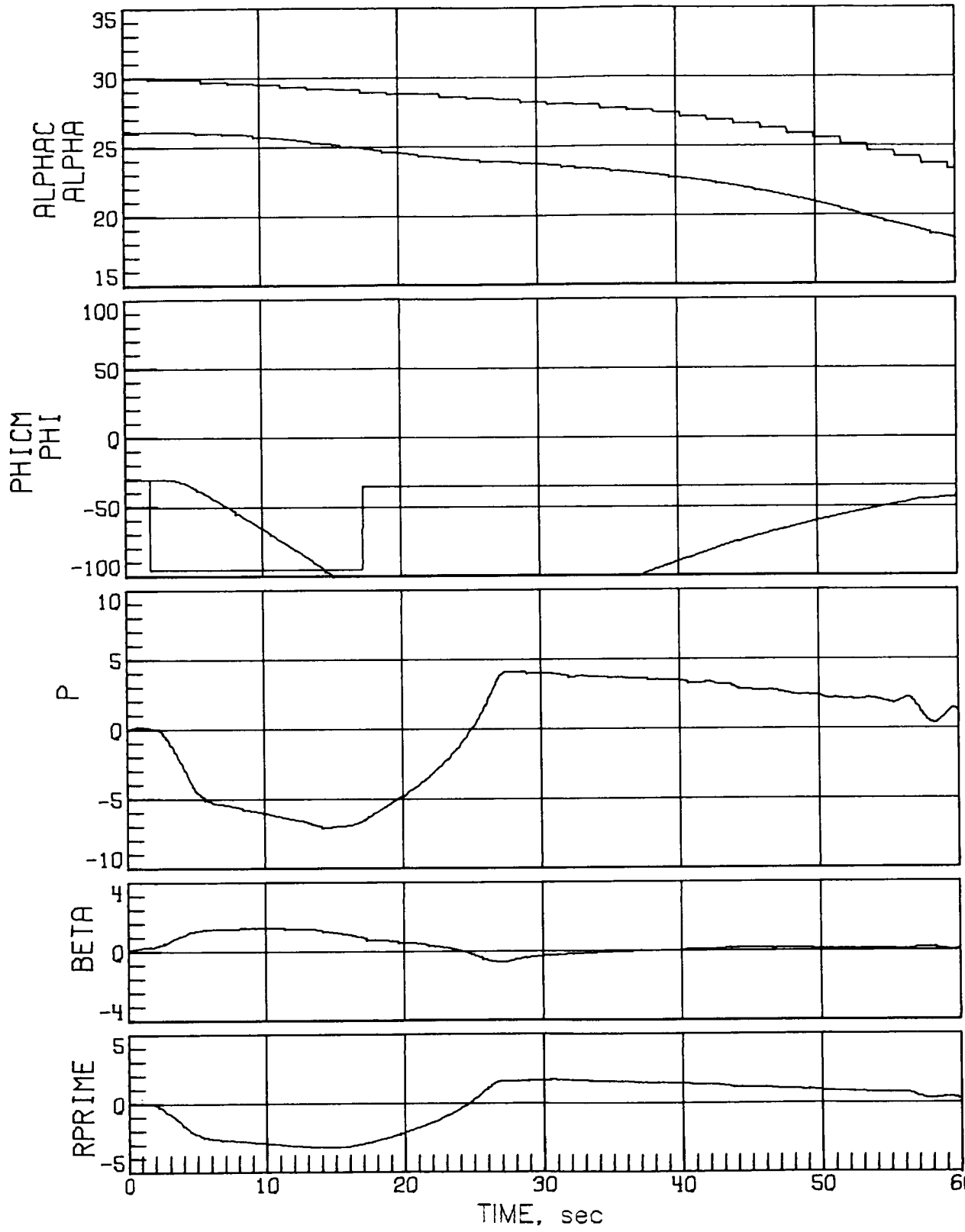

(c) N_Y misalignment of 1° and positive uncertainty increment in C_{Y_β}.

Figure 14.- Continued.

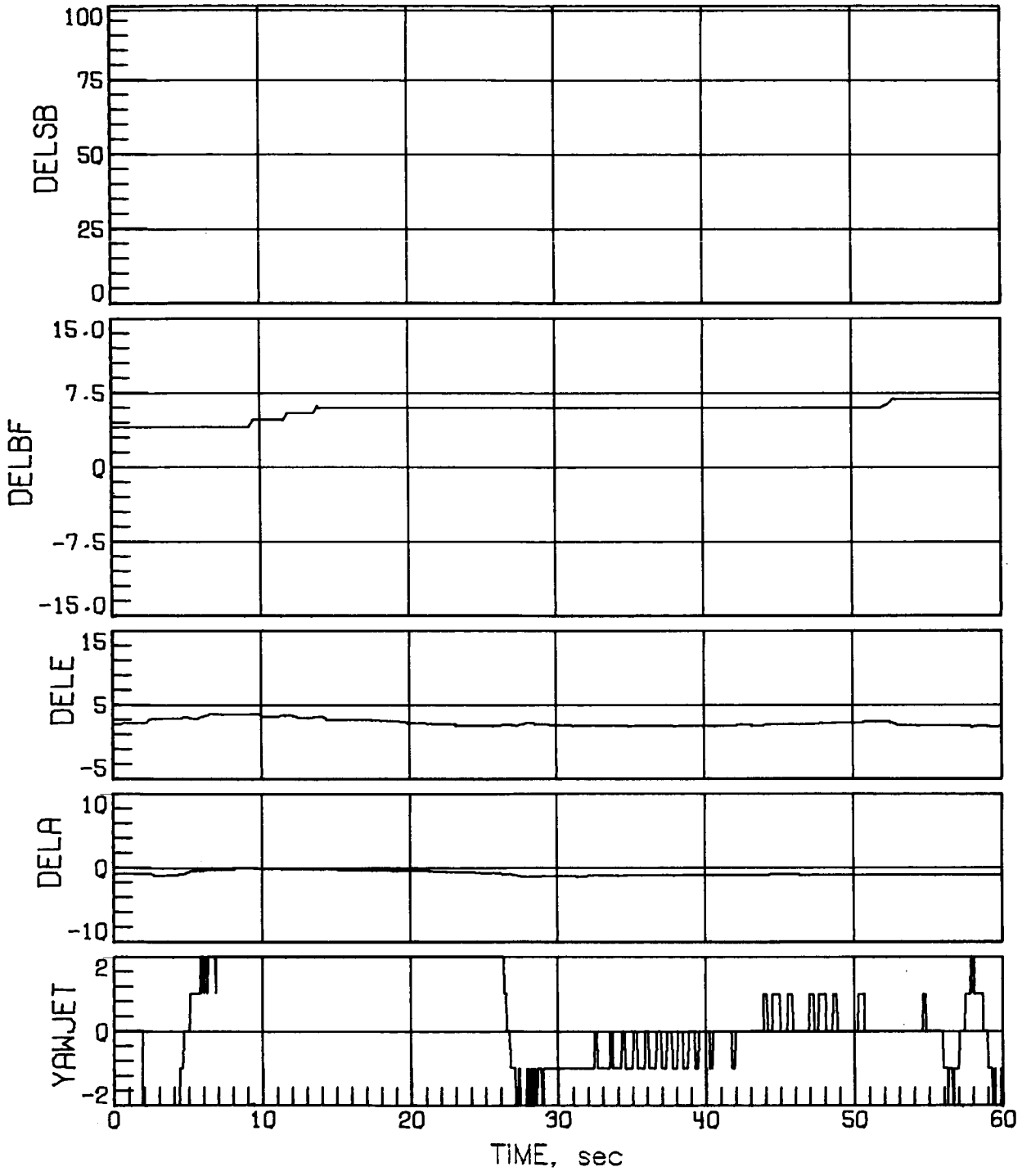

(c) Concluded.

Figure 14.- Continued.

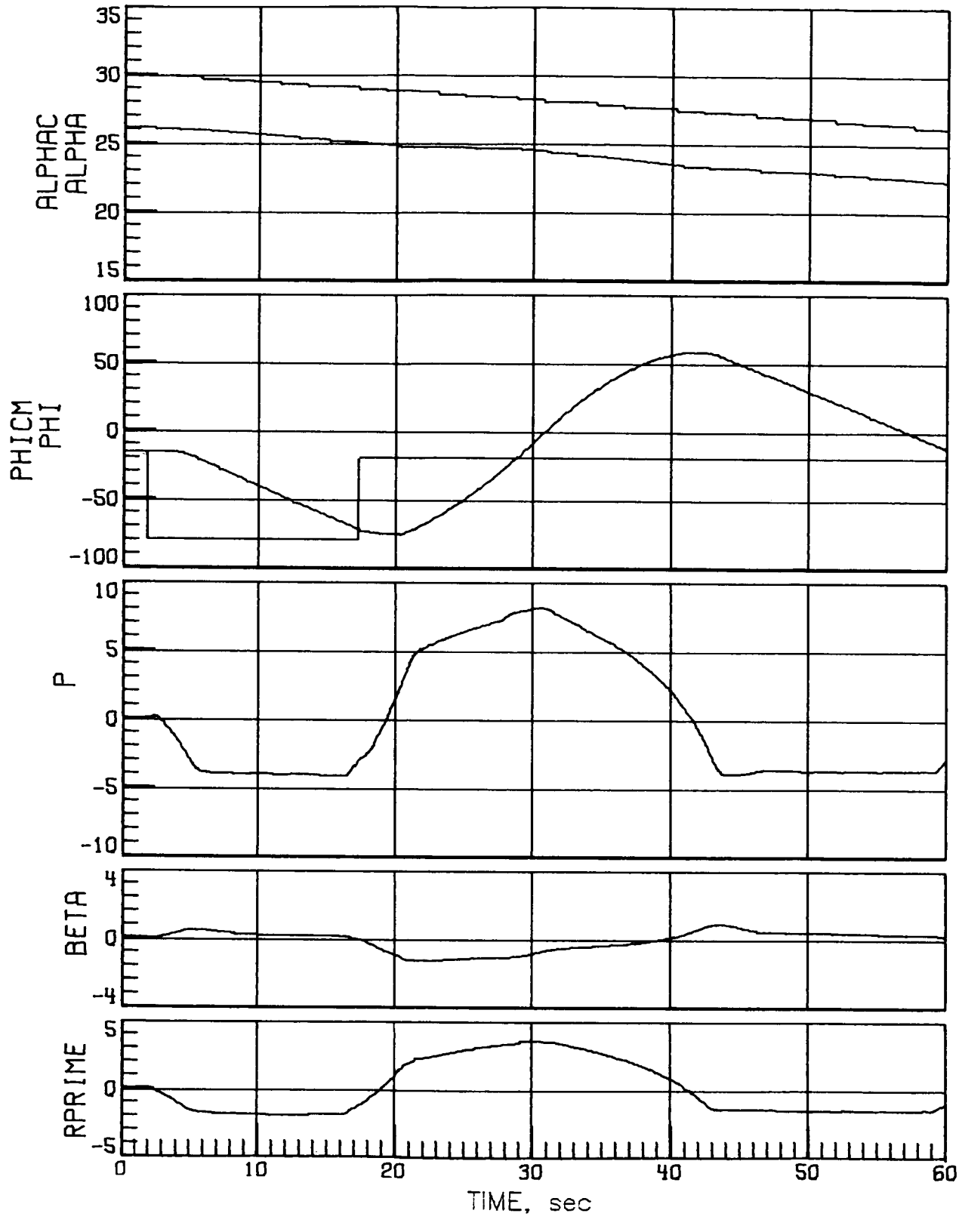

(d) N_Y misalignment of -1°.

Figure 14.- Continued.

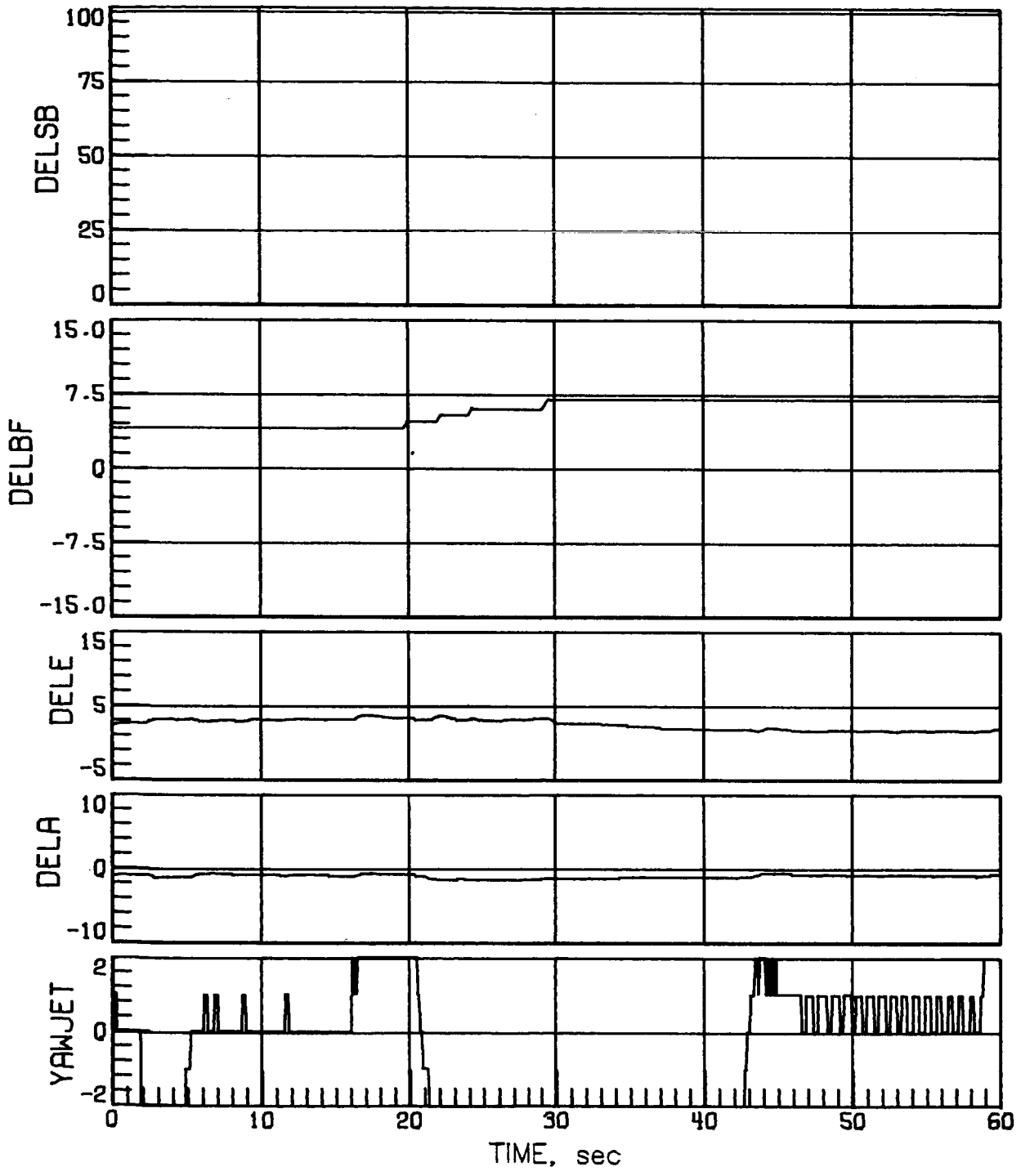

(d) Concluded.

Figure 14.- Continued.

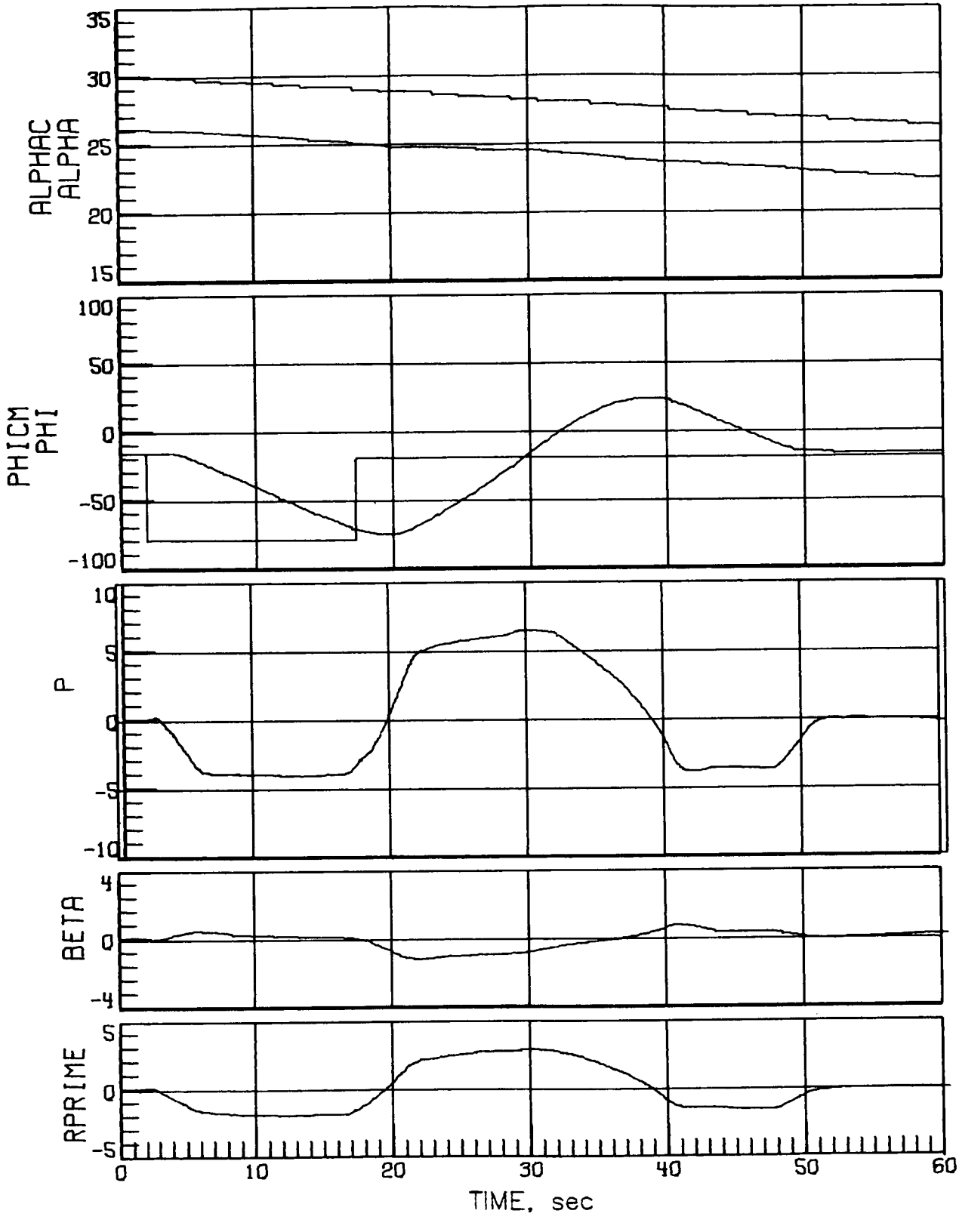

(e) N_Y misalignment of -1° and negative uncertainty increment in C_{Y_β}.

Figure 14.- Continued.

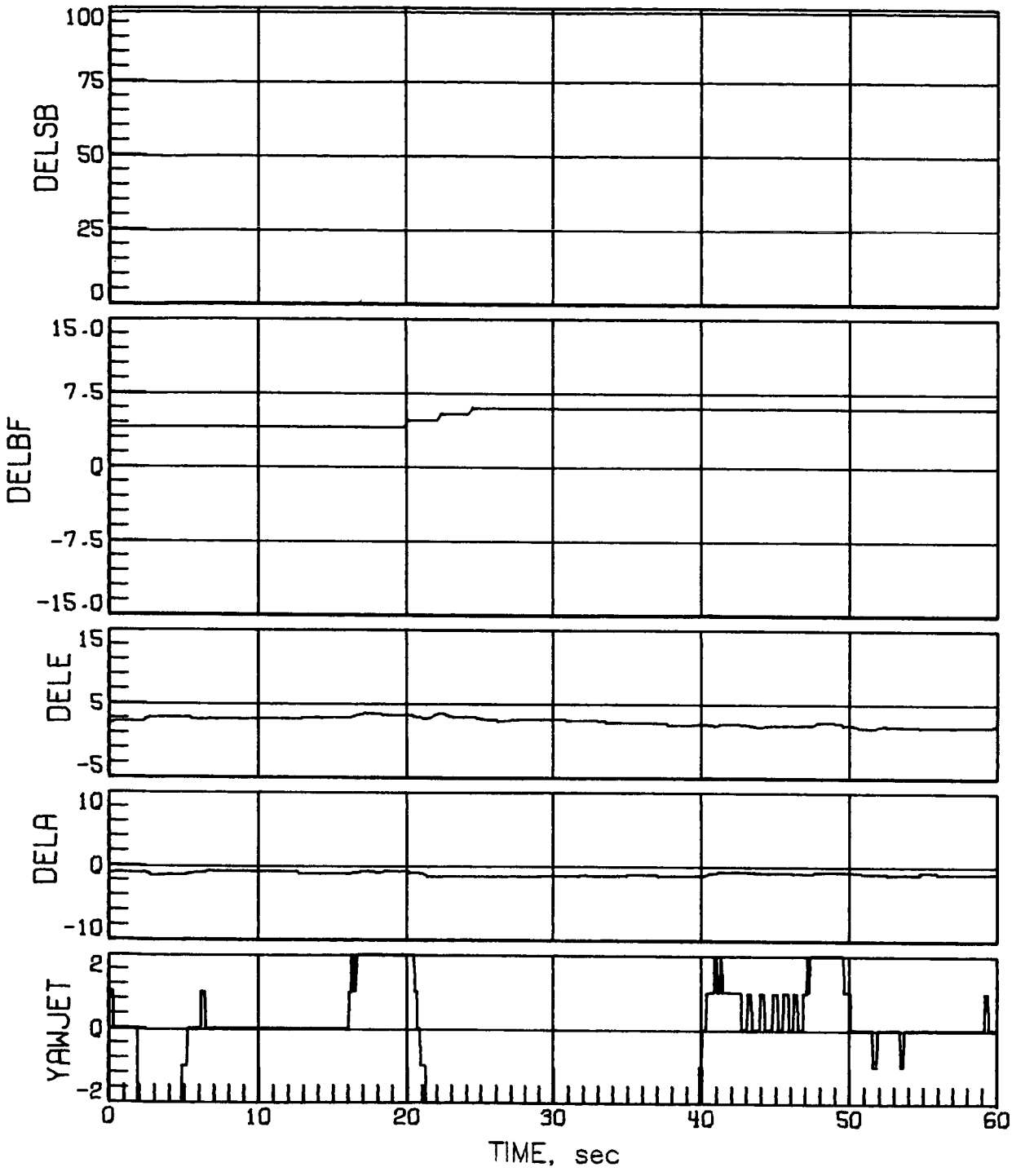

(e) Concluded.

Figure 14.- Continued.

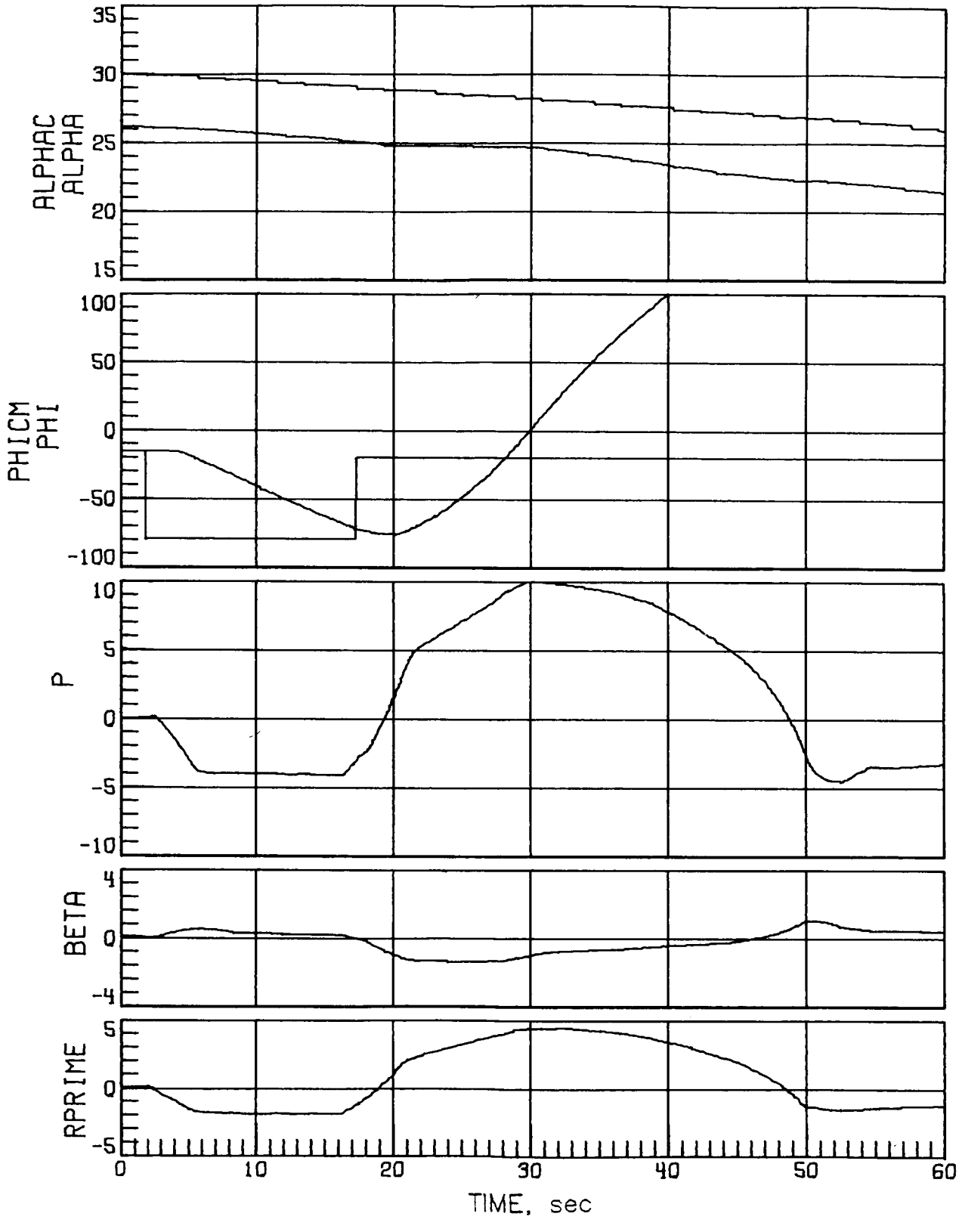

(f) N_Y misalignment of -1° and positive uncertainty increment in C_{Y_β}.

Figure 14.- Continued.

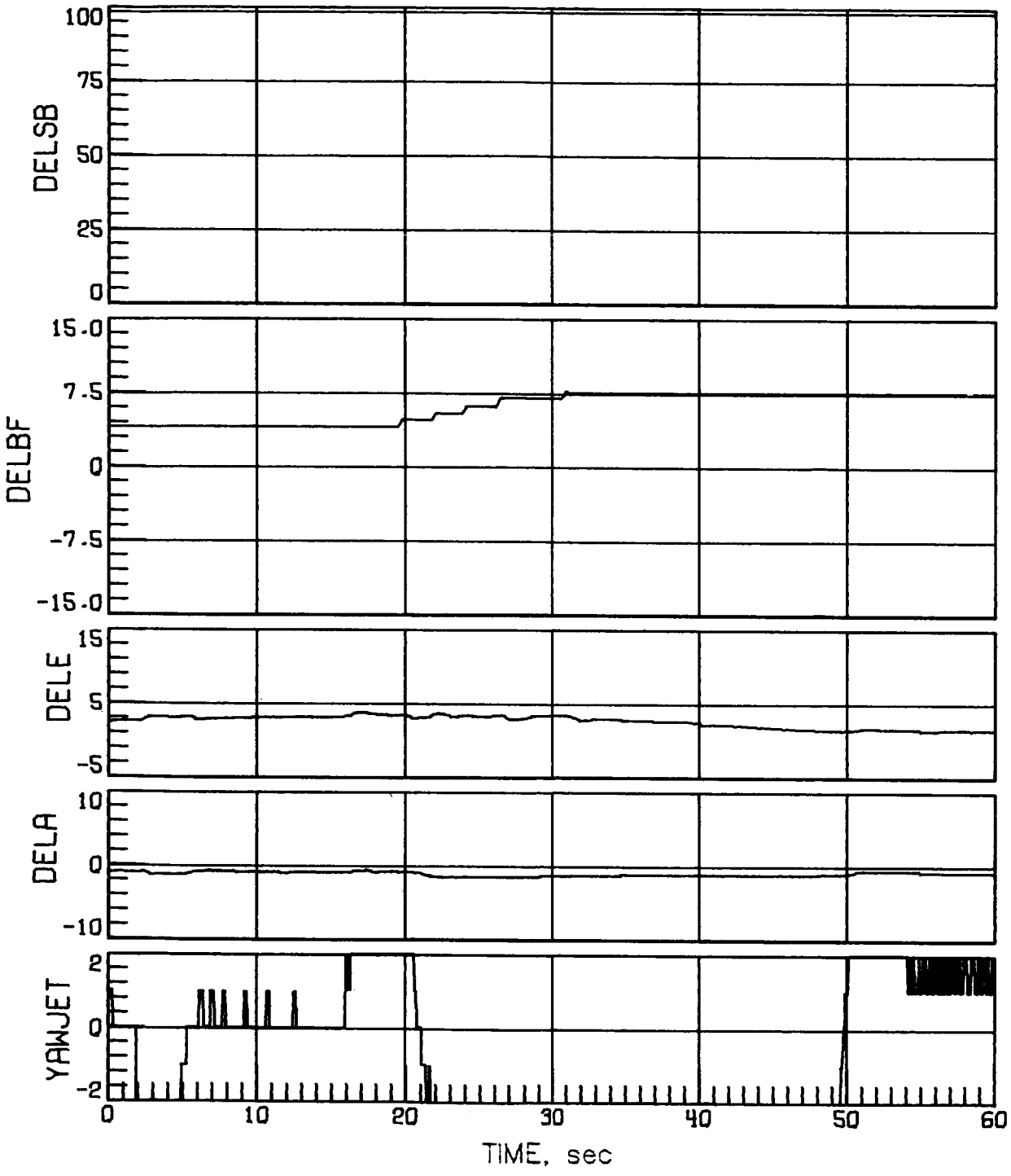

(f) Concluded.

Figure 14.- Continued.

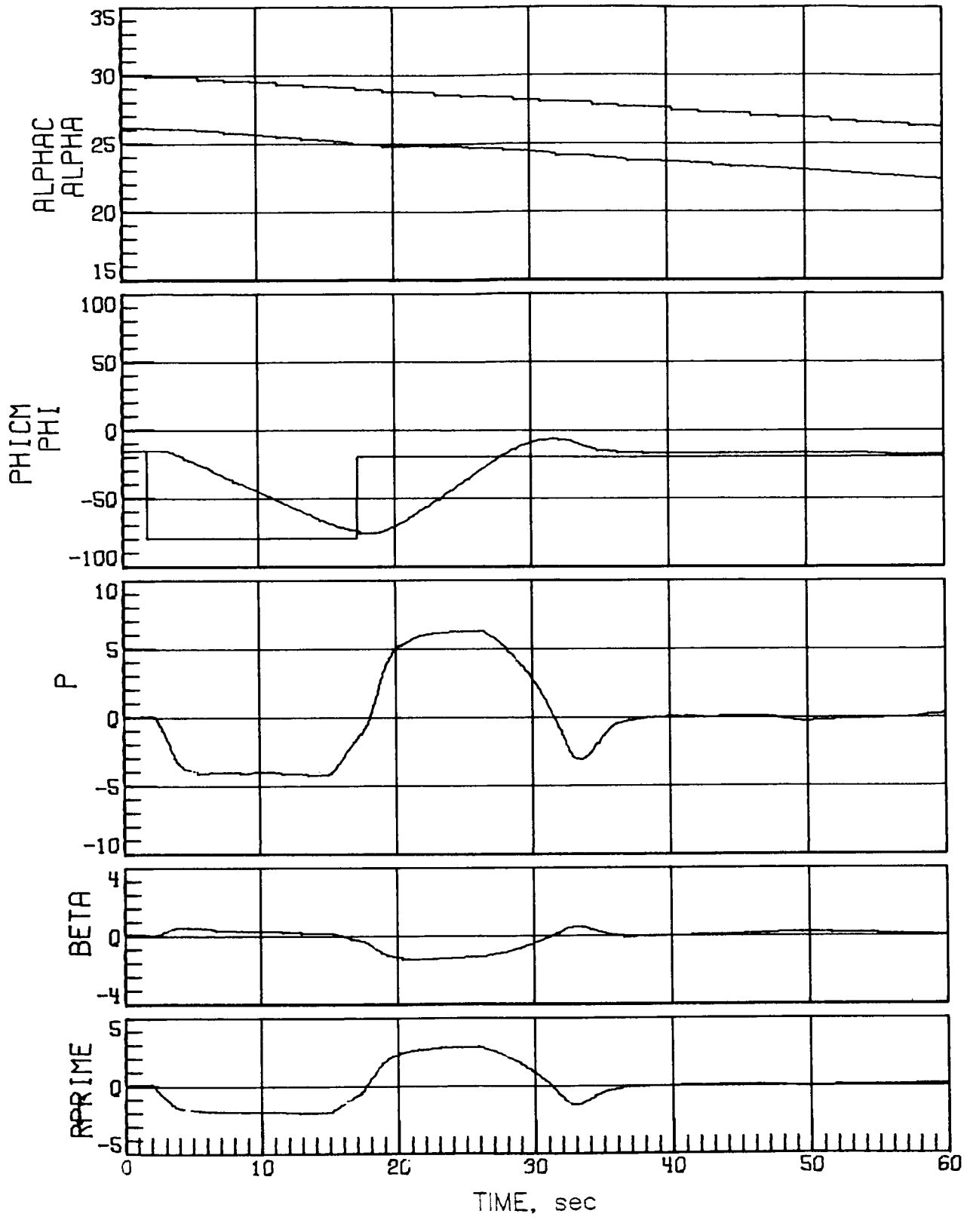

(g) N_Y misalignment of -1°, positive uncertainty increment in C_{Y_β}, and four yaw jets operating.

Figure 14.- Continued.

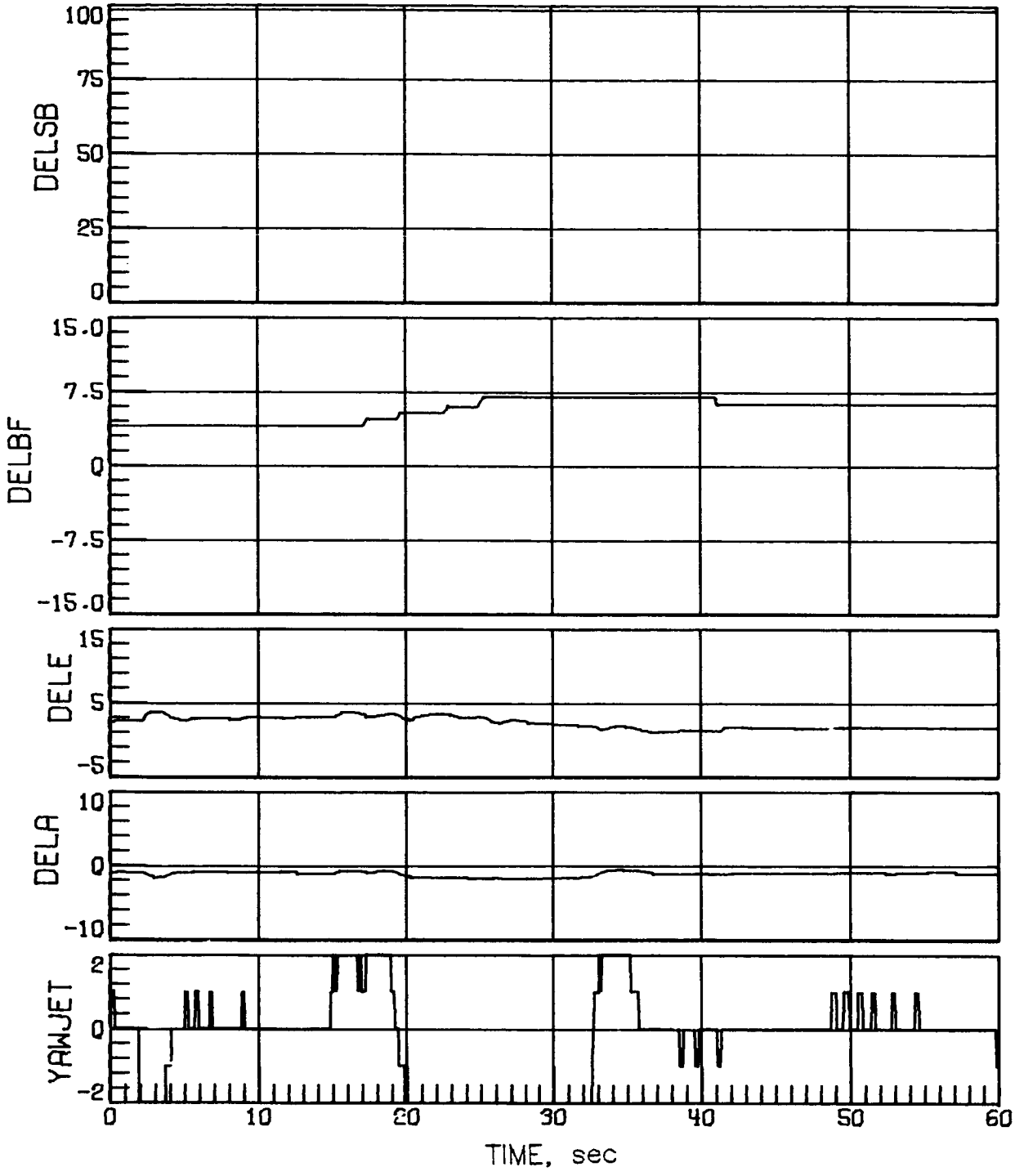

(g) Concluded.

Figure 14.- Concluded.

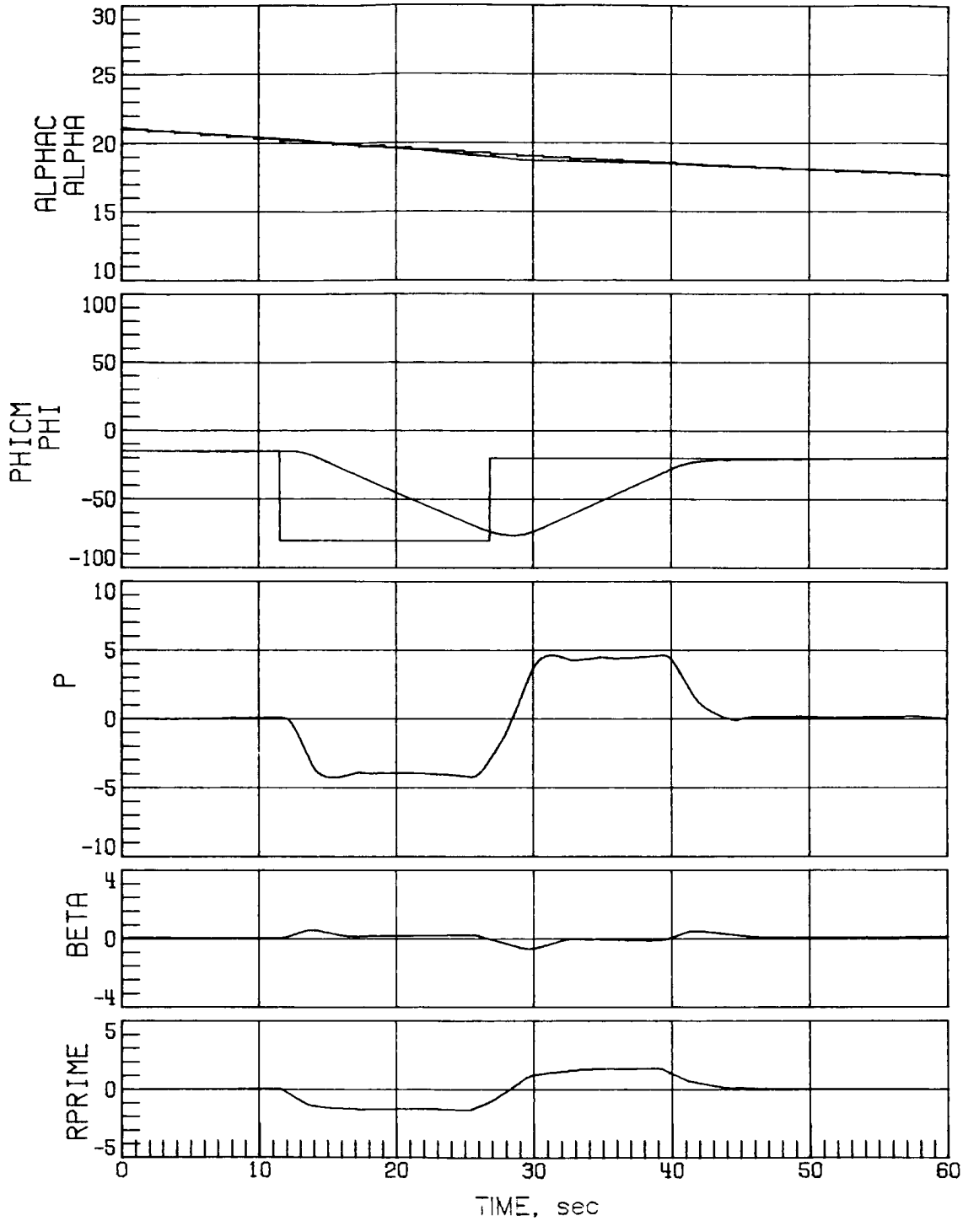

(a) Nominal α.

Figure 15.- Mach 5 maneuver performance with nominal aerodynamics. Maneuver initiated at different times.

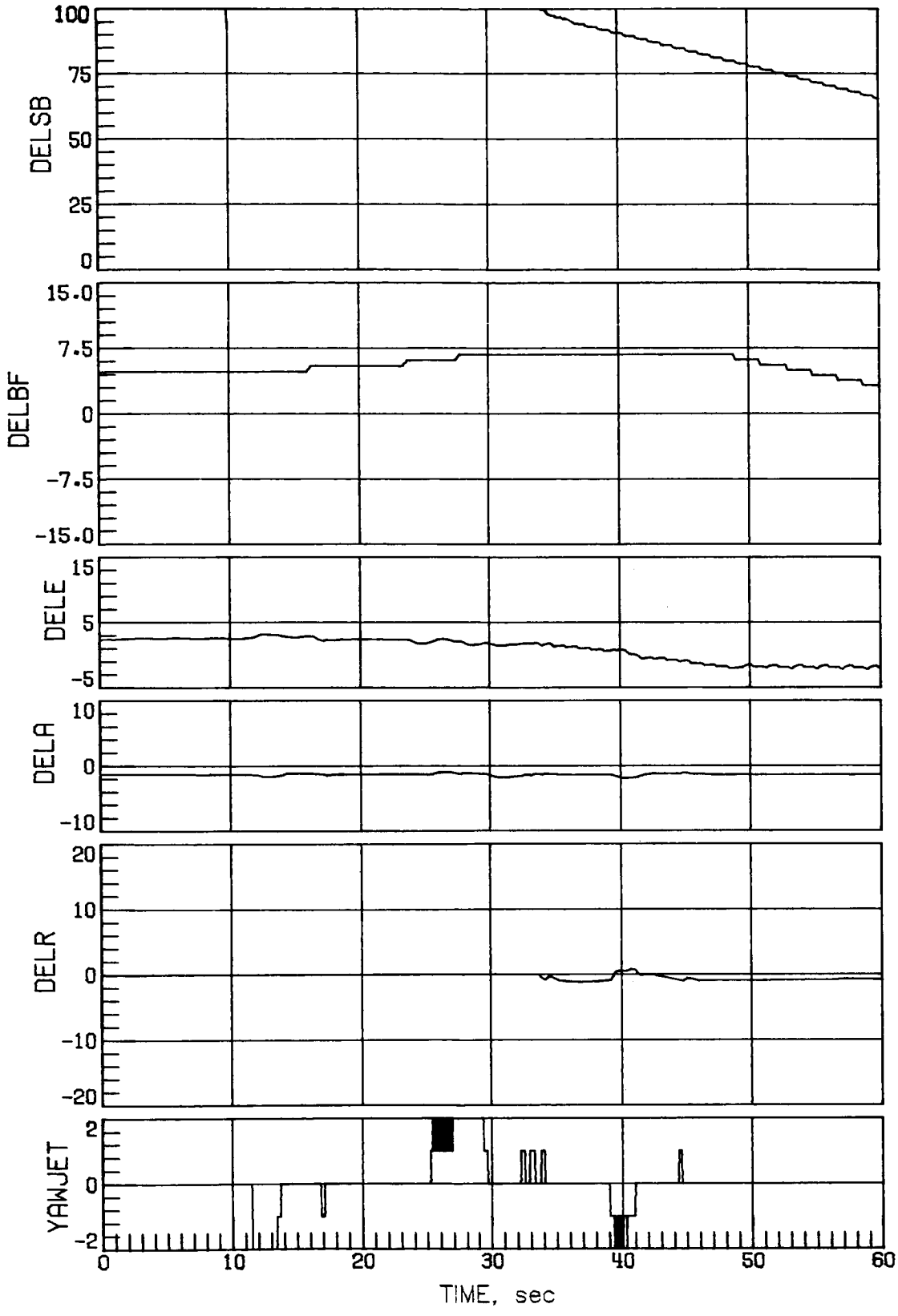

(a) Concluded.

Figure 15.- Continued.

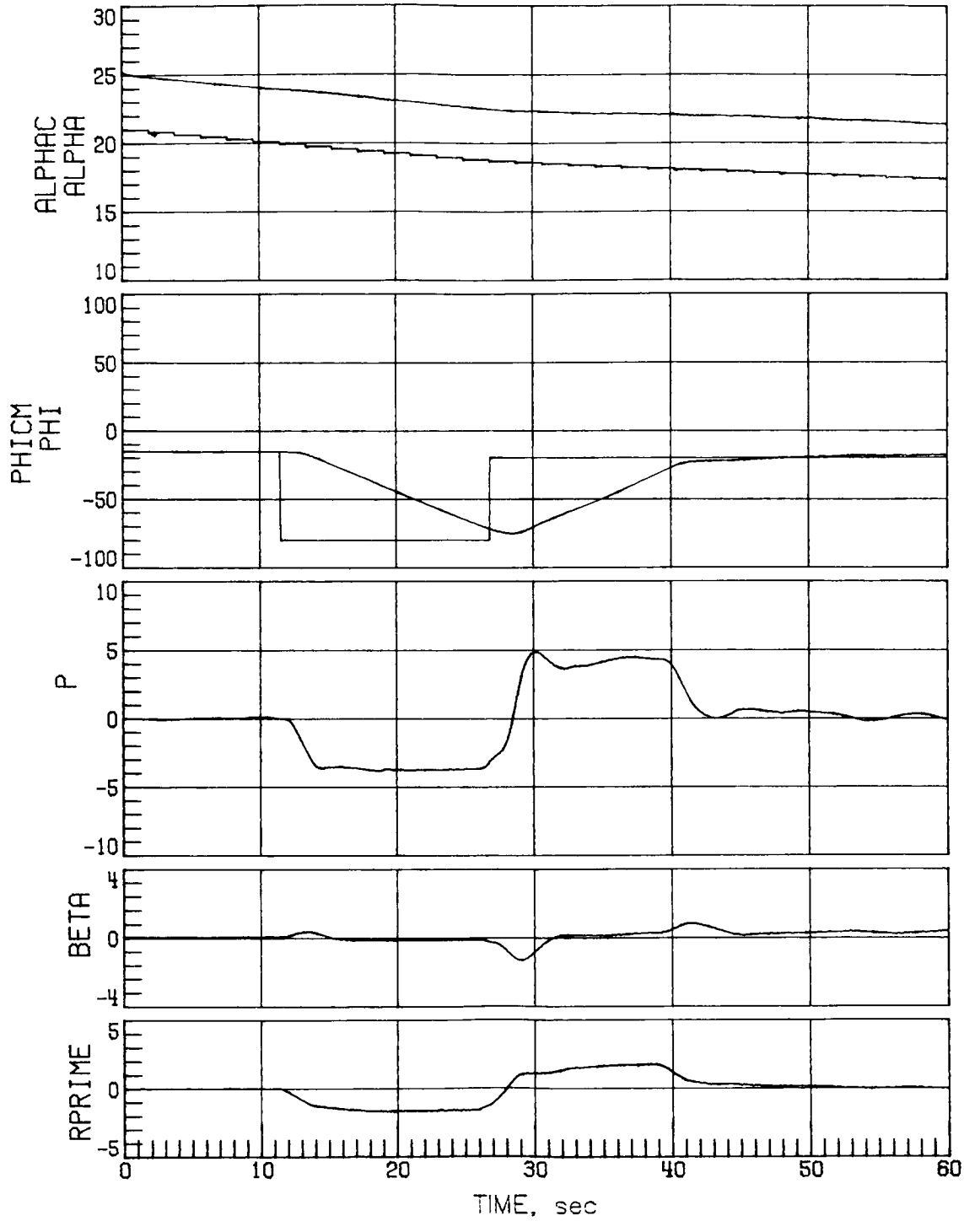

(b) Low-sensed α error of 4°.

Figure 15.- Continued.

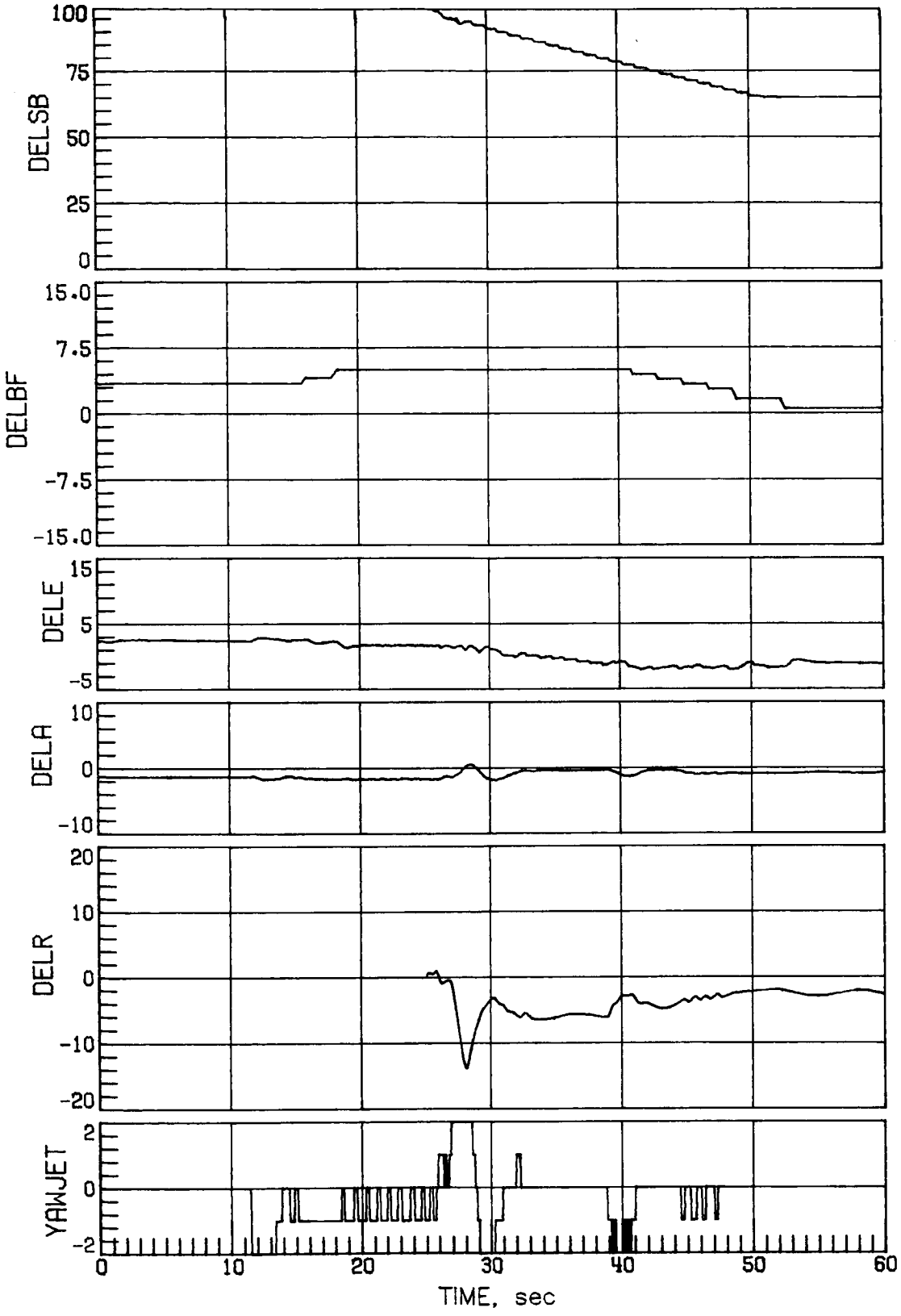

(b) Concluded.

Figure 15.- Continued.

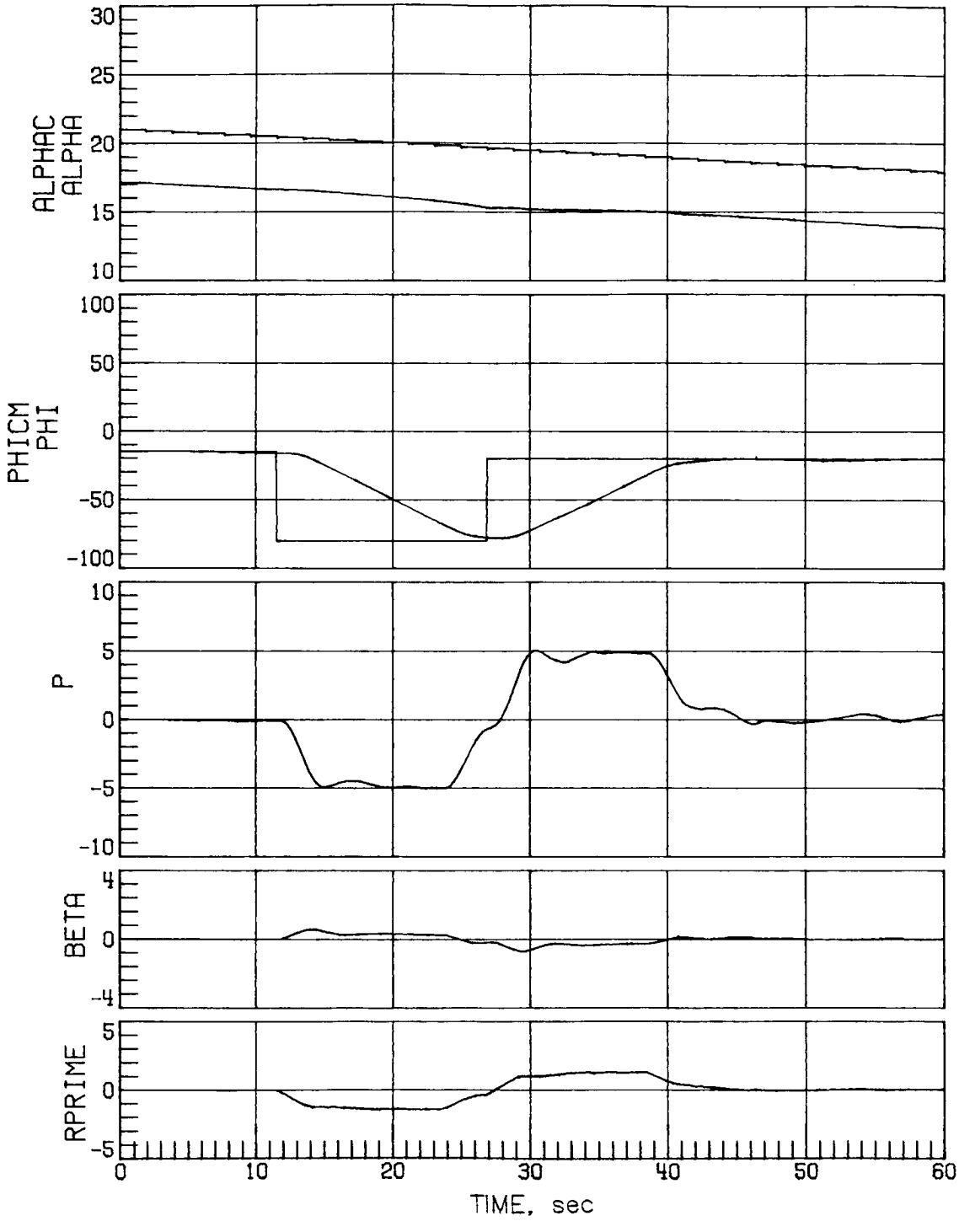

(c) High-sensed α error of 4°.

Figure 15.- Continued.

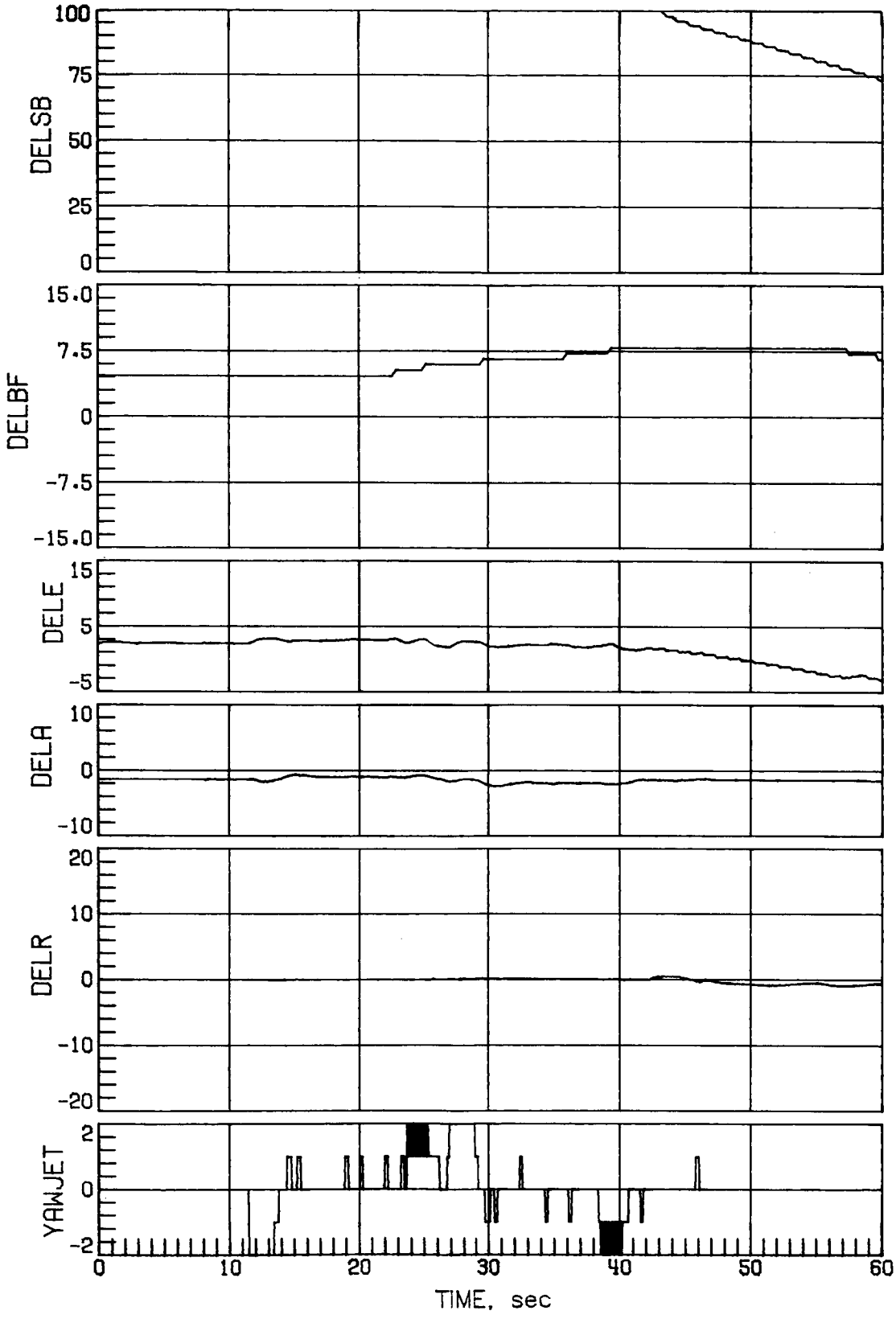

(c) Concluded.

Figure 15.- Continued.

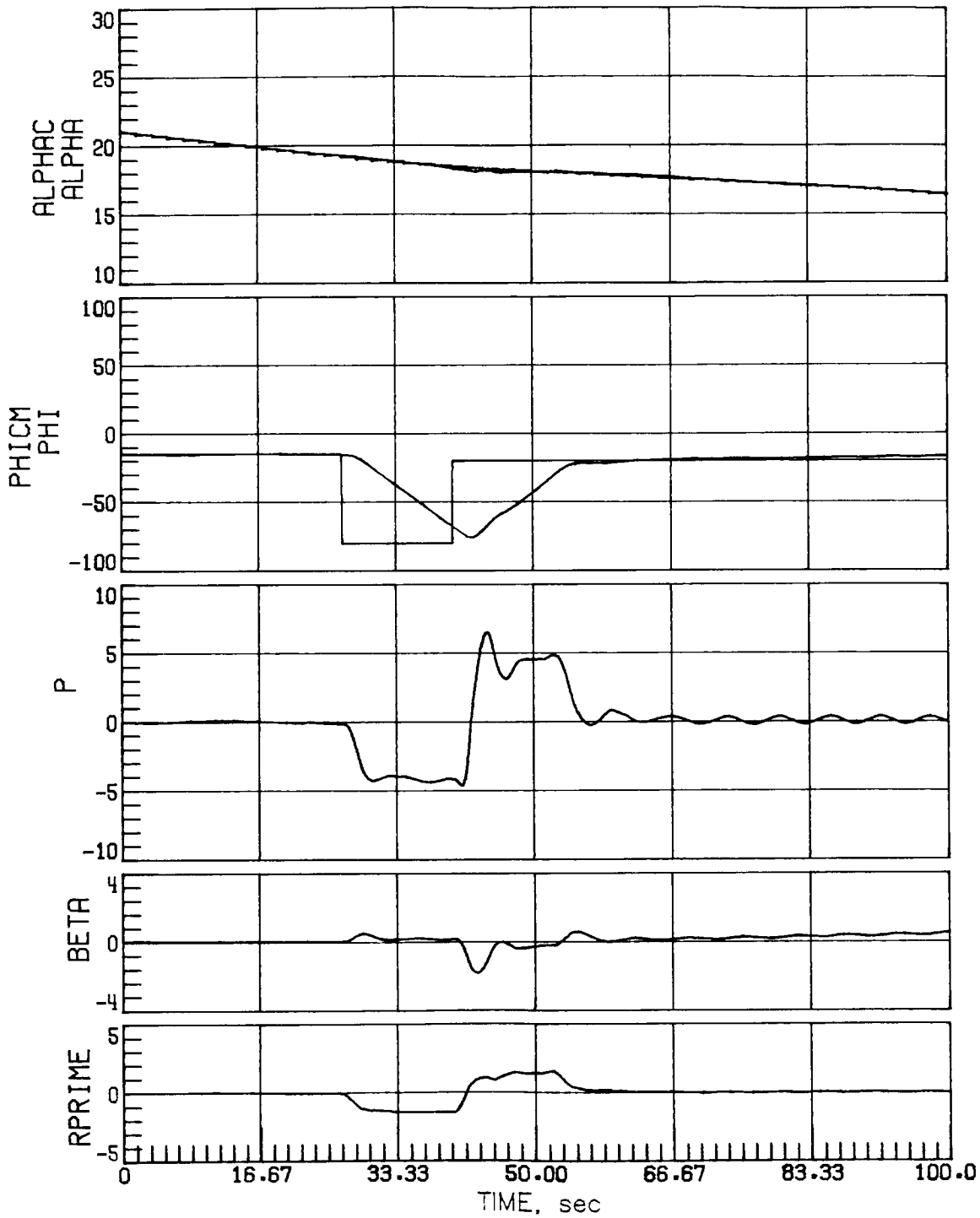

(d) Nominal α.

Figure 15.- Continued.

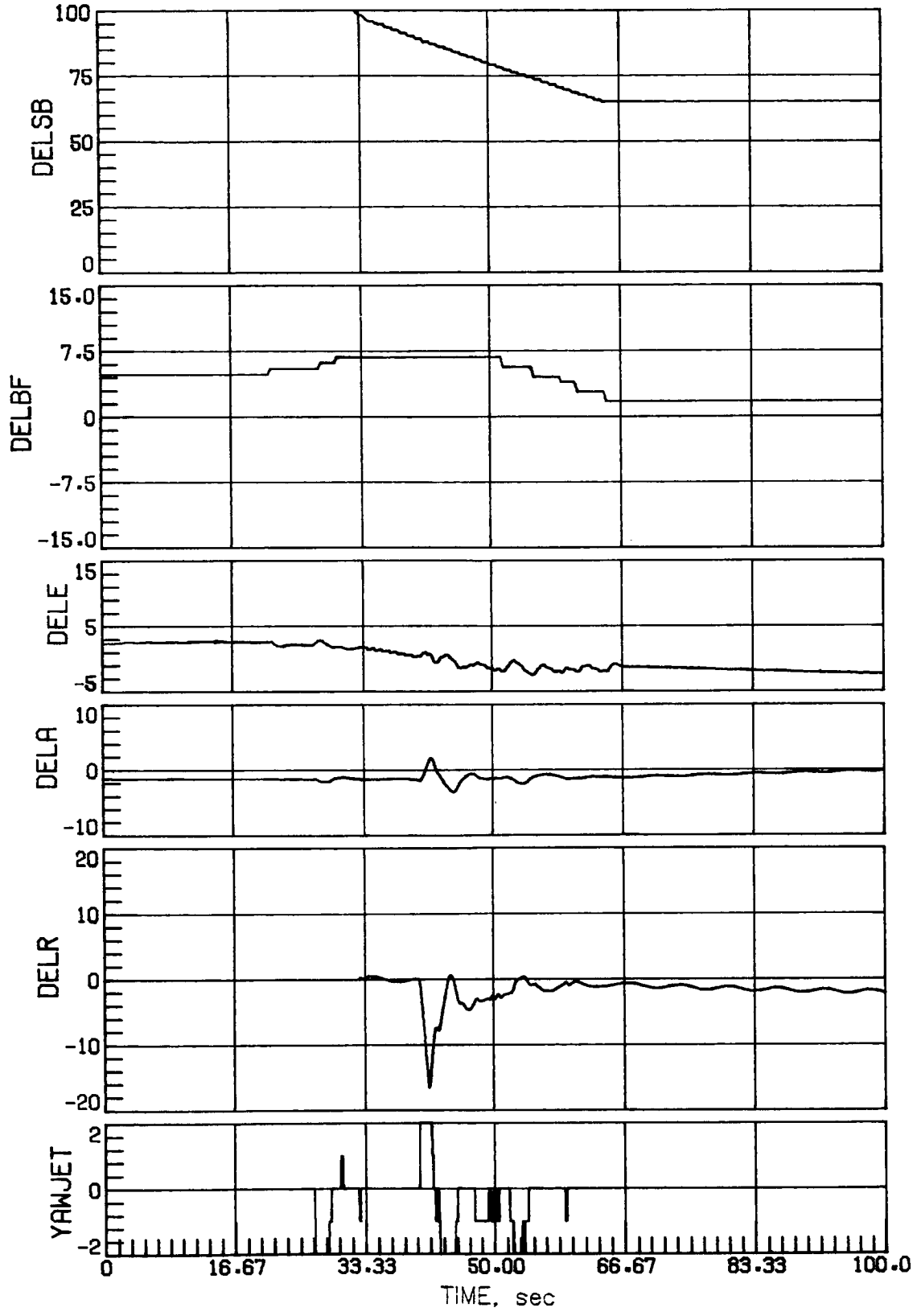

(d) Concluded.

Figure 15.- Continued.

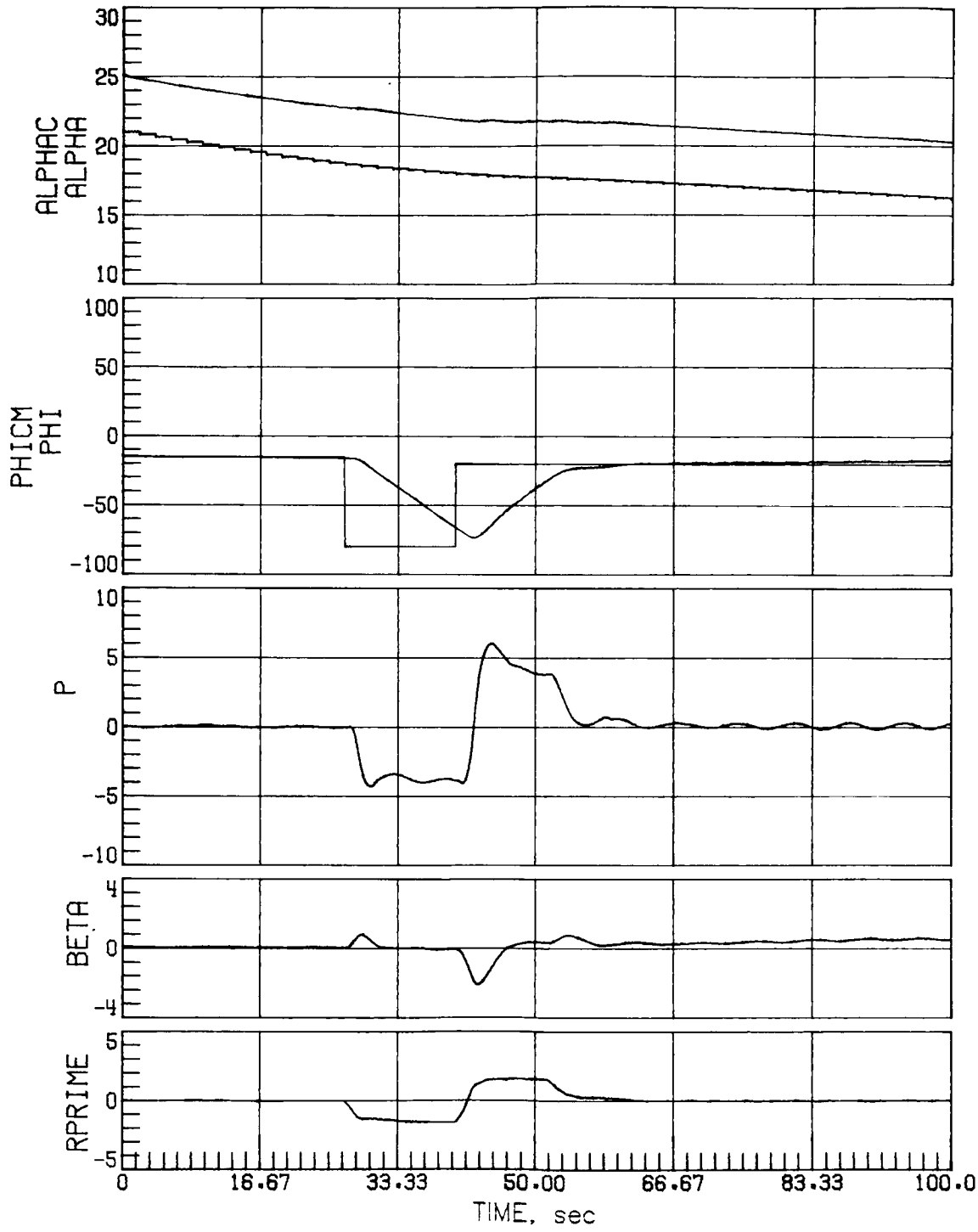

(e) Low-sensed α error of 4°.

Figure 15.- Continued.

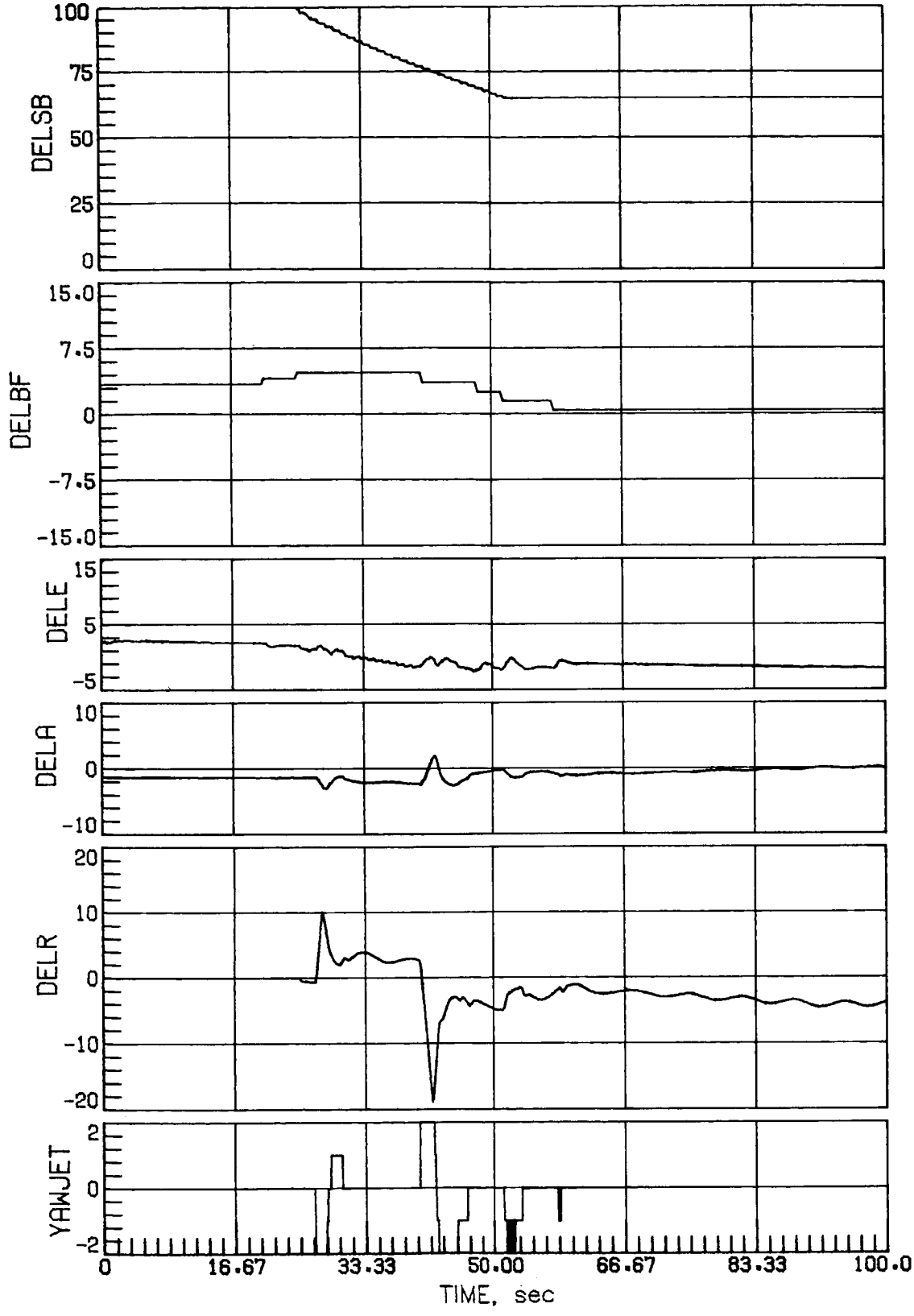

(e) Concluded.

Figure 15.- Continued.

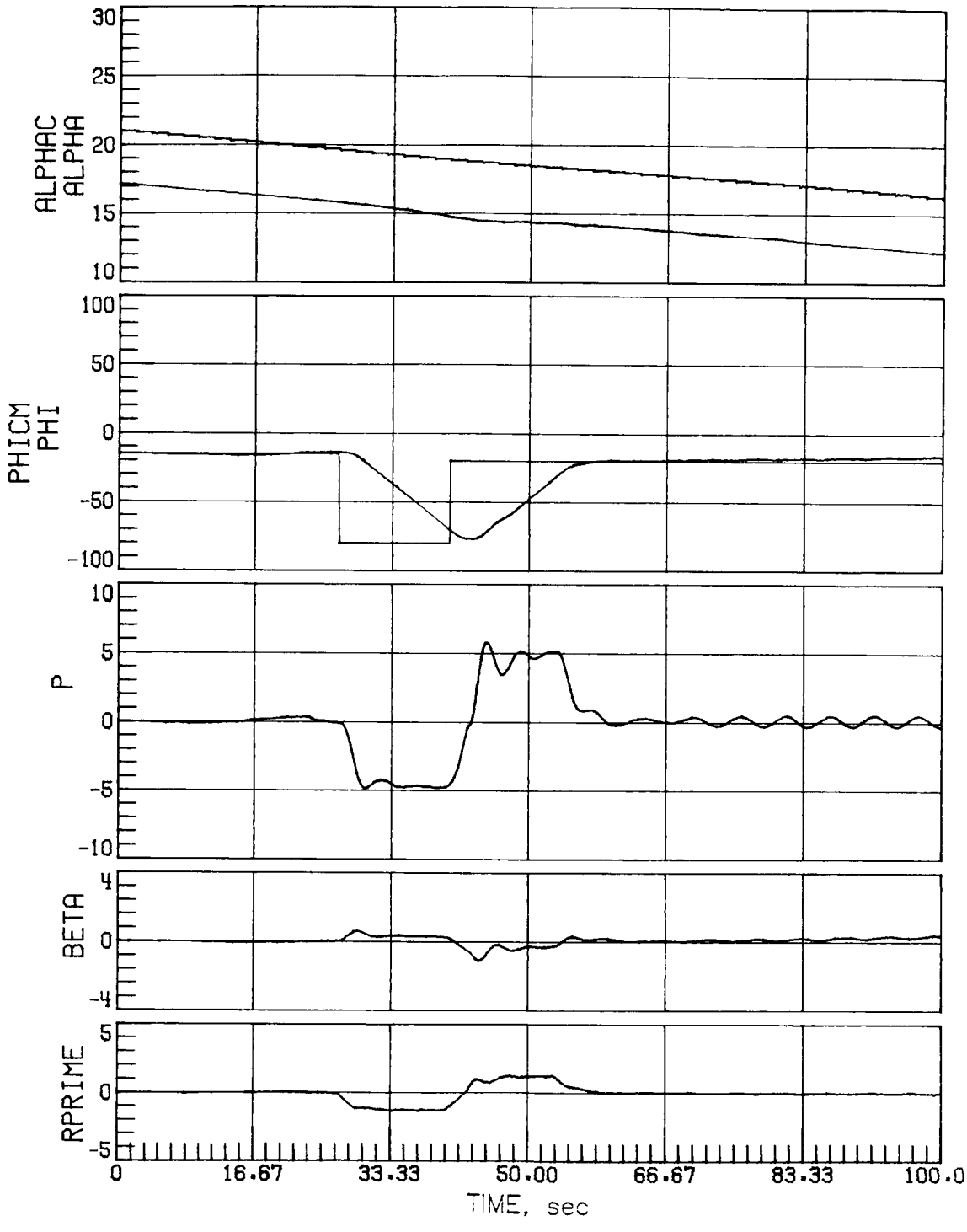

(f) High-sensed α error of 4°.

Figure 15.- Continued.

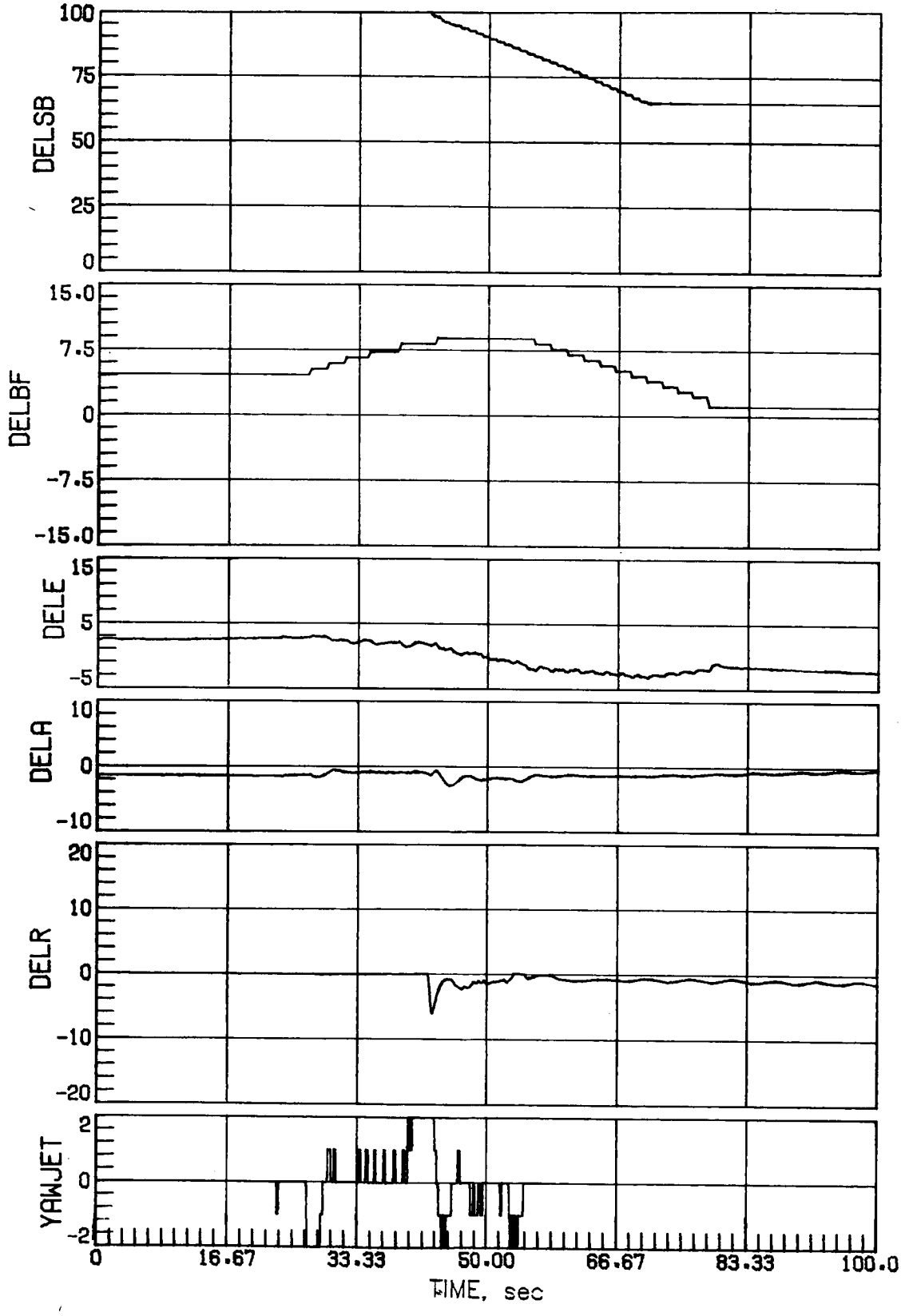

(f) Concluded.

Figure 15.- Concluded.

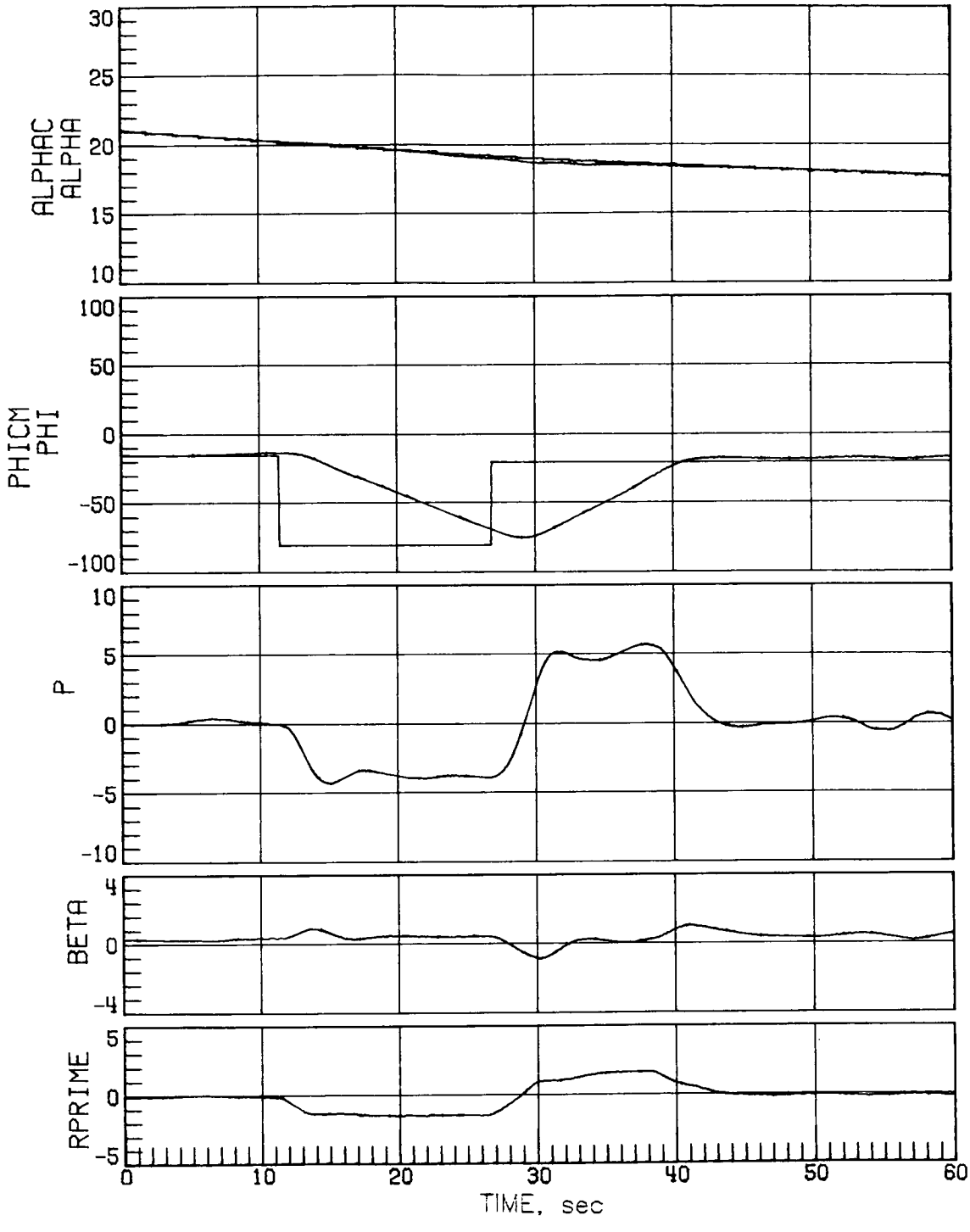

(a) Case 3.

Figure 16.- Mach 5 maneuver performance with off-nominal aerodynamics but with nominal rudder characteristics. Maneuver initiated at different times.

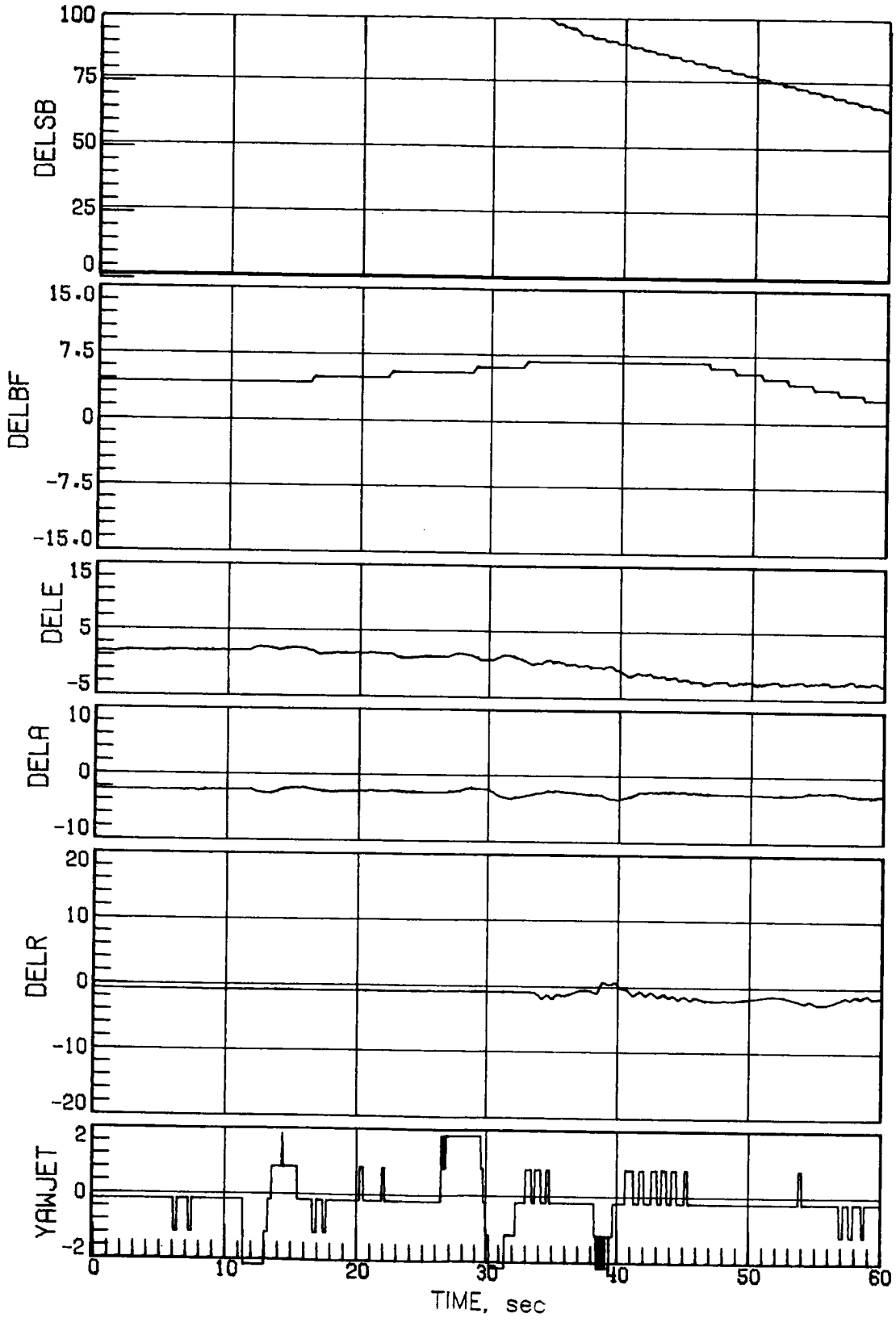

(a) Concluded.

Figure 16.- Continued.

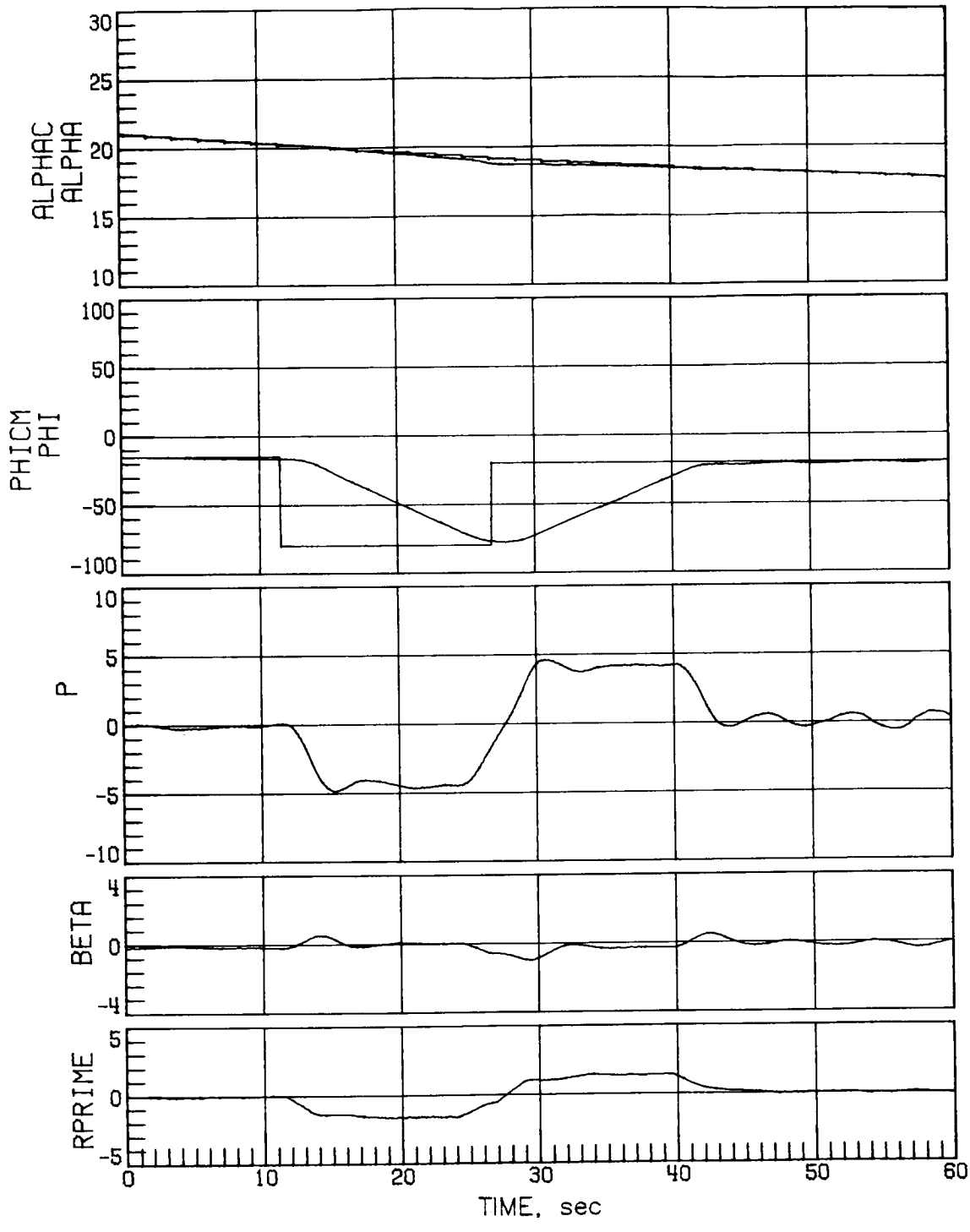

(b) Case 7.

Figure 16.- Continued.

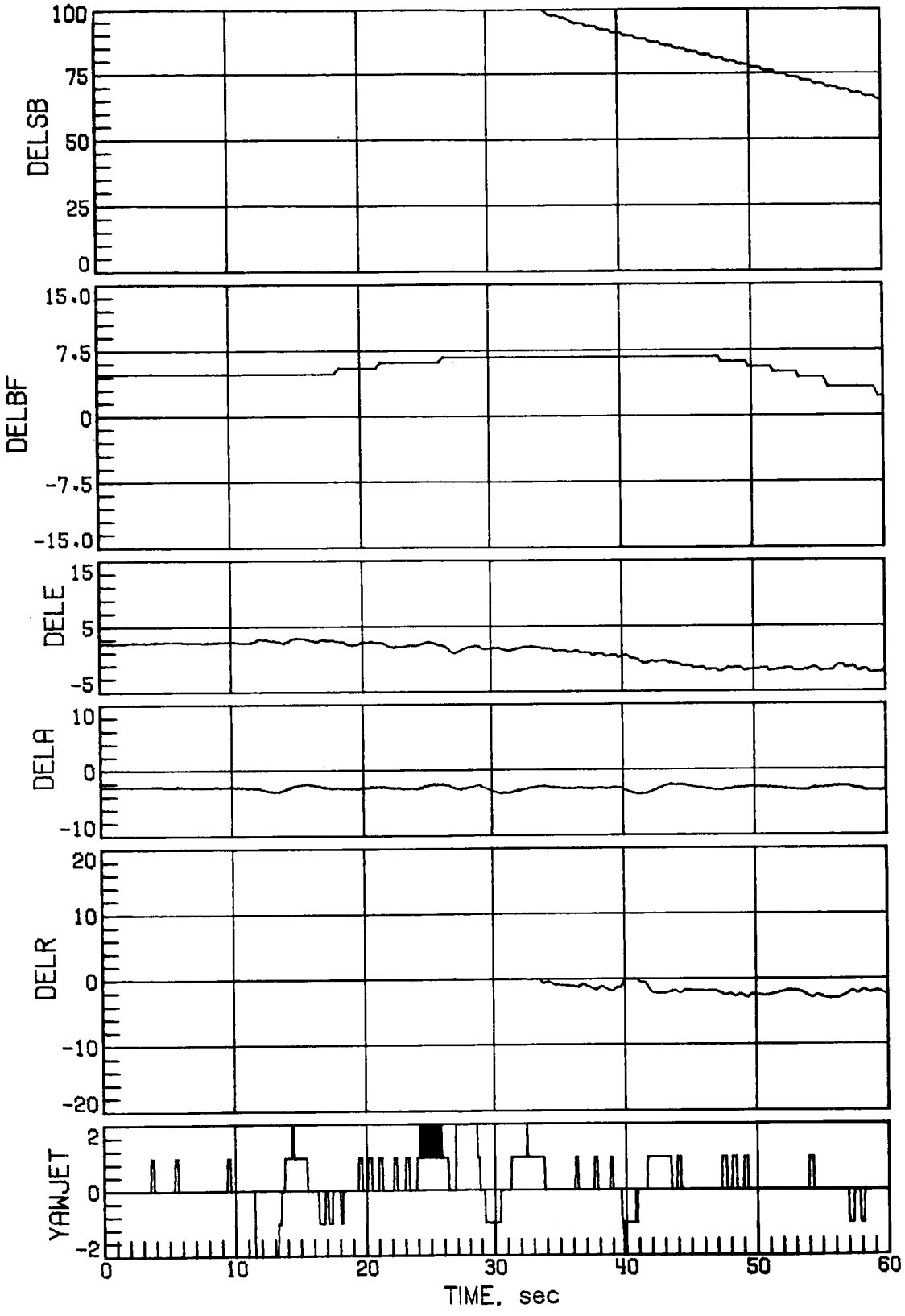

(b) Concluded.

Figure 16.- Continued.

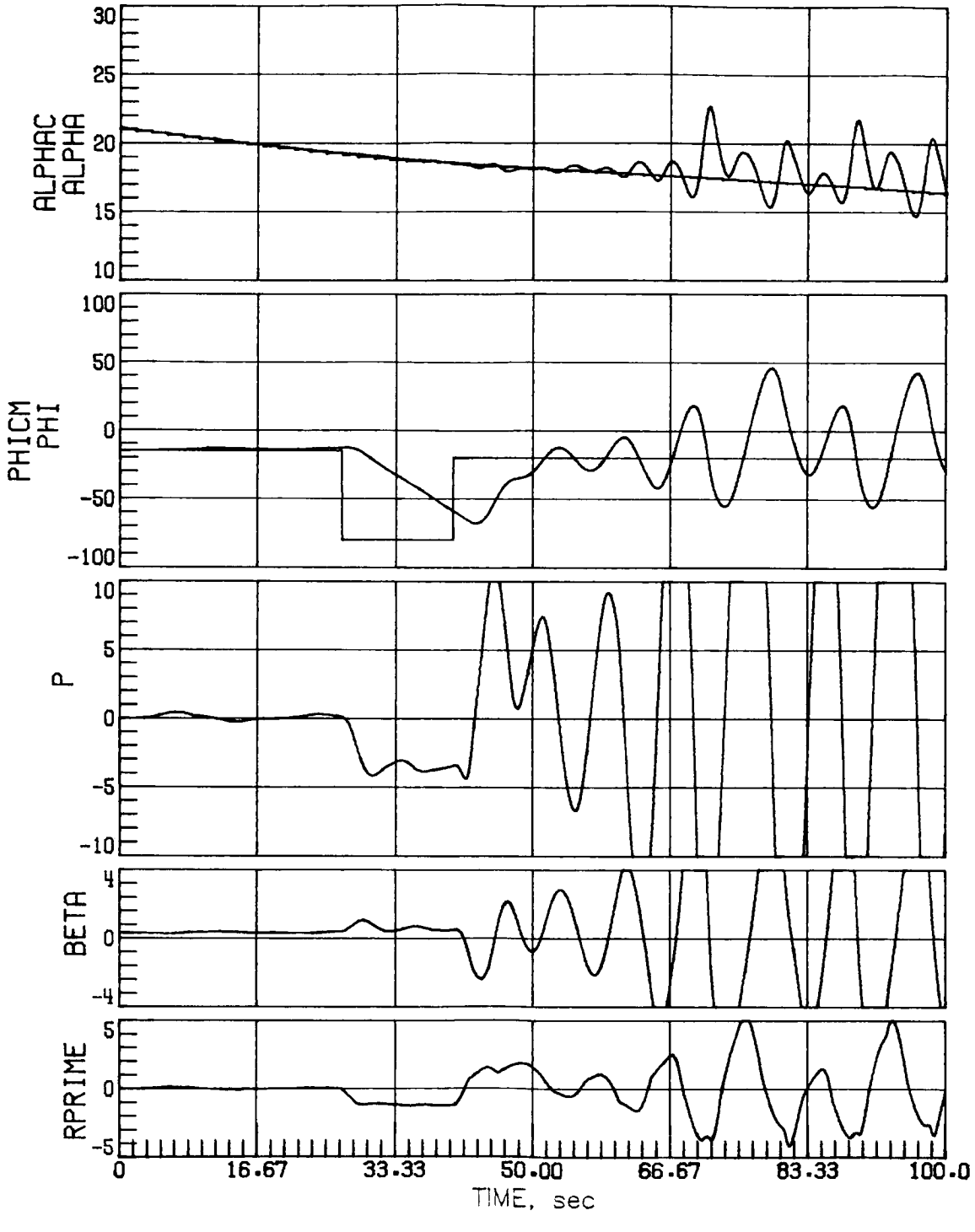

(c) Case 3.

Figure 16.- Continued.

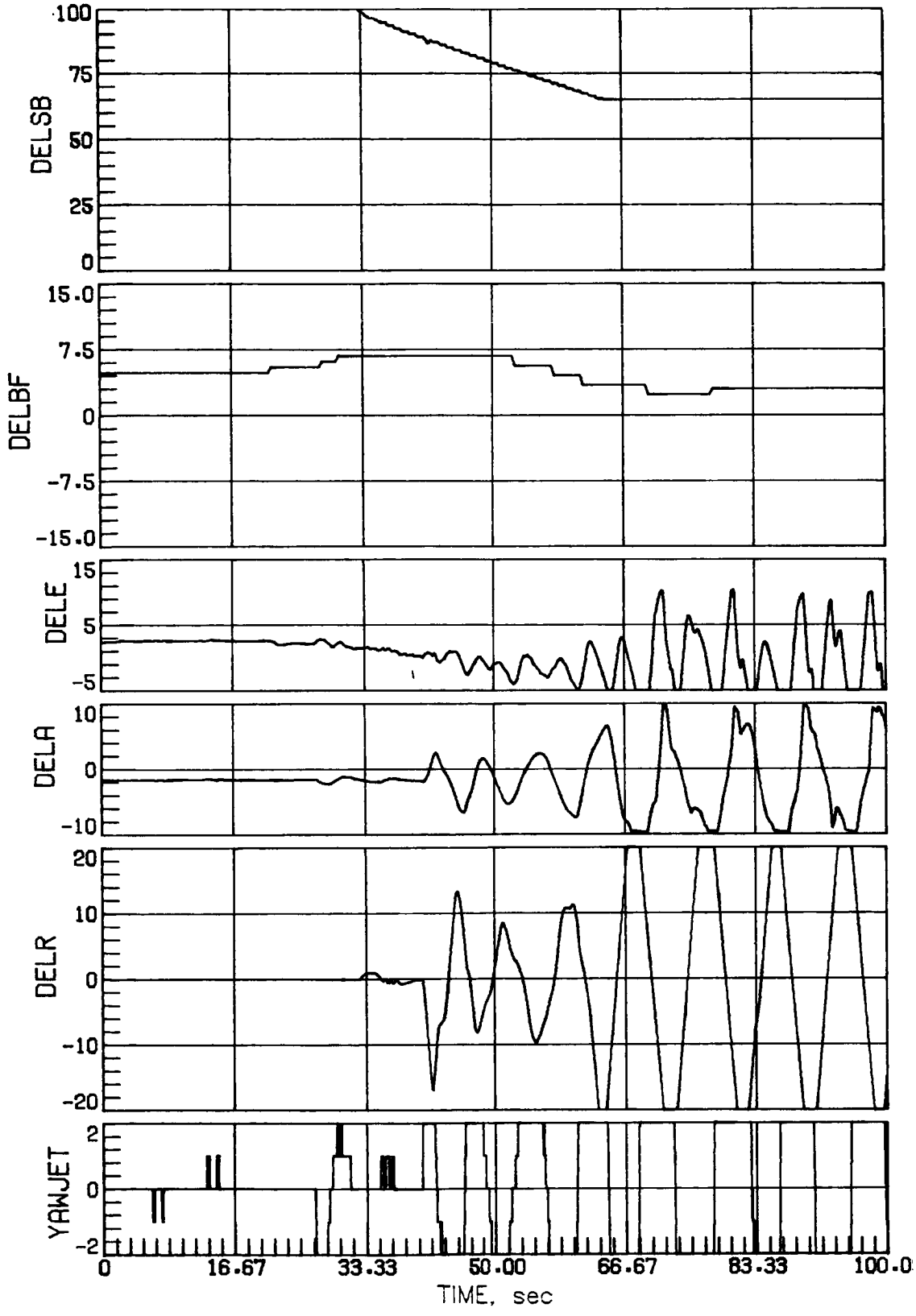

(c) Concluded.

Figure 16.- Continued.

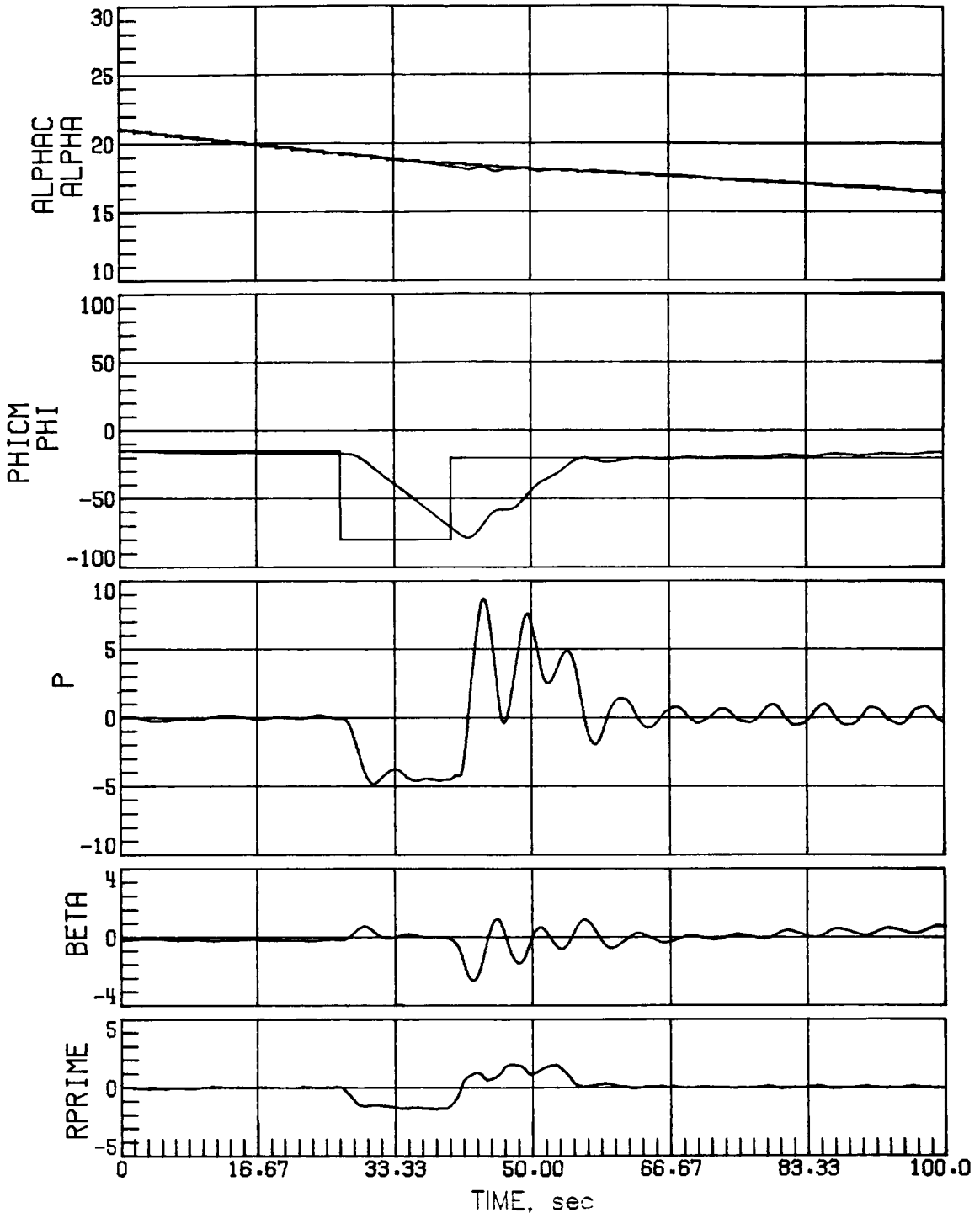

(d) Case 7.

Figure 16.- Continued.

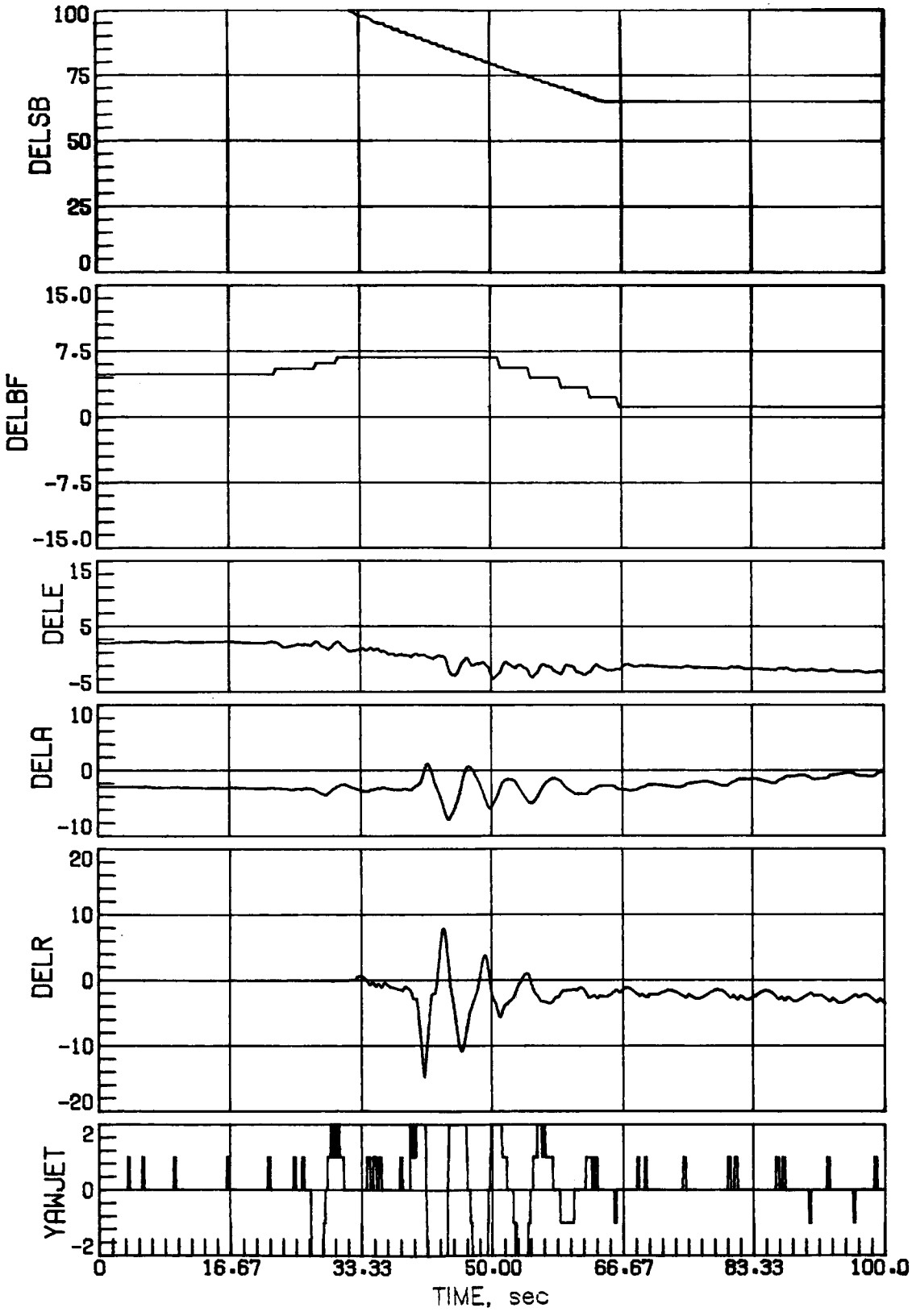

(d) Concluded.

Figure 16.- Concluded.

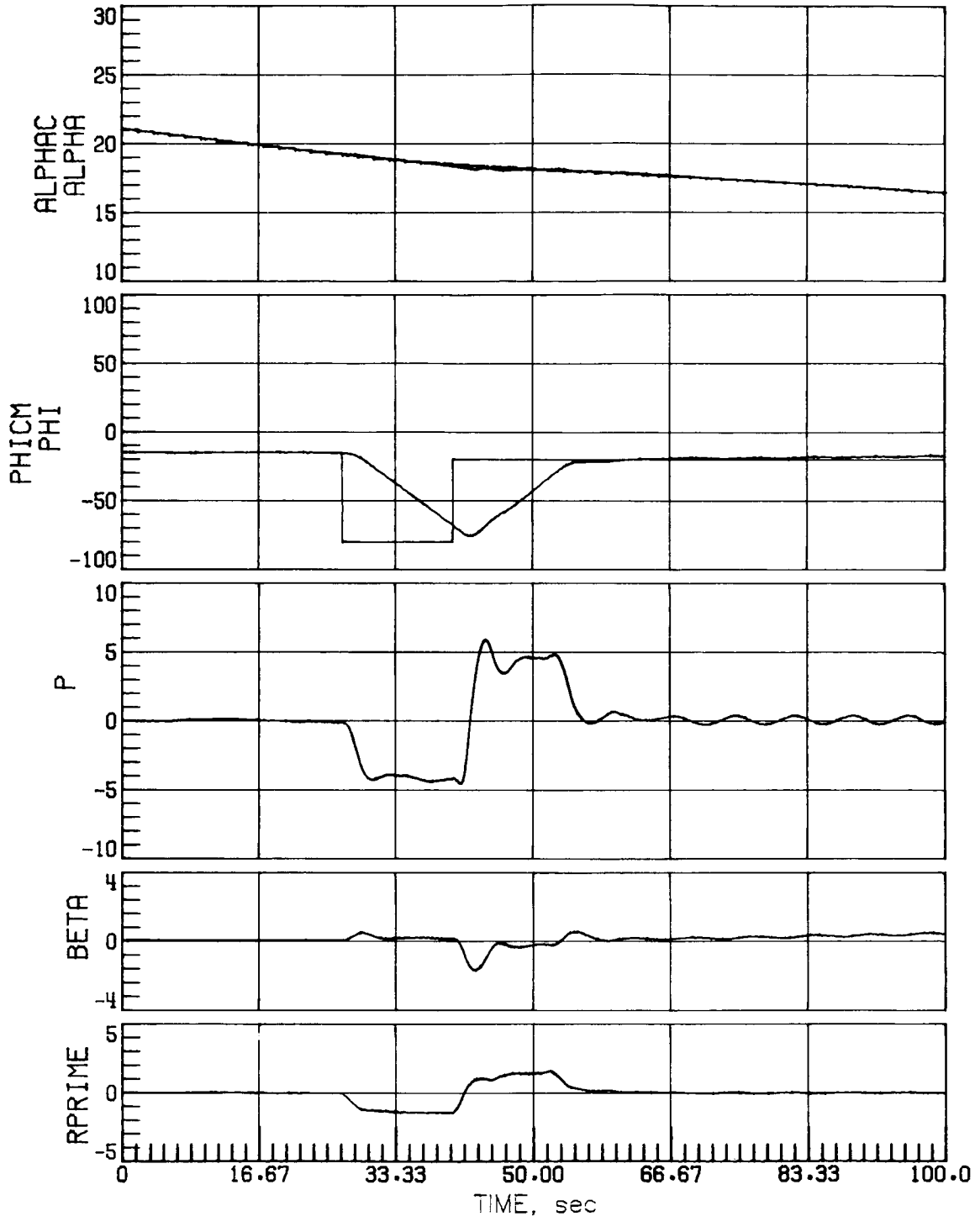

(a) Nominal aerodynamics.

Figure 17.- Mach 5 maneuver performance with nominal rudder characteristics and GDRC = 750. Maneuver initiated at different times.

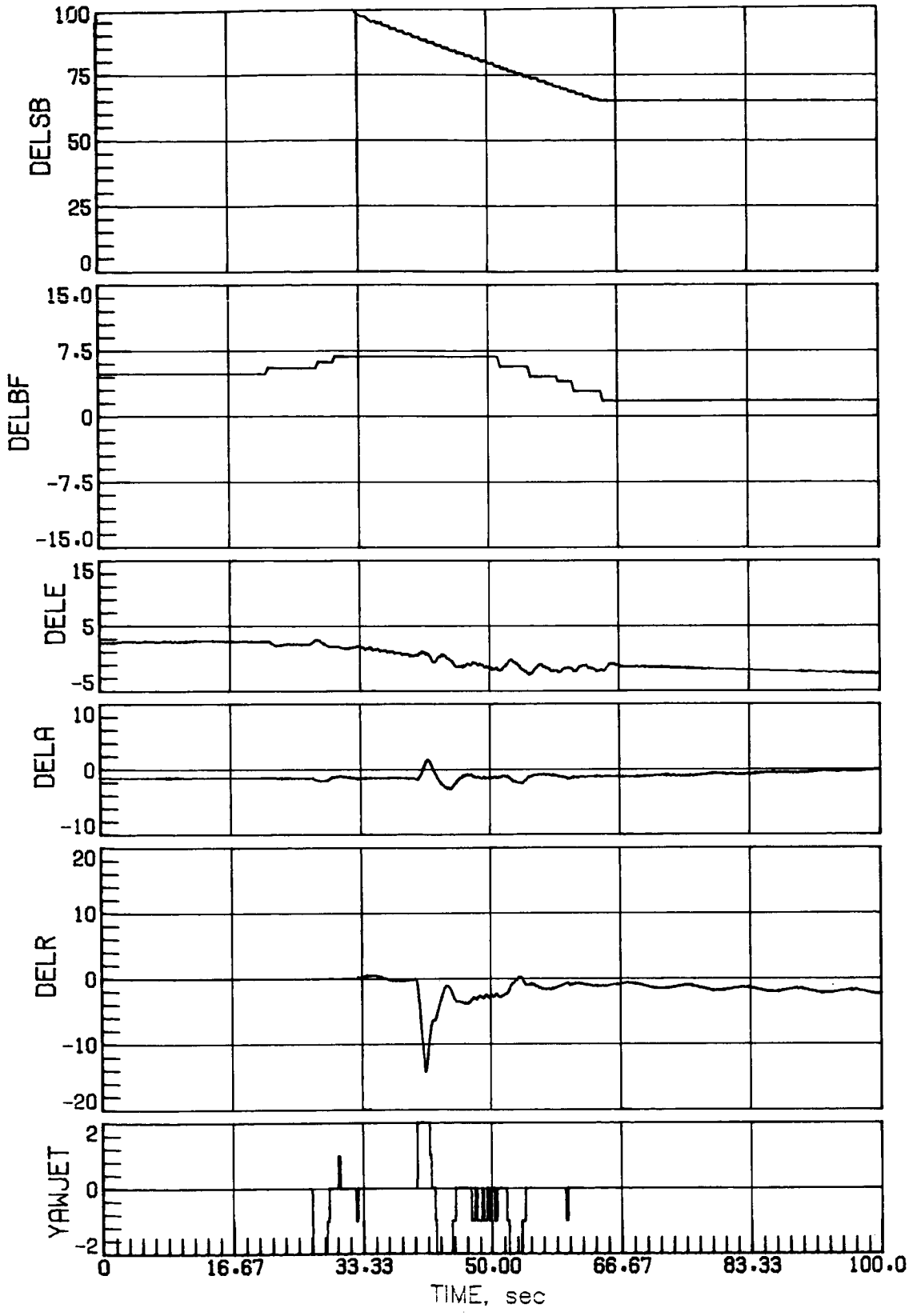

(a) Concluded.

Figure 17.- Continued.

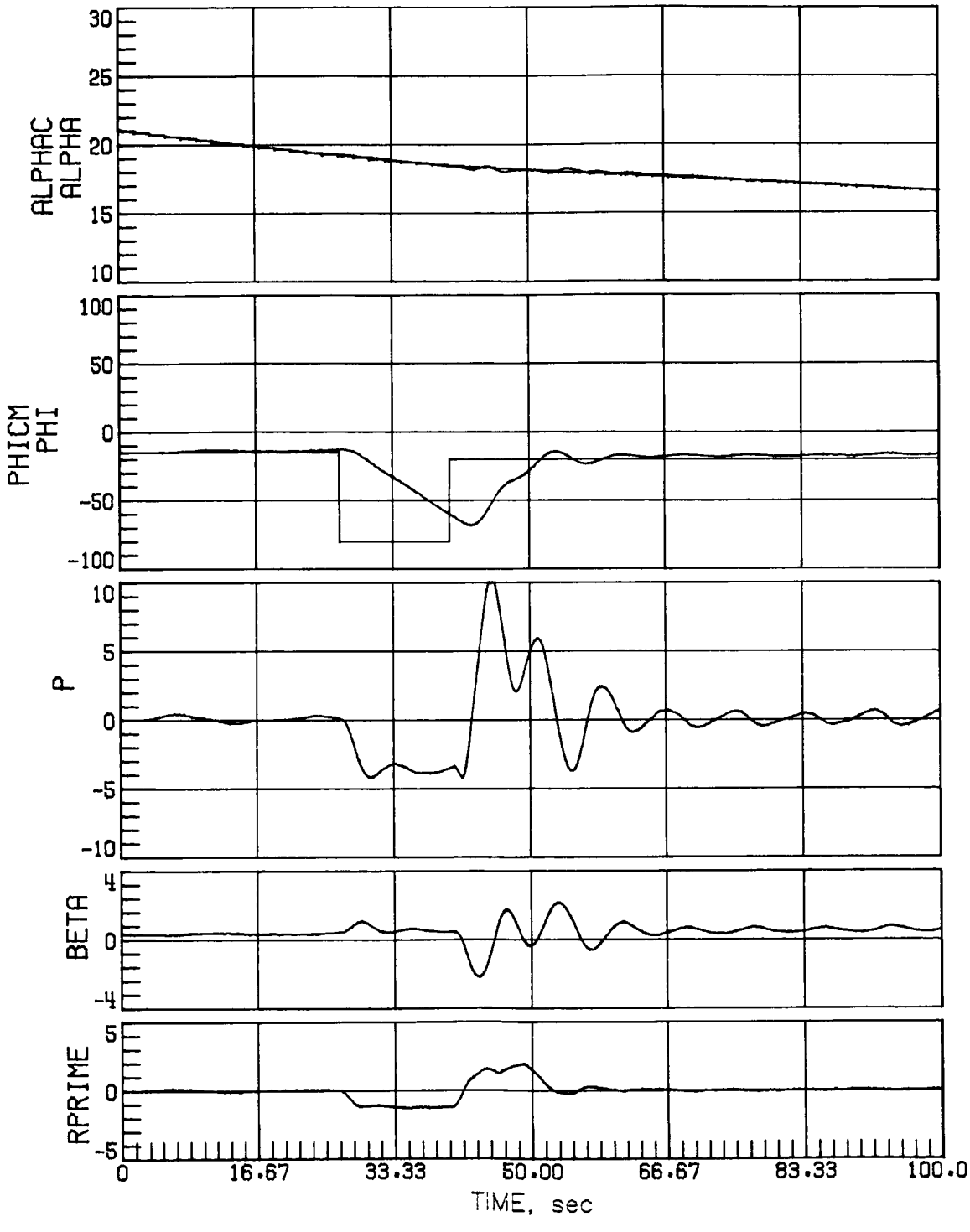

(b) Case 3.

Figure 17.- Continued.

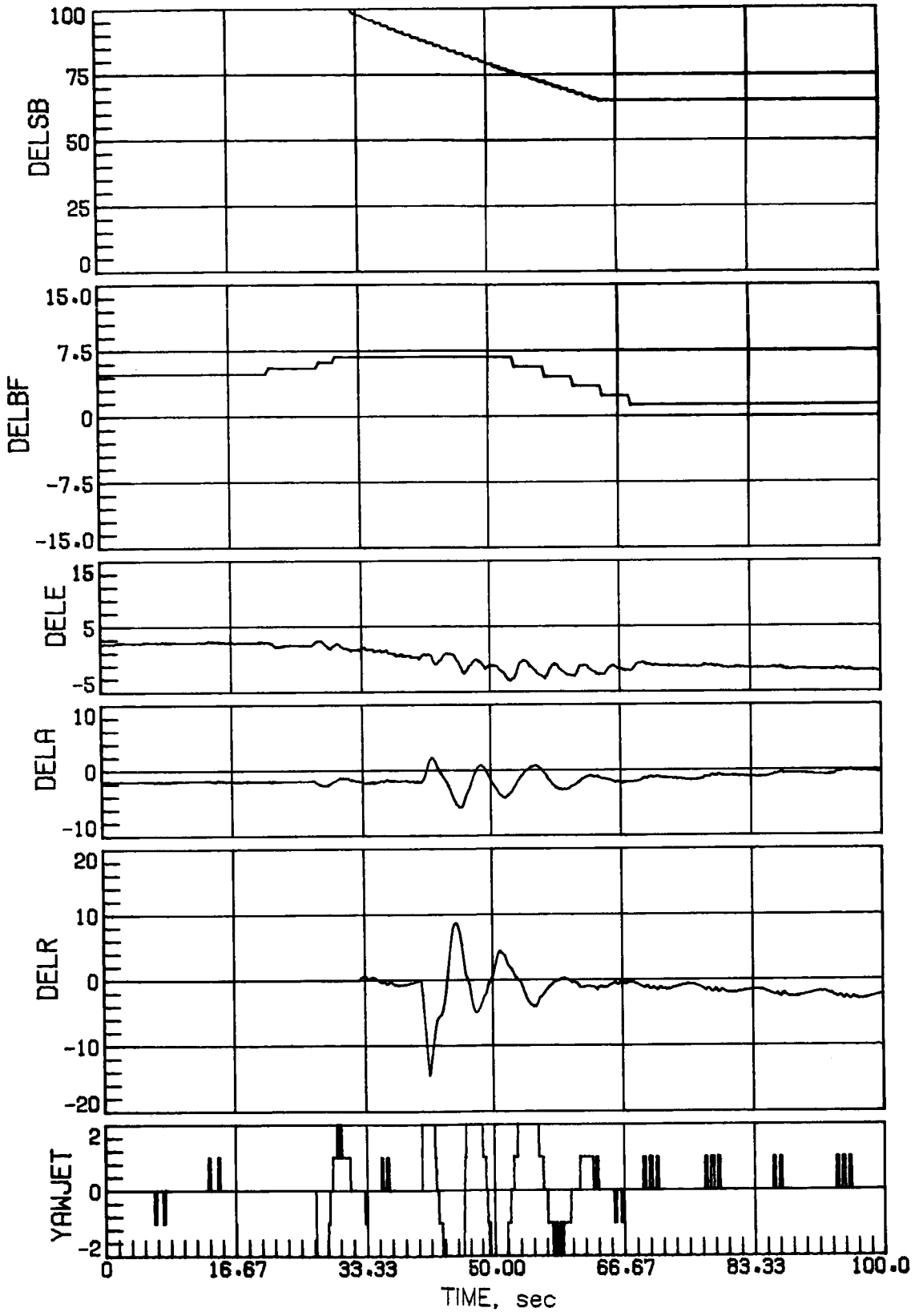

(b) Concluded.

Figure 17.- Continued.

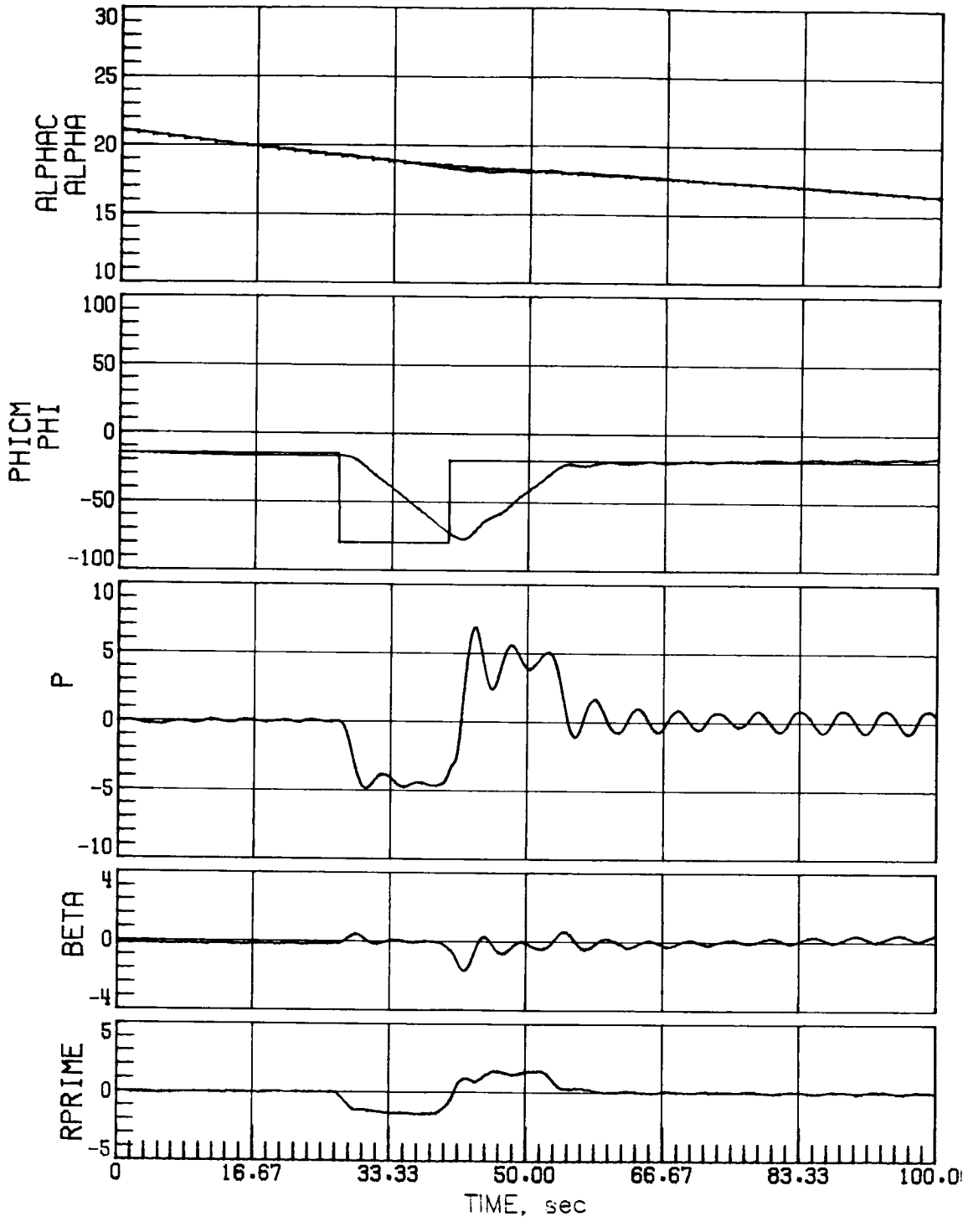

(c) Case 5.

Figure 17.- Continued.

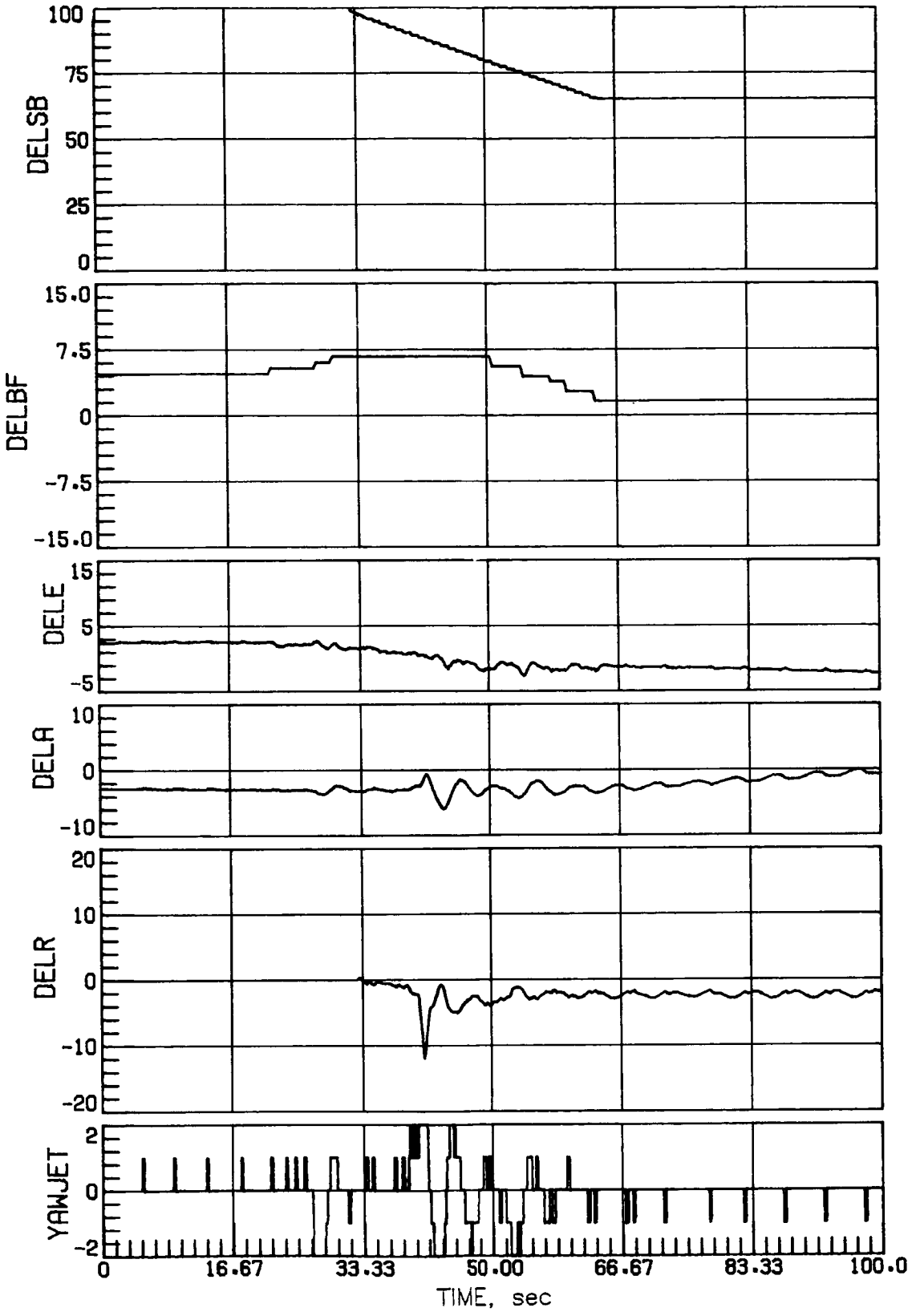

(c) Concluded.

Figure 17.- Continued.

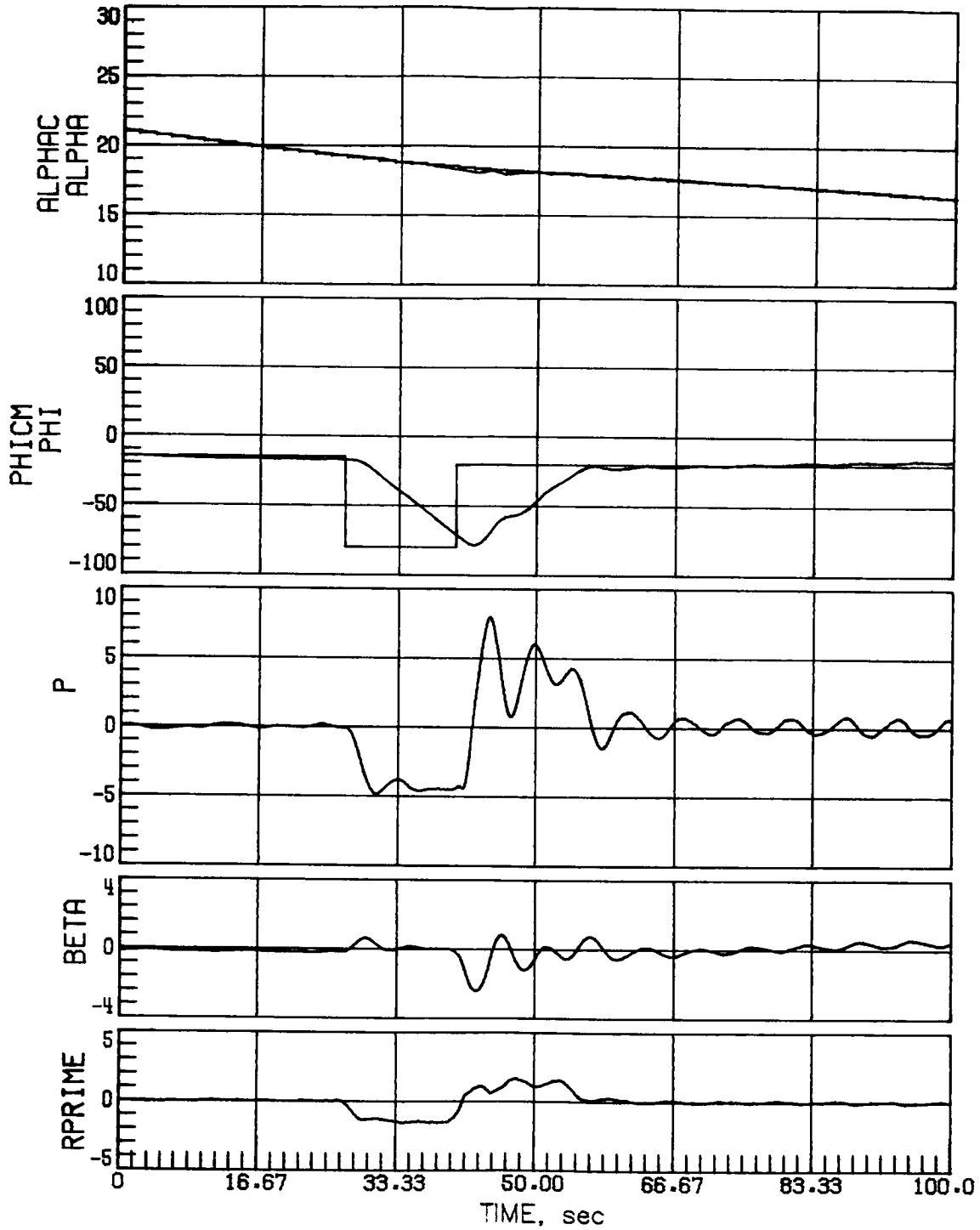

(d) Case 7.

Figure 17.- Continued.

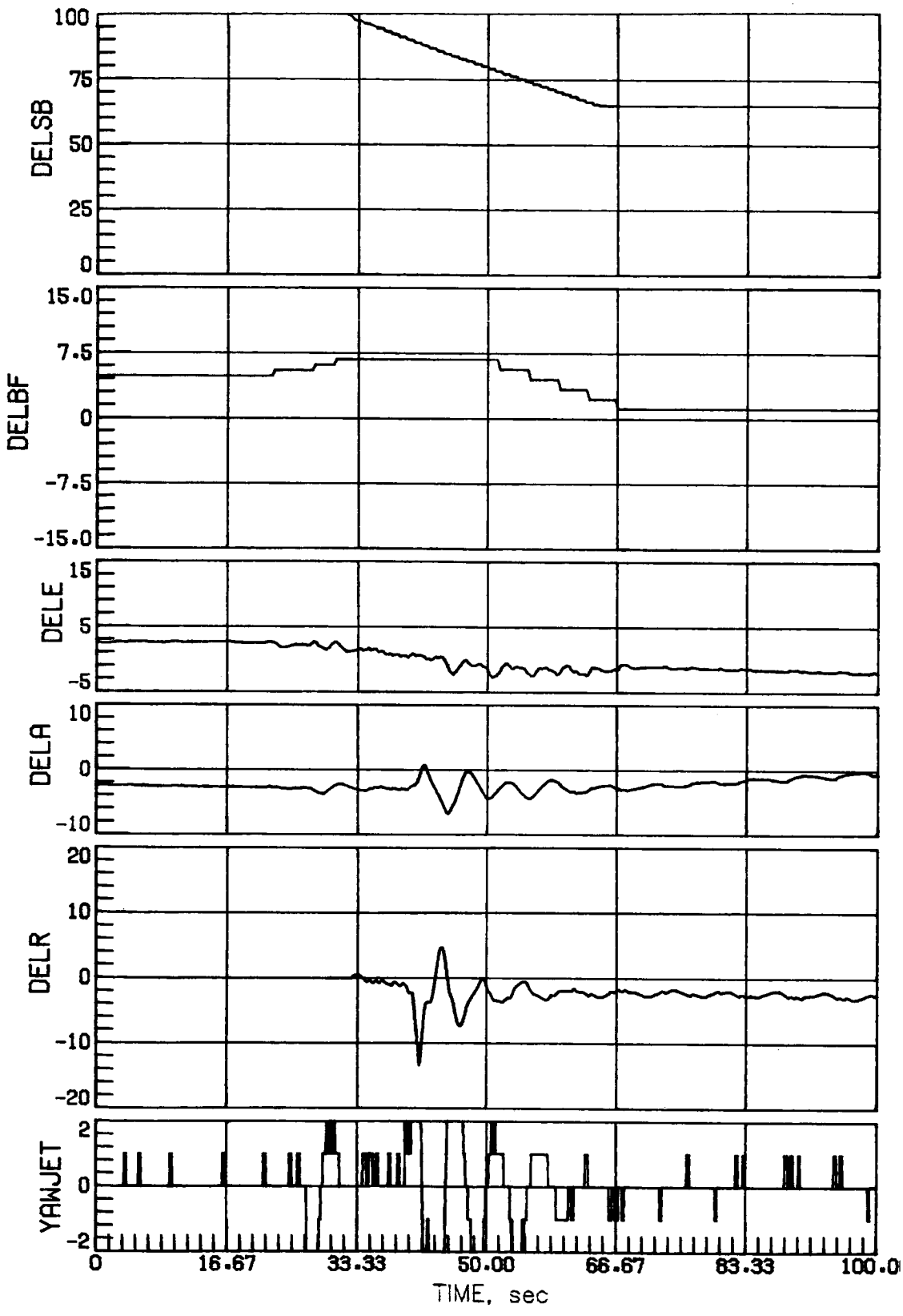

(d) Concluded.

Figure 17.- Continued.

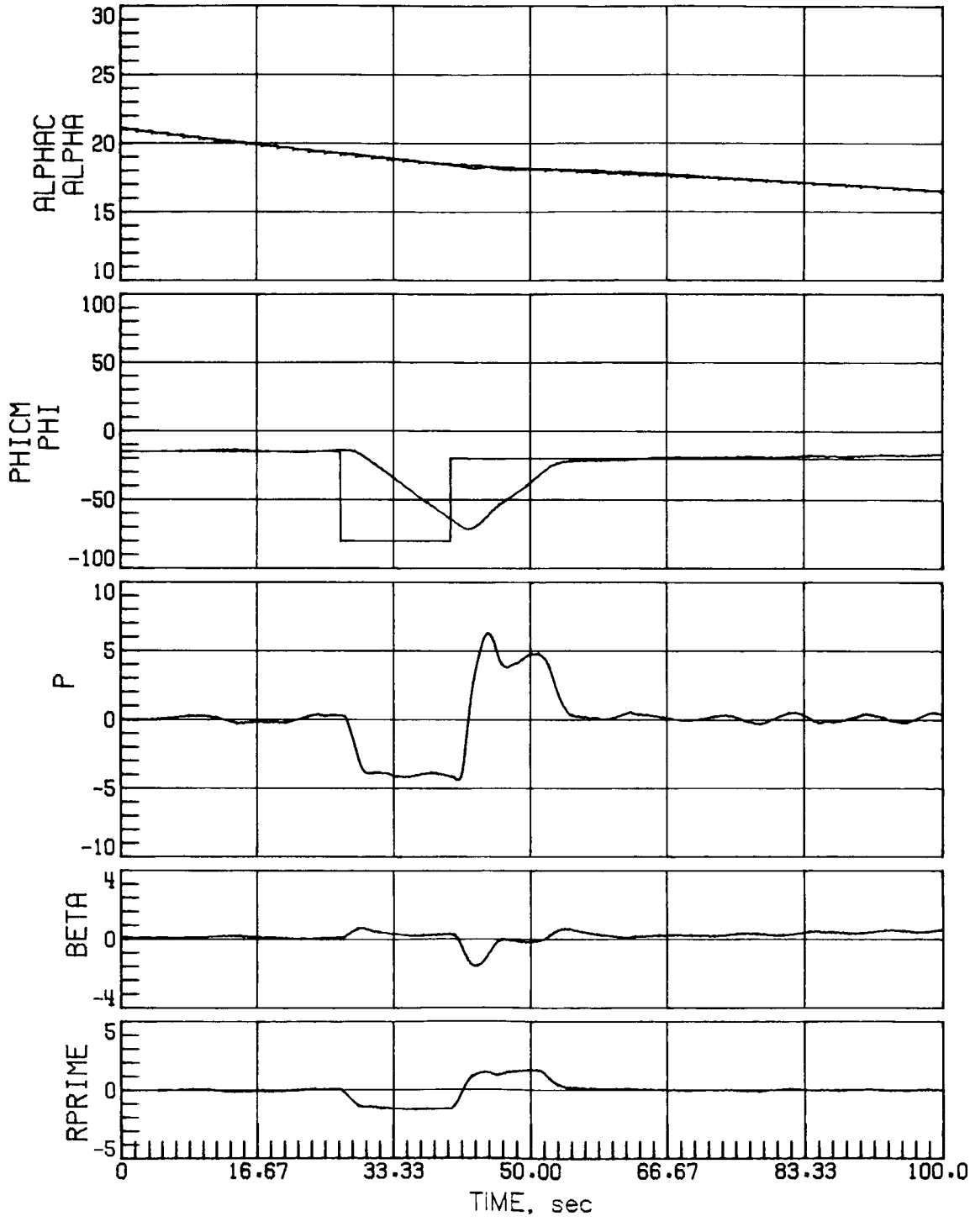

(e) Case 11.

Figure 17.- Continued.

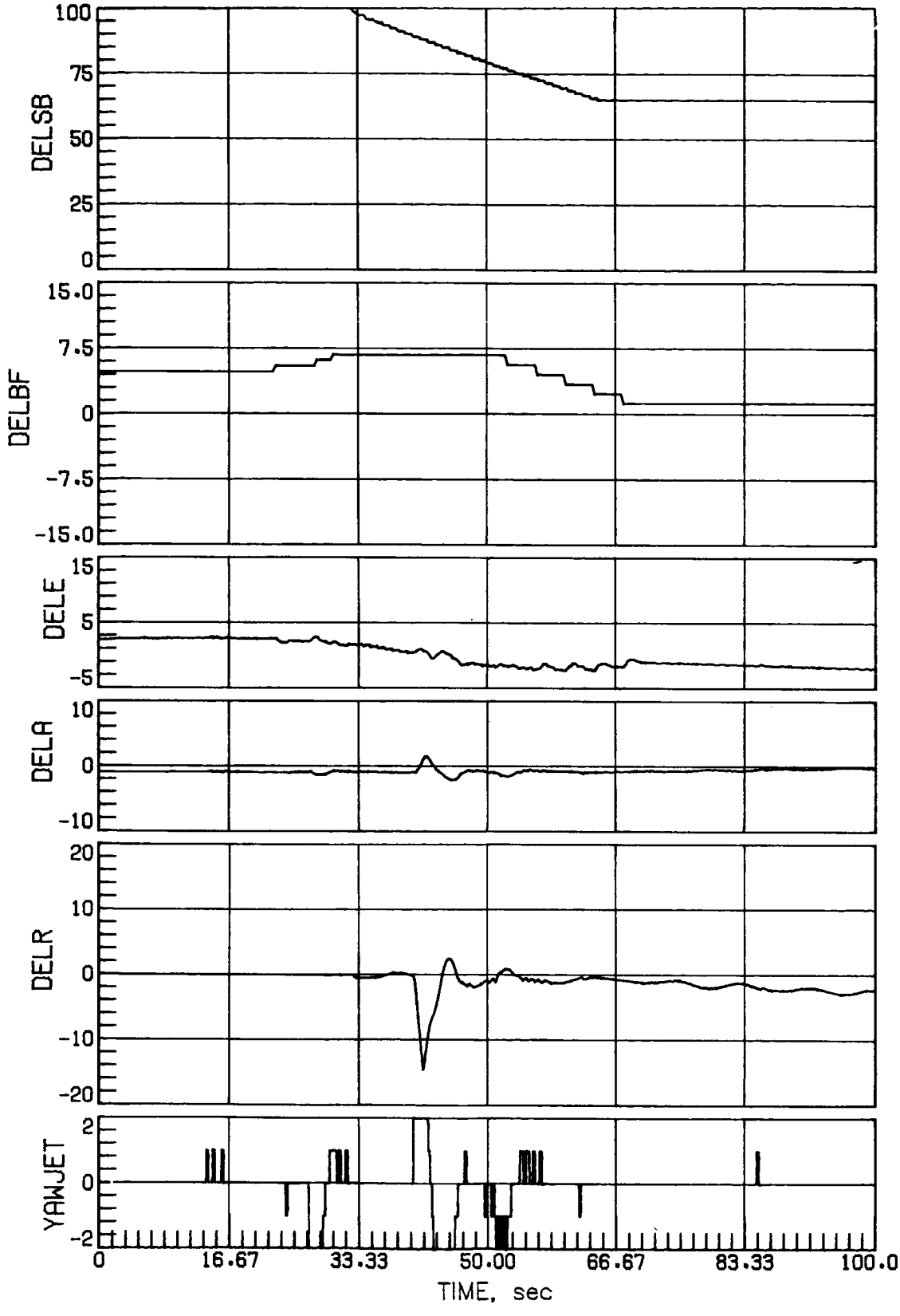

(e) Concluded.

Figure 17.- Continued.

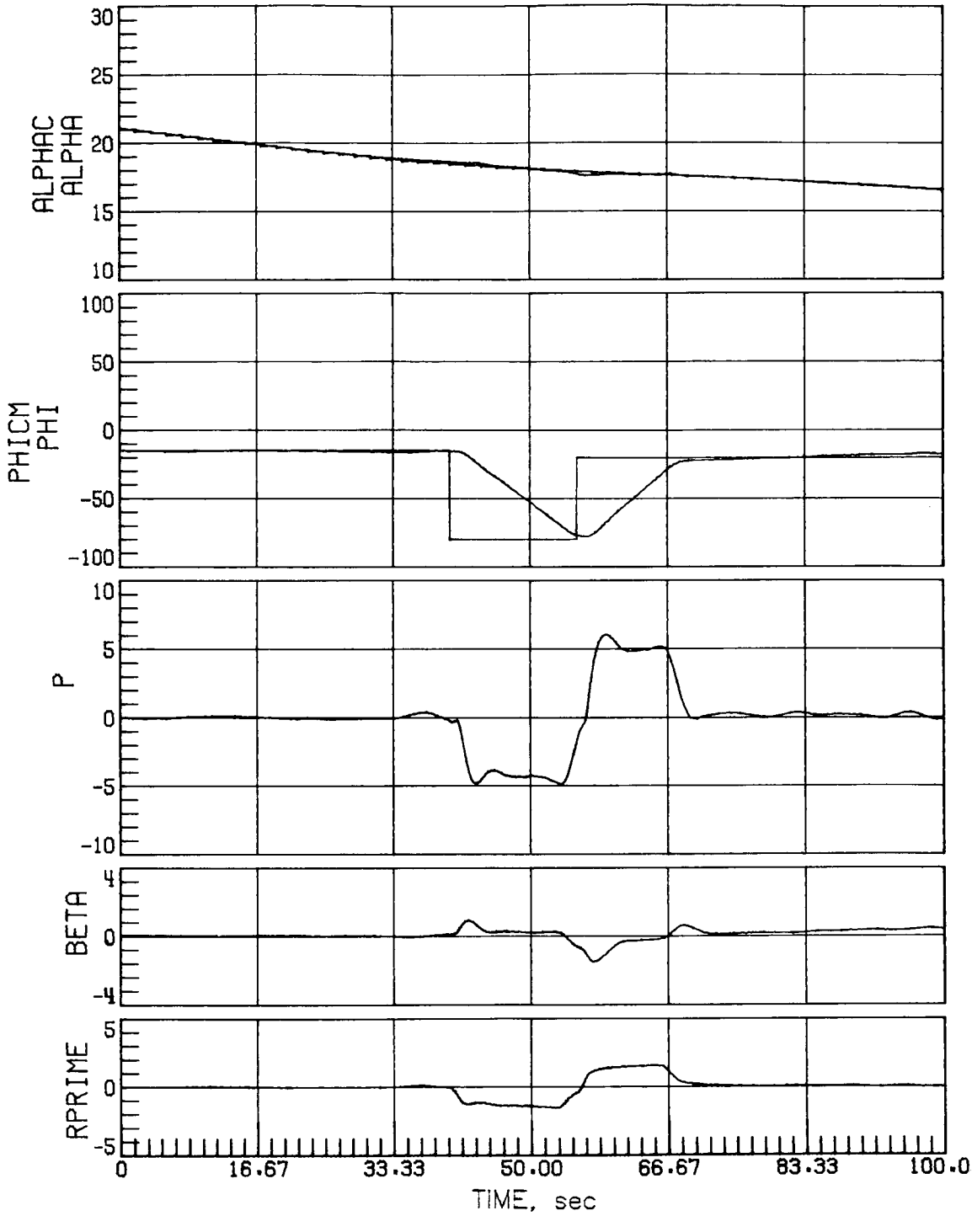

(f) Nominal aerodynamics.

Figure 17.- Continued.

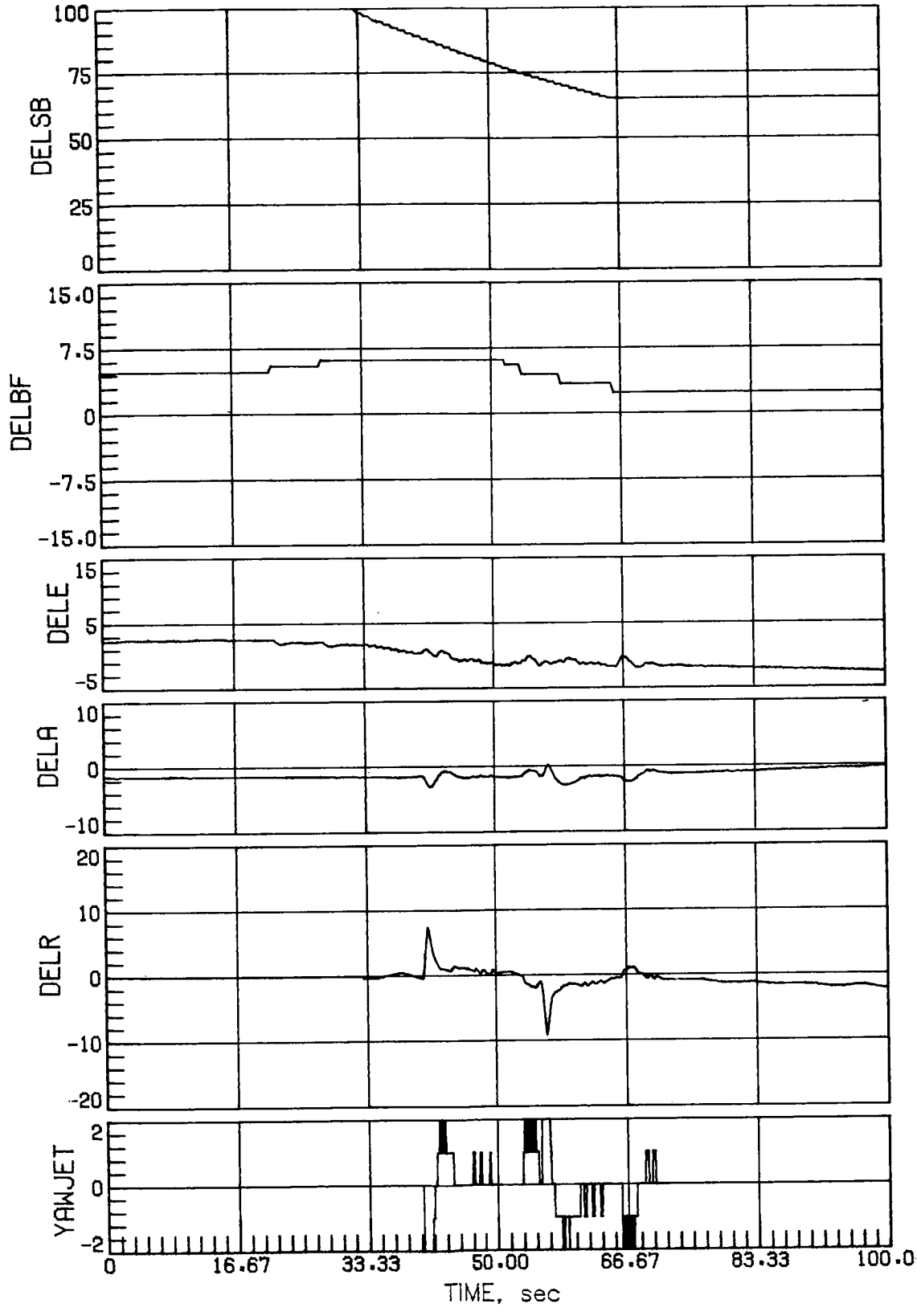

(f) Concluded.

Figure 17.- Continued.

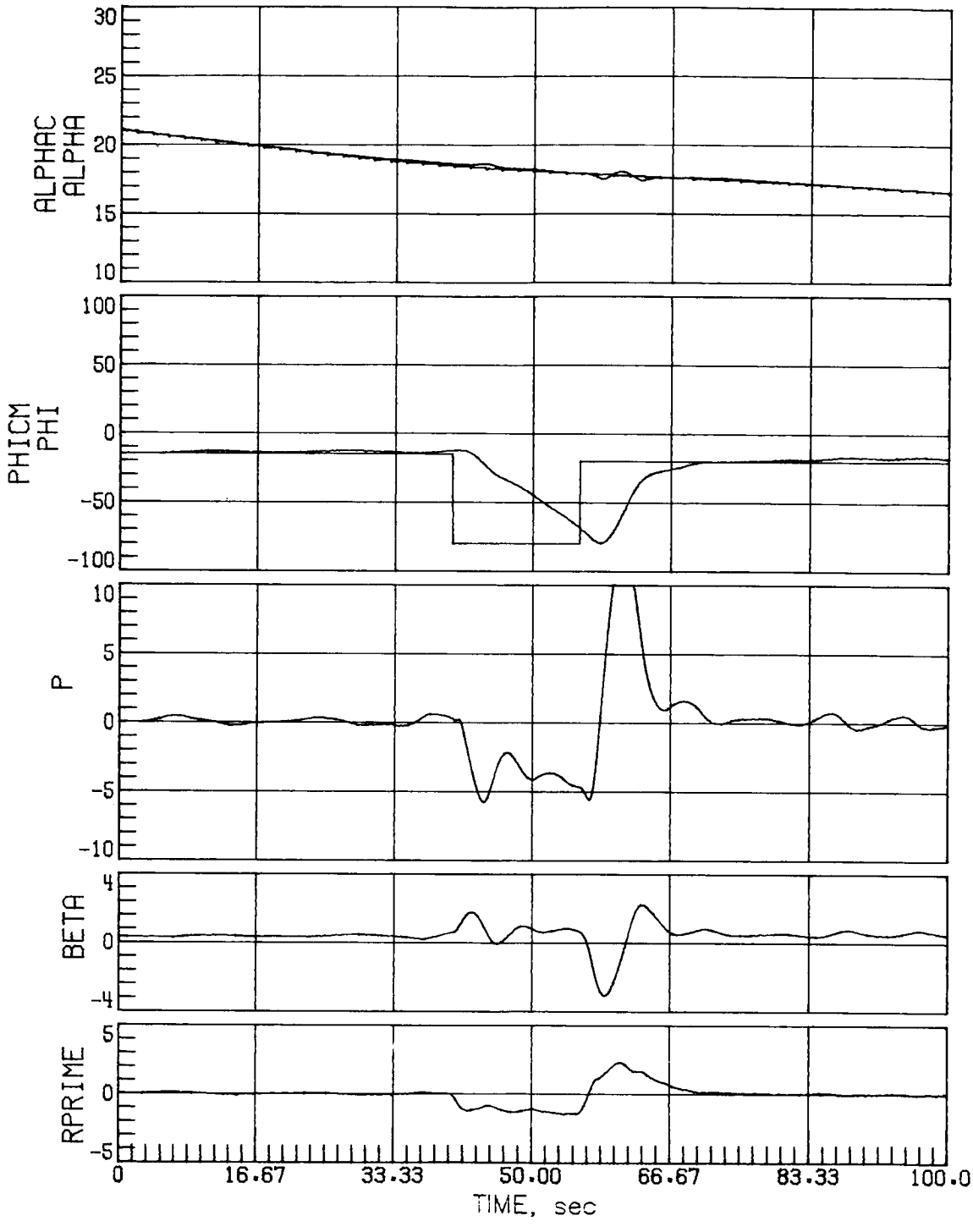

(g) Case 3.

Figure 17.- Continued.

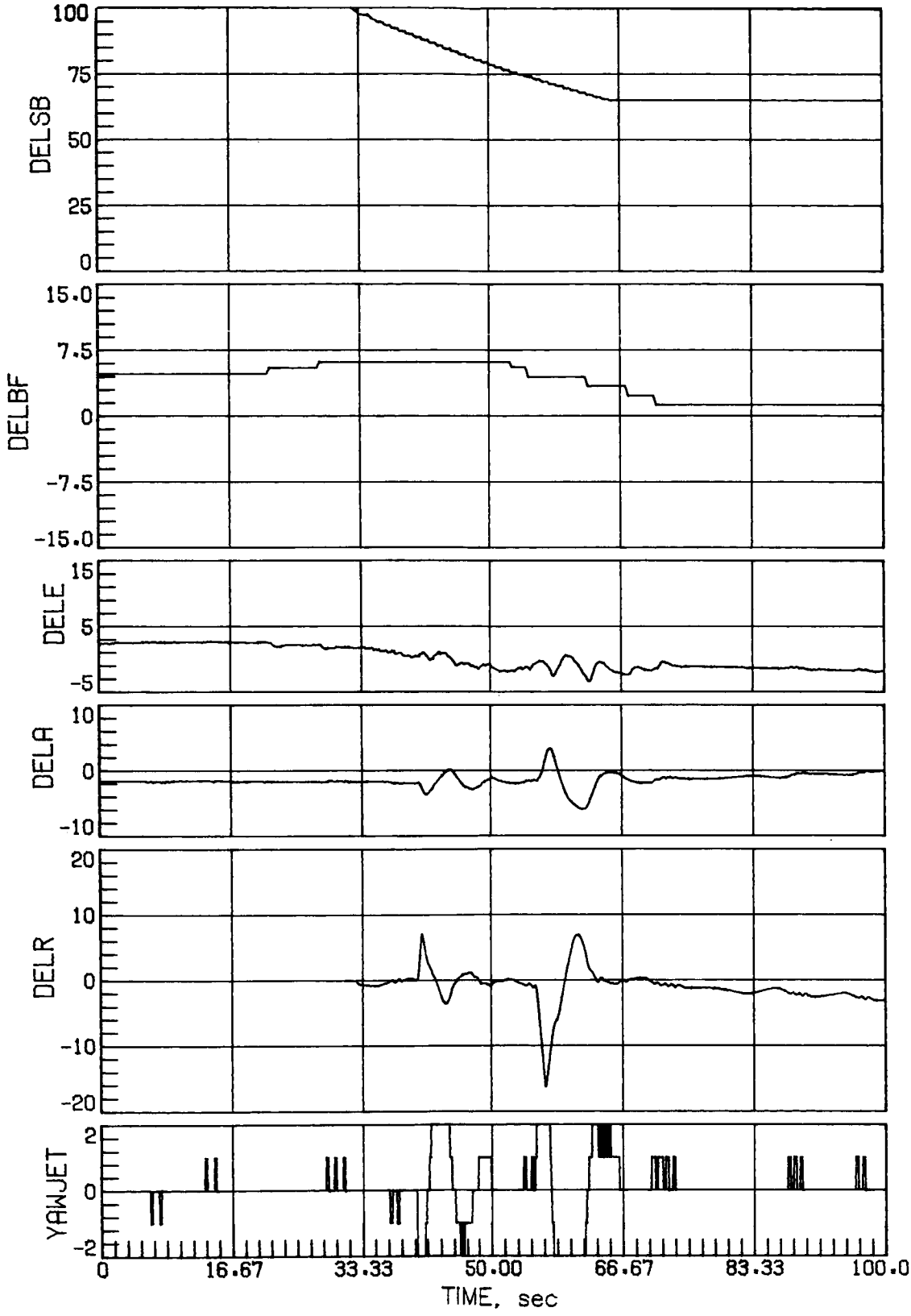

(g) Concluded.

Figure 17.- Continued.

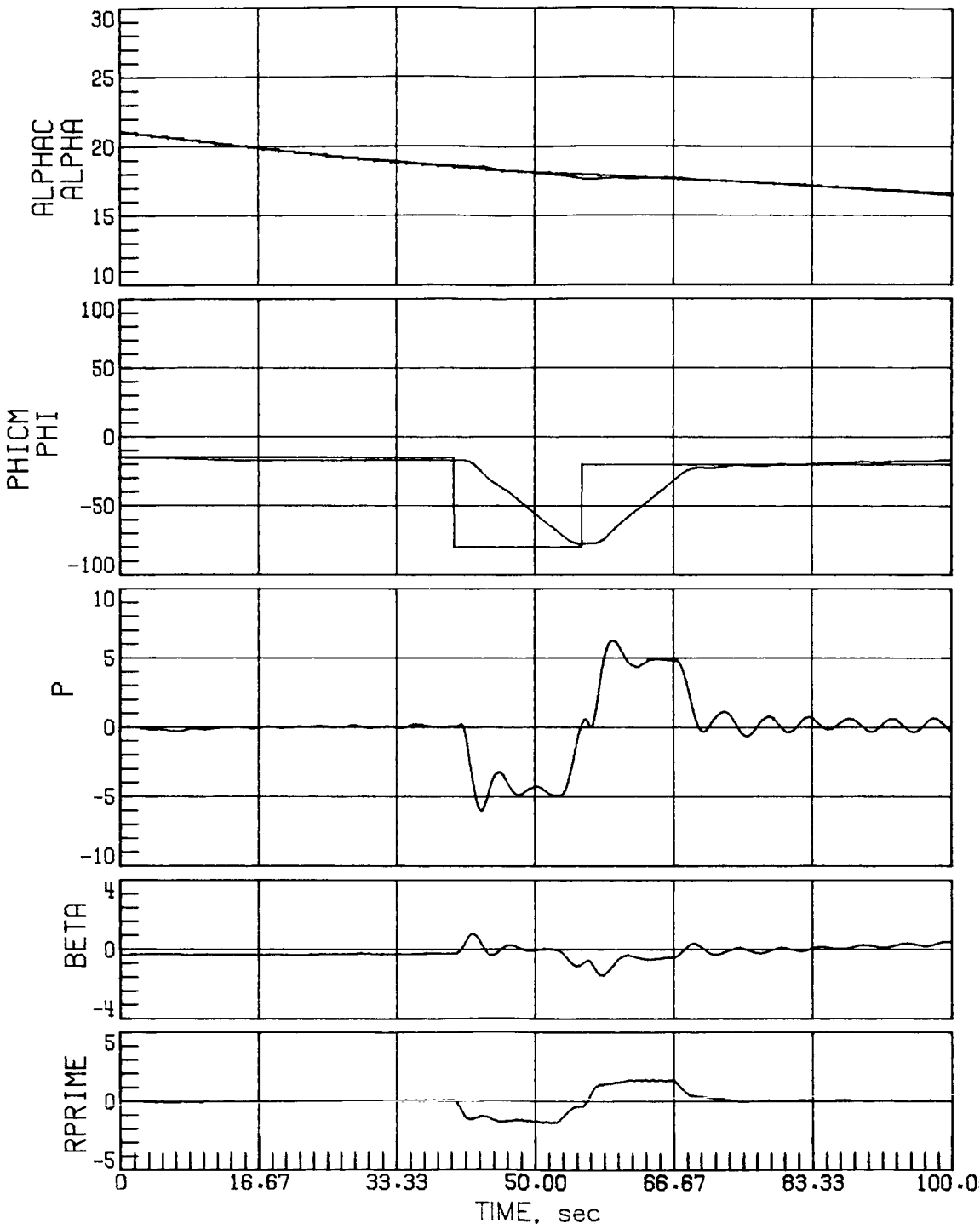

(h) Case 6.

Figure 17.- Continued.

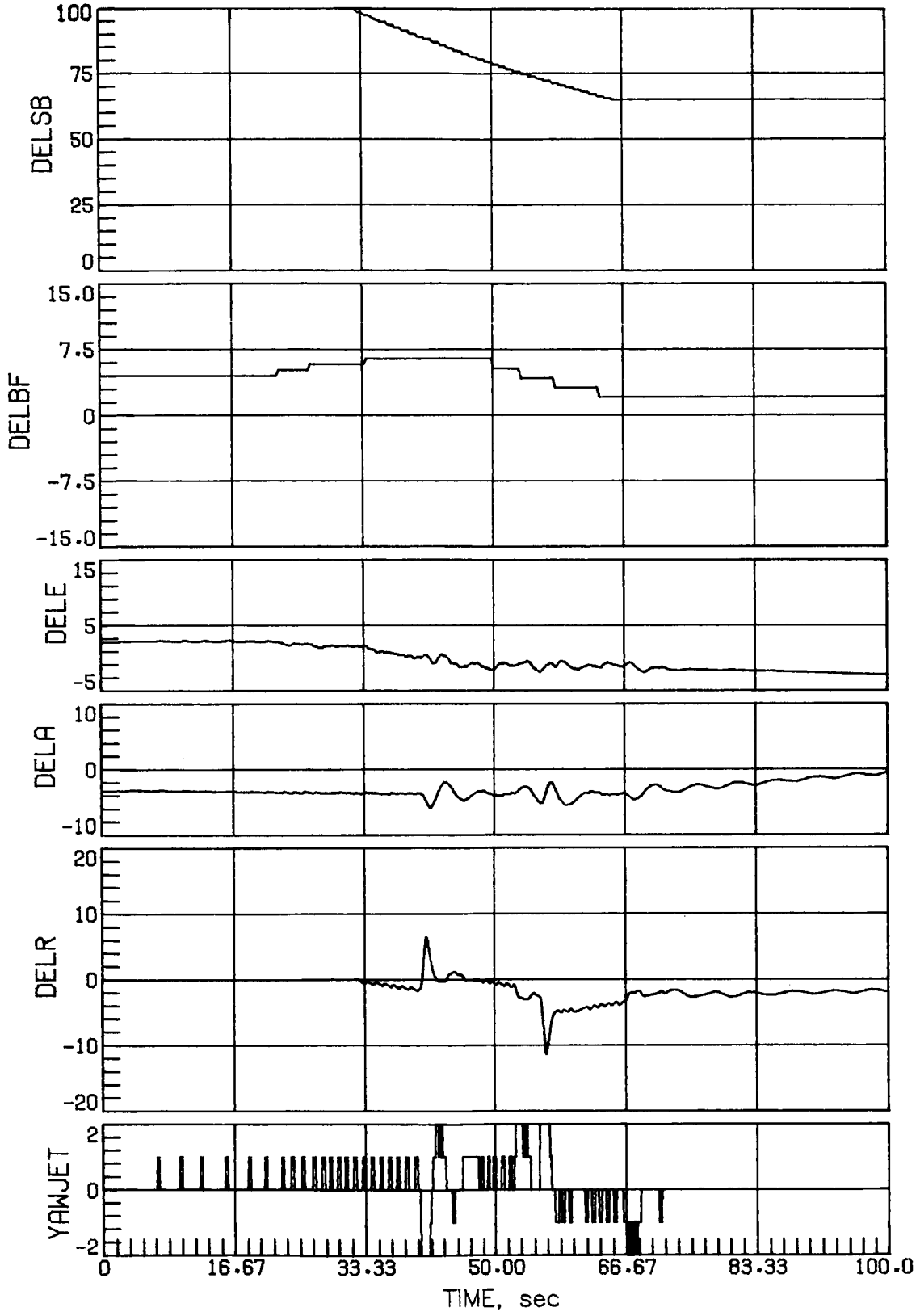

(h) Concluded.

Figure 17.- Continued.

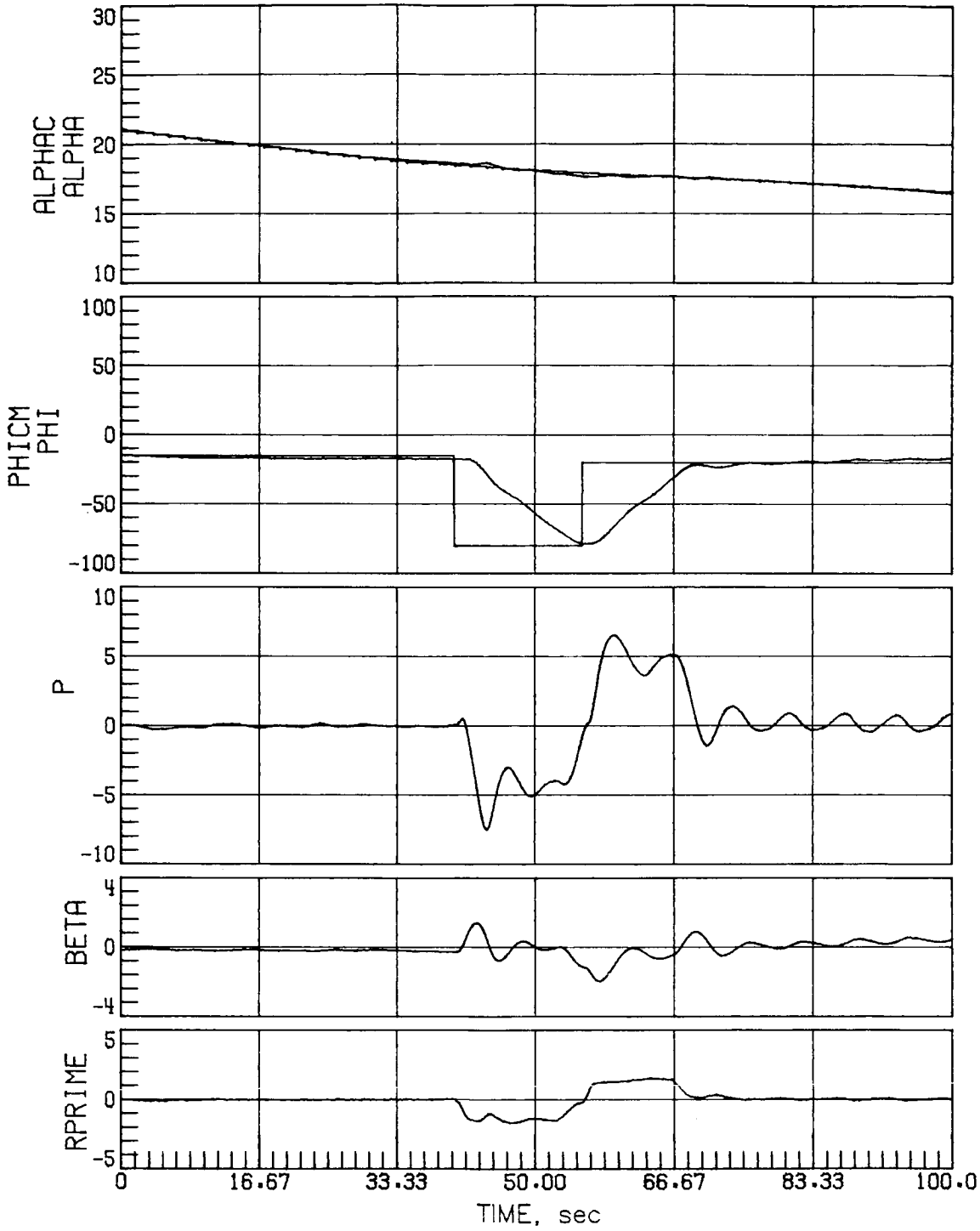

(i) Case 7.

Figure 17.- Continued.

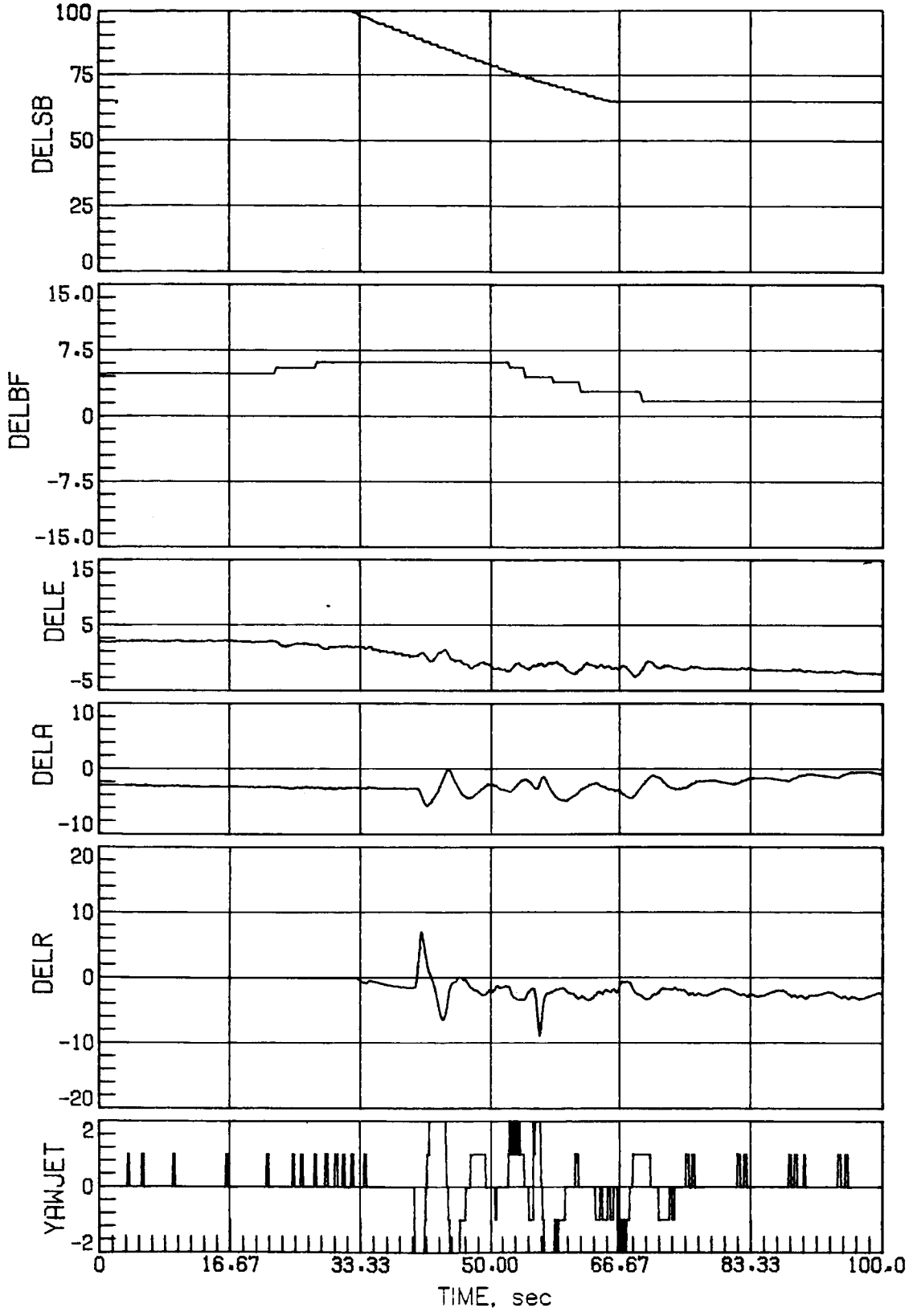

(i) Concluded.

Figure 17.- Concluded.

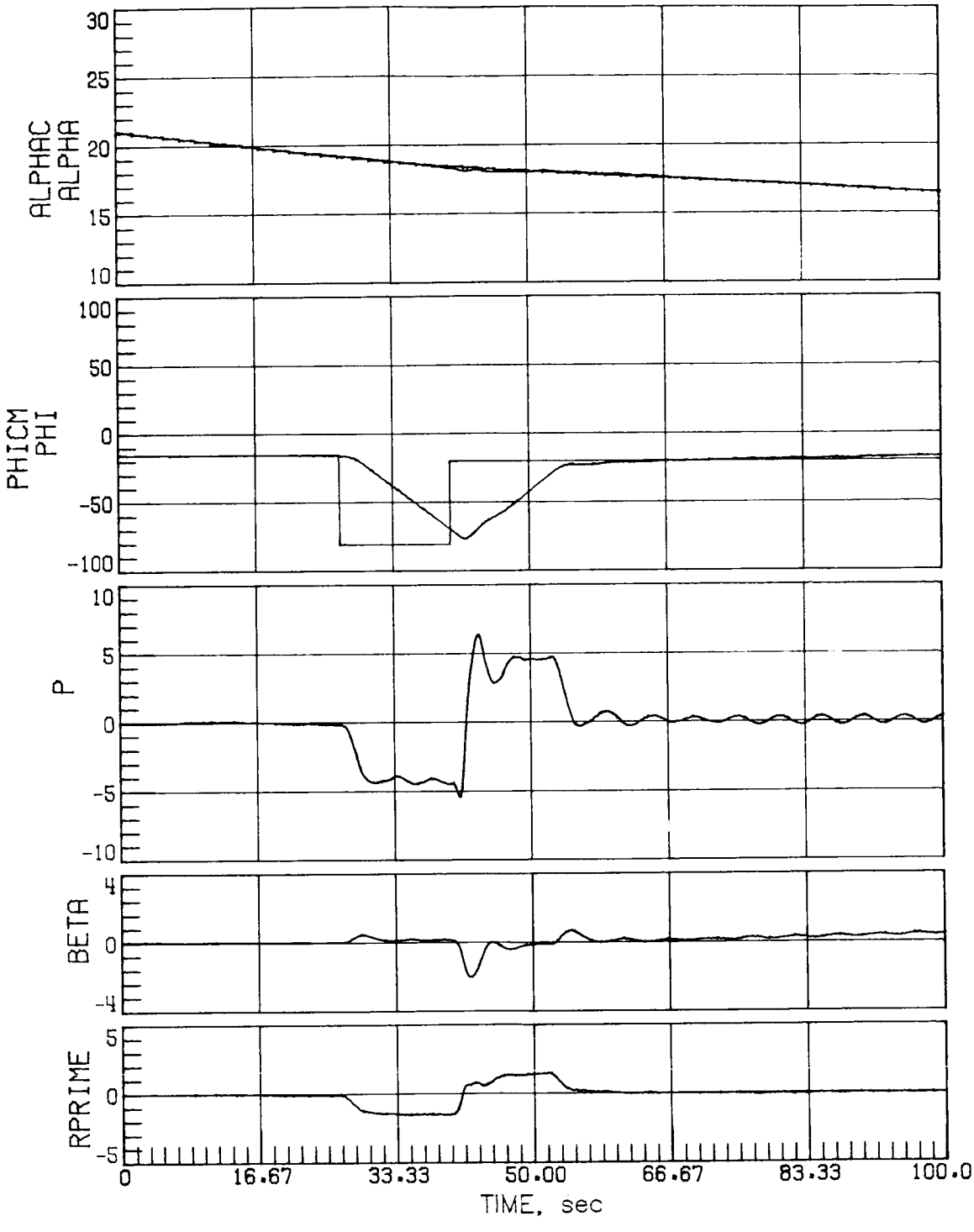

(a) Nominal aerodynamics.

Figure 18.- Mach 5 maneuver performance with increased rudder effectiveness.

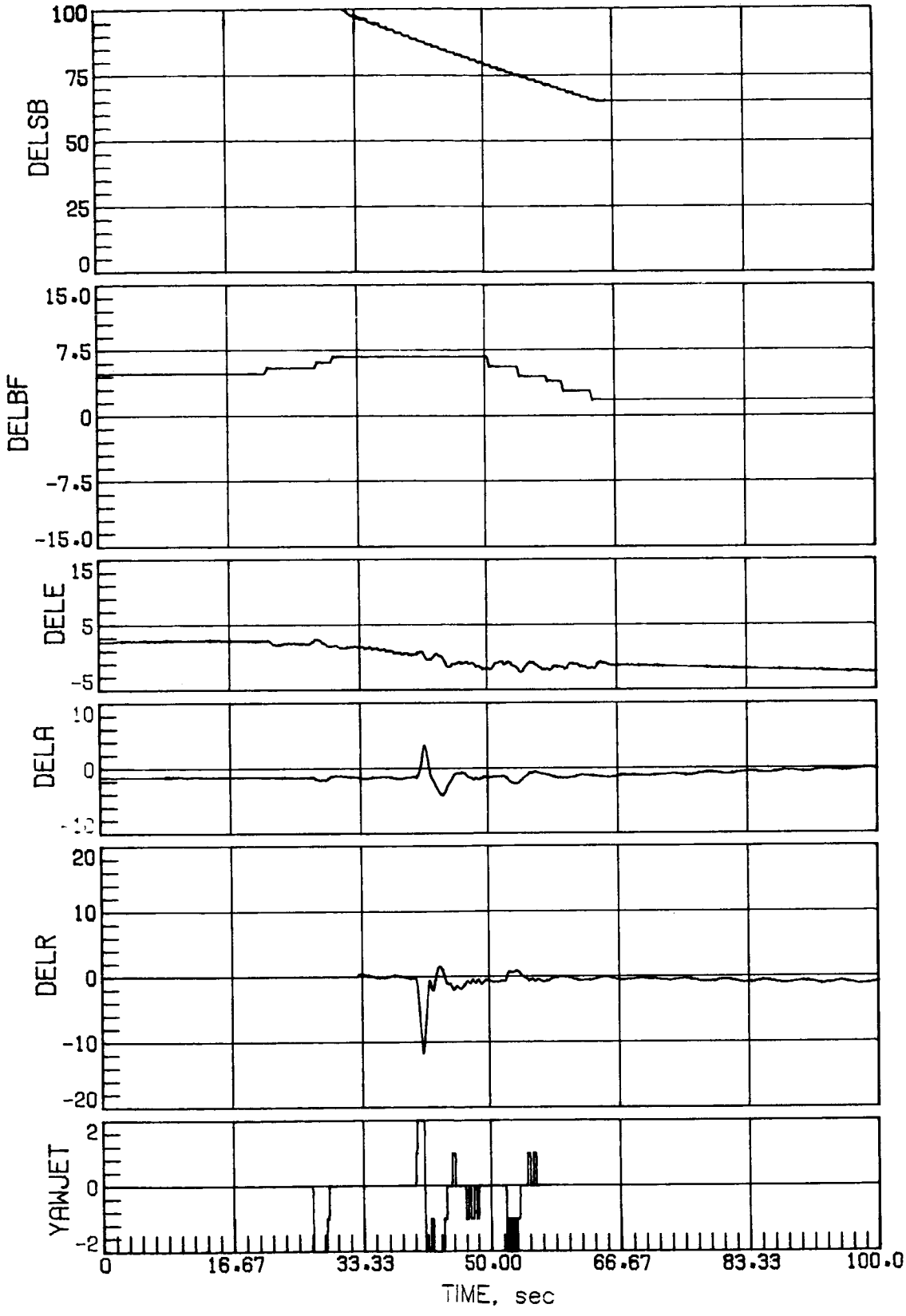

(a) Concluded.

Figure 18.- Continued.

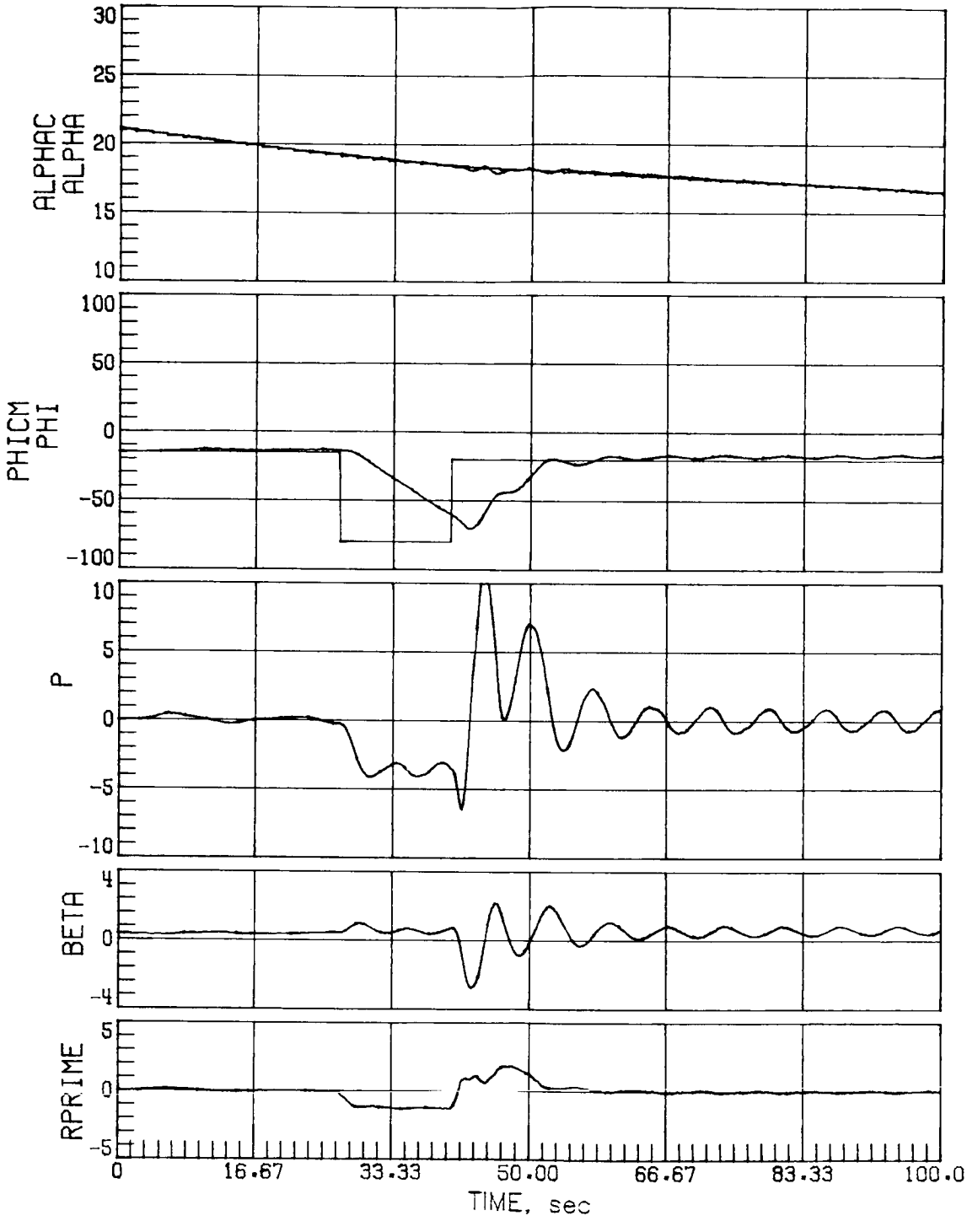

(b) Case 3.

Figure 18.- Continued.

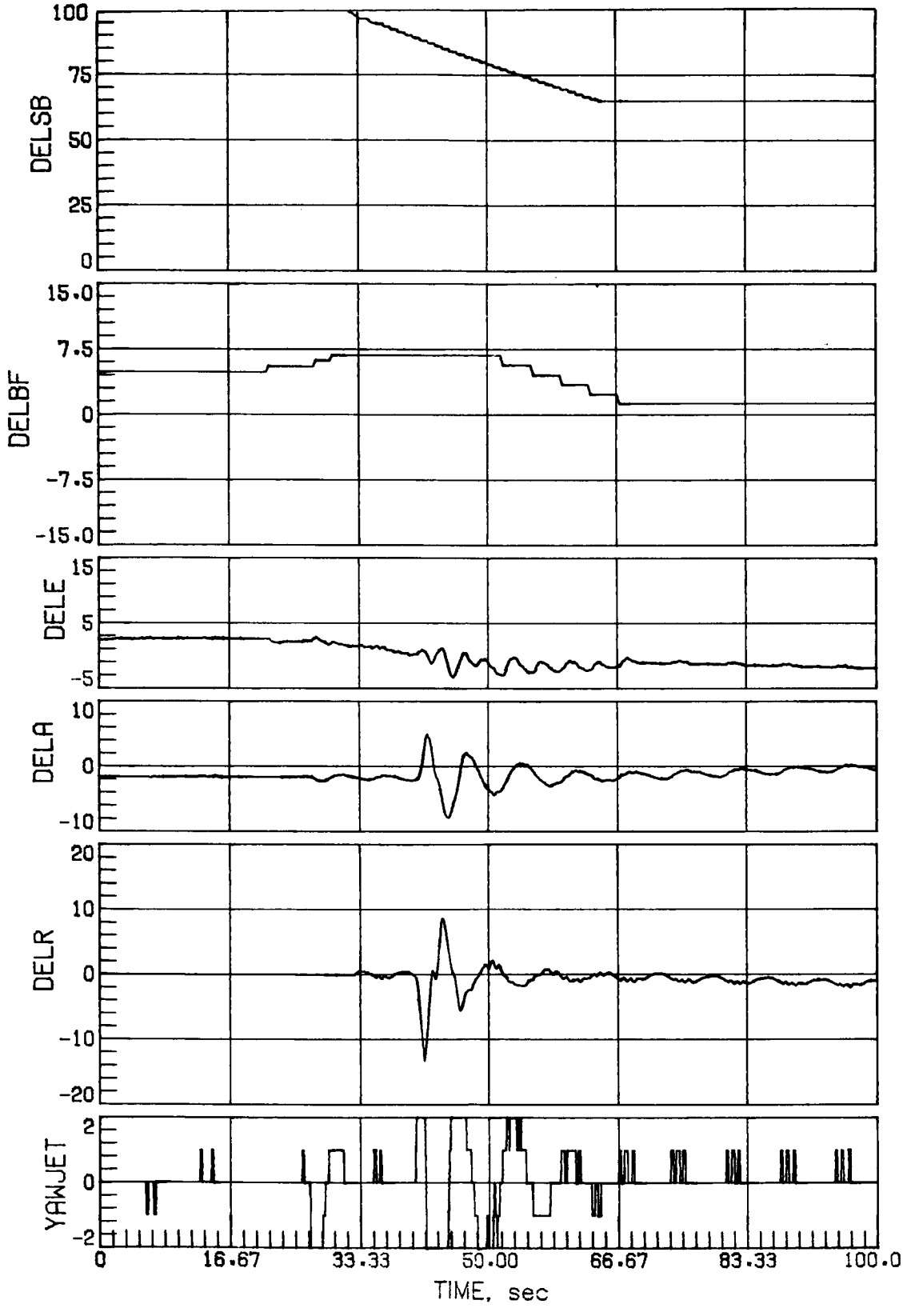

(b) Concluded.

Figure 18.- Continued.

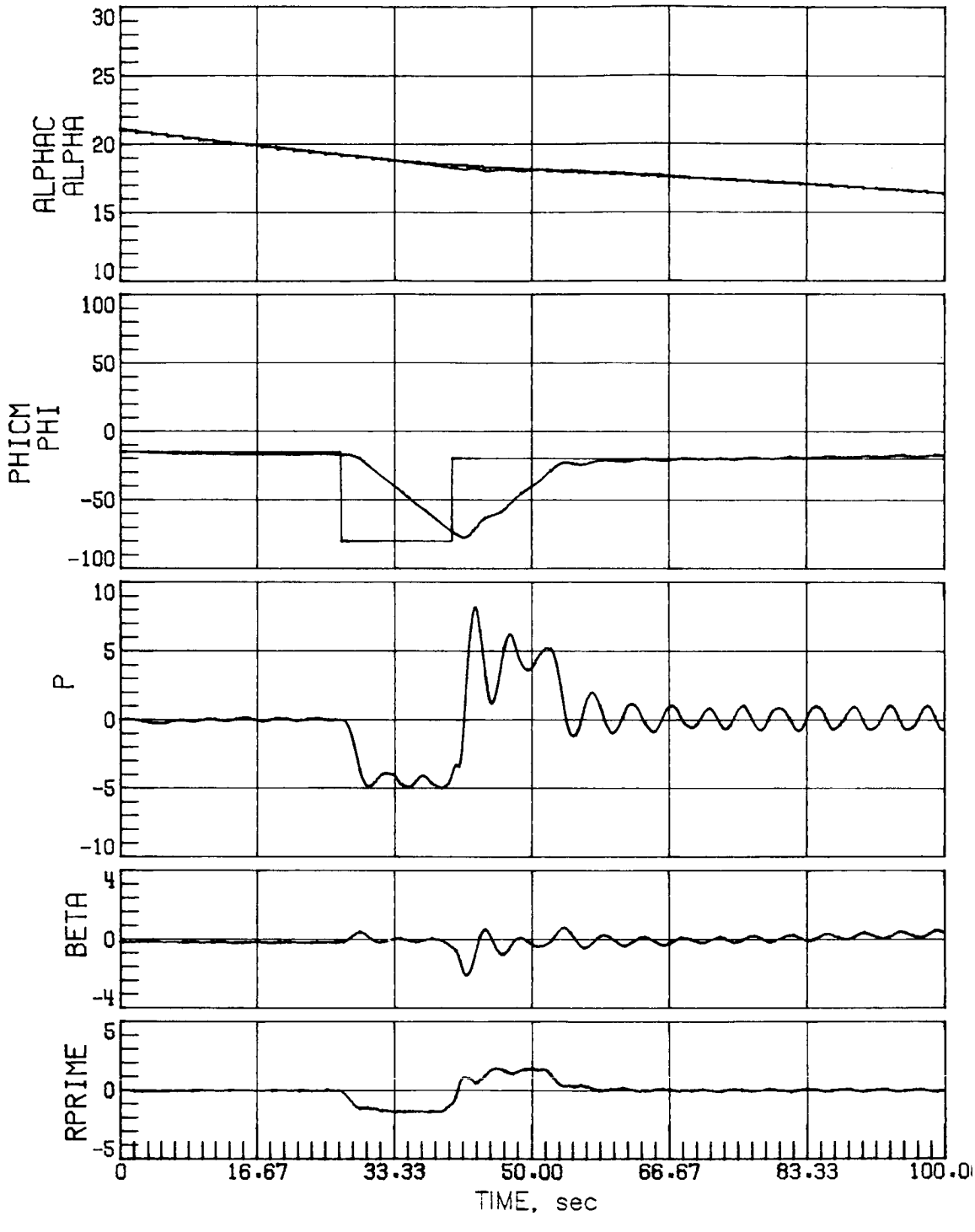

(c) Case 5.

Figure 18.- Continued.

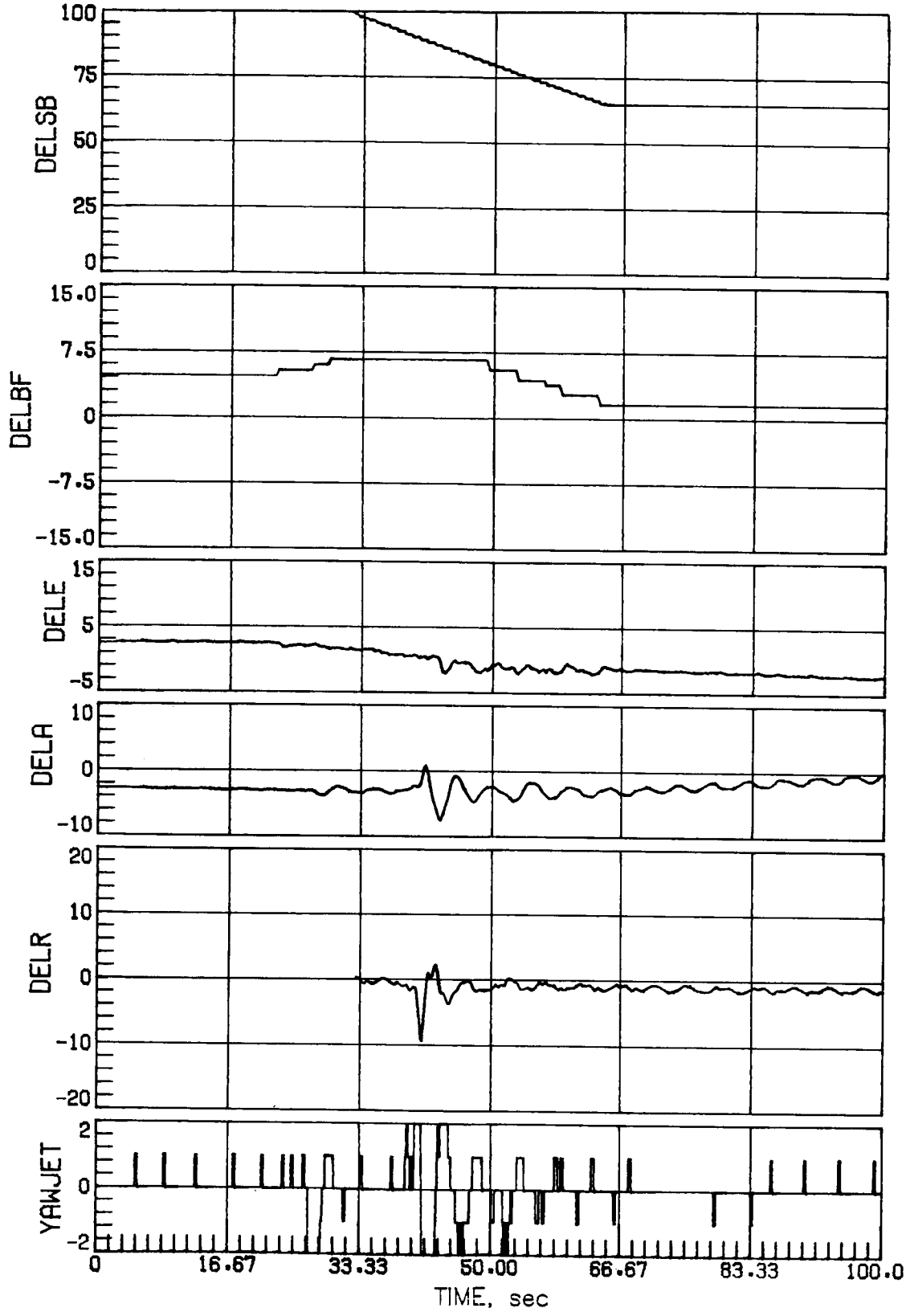

(c) Concluded.

Figure 18.- Continued.

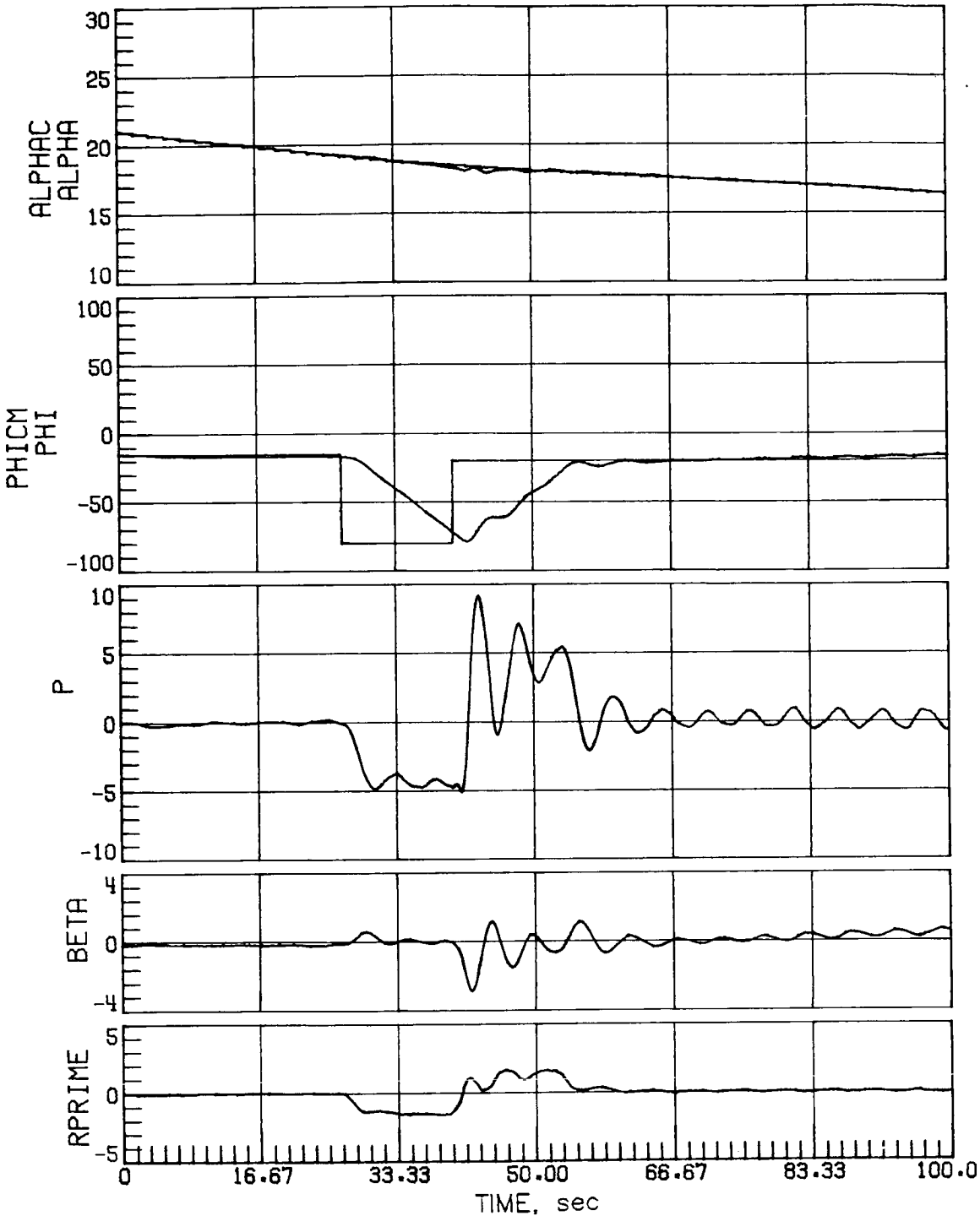

(d) Case 7.

Figure 18.- Continued.

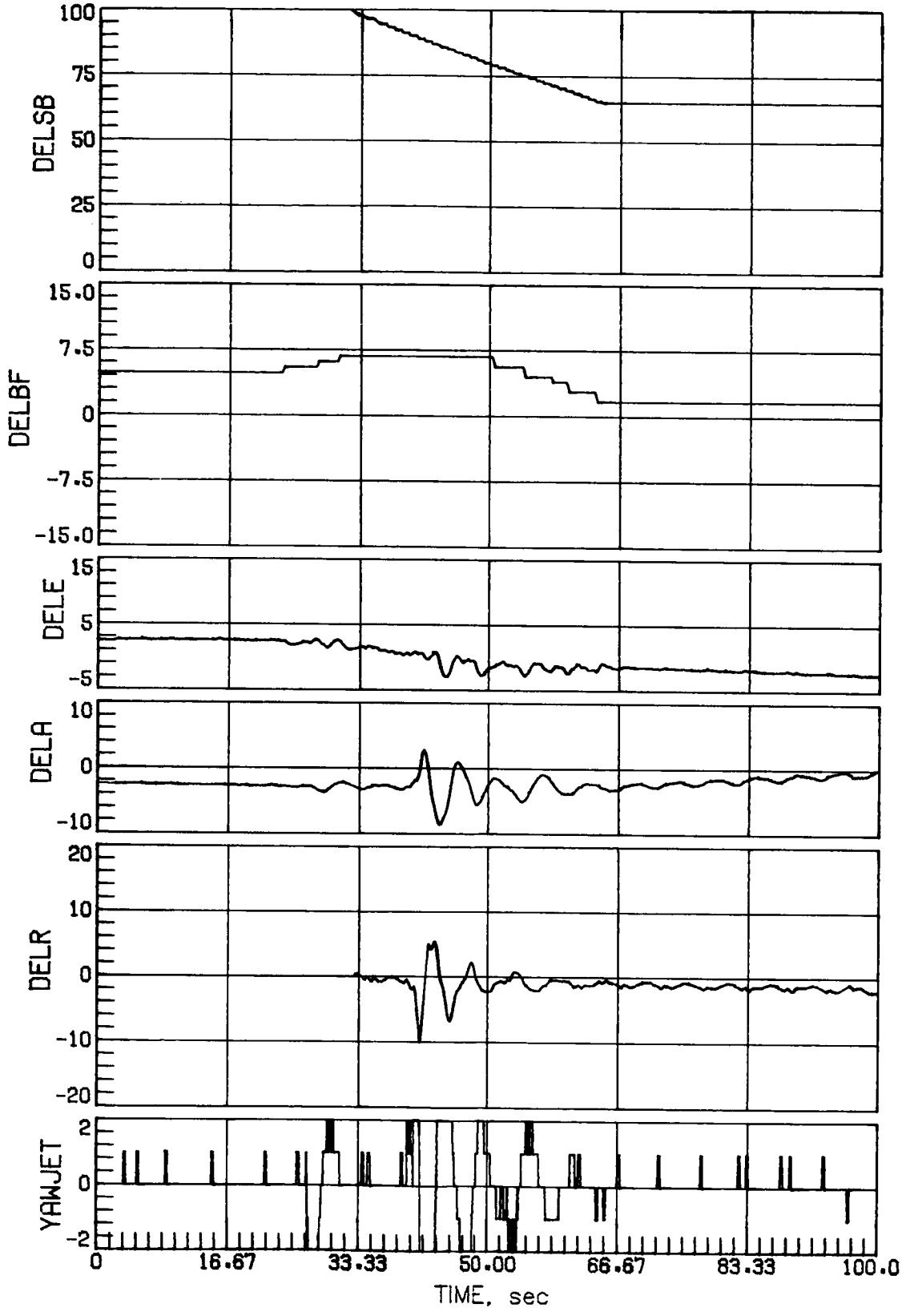

(d) Concluded.

Figure 18.- Concluded.

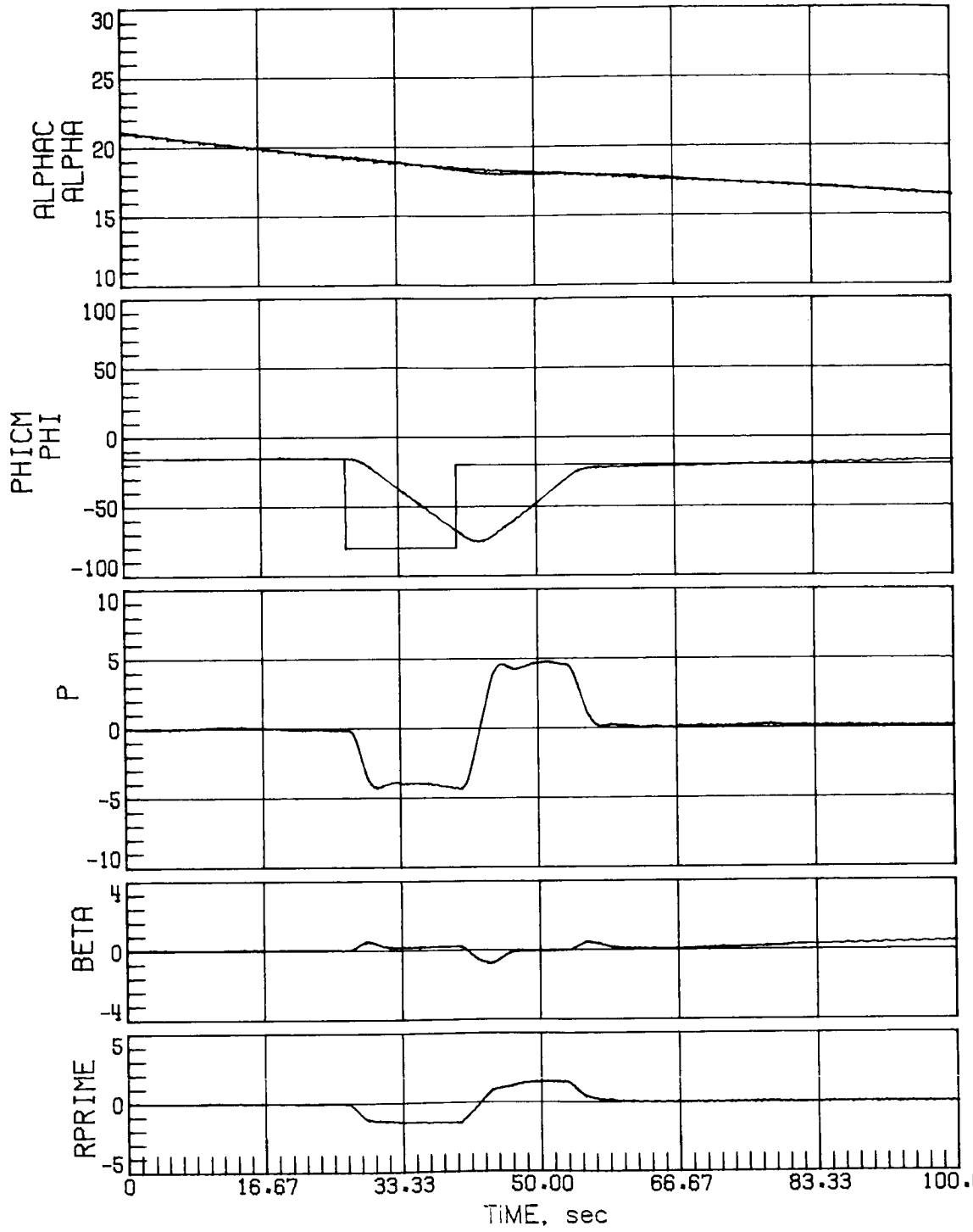

(a) Nominal aerodynamics.

Figure 19.- Mach 5 maneuver performance with decreased rudder effectiveness.

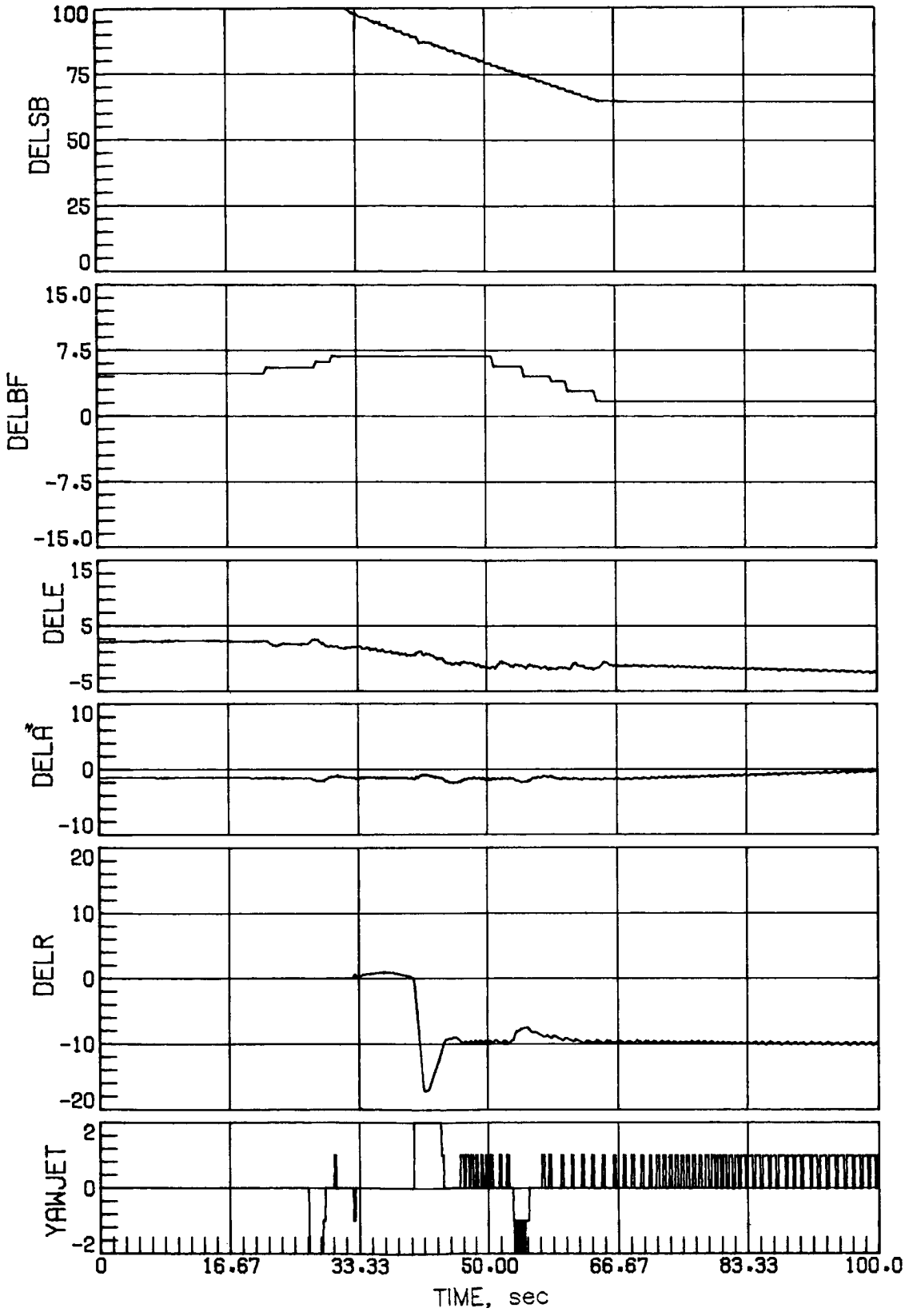

(a) Concluded.

Figure 19.- Continued.

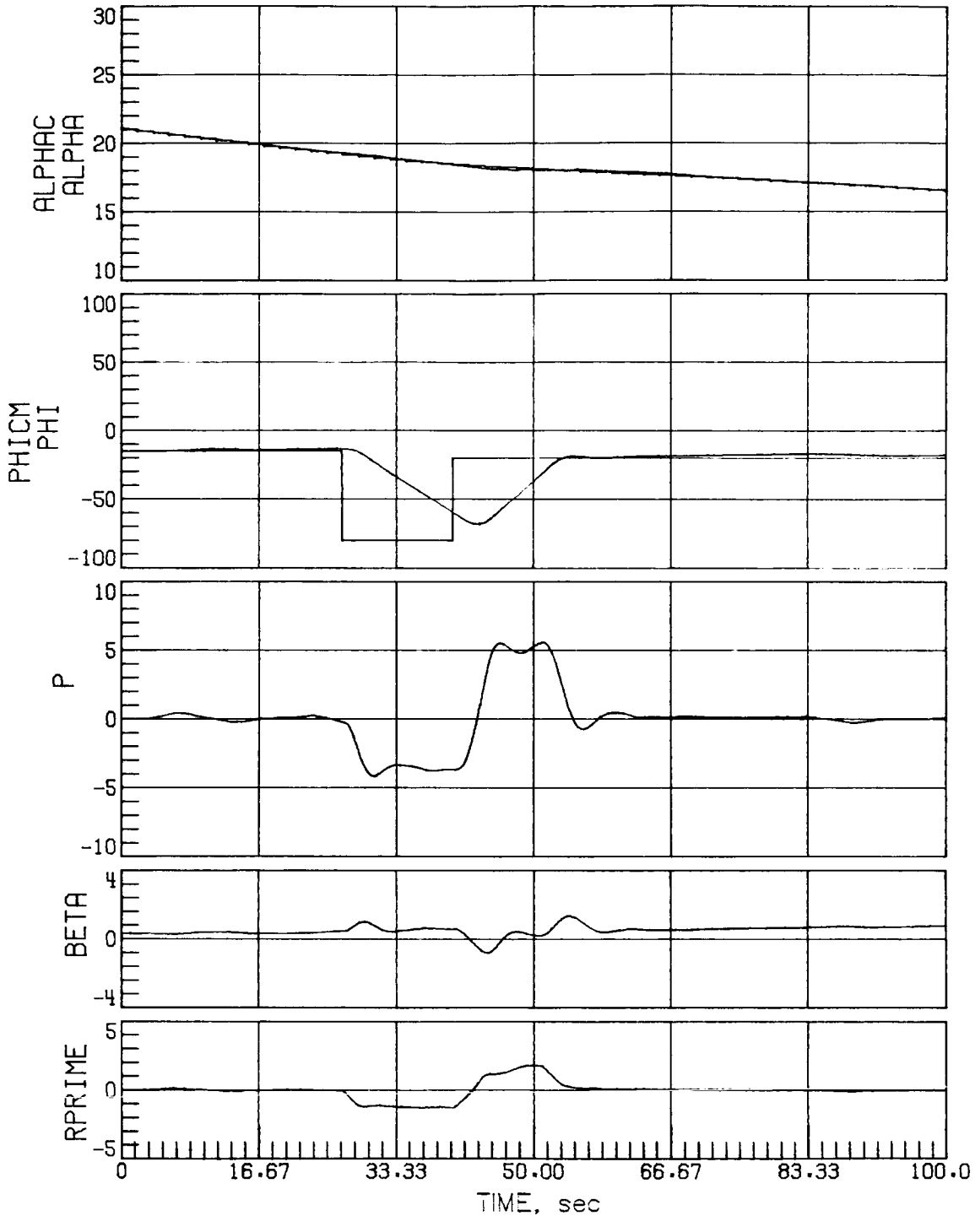

(b) Case 3.

Figure 19.- Continued.

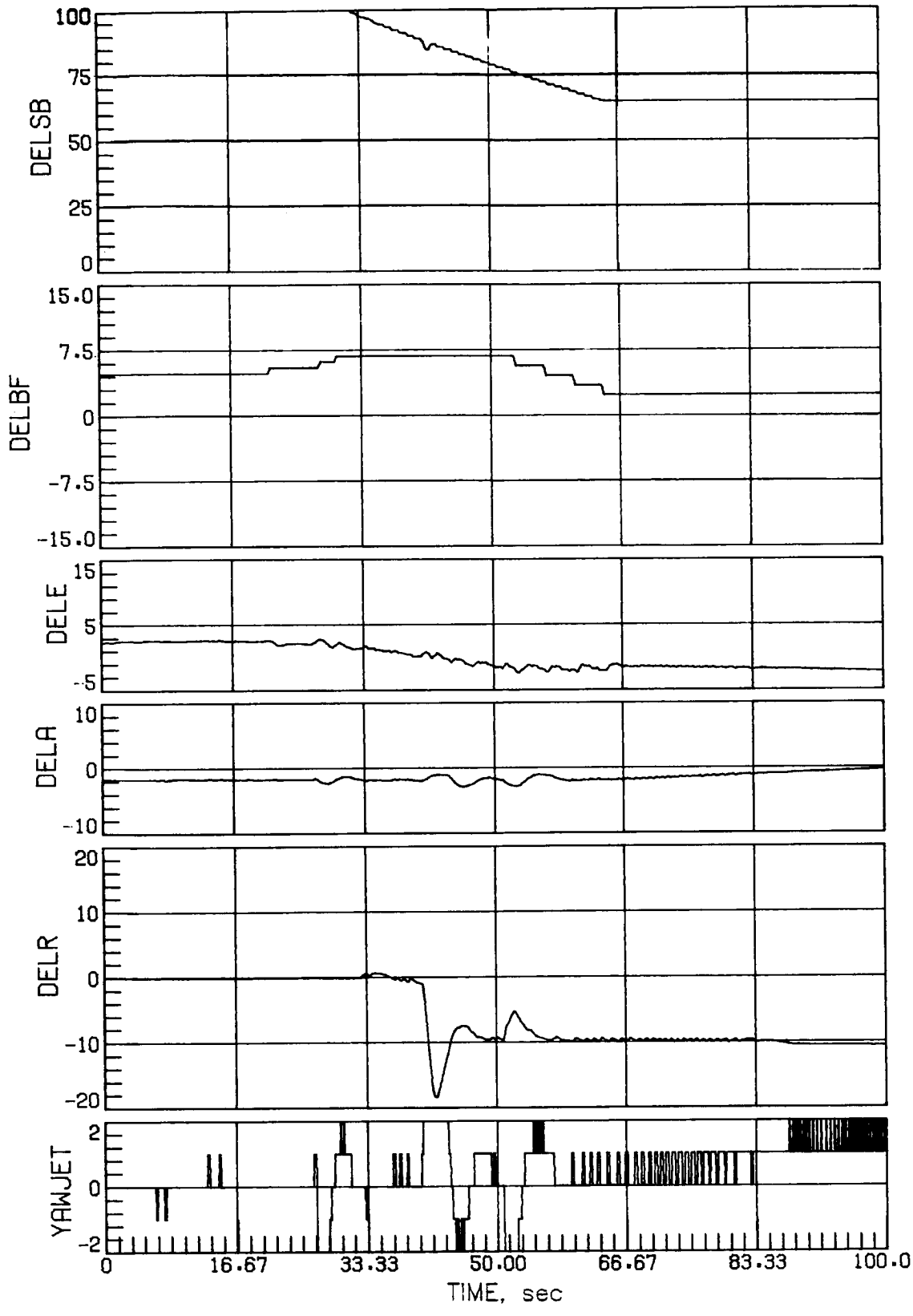

(b) Concluded.

Figure 19.- Continued.

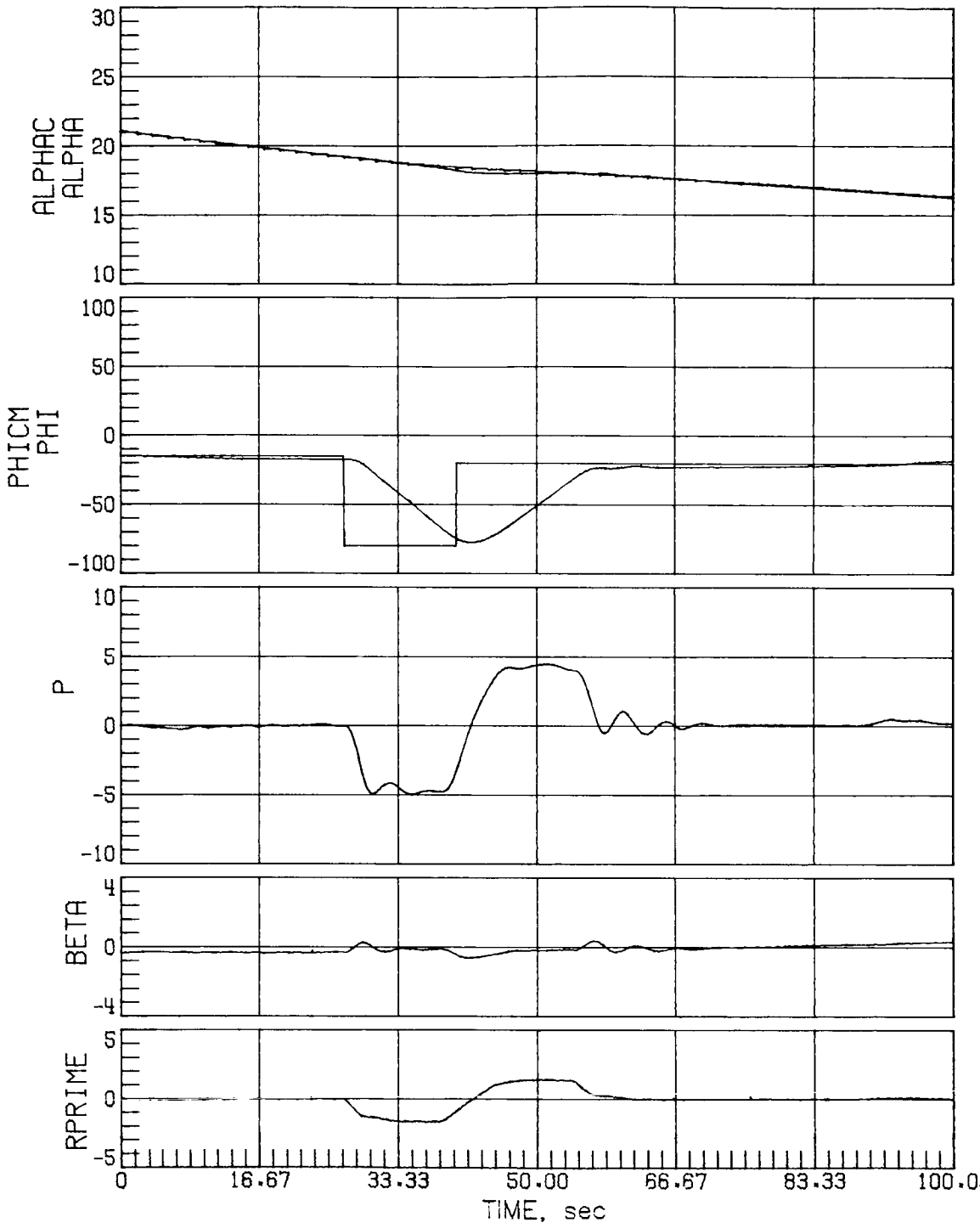

(c) Case 6.

Figure 19.- Continued.

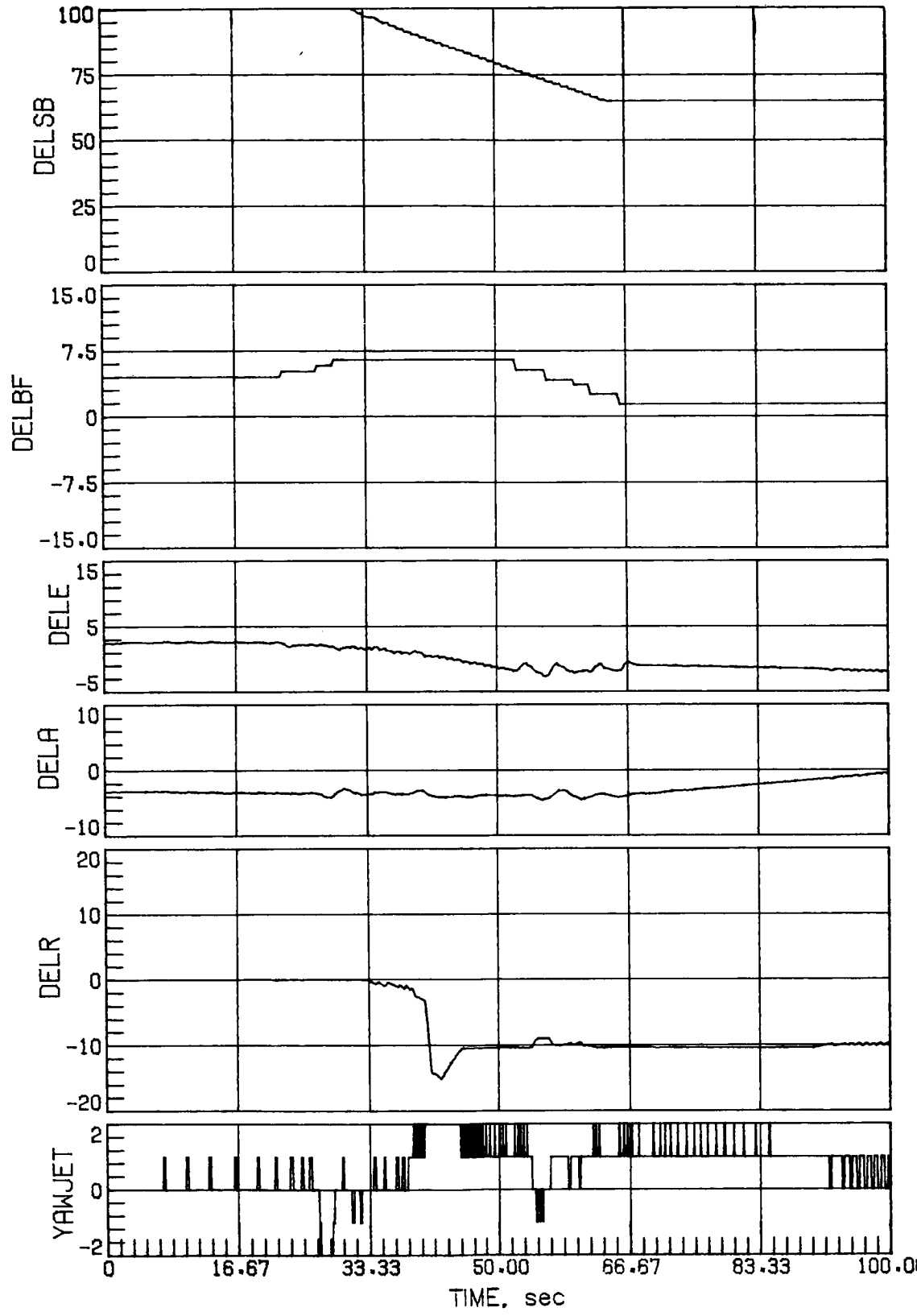

(c) Concluded.

Figure 19.- Continued.

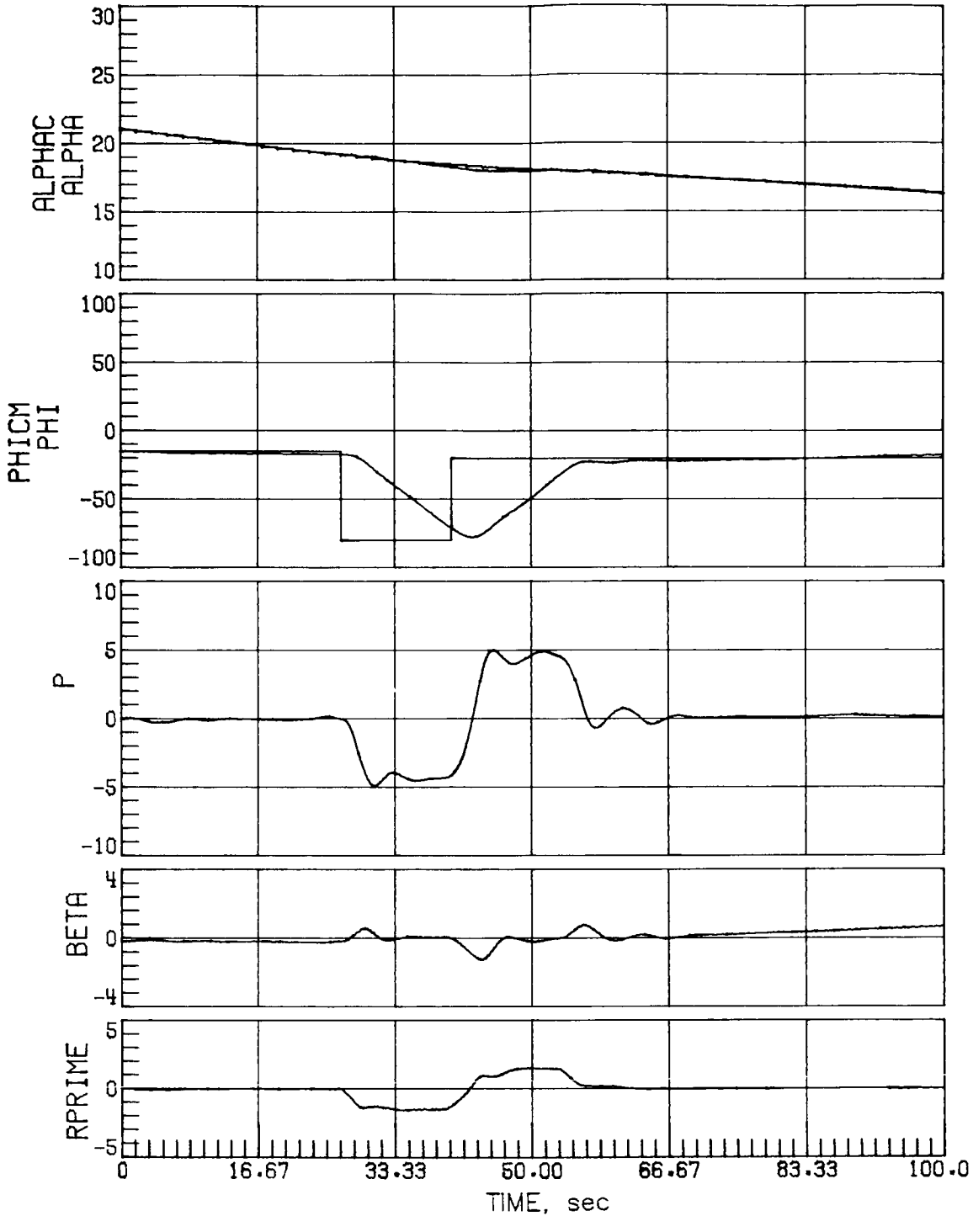

(d) Case 7.

Figure 19.- Continued.

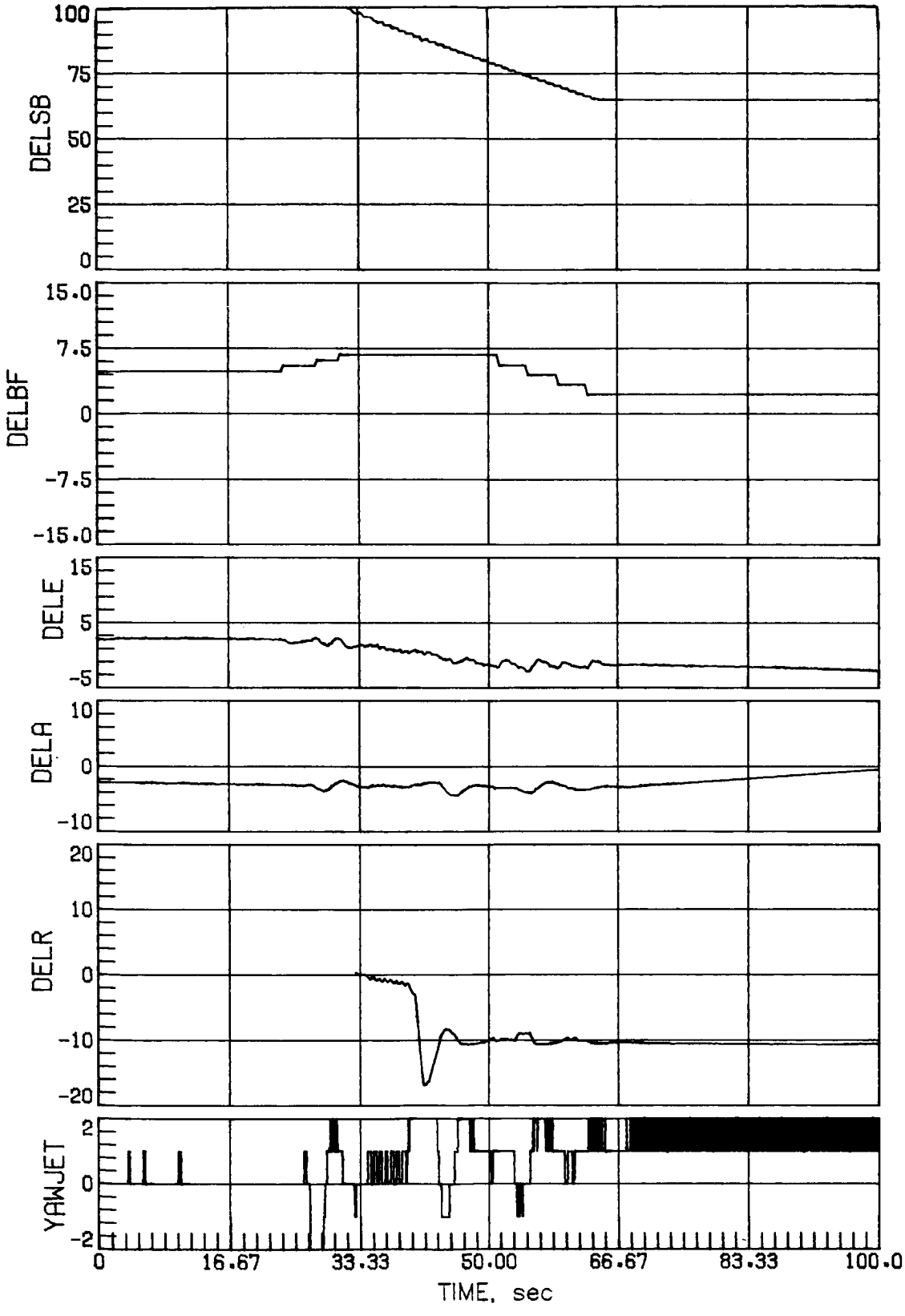

(d) Concluded.

Figure 19.- Continued.

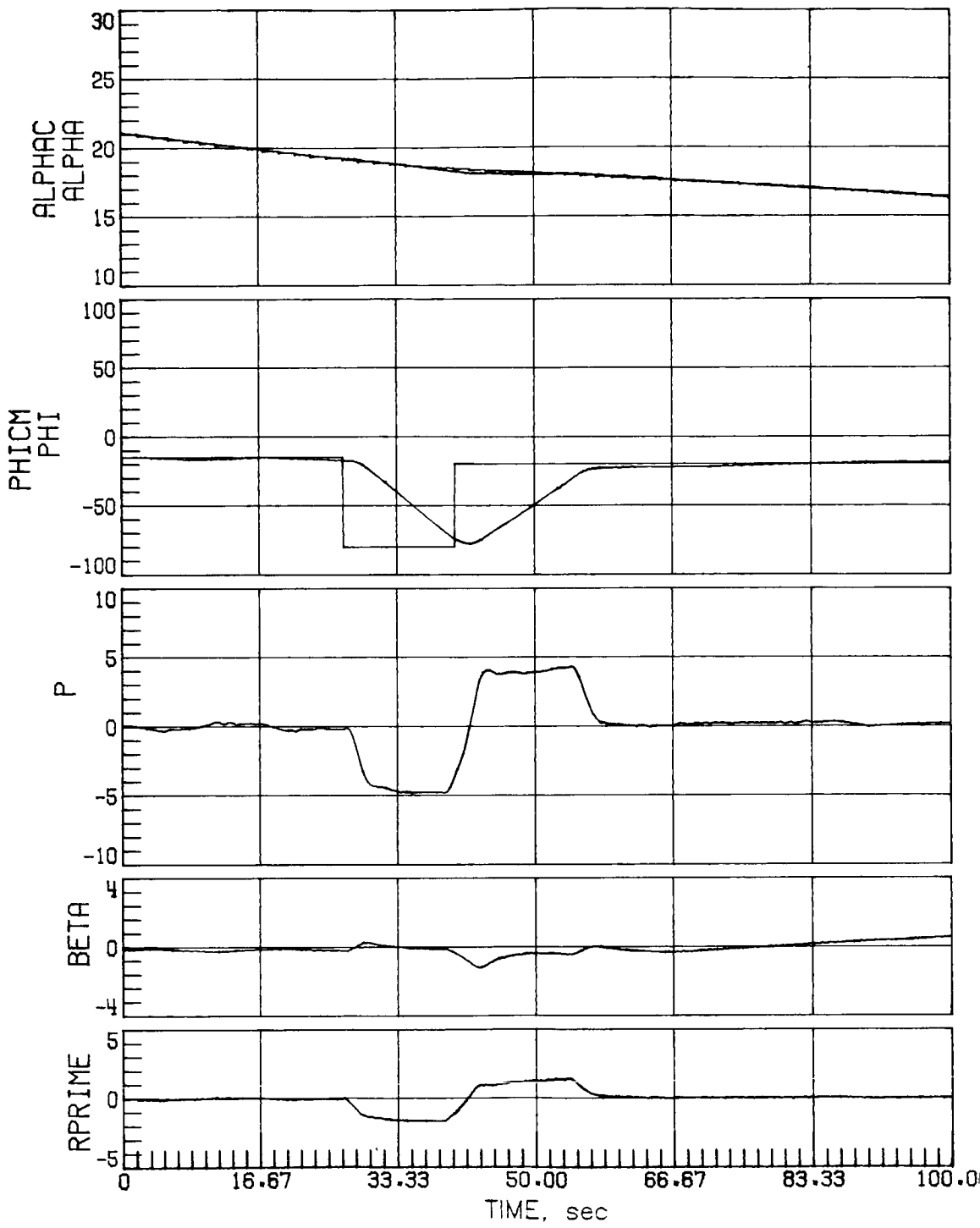

(e) Case 15.

Figure 19.- Continued.

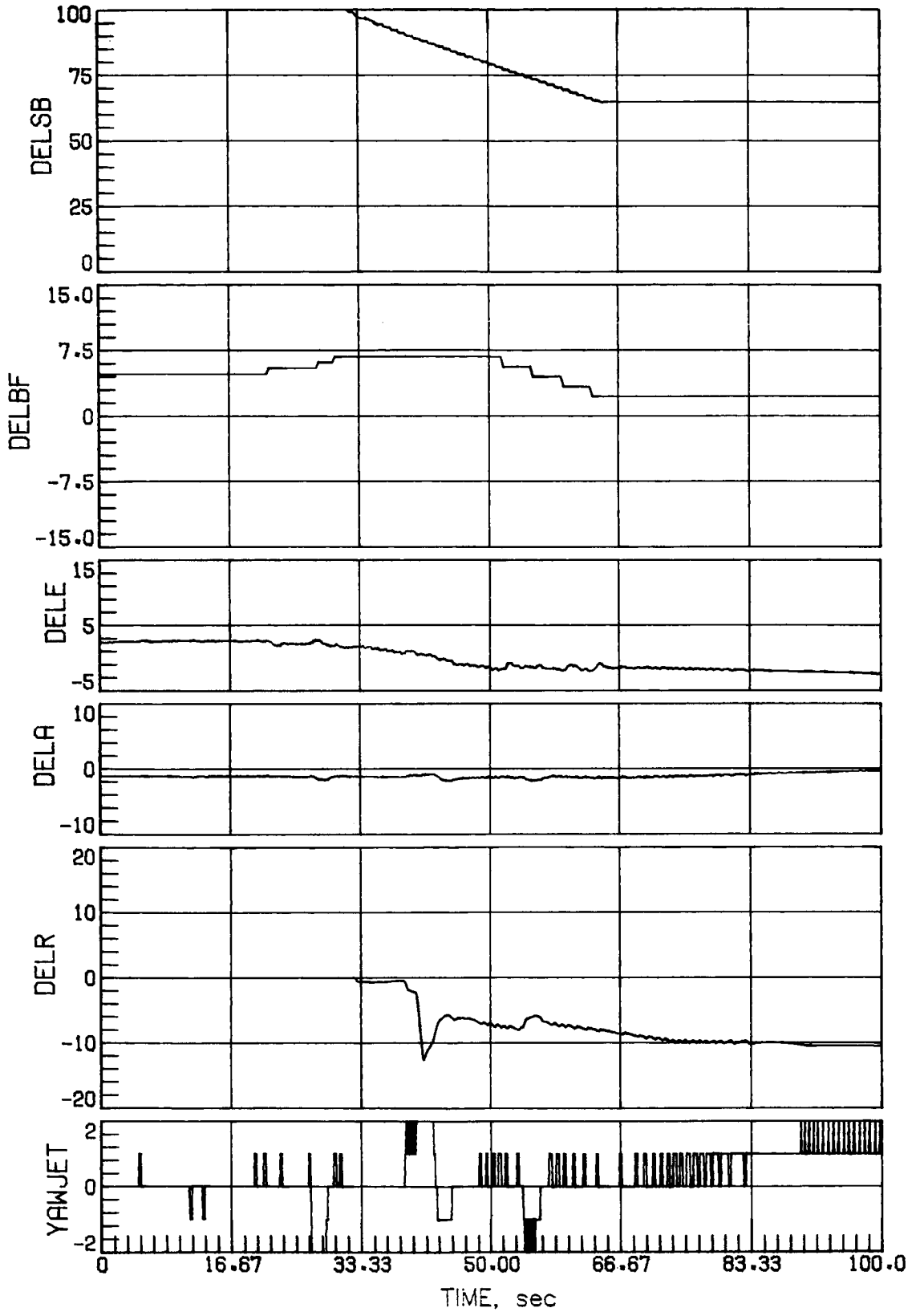

(e) Concluded.

Figure 19.- Concluded.

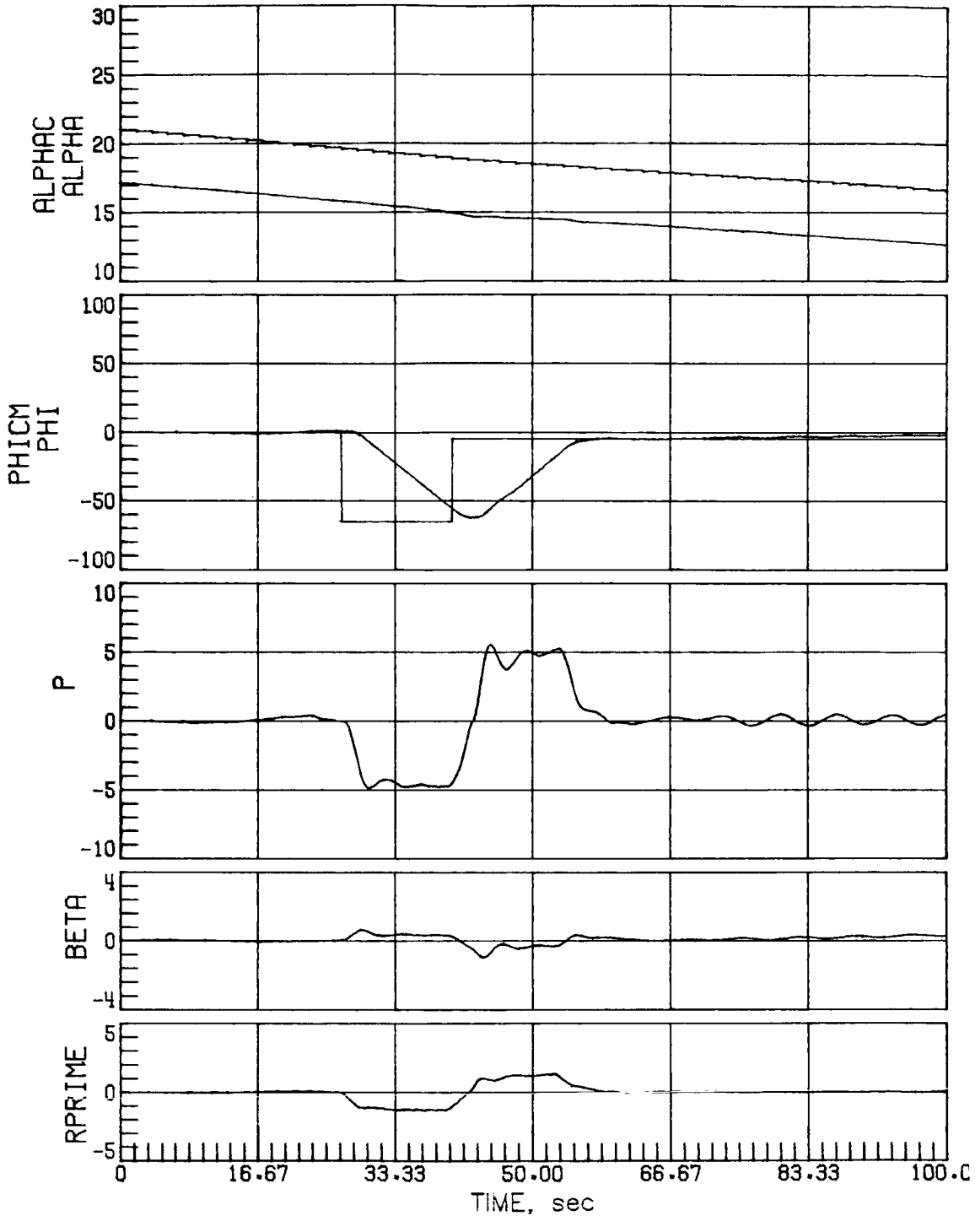

(a) Nominal aerodynamics.

Figure 20.- Mach 5 maneuver performance for a high-sensed α error of 4° with off-nominal aerodynamics and nominal rudder effectiveness.

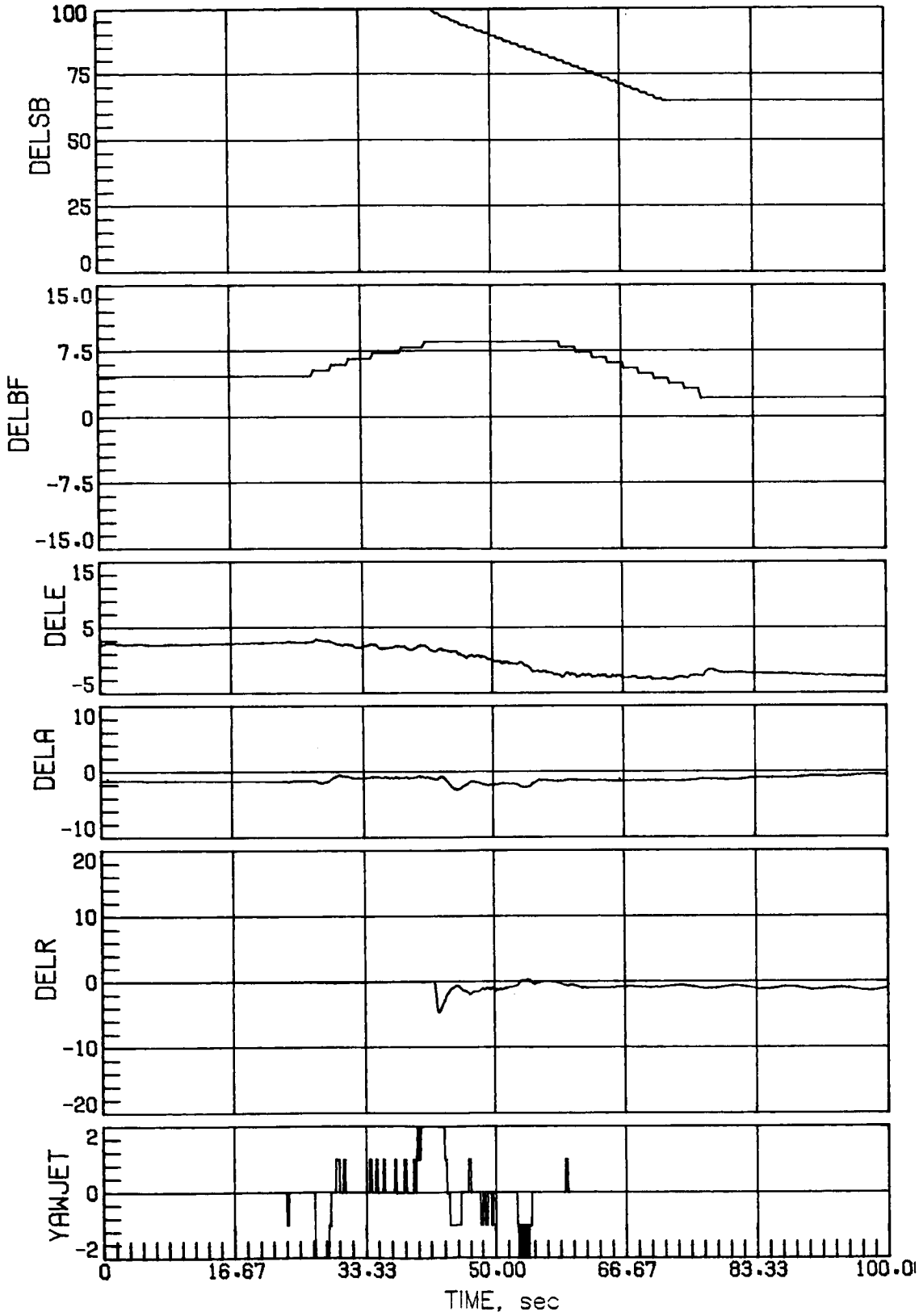

(a) Concluded.

Figure 20.- Continued.

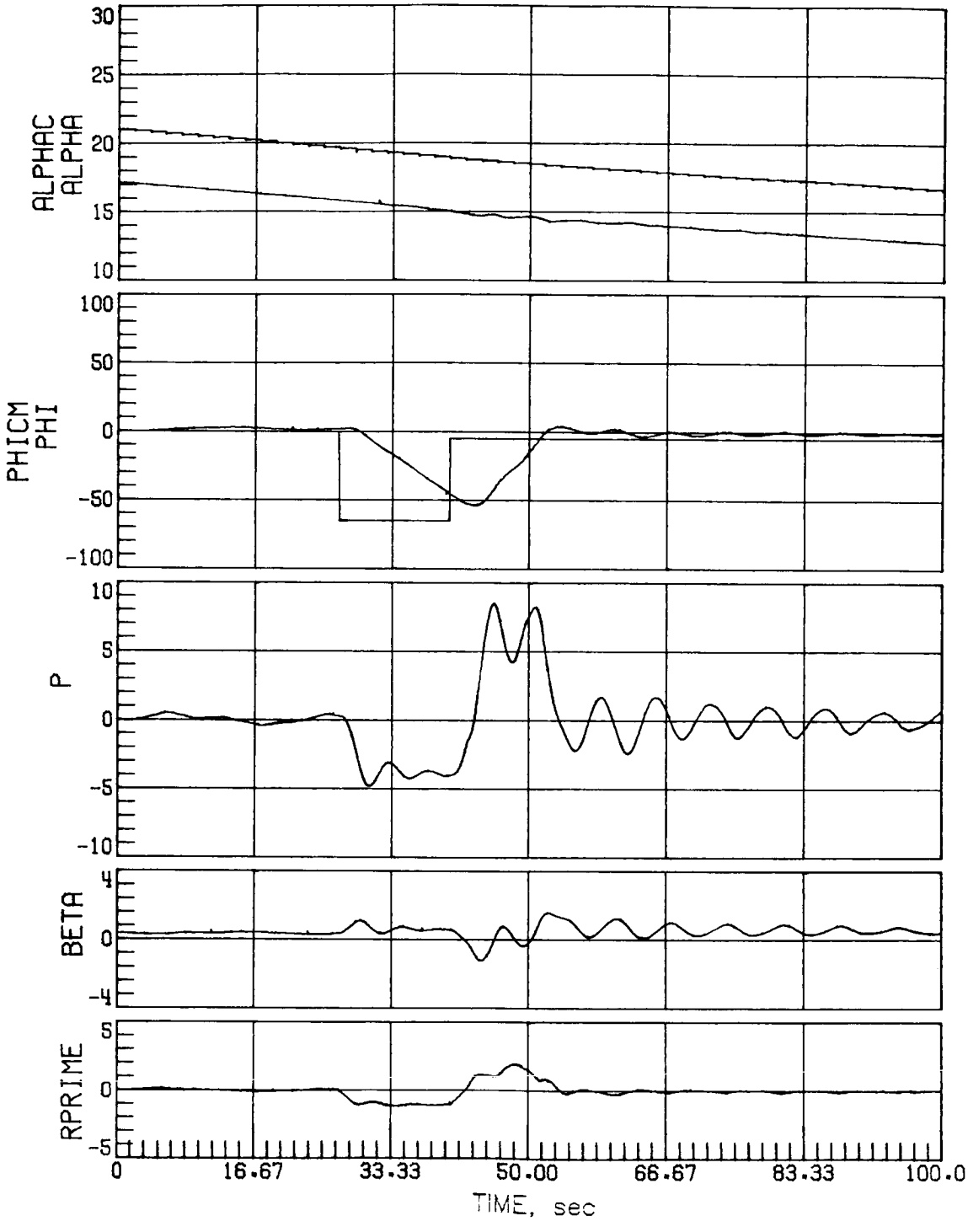

(b) Case 3.

Figure 20.- Continued.

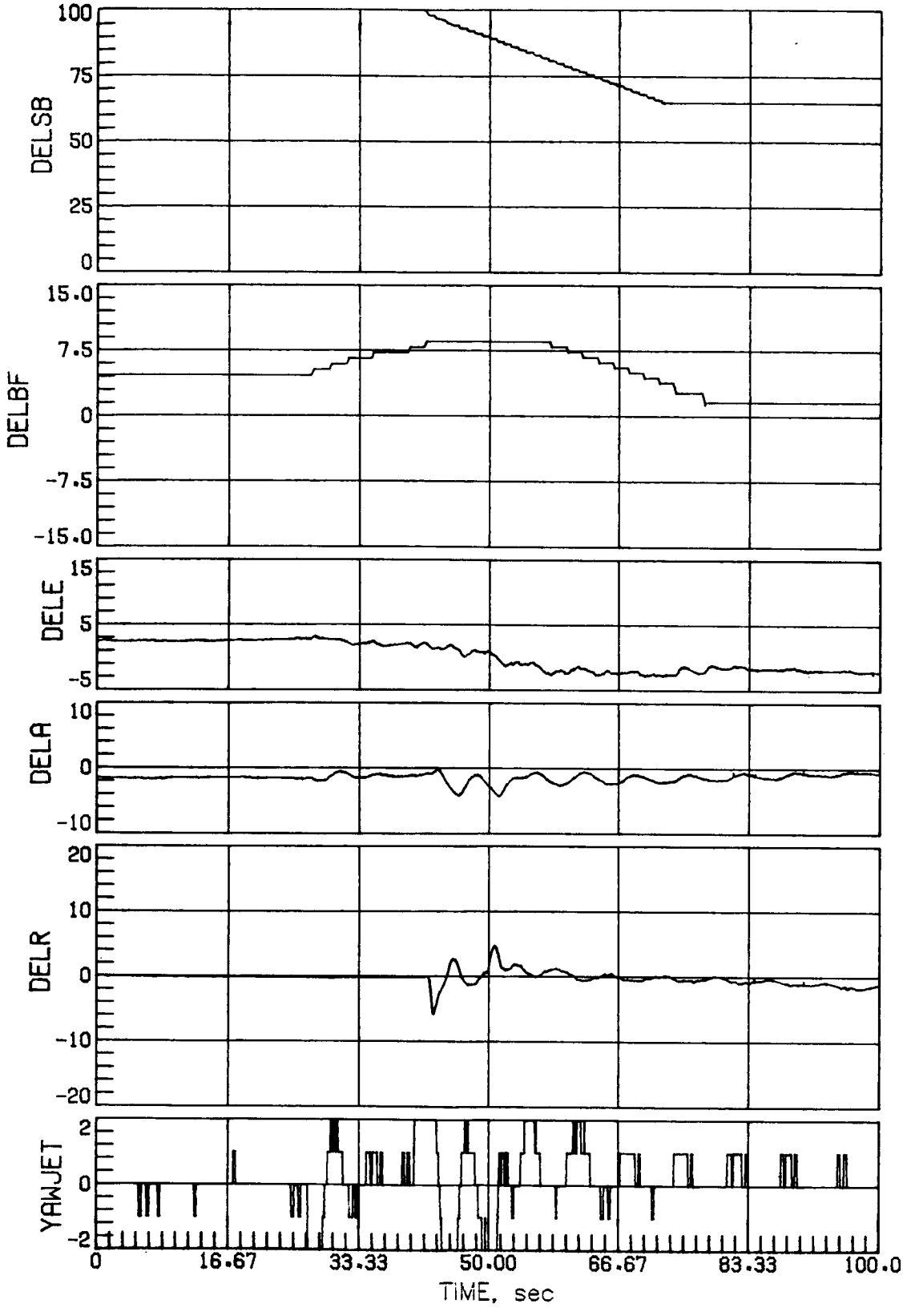

(b) Concluded.

Figure 20.- Continued.

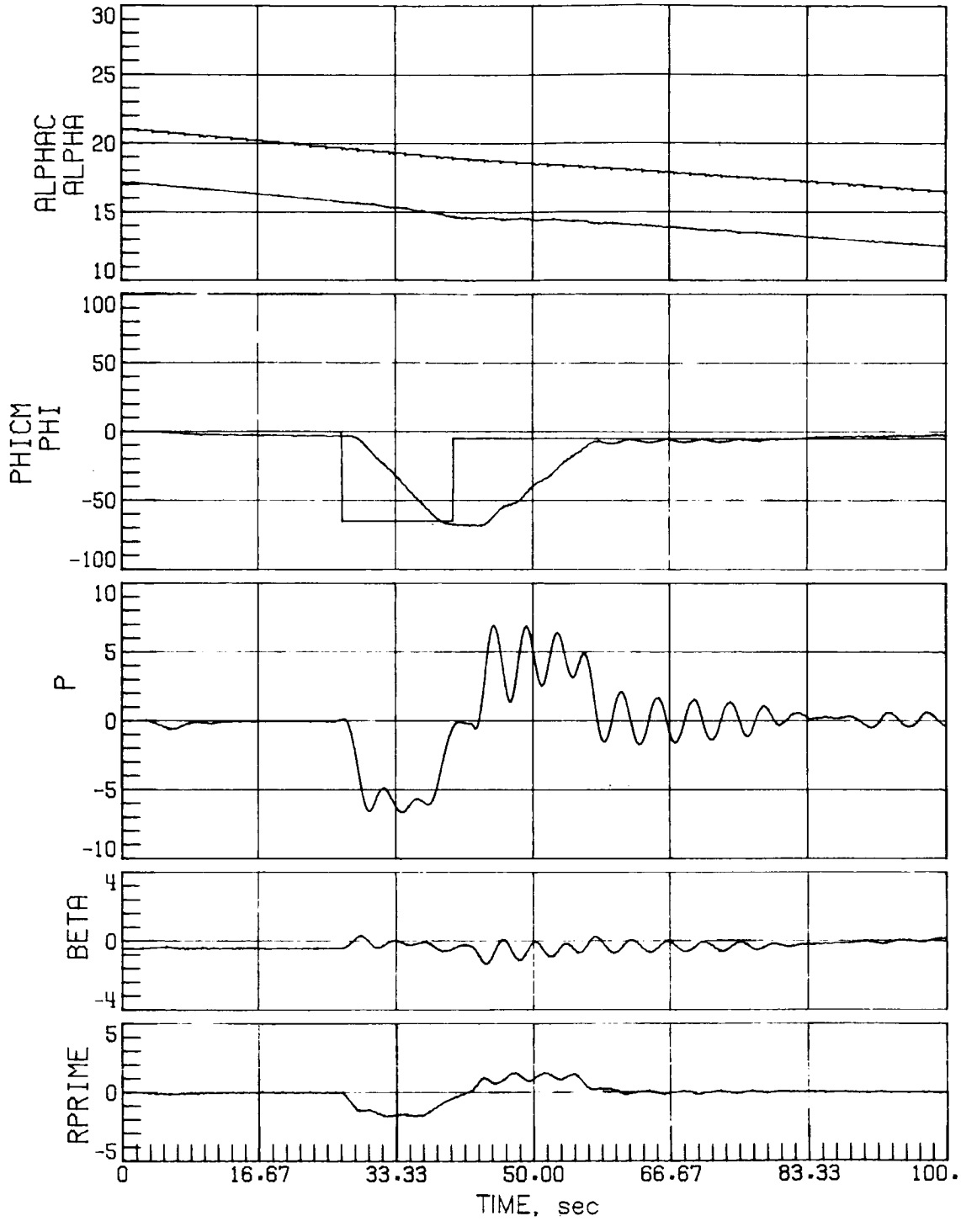

(c) Case 5.

Figure 20.- Continued.

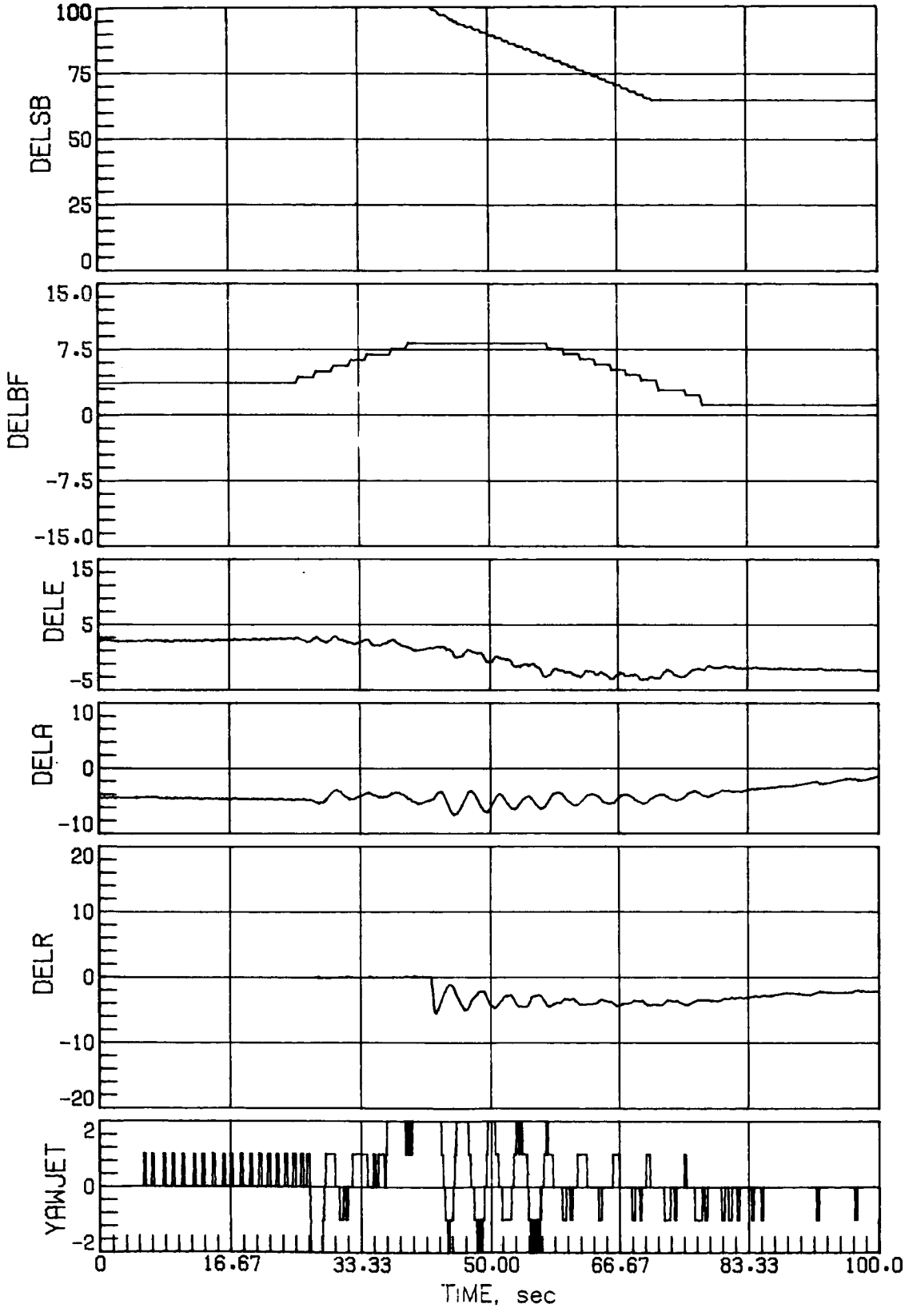

(c) Concluded.

Figure 20.- Continued.

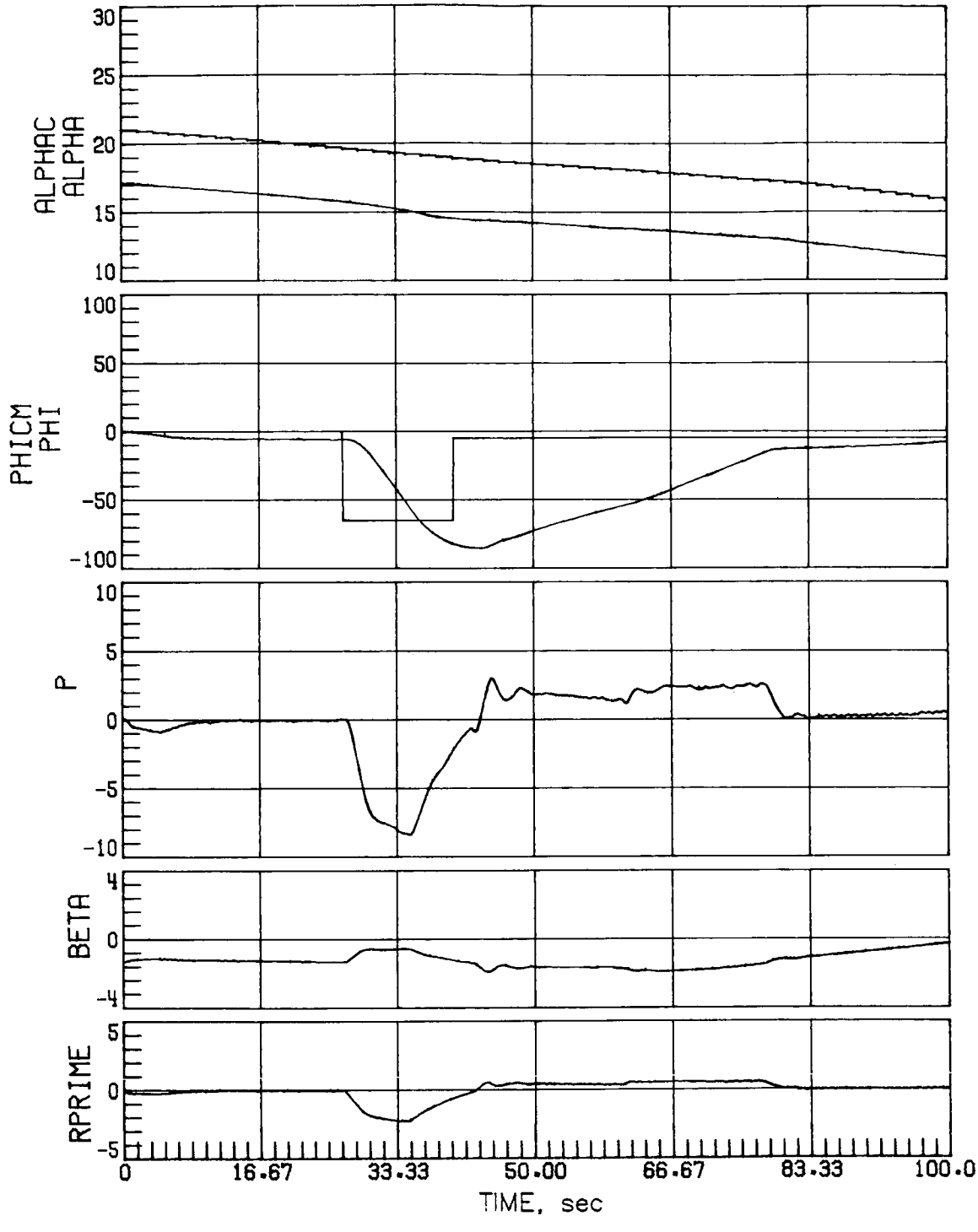

(d) Case 14.

Figure 20.- Continued.

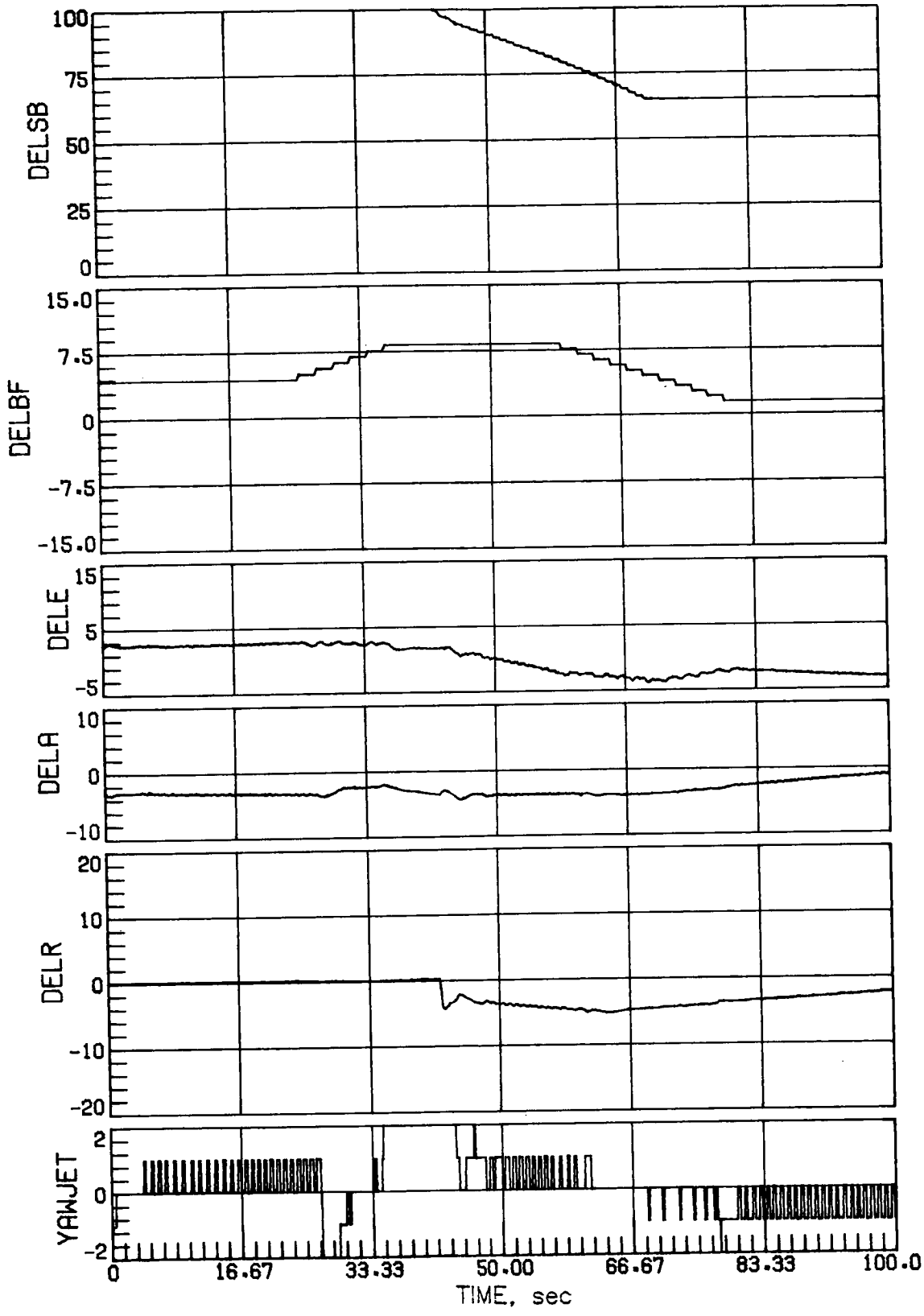

(d) Concluded.

Figure 20.- Concluded.

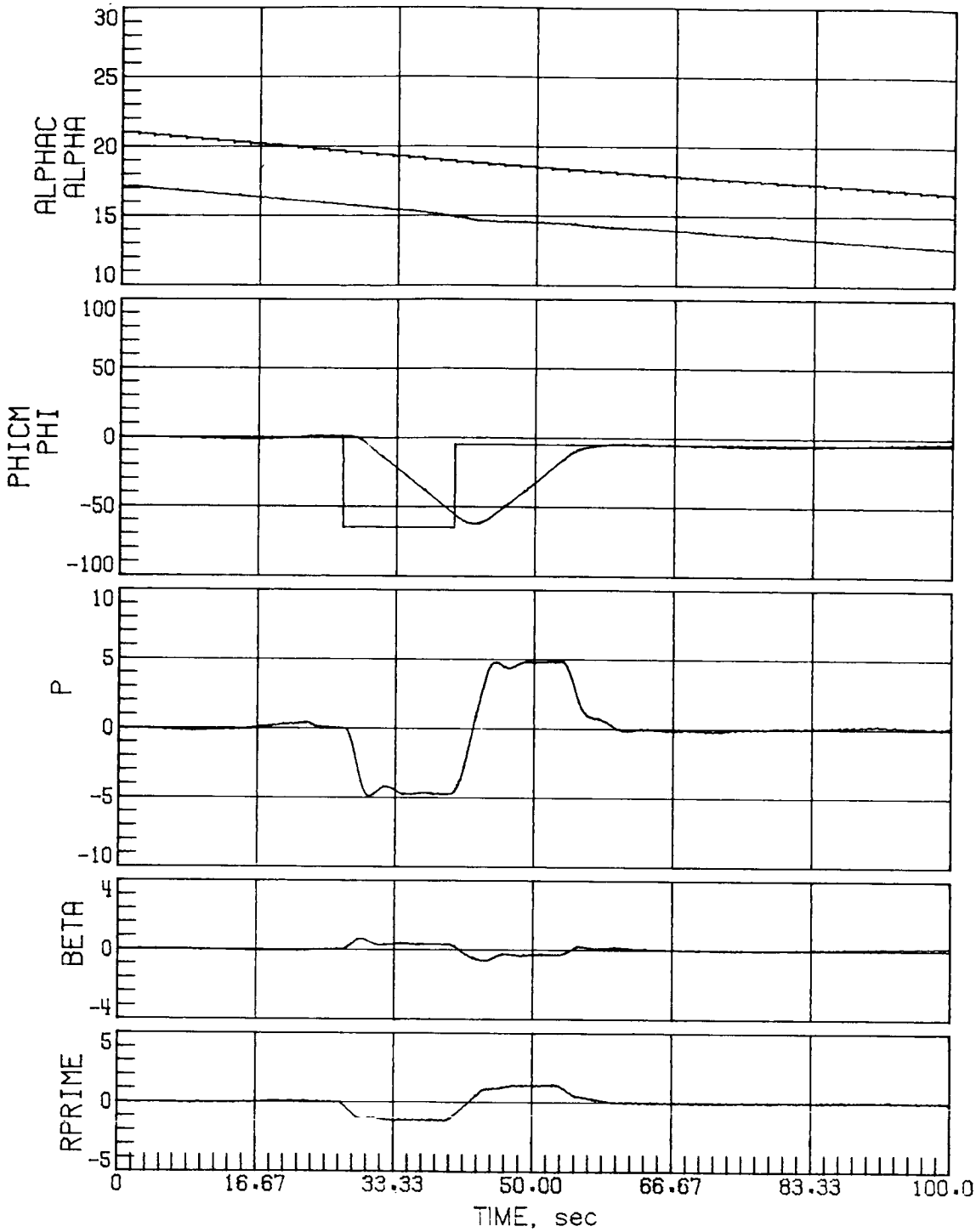

(a) Nominal aerodynamics.

Figure 21.- Mach 5 maneuver performance for a high-sensed α error of 4° with decreased rudder effectiveness.

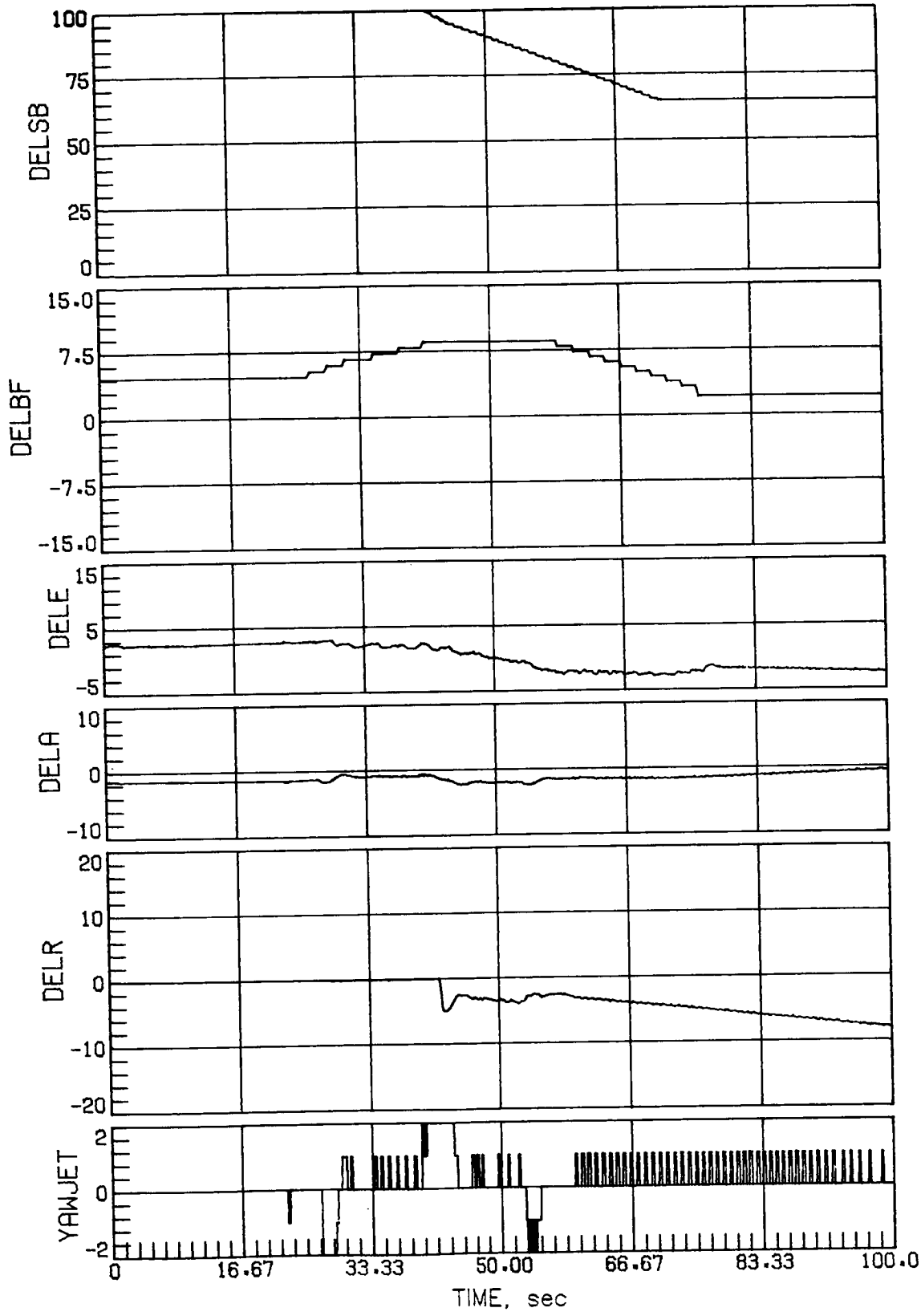

(a) Concluded.

Figure 21.- Continued.

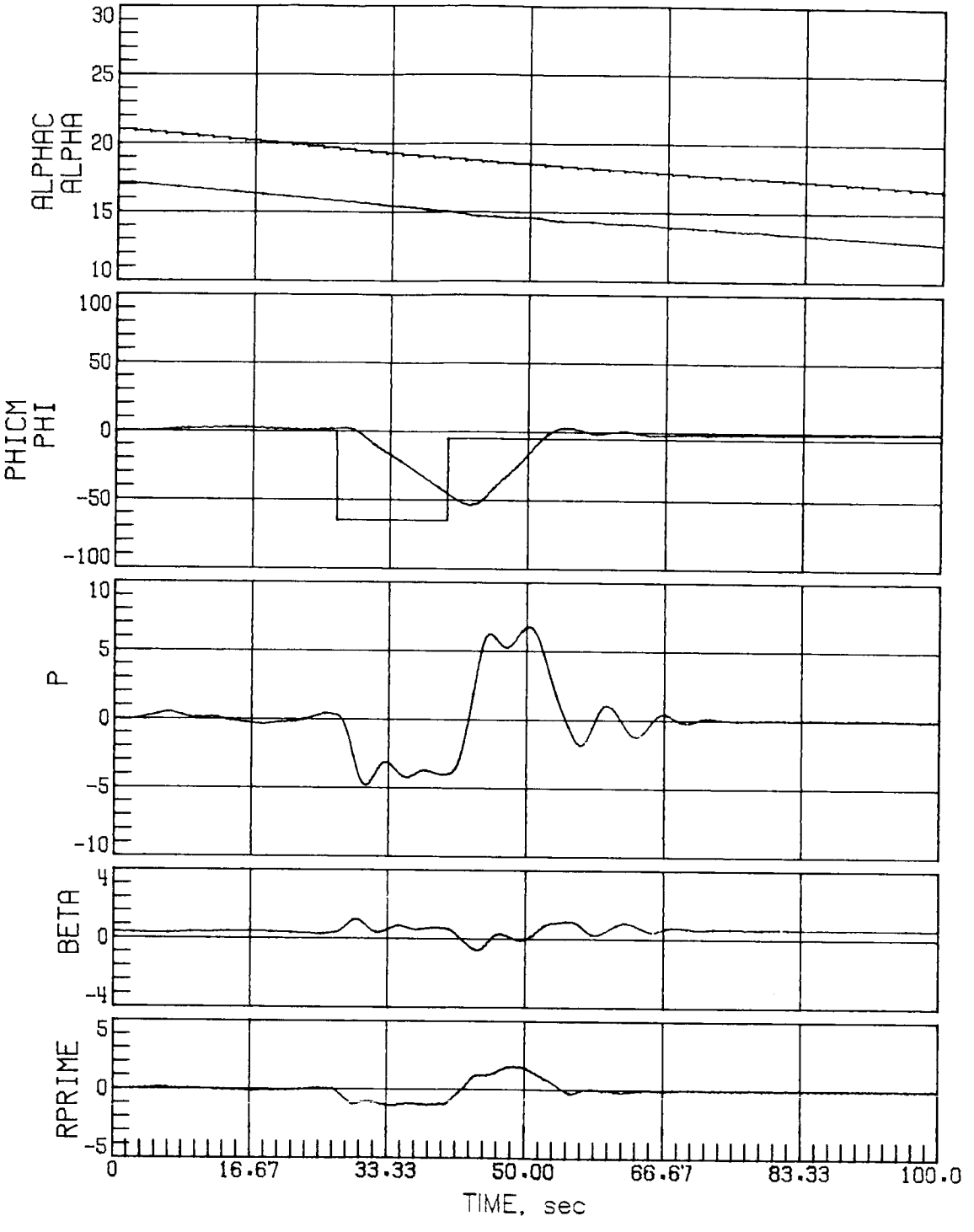

(b) Case 3.

Figure 21.- Continued.

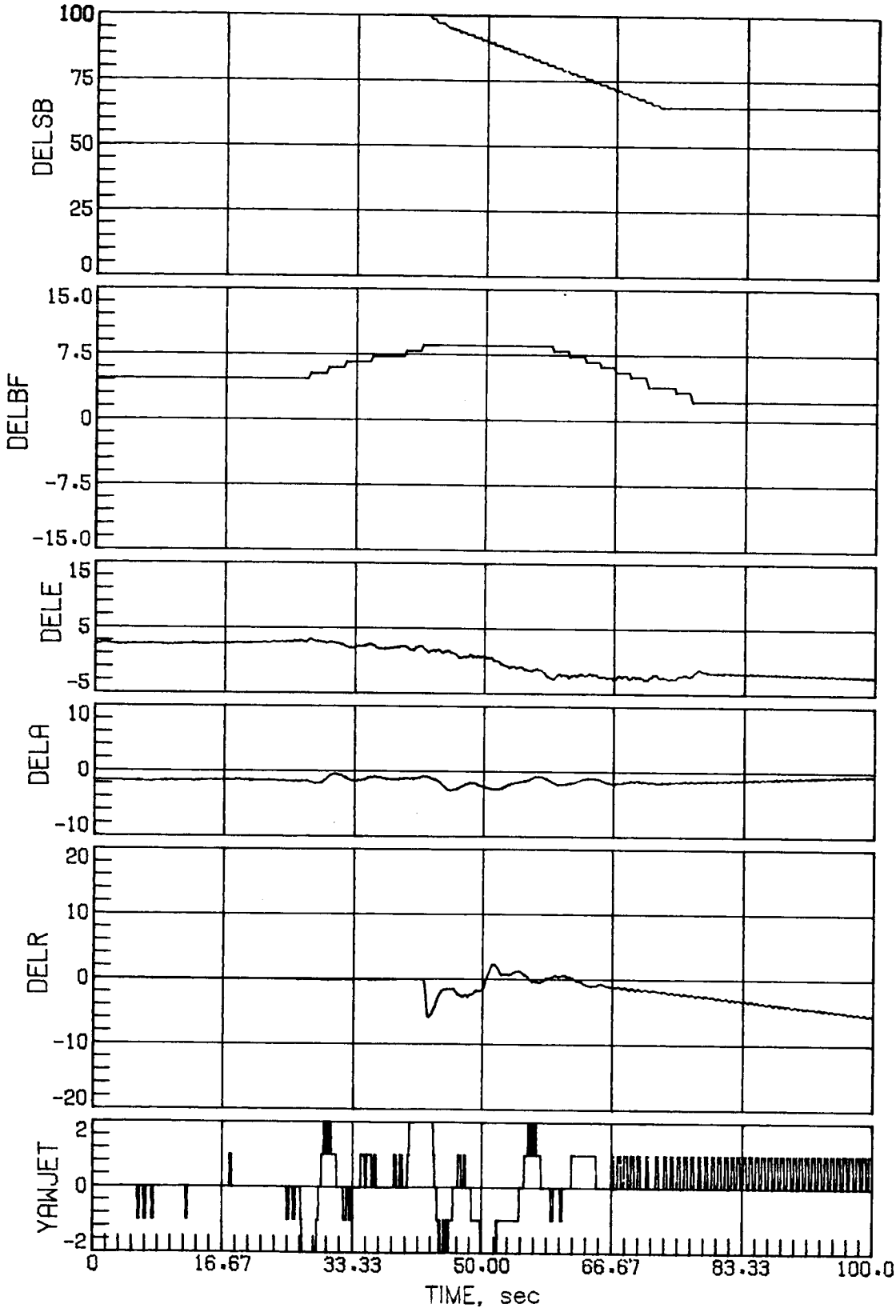

(b) Concluded.

Figure 21.- Continued.

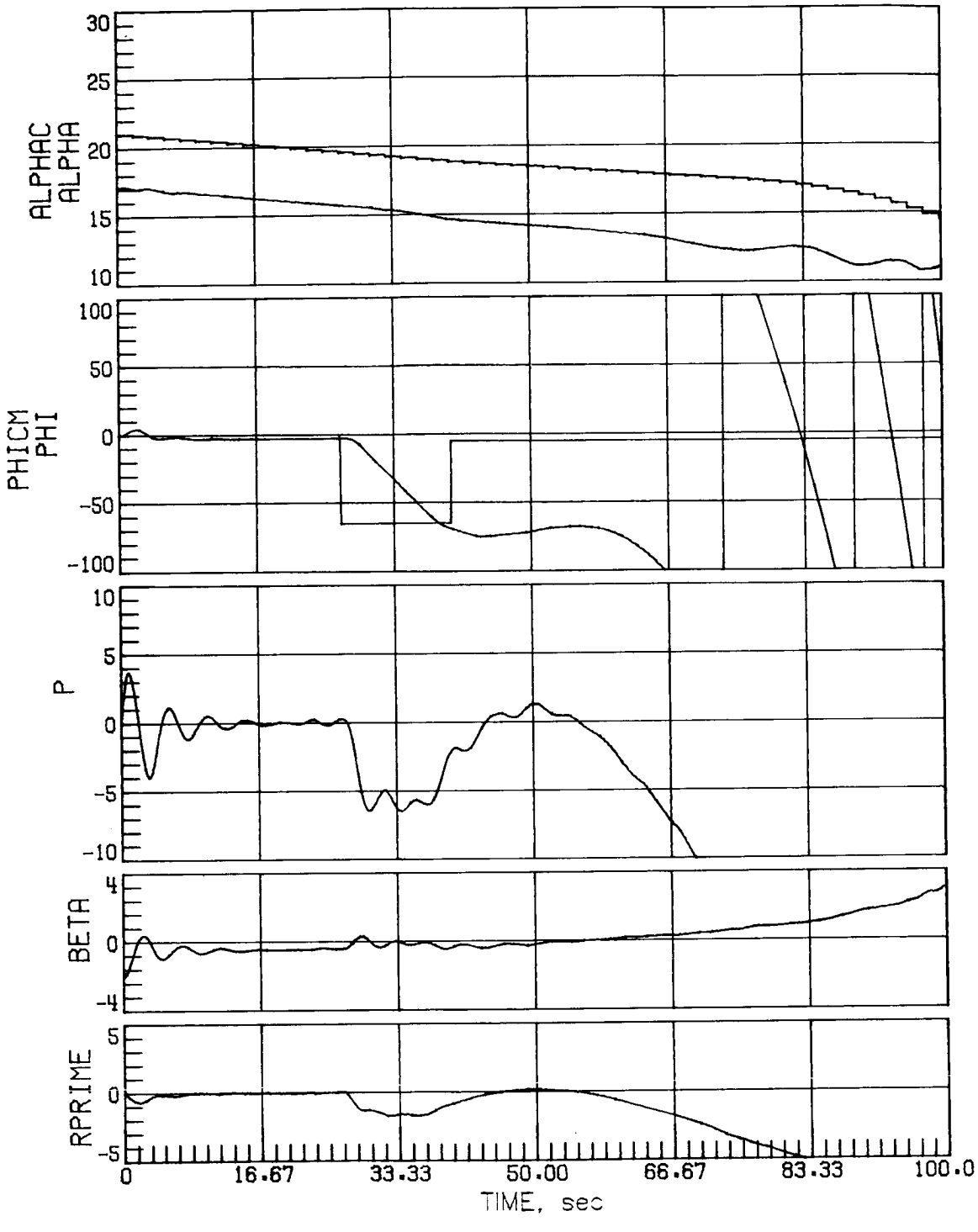

(c) Case 6.

Figure 21.- Continued.

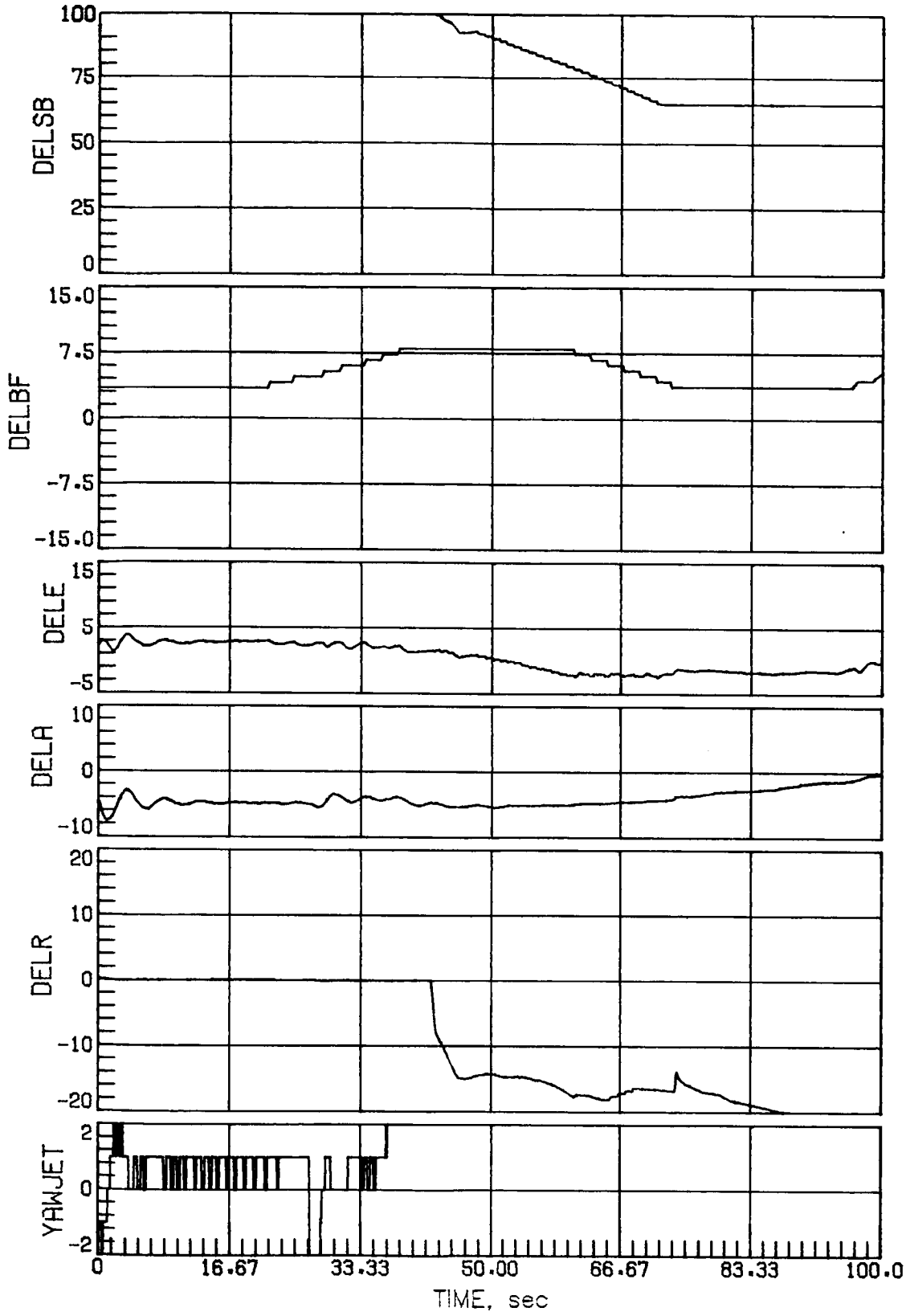

(c) Concluded.

Figure 21.- Continued.

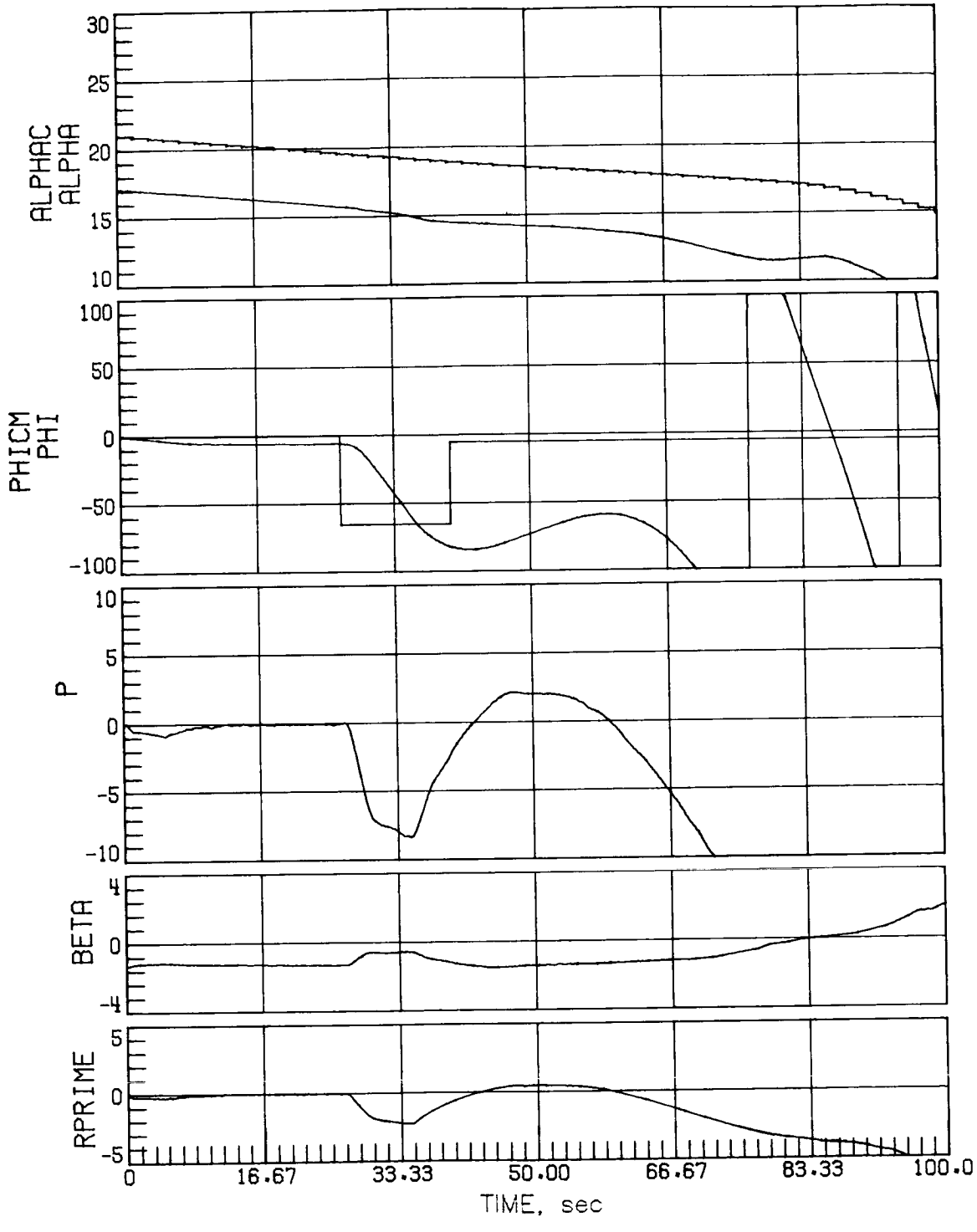

(d) Case 14.

Figure 21.- Continued.

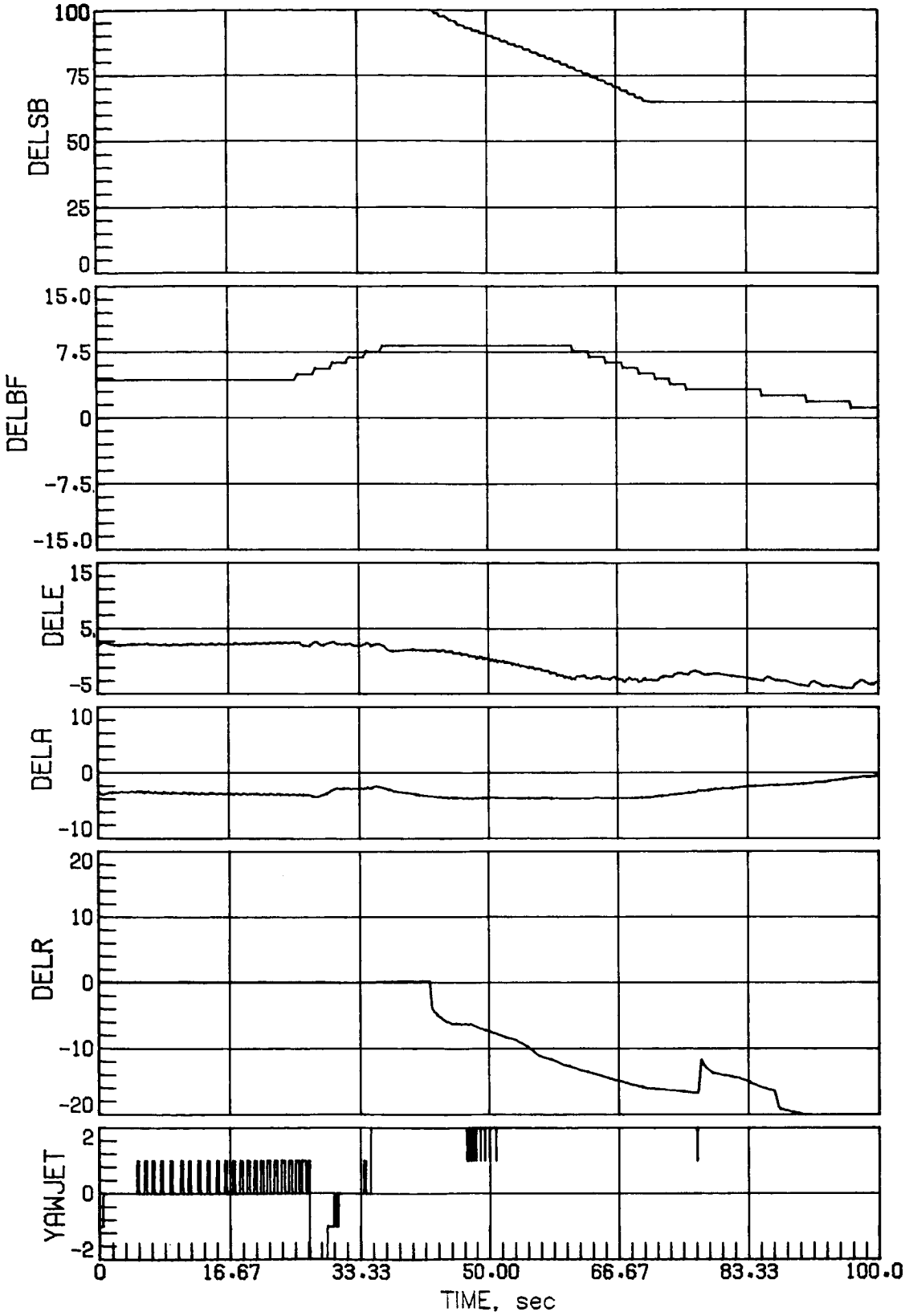

(d) Concluded.

Figure 21.- Concluded.

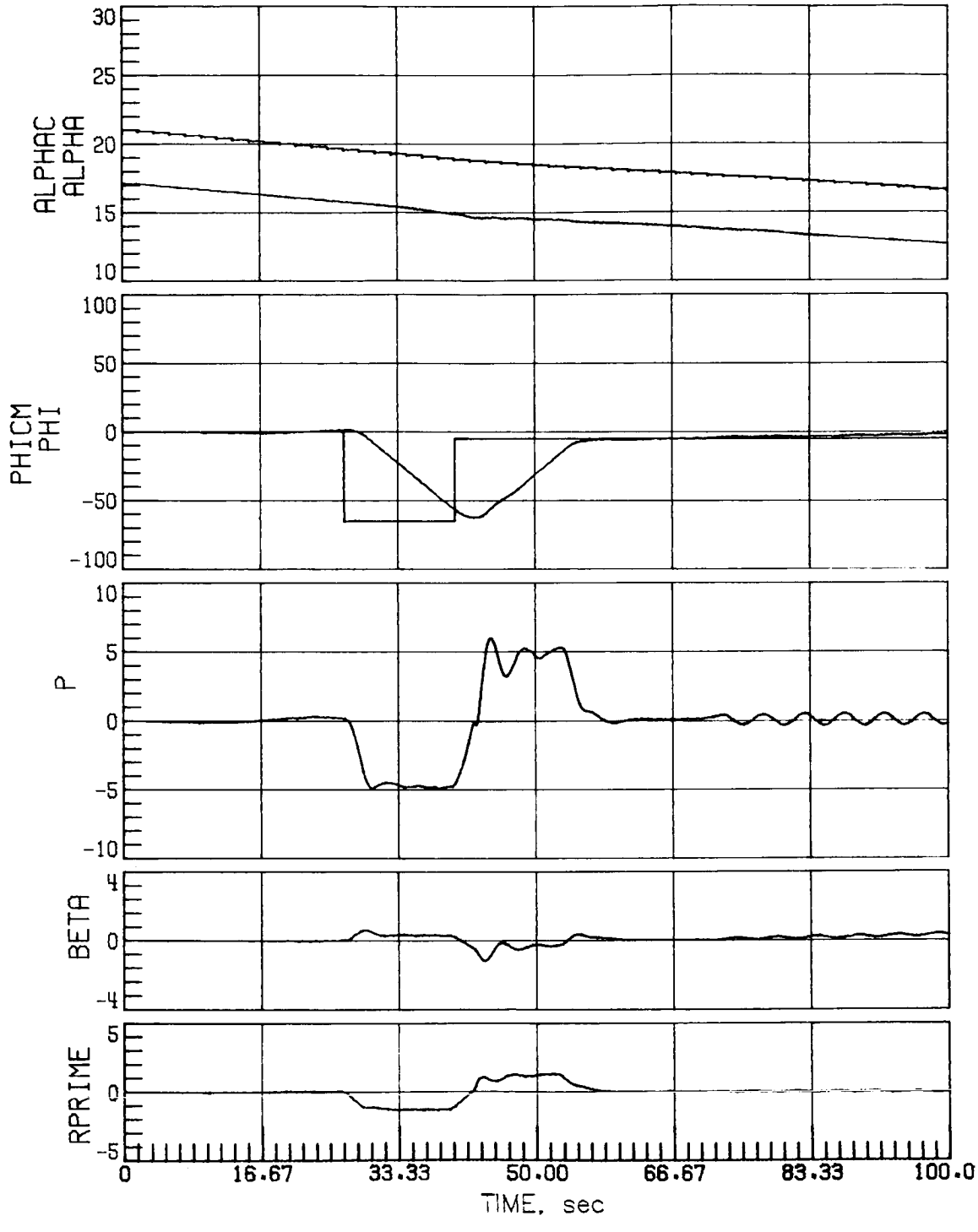

(a) Nominal aerodynamics.

Figure 22.- Mach 5 maneuver performance for a high-sensed α error of 4° with increased rudder effectiveness.

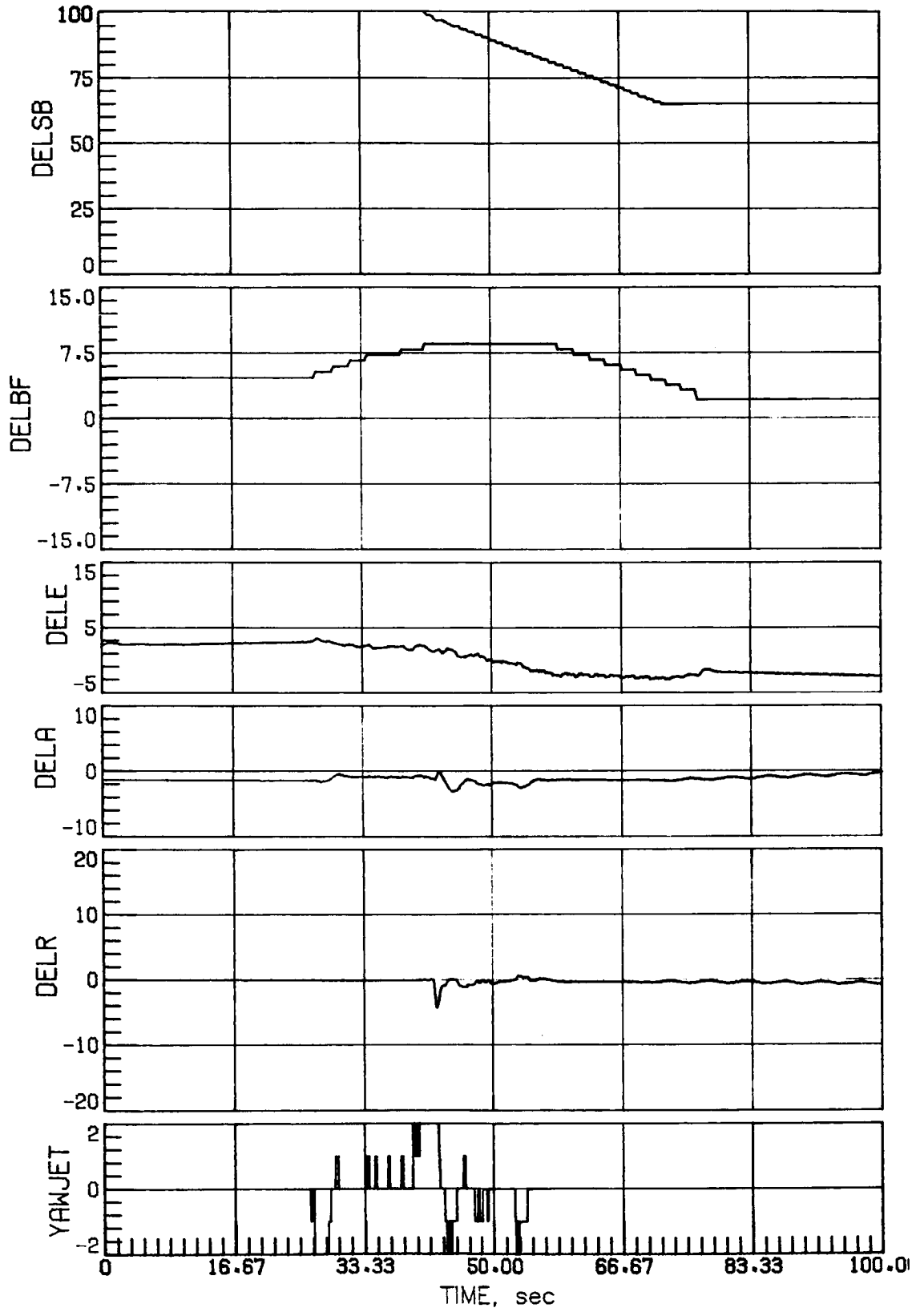

(a) Concluded.

Figure 22.- Continued.

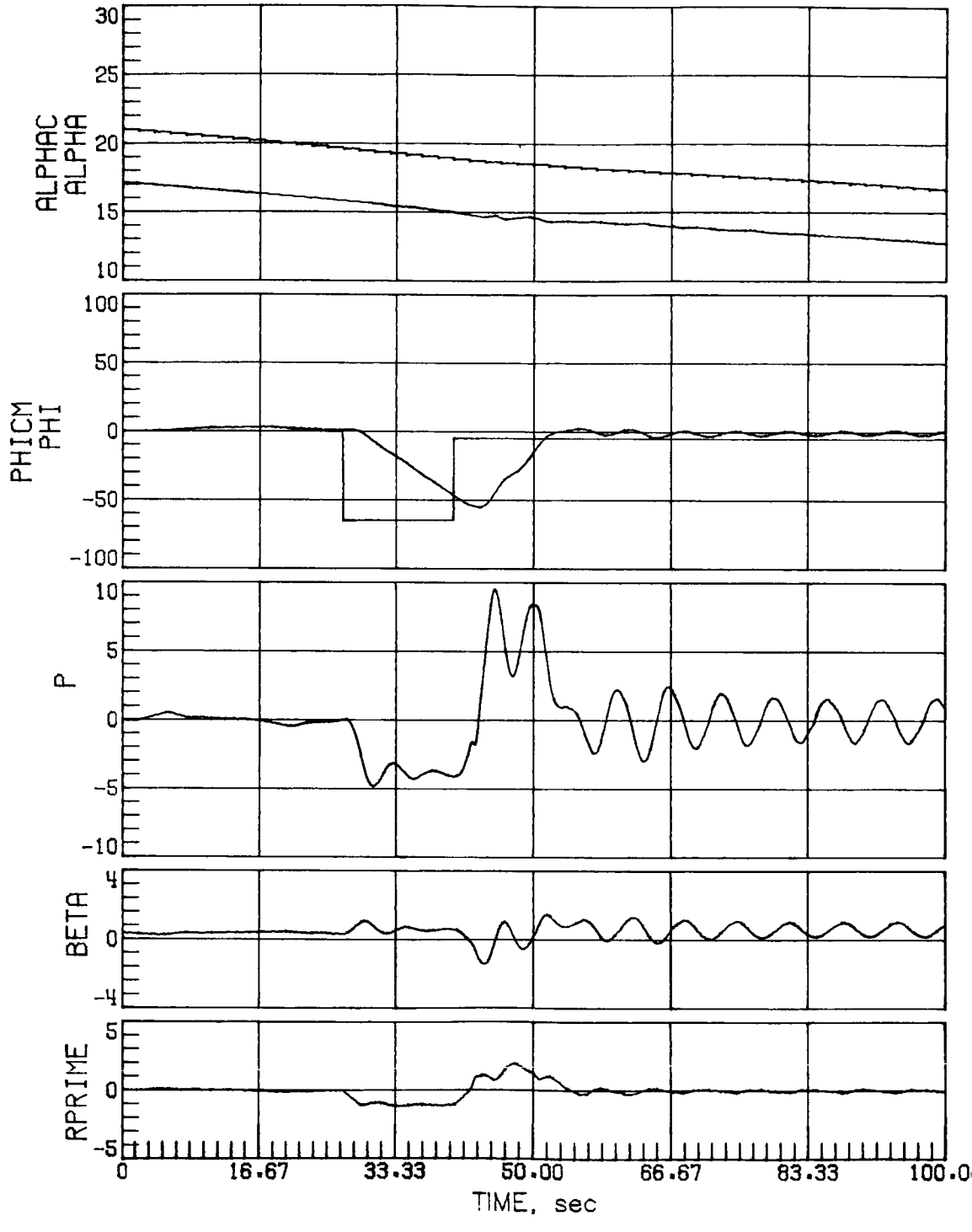

(b) Case 3.

Figure 22.- Continued.

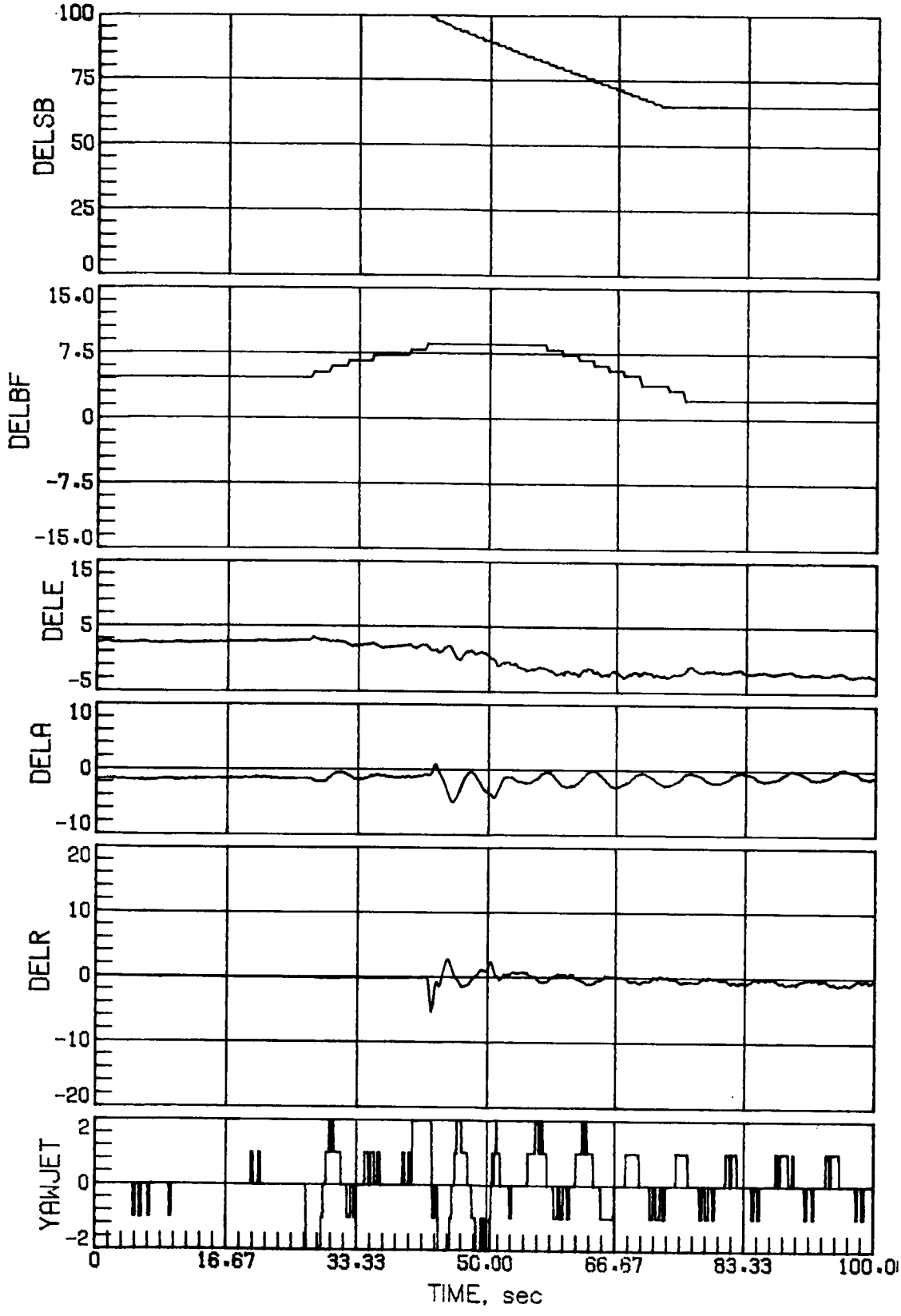

(b) Concluded.

Figure 22.- Continued.

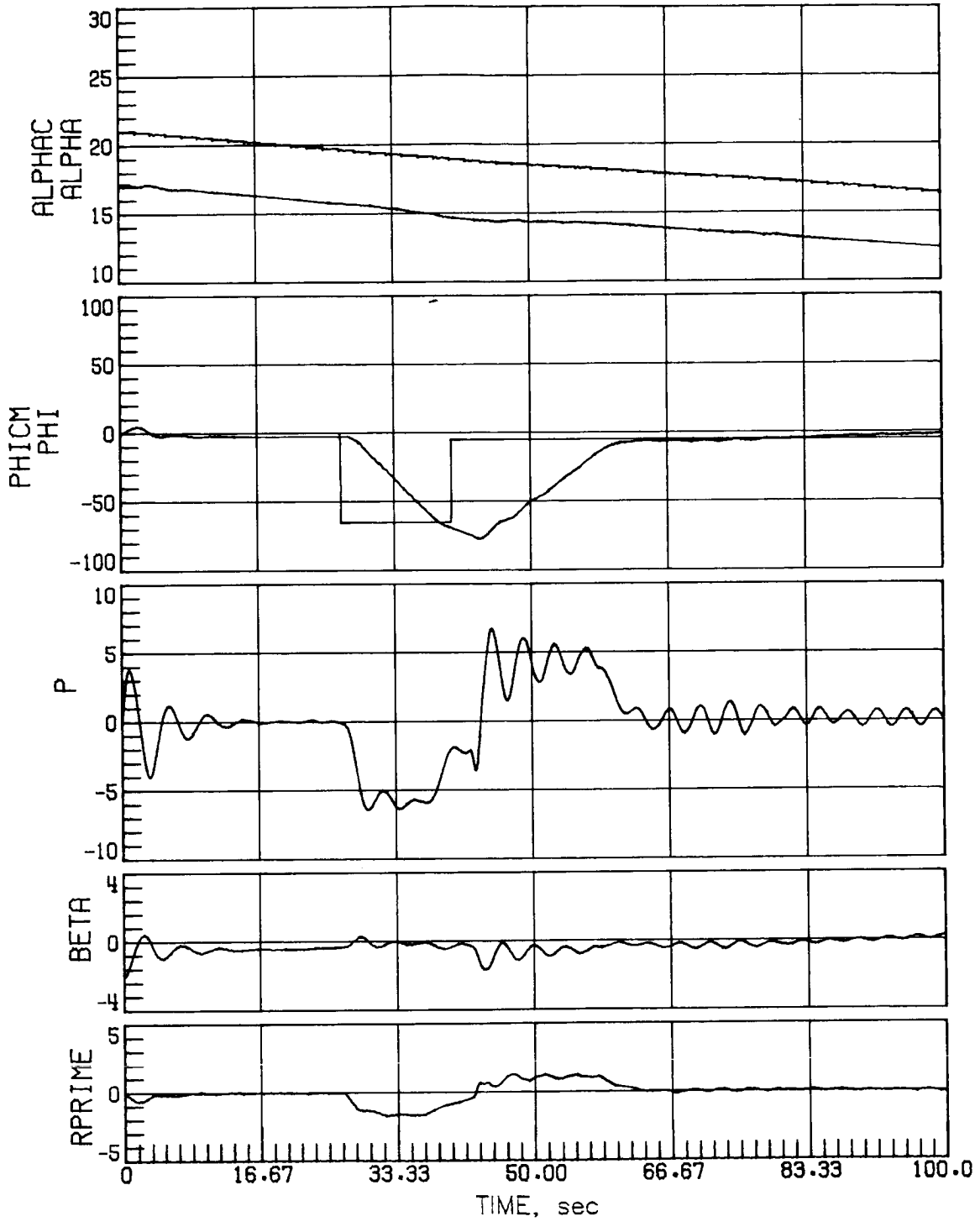

(c) Case 6.

Figure 22.- Continued.

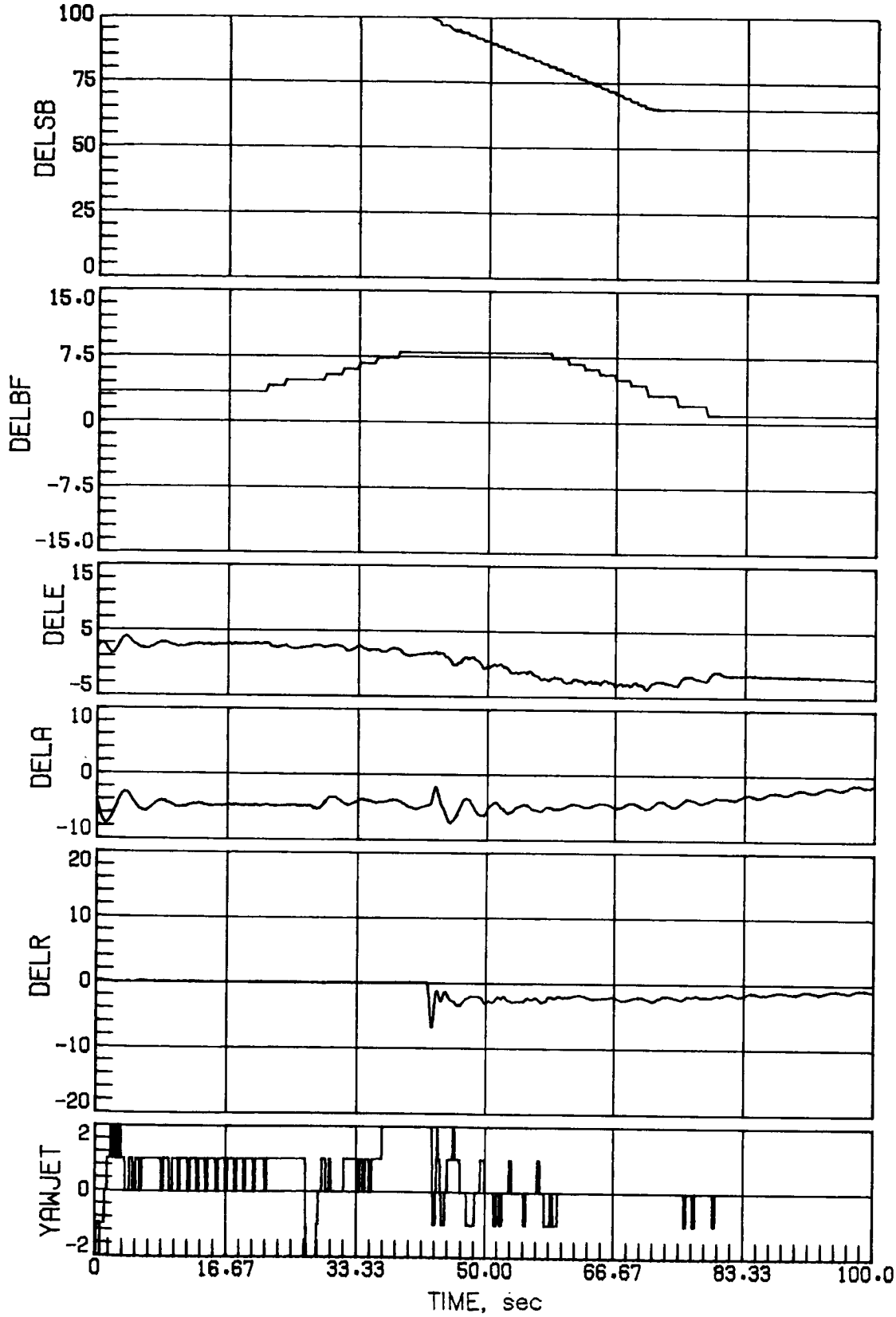

(c) Concluded.

Figure 22.- Continued.

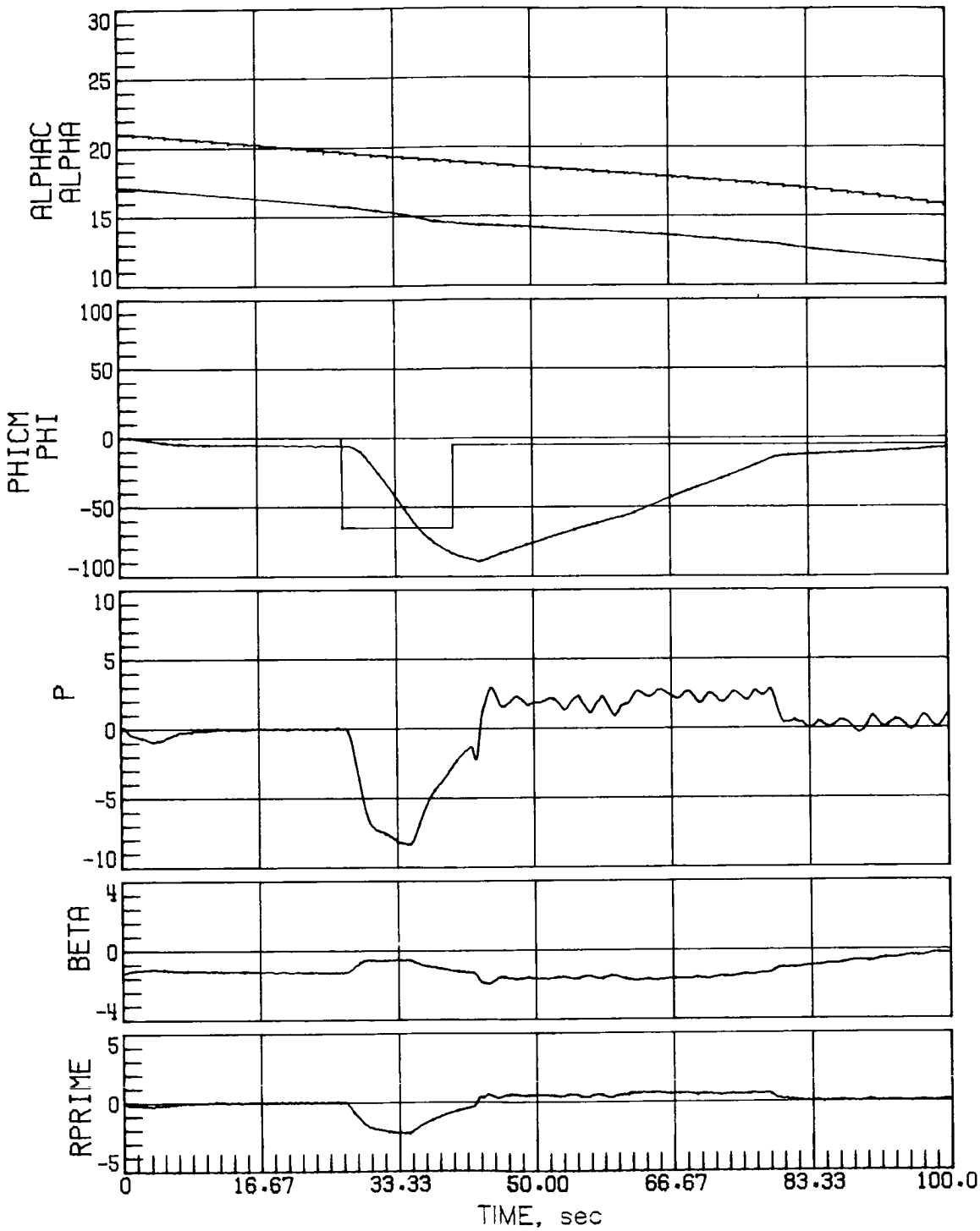

(d) Case 14.

Figure 22.- Continued.

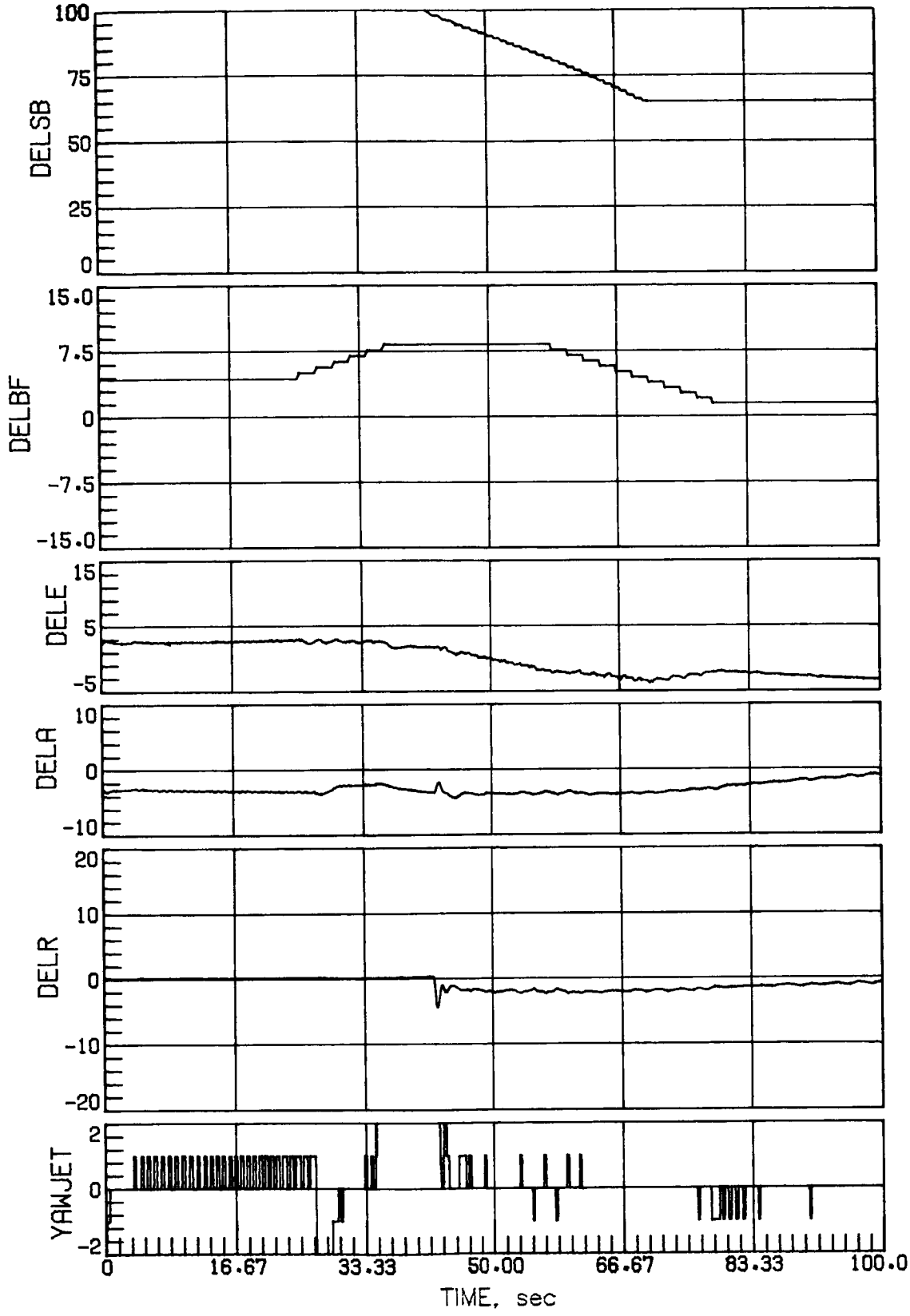

(d) Concluded.

Figure 22.- Concluded.

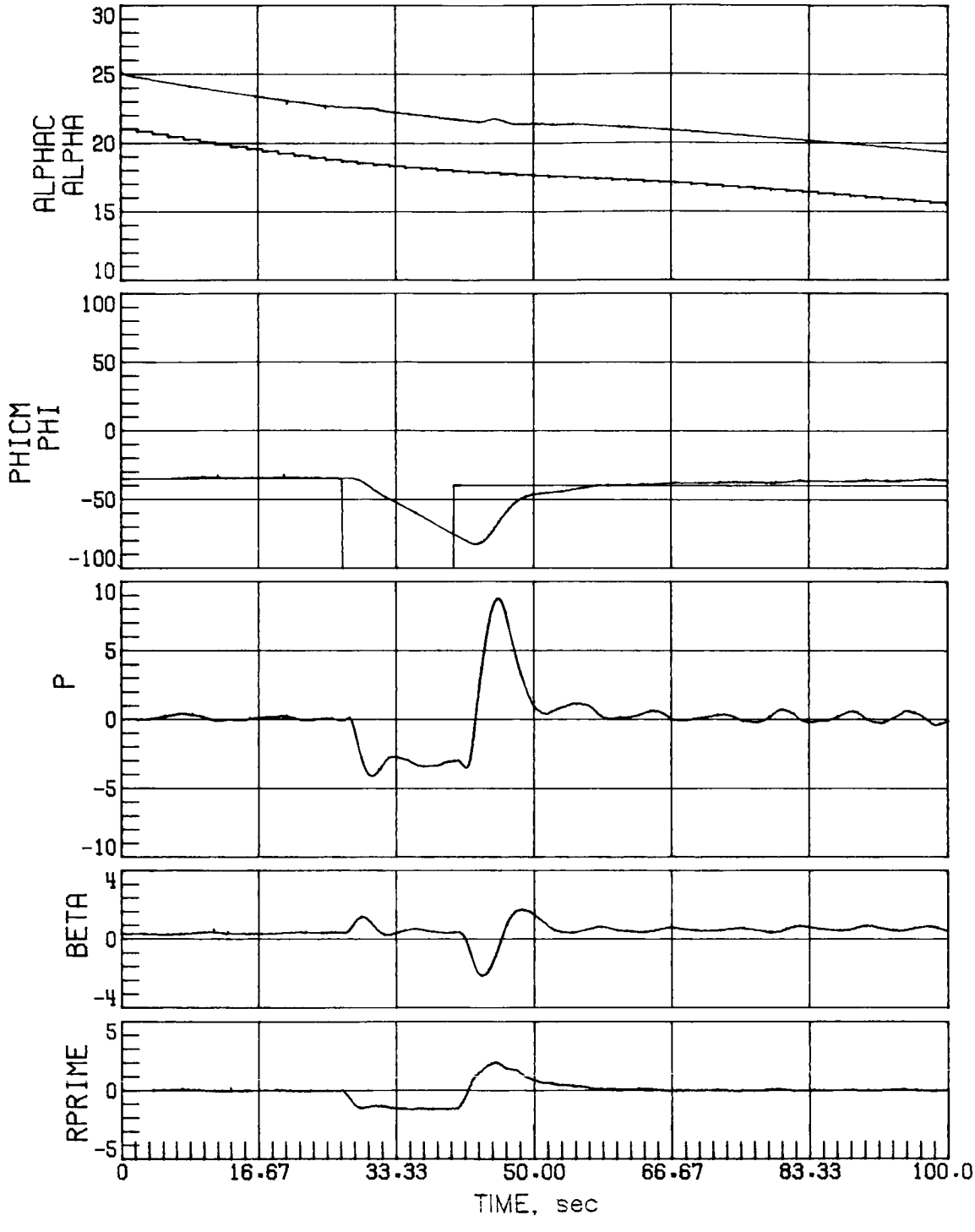

(a) Case 3.

Figure 23.- Mach 5 maneuver performance for a low-sensed α error of 4°.

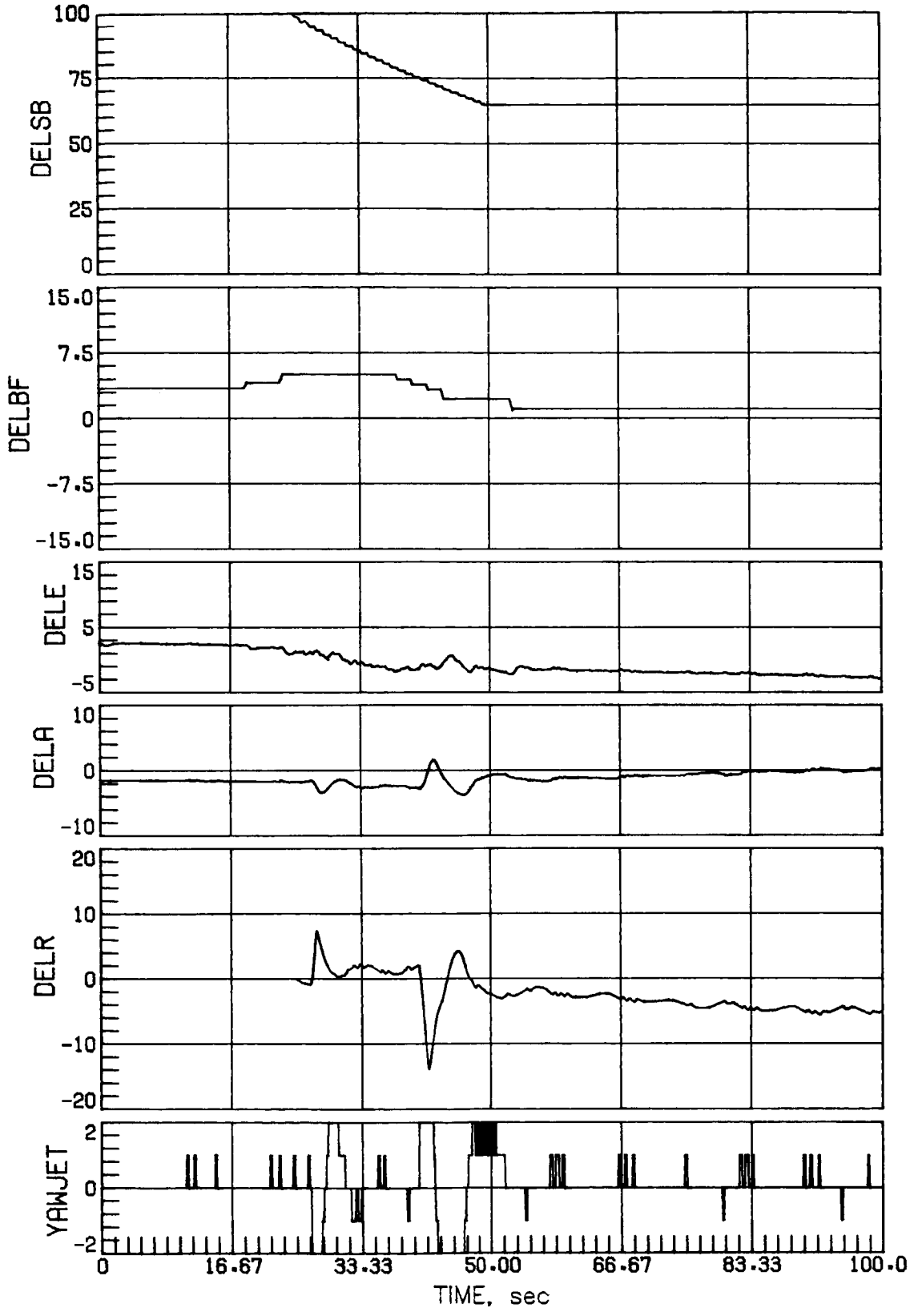

(a) Concluded.

Figure 23.- Continued.

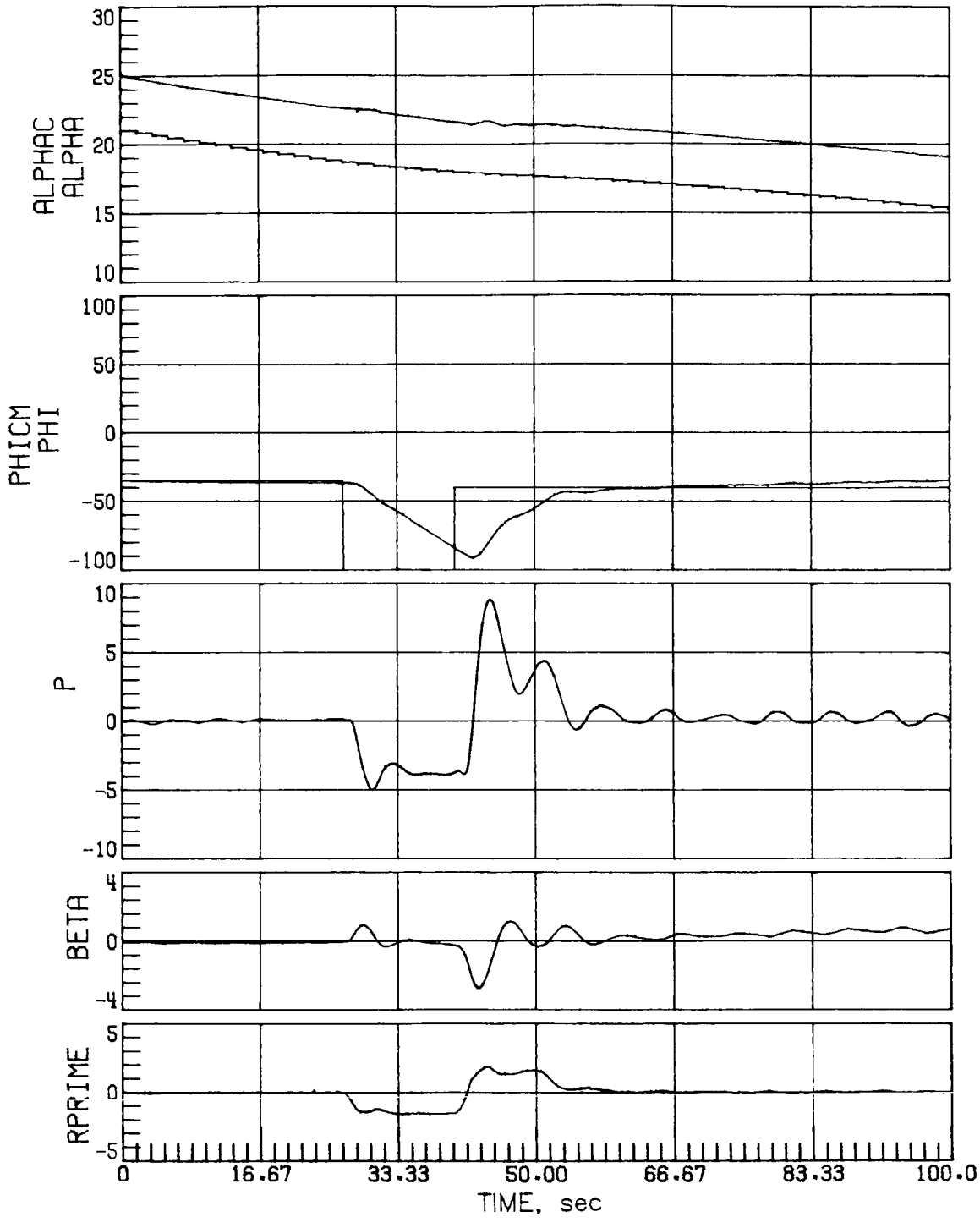

(b) Case 7.

Figure 23.- Continued.

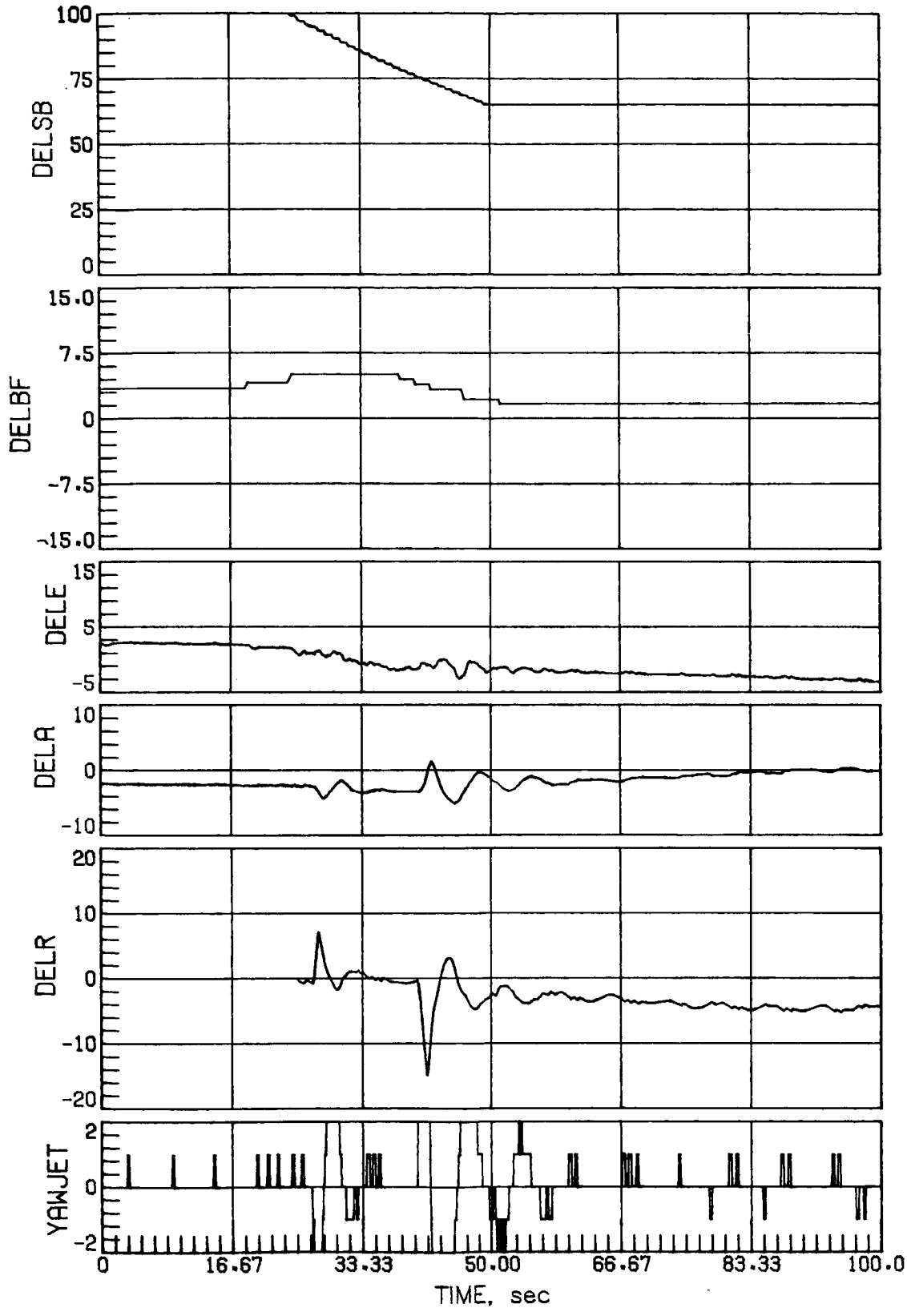

(b) Concluded.

Figure 23.- Continued.

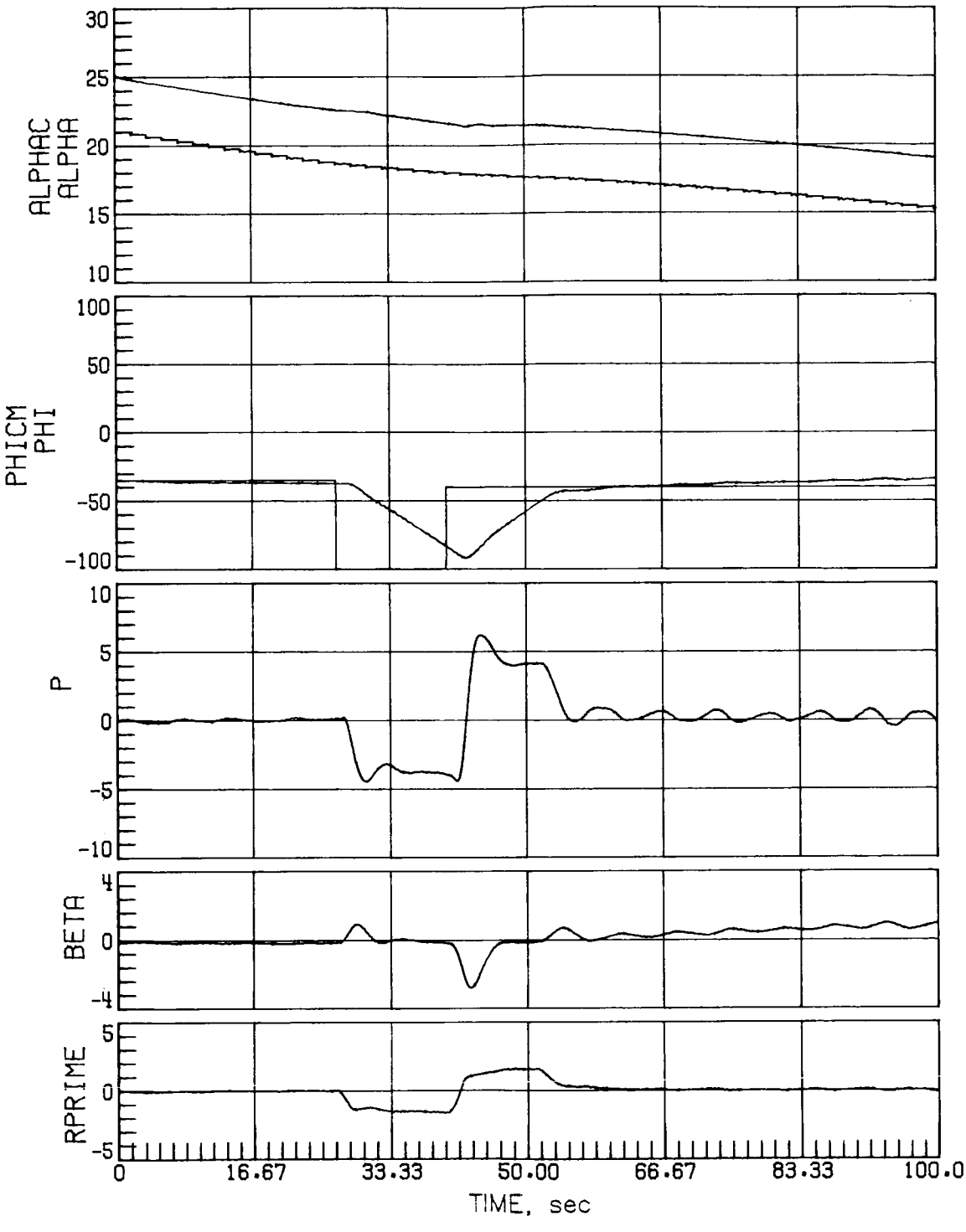

(c) Case 8.

Figure 23.- Continued.

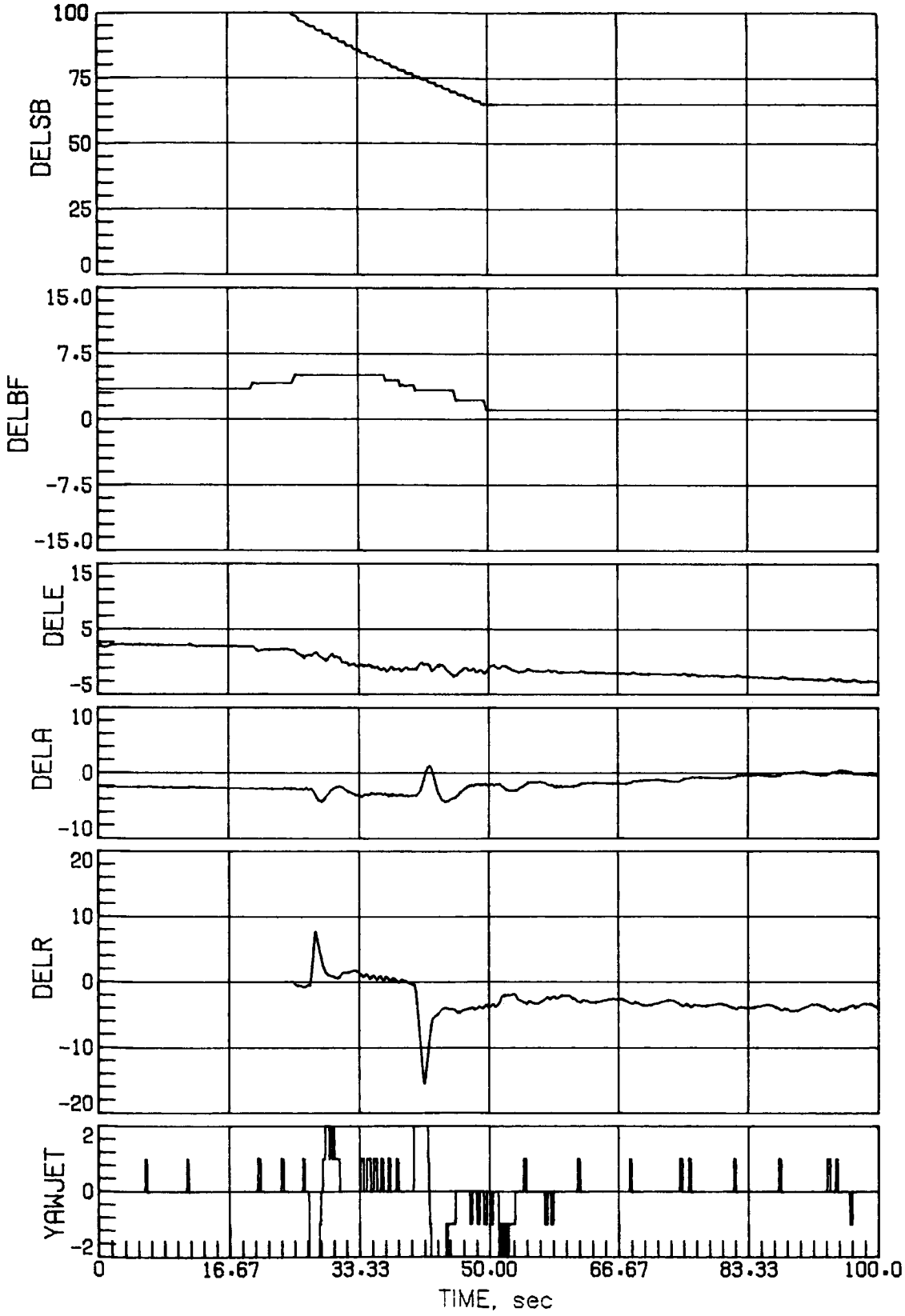

(c) Concluded.

Figure 23.- Continued.

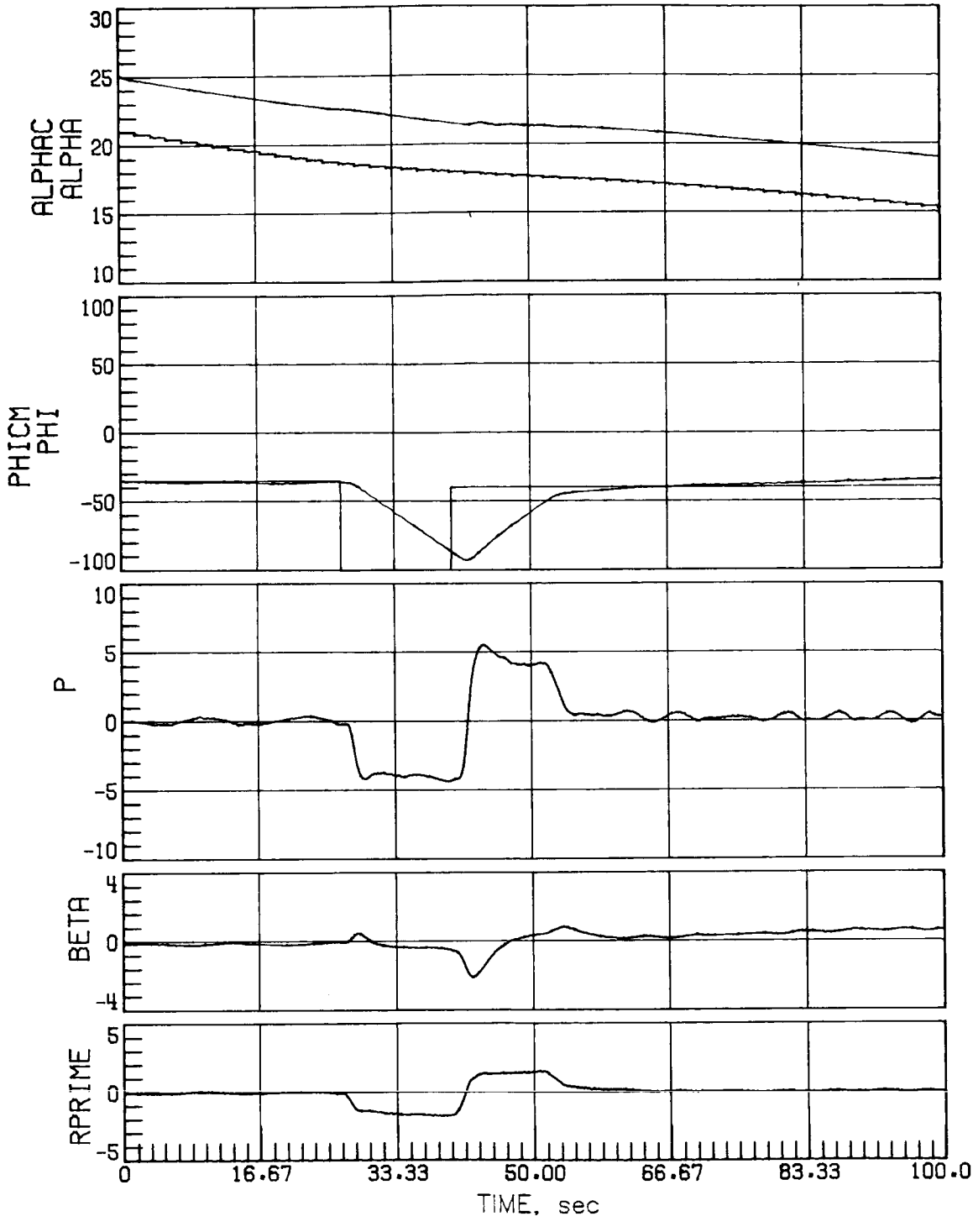

(d) Case 15.

Figure 23.- Continued.

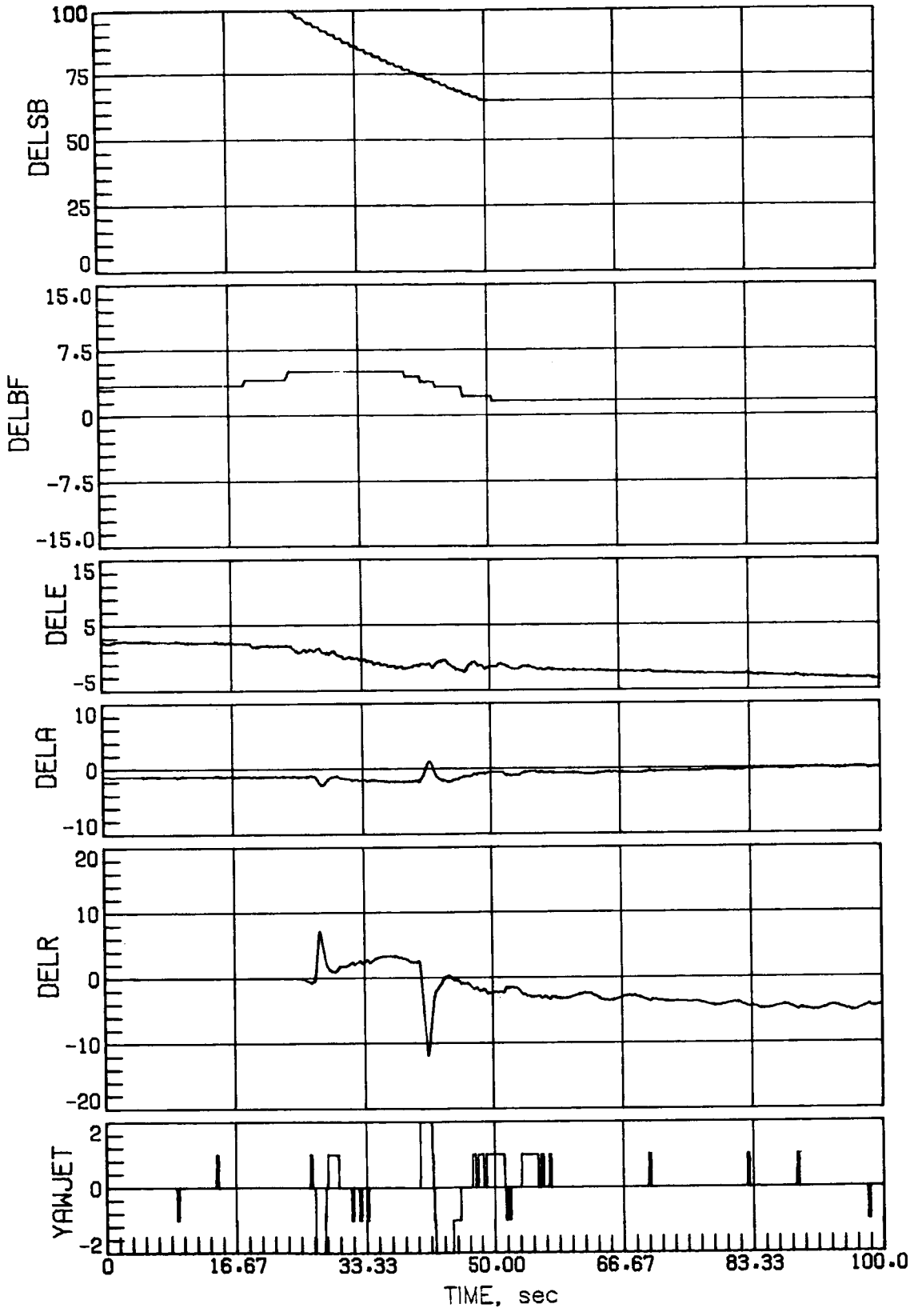

(d) Concluded.

Figure 23.- Concluded.

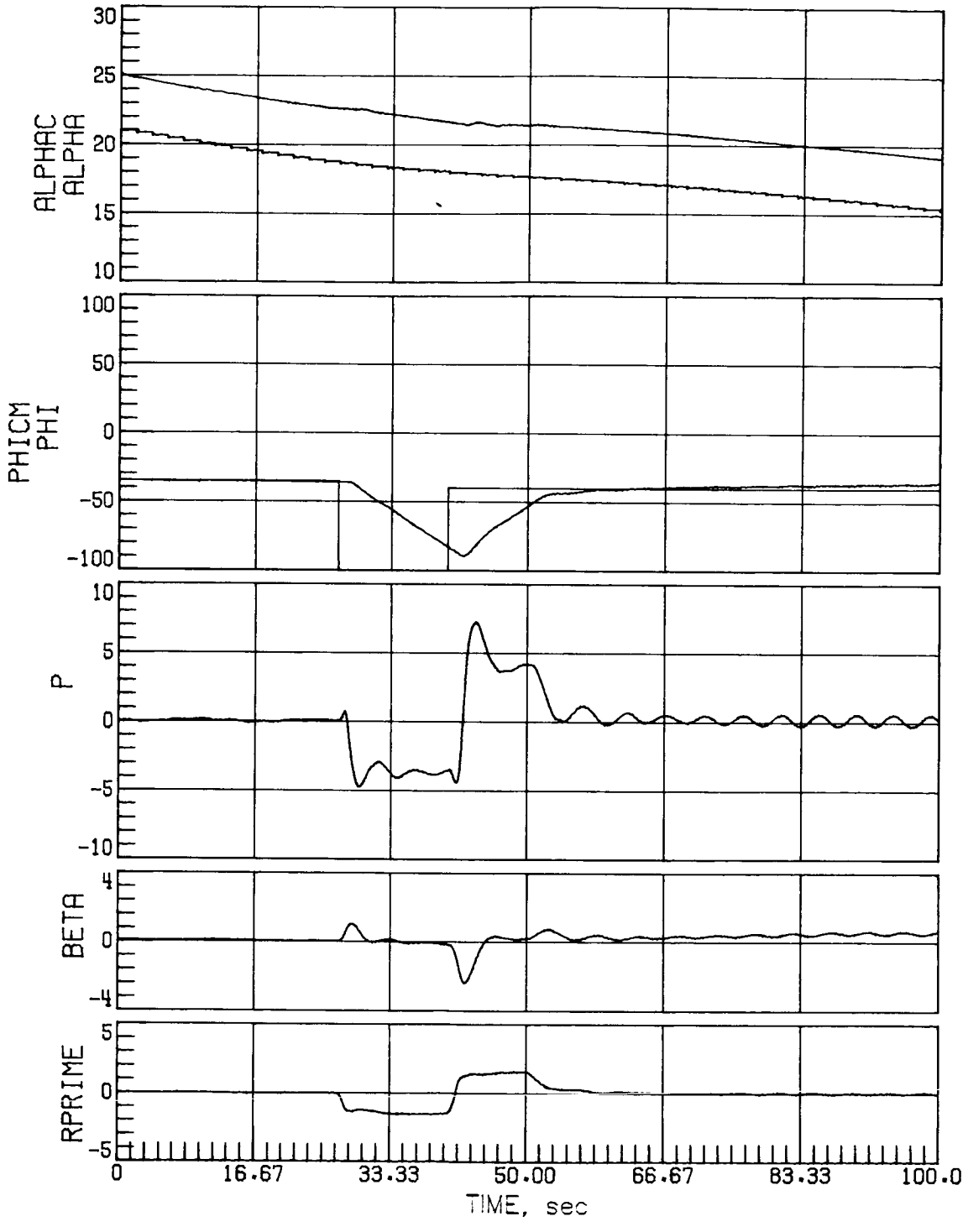

(a) Nominal aerodynamics.

Figure 24.- Mach 5 maneuver performance for a low-sensed α error of 4° with increased rudder effectiveness.

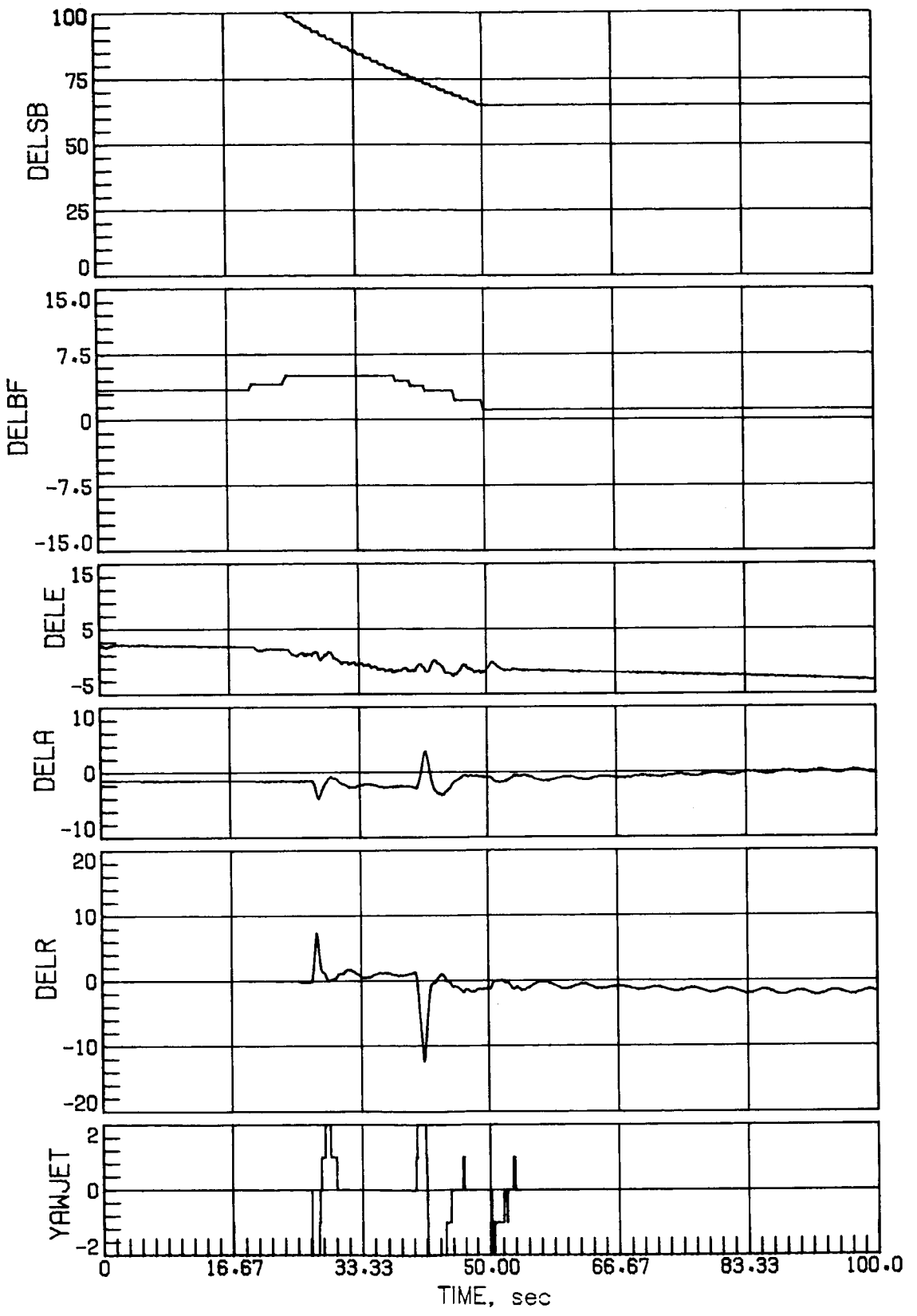

(a) Concluded.

Figure 24.- Continued.

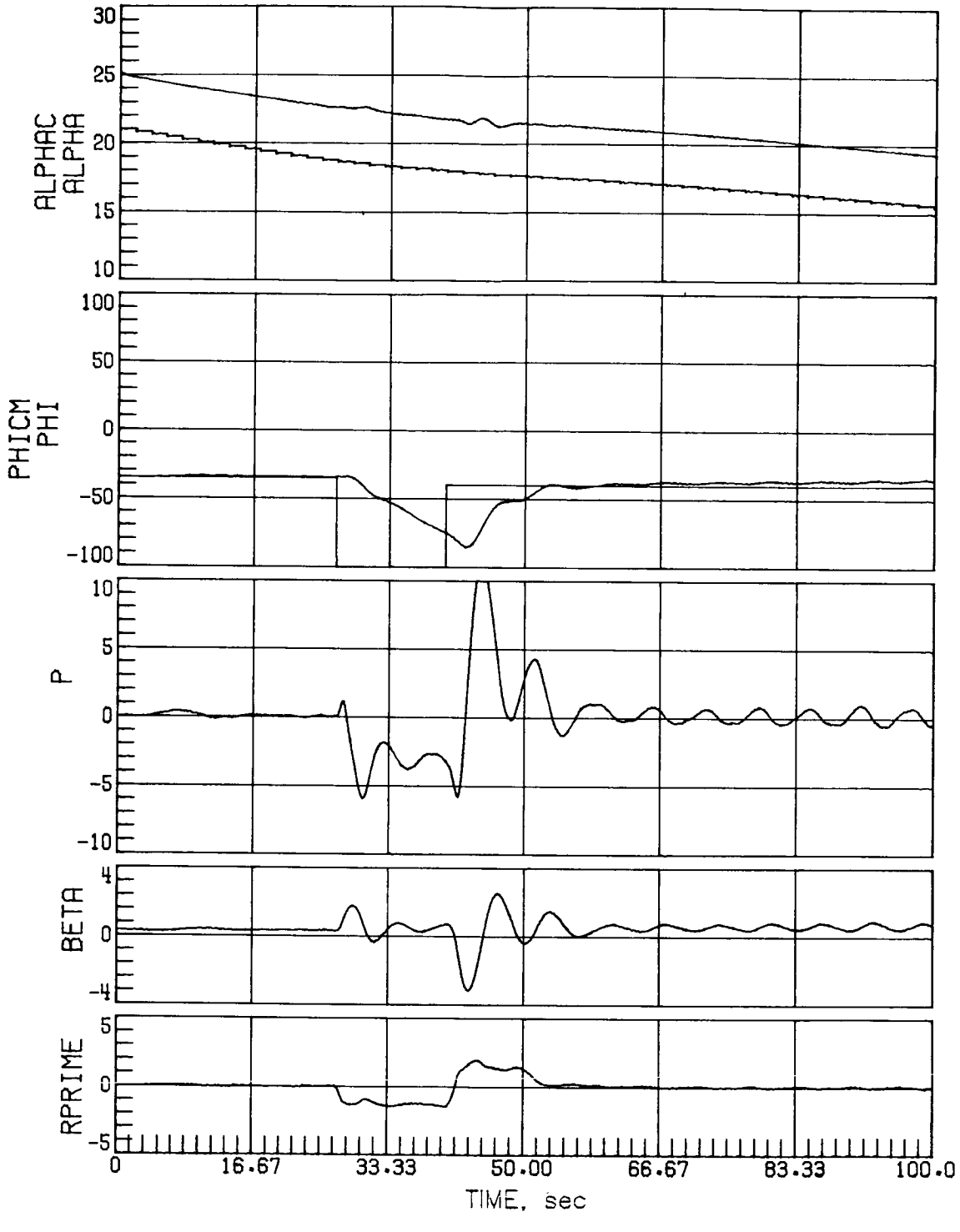

(b) Case 3.

Figure 24.- Continued.

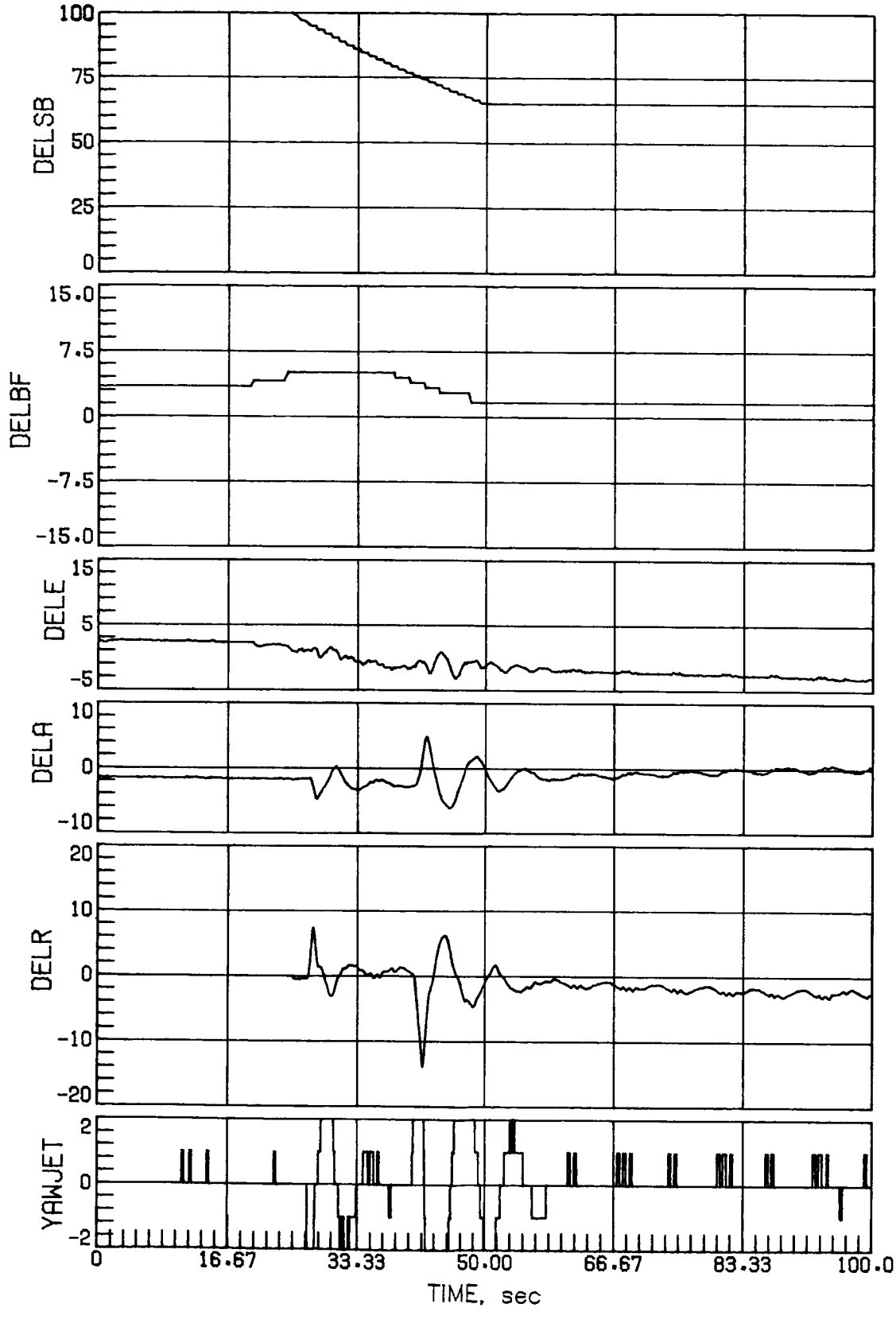

(b) Concluded.

Figure 24.- Continued.

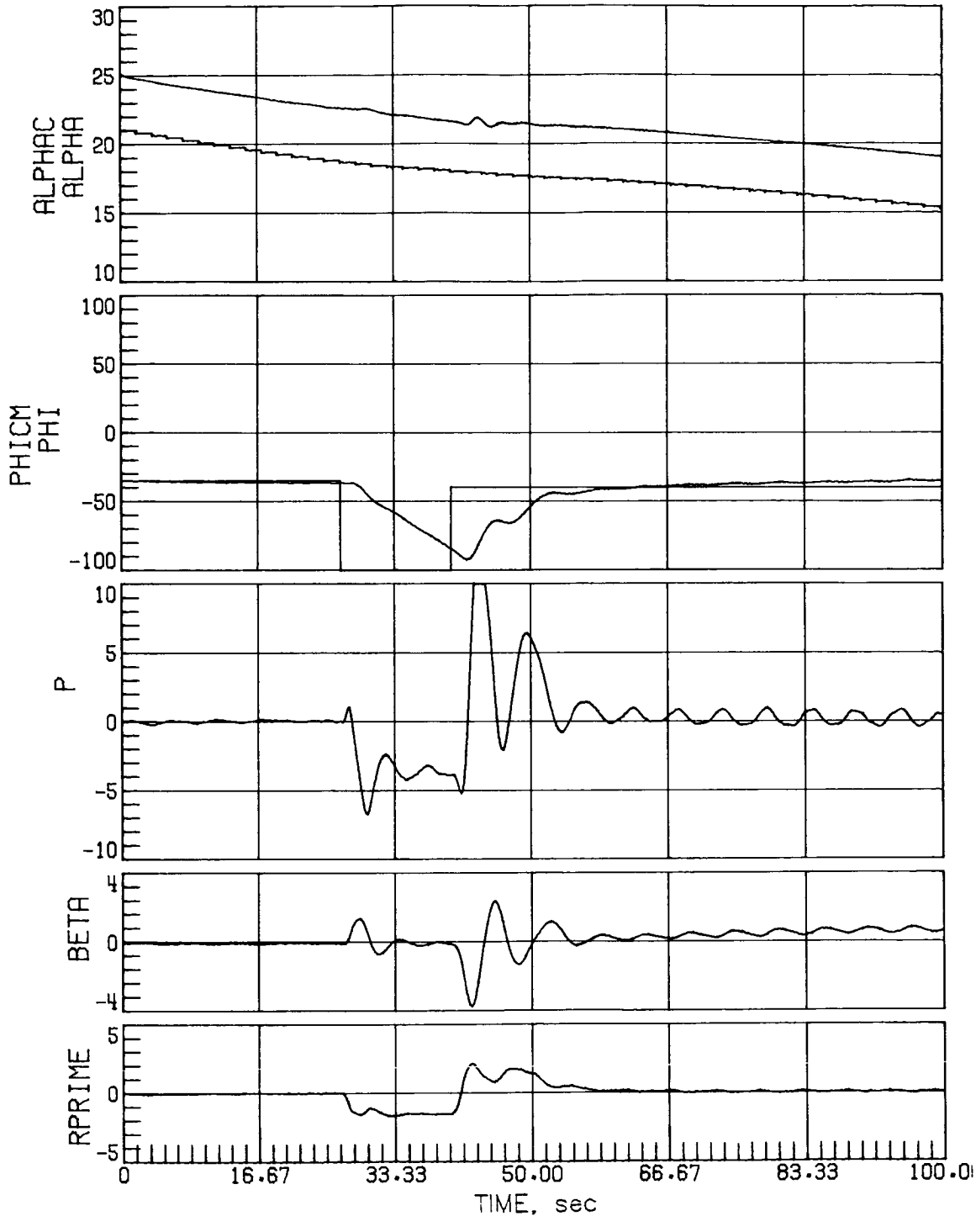

(c) Case 7.

Figure 24.- Continued.

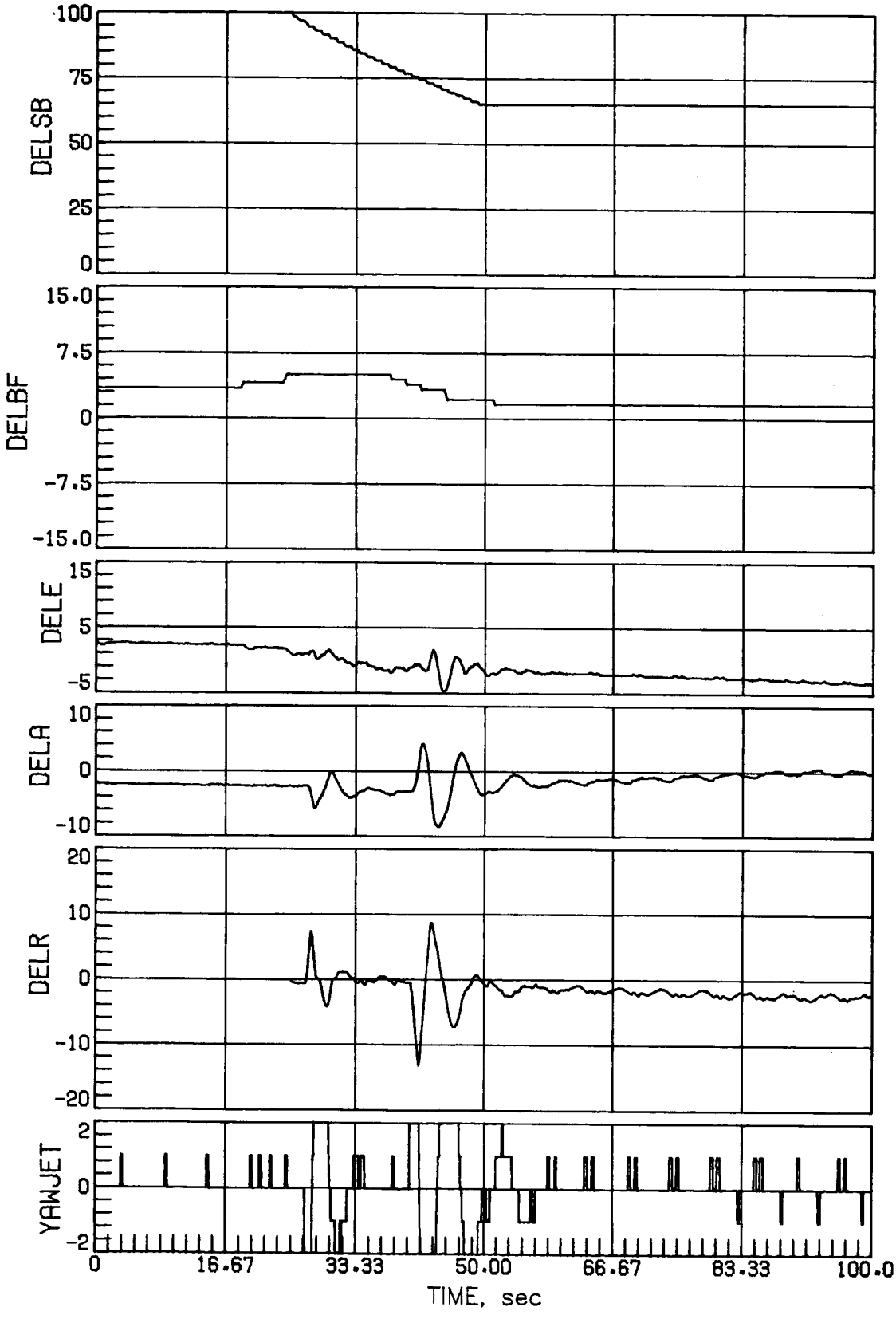

(c) Concluded.

Figure 24.- Concluded.

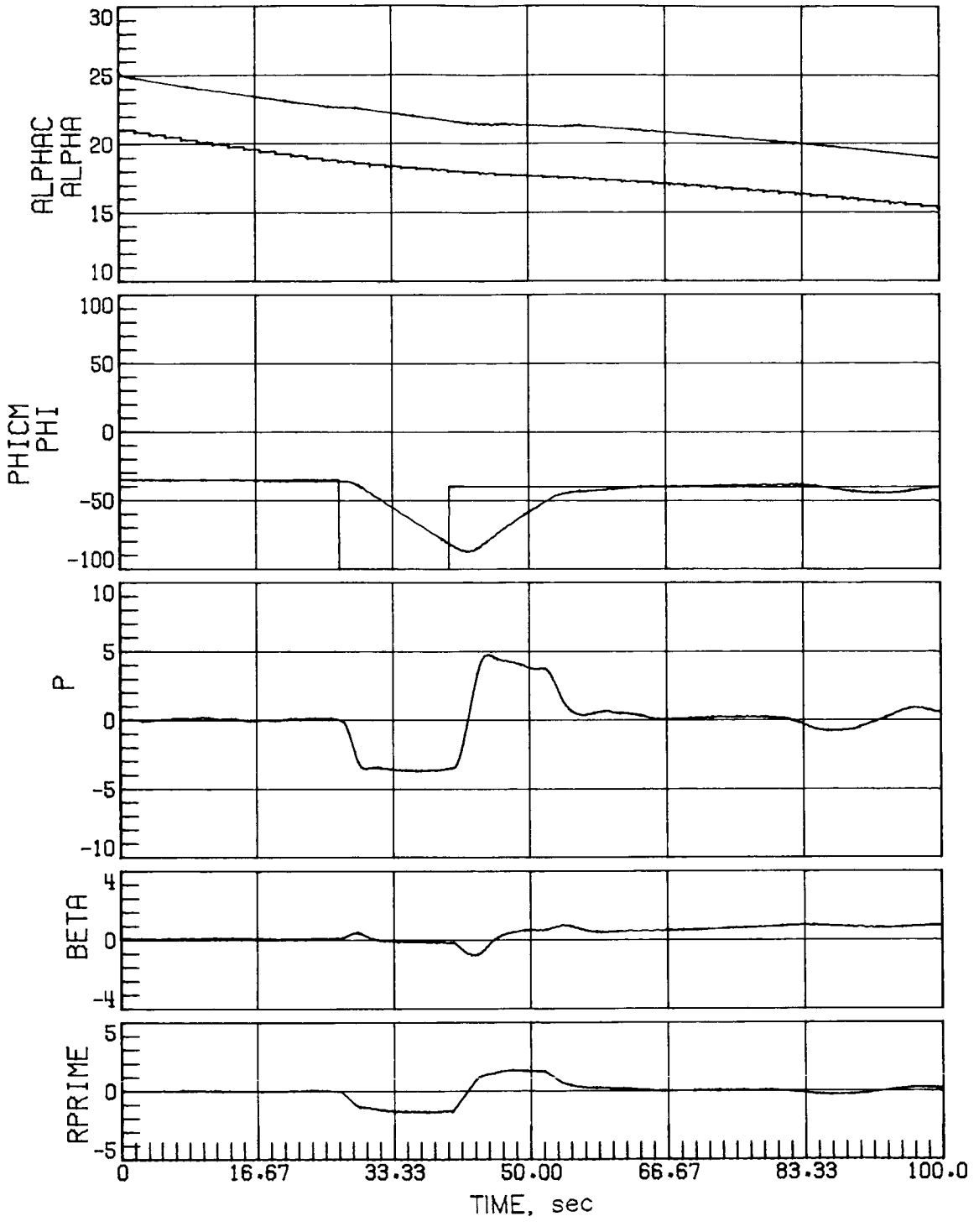

(a) Nominal aerodynamics.

Figure 25.- Mach 5 maneuver performance for a low-sensed α error of 4° with decreased rudder effectiveness.

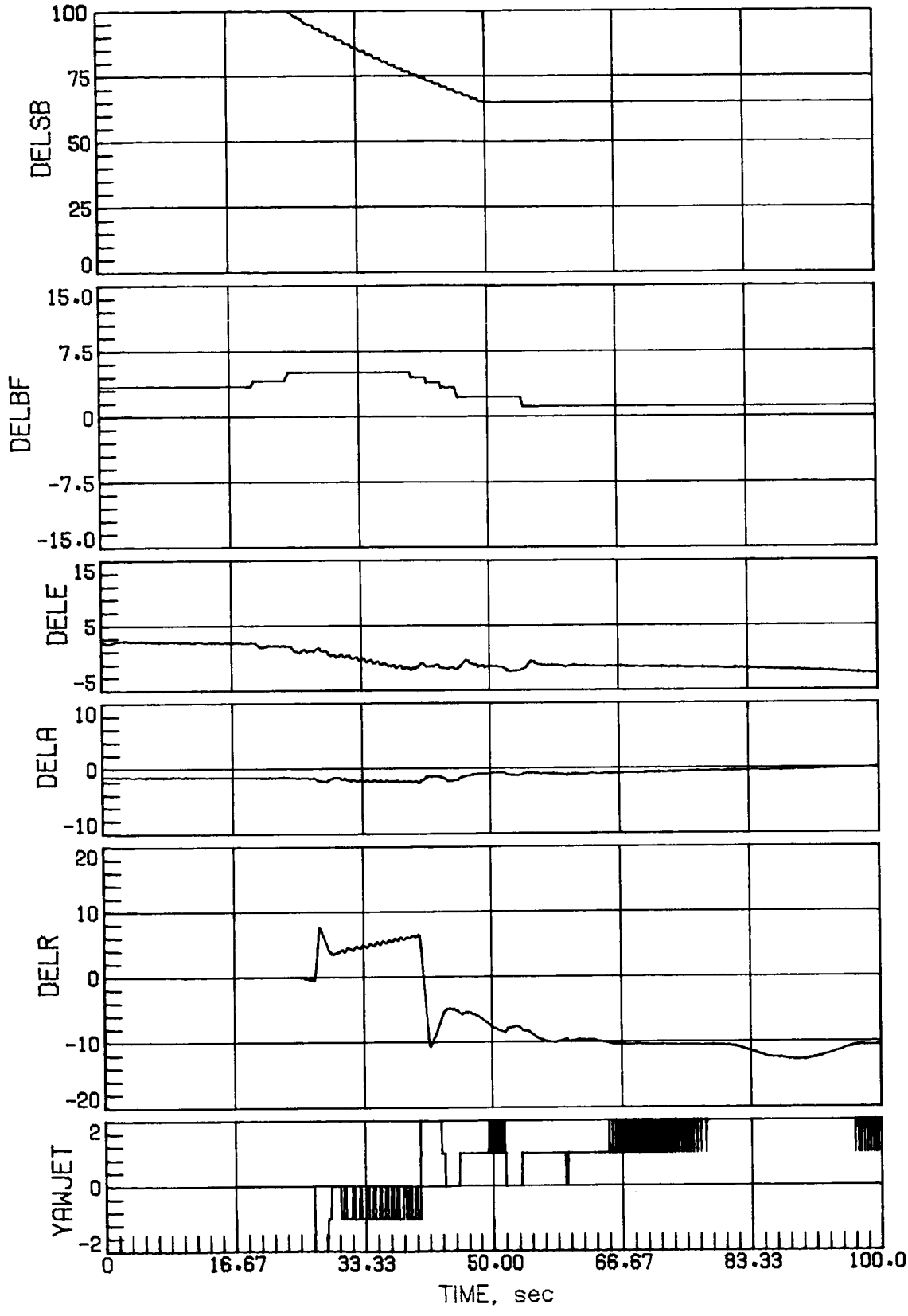

(a) Concluded.

Figure 25.- Continued.

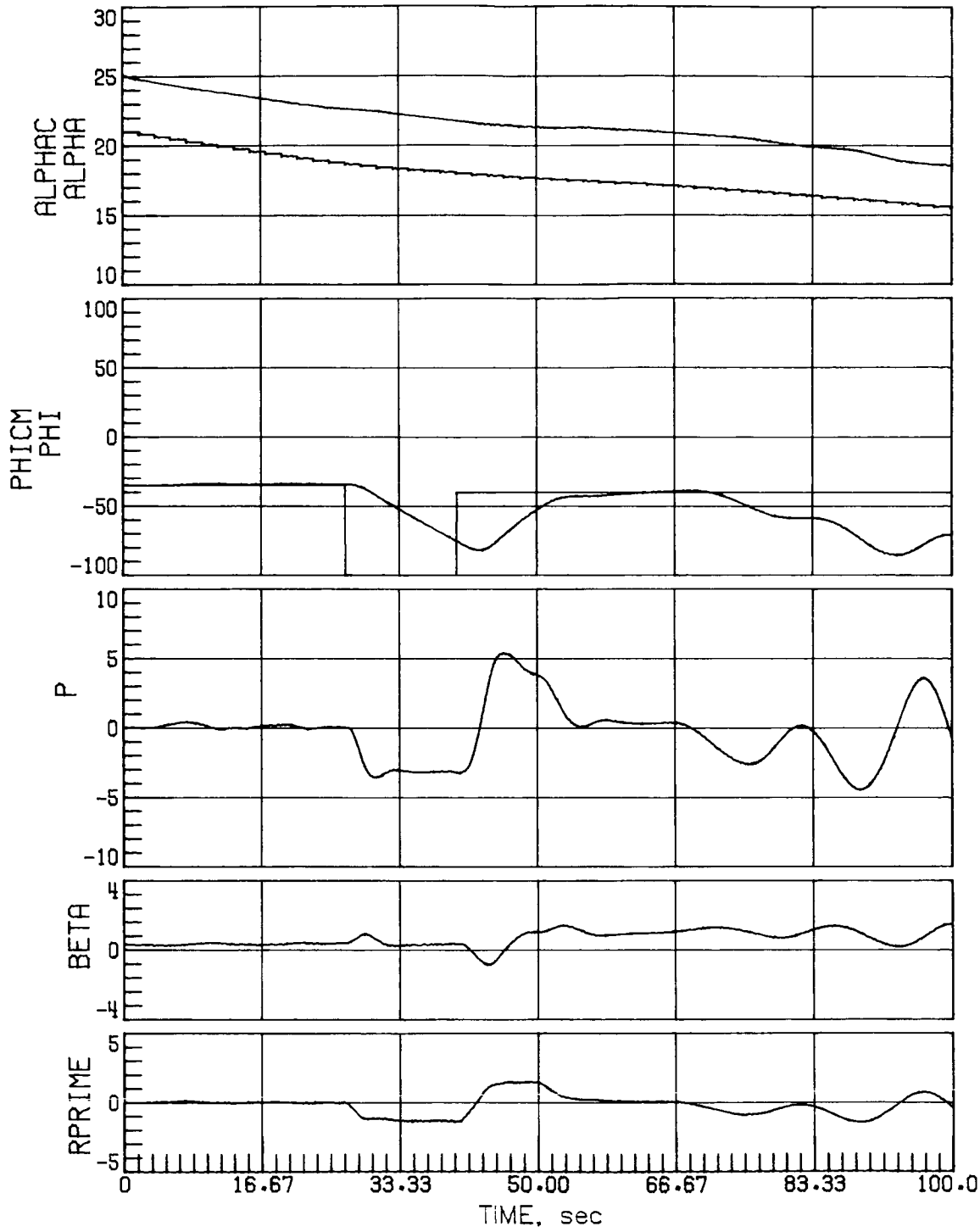

(b) Case 3.

Figure 25.- Continued.

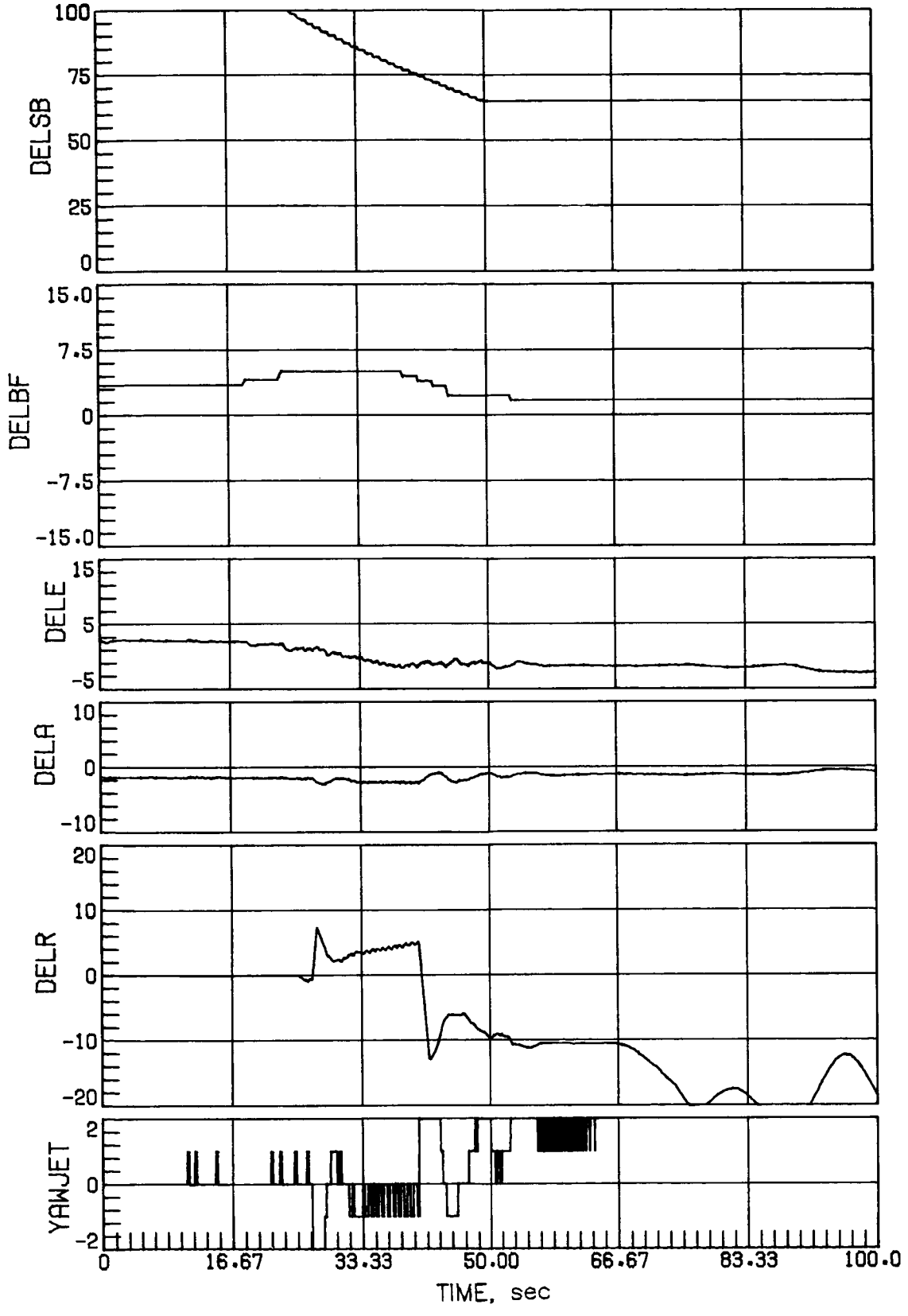

(b) Concluded.

Figure 25.- Continued.

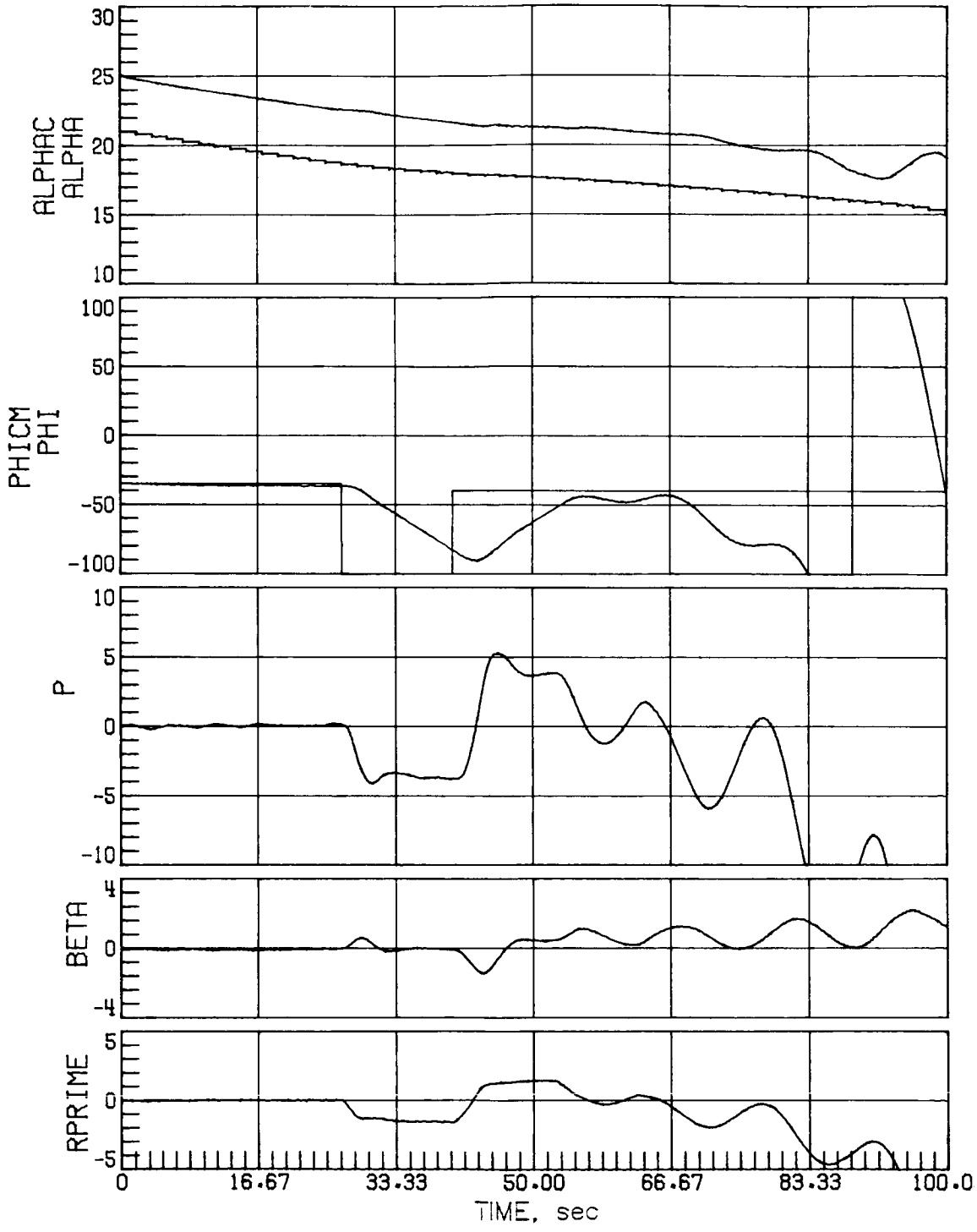

(c) Case 7.

Figure 25.- Continued.

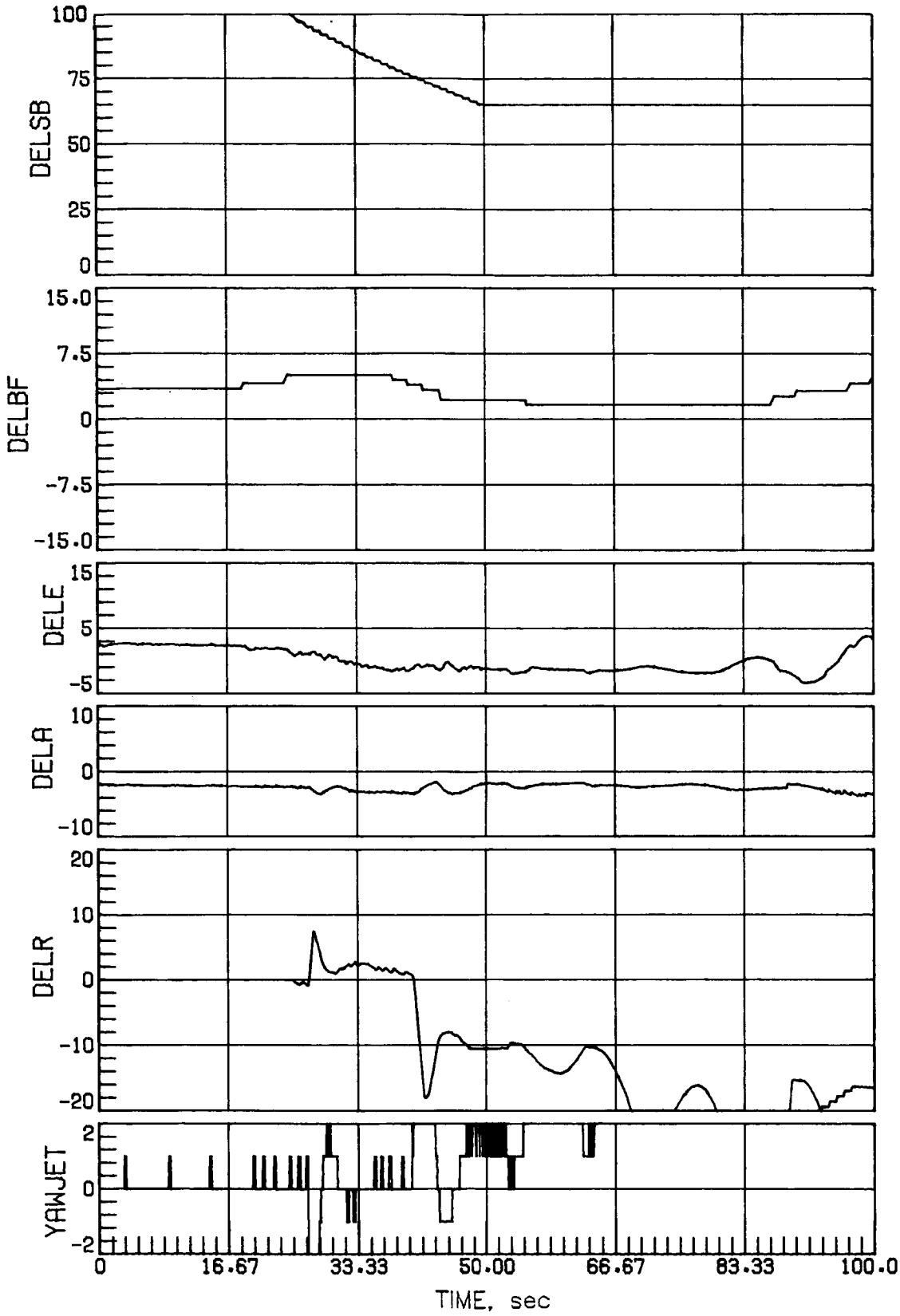

(c) Concluded.

Figure 25.- Continued.

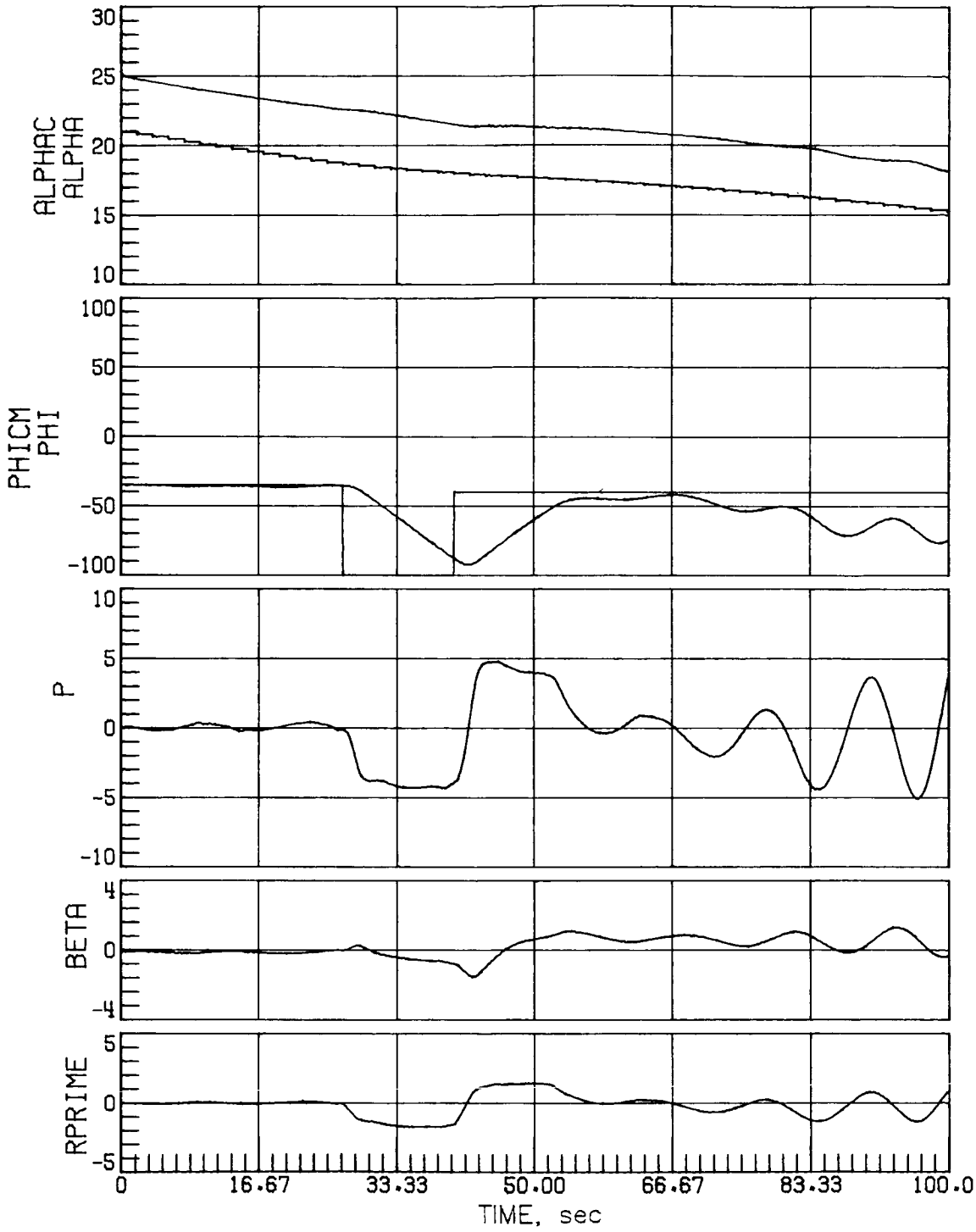

(d) Case 15.

Figure 25.- Continued.

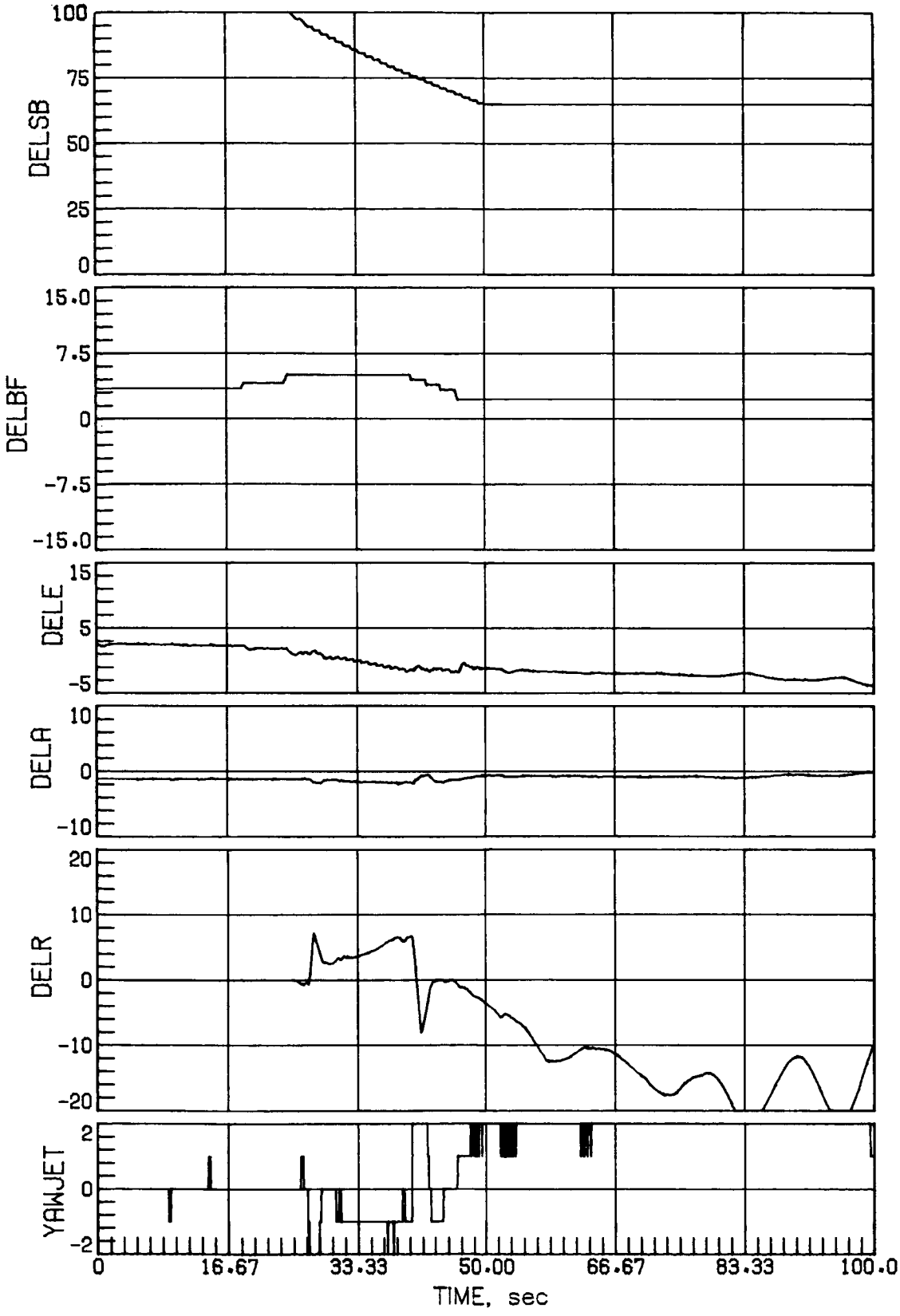

(d) Concluded.

Figure 25.- Concluded.

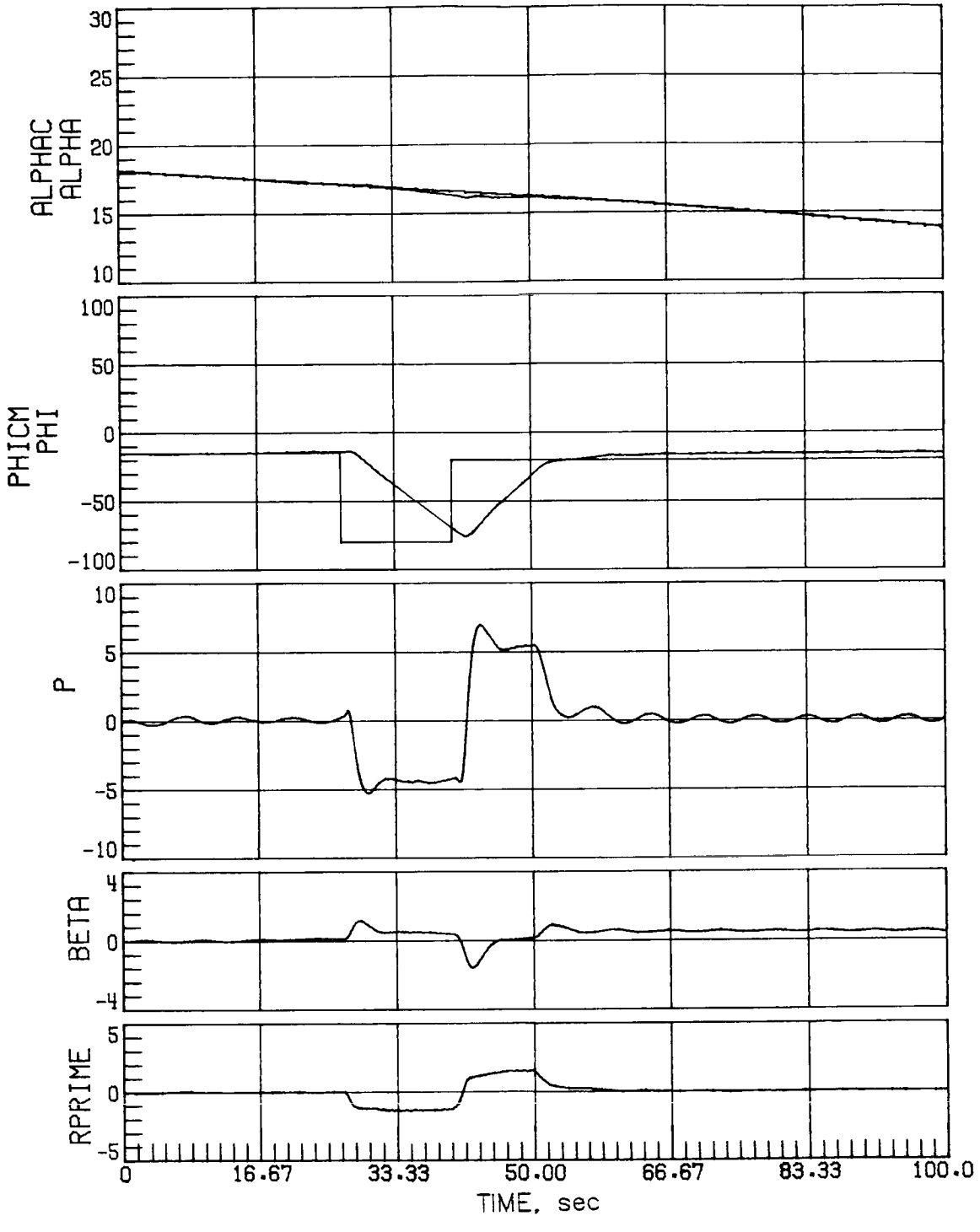

(a) Nominal α.

Figure 26.- Mach 4.2 maneuver performance with nominal aerodynamics.

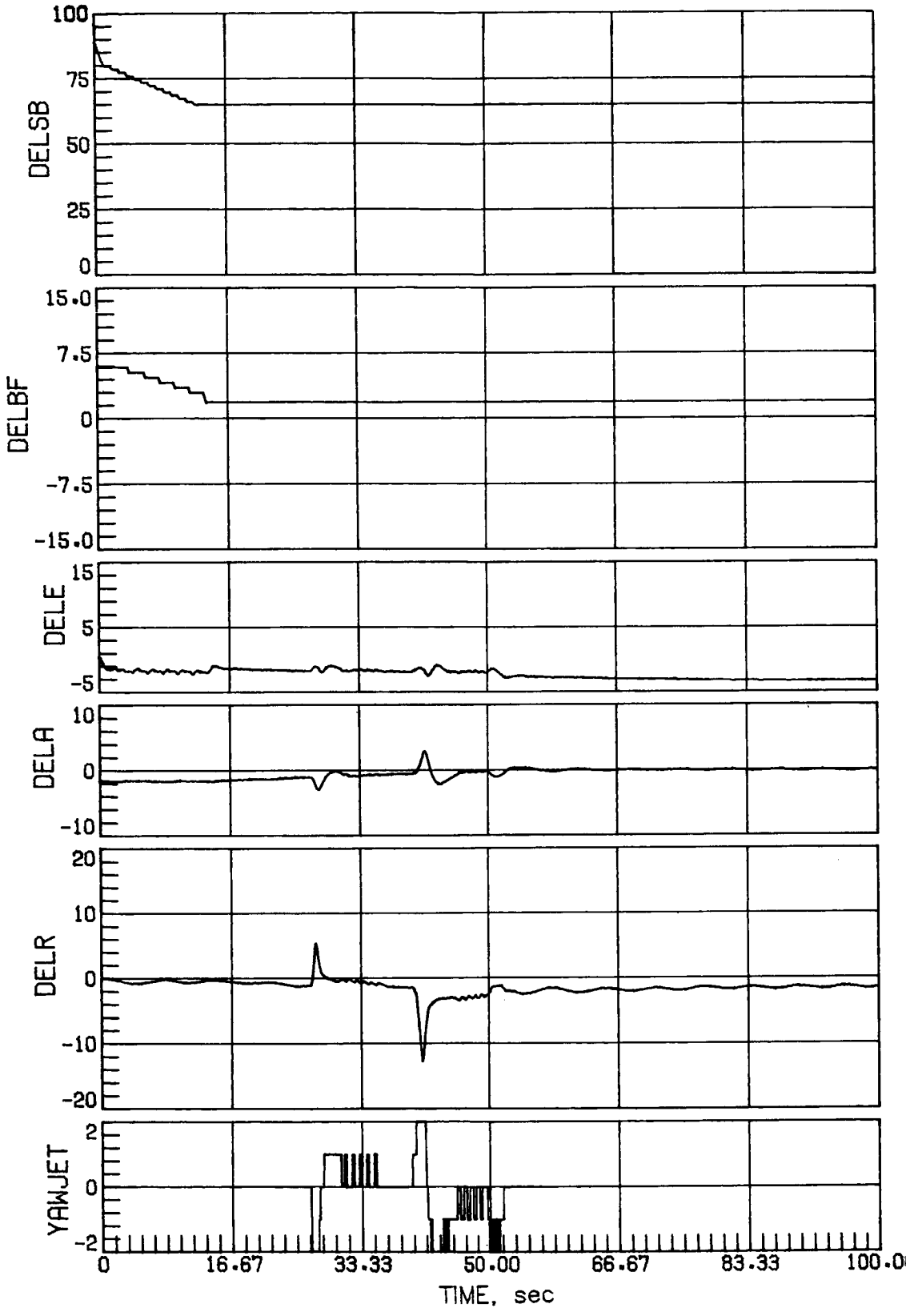

(a) Concluded.

Figure 26.- Continued.

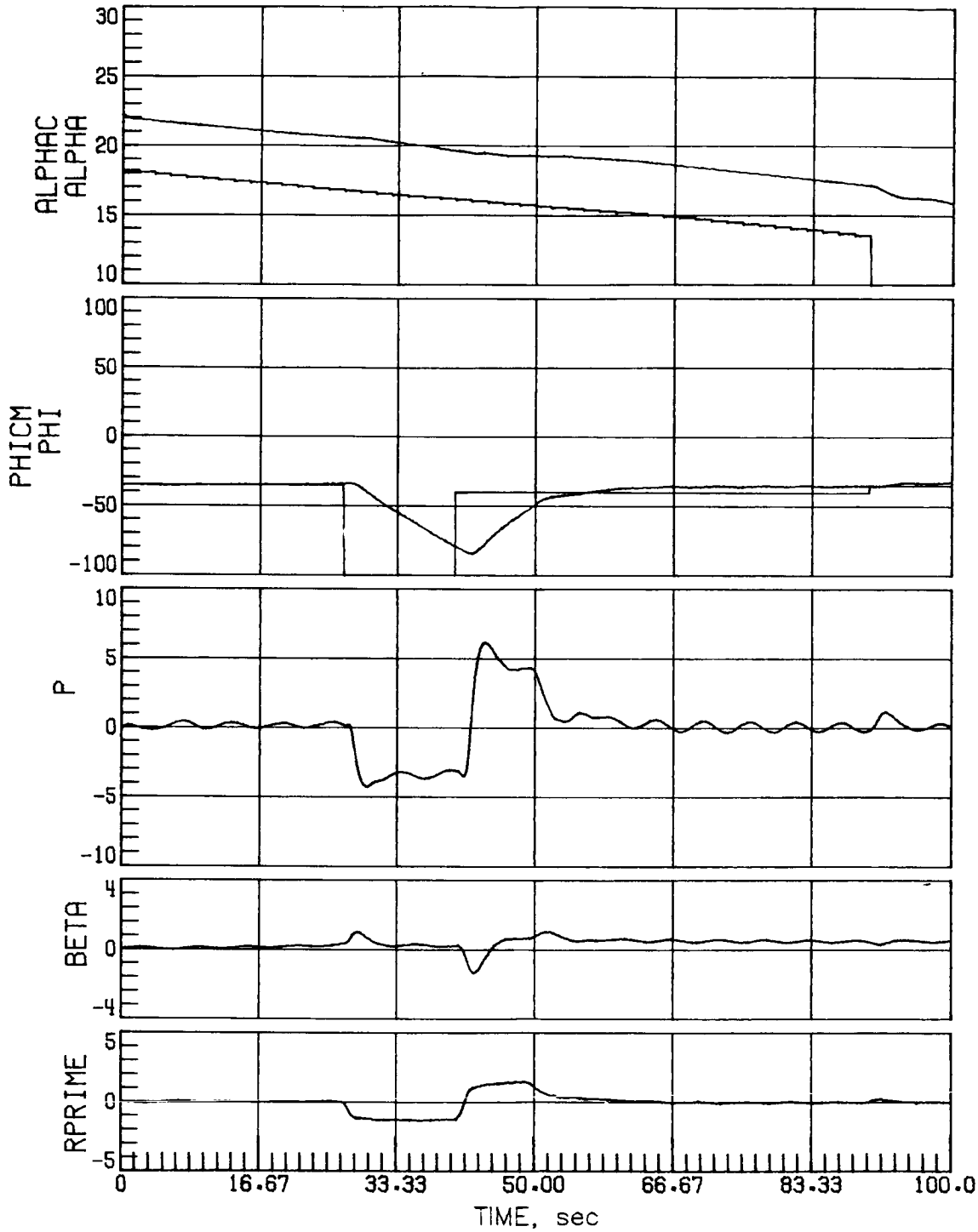

(b) Low-sensed α error of 4°.

Figure 26.- Continued.

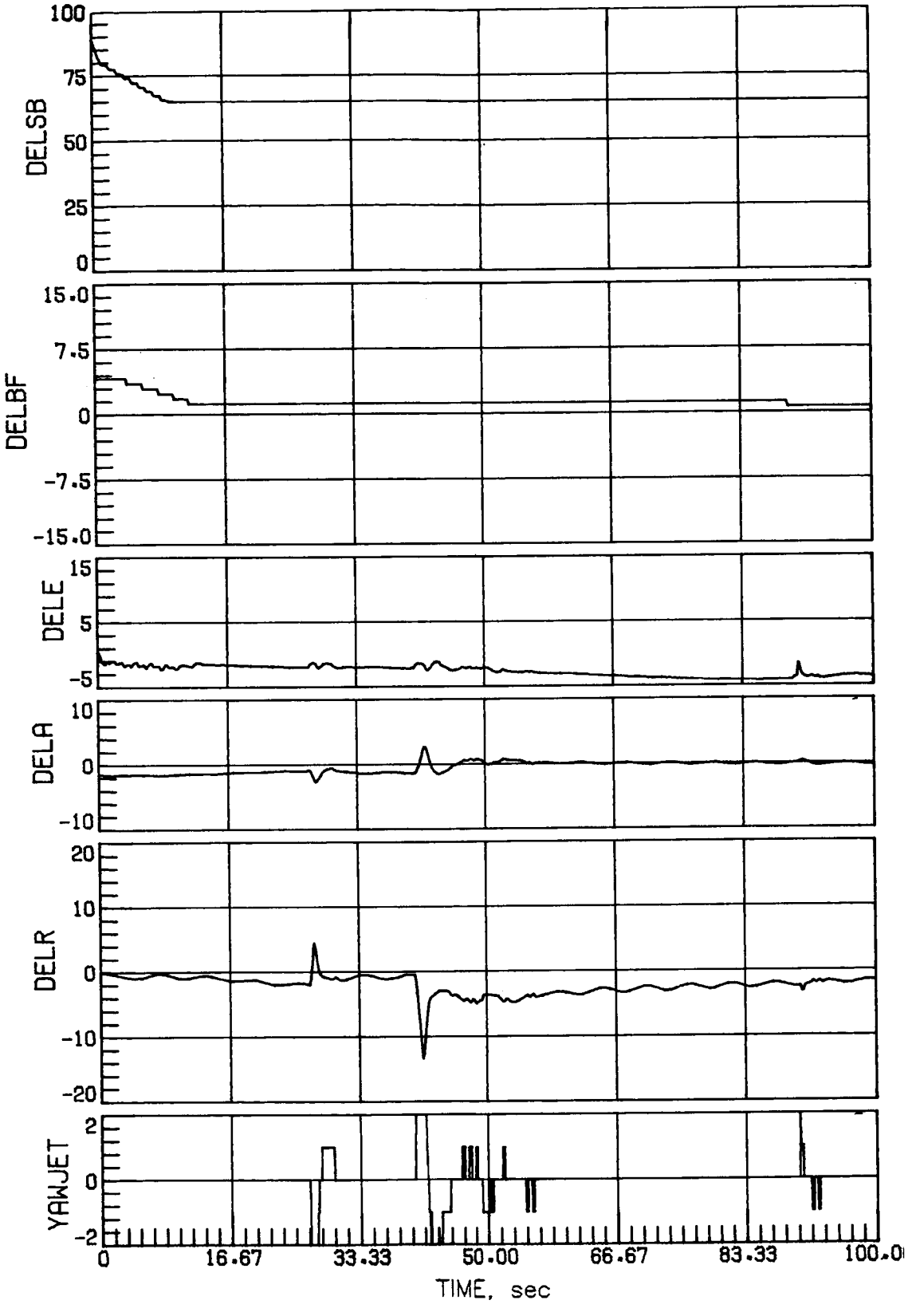

(b) Concluded.

Figure 26.- Continued.

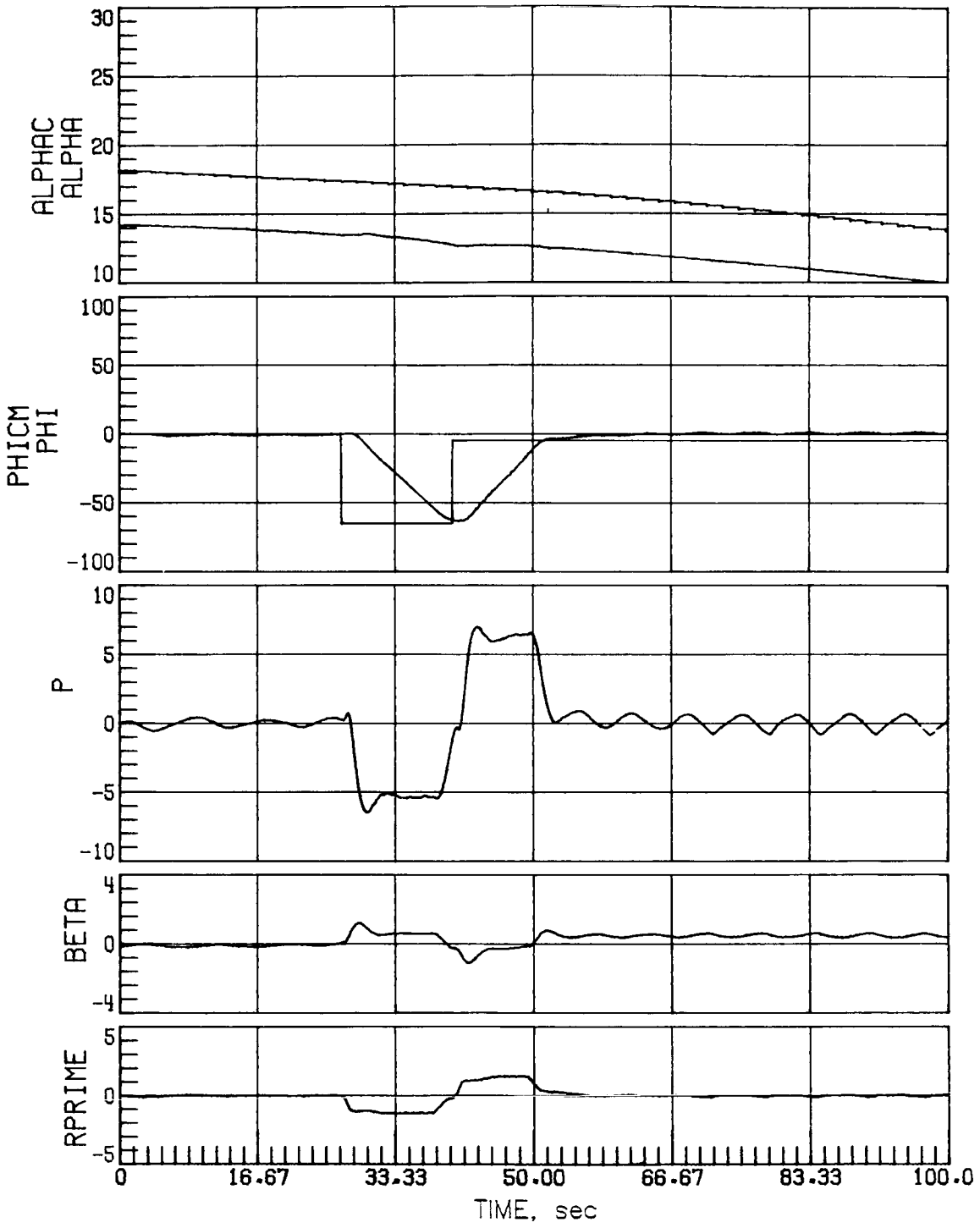

(c) High-sensed α error of 4°.

Figure 26.- Continued.

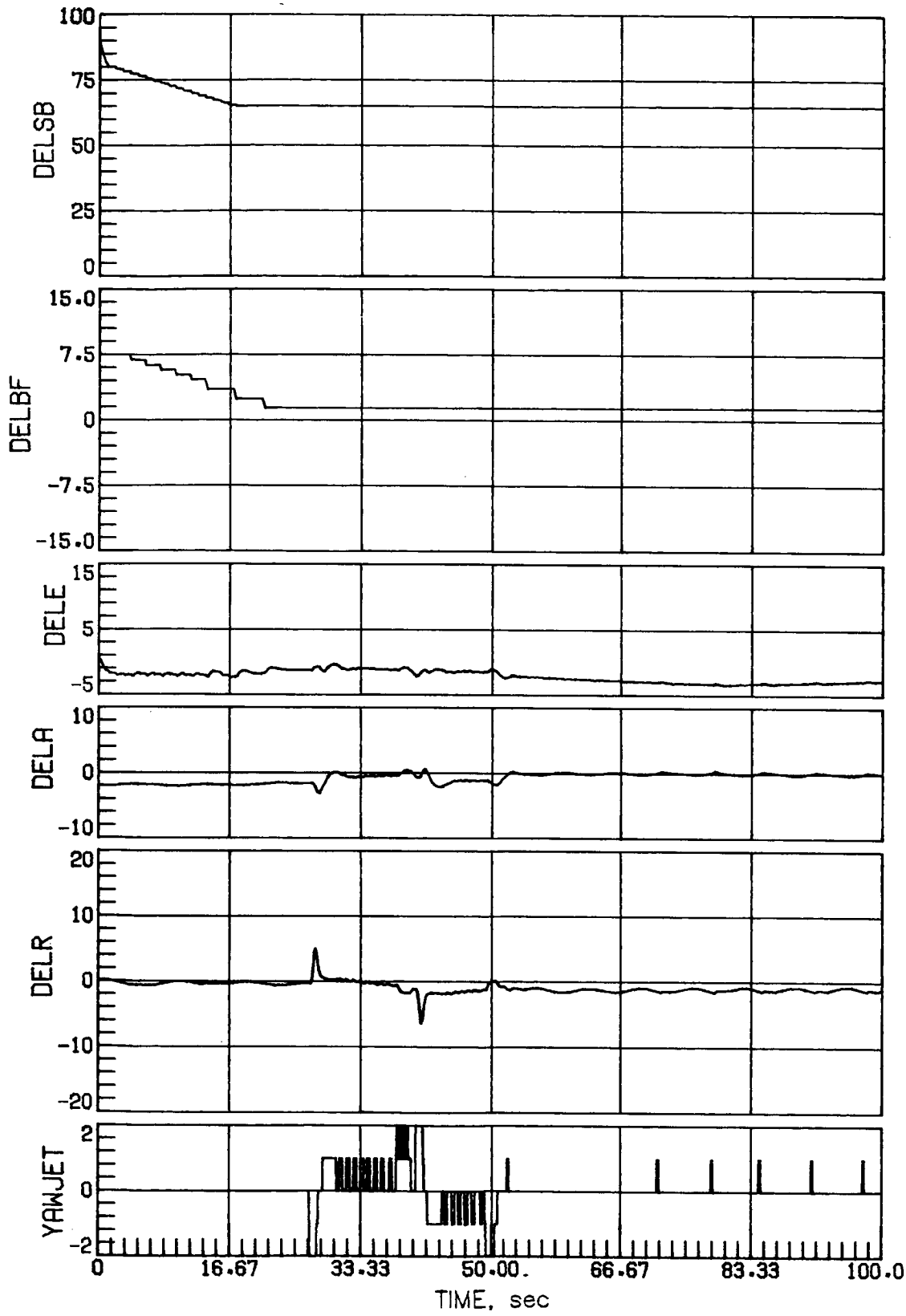

(c) Concluded.

Figure 26.- Concluded.

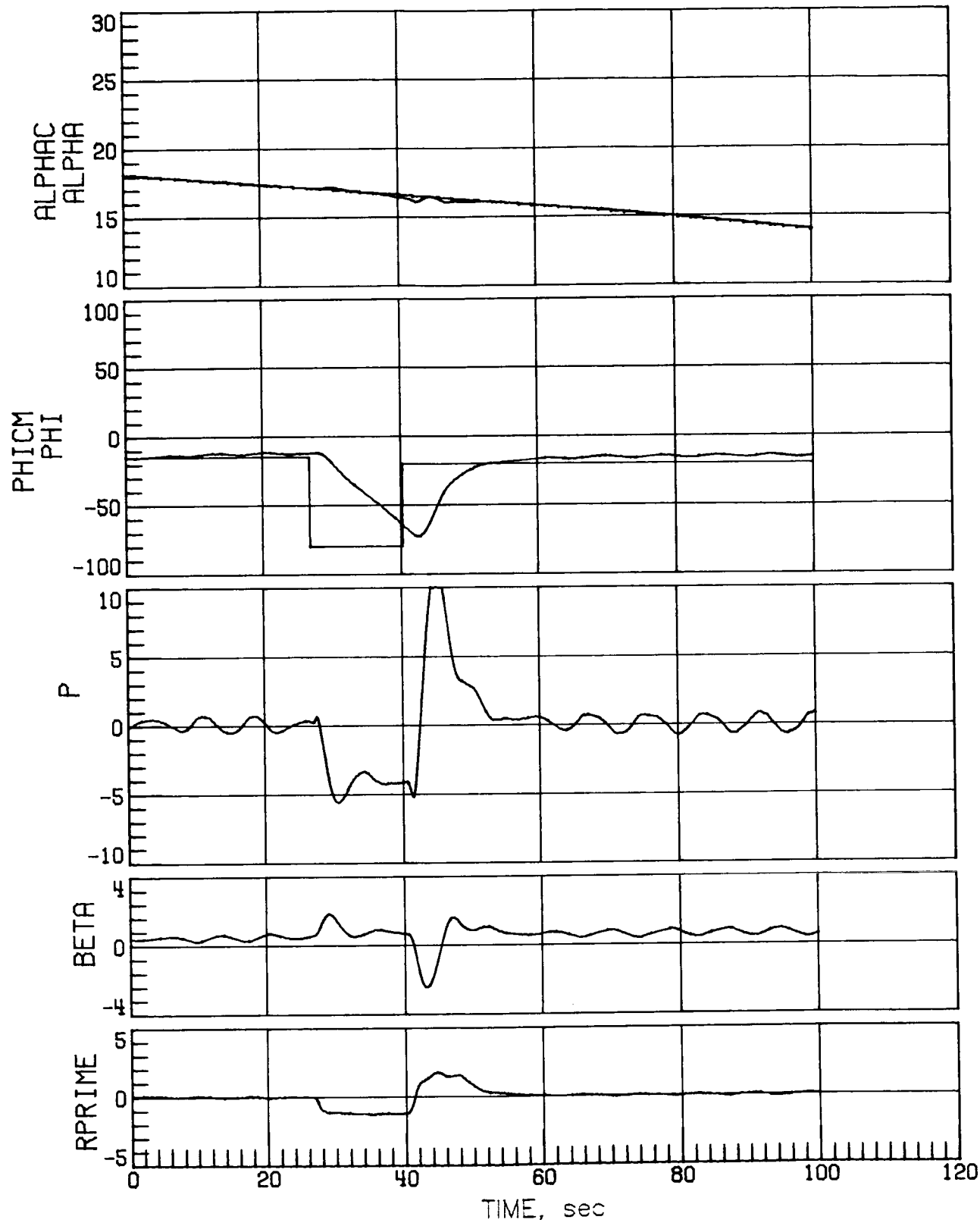

(a) Case 3.

Figure 27.- Mach 4.2 maneuver performance with nominal rudder effectiveness.

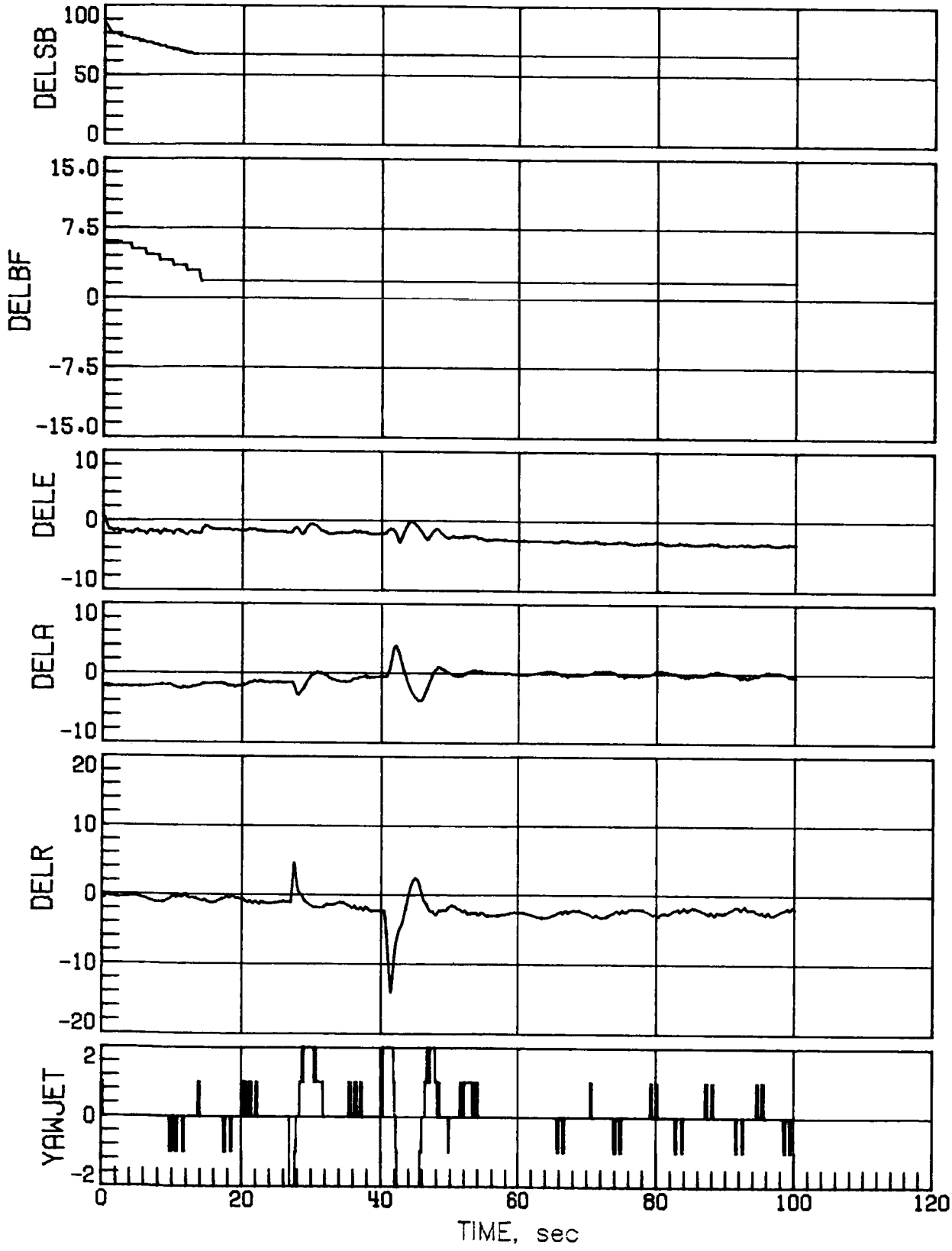

(a) Concluded.

Figure 27.- Continued.

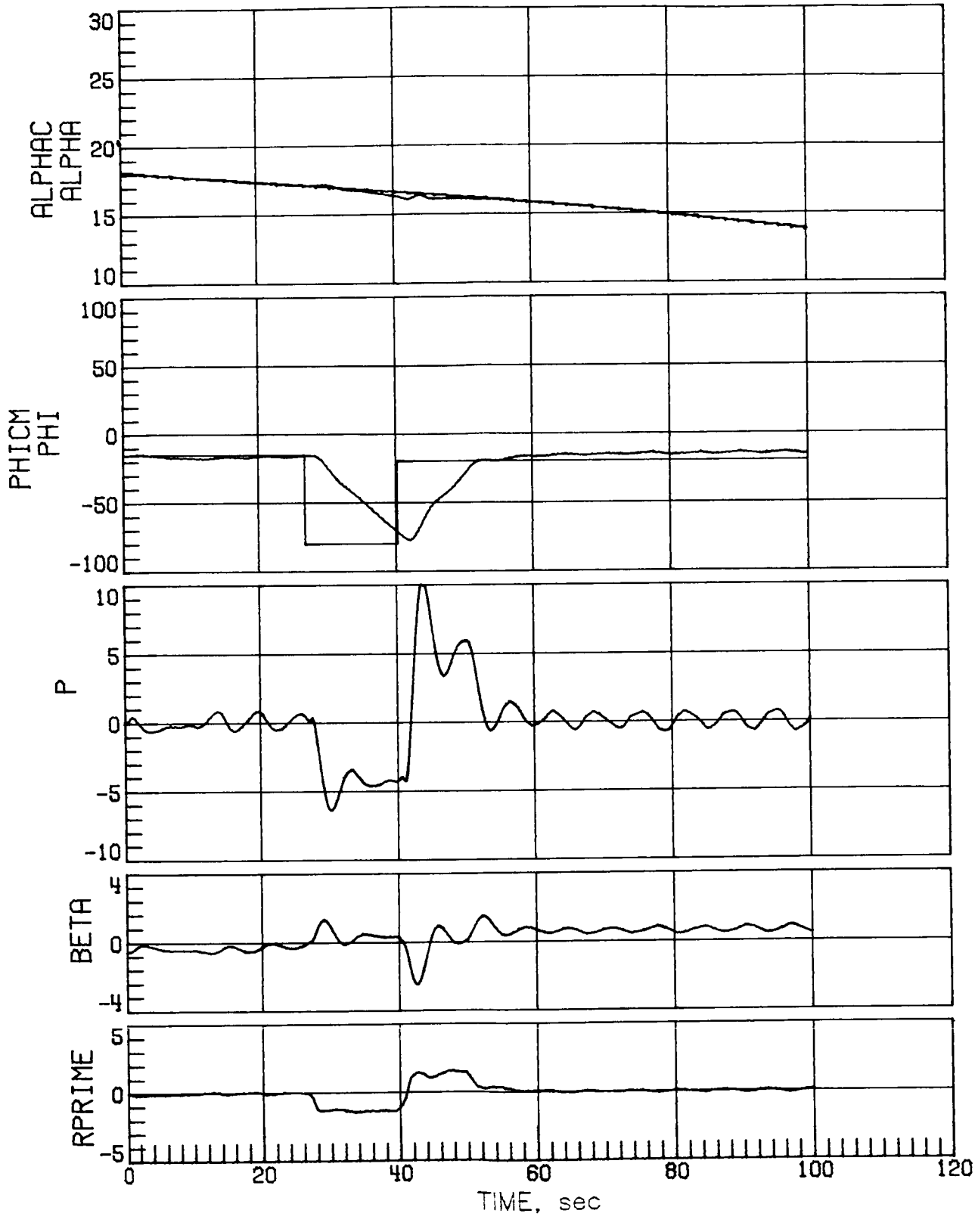

(b) Case 7.

Figure 27.- Continued.

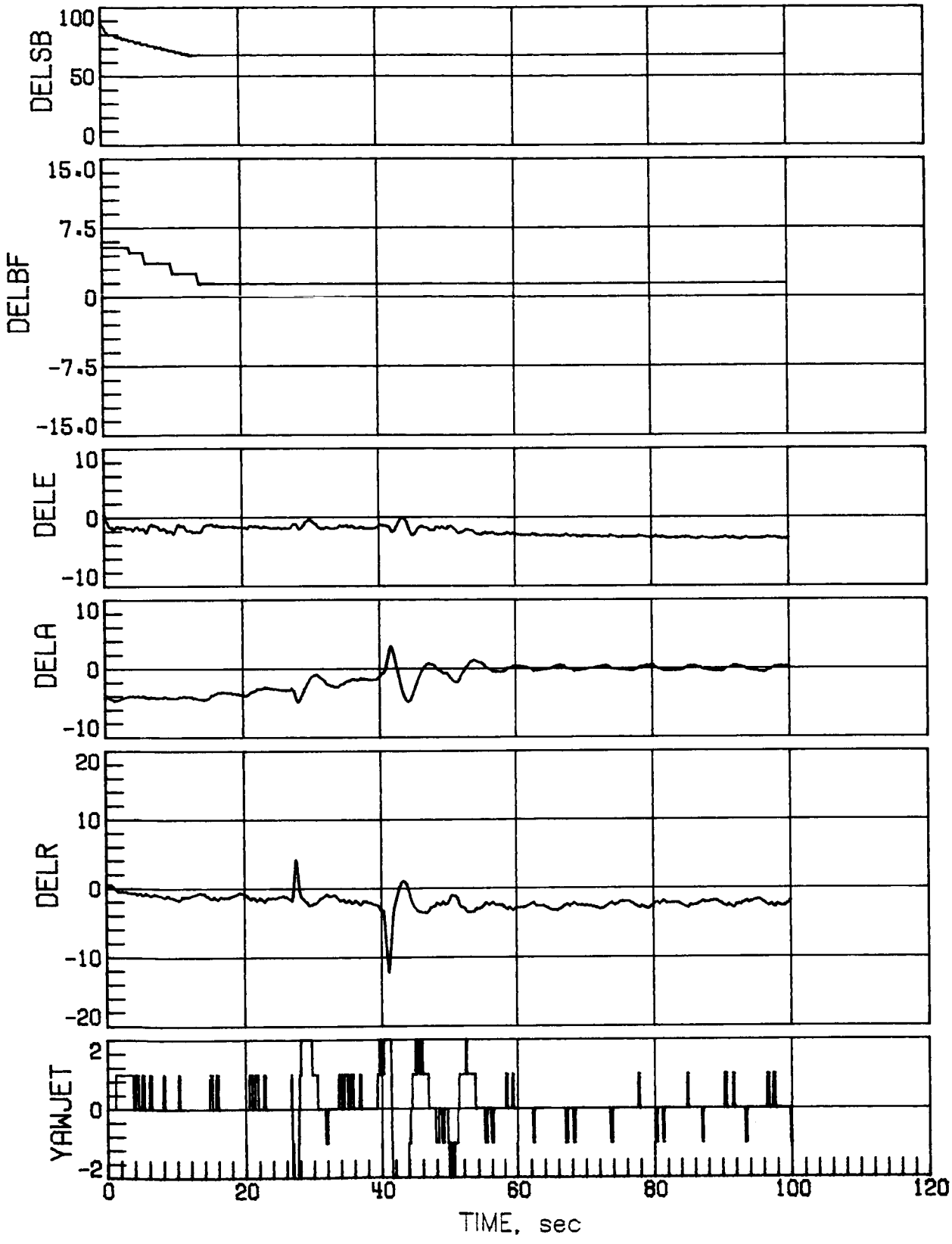

(b) Concluded.

Figure 27.- Concluded.

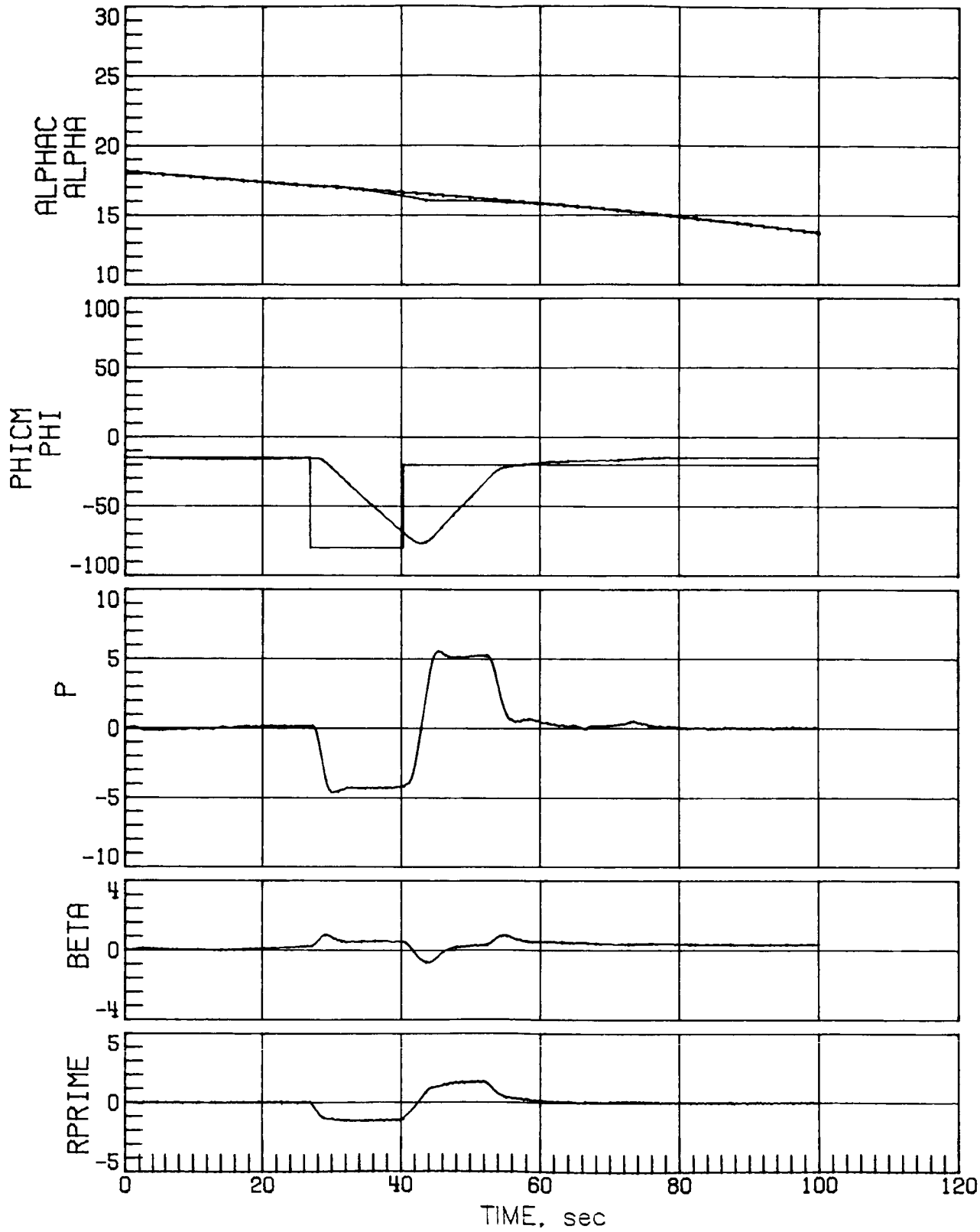

(a) Nominal aerodynamics.

Figure 28.- Mach 4.2 maneuver performance with decreased rudder effectiveness.

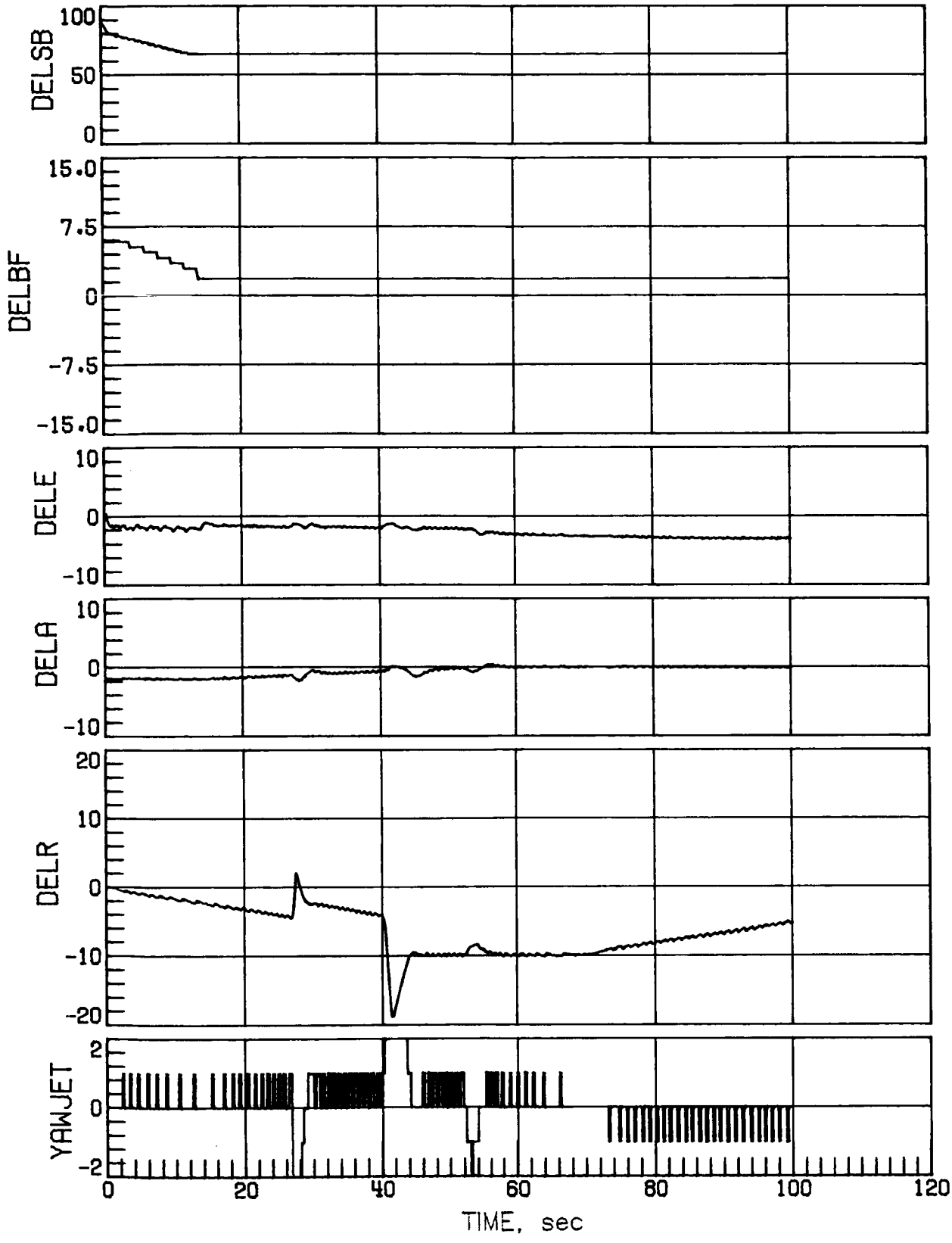

(a) Concluded.

Figure 28.- Continued.

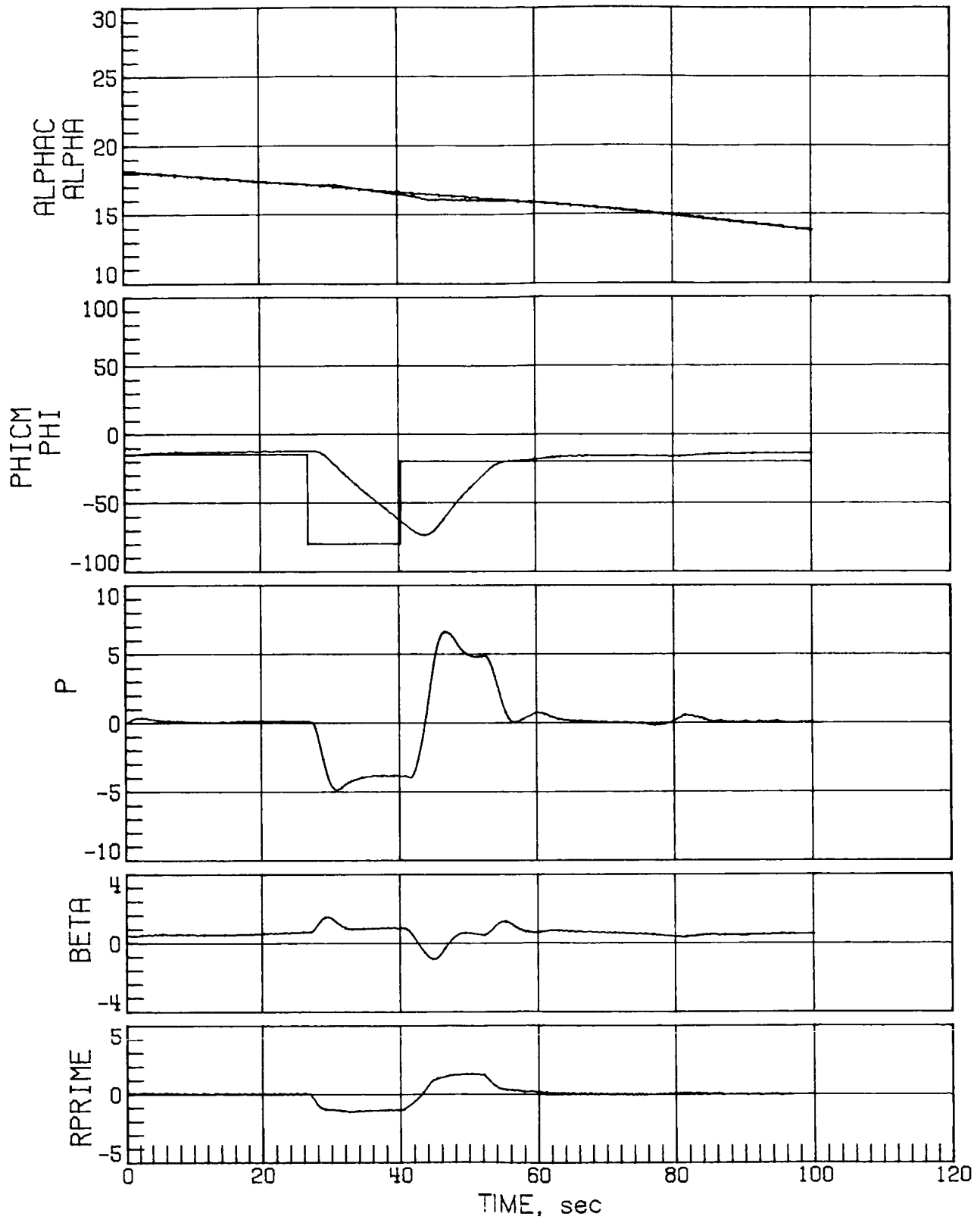

(b) Case 3.

Figure 28.- Continued.

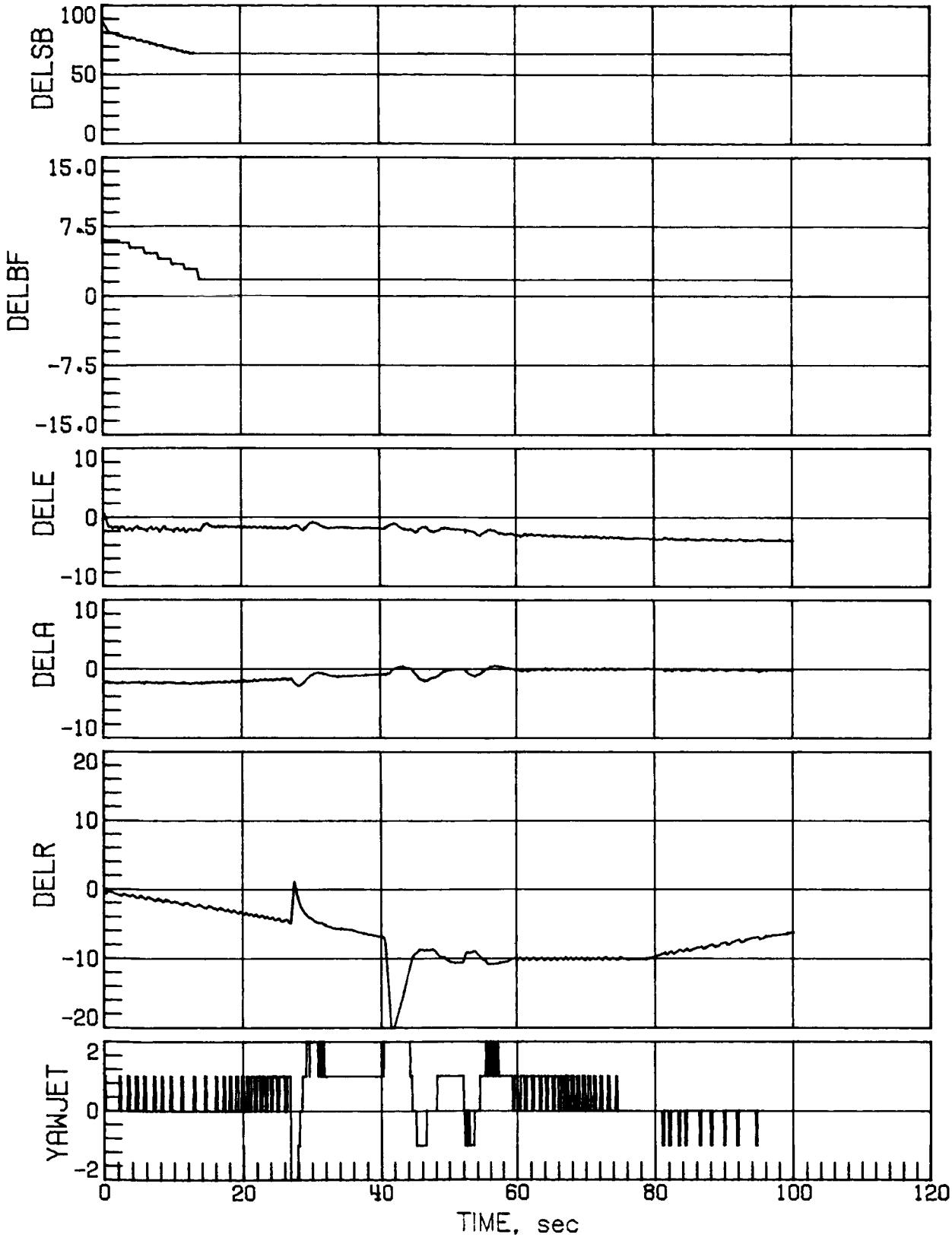

(b) Concluded.

Figure 28.- Continued.

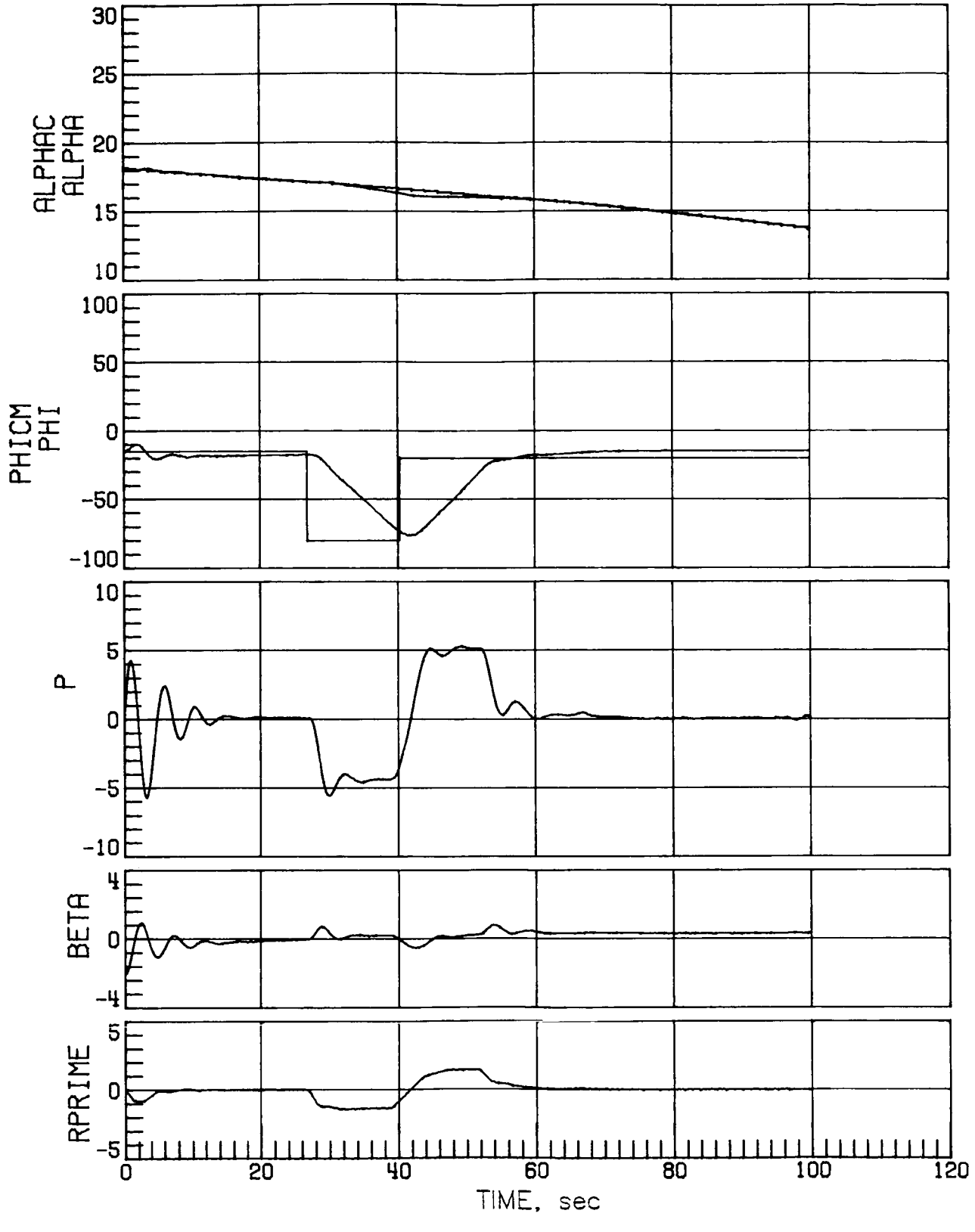

(c) Case 6.

Figure 28.- Continued.

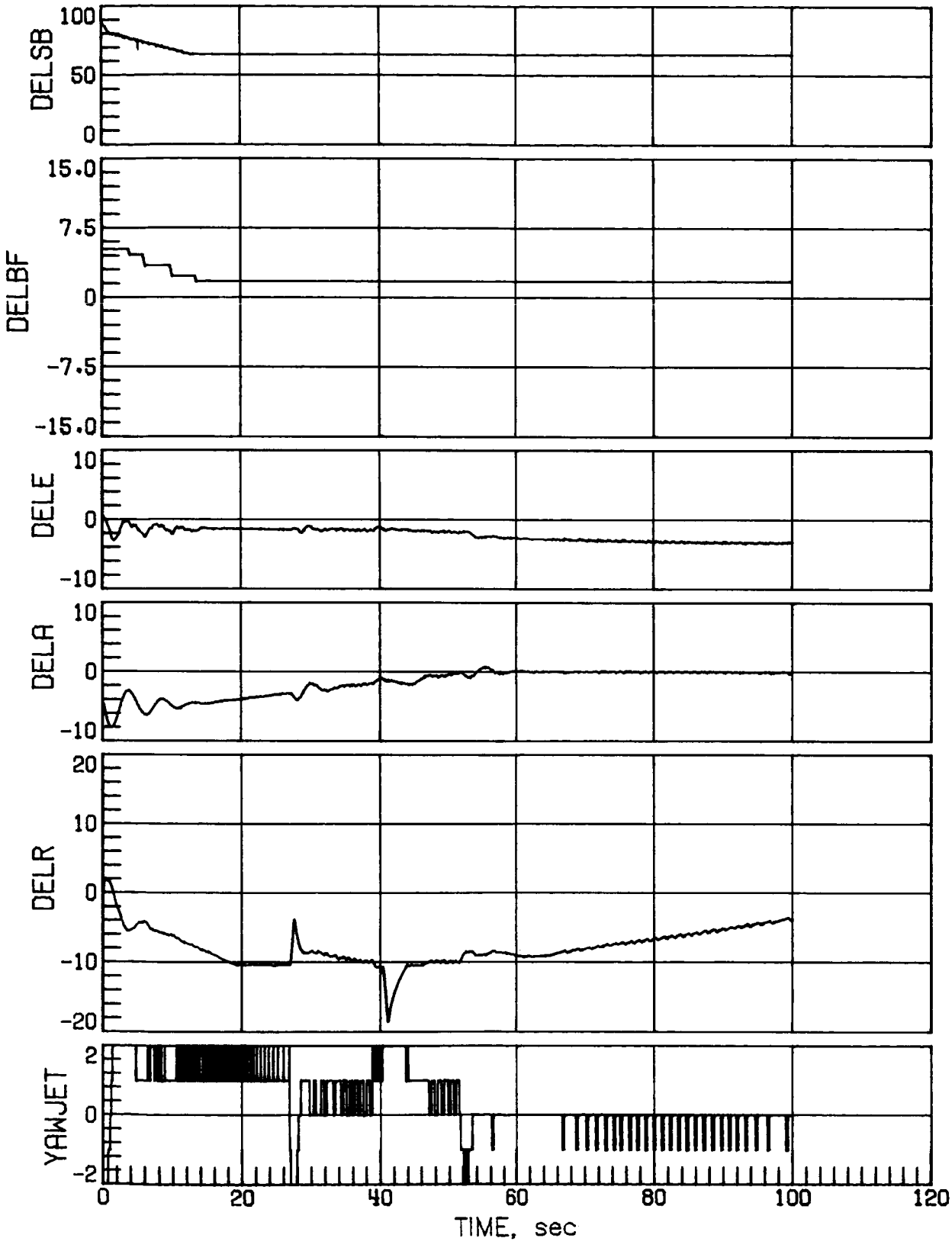

(c) Concluded.

Figure 28.- Concluded.

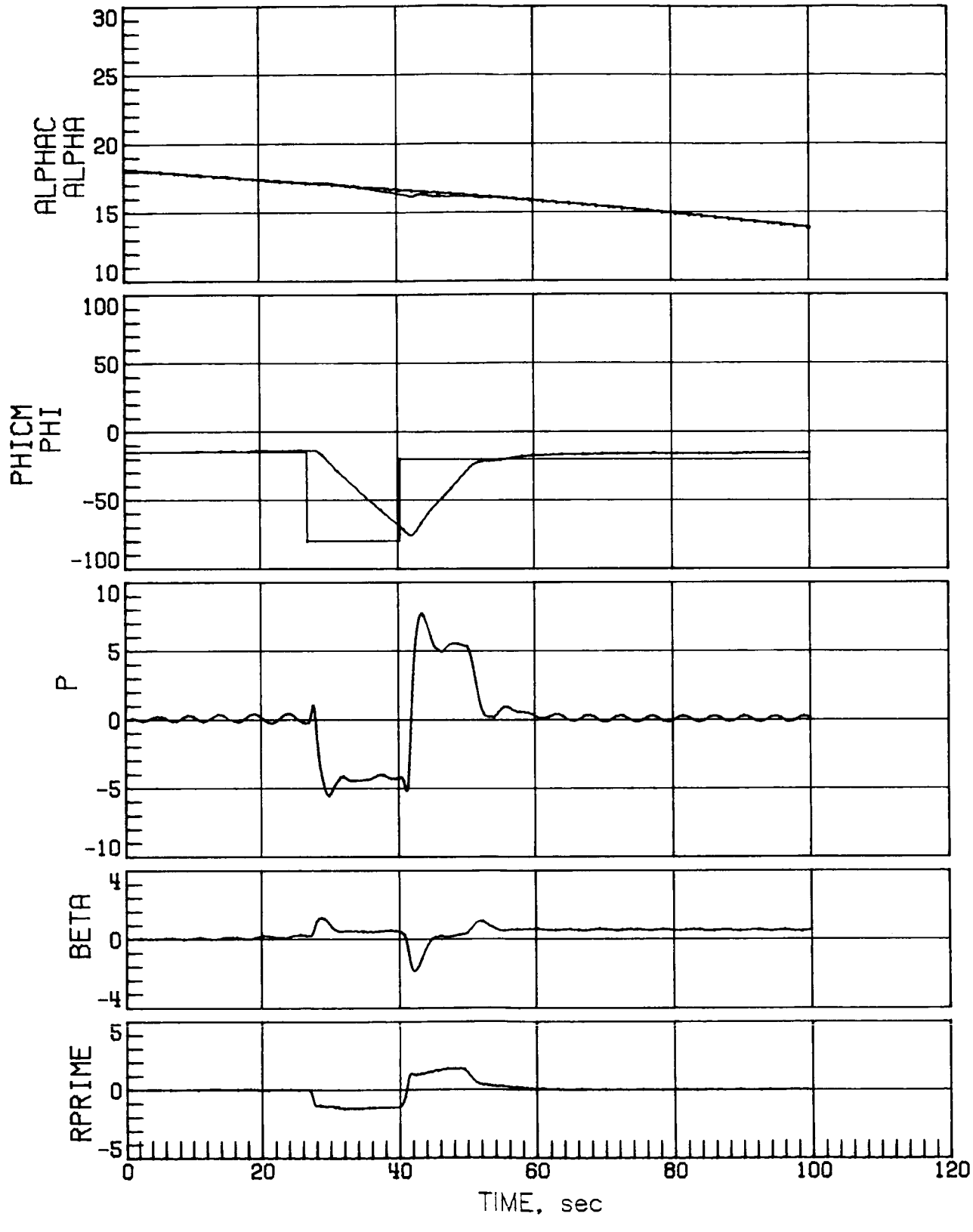

(a) Nominal aerodynamics.

Figure 29.- Mach 4.2 maneuver performance with increased rudder effectiveness.

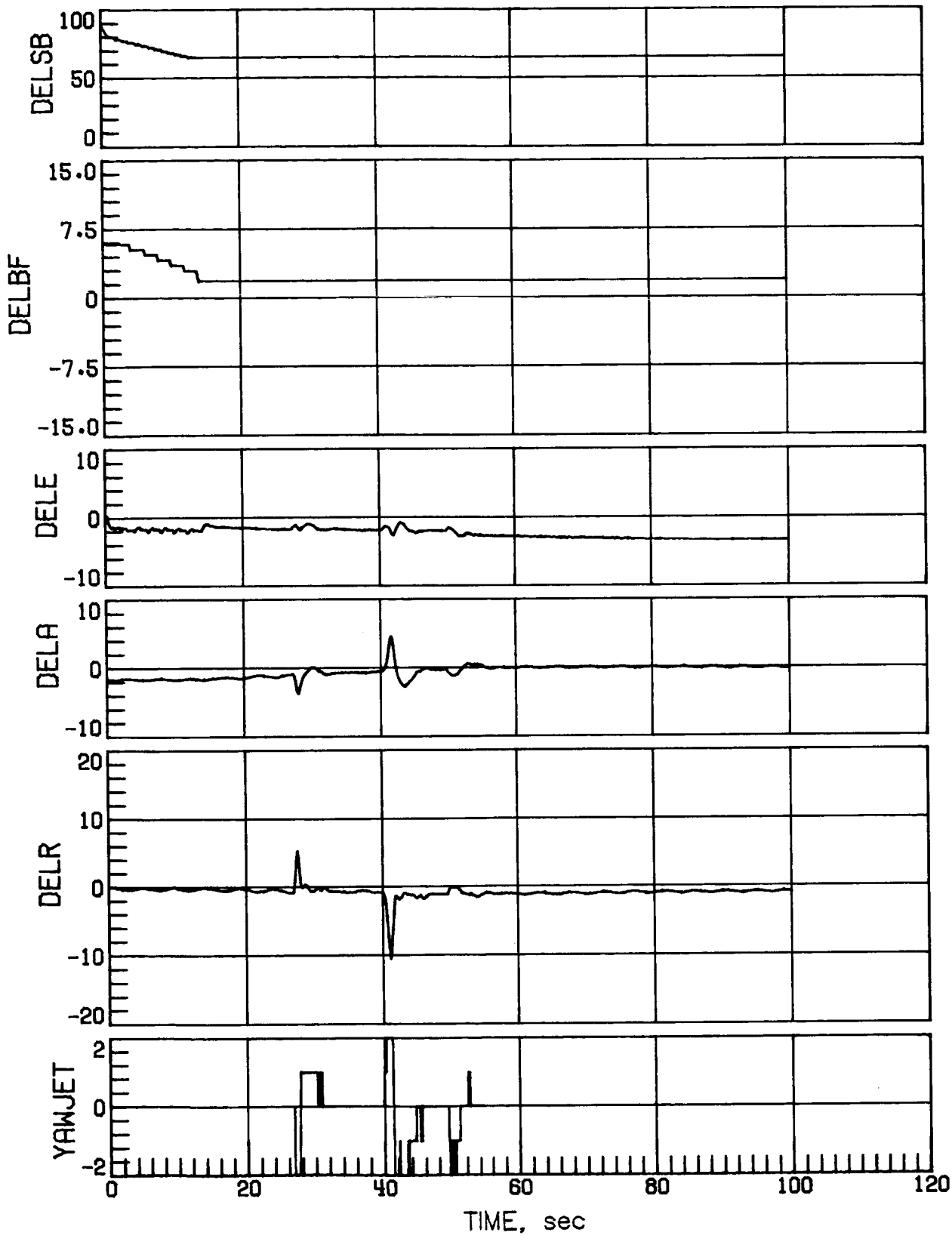

(a) Concluded.

Figure 29.- Continued.

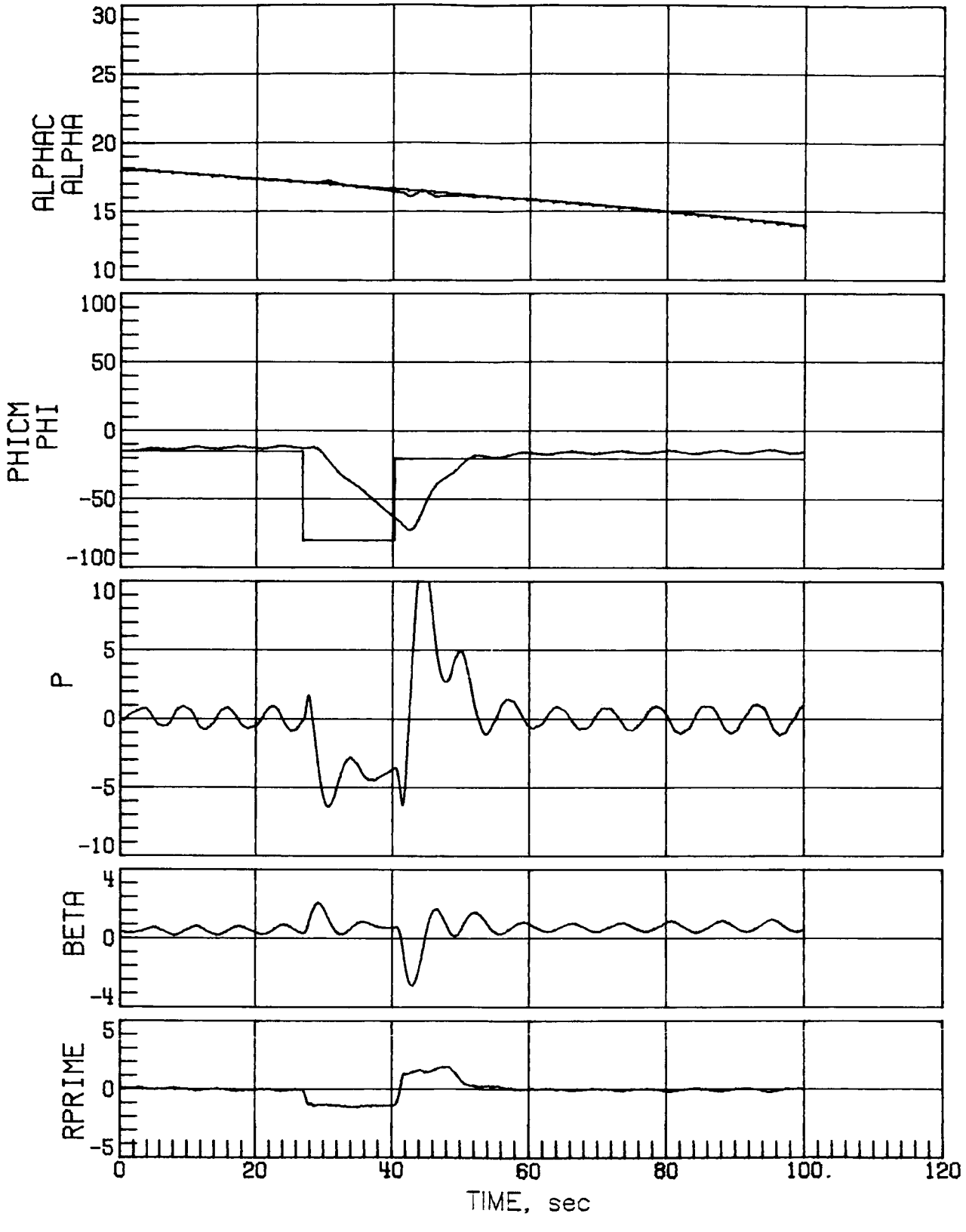

(b) Case 3.

Figure 29.- Continued.

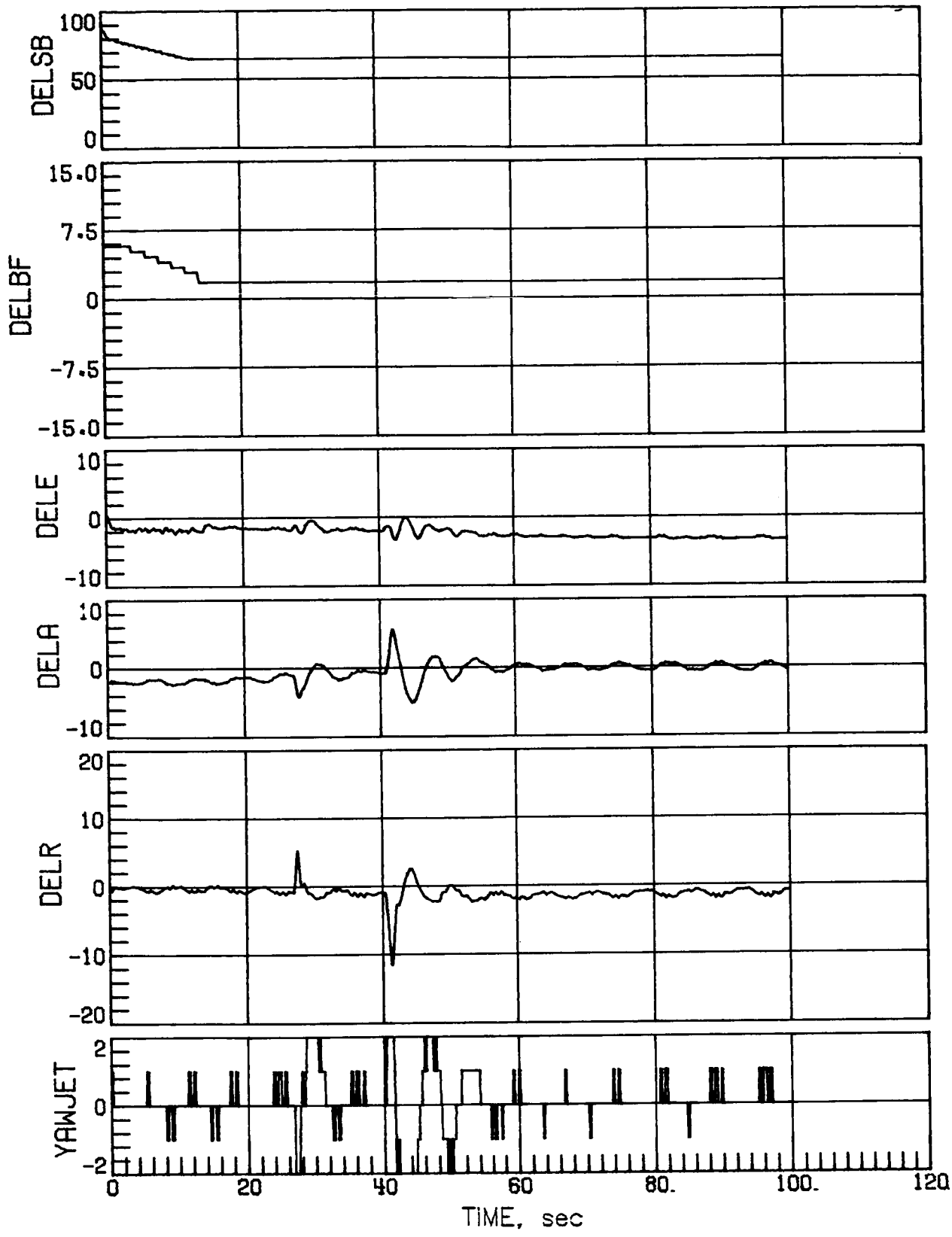

(b) Concluded.

Figure 29.- Continued.

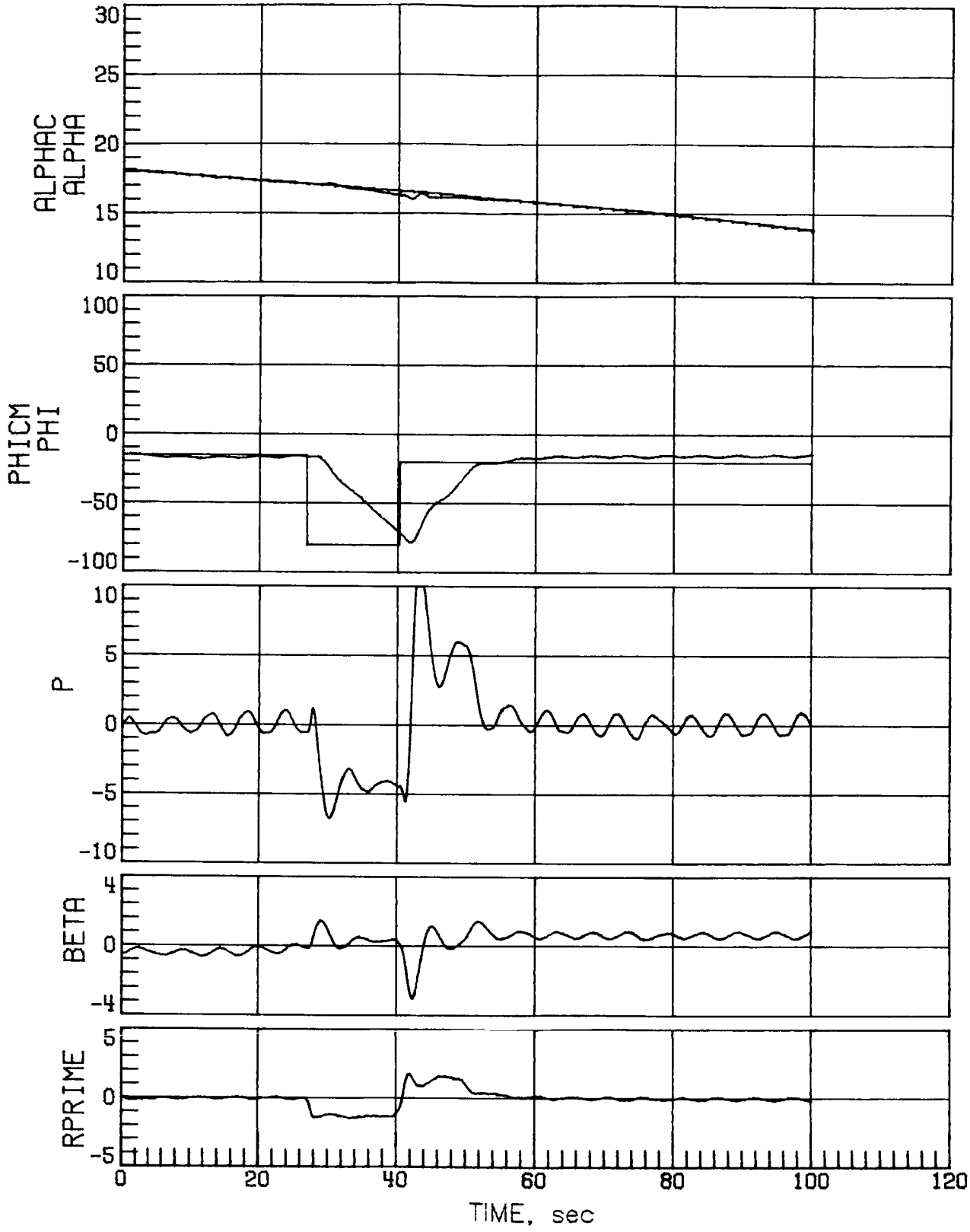

(c) Case 7.

Figure 29.- Continued.

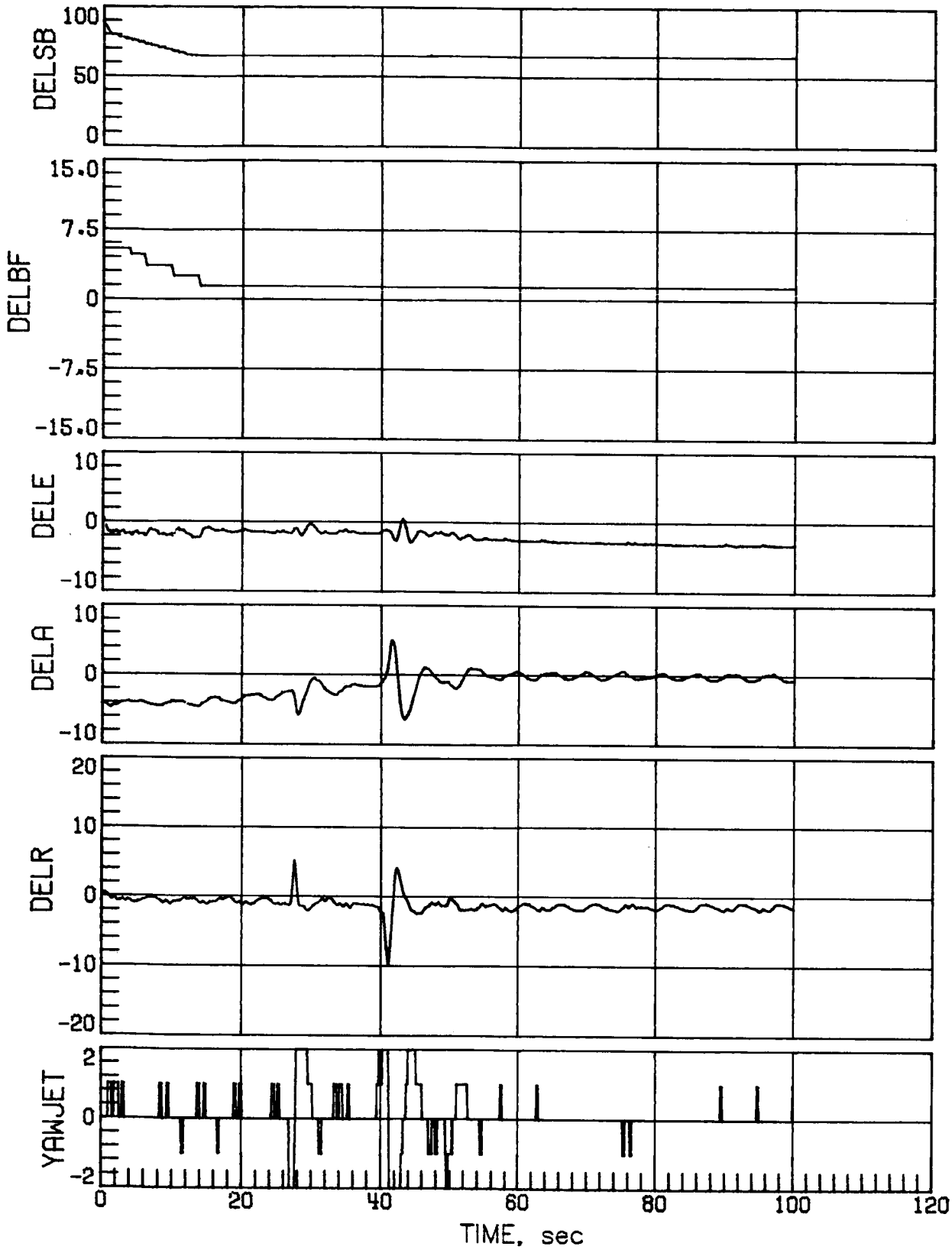

(c) Concluded.

Figure 29.- Concluded.

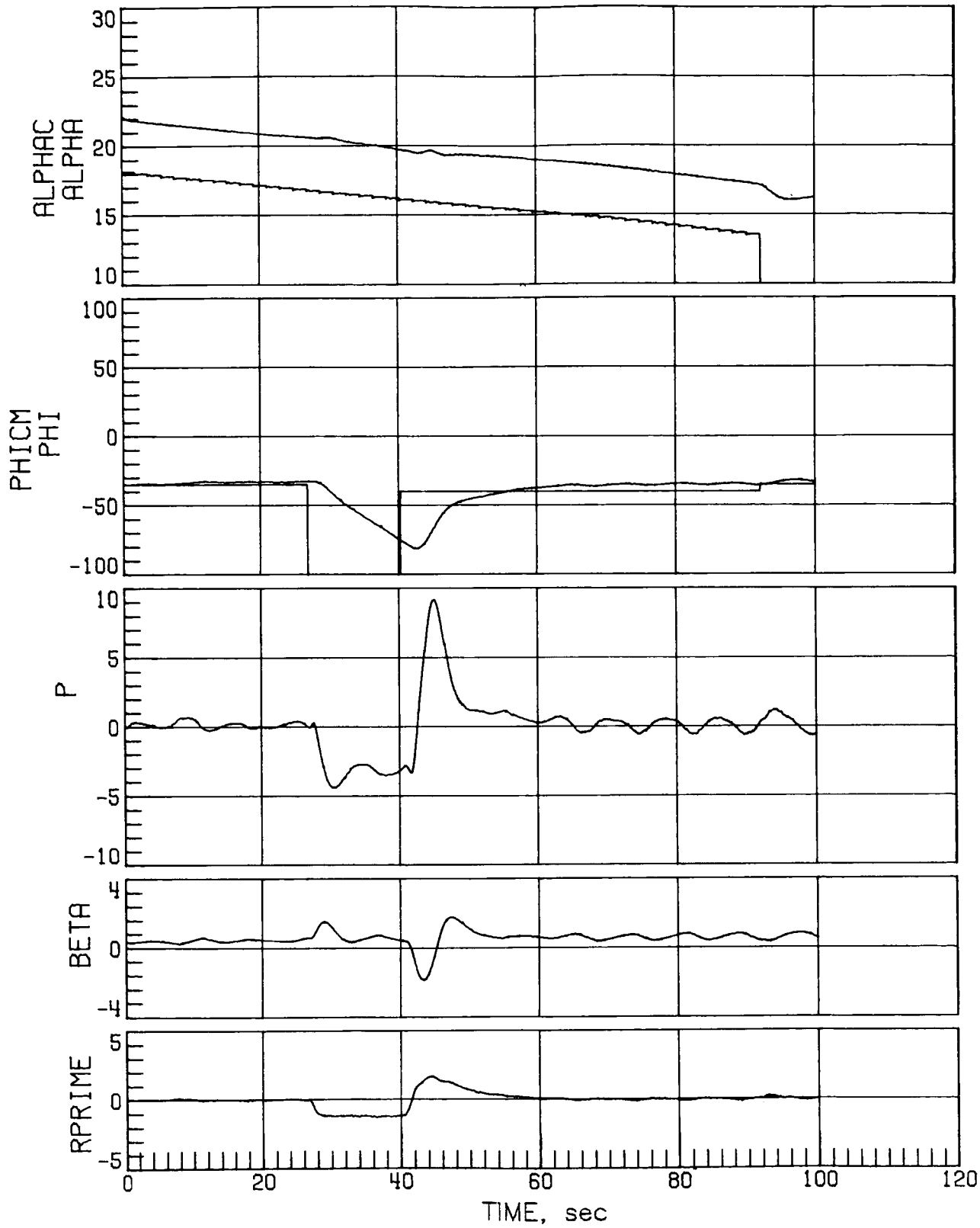

(a) Case 3.

Figure 30.- Mach 4.2 maneuver performance for a low-sensed α error of 4°.

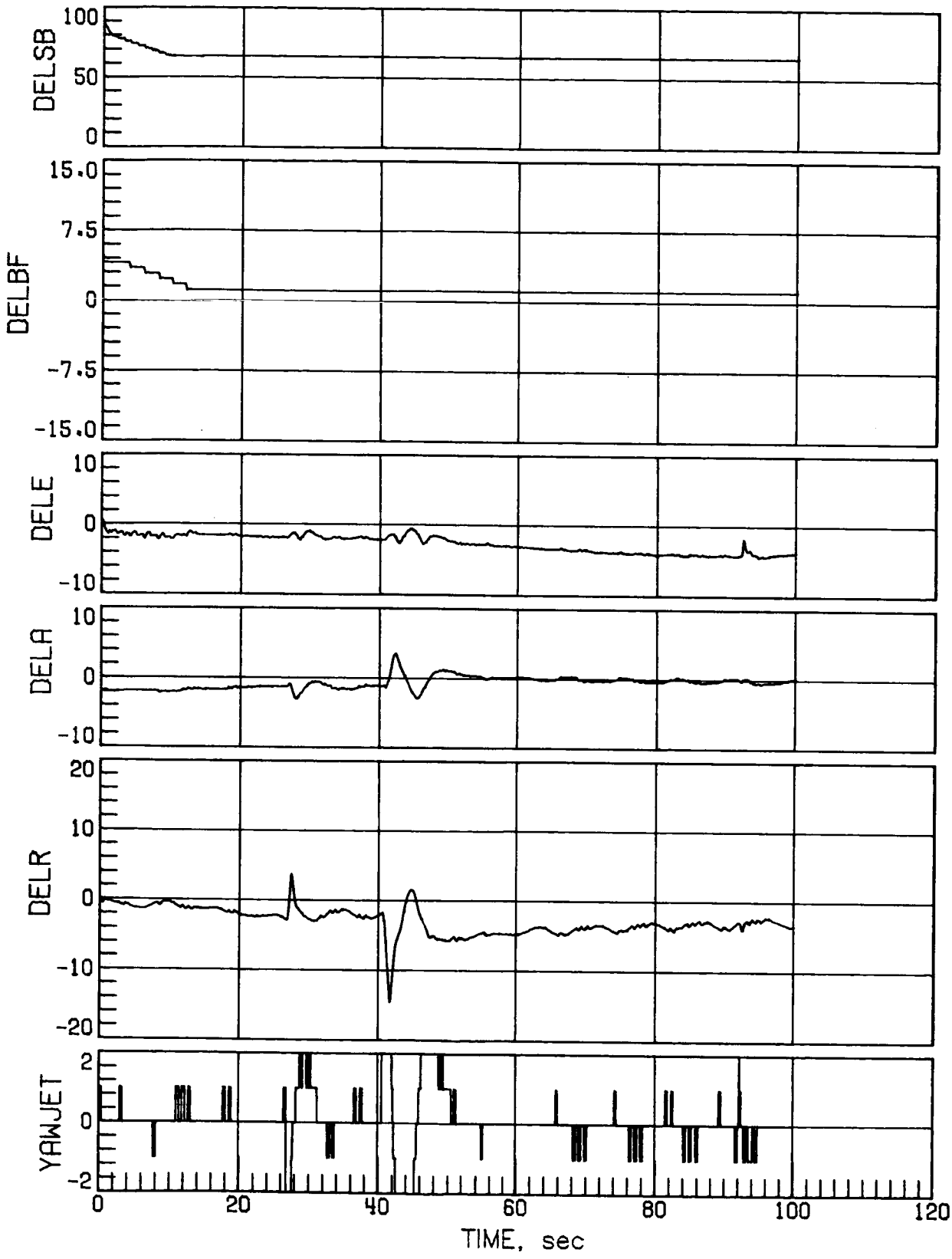

(a) Concluded.

Figure 30.- Continued.

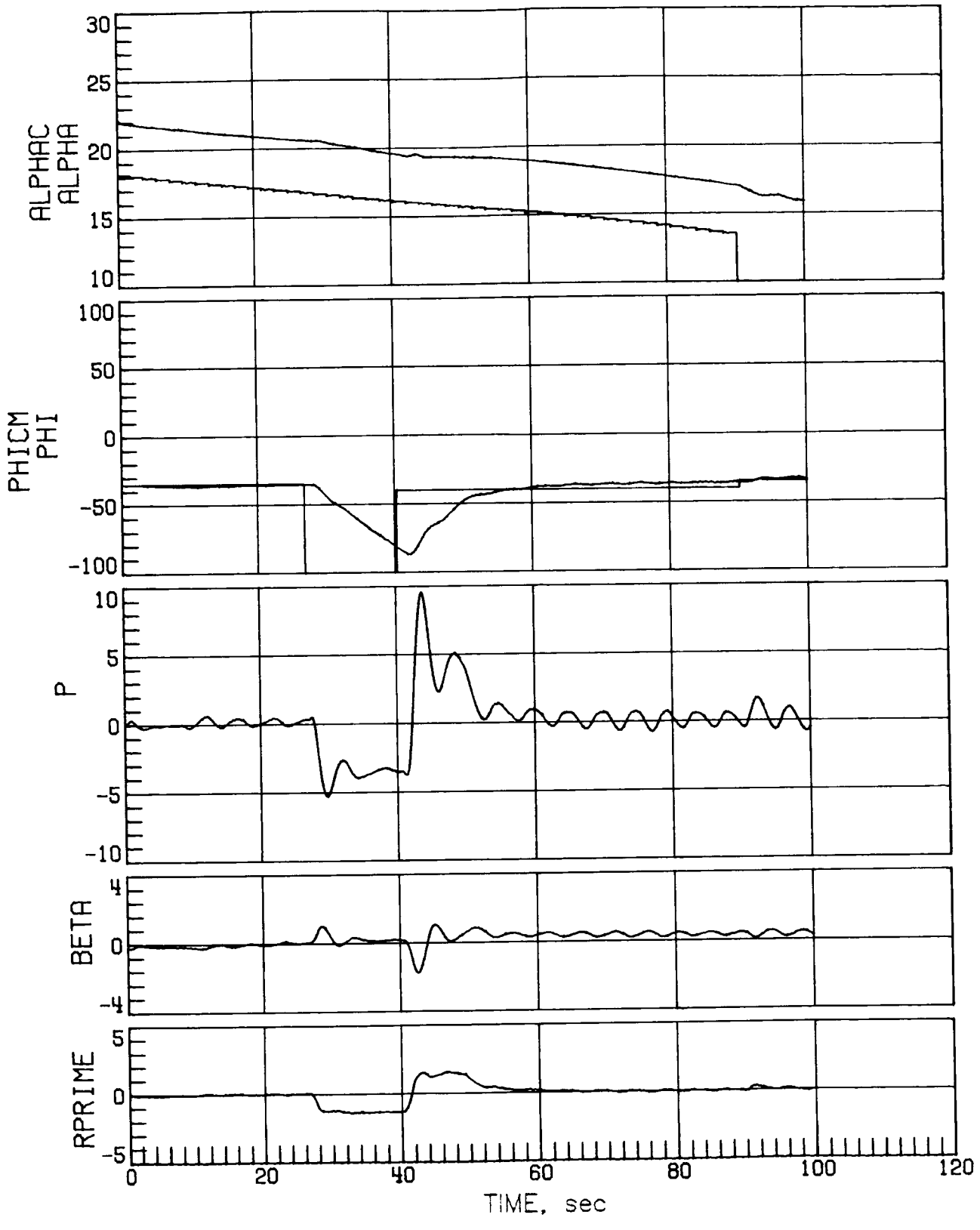

(b) Case 5.

Figure 30.- Continued.

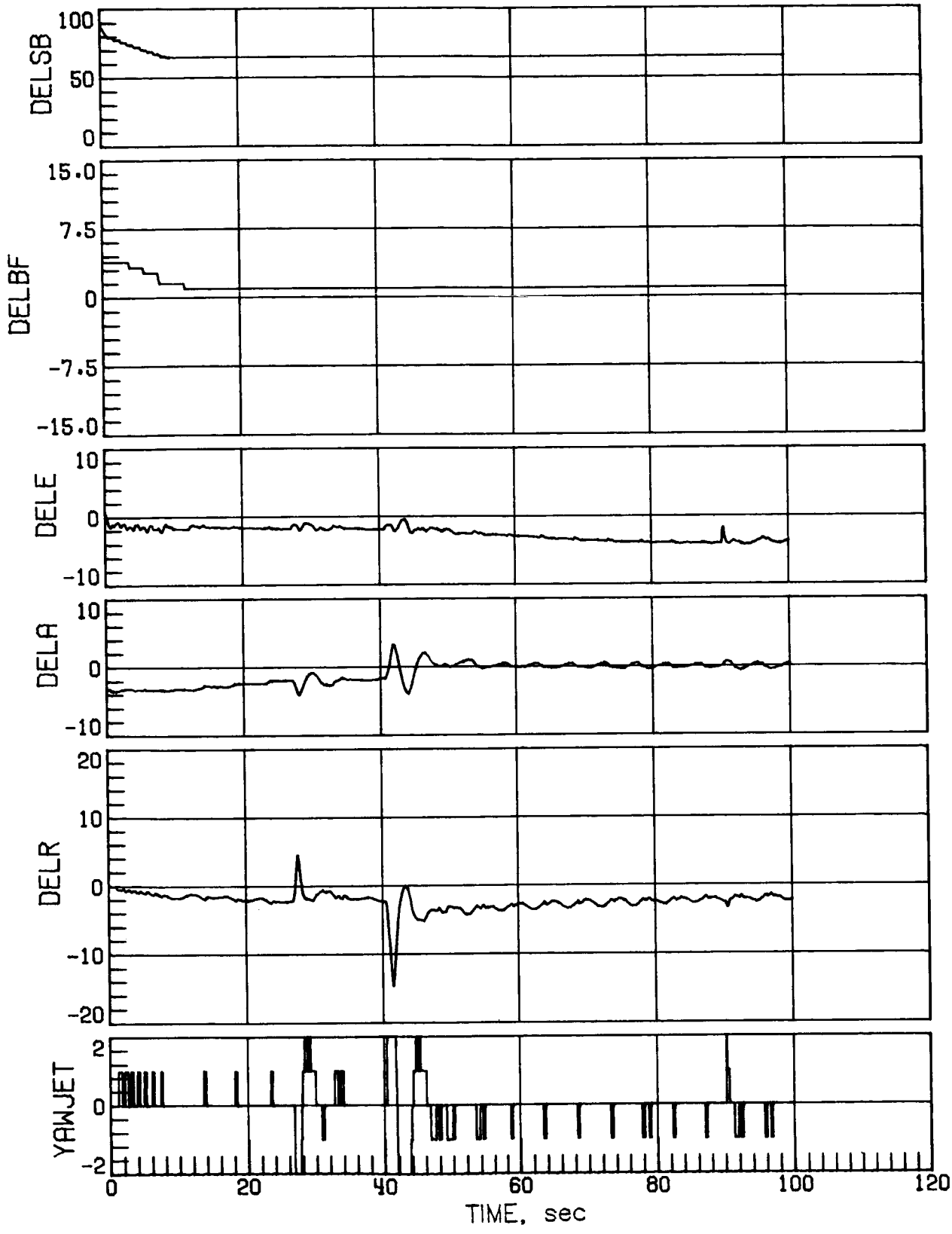

(b) Concluded.

Figure 30.- Continued.

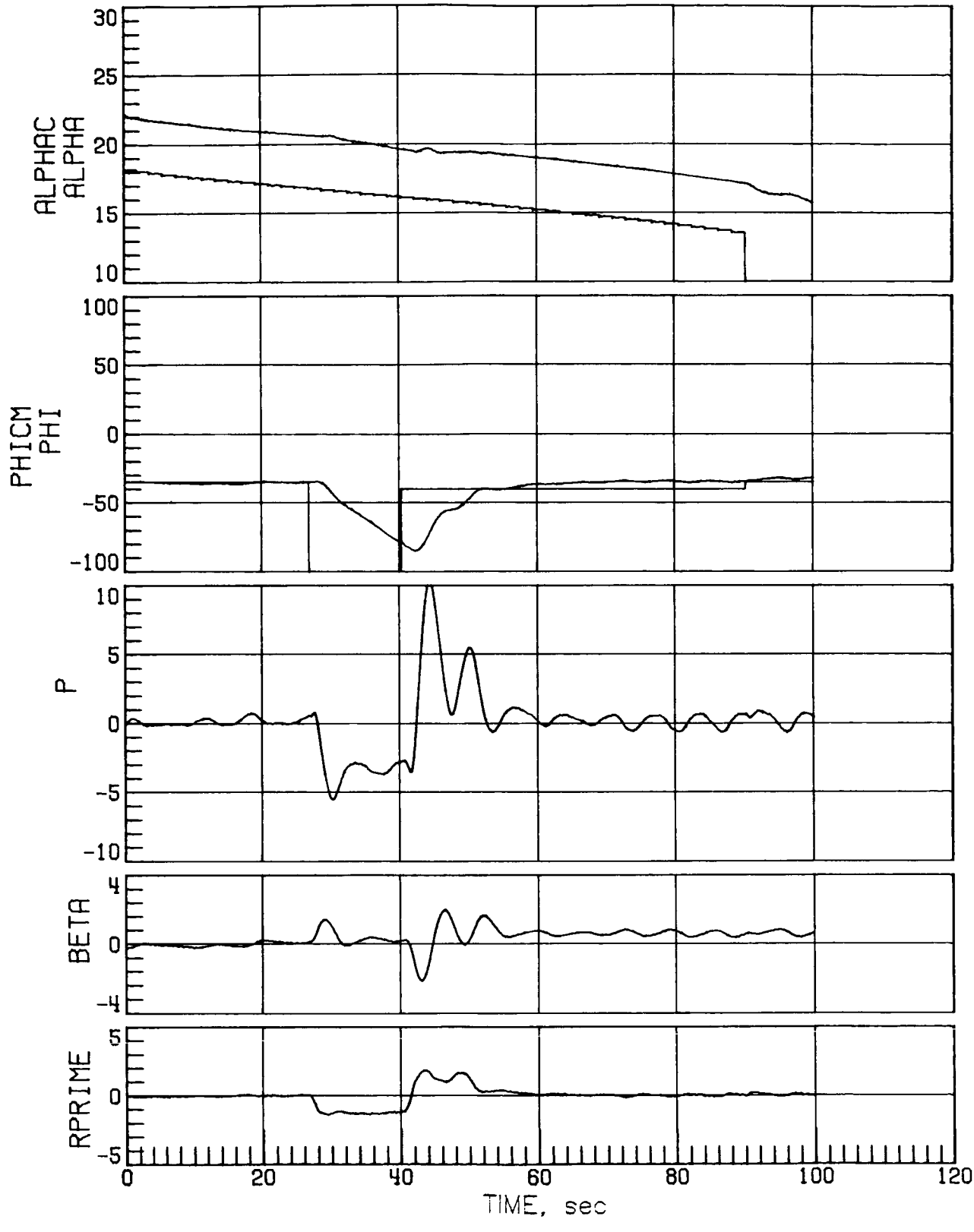

(c) Case 7.

Figure 30.- Continued.

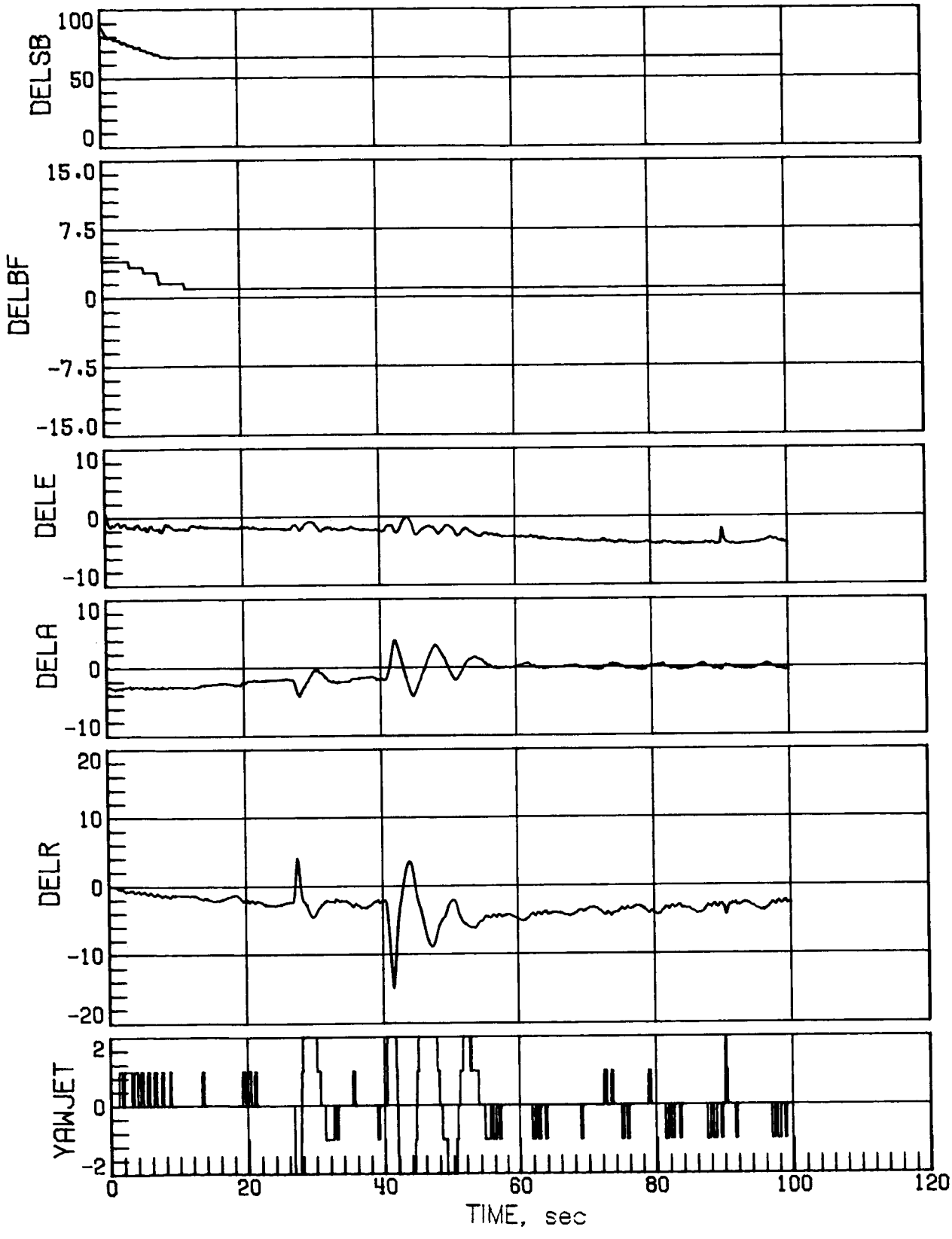

(c) Concluded.

Figure 30.- Concluded.

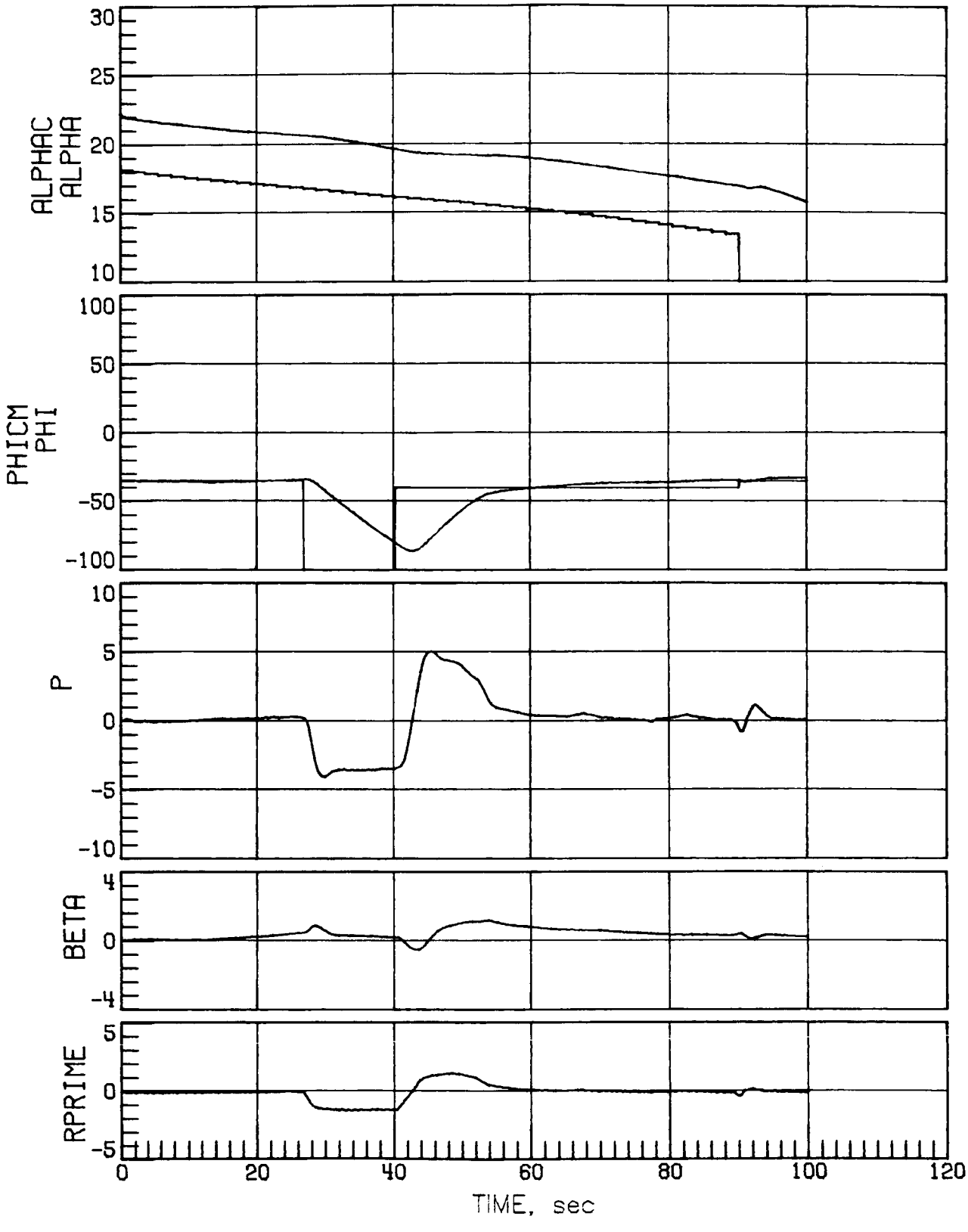

(a) Nominal aerodynamics.

Figure 31.- Mach 4.2 maneuver performance for a low-sensed α error of 4° with decreased rudder effectiveness.

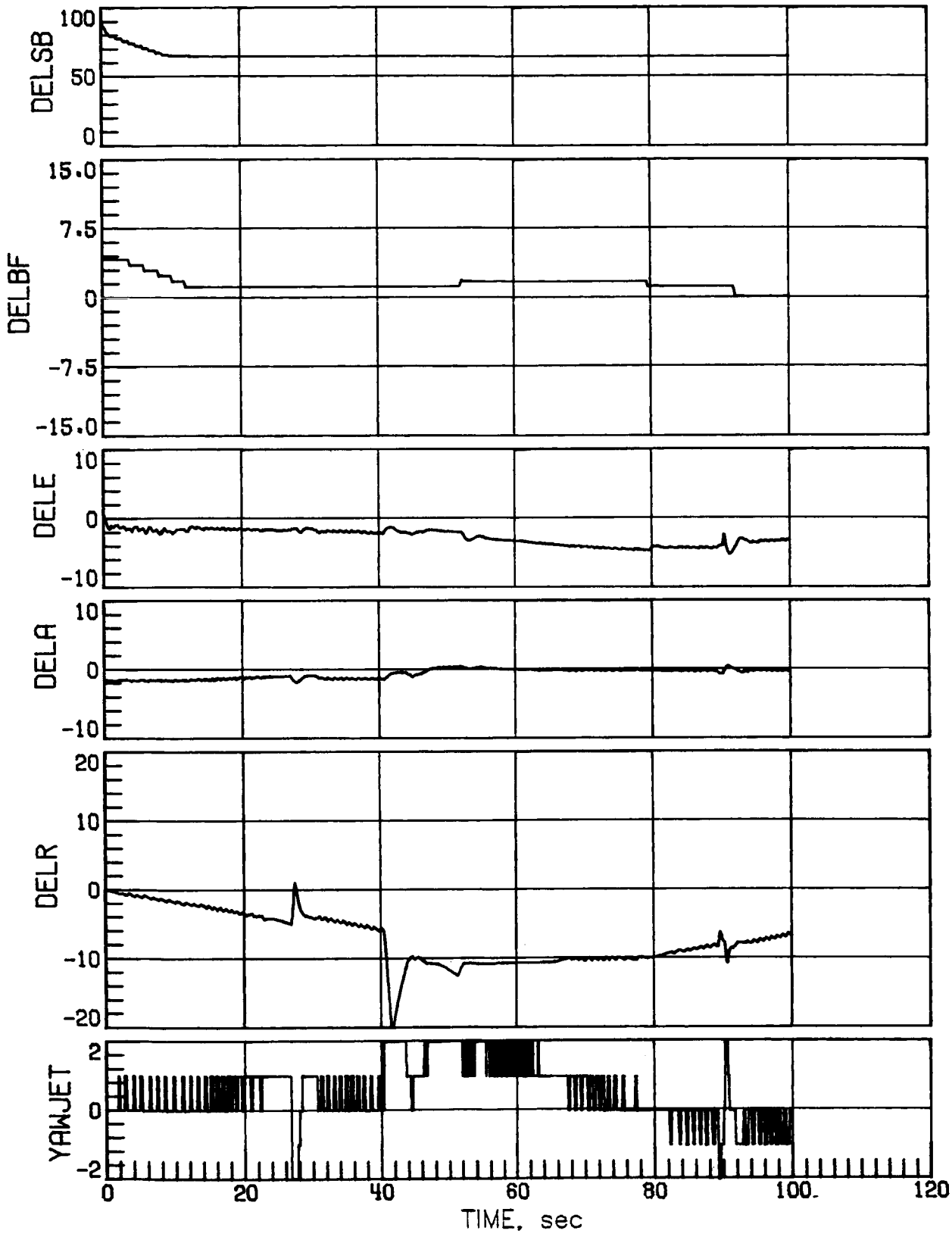

(a) Concluded.

Figure 31.- Continued.

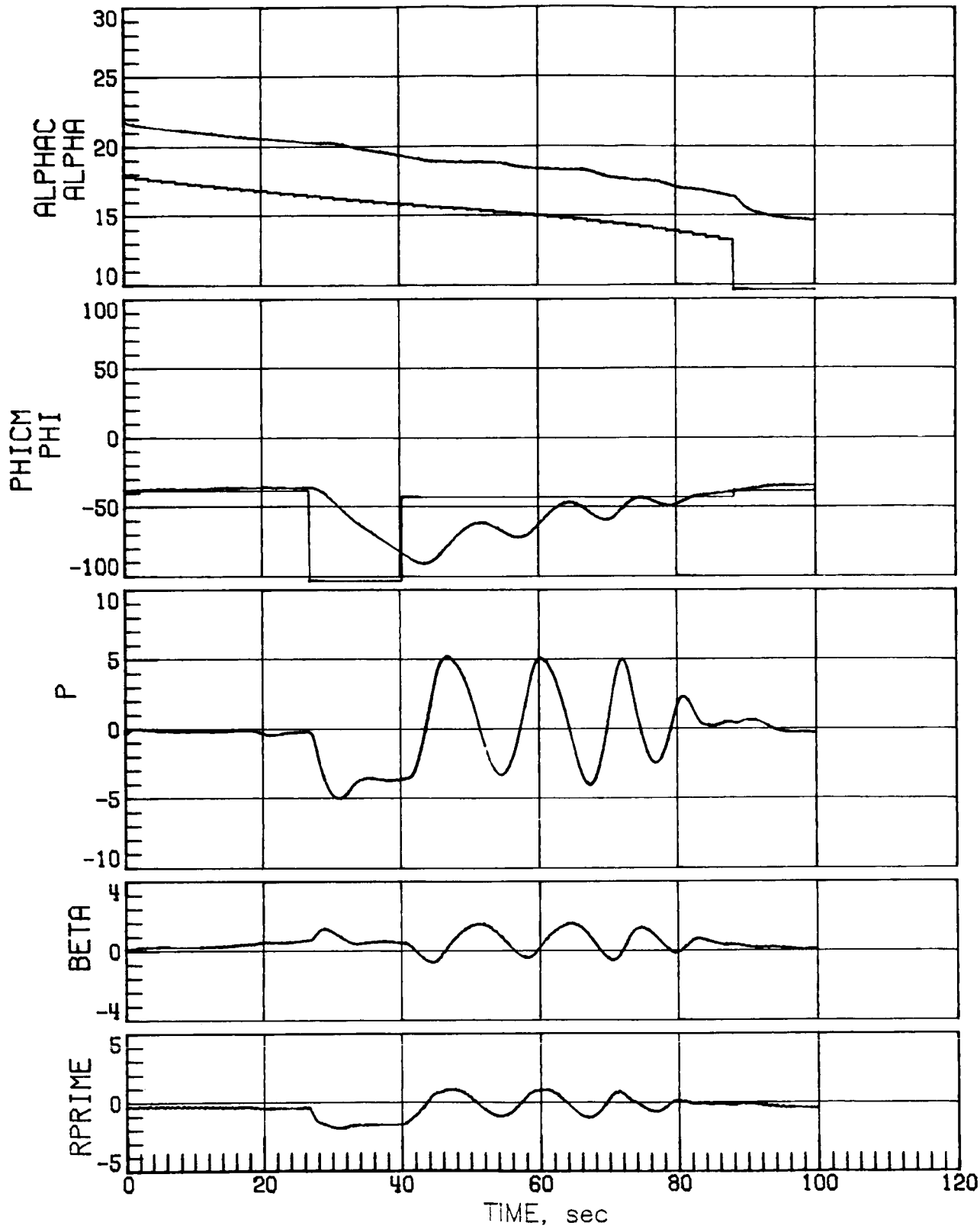

(b) Case 3.

Figure 31.- Continued.

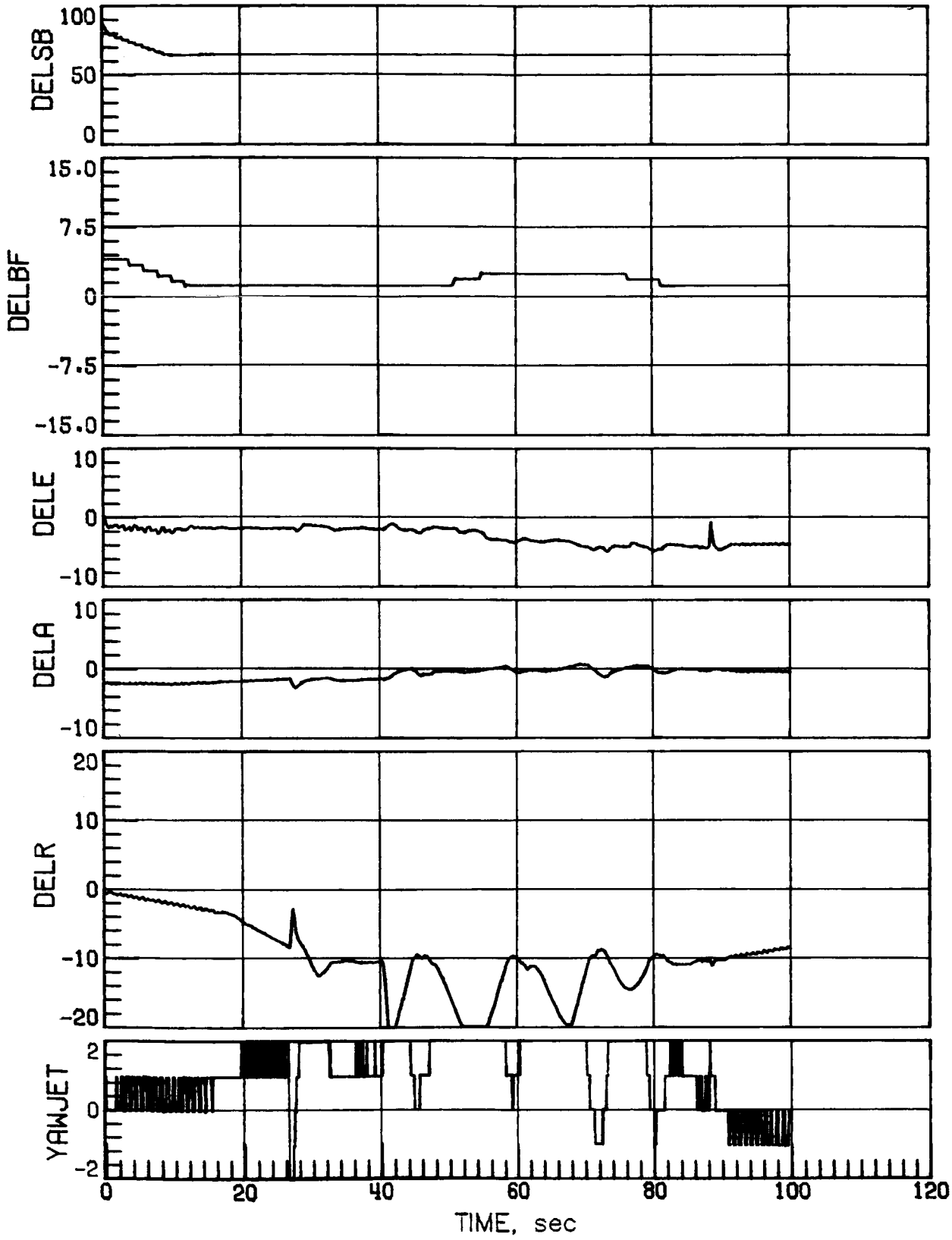

(b) Concluded.

Figure 31.- Continued.

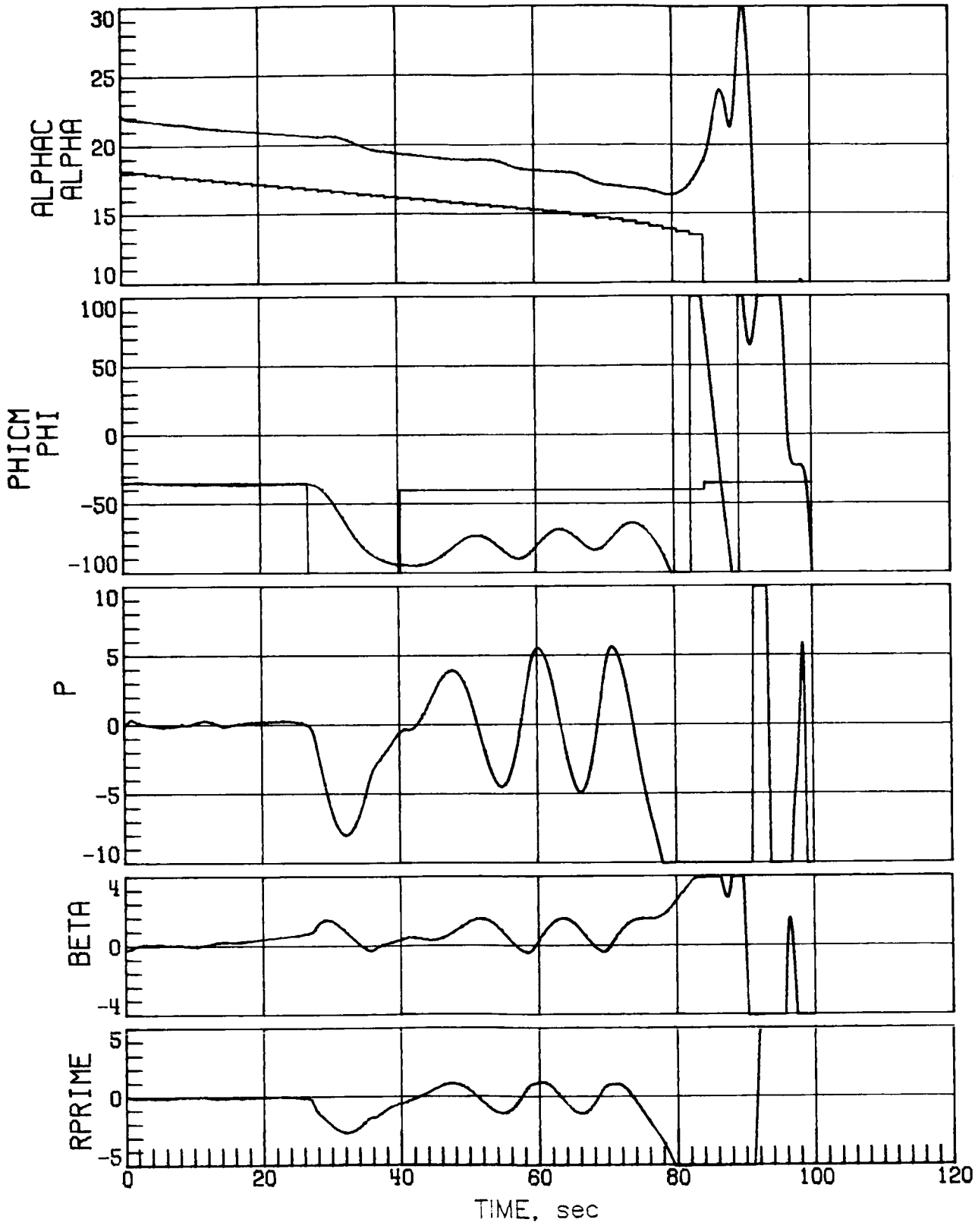

(c) Case 7.

Figure 31.- Continued.

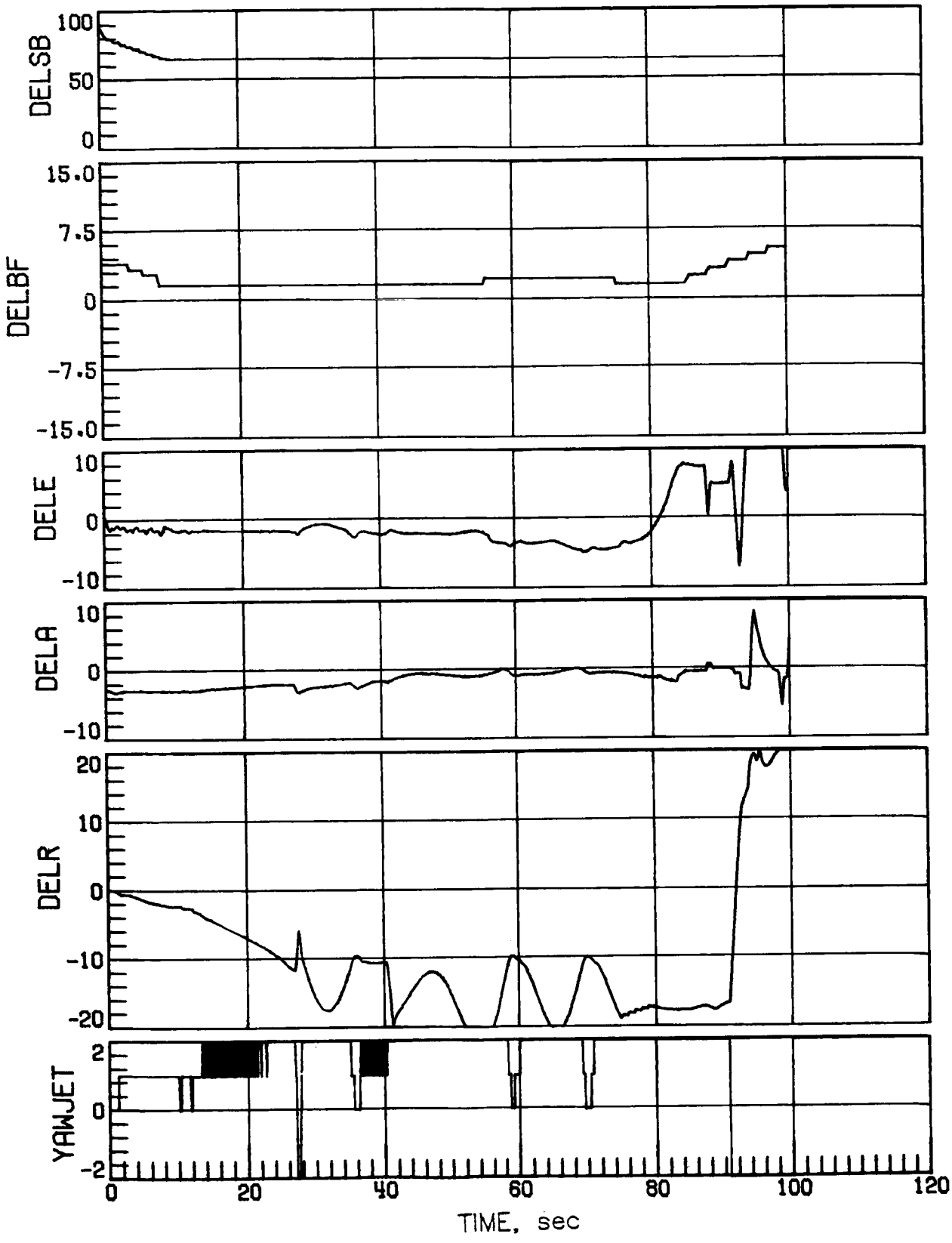

(c) Concluded.

Figure 31.- Concluded.

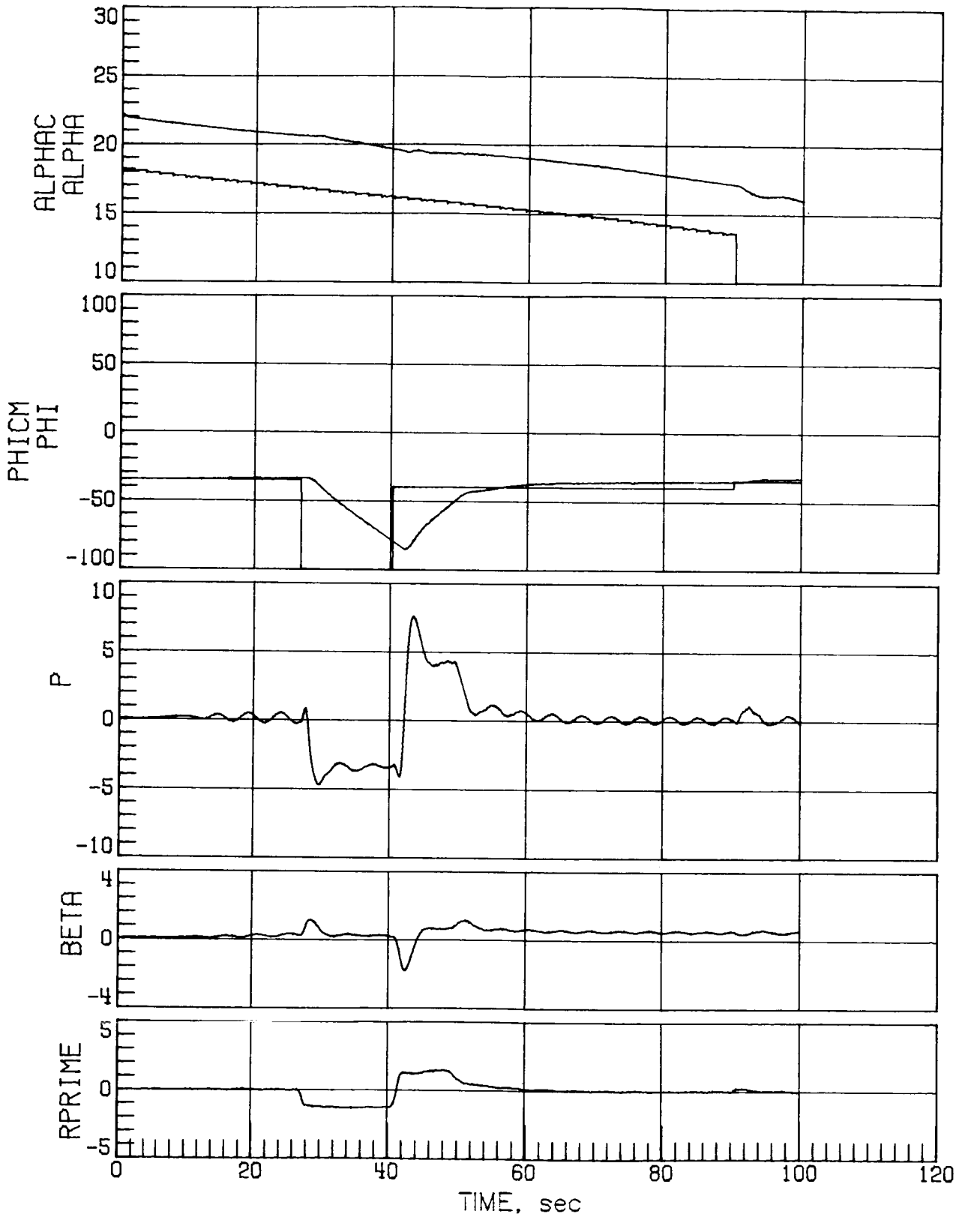

(a) Nominal aerodynamics.

Figure 32.- Mach 4.2 maneuver performance for a low-sensed α error of 4° with increased rudder effectiveness.

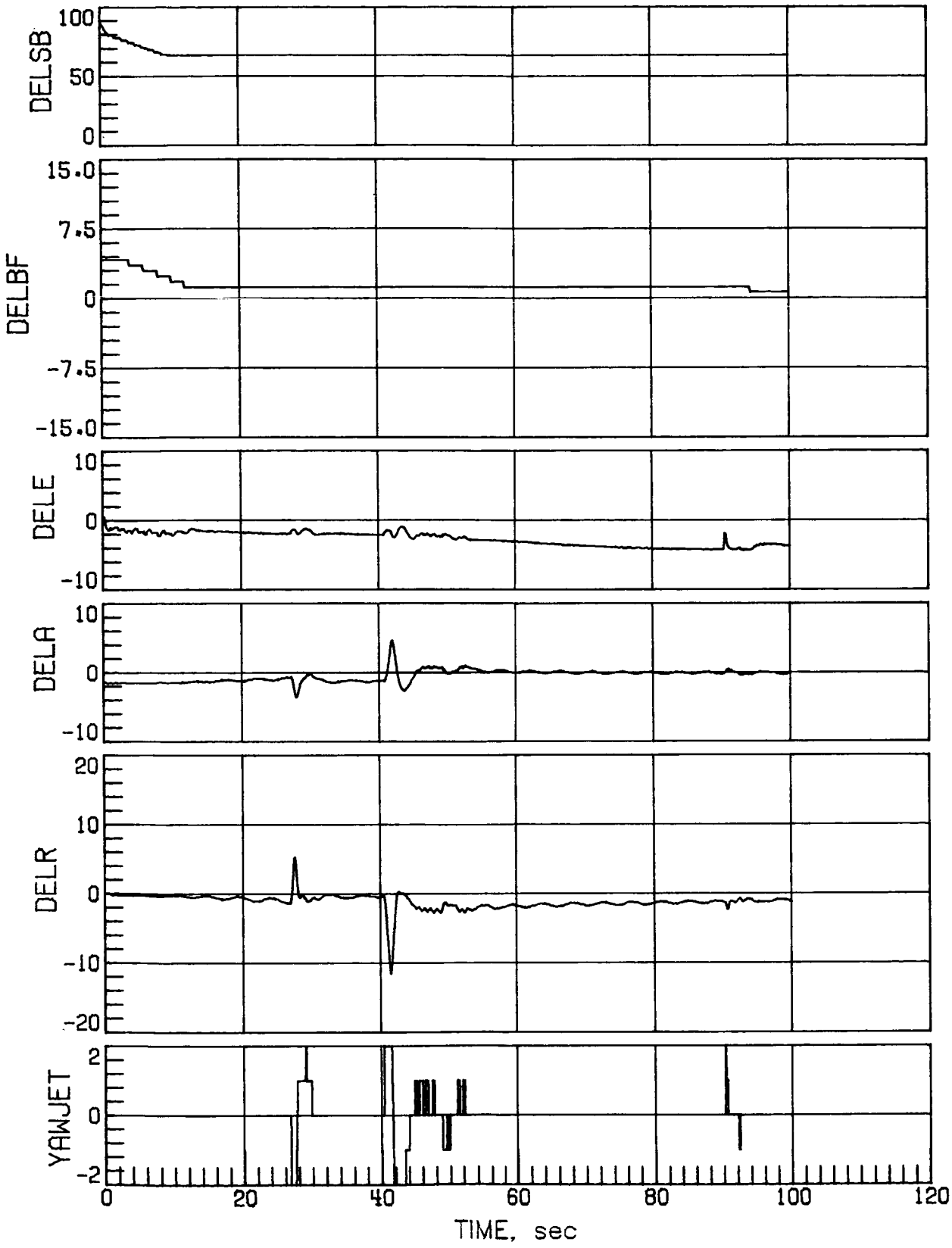

(a) Concluded.

Figure 32.- Continued.

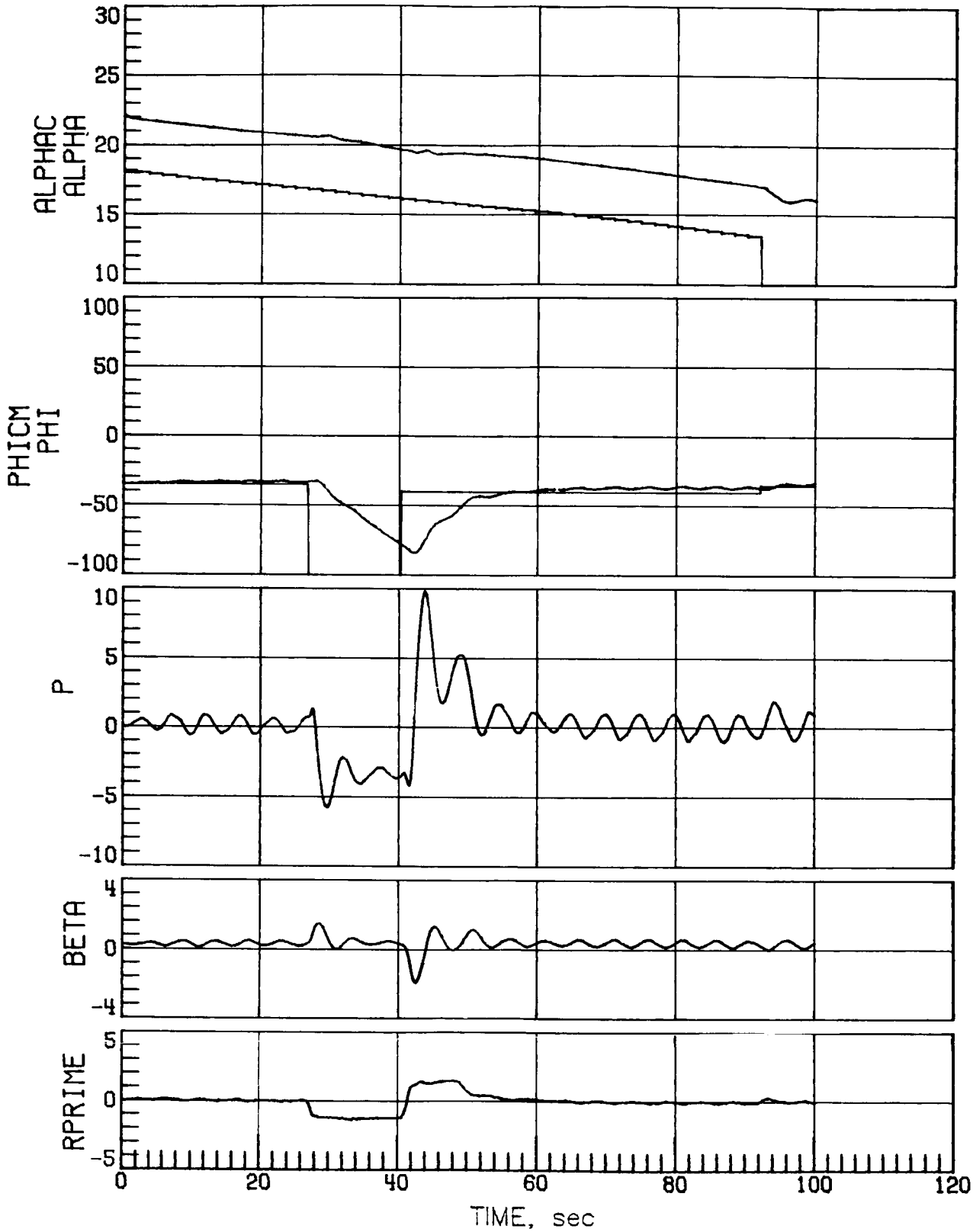

(b) Case 1.

Figure 32.- Continued.

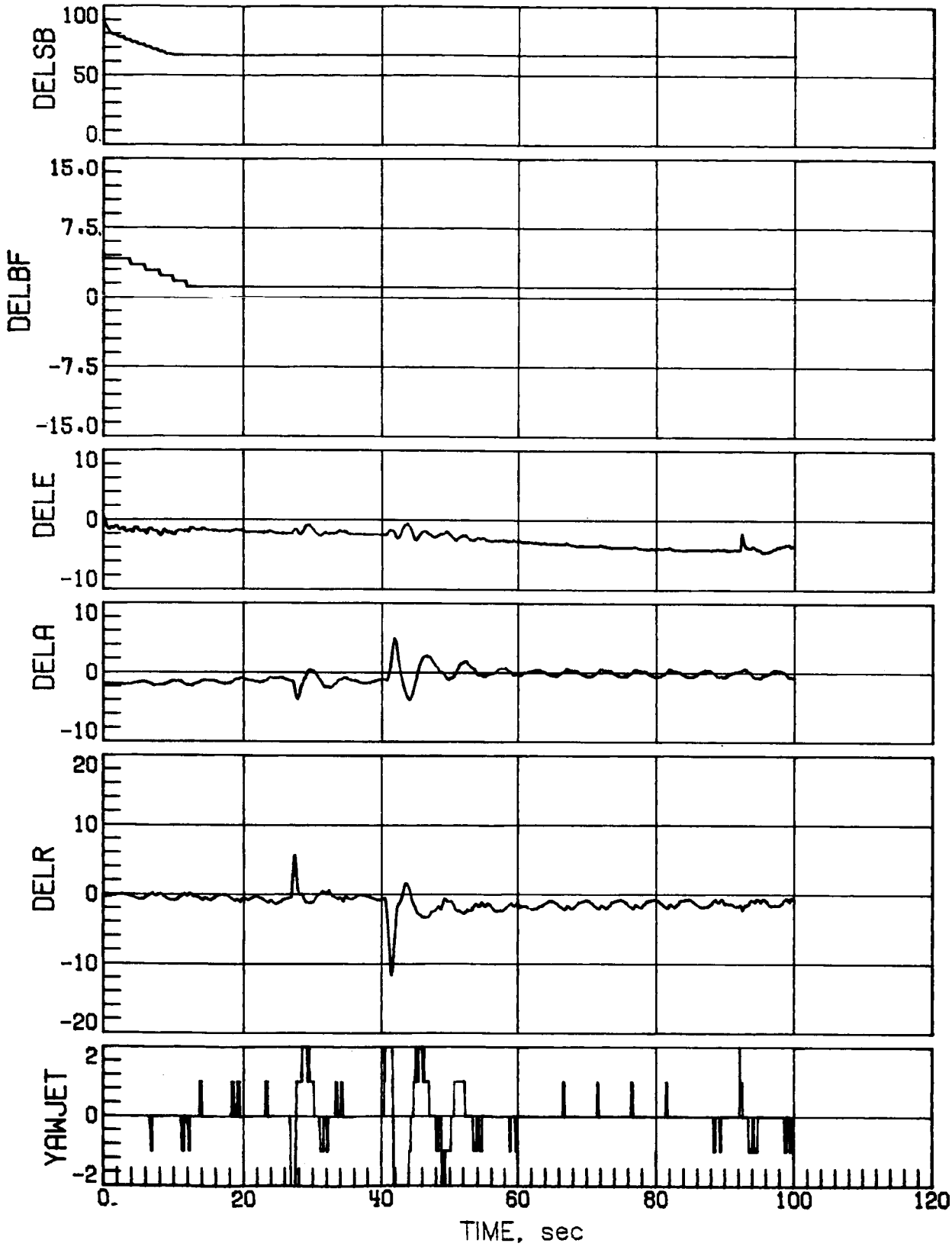

(b) Concluded.

Figure 32.- Continued.

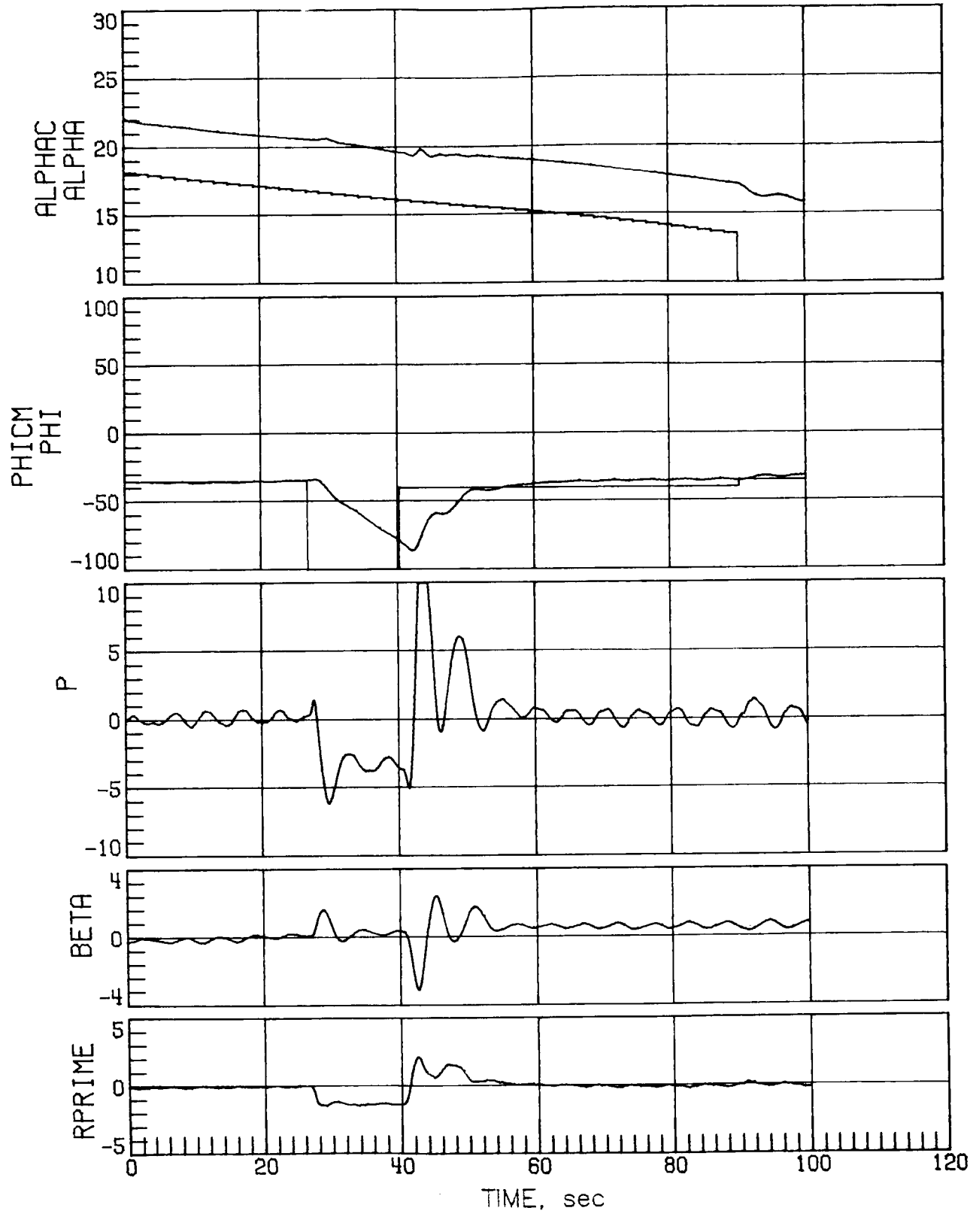

(c) Case 7.

Figure 32.- Continued.

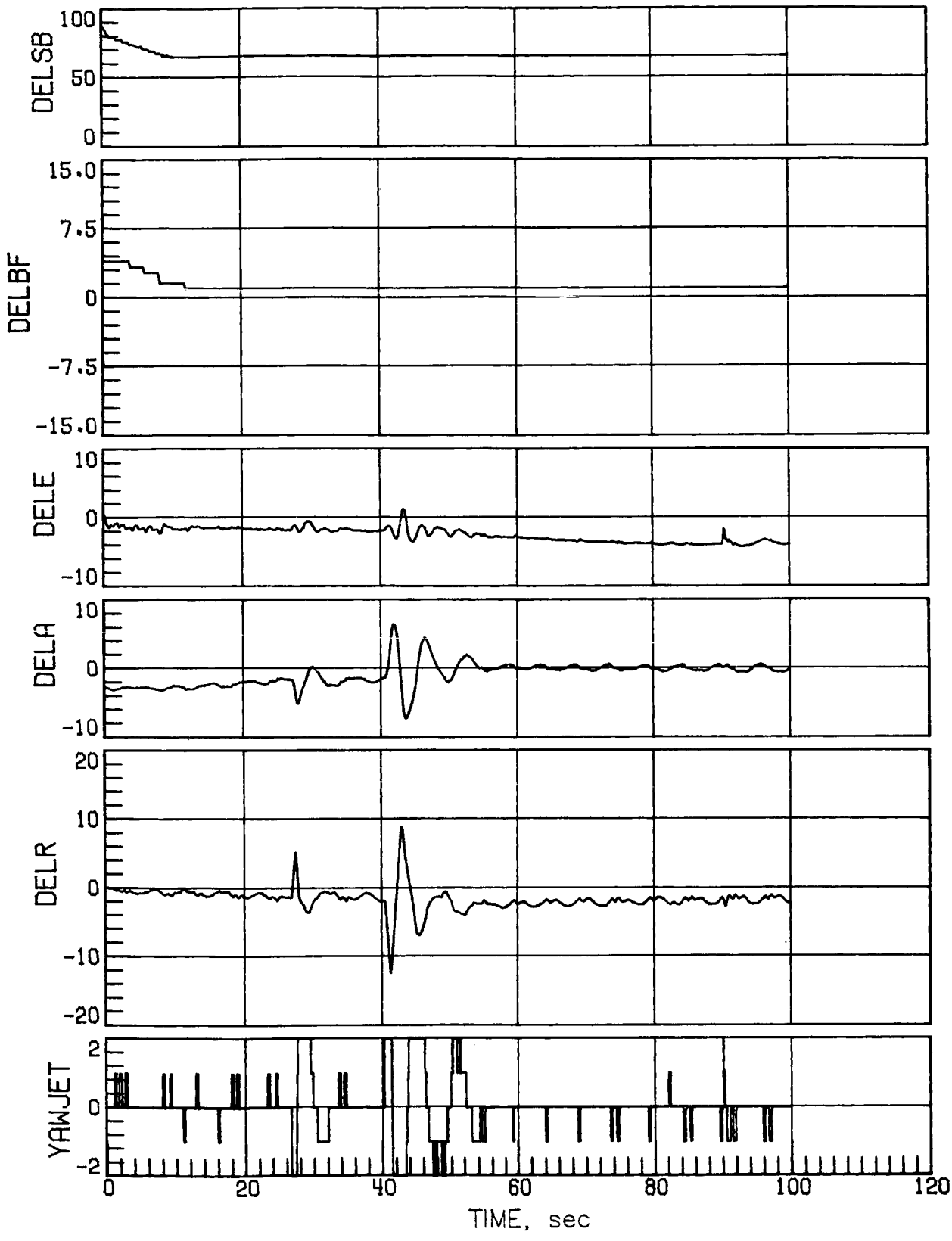

(c) Concluded.

Figure 32.- Concluded.

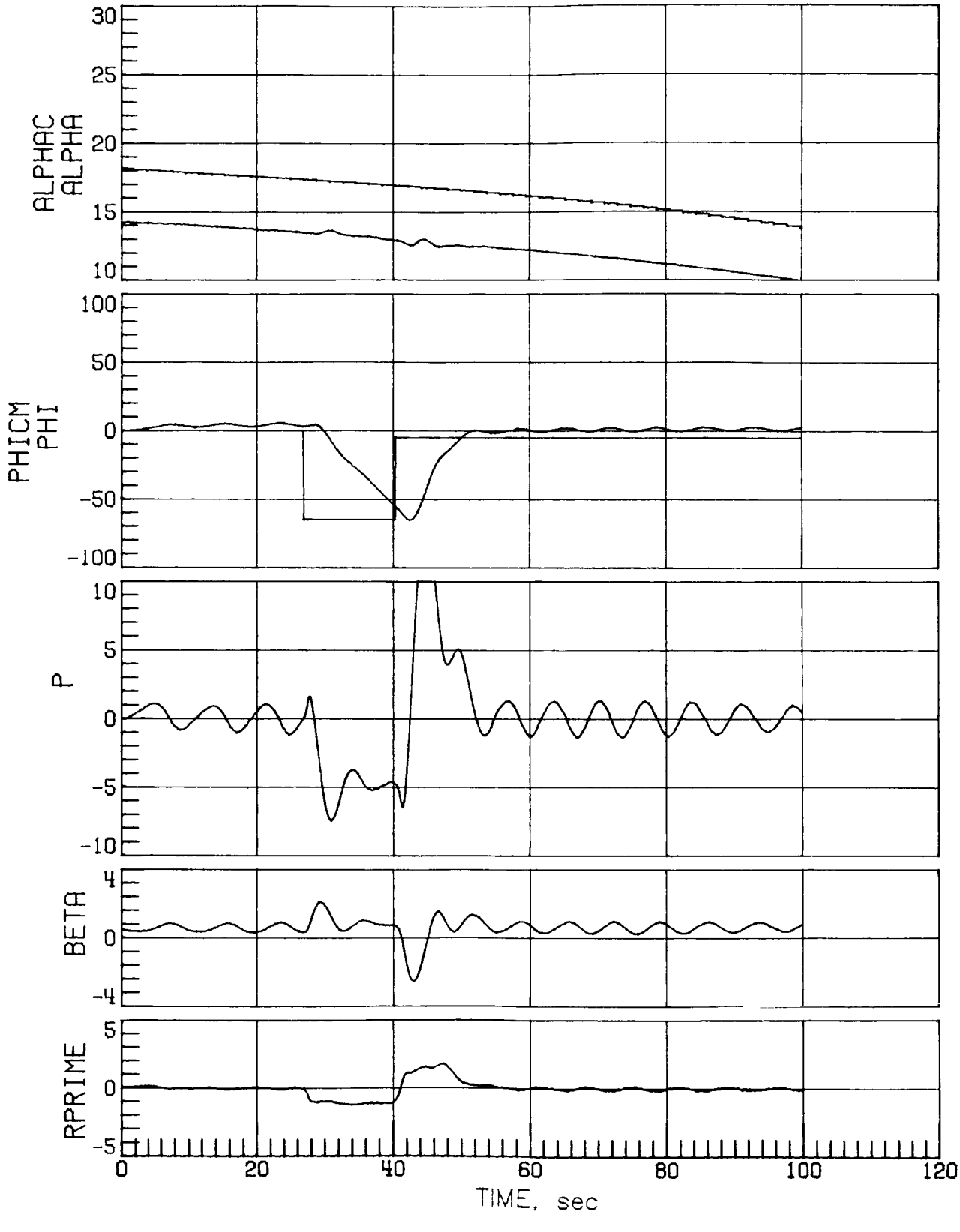

(a) Case 3.

Figure 33.- Mach 4.2 maneuver performance for a high-sensed α error of 4°.

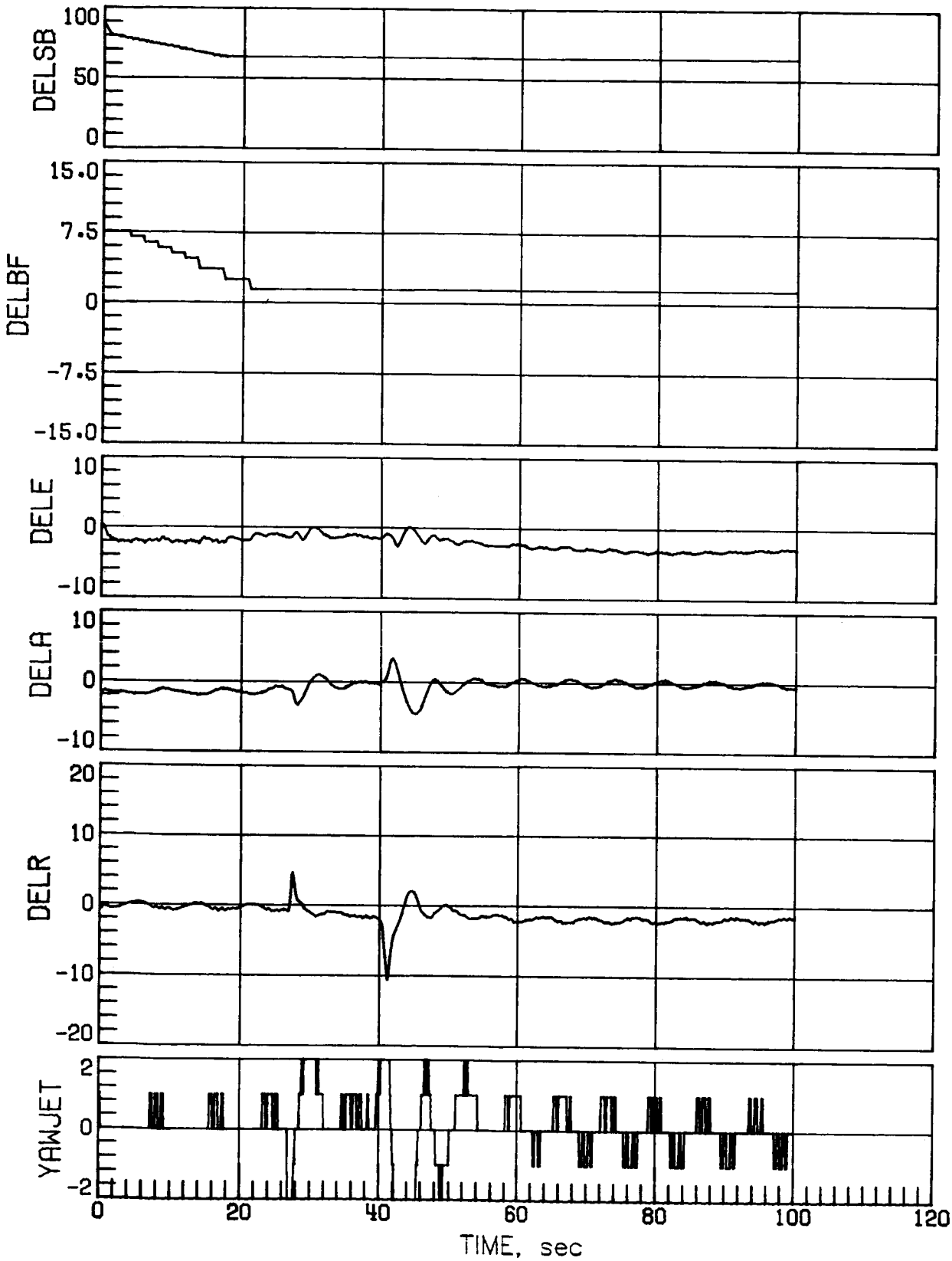

(a) Concluded.

Figure 33.- Continued.

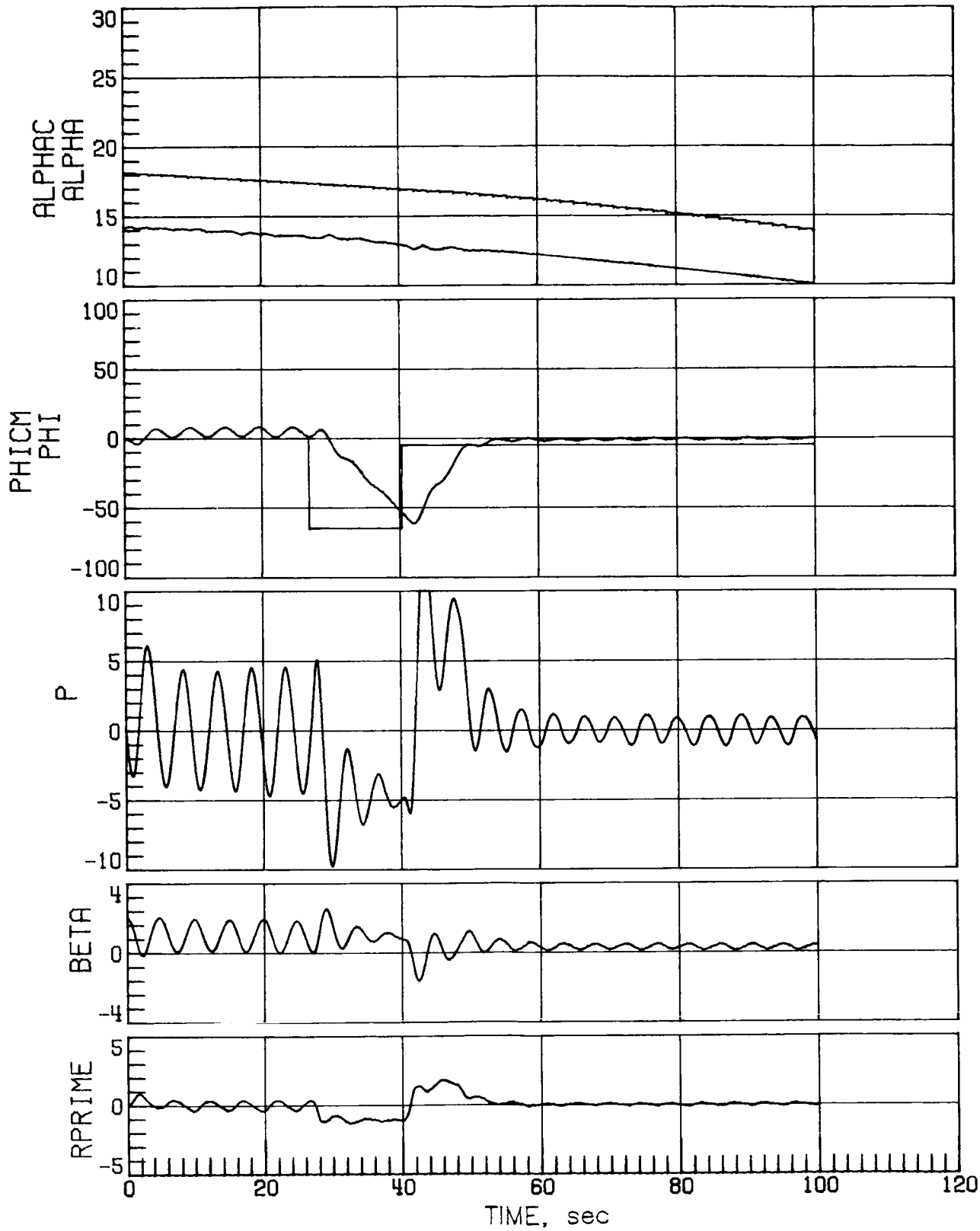

(b) Case 5.

Figure 33.- Continued.

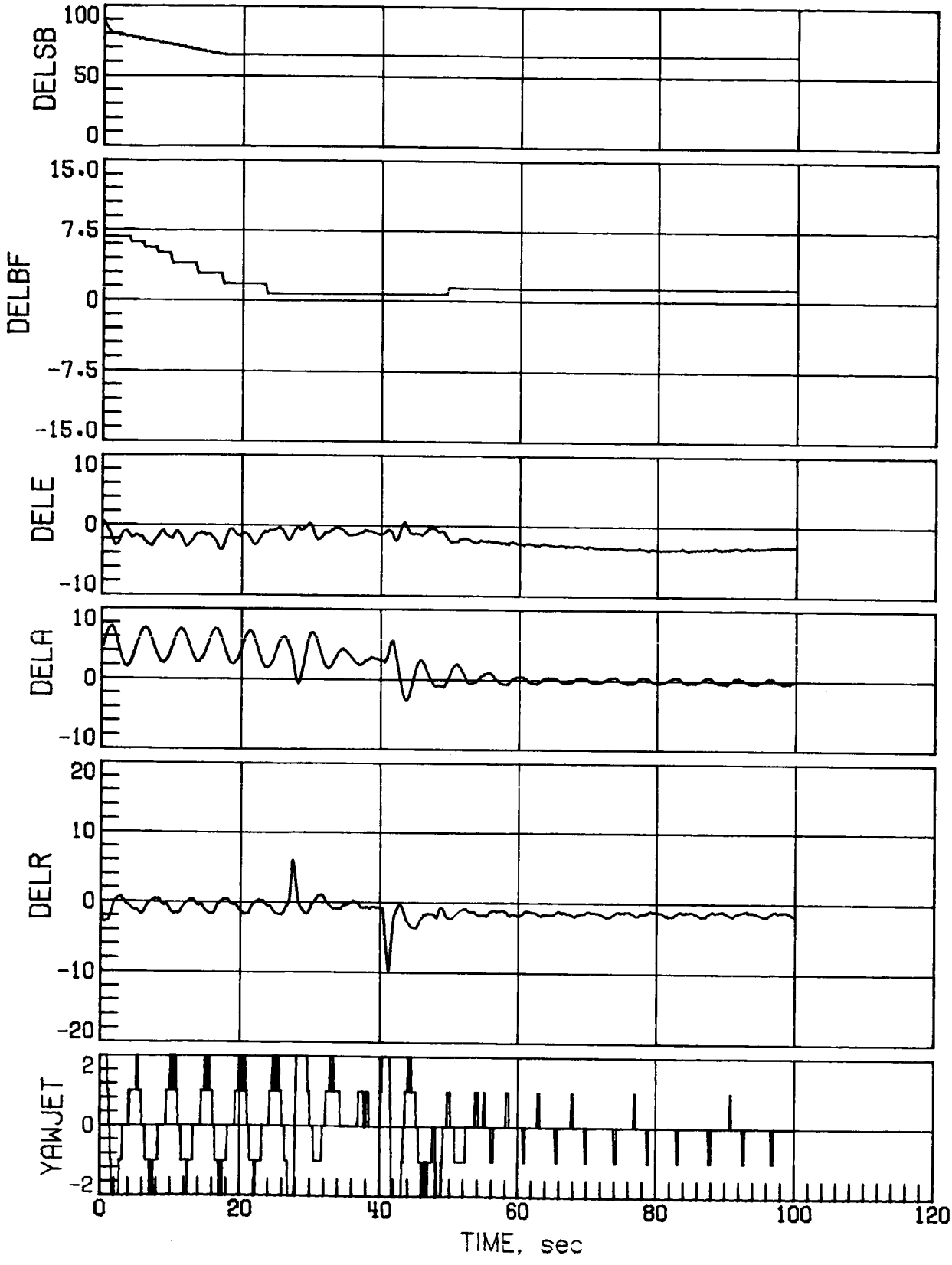

(b) Concluded.

Figure 33.- Concluded.

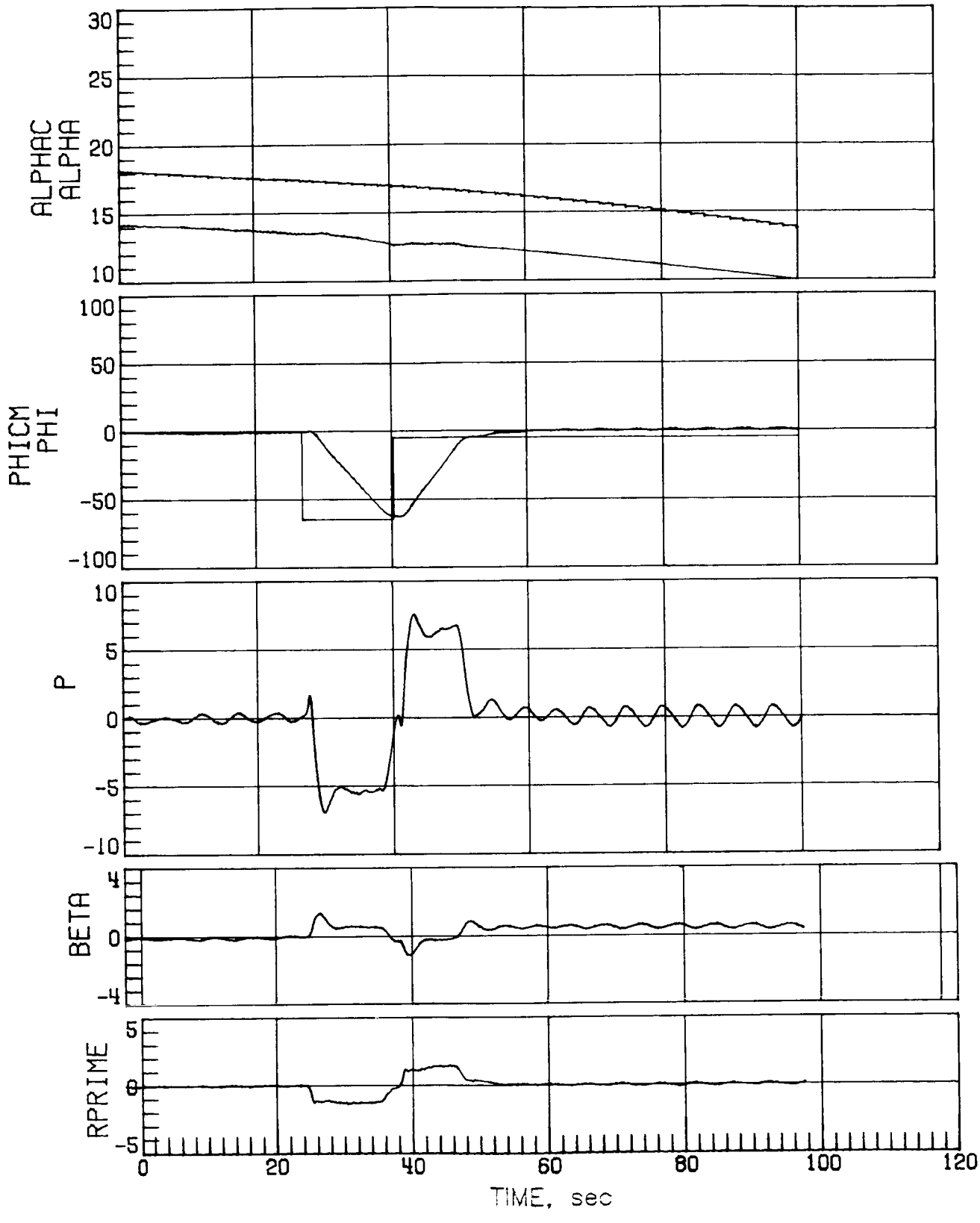

(a) Nominal aerodynamics.

Figure 34.- Mach 4.2 maneuver performance for a high-sensed α error of 4° with increased rudder effectiveness.

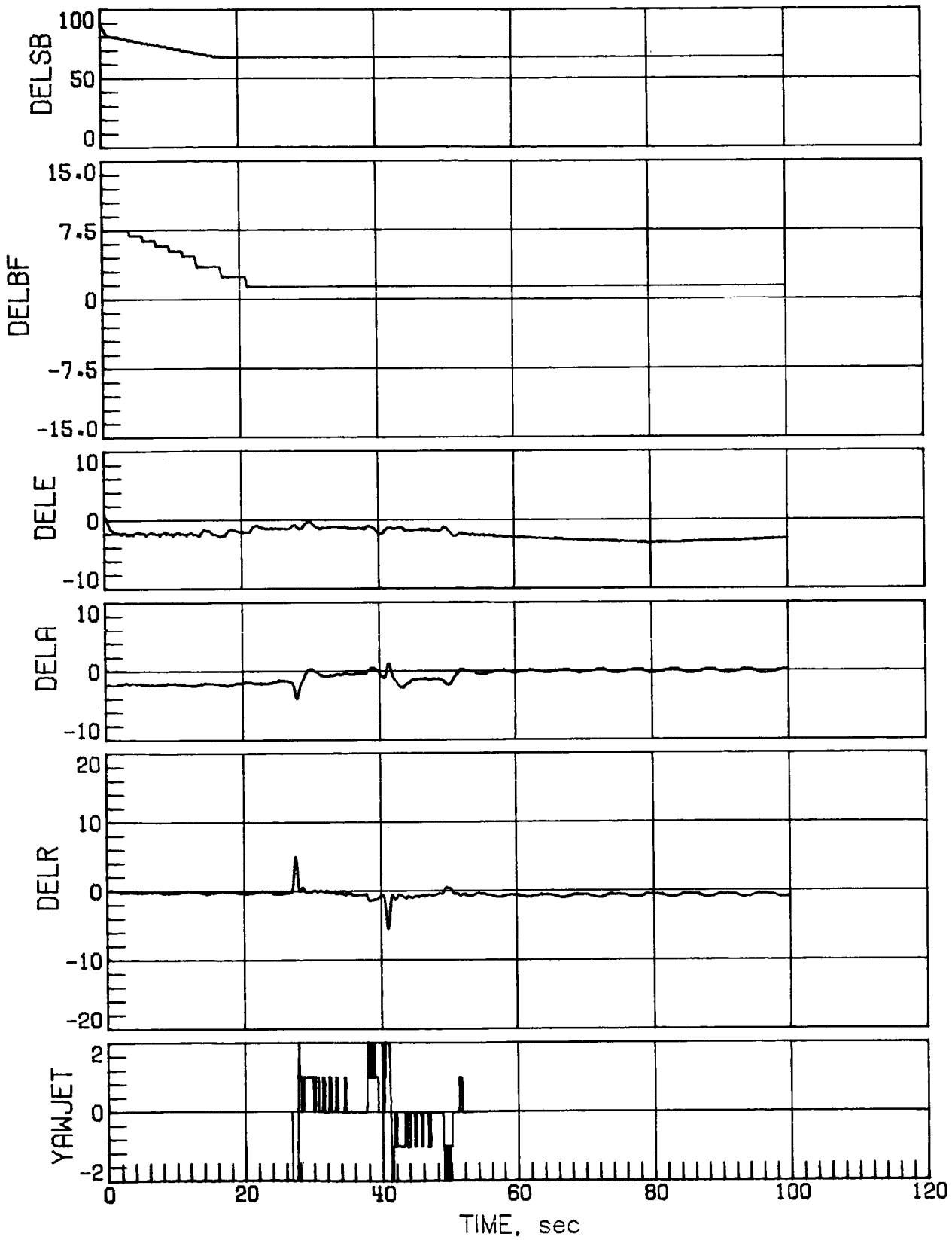

(a) Concluded.

Figure 34.- Continued.

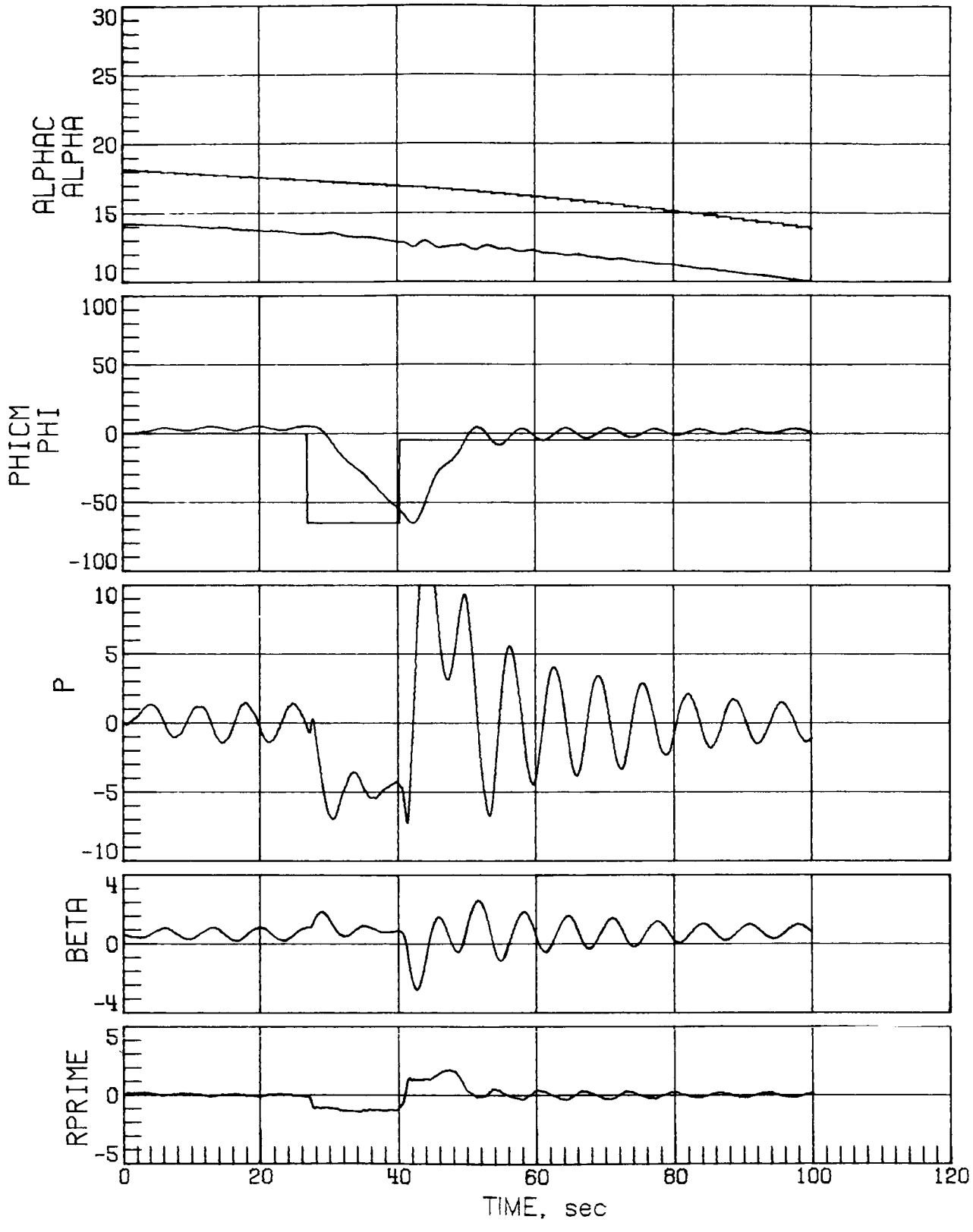

(b) Case 3.

Figure 34.- Continued.

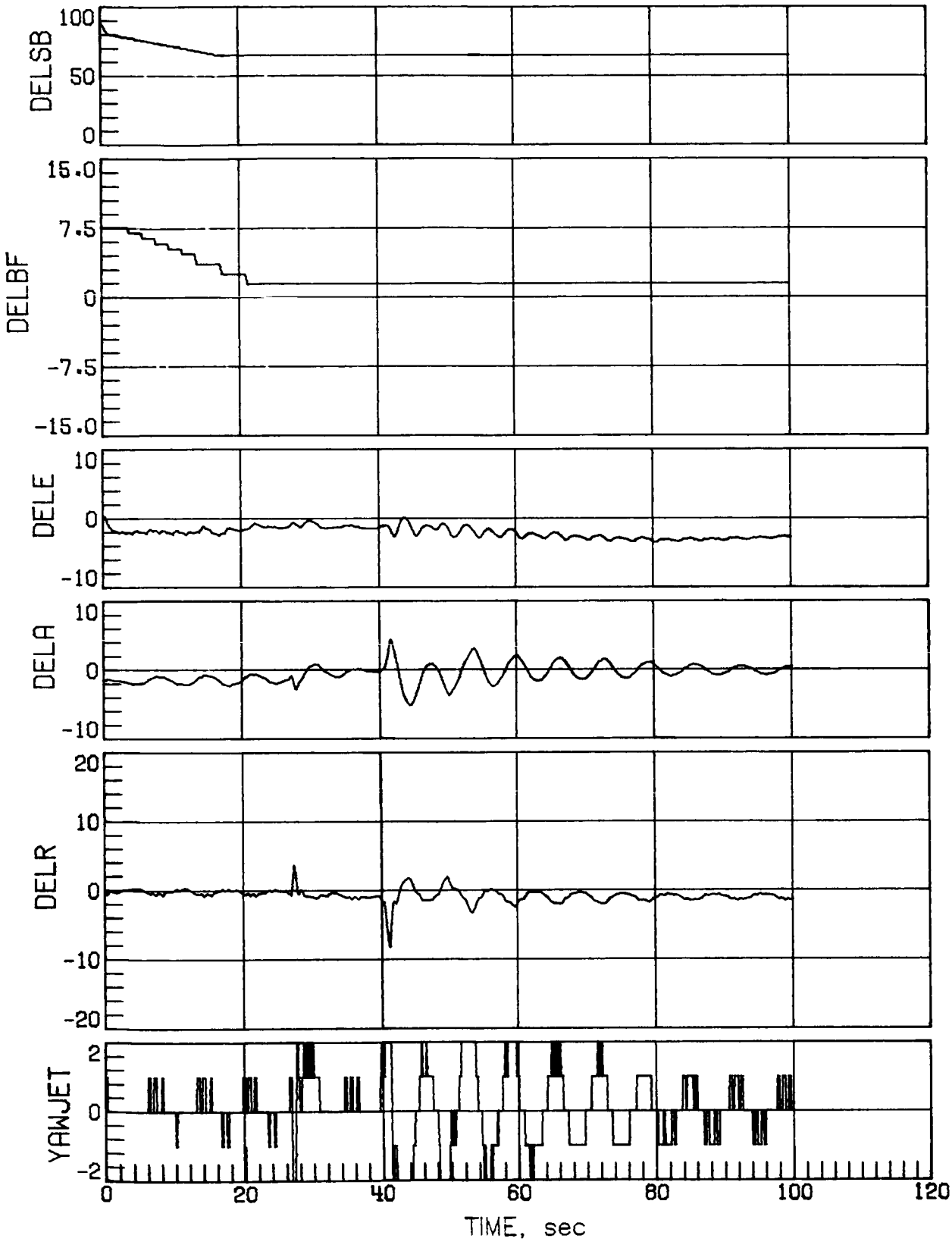

(b) Concluded.

Figure 34.- Continued.

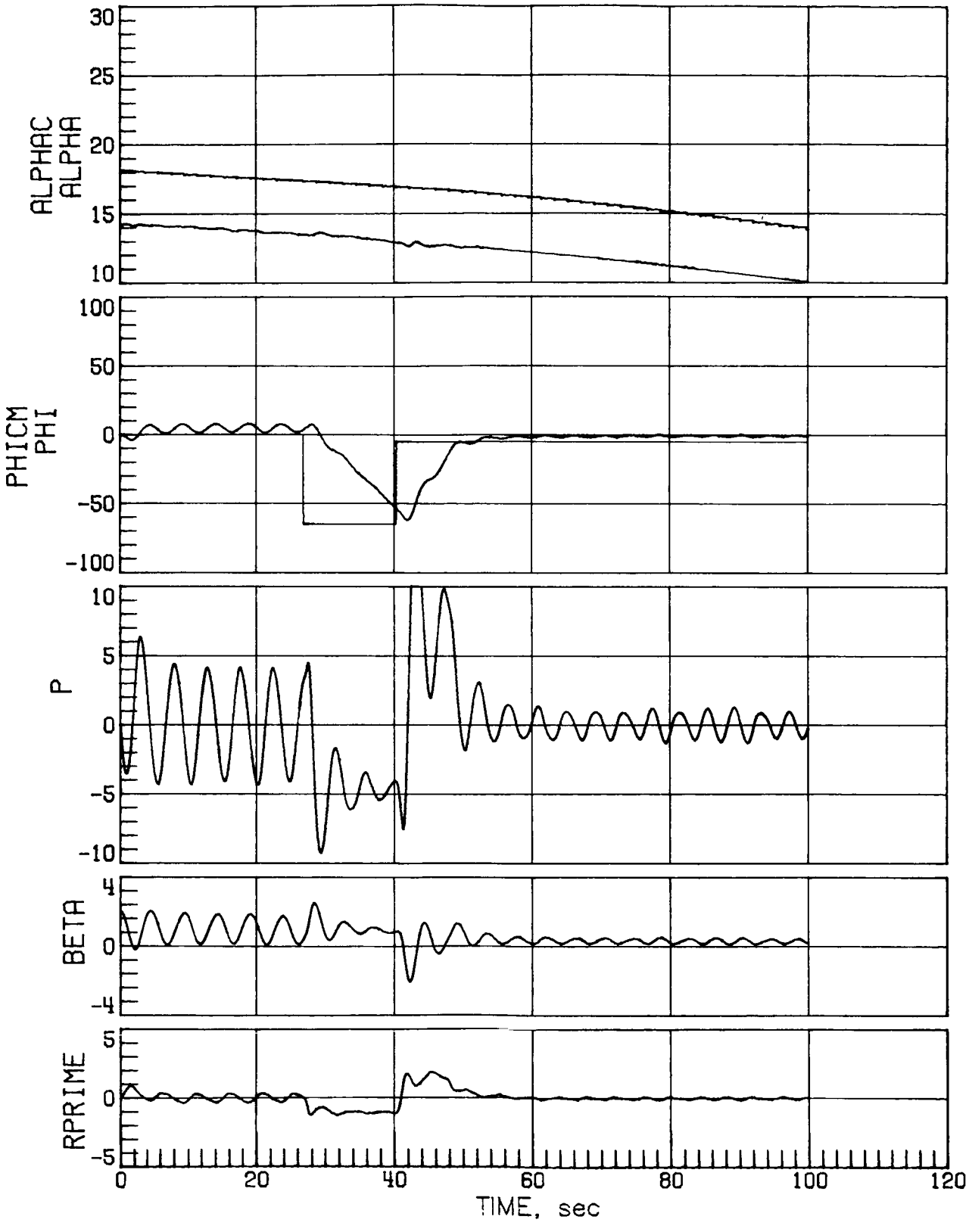

(c) Case 5.

Figure 34.- Continued.

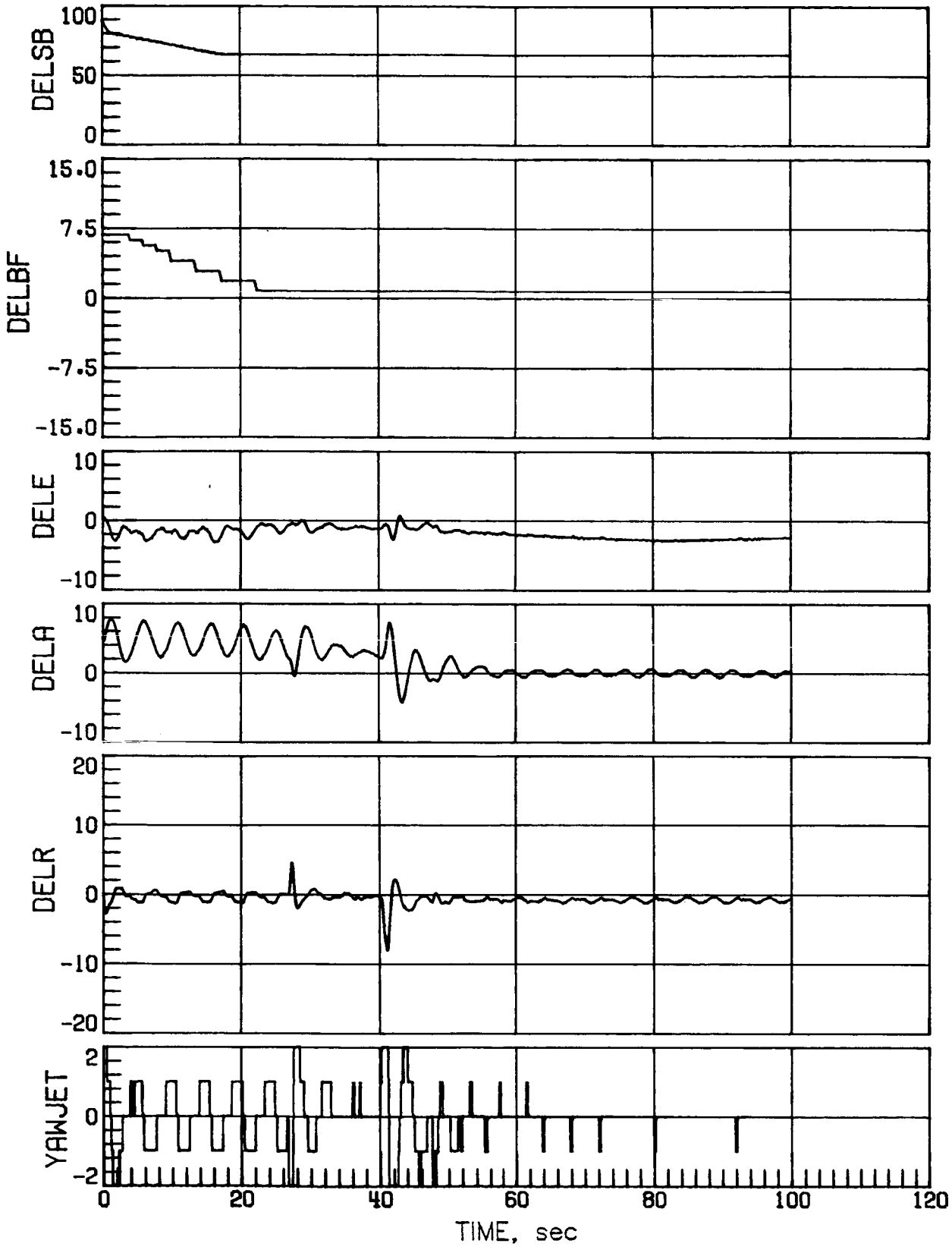

(c) Concluded.

Figure 34.- Concluded.

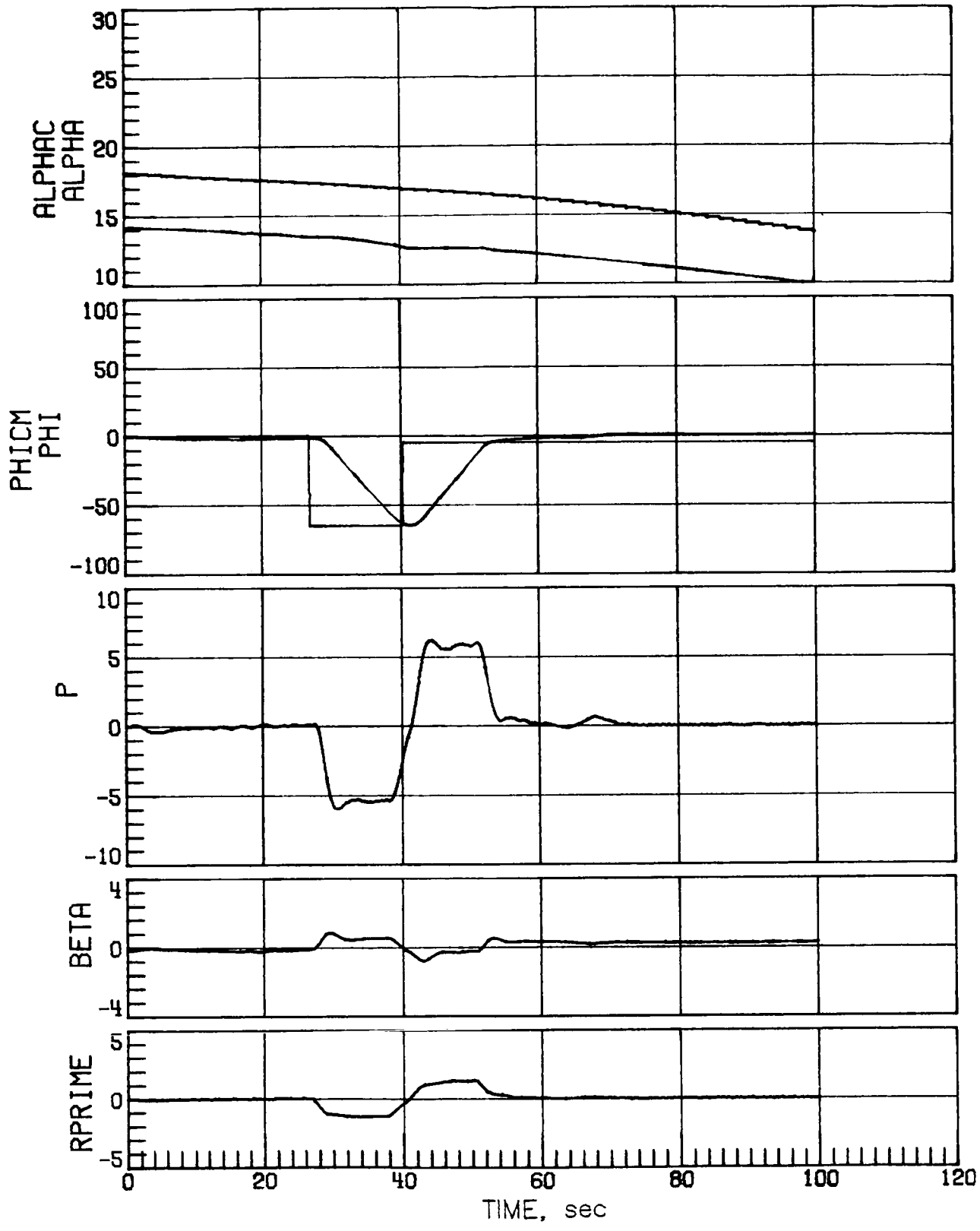

(a) Nominal aerodynamics.

Figure 35.- Mach 4.2 maneuver performance for a high-sensed α error of 4° with decreased rudder effectiveness.

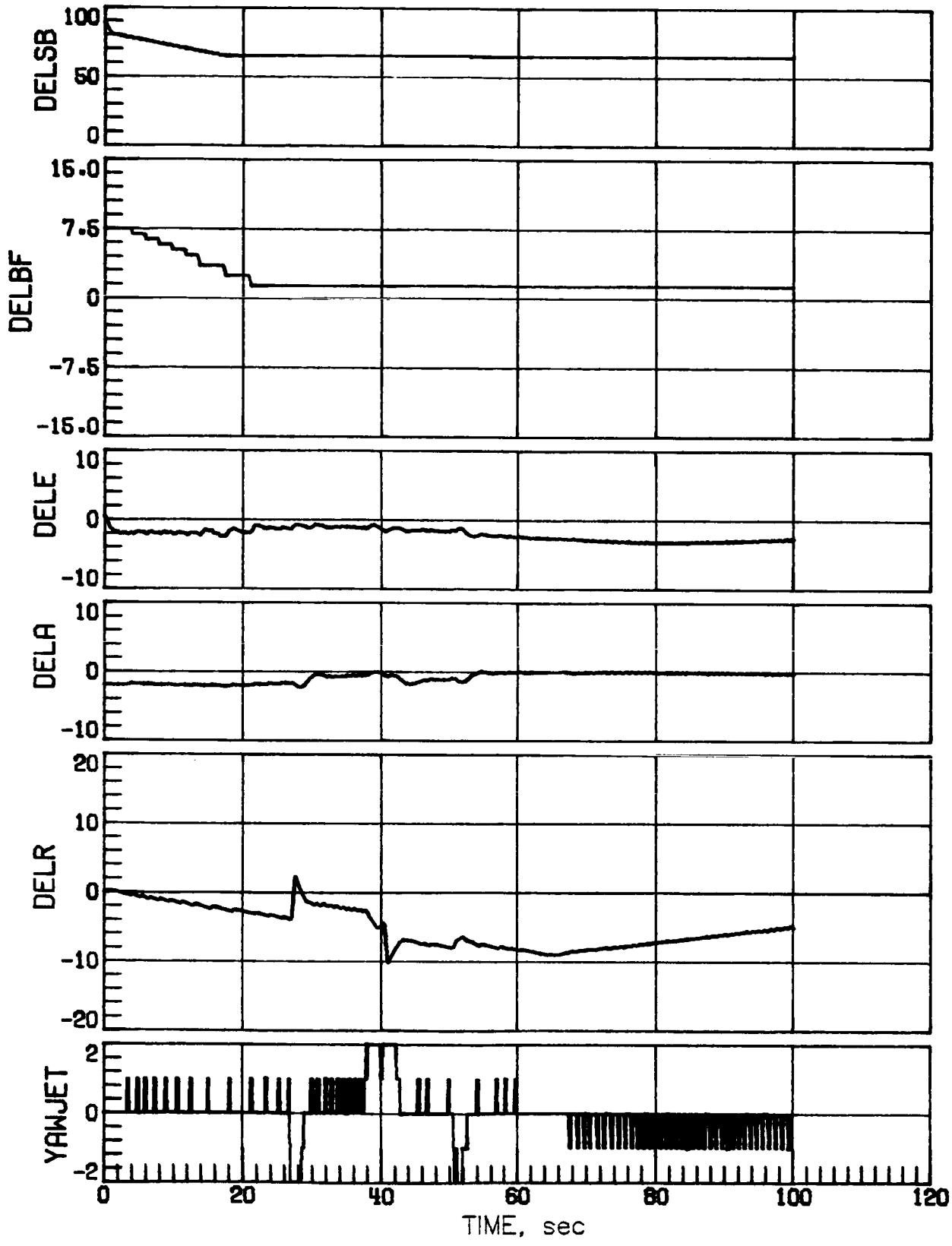

(a) Concluded.

Figure 35.- Continued.

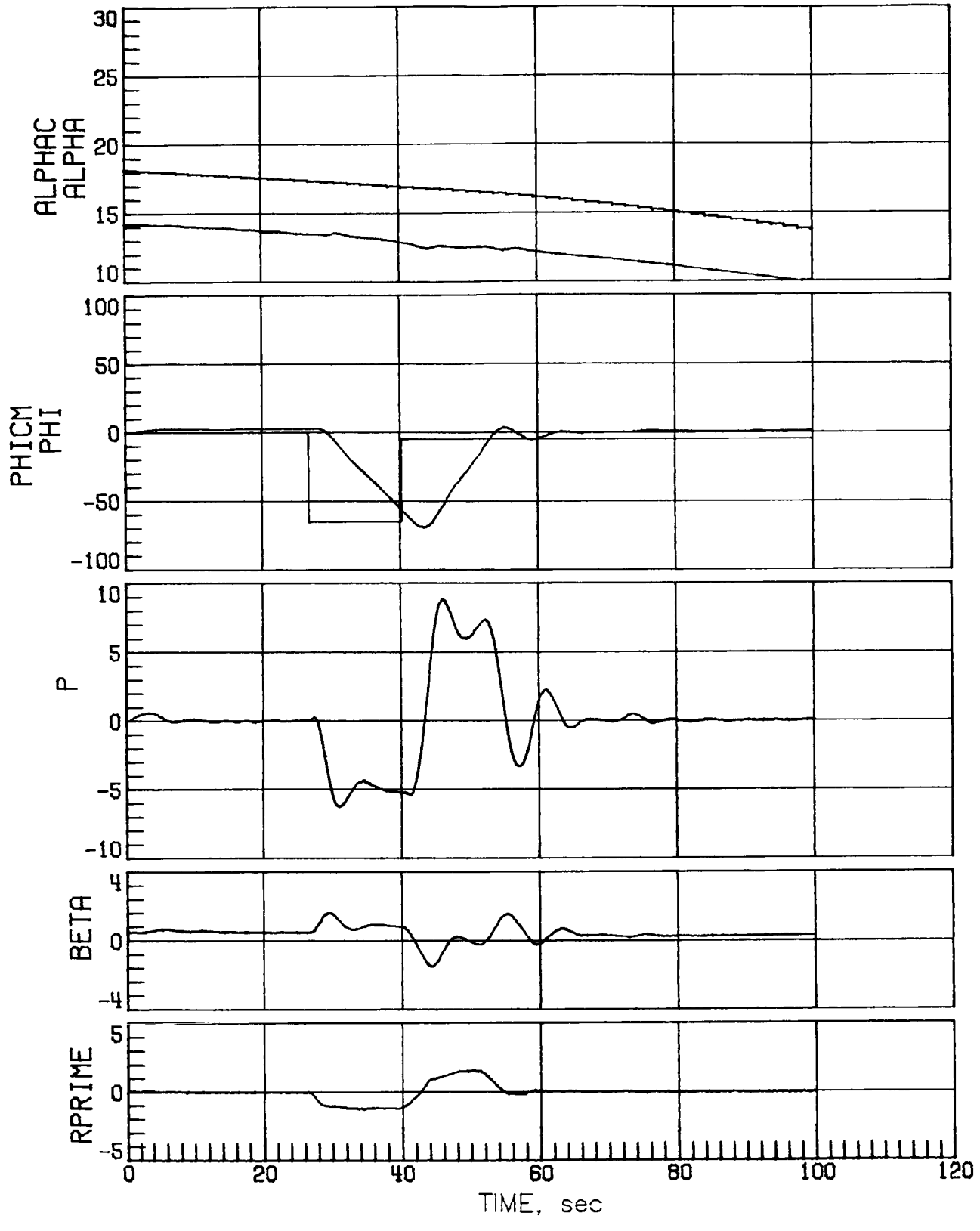

(b) Case 3.

Figure 35.- Continued.

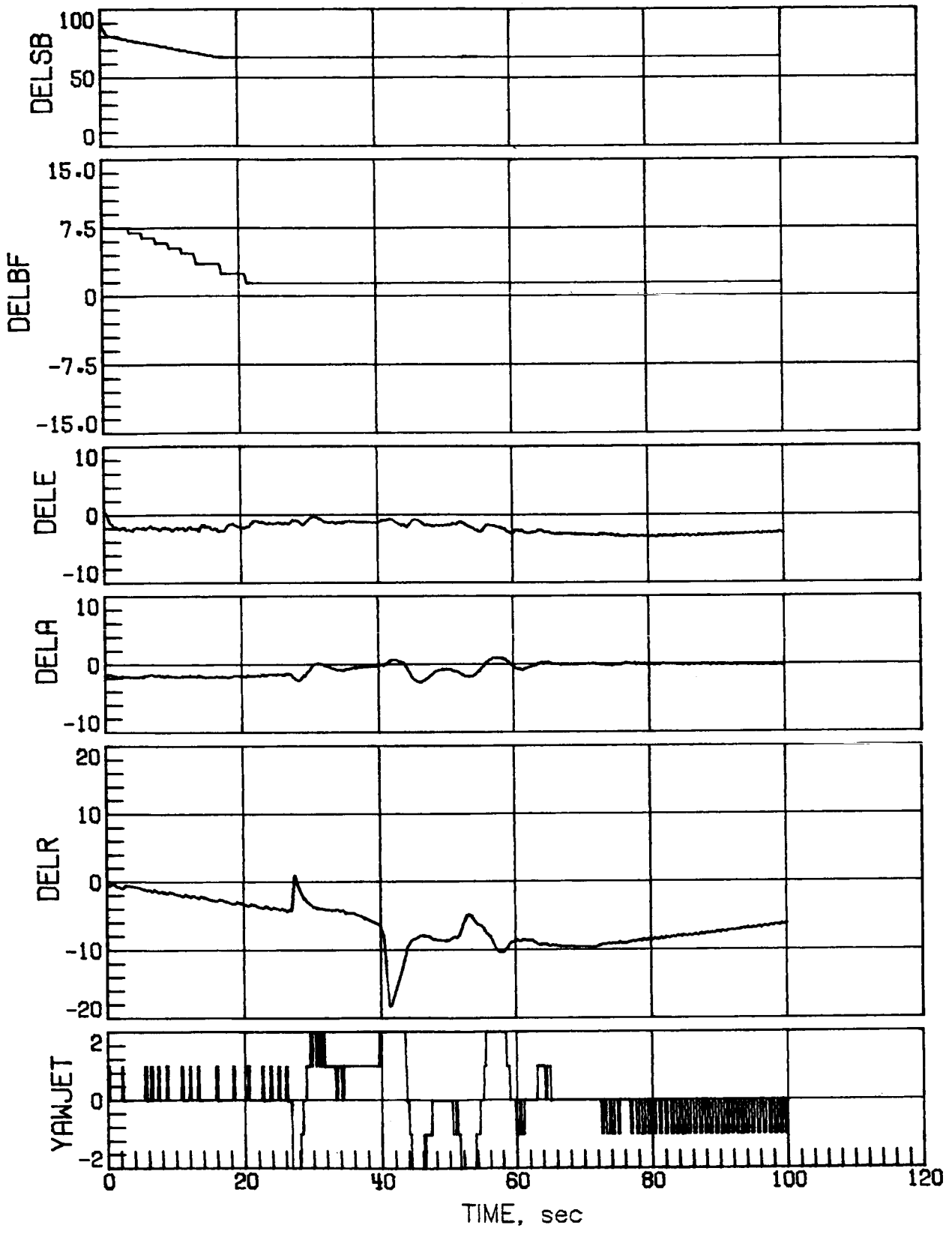

(b) Concluded.

Figure 35.- Continued.

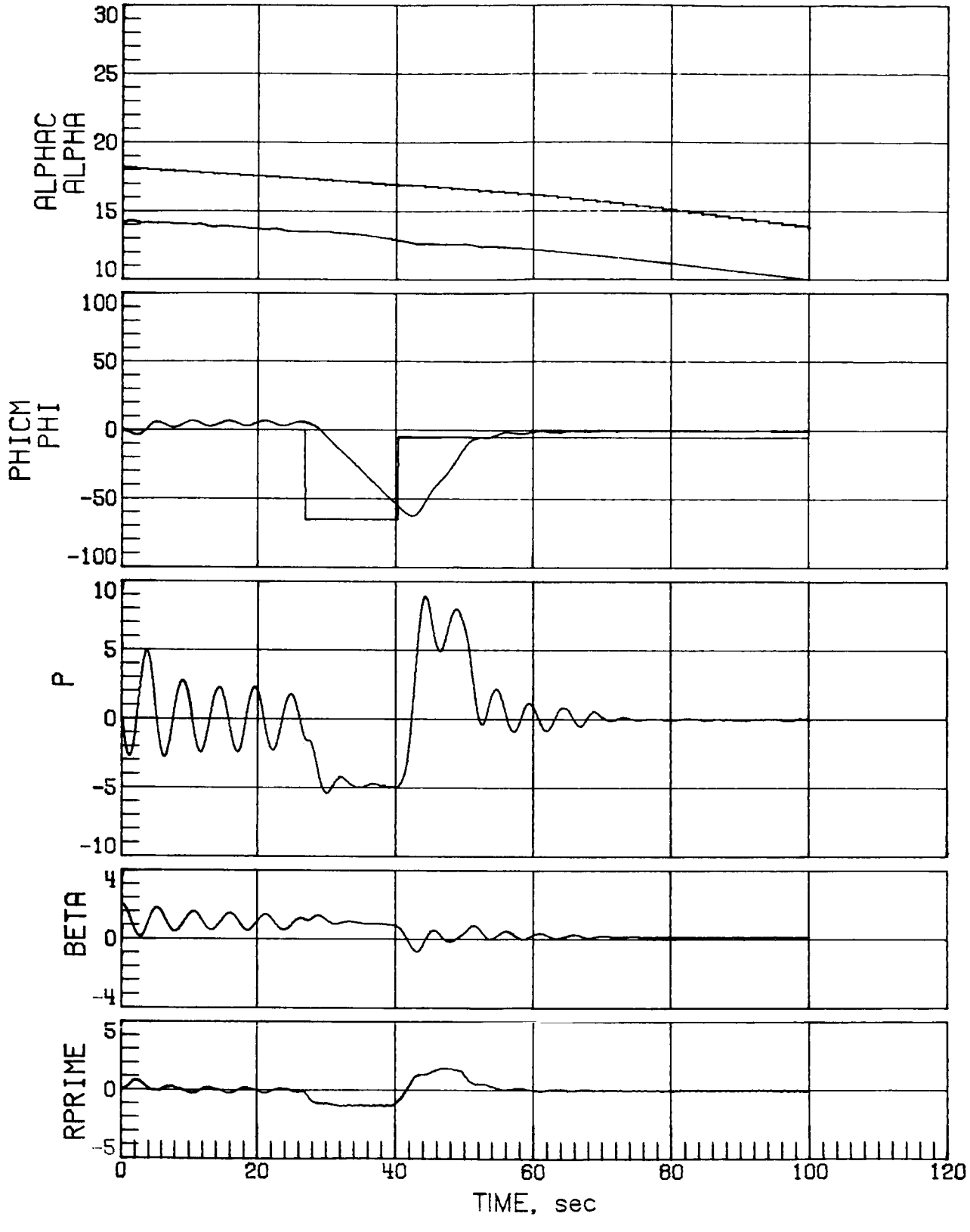

(c) Case 5.

Figure 35.- Continued.

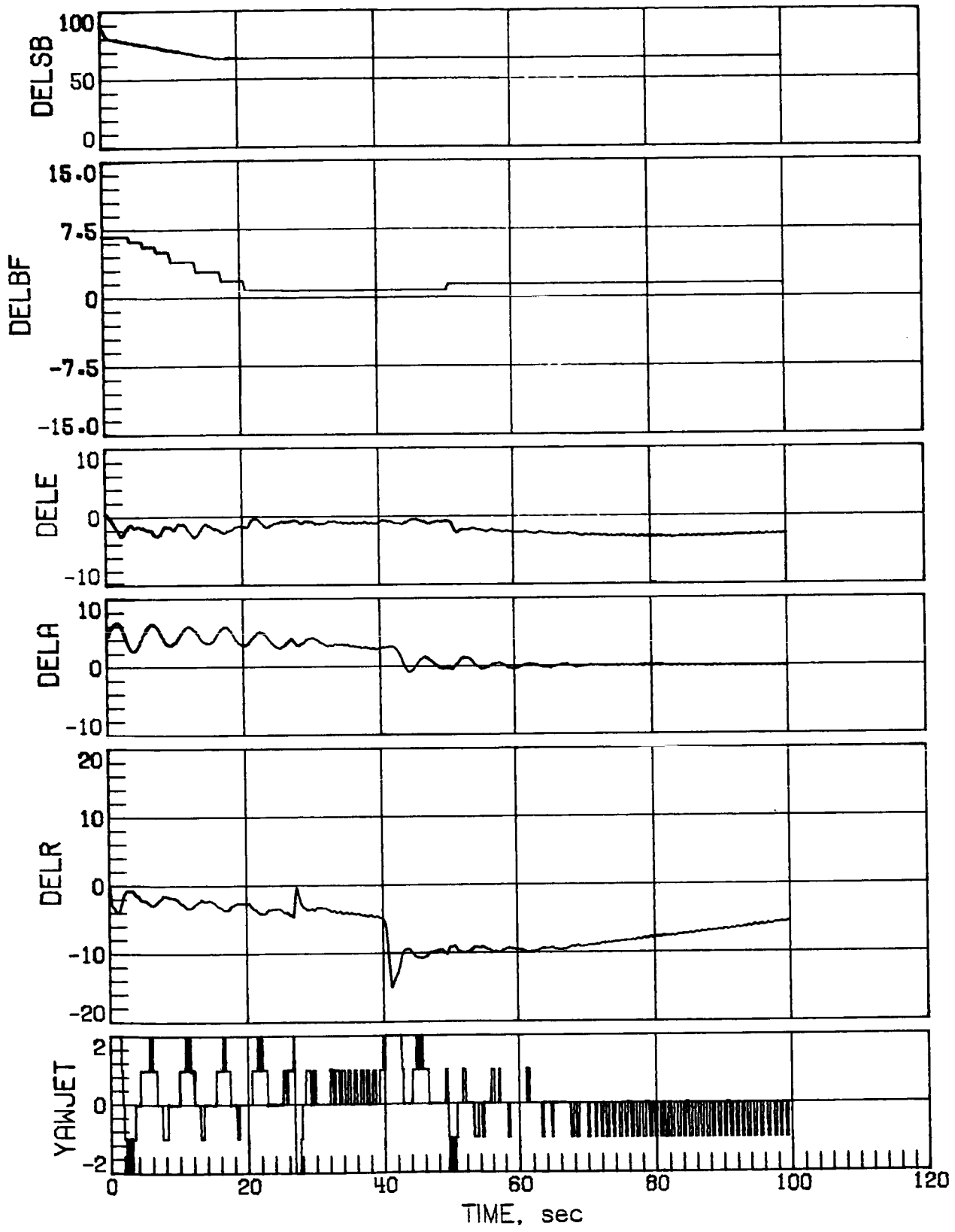

(c) Concluded.

Figure 35.- Concluded.

1. Report No.	2. Government Accession No.	3. Recipient's Catalog No.
NASA TP-2283		

4. Title and Subtitle	5. Report Date
EFFECT OF AERODYNAMIC AND ANGLE-OF-ATTACK UNCERTAINTIES ON THE BLENDED ENTRY FLIGHT CONTROL SYSTEM OF THE SPACE SHUTTLE FROM MACH 10 TO 2.5	April 1984
	6. Performing Organization Code: 506-51-13-07
7. Author(s): Howard W. Stone and Richard W. Powell	8. Performing Organization Report No.: L-15719
	10. Work Unit No.
9. Performing Organization Name and Address: NASA Langley Research Center, Hampton, VA 23665	11. Contract or Grant No.
12. Sponsoring Agency Name and Address: National Aeronautics and Space Administration, Washington, DC 20546	13. Type of Report and Period Covered: Technical Paper
	14. Sponsoring Agency Code

15. Supplementary Notes

16. Abstract

A six-degree-of-freedom simulation analysis has been performed for the Space Shuttle Orbiter during entry from Mach 10 to 2.5 with realistic off-nominal conditions using the entry flight control system specified in May 1978. The off-nominal conditions included the following: (1) aerodynamic uncertainties, (2) an error in deriving the angle of attack from onboard instrumentation, (3) the failure of two of the four reaction control-system thrusters on each side, and (4) a lateral center-of-gravity offset. With combinations of the above off-nominal conditions, the control system performed satisfactorily with a few exceptions. The cases that did not exhibit satisfactory performance displayed the following main weaknesses. Marginal performance was exhibited at hypersonic speeds with a sensed angle-of-attack error of 4°. At supersonic speeds the system tended to be oscillatory, and the system diverged for several cases because of the inability to hold lateral trim. Several system modifications were suggested to help solve these problems and to maximize safety on the first flight: alter the elevon-trim and speed-brake schedules, delay switching to rudder trim until the rudder effectiveness is adequate, and reduce the overall rudder loop gain. These and other modifications were incorporated in a flight-control-system redesign in May 1979.

17. Key Words (Suggested by Author(s))	18. Distribution Statement
Flight control Entry Space Shuttle	Unclassified - Unlimited Subject Category 08

19. Security Classif. (of this report)	20. Security Classif. (of this page)	21. No. of Pages	22. Price
Unclassified	Unclassified	290	A13

For sale by the National Technical Information Service, Springfield, Virginia 22161

NASA-Langley, 1984